UC Irvine
Faculty Publications

Title
Bounding the role of black carbon in the climate system: A scientific assessment

Permalink
https://escholarship.org/uc/item/1c68530v

Journal
Journal of Geophysical Research: Atmospheres, 118(11)

ISSN
2169897X

Authors
Bond, T. C
Doherty, S. J
Fahey, D. W
et al.

Publication Date
2013-06-16

DOI
10.1002/jgrd.50171

Peer reviewed

eScholarship.org Powered by the California Digital Library
University of California

Bounding the role of black carbon in the climate system: A scientific assessment

by

T. C. Bond[1], S. J. Doherty[2], D. W. Fahey[3], P. M. Forster[4], T. Berntsen[5], O. Boucher[6], B. J. DeAngelo[7], M. G. Flanner[8], S. Ghan[9], B. Kärcher[10], D. Koch[11], S. Kinne[12], Y. Kondo[13], P. K. Quinn[14], M. C. Sarofim[7], M. G. Schultz[15], M. Schulz[16], C. Venkataraman[17], H. Zhang[18], S. Zhang[19], N. Bellouin[20], S. K. Guttikunda[21], P. K. Hopke[22], M. Z. Jacobson[23], J. W. Kaiser[24], Z. Klimont[25], U. Lohmann[26], J. P. Schwarz[3], D. Shindell[27], T. Storelvmo[28], S. G. Warren[29], C. S. Zender[30]

Abstract

Black carbon aerosol plays a unique and important role in Earth's climate system. Black carbon is a type of carbonaceous material with a unique combination of physical properties. Predominant sources are combustion related; namely, fossil fuels for transportation, solid fuels for industrial and residential uses, and open burning of biomass. Total global emissions of black carbon using bottom-up inventory methods are 7500 Gg yr^{-1} in the year 2000 with an uncertainty range of 2000 to 29000. This assessment provides an evaluation of black-carbon climate forcing that is comprehensive in its inclusion of all known and relevant processes and that is quantitative in providing best estimates and uncertainties of the main forcing terms: direct solar absorption, influence on liquid, mixed-phase, and ice clouds, and deposition on snow and ice. These effects are calculated with models, but when possible, they are evaluated with both microphysical measurements and field observations. Global atmospheric absorption attributable to black carbon is too low in many models, and should be increased by about about 60%. After this scaling, the best estimate for the industrial-era (1750 to 2005) direct radiative forcing of black carbon is +0.43 W m^{-2} with 90% uncertainty bounds of (+0.17, +0.68) W m^{-2}. Total direct forcing by all black carbon sources in the present day is estimated as +0.49 (+0.20, +0.76) W m^{-2}. Direct radiative forcing alone does not capture important rapid adjustment mechanisms. A framework is described and used for quantifying climate forcings and their rapid responses and feedbacks. The best estimate of industrial-era (1750 to 2005) climate forcing of black carbon through all forcing mechanisms is +0.77 W m^{-2} with 90% uncertainty bounds of +-0.06 to +1.53 W m^{-2}. Thus, there is a 96% probability that black carbon emissions, independent of co-emitted species, have a positive forcing and warm the climate. With a value of +0.77 W m^{-2}, black carbon is likely the second most important individual climate-forcing agent in the industrial era, following carbon dioxide. Sources that emit black carbon also emit other short-lived species that may either cool or warm climate. Climate forcings from co-emitted species are estimated and used in the framework described herein. When the principal effects of co-emissions, including cooling agents such as sulfur dioxide, are included in net forcing, energy-related sources (fossil-fuel and biofuel) have a net climate forcing of +0.004 (-0.62 to +0.57) W m^{-2} during the first year after emission. For a few of these sources, such as diesel engines and possibly residential biofuels, warming is strong enough that eliminating all emissions from these sources would reduce net climate forcing (*i.e.,* produce cooling). When open burning emissions, which emit high levels of organic matter, are included in the total, the best estimate of net industrial-era climate forcing by all black-carbon-rich sources becomes slightly negative (-0.08 W m^{-2} with 90% uncertainty bounds of -1.23 to +0.81 W m^{-2}). The uncertainties in net climate forcing from black-carbon-rich sources are substantial, largely due to lack of knowledge about cloud interactions with both black carbon and co-emitted organic carbon. In prioritizing potential black-carbon mitigation actions, non-science factors, such as technical feasibility, costs, policy design, and implementation feasibility play important roles. The major sources of black carbon are presently in different stages with regard to the feasibility for near-term mitigation. This assessment, by evaluating the large number and complexity of the associated physical and radiative processes in black-carbon climate forcing, sets a baseline from which to improve future climate forcing estimates.

Submitted to the Journal of Geophysical Research-Atmospheres on 26 March 2012

[1]University of Illinois at Urbana-Champaign, Urbana, Illinois, USA.
[2]Joint Institute for the Study of the Atmosphere and Ocean, University of Washington, Seattle, Washington, USA.
[3]NOAA Earth System Research Laboratory, Boulder, Colorado, USA and Cooperative Institute for Research in Environmental Sciences, University of Colorado, Boulder, Colorado, USA
[4]University of Leeds, Leeds, UK.
[5]Center for International Climate and Environmental Research-Oslo and Department of Geosciences, University of Oslo, Oslo, Norway.
[6]Laboratoire de Météorologie Dynamique, IPSL/CNRS, Paris, France (Previously at Met Office Hadley Centre, Exeter, UK).
[7]US Environmental Protection Agency, Washington, DC, USA.
[8]University of Michigan, Ann Arbor, Michigan, USA.
[9]Pacific Northwest National Laboratory, Richland, Washington, USA.
[10]Deutsches Zentrum für Luft- und Raumfahrt Oberpfaffenhofen, Wessling, Germany.
[11]US Department of Energy, Washington, DC, USA.
[12]Max Planck Institute, Hamburg, Germany.
[13]University of Tokyo, Tokyo, Japan.
[14]NOAA Pacific Marine Environment Laboratory, Seattle, Washington, USA.
[15]Forschungszentrum Jülich GmbH, Jülich, Germany.
[16]Norwegian Meteorological Institute, Oslo, Norway.
[17]Indian Institute of Technology, Bombay, India.
[18]China Meteorological Administration, Beijing, China.

[19]Peking University, Beijing, China.
[20]Met Office Hadley Centre, Exeter, UK.
[21]Division of Atmospheric Sciences, Desert Research Institute, Reno, Nevada, USA
[22]Clarkson University, Potsdam, New York, USA.
[23]Stanford University, Stanford, California, USA.
[24]European Centre for Medium-range Weather Forecasts, Reading, UK.
[25]International Institute for Applied System Analysis, Laxenburg, Austria.
[26]Eidgenössische Technische Hochschule Zürich, Zurich, Switzerland.
[27]NASA Goddard Institute for Space Studies, New York, New York, USA.
[28]Yale University, New Haven, Connecticut, USA.
[29]University of Washington, Seattle, Washington, USA.
[30]University of California, Irvine, California, USA.

Table of Contents

0. Executive Summary

0.1. Background and motivation

Black carbon is emitted in a variety of combustion processes and is found throughout the Earth system. Black carbon has a unique and important role in the Earth's climate system because it absorbs solar radiation, influences cloud processes, and alters the melting of snow and ice cover. A large fraction of atmospheric black carbon concentrations is due to anthropogenic activities. Concentrations respond quickly to reductions in emissions because black carbon is rapidly removed from the atmosphere by deposition. Thus, black carbon emission reductions represent a potential mitigation strategy that could reduce global climate forcing from anthropogenic activities in the short term and slow the associated rate of climate change.

Previous studies have shown large differences between estimates of the effect of black carbon on climate. To date, reasons behind these differences have not been extensively examined or understood. This assessment provides a comprehensive and quantitative evaluation of black carbon's role in the climate system and explores the effectiveness of a range of options for mitigating black carbon emissions. As such, this assessment includes the principal aspects of climate forcing that arise from black carbon emissions. It also evaluates the net climate forcing of combustion sources that emit large quantities of black carbon by including the effects of co-emitted species such as organic matter and sulfate aerosol precursors. The health effects of exposure to black carbon particles in ambient air are not considered in this assessment.

0.2. Major Findings

0.2.1. Black carbon properties

1. *Black carbon is a distinct type of carbonaceous material that is formed primarily in flames, is directly emitted to the atmosphere, and has a unique combination of physical properties.* It strongly absorbs visible light; is refractory with a vaporization temperature near 4000 K; exists as an aggregate of small spheres; and is insoluble in water and organic solvents. In measurement and modeling studies, the use of the term 'black carbon' frequently has not been based on this rigorous definition, resulting in a lack of comparability among results.
2. *Many methods used to measure black carbon can be biased by the presence of other chemical components.* Measured mass concentrations can differ between methods by up to 80% with the largest differences corresponding to aerosol with low black carbon mass fractions.
3. *The atmospheric lifetime of black carbon, its impact on clouds and its optical properties depend on interactions with other aerosol components.* Black carbon is co-emitted with a variety of other aerosols and aerosol precursor gases. Soon after emission, black carbon becomes mixed with other aerosol components in the atmosphere. This mixing increases light absorption by black carbon, influences its atmospheric removal rate, and increases its capacity to form liquid-cloud droplets.

0.2.2. Black carbon emissions and abundance

1. *Sources whose emissions are rich in black carbon ('BC-rich') can be grouped into a small number of categories, broadly described as diesel engines, industry, residential solid fuel and open burning.* The largest global sources are open burning of forests and savannas. Dominant emitters of black carbon from other types of combustion depend on the location. Residential solid fuels (*i.e.,* coal and biomass) are 60 to 80% of Asian and African emissions, while on-road and non-road diesel engines are about 70% of emissions in Europe, North America and Latin America. Residential coal contributes significantly in China, the former USSR and a few Eastern European countries. These categories represent about 90% of black-carbon mass emissions. Aircraft and shipping emissions are minor contributions to emitted mass.
2. *Total global emissions of black carbon using bottom-up inventory methods are 7500 Gg yr^{-1} in the year 2000 with an uncertainty range of 2000 to 29000.* Emissions of 4800 (1200 to 15000) Gg yr^{-1} black carbon are from energy-related combustion, which includes all but open burning, and the remainder is from open burning of forests, grasslands, and agricultural residues.
3. *An estimate of background black carbon abundances in a pre-industrial year is used to evaluate climate effects.* In this assessment, we use the term 'industrial era' to denote differences in the atmospheric state between present day and the year 1750. We use a pre-industrial value of 1400 Gg of black carbon per year from biofuel and open biomass burning, although some fraction was anthropogenic at that time.
4. *Current emission estimates agree on the major sources and emitting regions, but significant uncertainties remain.* Information gaps include the amounts of biofuel or biomass combusted, and the type of technology or burning, especially in developing countries. Emission estimates from open-biomass burning lack data on fuel consumed, and black-carbon emission factors from this source may be too low.
5. *Black carbon undergoes regional and intercontinental transport during its short atmospheric lifetime.* Atmospheric removal occurs within a few days to weeks via precipitation and contact with surfaces. As a result, black carbon is found in remote regions of the atmosphere at concentrations much lower than in source regions.
6. *Comparison with remote sensing observations indicates that global atmospheric absorption attributable to black carbon is too low in many models.* Scaling the aerosol absorption to match observations increases the modeled globally averaged, industrial-era absorption by 60%. Much, but not all, of the model underestimates can be attributed to the models lacking treatment of enhanced absorption caused by mixing of black carbon with other constituents. The remainder is attributed to underestimates of the amount of black carbon in the atmosphere. Underestimates of 50 to 160% are found in South Asia, Southeast Asia, Latin America, and the Pacific region. In contrast, models generally overestimate black carbon amounts in Europe, Central Asia, and the Middle East while amounts in North America, East Asia and Africa are approximately correct.
7. *If all differences in modeled black carbon abundances were attributed to emissions, total emissions would be 10000 Gg yr^{-1} compared to the bottom-up inventory estimates of 7300 Gg yr^{-1}.* The industrial-era value of about *8700 Gg yr^{-1}*, obtained by subtraction of the pre-industrial value, is used as the best estimate of emissions to determine final forcing values in this

assessment. However, some of the difference could be attributed to poorly modeled removal rates instead of emissions.

0.2.3. Synthesis of black-carbon climate forcing terms

1. Radiative forcing used alone to estimate black-carbon climate effects fails to capture important rapid adjustment mechanisms. Black-carbon-induced atmospheric heating and cloud microphysical effects cause rapid adjustments within the climate system, particularly in clouds and the snow-pack. These rapid adjustments cause radiative imbalances that should be captured as adjusted or effective forcings. Use of these adjusted measures gives a more complete understanding of the global response to black carbon. The effective forcing accounts for the larger response of surface temperature to a radiative forcing by black carbon in snow and ice compared to other forcing mechanisms. These factors are included in the climate forcing values reported in this assessment.

2. The best estimate of industrial-era effective climate forcing of black carbon through all forcing mechanisms is +0.77 W m^{-2} with 90% uncertainty bounds of -0.06 to +1.53 W m^{-2}. This is greater than the direct forcing given in the fourth Intergovernmental Panel on Climate Change (IPCC) report. There is a 96% probability that black carbon emissions, independent of co-emitted species, have a positive forcing and warm the climate. This black carbon climate forcing is based on the change in atmospheric abundance over the industrial era (1750 to 2005). The black-carbon climate-forcing terms that make up this estimate are listed in Table 0.1. For comparison, the radiative forcings from the two most significant long-lived greenhouse gases, carbon dioxide (CO_2) and methane (CH_4), in 2005 were +1.66 and +0.48 W m^{-2}, respectively.

3. The fossil-fuel direct effect of black carbon of +0.15 W m^{-2} agrees with the value provided by the IPCC in 2007. The black-carbon-in-snow forcing estimate in this assessment is also comparable, although more sophisticated. Our total climate forcing estimate of +0.77 W m^{-2} includes biofuel and open-biomass sources of black carbon, as well as cloud effects that the IPCC report did not explicitly isolate for black carbon.

0.2.4. Black-carbon direct radiative forcing

1. Direct radiative forcing of black carbon is caused by absorption and scattering of sunlight. Absorption heats the atmosphere where black carbon is present and reduces sunlight that reaches the surface and that is reflected back to space. Direct radiative forcing is the most commonly cited climate forcing associated with black carbon.

2. The best estimate for the industrial-era (1750 to 2005) direct radiative forcing of black carbon in the atmosphere is +0.43 W m^{-2} with 90% uncertainty bounds of +0.17 to +0.68 W m^{-2}. Previous direct forcing estimates ranged from +0.2 to +0.9 W m^{-2}. This range is altered because we constrain global aerosol models with observational estimates of black carbon amounts.

3. Direct radiative forcing from all present-day sources of black carbon (including pre-industrial background sources) is estimated to be +0.49 W m^{-2} with 90% uncertainty bounds of +0.20 to +0.76 W m^{-2}. This value is 14% larger than industrial-era forcing because of appreciable pre-industrial emissions from open burning and biofuel use.

0.2.5. Black-carbon cloud effects

1. Black carbon influences the properties of ice clouds and liquid clouds through diverse and complex processes. These processes include: changing the number of liquid cloud droplets, enhancing precipitation in mixed-phase clouds, and changing ice particle number and cloud extent. The resulting radiative changes in the atmosphere are considered climate *indirect effects* of black carbon. In addition, in the semi-direct effect, light absorption by black carbon alters the atmospheric temperature structure within, below, or above clouds and consequently alters cloud distributions. Liquid-cloud and semi-direct effects may have either negative or positive climate forcings. Mixed-phase cloud changes cause positive climate forcing (warming). At present, even the sign of BC ice-cloud forcing is unknown.

2. The best estimate of the industrial-era climate forcing from black carbon cloud effects is positive with substantial uncertainty (+0.17 W m^{-2} with a -0.45 to +0.86 W m^{-2} 90% uncertainty range). The cloud effects are quantified in Table 0.1. Cloud effects are the largest source of uncertainty in the evaluation of black carbon's role in the climate system. Very few model studies have isolated the influence of black carbon in these indirect effects.

0.2.6. Black-carbon snow and ice effects

1. Black carbon deposition on snow and ice causes positive climate forcing. Even aerosol sources with negative globally averaged, climate forcing, such as biomass combustion, can produce positive climate forcing in the Arctic because of their effects on snow and ice.

2. The best estimate of climate forcing from black carbon deposition on snow and sea ice in the industrial era is +0.14 W m^{-2} with 90% uncertainty bounds of +0.04 to +0.34 W m^{-2}. The all-source present-day climate forcing estimate is somewhat higher at +0.16 W m^{-2}. This climate forcing results from a combination of radiative forcing, rapid adjustments, and the higher efficacy of this forcing compared to an equivalent, globally averaged forcing from carbon dioxide. The high efficacy is driven by the snow albedo feedback and the high latitude of the forcing.

3. Species other than black carbon are a large fraction of the absorbing aerosol mass that reduces reflectivity of snow and ice cover. These species include dust and absorbing organic carbon; the latter is co-emitted with black carbon or may come from local soils.

4. The role of black carbon in the melting of glaciers is still highly uncertain. Few measurements of glacial black-carbon content exist, and studies of the impact on glacial snow melt and sea ice have not sufficiently accounted for natural impurities such as soil dust and algae or for the difficulty in modeling regions of mountainous terrain.

0.2.7. Impacts of black-carbon climate forcing

1. The black-carbon climate forcings from the direct effect and snowpack changes cause the troposphere and the top of the cryosphere to warm, inducing further climate response in the form of cloud, circulation, surface temperature and precipitation changes. In climate model studies, black-carbon direct effects cause equilibrium, globally averaged, surface warming between +0.1 and +0.7 K, with the warming concentrated in the Northern Hemisphere. Black-carbon snow

forcing causes equilibrium, globally averaged, climate warming of +0.05 to +0.20 K. The warming response to snow forcing is greatest during local spring and over mid-to-high northern latitudes.

2. *Regional circulation and precipitation changes may occur in response to black-carbon climate forcings.* These changes include a northward shift in the Inter-Tropical Convergence Zone and changes in Asian monsoon systems where concentrations of absorbing aerosols are large. Black-carbon cloud indirect effects are also expected to induce a climate response. However, the responses to these complex and uncertain climate-forcing mechanisms is not a robust feature of global models.

0.2.8. Net climate forcing by black-carbon-rich source categories

1. *Other species co-emitted with black carbon influence the sign and magnitude of net climate forcing by black-carbon-rich source categories.* The net climate forcing of a source sector is a useful metric when considering mitigation options. Principal co-emitted species that can change the sign of forcing are organic matter and sulfur species. The direct radiative forcing is positive for almost all black-carbon-rich source categories (about 95% of the black carbon mass), even when negative direct forcings by sulfate and organic matter are considered. Liquid-cloud forcing by co-emitted aerosol species can introduce large negative forcing. Therefore, high confidence in net positive effective forcing is possible only for black-carbon source categories with low co-emitted species, such as diesel engines.
2. *The best estimate of the net industrial-era climate forcing by short-lived effects from all black-carbon-rich sources is near zero with large uncertainty bounds.* Short-lived effects are defined as those lasting less than one year. This total is +0.004 (-0.62 to +0.57) W m^{-2} for fossil-fuel and biofuel emissions, and -0.08 W m^{-2} with 90% uncertainty bounds of -1.24 to +0.81 W m^{-2} when open burning emissions are included.
3. *The climate forcings from specific sources within black-carbon source categories can be highly variable.* Some subsets of a category may have net positive climate forcing even if the whole category does not. Selecting such individual source types from each category can yield a group of measures that, if implemented, would reduce climate forcing. However, the positive forcing reduction would be much less than the +0.77 W m^{-2} attributable to all industrial-era black-carbon emissions in 2005.
4. *Short-lived forcing effects from black-carbon-rich sources are substantial compared with the effects of long-lived greenhouse gases from the same sources, even when the forcing is integrated over 100 years.* Climate forcing from changes in short-lived species integrated over 100 years amounts to 5 to 60% of the combined longer-lived forcing by methane, effects on the methane system, and CO_2.

0.2.9. Climate metrics for black carbon emissions

1. *The 100-year global-warming-potential (GWP) value for black carbon is 800 (35 to 1700 range) with all forcing mechanisms included.* The large range derives from the uncertainties in the climate forcings for black carbon effects. The GWP and other climate metric values vary by about ±30% between emitting regions. Black-carbon metric values decrease with increasing time horizon due to the short lifetime of black carbon emissions compared to CO_2. Black carbon and CO_2 emission amounts with equivalent 100-year GWPs have different impacts on climate, temperature, rainfall, and the timing of these impacts. These and other differences raise questions about the appropriateness of using a single metric to place black carbon and greenhouse gases on a common scale.

0.2.10. Perspective on mitigation options for black carbon emissions

1. *Prioritization of black-carbon mitigation options is informed by both scientific and non-scientific factors.* Scientific issues include the magnitude of black carbon emissions by sector and region, and net climate forcing including co-emissions and impacts on the cryosphere. Non-science factors, such as technical feasibility, costs, policy design, and implementation feasibility also play roles. The major sources of black carbon are presently in different stages with regard to technical and programmatic feasibility for near-term mitigation.
2. *Diesel-engine sources of black carbon appear to offer the best mitigation potential to reduce near-term climate forcing.* Mitigating emissions from residential solid fuels also may yield a reduction in net positive forcing, especially when the longer-term effects on methane are considered. The net effect of small industrial sources depends on the sulfur content, so that net climate benefits are possible by mitigating some individual source types.

0.2.11. Implications for policymakers

1. *Black carbon is likely to be the second most important individual climate-forcing agent after carbon dioxide, with a total climate forcing of +0.77 W m^{-2} (+0.06 to +1.53 W m^{-2} range).* This forcing estimate includes all known effects: direct effects, cloud effects, and snow and ice effects. The uncertainty in the total climate-forcing estimate is large, at approximately ±100% (+0.06 to +1.53 W m^{-2} range). The large uncertainty derives principally from the indirect climate-forcing effects associated with the interactions of black carbon with cloud processes.
2. *Black carbon forcing concentrates climate warming in the mid-high latitude Northern Hemisphere.* As such, black carbon could induce changes in the precipitation patterns from the Asian Monsoon. It is also likely to be one of the causes of Arctic warming in the early 20th century.
3. *The species co-emitted with black carbon also have significant climate forcing.* For a subset of black-carbon-rich sources, including diesel engines and possibly residential solid-fuel emissions, the net impact of reductions can be a lessening of positive climate forcing (cooling). However, the impact of all emissions from BC-rich sources is slightly negative (-0.08 W m^{-2}) with a large uncertainty range (-1.24 to +0.81 W m^{-2}). The implication of this estimate is that uniform elimination of all emissions from black-carbon-rich sources could lead to no change in climate warming. Therefore, sources and mitigation measures chosen to reduce positive climate forcing should be carefully identified. The uncertainty in the response to mitigation is larger when more aerosol species are co-emitted.
4. *The majority of aerosol negative forcing is concentrated in sectors with no black carbon emissions.* This means that any black-carbon-rich source category is a good candidate for

reducing aerosol concentrations, which affect public health, without adversely affecting climate.

5. *Forcings by greenhouse-gases alone from emission sources do not convey the full climate impact of individual actions.* For black-carbon-rich sectors, climate forcing by short-lived emissions (black carbon, other aerosols and precursors, and some gases) is substantial (up to 60%) in comparison with the co-emissions of long-lived greenhouse gases (*e.g.,* CO_2 and CH_4) from these sources, even when both forcings are integrated over 100 years.

1. Introduction

[1] In the year 2000, a pair of papers [*Jacobson*, 2000; *Hansen et al.*, 2000] pointed out that black carbon— small, very dark particles resulting from combustion—might presently warm the atmosphere about one-third as much as CO_2. Because black carbon absorbs much more light than it reflects, it warms the atmosphere through its interaction with sunlight. This warming effect contrasts with the cooling effect of other particles that are primarily scattering and thus reduce the amount of energy kept in the Earth system. Radiative forcing (RF) by atmospheric BC stops within weeks after emissions cease because its atmospheric lifetime is short unlike the long timescale associated with the removal of CO_2 from the atmosphere. Thus, sustained reductions in emissions of BC and other short-lived climate warming agents, especially methane and tropospheric ozone (O_3), could quickly decrease positive climate forcing and hence climate warming. While such targeted reductions will not avoid climate change, their value in a portfolio to manage the trajectory of climate forcing is acknowledged in the scientific community [*e.g.*, *Molina et al.*, 2009; *Ramanathan and Xu,* 2010].

[2] In the decade since the initial proposals, the speed of Arctic climate change and glacial melt has increased the demand for mitigation options which can slow near-term warming, such as reductions in the emissions of short-lived warming agents. The impact of air quality regulations that reduce sulfate particles is also being recognized. Most particles, including sulfates, cool the climate system, masking some of the warming from longer-lived greenhouse gases (GHGs) and BC. Thus, regulating these particles to protect human health has the unintended consequence of increasing warming, a rapid change that could be offset by BC reductions. BC also plays a direct role in surface melting of snow and ice and, hence, may have an important role in Arctic warming [*Quinn et al.,* 2008]; if so, targeted reductions could have disproportionate benefits for these sensitive regions.

[3] Particulate matter was originally regulated to improve human health. Evidence supporting the link between particles and adverse respiratory and cardiovascular health continues to mount [*Pope et al.,* 2009]. High human exposures to particulate matter in urban settings are linked to sources that emit black carbon [*Grahame and Schlesinger,* 2007; *Naeher et al.*, 2007; *Janssen et al.*, 2011] and to intense exposures in indoor air [*Smith et al.,* 2010]. Thus, reducing particulate matter is desirable to improve human welfare, regardless of whether those reductions reduce climate warming.

[4] For the past few years, the opportunity to reduce black carbon has received pervasive policy attention at high levels. The G8 declaration, in addition to promising GHG reductions, committed to "…taking rapid action to address other significant climate forcing agents, such as black carbon." [9 July 2009, L'Aquila, Italy]. The Arctic Council, recognizing that "…reductions of emissions have the potential to slow the rate of Arctic snow, sea ice and sheet ice melting in the near-term…," established a task force in 2009 to offer mitigation recommendations [29 April 2009, Tromsø, Norway] and "encouraged" the eight member states to implement certain black-carbon reduction measures [12 May 2011, Nuuk, Greenland]. The United States has complemented this international interest with passage of a bill [H.R. 2996] requiring a study of the sources, climate and health impacts, and mitigation options for black carbon both domestically and internationally. A proposed revision to the Gothenburg Protocol [*UNECE*, 1999] states that parties "should, in implementing measures to achieve their national targets for particulate matter, give priority, to the extent they consider appropriate, to emission reductions measures which also significantly reduce black carbon." [*UNECE*, 2011].

[5] The prospect of achieving quick climate benefits by reducing BC emissions is tantalizing, but the scientific basis for evaluating the associated policy choices has not yet been fully established. This assessment is intended to provide a comprehensive and quantitative scientific framework for such an evaluation. In the remainder of this section, we briefly define black carbon, provide an overview of its role in the climate system, and describe the assessment's principal sections. This introductory section closes by discussing the guiding principles used in this assessment in light of the scientific complexity of the topic.

1.1. What is black carbon?

[6] Black carbon is a distinct type of carbonaceous material, formed only near flames during combustion of carbon-based fuels. It is distinguishable from other forms of carbon and carbon compounds contained in atmospheric aerosol because it has a unique combination of the following physical properties:

1. It *strongly absorbs visible light* with a mass absorption cross section of at least 5 $m^2 g^{-1}$ at a wavelength of 550 nm.

2. It is *refractory;* that is, it retains its basic form at very high temperatures, with a vaporization temperature near 4000K.

3. It is *insoluble* in water, in organic solvents including methanol and acetone, and in other components of atmospheric aerosol, and

4. It exists as an *aggregate* of small carbon spherules.

[7] The strong absorption of visible light by black carbon is the distinguishing characteristic that has raised interest in studies of atmospheric radiative transfer. No other substance with such strong light absorption per unit mass is present in the atmosphere in significant quantities. The aggregate nature of black carbon results from its formation in combustion, differentiating it from graphite. BC has very low chemical reactivity in the atmosphere; its primary removal process is wet or dry deposition to the surface. BC is generally found in atmospheric aerosol particles containing a number of other materials, many of which are co-emitted with BC from a variety of sources.

[8] In this assessment, the term 'black carbon' and the abbreviation 'BC' will be used to denote ambient aerosol material with the above characteristics. Note that this definition of black carbon has not been used rigorously or consistently throughout most previous literature describing absorbing aerosol and its role in the atmosphere. Section 2 gives further discussion of terminology.

1.2. How does black carbon affect the Earth's radiative budget?

[9] The principal goal of this assessment is to synthesize the current state of science regarding BC as a climate forcing agent. Figure 1.1 illustrates the multi-faceted interaction of BC with

the Earth system. A variety of combustion sources, both natural and anthropogenic, emit BC directly to the atmosphere. The largest global sources are open burning of forests and savannas, solid fuels burned for cooking and heating, and on-road and off-road diesel engines. Industrial activities are also significant sources, while aircraft and shipping emissions represent minor contributions to emitted mass at the global scale. The difficulty in quantifying emissions from such diverse sources contributes to the uncertainty in evaluating BC's climate role. Once emitted, BC aerosol undergoes regional and intercontinental transport and is removed from the atmosphere through wet (*i.e.,* in precipitation) and dry deposition to the Earth's surface, resulting in an average atmospheric lifetime of one to two weeks.

[10] Radiative forcing over the industrial era (1750 –present) has typically been used (*e.g.*, by the IPCC [*Forster et al.,* 2007]) to quantify and compare first-order climate effects from different climate change mechanisms. Many of BC's effects on clouds and within the cryosphere are not easily assessed within this framework. These effects result in rapid adjustments involving the troposphere and land surface that lead to a perturbed energy balance that can also be quantified in units of radiative forcing. We employ the term 'climate forcing' to encompass both traditional radiative forcing and the rapid adjustment effects on clouds and snow (Table 1.1); this will be discussed further in Section 1.3.

[11] The best quantified climate impact of BC is its atmospheric *direct radiative forcing* — the consequent changes in the radiative balance of the Earth due to an increase in absorption of sunlight within the atmosphere. When BC is located above a reflective surface, such as clouds or snow, it also absorbs solar radiation reflected from that surface. Heating within the atmosphere and a reduction in sunlight reaching the surface can alter the hydrological cycle through changes in latent heating, and also by changing convection and large-scale circulation patterns.

[12] A particularly complex role of BC and other aerosols in climate is associated with changes in the formation and radiative properties of liquid-water and ice clouds. BC particles may increase the reflectivity and lifetime of warm (liquid) clouds, causing net cooling, or they may reduce cloudiness, resulting in warming. Aerosol particles can change cloud droplet number and cloud cover in ice clouds, or in mixed-phase clouds made up of both ice and liquid water. Changes in droplet number may also alter cloud emissivity, affecting longwave radiation.

[13] BC also produces warming when it is deposited on ice or snow because BC decreases the reflectivity of these surfaces, causing more solar radiation to be absorbed. The direct absorption of sunlight produces warming which affects snow and ice packs themselves, leading to additional climate changes, and ultimately to earlier onset of melt and amplified radiative forcing.

[14] An important consideration in evaluating the climate role of BC emissions is the role of co-emitted aerosols, aerosol precursors and other gases. Many of these co-emitted species arise in the same combustion sources that produce BC. The greatest emissions by mass include sulfur-containing particles or precursors; organic aerosols that are directly emitted; organic compounds that are precursors to aerosols and ozone; nitrogen oxides that play roles in ozone formation and methane destruction and are precursors to nitrated aerosols; and long-lived GHGs. Sources also emit smaller quantities of ionic species such as potassium and chloride. The non-BC particles absorb little or no light, so they often cool rather than warm climate. They also play a role in many, but not all, of the same cloud processes as BC.

[15] In contrast to BC, most other aerosols and precursors are chemically reactive in the atmosphere. Because of transport and chemical and microphysical transformation after emission, the atmospheric aerosol becomes a complex array of atmospheric particles, some of which contain BC. Pure BC aerosol rarely exists in the atmosphere and, because it is just one component of this mixed aerosol, it cannot be studied in isolation. Compared with pure BC, mixed-composition particles differ in their lifetimes, interaction with solar radiation, and interactions with clouds. The components of these mixed particles may come from the same or different sources than BC.

[16] The overall contribution of natural and anthropogenic sources of BC to climate forcing requires aggregating the multiple aspects of BC's interaction with the climate system, as well as the climate impacts of constituents that are co-emitted with BC. Each contribution may lead to positive climate forcing (generally leading to a warming) or negative climate forcing (generally cooling). As discussed in the body of this assessment, BC impacts include both warming and cooling terms. A principal goal of this assessment is to provide an aggregation of impacts by BC only, along with their uncertainties. A second major goal is estimating the impacts by BC plus co-emitted species to estimate a net climate forcing contribution of particular sources. Quantifying this net value is fundamental to understanding the climatic impact of reducing BC emissions.

[17] While globally averaged climate forcing is a useful concept, BC concentration and deposition are spatially heterogeneous. This means that climate forcing by aerosols and climate response to aerosols may be distributed differently than those of well-mixed GHGs. In this assessment, we briefly discuss regional variations in BC impacts. Also discussed are climate impacts of BC emissions beyond climate forcings *per se,* such as changes in precipitation. However, a thorough quantification of these impacts is not included here.

[18] This assessment is divided into the following sections, which address specific aspects of BC and its role in Earth's climate:

2. Microphysical properties. The assessment begins with a review of BC-specific properties, including the techniques used to measure BC. The interactions of BC with the climate system depend upon its microphysical properties, optical properties, and mixing with other aerosol components. These govern all impacts shown in Figure 1.1.

3. Emissions. The origins and emission rates of BC are basic components of understanding its total impact. This section identifies major sources of BC, and those containing high fractions of black carbon ('BC-rich sources'). It also identifies other climate-active aerosols or aerosol precursors emitted from these sources. Finally, data from ambient measurements are reviewed to evaluate emission estimates and the contributions of particular source types.

4. Atmospheric abundance. The burden of BC in the atmosphere and its geographic distribution are basic quantities that directly affect all climate-forcing estimates. Observations that constrain the magnitude and location of modeled atmospheric burdens are discussed here.

5. Direct atmospheric radiative forcing. The direct interaction between BC and sunlight unquestionably results in a net positive radiative forcing of climate. This section discusses the basic components that affect direct radiative forcing and the best estimates for each of these components, and it explores the reasons for differences in published radiative forcing values.

6. Cloud changes. BC influences clouds by changing droplet formation and microphysical properties and by altering the thermal structure of the atmosphere. BC is not evenly distributed at different altitudes. It directly warms the atmosphere where it is located and alters atmospheric dynamics, the meteorological conditions affecting cloud formation, and the quantity of clouds. In addition, BC, as well as other particles, influences the size and number of water droplets and ice crystals in water and ice clouds through microphysical interactions. All of these changes produce radiative forcing by altering cloud properties. This section reviews the magnitude of changes in water clouds, mixed-phase clouds and ice clouds. The section emphasizes changes caused by BC alone, instead of the more common examination of cloud changes by all particles.

7. Cryosphere changes. BC is removed from the atmosphere both in precipitation and through dry deposition and thereby is incorporated into surface snow and ice, reducing their reflectivity. This initial radiative forcing is amplified by a series of rapid adjustments. Section 7 reviews modeled cryosphere forcing estimates, including discussion of the microphysical factors that affect radiative transfer in snow and ice packs and model choices that affect the amplification of that forcing through rapid adjustments. The section also compares the sources and magnitudes of modeled cryospheric BC concentrations with observations and uses this comparison to scale model estimates of forcing for a best estimate.

8. Climate response. Forcing is a common measure of radiative impact, but of ultimate concern is the climate response to BC, especially if it differs from that of other forcing agents. This section discusses the rapid adjustments in the climate system that affect the efficacy of the forcing by BC in the atmosphere and cryosphere. It also reviews the sparse knowledge about how regional and global climate respond to changes in top-of-atmosphere (ToA) forcing and atmospheric heating.

9. Synthesis. In this section, best estimates of climate forcing from direct atmospheric light absorption, microphysical cloud changes, the rapid adjustment to direct atmospheric absorption, and the darkening of surface snow and ice by BC are combined with estimates of the forcing efficacy to estimate the total climate forcing of BC in the industrial era (1750 to 2000). Total present-day (*i.e.,* 'all-source') forcing is also given for direct radiative forcing and snow and ice forcings.

10. Net climate forcing by BC-rich source categories. Because BC emissions are always accompanied by other species, this section examines the total atmospheric impacts of sources rich in BC, accounting for co-emitted species. While the preceding sections of the assessment examined total impact for all BC emissions, this section moves toward quantifying impact per emission of all species from a given source.

11. Metrics. Cost effectiveness is a key factor in policy discussions. To evaluate the cost effectiveness of BC mitigation versus mitigation of other climate forcing emissions like CO_2, the first step is to put climate impacts per kg emitted of different compounds on a common scale. This involves scientific issues as well as value judgments. This section expands the discussion of impact per emission, presenting how metrics commonly used in climate policy discussions may be applied to BC. The section also compares appropriate uses of each impact measure.

12. Mitigation of BC-rich sources. The preceding sections estimate the contributions to net climate forcing of BC emissions alone and of BC and co-emitted species from BC-rich sources. Although the questions to this point were largely scientific, mitigation choices aimed at reducing climate warming need to consider the feasibility of implementation. We therefore discuss some of the technological and logistical elements involved in enacting emission reductions, considering that emission types, control measures, and policies differ worldwide.

1.3. How can we quantify the climate effect of black carbon?

[19] Most discussions about climate change refer to measures that are variously called 'radiative forcing' or 'climate forcing.' Our use of the term 'radiative forcing' follows the IPCC definition given by Forster *et al.* [2007] that keeps tropospheric and surface temperatures fixed. However, many aerosol effects (*e.g.,* rapid adjustments in aerosol, cloud or snow distributions in response to the initial radiative forcing) can also be measured as changes in fluxes at the tropopause, making them amenable to comparison with radiative forcings. The sum of the radiative forcing and forcing due to these rapid adjustments yields the adjusted forcing. For the atmosphere and most of the land surface such rapid adjustments occur with a few days of applying the forcing. For the cryosphere, there is more of a continuum of adjustment processes and timescales, and rapid adjustments are usually considered to occur on seasonal timescales or less. For comparability to other forcing agents such as long-lived GHGs, these forcings can be scaled by their efficacy to yield the 'effective radiative forcing.' Our definitions for these terms are listed in Table 1.1, including descriptions of how they are determined from climate models. We give the sum of radiative forcing and all other forcing-like terms the name 'climate forcing,' and this usage is similar to that in the IPCC assessments [*IPCC,* 2007].

[20] Radiative forcing employed in IPCC reports assumes that anthropogenic impact is well represented by the difference between present day and the year 1750, the beginning of the industrial era. This may not be true for BC, where there is evidence of considerable anthropogenic biofuel and open burning before 1750. For the purposes of this assessment, the global climate forcings of BC and co-emitted species are evaluated from the beginning of the industrial era (1750). This

definition gives forcing that can be compared with the temperature change since that time, without requiring attribution to a particular cause. Rather than assuming that this value represents the present-day contribution of humans to climate forcing, we refer to the difference between year-2000 forcing and year-1750 forcing as 'industrial-era forcing.' For direct and cryosphere forcing, we also estimate forcing from all sources, even those that might have been ongoing before 1750. This total forcing is referred to as the 'all-source' forcing.

1.4. Guiding principles

[21] This assessment distills the scientific understanding of aerosol-climate interactions to estimate how BC-rich sources affect the climate system. A few principles guide the results presented here.

1. Quantification. We provide central values and ranges of physically reasonable estimates for each impact, with the goal of bounding the impact of BC and identifying key knowledge gaps that cause uncertainties to persist. Estimates of the climate impacts of BC vary among studies. The causes of some of the variation are identifiable, while some of the variation stems from inherent uncertainty. Diagnosis of this variation among estimates is a goal of this work. Our goal is to provide a best estimate and physically reasonable ranges or uncertainties for each impact, considering all available studies. To accomplish this, we have applied simplified adjustments to some study results in order to compare dissimilar results, with a philosophy of drawing information from as many studies as possible. Ranges are, therefore, based on quantitative analysis of publications combined with expert judgment and, unless otherwise specified, represent a 90% confidence interval.

2. Comprehensiveness with regard to physical effect. As discussed in the foregoing section, BC affects multiple facets of the Earth system, all of which respond to changes in emissions. In evaluating the net impact of BC emissions, we aggregate the best estimates of multiple effects, either from new analysis or from previous separate evaluation and presentation in the literature.

3. Comprehensiveness with regard to source contribution. A suite of pollutants is emitted from each combustion source of BC. Mitigation of those sources will reduce warming by BC aerosol, but it will also alter emissions of cooling particles or their precursors, short-term warming gases such as ozone precursors, and long-lived GHGs. Multi-pollutant analyses of climate impacts have been demonstrated in other work, and we continue that practice here.

4. Connection to action. Atmospheric science has historically focused on individual pollutants rather than the net impacts of sources. However, each pollutant generally comes from many sources, and each source produces multiple pollutants. For many purposes, an ideal measure of benefit would be the change in total climate forcing or response per change in activity—in mathematical terms, the partial derivative of forcing with respect to activity. In this assessment, we begin by examining the physics and net climate forcing of BC, and finish by evaluating the total climate forcing of key sources that account for most of the BC emissions and that may be the focus of mitigation actions. We scale model results for each pollutant to infer forcing from groups of sources that are rich in BC. Although such scaling may yield imprecise estimates of impact, we assert that ignoring species or effects could result in misconceptions about the true impact of mitigation options. In light of the scientific assessment of BC, we address the question: How certain are we of the forcing and climate responses to mitigation actions that target specific BC-rich sources, considering all emitted species and physical effects?

2. Measurements and microphysical properties of black carbon

2.1. Section summary

[1]

1. The term 'black carbon' has not been used rigorously or consistently in measurement studies or in modeling studies that use measurements. For future work, we recommend that the term 'refractory black carbon', or rBC, be adopted for the distinctive material defined herein as black carbon.

2. Either during or soon after emission, BC becomes internally mixed with other aerosol components such that it and other chemical species exist together within the same particle. This mixing can alter the optical properties of BC and influence its atmospheric lifetime and ability to form cloud droplets and ice crystals. Hence, the climate impacts of BC must be evaluated in the context of changes in its physico-chemical properties due to interactions with other aerosol components.

3. Freshly emitted BC particles are small in diameter and hydrophobic and, therefore, make very poor cloud condensation nuclei. Aging of BC after emission and associated accumulation of soluble mass increases the size and hygroscopicity of the internally mixed BC and enhances its cloud condensation nuclei (CCN) activity.

4. The mass absorption cross section of BC (MAC_{BC}) is a fundamental model input; it is needed to translate the BC mass concentration simulated by chemical transport models to the impact of BC on radiative transfer. Measured values for freshly generated BC fall within a relatively narrow range of 7.5 ± 1.2 m^2g^{-1} at 550 nm. MAC_{BC} increases by approximately 50% as BC becomes internally mixed with other aerosol chemical components.

5. Filter-based measurements of both absorption coefficient and BC mass concentrations can be biased by the presence of other chemical components in internally or externally mixed aerosol. Measured mass concentrations can differ between methods by up to 80% with the largest differences corresponding to aerosol with lower BC to organic carbon (OC) ratios. These measurement uncertainties may confound our understanding of trends, spatial and temporal variability, and impacts on climate.

2.2. Definitions

2.2.1. Black carbon

[2] Black carbon (BC) is distinct from other forms of carbon and carbon compounds contained in atmospheric aerosol. It has a unique combination of properties, as summarized in Section 1.1. These properties include strong visible light absorption of at least 5 m^2 g^{-1} at 550 nm, refractory nature, aggregate morphology, and insolubility in most organic solvents. The combination of these properties distinguishes BC from other light absorbing material, such as some organic carbon compounds.

[3] In this assessment, the term 'black carbon' and the notation 'BC' will be used to denote ambient aerosol material that has the above characteristics. The definition of 'black carbon' given here has not been used rigorously or consistently throughout all previous modeling and measurement literature, and as we discuss later in this section, most measurement techniques do not respond uniquely to this substance. For future studies, we suggest that the term 'refractory black carbon' (rBC) will be less ambiguous if the substance can be uniquely identified. Here, we continue the use of the term 'black carbon' for consistency with the literature published to date.

2.2.2. Organic matter and other carbon aerosols

[4] 'Organic aerosol' (OA) is a broad term indicating carbon-containing compounds that contain hydrogen and, usually, oxygen. This term excludes primary organic material directly emitted from plants [*Heald and Spracklen*, 2009]. All sources that emit BC also emit primary organic aerosol (POA), as well as gases that may become secondary organic aerosol (SOA) in the atmosphere. In atmospheric chemistry, the combination of BC and OA is often called 'carbonaceous aerosol.' Mineral dust also contains carbon as carbonate; this type of aerosol has different sources and is not covered in this assessment.

[5] The term 'organic carbon' (OC) refers to the carbon mass within OA, excluding the associated oxygen and hydrogen content. Although OA is the quantity most relevant to climate, measurements and emission inventories usually report values of OC because it is easier to measure. The ratio between OA and OC mass (OA:OC ratio) depends on the amount of oxygen incorporated in the organic molecules. It varies from about 1.1 to 2.2 [*Russell*, 2003], depending on the combustion source, with lower values of OA:OC from coal or diesel and higher values from biomass combustion. A default value for POA:OC of 1.3 or 1.4 is often assumed.

2.2.3. Other particulate light absorbers

[6] Two other types of atmospheric particles absorb visible light: dust and 'brown carbon.' Most of the dust in the atmosphere originates from deserts [*e.g.*, *Chin et al.,* 2009], and smaller amounts come from construction, on-road and off-road traffic, and agriculture. Dust particles can be distinguished from BC particles because they are typically large, nonspherical, formed from crustal elements, more weakly absorbing per mass than BC (about 0.009 m^2g^{-1} at 550nm for Asian dust [*Clarke et al.,* 2004]), and are 'colored' (*i.e.*, have relatively more absorption at shorter versus longer wavelengths). Although dust is more weakly absorbing than BC, globally averaged total absorption by dust is significant due to its relatively high mass abundance.

[7] Brown carbon, a subset of OA, does not have a formal analytical definition. Unlike BC, it is soluble in some organic solvents. It is a complex mixture of organic compounds that absorbs light weakly; its MAC is less than 1 m^2g^{-1} at 550 nm [*Sun et al.*, 2007]. Particles containing brown carbon are similar in size to BC. Brown carbon particles have been detected by analytical techniques that isolate humic-like substances [*Andreae and Gelencser*, 2006; *Graber and Rudich*, 2006] and can be distinguished from BC by their strong wavelength dependence of absorption [*Wonaschutz et al.*, 2009].

2.3. Black carbon formation and evolution

[8] BC is produced during the combustion of carbon-based fuels when oxygen is insufficient for complete combustion. Even if adequate oxygen is supplied overall, fuel-rich, oxygen-poor zones can occur when the reactants are not well mixed. A complex series of reactions involving polycyclic aromatic hydrocarbon molecules forms precursors of BC. These precursors coagulate to sizes large enough to serve as particle

nuclei and grow through reactions on the surface. Electron microscopy images show that these spheres are unique among atmospheric particles, with wrinkled graphite layers forming a shell around a hollow or disordered interior [*Heidenreich et al.*, 1968]. They have diameters on the order of tens of nanometers [*e.g., Martins et al.,* 1998a; *Posfai et al.,* 1999; *Li et al.,* 2003] and high carbon-to-hydrogen ratios. Soon after formation, the graphitic spheres coagulate to form aggregates or chain-like structures consisting of hundreds or thousands of spheres [*e.g., Medalia and Heckman*, 1969; *Li et al.,* 2003] (Figure 2.1). If the combustion exhaust is kept hot, and if sufficient oxygen is well mixed with the flame products, these carbon particles may be eliminated by oxidation reactions before they leave the combustor [*e.g., Lee et al.,* 1962]. Otherwise, they will be emitted.

[9] The morphology of emitted chain-like aggregates change rapidly after emission as they collapse into densely packed clusters [*Martins et al.,* 1998b]. Further changes occur as water vapor and other gas phase species, primarily organic material co-emitted during combustion, condense upon the aggregates, and the combustion aerosol coagulate and react heterogeneously with particulate and gas phase species present in the surrounding atmosphere. Electron microscopy images indicate that freshly emitted particles often exist as an external mixture in which scattering components (organic and inorganic) and strongly absorbing components (chain aggregates of BC) reside in different particles [*Posfai et al.,* 2003; *Li et al.,* 2003]. Within hours after emission, atmospheric reactions, condensation and coagulation occur, resulting in individual chemical components becoming internally mixed (*i.e.,* different aerosol components existing together within a single particle). Such particles are no longer pure BC, but contain sulfate and organic material [*Lee et al.,* 2002; *Moteki et al.,* 2007; *Shiraiwa et al.,* 2007]. We refer to these internally mixed particles as 'BC-containing' particles.

[10] The top portion of Figure 2.2 summarizes particle properties that are used as input into global and radiative transfer models and that can be constrained by measurements. Each characteristic may affect the representation of atmospheric processes and resulting modeled concentrations, as shown in the lower portion of Figure 2.2. Pure BC and BC-containing particles are separated in Figure 2.2 because their microphysical, optical, hygroscopic and cloud-nucleating properties differ [*Abel et al.,* 2003; *Slowik et al.,* 2004]. For example, as BC ages, it becomes coated or internally mixed with non-BC components and the resulting BC-containing particles become more hydrophilic, which can lead to a reduced lifetime and atmospheric loading [*Stier et al.,* 2006a]. Internal mixing with other compounds can enhance absorption of solar radiation according to both models [*Fuller et al.,* 1999; *Jacobson*, 2001a*; Lack and Cappa*, 2010] and measurements, primarily laboratory-based [*Schnaiter et al.,* 2005; *Slowik et al.,* 2007]. As a result, when modeling the climate impacts and atmospheric lifetime of BC, the additional material in BC-containing particles must be taken into account [*Stier et al.,* 2006b].

[11] In the remainder of this section, we discuss the physical properties that affect estimates of radiative forcing, measurements of these properties and representation of these properties in global models. We begin with a discussion of BC mass concentration in Section 2.4. Important optical properties of BC, including absorption, are discussed in Section 2.5, followed by a review of absorption measurements in Section 2.6. Section 2.7 reviews measurements and models of a key optical property, the mass absorption cross-section. Section 2.8 discusses properties of BC and BC-containing particles that are relevant to nucleating liquid cloud droplets. The discussion of microphysical properties, which also affect the interaction of BC-containing particles with ice clouds, appears in Section 6.6.

2.4. Measurement of BC mass

[12] Ambient air samples of particulate populations that contain BC always contain a mix of BC and other constituents. The mass fraction of BC in atmospheric aerosol is typically less than 10%. Thus, BC mass concentration (in g m^{-3}) cannot be measured directly by collecting aerosol in an air sample and weighing it. Instead, BC mass must be determined indirectly, usually through optical methods, thermal heating combined with optical methods, or via laser-induced incandescence (Table 2.1). The measurement of BC mass concentrations by some methods can be biased when BC is sampled with other aerosol components. This mixing can take place either within ambient aerosol particles before sampling, or in the sample itself if BC and other particles are collected and measured simultaneously. Biases occur either because the mixing increases absorption or extinction (see Section 2.6), because BC is incorrectly classified as another material, or because another material is incorrectly classified as BC (*i.e.,* lack of specificity). Most techniques measure similar BC mass concentrations when they are applied to pure BC or when other aerosol components are removed by applying heat [*Knox et al.,* 2009; *Kondo et al.*, 2009] or by solvent rinsing [*Subramanian et al.*, 2006]. For that reason, measurements on untreated samples are usually in closer agreement for diesel exhaust, which contains little non-BC material, than they are for aged (*i.e.,* internally mixed) aerosol [*Schmid et al.*, 2001; *Chow et al.,* 2004] or biomass burning (BB) aerosol, which has a high content of organic matter and other inorganic substances that could cause interferences [*Novakov and Corrigan*, 1995; *Reid et al.,* 1998]. The major uncertainty in some measurements of BC mass is associated with isolating BC from the other constituents with which it is internally or externally mixed. A summary of measurement techniques for BC mass is listed in Table 2.1 along with common terminology and any directions and causes of bias. In addition, more explicit names for the measured quantities are suggested; some of these follow *Andreae and Gelencser* [2006]. Details of the measurement of BC mass concentrations by existing methods are given below.

[13] The most common separation between BC and OC is accomplished by volatilizing and combusting material collected on a filter and by detecting the CO_2 produced. The discrimination between these two classes of aerosol is based on the idea that BC is non-volatile or refractory, whereas OC is volatile. This thermal method does not detect BC directly, and the amount of refractory material detected depends on the details of the method. The analytical result is therefore an operational definition and is traditionally called elemental carbon (EC).

[14] In thermal methods based on volatility, the sample filter is first heated in inert gas to volatilize OC, cooled, and then

heated again with oxygen to combust the EC [*e.g., Chow et al.,* 1993; *Birch and Cary,* 1996]. A complication is 'charring' of OC (*i.e.,* conversion of OC to EC) at high temperatures, which reduces its volatility and causes it to become an artifact in the EC/OC determination. Variations of this method include different temperature ramping schemes, and correcting for the charring of OC during pyrolysis by monitoring the optical reflectance of the sample filter [*Huntzicker et al.,* 1982] or light transmission [*Turpin et al.,* 1990]. Comparisons between temperature and optical-correction protocols show that derived EC concentrations can differ by over an order of magnitude [*Schmid et al.,* 2001], and that much of this difference is caused by the lack of correction for charring, which leads to considerable overestimates of EC. In addition, there are significant differences between methods that correct for charring using the dependence of thermal optical reflectance or light transmission [*Chow et al.,* 2001; *Chow et al.,* 2004]. The use of reflectance and transmission corrections for charring yield comparable EC concentrations if the filter contains a shallow surface deposit of EC or if OC is uniformly distributed through the filter. If EC and OC both exist at the surface and are distributed throughout the filter, the two types of corrections yield different concentrations of EC, and the variability also depends on the temperature protocol used. Hence, the difference between the two methods depends, in part, on the OC/EC ratio in the sample. As a result, the correction schemes yield similar results for diesel exhaust, which is dominated by EC, but can differ widely for complex atmospheric mixtures.

[15] The Single Particle Soot Photometer (SP2) has become increasingly recognized as a valuable tool for quantifying aerosol refractory BC (rBC) mass in individual particles [*Schwarz et al.,* 2006, 2008a]. It is able to provide continuous, real-time, size and coating information on individual particles containing rBC over a wide dynamic range of mass loadings. In the SP2, the rBC component of individual particles is heated to vaporization temperatures (*i.e.,* about 4000K) with an infrared intracavity laser and incandescence proportional to rBC mass is detected. Essentially all rBC cores between 70 and 700 nm mass-equivalent diameter (MED) are measured, assuming void-free rBC has a density of 2 g cm^{-3}. The response of the SP2 to rBC mass and the lack of interference in measuring rBC mass from the presence of non-rBC aerosol components (*i.e.,* coatings) have been evaluated in the laboratory [*Schwarz et al.,* 2006; *Slowik et al.,* 2007; *Moteki and Kondo,* 2007]. The dominant uncertainty in the measured mass lies in calibrating its sensitivity to ambient rBC material. The range of this sensitivity is around 15% [*Moteki and Kondo*, 2010; *Laborde et al.*, 2012]. However, the limitations of the size range detected by the SP2 may introduce additional uncertainty, depending on the airmass. Typically, in remote regions the size range captured by the SP2 contains most of the rBC mass and about 50% of the rBC number [*Schwarz et al.,* 2008b; *Shiraiwa et al.,* 2008]. In urban environments a correction to total measured mass of about 25% may be required.

2.5. Optical properties of black carbon

[16] Models of radiative transfer require the concentration of absorption and scattering in the atmosphere, known as the absorption and scattering coefficients (m^2 m^{-3} or simply m^{-1}). Atmospheric models convert modeled mass concentrations to these optical coefficients using intensive properties (*i.e.,* optical cross-section per mass, or m^2 g^{-1}) known as the mass absorption cross-section (MAC) and mass scattering cross-section (MSC). Estimates of these values are needed at all wavelengths, and the directional distribution of scattering (dimensionless) is also needed for radiative transfer models.

[17] From atmospheric measurements, MAC can be calculated in reverse: the light-absorption coefficient divided by mass concentration. Throughout this assessment, we often refer to MAC that is determined by dividing by BC mass concentration (MAC_{BC}). The simple term MAC will indicate the value determined by dividing by the total mass of BC-containing particles, which is smaller than MAC_{BC}. All other properties are usually measured for BC-containing particles, not for pure BC. Optical properties depend on refractive index, density, size distribution, mixing state and particle shape. The propensity for water uptake affects the MSC and MAC of BC-containing particles, as well as their lifetime, removal from the atmosphere and ability to form cloud droplets. For sub-saturated conditions (relative humidity below 100%), this water uptake is characterized in terms of hygroscopicity or growth factor. When air is saturated, the climate-relevant quantity is the fraction of particles that act as CCN.

[18] The MAC was mentioned earlier as a distinguishing feature of BC. Values of MAC and MSC are fundamental model inputs for all aerosols or aerosol components. These quantities are necessary to translate mass concentrations simulated by chemical transport models to their effects on radiative transfer. The wavelength-dependence of MAC must also be represented in models for the full solar spectrum. As its name implies, BC strongly absorbs light at all visible wavelengths. In contrast, other atmospheric aerosols that absorb light (OA, soil, and dust) are more yellow, brown or red, meaning they absorb more blue light than red light. The quantity generally used to characterize the spectral dependence of light absorption is the absorption Ångstrom exponent:

$$Å_{abs} = -\log(MAC(\lambda_1)/MAC(\lambda_2))/\log(\lambda_1/\lambda_2) \quad (2.1)$$

where $MAC(\lambda_1)$ and $MAC(\lambda_2)$ are the mass absorption cross sections at wavelengths λ_1 and λ_2, respectively. Two wavelengths spanning the visible range are commonly used, such as 450 and 650 nm. Alternatively, $Å_{abs}$ can be calculated from absorption coefficients at the two wavelengths.

[19] Both measurements and modeling have shown that for pure, uncoated BC, $Å_{abs}$ is near 1.0 at visible wavelengths [*Rosen et al.,* 1978; *Bergstrom et al.,* 2002, 2007; *Kirchstetter et al.,* 2004; *Clarke et al.,* 2007]. When BC becomes coated, $Å_{abs}$ can theoretically be as low as 0.8 or as high as 1.9 [*Lack and Cappa*, 2010]. In contrast, $Å_{abs}$ for OA has been observed to be between 3.5-7 [*e.g. Kirchstetter et al.,* 2004; *Sun et al.,* 2007; *Lewis et al.,* 2008; *Yang et al.,* 2009]. $Å_{abs}$ for dust is typically about 2 to 3, but can be higher for very red (iron-rich) dust [*e.g., Fialho et al.,* 2006; *Alfaro et al.,* 2004; *Bergstrom et al.,* 2007]. This difference in the wavelength-dependence of absorption of BC versus other absorbing aerosol has been used to approximate relative fractions of BC versus other light-absorbing constituents.

[20] The single-scattering albedo, ω_0, is scattering divided by extinction (*i.e.,* the sum of scattering and absorption), or

$$\omega_0 = MSC / (MSC + MAC) \quad (2.2)$$

Values of ω_0 near one indicate that the aerosol is mainly scattering. Values below about 0.8 indicate that the particles are strongly absorbing and could have a net warming effect [*Haywood and Shine,* 1995]. The critical value that divides warming from cooling also depends on the environment, particularly the albedo of the underlying surface or clouds.

2.6. Measurement of absorption

[21] The most widely used technique to measure the absorption coefficient involves collecting aerosol on a filter and inferring atmospheric absorption from the resulting change in transmission of light through the filter [*Gundel et al.*, 1984], often at one mid-visible wavelength but sometimes at multiple wavelengths. Common instruments using this approach are the Particle Soot Absorption Photometer (PSAP) [*Bond et al.,* 1999; *Virkkula et al.,* 2005], which has been used to obtain a worldwide data base through the Global Atmospheric Watch program; the Hybrid Integrating Plate System (HIPS), which has been used to collect data by the Interagency Monitoring of Protected Visual Environments (IMPROVE) in U.S. National Parks [*Malm et al.,* 1994]; and the Aethalometer [*Hansen et al.,* 1982]. Other filter-based absorption instruments include the Integrating Plate [*Lin et al.,* 1973], and the Multi-Angle Absorption Photometer (MAAP) [*Petzold et al.,* 2005a]. These filter-based methods overestimate absorption if light transmission is also affected by particulate light scattering [*Horvath*, 1997*; Bond et al.,* 1999]. With the application of empirical corrections to overcome this artifact, accuracies of the PSAP, IP, and HIPS range between 20 and 30% [*Bond et al.,* 1999; *Weingartner et al.,* 2003, *Virkkula et al.,* 2005]. However, these correction schemes are based on laboratory-generated aerosols that may limit their application and accuracy for the measurement of atmospheric aerosols. In addition, coating of BC with volatile compounds can greatly contribute to variation in filter-based measurements of light absorption [*Lack et al.*, 2008; *Cappa et al.,* 2008; *Kondo et al.,* 2009]. For example, PSAP absorption coefficients can be biased high (50 to 80%) when the ratio of organic aerosol to BC is high (15 to 20). *Lack et al.* [2008] postulated that this high bias was due to the redistribution of liquid-like OC that affected either light scattering or absorption. This difficulty can be overcome by removing most of the mass of volatile aerosol components before the BC particles are collected on filters. This removal can be accomplished without significant charring of organic compounds with a heated sampling inlet. This technique is used for the Continuous Soot Monitoring System (COSMOS) instrument [*Kondo et al.,* 2011a]. Under those conditions, comparisons of ambient BC mass concentrations measured by light absorption (COSMOS), thermal-optical measurements, and laser-induced incandescence (*i.e.,* SP2) measurements have been found to agree within 10% [*Kondo et al.,* 2011a].

[22] Filter-based optical measurements of absorption are sometimes used to derive 'effective' BC mass concentrations by using an assumed MAC_{BC} to convert measured absorption to BC mass [*e.g., Sharma et al.,* 2002]. Given the artifacts and uncertainties associated with filter-based measurements and the choice of MAC_{BC}, the resulting BC mass concentrations also can be highly uncertain.

[23] Non filter-based techniques also are available for the measurement of absorption by BC. In the photoacoustic spectrometer (m) [*e.g., Arnott et al.,* 1997; *Lack et al.,* 2006], particles are drawn into an acoustic cavity and irradiated by laser light. The heat that is produced when the particles absorb laser light is transferred to the surrounding gas creating an increase in pressure. Sensitive microphones are used to detect the standing acoustic wave that results from the pressure change. The detected signal together with instrument parameters are used to calculate the absorption coefficient. Gas phase absorbers can interfere with BC detection in PAS systems. The overall uncertainty of the PAS with respect to aerosol absorption has been reported at about 5% [*Lack et al.,* 2006].

[24] Absorption techniques, whether filter-based or non-filter based, are not specific for BC. Any light-absorbing aerosol other than BC that absorbs at the measurement wavelength is detected. The degree to which other light absorbing species interfere with the measurement of BC absorption depends on the relative abundance of light absorbing species and the size range and wavelength of the measurement. Measurement of the chemical composition of the aerosol and measurement of absorption at several wavelengths can help determine the interference from all atmospheric species. BC-containing aerosol generally fall into the submicron size range, so measurements of the submicron aerosol only can also reduce the interference of dust absorption.

2.7. Mass absorption cross section

2.7.1. MAC_{BC} derived from measurements

[25] Empirical values of MAC_{BC} have been obtained from measurements of light absorption by filter or photoacoustic methods, divided by measurements of EC mass from thermal evolution methods [*e.g., Martins et al.,* 1998a; *Moosmüller et al.,* 2001]. Measured values for freshly generated BC, where care has been taken to eliminate non-BC material, fall within a relatively narrow range of 7.5 ± 1.2 m^2g^{-1} [*Clarke et al.,* 2004; *Bond and Bergstrom,* 2006]. The MAC_{BC} may be reduced as the highly fractal particles collapse into less fractal forms [*Schnaiter et al.*, 2003].

[26] Internal mixing between BC and other compounds increases BC absorption of visible light, partly because of light refraction by the non-absorbing shell surrounding an absorbing BC core. The absorption increase is low for very thin coatings [*Slowik et al.,* 2007] and reaches a factor of 1.8 to 2 for thicker coatings [*Schnaiter et al.,* 2005; *Khalizov et al.* 2009; *Shiraiwa et al.,* 2010; *Cross et al*., 2010; *Bueno et al.*, 2011]. Filter-based and photoacoustic measurements report different degrees of enhancement in the measured absorption [*Slowik et al.,* 2007; *Knox et al.*, 2009], possibly due to artifacts (see Table 2.1). Artifacts in measurements of both absorption and BC mass may confound inferences of MAC_{BC}. Basing the measurement on instruments with fewer artifacts, such as the photoacoustic spectrometer and SP2, could provide this important quantity more precisely for ambient and laboratory BC (*e.g., Cross et al.* [2010]), but these instruments are relatively new and have been used in fewer measurement programs.

[27] *Knox et al.* [2009] confirmed near source regions that enhancement of absorption by a factor of 1.2 to 1.6 occurs in atmospheric particles by measuring MAC_{BC} before and after removal of coatings. Measurements made downwind (up to hundreds of kilometers) of BC source regions give a wider range of reported enhancements. MAC_{BC} values from a series

of intensive experiments downwind of BC sources, all derived with use of identical sampling and analysis protocols, ranged from 6 to 20 m^2g^{-1} [*Quinn and Bates,* 2005]. These measurements were made far from sources, so they included BC as well as other chemical components that may contribute to measured light absorption.

[28] Most of the above measurements of MAC_{BC} after mixing with non-BC material were made under dry conditions or at relatively low humidity. However, water is also a component of mixed aerosols, both in clear air at high relative humidity and in clouds. Particles that have taken up water become even larger than mixed, dry atmospheric particles, but measurements at such elevated humidities are difficult. *Mikhailov et al.* [2006] measured a three-fold increase in absorption of BC at 100% relative humidity. *Brem et al.* [2012] also found an amplification factor of up to 2.7 for an absorbing organic aerosol core at 95% relative humidity.

2.7.2. Microphysical properties for modeling MAC

[29] Values of MAC can be predicted with several theories describing how the particles interact with light. These models require material properties (*i.e.,* refractive index and density), as well as a choice of particle shape. The calculation is usually based on Mie theory, which describes homogeneous or core-shell spherical particles. BC particles are assumed to be either externally or internally mixed with other aerosol components. For external mixing, the calculation uses the material properties of pure BC. If internal mixing is assumed, the non-BC material is either placed in a spherical shell around a BC core, or the refractive index and density of BC and non-BC material are averaged and a homogeneous particle is modeled. Very few models use theories such as the Rayleigh-Debye-Gans approximation that account for the nonspherical shape of freshly emitted BC particles.

[30] The fact that BC particles are aggregated spherules rather than single spheres creates difficulties in the determination of all properties used for modeling. Measurements usually examine either particles that are assumed to be spherical, or particles that are collected and compacted. In either case, the material is not pure BC, but contains an unknown fraction of voids. The non-spherical nature of BC also affects measurements of particle size. Air drag is different for non-spherical particles and affects measurements based on mobility [*Lall and Friedlander,* 2006]. The SP2 measurement detects BC mass and provides equivalent spherical diameters. The ideal refractive index, density and size used for modeling would be obtained for the pure material, but observed properties may be obtained for material with unknown and inconsistent void fractions. Despite these uncertainties, measurements of material properties and sizes are described below along with recommended values.

2.7.2.1. Refractive Index

[31] The refractive index of a material is critical in determining the scattering and absorption of light, with the imaginary part of the refractive index having the greatest effect on absorption. Refractive index values are derived by invoking a model for the expected interaction of BC with light (*i.e.,* reflectance or absorption) and adjusting model parameters (including the refractive index) until predictions match measurements. Three methods that have been used include: 1) fitting Fresnel's formula to reflectance and transmittance data measured for a compressed pellet; 2) fitting Mie theory to light-scattering data for individual spherical particles; and 3) fitting either Mie theory or an approximation formula to scattering and extinction data for particle ensembles. Method 1 has been used widely to estimate refractive indices of solid aerosols like combustion-generated BC [*Mullins and Williams,* 1987]. However, direct evidence of the optical flatness of pellet surfaces, which is necessary for application of Fresnel's formula, has never been shown for wavelengths shorter than the infrared region [*Janzen,* 1979]. Method 2, which is limited to spherical particles, uses measurements of resonance structures in Mie scattering to determine the refractive index [*Chylek et al.,* 1983a]. In method 3, the refractive index and a size distribution function are inferred simultaneously from extinction or scattering data for an ensemble of particles. Solving this inversion problem requires a theory to connect microphysical and light-scattering properties; Mie theory has been used for spherical particles [*Lack et al.,* 2009] and the Rayleigh-Gans approximation for nonspherical particles [*Charalampoulos et al.,* 1989; *Van-Hulle et al.,* 2002]. For polydisperse or nonspherical particles, the inversion results may have large errors if the assumed size distributions or shapes are simplified compared with the actual particles. *Moteki et al.* [2010] developed a method to estimate refractive indices that accounted for non-spherical particles by measuring the relationship between the scattering cross-section and the particle volume.

[32] A variety of values for the refractive index of BC has been used in global climate models including the OPAC (Optical Properties of Aerosols and Clouds) value of 1.74 - 0.44*i* [*Hess et al.,* 1998]. As reviewed by *Bond and Bergstrom* [2006], reported values of the refractive index of light absorbing carbon vary widely; the real part, *n,* appears to vary from that of water to that of diamond and the imaginary part, *k,* varies from that of negligibly absorbing material to that of graphite. *Bond and Bergstrom* [2006] hypothesize that strongly absorbing carbon with a single refractive index exists and that some of the variation in reported values results from void fractions in the material. Based on agreement between measured real and imaginary parts of the refractive index of light absorbing carbon, *Bond and Bergstrom* [2006] recommended a value of 1.95 – 0.79*i* at 550 nm. They caution, however, that this value may not represent void-free carbon. *Stier et al.* [2007] found that this value led to better agreement with observed atmospheric absorption, compared with the OPAC value. *Moteki et al.* [2010] found that the refractive index of ambient BC in the Tokyo urban area was about 2.26 – 1.26*i* at 1064 nm. The OPAC assumption for imaginary refractive index is not taken from combustion-generated particles, is lower than either of the latter two recommendations and would lead a MAC prediction about 30% lower if all other factors were equal.

[33] Applying a radiative inversion method [*Dubovik and King,* 2000] to passive remote sensing can also provide values for refractive indices, but only for the entire mixed aerosol, which includes water. Currently, data are available from about 500 globally distributed Aerosol Robotic Network (AERONET) surface sites [*Holben et al.,* 1998]. These refractive index

estimates are more accurate for higher aerosol optical depth (AOD), as discussed in Section 4.4.2.

2.7.2.2. Density

[34] *Fuller et al.* [1999] compiled reported densities for several types of graphitic material and found values ranging from 0.625 to 2.25 g cm^{-3}. Based on the type of BC emitted from diesel combustion, they adopted the highest density, which was measured for paracrystalline graphite, as representative of strongly absorbing atmospheric BC. BC is not perfectly crystalline, so its microstructure, density, and refractive index differ from those of graphite. The density of pure graphite is 1.9 to 2.1 g cm^{-3} [*Hess and Herd*, 1993]. Densities for pressed pellets of BC with corrections for air volume fractions in the surface layer are slightly lower at 1.8 to 1.9 g cm^{-3} [*Medalia and Richards*, 1972; *Janzen*, 1980]. *Park et al.* [2004] reported a density of 1.8 g cm^{-3}, and *Kondo et al.* [2011a] found 1.718 ± 0.004 g cm^{-3} for fullerene soot. Some models still use the OPAC-recommended density of 1 g cm^{-3}, which will result in an overestimate of absorption if all other factors are correct.

2.7.2.3. Size and Particle Shape

[35] Size distributions of BC cores in ambient aerosol are determined by the atmospheric mixing of nascent particle size distributions from a variety of sources and any subsequent BC coagulation. The latter generally occurs only near BC sources before emissions are diluted. Formation of coatings on the BC cores and other processes change the overall aerosol size distribution, but the underlying size distribution of BC cores does not change except through coagulation. BC size can be diagnosed separately; the SP2 technique has provided such measurements in fresh urban plumes dominated by fossil-fuel (FF) combustion [*e.g., Kondo et al.,* 2011a, *Schwarz et al.,* 2008b], in aged plumes in Asian outflow [*Shiraiwa et al.,* 2008] and in the remote upper troposphere and lower stratosphere [*Schwarz et al.,* 2006; 2008b]. In the urban areas of Tokyo and Nagoya (Japan) and Seoul (Korea), the mass median diameter (MMD) and count median diameter (CMD) of fresh BC ranged from 120 to 160 nm and 50 to 80 nm, respectively. In plumes associated with wildfires, the MMD was measured to be about 200 nm and the CMD to be 120 nm [*Kondo et al.*, 2011b]. The distinct difference in the size between BC particles from fossil-fuel combustion and biomass burning seems to be a general feature (Figure 2.3). The CMD and MMD of BC observed in the Asian outflow were significantly higher than those in fresh urban plumes [*Shiraiwa et al.,* 2008], suggesting the growth of BC size by coagulation during transport after emissions. BC particles are largely found in the Aitken mode (< 100 nm) and the accumulation mode because of their formation mechanism. Large concentrations of BC in the Aitken mode size range result from high combustion temperatures and efficient fuel burn. For example, BC particles produced by aircraft jet engines have mean number diameters of about 30 nm [*Petzold et al.,* 2005b].

2.7.3. Microphysical model ability to simulate MAC_{BC}

[36] As discussed above, most model treatments of absorption and scattering rely upon Mie theory with prescribed size distributions and the assumption of spherical particles. We first review whether these microphysical models can simulate observed MAC_{BC}. Then, we discuss how these representations are implemented in global models.

2.7.3.1. MAC_{BC} of unmixed BC

[37] Particle size distribution has almost no influence on calculated MAC when particle diameter is below about 80 nm [*Bergstrom*, 1973]. The simplest theory that accounts for aggregate particles indicates that MAC depends only on the size of the component spherules, which are smaller than 80 nm. Therefore, MAC_{BC} should not be very sensitive to particle size. *Bond and Bergstrom* [2006] find a relatively constant MAC_{BC} value obtained from measured absorption and mass of unmixed BC, 7.5 ± 1.2 m^2g^{-1}. However, this value is about 30% higher than values calculated using Mie theory or theory for simple aggregates with best estimates of refractive indices and a density of 1.8 g cm^{-3}. This comparison remains unchanged even with the higher refractive index values found by *Moteki et al.* [2010]. *Bond and Bergstrom* [2006] suggest that the 30% higher absorption of actual particles could be caused by interactions between neighboring BC spherules. However, *Kahnert* [2010] showed that this interaction alone could not account for the observed discrepancy. The inability of microphysical models to reproduce measured MAC from best estimates of refractive index and density remains unresolved.

[38] Although MAC_{BC} is sensitive to the large differences in both refractive index and density used by different models, *Bond and Bergstrom* [2006] note some compensating errors. For models using OPAC refractive index and density, the low refractive imaginary index would underestimate MAC_{BC}, while the low assumed density (1 g cm^{-3}) would overestimate it. Therefore, the MAC_{BC} simulated with the erroneous OPAC refractive index and density is comparable to MAC using the values of refractive index and density recommended by *Bond and Bergstrom* [2006], although the model inputs are quite different. However, it may not be possible to simulate the MAC of mixed particles using these erroneous values.

2.7.3.2. MAC of BC mixed with other substances

[39] For internal mixtures of BC and non-absorbing material, including water, the mixed particle may be either treated as a coating surrounding a BC core ('core-shell') or as homogeneous particle for which the effective refractive index is obtained using 'mixing rules' [*Heller*, 1965; *Stier et al.*, 2007]. Some frequently used mixing rules are the volume mixing approach, in which refractive indices are proportional to substance volume, or the Bruggeman or Maxwell-Garnet effective medium approximations. The increase in MAC_{BC} is included in neither the OPAC recommendations nor the *Bond and Bergstrom* [2006] values, which describe unmixed BC.

[40] Different representations of mixing often produce comparable estimates of absorption. For example, using the *Bond and Bergstrom* [2006] refractive index and density, *Adachi et al.* [2010] calculated the mass absorption cross section for uncoated spheres (6.4 m^2g^{-1}), uncoated aggregates (6.1 m^2g^{-1}), volume mixing (13.6 m^2g^{-1}), core-shell (13.3 m^2g^{-1}), Maxwell-Garnet effective medium approximation (12.0 m^2g^{-1}), and realistic coated BC particles (9.9 m^2g^{-1}) at 550 nm wavelength. The assumption of a perfectly concentric core within a shell gives the highest absorption among core-shell particles [*Fuller*, 1995]. However, *Jacobson* [2006] showed that the dynamic effective medium approximation suggested for

cloud droplets by *Chýlek et al.* [1996] produced a much higher MAC_{BC} than a core-shell treatment.

[41] Sensitivity to mixing depends on the relative concentrations of BC and non-BC components, which may include water, liquid and solid components; hence, mixing varies widely in space and time. A single value of MAC for an internally mixed aerosol is not appropriate due to the widely varying amounts of non-absorbing material surrounding BC cores. *Moffet and Prather* [2009] estimate that the increase above unmixed aerosol could be 80-200% for individual particles. This increase depends upon the relative sizes of the shell and the core, and the location of the core within the particle [*Fuller,* 1995]. *Bond et al.* [2006] suggest a smaller enhancement, concluding that MAC_{BC} is 80% higher for mixed than for unmixed spheres. However, because the absorption of aggregate BC appears to be 30% higher than that of spheres, the increase between uncoated, aggregate BC to coated, mixed spherical particles might be only 50%. The MAC_{BC} of 7.5 m^2g^{-1} for freshly emitted BC, plus an enhancement of 50%, agrees approximately with observed MAC_{BC} at dry conditions. However, a more precise evaluation of the agreement between models and observations is hampered by artifacts in the measurements.

2.7.3.3. Global model treatment of mixing and MAC_{BC}

[42] All models consider how aging affects removal rates of BC, but they have been slow to incorporate the effect of mixing on MAC_{BC}. In early models of atmospheric BC, including some summarized in Section 5, the aging of BC is expressed by prescribing a timescale for converting hydrophobic BC to hydrophilic BC, typically about one day [*Koch et al.,* 2009a]. Many models have evolved to express aging explicitly in terms of coagulation with sulfate particles and condensation of sulfuric acid (H_2SO_4) and secondary organic vapor on BC, converting freshly emitted BC to an aged accumulation mode after it is coated by soluble material. Some models represent BC-containing aerosol with discrete size-resolved bins [*Jacobson*, 2001a; 2010]. Others, known as "multi-modal" models, represent different aerosol classes, such as unmixed BC versus BC coagulated with other material [*Kirkevag and Iversen,* 2002; *Vignati et al.,* 2004; *Stier et al.,* 2005; *Bauer et al.*, 2008; *Ghan et al.,* 2012]. Removal representations vary from empirical removal rates to rates that depend on aerosol and cloud droplet size, as in GATOR [*Jacobson*, 2002].

[43] Although models of BC have always considered how aging affects removal rates, they have been slow to incorporate the effect of mixing on MAC_{BC}, despite observations showing the prevalence of internal mixing of BC with other constituents. Values of MAC_{BC} used in global models range from 2.3 to 10 m^2g^{-1} [*Koch et al.,* 2009a]. Much of this diversity arises from differences in the assumed mixing state. As internal mixing and absorption enhancement have been shown to be realistic, models without these treatments predict MAC_{BC}, and hence radiative forcing, that is too low (Section 5).

[44] All models that represent internal mixing report a large increase in absorption and positive forcing for internally mixed particles. One long-standing model, GATOR-GCMOM [*Jacobson*, 2001a] reported doubled forcing when BC-containing particles were treated as core-shell rather than externally mixed. *Chung and Seinfeld* [2002] found a forcing increase of 36% for BC with homogeneous internal mixing compared with external mixing. *Bauer et al.* [2010] included a core-shell representation in a multi-modal model. *Flanner et al.* [2007] and *Myhre et al.* [2009] associated internally mixed values of MAC_{BC} with aged BC, and *Adachi et al.* [2010] explored several mixing assumptions in a global model. Model treatment of aging and mixing affects both absorption and lifetime, often with compensating effects. *Ghan et al.* [2012] found that two different treatments of BC produced similar forcing estimates, as internally mixed BC had higher MAC_{BC} but was removed faster.

2.8. CCN activity of black carbon

[45] Particle size, hygroscopicity, and mixing state also affect the interaction of particles and clouds. While BC-induced cloud changes are mainly discussed in Section 6, we review the processes of CCN activation here because they are closely related to the microphysical properties of BC-containing aerosol.

[46] Aerosol particles serve as nucleation sites for forming cloud droplets through a process known as *activation*. The ability of an aerosol particle to act as a cloud condensation nucleus depends on its size, composition, and mixing state, and the supersaturation with respect to water vapor within the cloud. The *critical supersaturation* for a given particle is the lowest supersaturation at which that particle will activate and produce a cloud droplet. Any particle can activate in extremely supersaturated air. Particles that activate more easily (*i.e.,* that have a lower critical supersaturation) have a greater chance of affecting cloud droplet number and cloud reflectivity, and they may also be more easily removed by wet deposition.

[47] If all other factors are equal, small particles require greater supersaturation than large particles. Less hygroscopic particles have larger critical supersaturations than more hygroscopic particles. Because freshly emitted BC particles are small in diameter and hydrophobic, they have very large critical supersaturations and make very poor CCN. Aging of BC after emission lowers its critical supersaturation, as the addition of soluble mass increases both particle volume and hygroscopicity.

[48] The dependence of the CCN activity of BC on the amount of non-BC material has been probed empirically. In one approach, the comparison of heated and unheated particle size distributions was used to indicate the quantity of non-refractory material in the particles [*Sakurai et al.,* 2003; *Philippin et al.,* 2004; *Kuwata et al.,* 2007]. Figure 2.4 shows the relationship between the condensed mass per particle and the CCN activity of 100-nm BC particles observed in Tokyo [*Kuwata et al.,* 2009]. The number fraction of CCN-active BC particles increases with increasing condensed mass, indicating that 0.18 x 10^{-15} g of condensed coating material is required to activate these BC-containing particles at 0.9% supersaturation. In this case, the chemical composition of condensed compounds was found to be primarily organic. Figure 2.5 shows the dependence of the critical supersaturation on particle diameter and BC mass fraction as simulated by a particle-resolved model [*Riemer et al.,* 2009]. Larger particles have a lower critical supersaturation and, for a given particle size, a higher BC mass fraction increases the critical supersaturation.

[49] The treatment of BC in global climate models (GCMs) does not always reflect this dependence on size and

hygroscopicity. In some GCMs, the activation of BC by cloud droplets is not considered at all. The next level of complexity, a *mass-based* parameterization, simply assumes that the number of cloud droplets activated are empirically related to the submicron aerosol mass. In turn, that mass is determined from the hydrophilic aerosol species sulfate, submicron sea salt, and hydrophilic carbonaceous aerosol, where carbonaceous aerosol is the sum of OA and BC [*Rotstayn et al.,* 2009]. This simple parameterization ignores differences in activation behavior for particles of different sizes and composition, but many models have advanced to treat these physical processes. GATOR represents size-resolved incorporation of aerosols in cloud droplets and removal for aerosol bins resolved by size [*Jacobson*, 2006]. In the ECHAM GCM, the cloud droplet number concentration is empirically related to the aerosol number concentration with wet radii greater than 35 nm and the updraft velocity without distinguishing aerosol types [*Lohmann et al.,* 2007]. More sophisticated parameterizations of cloud droplet formation derived from *Köhler theory* have been developed by *Abdul-Razzak and Ghan* [2000] and *Nenes and Seinfeld* [2003]. In these schemes, the dependence on size and hygroscopicity can be taken into account, including the competition between different types of particles. For example, large hygroscopic particles take up water, reduce supersaturation, and therefore result in less activation of smaller or less hygroscopic particles such as those containing BC [*Ghan et al.,* 1998]. The *Abdul-Razzak and Ghan* [2000] scheme and its subsequent refinements are included in the CAM-Oslo GCM [*Storelvmo et al.,* 2008], in a modified version of CAM3 [*Morrison and Gettelman,* 2008], in CAM5 [*Liu et al.,* 2011], in the SPRINTARS model [*Takemura et al.,* 2005] and in the GISS model [*Bauer et al.,* 2010]; however, earlier published results from models with the same names may not reflect these advances.

3. Emission magnitudes and source sectors

3.1. Section summary

[1]

1. Global emission estimates use the 'bottom-up' method of multiplying emission factors by activity data. With this method, a bottom-up estimate of total global emissions in the year 2000 is about 7500 Gg BC yr^{-1}, with an uncertainty range of 2000 to 2900 Gg yr^{-1}. About 4770 Gg BC yr^{-1} is from energy-related burning, with the remainder of about 2500 Gg BC yr^{-1} from open biomass burning. Total primary organic aerosol (POA) emissions are 47000 Gg POA yr^{-1} for the global total, with an uncertainty range of 1800 to 180000 Gg POA yr^{-1}. Energy-related burning and open burning produce 16000 and 31000 Gg POA yr^{-1}, respectively; the largest uncertainties are in open burning.

2. Industrial-era emissions are the difference between present-day and the pre-industrial background year, 1750. These values are 6100 Gg BC yr^{-1} (4400 Gg BC yr^{-1} from energy-related burning and the remainder of about 1700 Gg BC yr^{-1} from open burning) and 33000 Gg POA yr^{-1} (14000 Gg POA yr^{-1} from energy-related sources and the rest from open burning).

3. Sources whose emissions are rich in BC can be grouped into a small number of categories, broadly described as diesel engines, industry, residential solid fuel and open burning. Dominant emitters of BC from energy-related combustion depend on the location. Asia and Africa are dominated by residential coal and biomass fuels (60-80%), while on-road and non-road diesel engines are leading emitters (about 70%) in Europe, North and Latin America. Residential coal contributes significantly in China, the former USSR and a few Eastern European countries.

4. Estimates of energy-related emissions agree broadly on major sectors and approximate magnitudes of BC emission. However, current inventories in many world regions lack information regarding the factors governing emissions. These include the type of technologies or burning, and the amounts of biofuel (BF) combusted. Major differences in estimates of energy-related emissions result from a few knowledge gaps. For energy-related emissions, these include sparse emission measurements of sources with the highest emissions. In industrialized countries, these may be a small fraction of the emitting sources. Only energy-use inventories in North America, Europe and urban East Asia provide a high level of detail. Measurements in developing countries are scarce for all source types.

5. Current emission factors from biomass burning, and thus emission estimates, might be biased low by a factor of at least two. While emission estimates from open burning are generally uncertain due to insufficient data on burned area and fuel consumed, quantification of BC emissions from this source is particularly difficult because they strongly depend on the burning behavior and because of inherent problems with sampling and analyzing BC in smoke plumes from vegetation fires.

6. The majority (80%) of open fire emissions occurs in tropical latitudes, and interannual variability of BC emissions from forest or savanna fires can exceed one order of magnitude in some regions.

7. Black-carbon emission sources are changing rapidly due to greater energy consumption, which increases emissions, and cleaner technology and fuels, which decreases them.

8. Because the net aerosol effect on climate depends on the ratio of absorbing to reflective particles such as OA and sulfate, we group emission sources into categories based on their combustion type and co-emissions. Major sources of BC, ranked in order of increasing POA:BC ratio, are diesel vehicles, residential burning of coal, small industrial kilns and boilers, burning of wood and other biomass for cooking and heating, and all open burning of biomass. A few of these sources also emit significant quantities of SO_2.

9. Receptor modeling studies of BC in urban areas that use chemical composition to identify dominant emission sources find source categories that are qualitatively similar to those in bottom-up inventories based on activity data.

3.2. Introduction

[2] Emission inventories, or global and regional tabulations of emission quantities, have a dual role. They are required inputs for atmospheric models that assess the environmental consequences of these emissions, and they also provide necessary information for the development of air quality and climate policies by indicating the largest or most easily manageable sources of emission. For BC and POA, inventories used in global models are typically 'bottom-up' tabulations constructed from estimates of activity (*e.g.,* number of km driven) combined with emission factors (*e.g.,* grams BC emitted per km driven). To address major fractions of particulate air pollution, or radiative forcing related to BC, identification of the sources that contribute to total emissions is needed. The identification of emitting sectors is important not only for mitigation policies, but also for historical reconstructions and future projections, as each sector has a different temporal evolution. The major BC emitters in each country or region depend on technological development and on practices common in each society.

[3] In this section, we first provide definitions of the terms, groupings of emission sources, and groupings of countries used throughout this assessment. Section 3.2 outlines general procedures for producing bottom-up inventories. We then present global totals, major source sectors, and regional contributions in Section 3.3. Section 3.4 discusses major sources of uncertainty in emission estimates, focusing on the sectors identified as most important. In Section 3.5, we discuss studies that have inferred the major sources of particulate matter based on the chemical composition of ambient aerosol, known as receptor modeling. These studies have been conducted primarily in urban areas. Finally, Section 3.6 gives an overview of inverse modeling results, where three-dimensional chemical and transport models are used to infer emission fluxes from the spatial and temporal characteristics of the concentration field.

[4] The forcing by species co-emitted with BC is important in determining the net radiative forcing by BC sources (see Section 5). In this section, we also discuss emissions of POA, the aerosol species most commonly emitted with BC. For BC sources, we also summarize co-emissions of SO_2, which is a precursor to sulfate. Dust and sea salt are other major aerosol components, but they are generally not co-emitted with BC and they usually have larger particle sizes than BC or its co-

emissions. Aged aerosol, however, may contain all of these components. The discussion of uncertainties in this section emphasizes BC emissions.

3.2.1. Geographic aggregation

[5] In this assessment, we summarize emissions and concentrations based on ten groups of countries (called 'regions'), depicted in Figure 3.1. These groups were chosen based on proximity, development status, and basic meteorological similarity, although there is heterogeneity within each region. Countries in each region are listed in the Supplemental Information (Table S1).

3.2.2. Definitions and aggregation of emission sources

[6]

1. Activity. The term 'activity,' as it is commonly used in the emission community, indicates a quantitative measure of an event that leads to emission, such as the quantity of fuel burned, product manufactured, or kilometers driven.

2. Emission factor. The term 'emission factor' gives mass of BC emission per activity, as opposed to total emissions. Emission factors for BC vary by region and end-use, even for the same fuel.

3. Source categories. Because this assessment focuses on BC sources and their impacts, we isolate sources that contain large fractions of BC relative to other aerosol components or precursors. We group sources with some similarities into aggregates called 'source categories,' although there is some heterogeneity within these category. For example, we lump both modern diesel engines with emission reduction technology and high-emitting, poorly maintained diesel engines into the category 'on-road diesel engines.' These categories are discussed further in Section 3.3.

4. Sectors. The term 'sectors,' as used throughout emission literature, refers to broad activity categories used for reporting by the International Energy Agency and the United Nations. These sectors are energy or transformation (which includes electricity generation), industrial activity, transportation, agriculture, and residential. The sector frequently termed 'residential combustion' may also contain commercial, agriculture, and miscellaneous activity. Energy-related combustion is conducted deliberately to produce economic activity or to meet energy demands. Open biomass burning also produces large quantities of atmospheric pollutants, and this activity has also become known as a sector in atmospheric literature. Because sectors consist of many types of activity, they include both BC-rich sources and sources that emit little BC. For that reason, we present emissions from source categories rather than from sectors.

5. Aggregated emissions. We use some additional terms to describe aggregated emission categories. 'Energy-related' emissions include power plants, industrial activity, transportation, and residential fuel use. 'Open burning' includes combustion of forests and grasslands or savannah, regardless of the cause of the fire. We also include open burning of waste for disposal, including crop residue or urban waste, in the latter category. The term 'fossil fuel' indicates emissions from combustion of all fossil fuels, including diesel fuel and coal used in residential and industrial sectors. The term 'biofuel' denotes biomass burned intentionally to meet energy needs and includes solid, unprocessed biofuel such as wood and agricultural waste.

6. Industrial-era versus anthropogenic emissions. A distinction of importance to the IPCC, among others, is the identification of 'anthropogenic' emission sources. As discussed in Section 1.3, we follow IPCC practice and use a time-based definition of climate forcing that is more accurately described as 'industrial-era' forcing: the difference between the near-current year 2000 and the background year 1750. Nominally, energy-related sources are all anthropogenic, as are sources associated with disposal. Vegetation fires are the only BC emission source that sometimes occurs without human activity. Industrial-era emissions are required to evaluate climate changes since 1750. 'All-source' emissions include the component that occurred both in 1750 and in the present day. Industrial-era emissions are more uncertain than all-source emissions because of the large uncertainties in activity during the background year, especially for open biomass burning.

3.3. Bottom-up inventory procedures

[7] Emissions from energy-related combustion and from open vegetative burning are derived from different types of input data and often created by separate communities. In this section, we summarize information needed to create inventory estimates to clarify the sources of uncertainties.

3.3.1. Energy-related emissions

[8] Emission estimates for activities related to energy use were first developed to evaluate air quality in urban areas, where both high concentrations and high population led to severe exposure to health risks. Urban regulations have historically targeted total particulate matter mass concentrations, not individual chemical species. For that reason, early source characterization focused on mass emissions, and many source measurements did not provide emission rates of individual components such as BC.

[9] Bottom-up inventory estimates from energy use are based on the following simple equation:

$$Emission = \sum_i A_i \, EF_i \, (1 - eff_i) \qquad (3.1)$$

In the equation above, A_i represents activity of a particular type (*e.g.,* fuel consumption or commodity production, conducted in a specific way); EF_i is an emission factor in grams per activity; and eff_i is the pollutant removal efficiency by a particular type of abatement. The subscript i represents different types of activity that result in emissions of the same pollutant. Both emission factors and removal efficiency depend on the type of activity and the pollutant.

[10] BC emission inventories from energy-related emissions are available for all countries. However, the level of detail used in each inventory varies greatly. Quantification of emissions and the identification of major contributing sources could be substantially refined by disaggregating the activity definitions used in Equation 3.1. For example, activity for a country might be given as total coal consumption in the residential sector, with a single emission factor used for all coal burning installations. This lumping ignores the fact that large boilers might have very

different emission factors or better control devices than small coal stoves.

[11] Table 3.1 proposes inventory grades based on the level of refinement in estimates of emissions from energy-related combustion. Major uncertainties in current bottom-up inventories include insufficient knowledge of activity rates and emission characteristics. Emission factors are not as well understood for sources largely found in rural areas, such as off-road diesel engines. Furthermore, measurement resources have been concentrated in developed countries, so there are still relatively few measurements of key emission sources in developing countries. Section 3.7 gives further details on uncertainties, which vary by emission sector and by region.

3.3.2. Open burning emissions

[12] In contrast to energy use, open burning emissions are usually not included in national activity reports. There are thousands of open fires burning globally each day, and most of these are caused by humans, either purposefully or involuntarily. Open fires are ignited for many purposes, and their emissions differ by region and ecosystem type. In contrast to residential and industrial emission sources, which are predominantly located in the northern hemisphere mid latitudes, open fires occur largely in tropical regions, with 80% of emissions occurring there. National regulations about fire use and their enforcement vary among countries. Another important distinction between emissions from open fires and emissions from energy use is the very large inter-annual variability of the former. This is caused by variations in the accumulation of wooded or grass fuels, in fuel characteristics such as dryness, and in other factors influencing fire spread and fire severity. An extreme case in point is fires in Indonesia that are strongly influenced by the El Niño-Southern Oscillation in combination with the draining of peatlands. According to *Schultz et al*. [2008] BC emissions from Indonesian fires ranged between 40 and 1400 Gg yr^{-1} during the 1990s. Such large fires can occur at any latitude; for example *Mack et al*. [2011] report a tundra fire that released approximately 2100 Gg of carbon as CO_2, similar in magnitude to the annual net carbon sink for the entire Arctic tundra biome.

[13] The method for estimating emissions from large open fires is similar to Equation 3.1, but using different input data.

$$M_{emitted} = \sum_i BA_i \, FL_i \, CC_i \, EF_i \qquad (3.2)$$

Here, BA_i is the burned area (km^2), FL_i the available fuel load (kg dry matter per km^2), CC_i the combustion completeness (fraction) and EF_i the emission factor (g compound per kg dry matter). The first three parameters combine to produce activity, or total mass burned. The index *i* usually stands for one ecosystem type in each inventory grid cell. As fire activity has a pronounced seasonal cycle, *BA, FL,* and *CC* must also consider temporal variability of fires, although this is not yet state-of-the-art in global inventories for *FL* and *CC*. Similar to estimates of energy-related combustion, emissions for open burning can be accomplished at different levels of refinement, as summarized in Table 3.2.

[14] Burned area is either derived from aerial surveillance or retrieved from satellite instruments that measure surface temperature and reflectance [*Stocks et al.,* 2002; *Kasischke and French*, 1995]. Space-borne retrievals of burned area are generally based on the changes in surface reflectance as a result of the dark burn scar after a fire, but they occasionally make use of active fire detection as well [*Giglio et al*., 2009]. These retrievals can be confounded by apparent changes caused by the viewing geometry, cloud shadows, snow melt or temporary flooding, and other factors [*Roy et al.*, 2002; *Simon et al.,* 2004]. Some studies have also related fire radiative power from active burns to the amount of biomass combusted [*e.g., Wooster et al.,* 2005; *Kaiser et al.* 2009; *Kaiser et al.,* 2011] or to the amount of aerosol emitted [*e.g.*, *Ichoku and Kaufman*, 2005; *Sofiev et al.,* 2009].

[15] Fuel loads and combustion completeness are normally extrapolated from smaller-scale field studies. Grassland fires often consume nearly 100% of the above-ground biomass [*e.g., Shea et al.,* 1996; *Keene et al.,* 2006]. In contrast, the combustion completeness in forests varies strongly depending on the fuel and burning conditions. If the fuel is sufficiently dry, the dead plant material and plant litter are often consumed almost completely. Larger branches and stems rarely burn entirely and living biomass is generally affected only in severe fires. The actual consumption of biomass in a given fire depends strongly on the ecosystem type and the fire size, severity and persistence. Fires can consume substantial amounts of soil material, which can dominate fire emissions, for example in peat areas of Indonesia or Siberia [*e.g., Goldammer and Seibert,* 1990; *Soja et al.,* 2004].

[16] Emission factors are obtained from laboratory experiments or field measurements in the smoke plumes of actual open burns. Different measurement methods for BC in each field study, systematic sampling biases, and the use of ecosystem mean emission factors to represent both flaming and smoldering combustion introduce uncertainties in the estimated emissions (see Section 3.7.2.3).

3.3.3. Waste burning emissions

[17] Combustion may be used to dispose of agricultural, household, or industrial waste. Well-controlled combustion systems, such as incinerators, emit little particle mass, and the discussion here focuses on uncontrolled burning. Activity data are among the most difficult to estimate, as they are not of economic interest and, therefore, not quantified by any organization. Large agricultural fires are detected with remote sensing, but the smaller fires are not and may be excluded from open burning emission estimates.

[18] Agricultural waste, such as cereal straws, woody stalks, and sugarcane leaves and tops, are generated during harvest periods. Some of this biomass finds use as animal fodder, thatching for rural homes, and fuel for residential cooking and agricultural and rural industry. A fraction of agricultural waste is burned in fields, often to clear them for a new sowing season, or sometimes as part of the harvesting process. The practice of agricultural waste burning has strong regional and crop-specific differences, and has large seasonal variations. Emissions from agricultural waste burning are typically calculated by multiplying crop production of a particular type, a fraction of residue per product, a fraction burned in the field, a fraction of dry matter, and the combustion completeness. Reported residue-to-product ratios [*Koopmans and Koppejan,* 1997] are larger for straw and stalks of crops like cereals (rice, wheat,

millets) and legumes, but smaller for husks and hulls from rice and groundnut. Reported ranges of dry matter fraction are 0.71 to 0.85 and combustion efficiencies range from 0.68 to 0.89 [*Streets et al.*, 2003a]. However, the assumed fraction burned in field is subject to large uncertainties and is sometimes computed based on local practice and knowledge of competing uses of the agricultural waste [*Venkataraman et al.,* 2006].

[19] Emissions from garbage burning are estimated using per-capita waste generation rates, along with fraction burned and emission factors. Both waste generation rates and fraction burned are location-specific [*e.g.*, *Christian et al.,* 2010]. Waste generation is higher in industrialized countries and urban areas, but the fraction burned is higher in developing countries. Burning of industrial waste is quantified in industrialized countries, but it is highly controlled so that emissions are small. In contrast, informal disposal of industrial waste has not been quantified in developing countries and these emissions are not included in these estimates.

3.4. Total BC emissions and major source categories

[20] Table 3.3 summarizes the best estimates and their ranges for BC and POA emissions in the year 2000 as derived in this assessment from a variety of information sources described in this section. Figure 3.2 summarizes sources of global BC emissions from two global inventories, along with estimates of their uncertainty; it also shows emission ratios for co-emitted, cooling aerosol species or precursors. Estimates from SPEW (Speciated Pollutant Emissions Wizard [*Bond et al.*, 2004, 2007; *Lamarque et al.*, 2010]) and GAINS (Greenhouse Gas and Air Pollution Interactions and Synergies [*Kupiainen and Klimont*, 2007; *Cofala et al.*, 2007; *Amann et al.,* 2011; *UNEP*, 2011]) are used as a reference for energy-related emissions throughout this assessment because they have the technological detail required to explore mitigation. SPEW estimates contain bottom-up uncertainties and are therefore used as the basis for Figure 3.2. GAINS estimates have the advantage of providing all co-emitted species, including gaseous emissions, and are used in the discussion of source category impacts in Section 10. Section 3.6 discusses differences between these inventories and compares other global and regional emission estimates.

[21] Figure 3.2 and Table 3.4 also give bottom-up estimates from open burning. Both RETRO (Reanalysis of the TROposphere over the last 40 years) [*Schultz et al.*, 2008]) and GFED (Global Fire Emissions Database [*van der Werf et al.*, 2006]) incorporate remote sensing information on fires to provide seasonal and interannual emission variation, and are frequently used by atmospheric models. However, because remote sensing poorly detects small agricultural fires, we rely on estimated activity data (SPEW and GAINS) for agricultural waste burning emissions. The figure and table also compare SPEW open-burning emissions, which are based on country information about total quantities burned.

[22] The left panel of Figure 3.2 presents total BC emissions for each source category, also indicating the regions of emission. This panel shows ranges calculated from uncertainties in both activity data and emission factors in SPEW, and a comparison with the same sectors in the GAINS database. Although totals for each category vary, there is general agreement that the three largest contributors are open burning, diesel engines, and residential solid fuels. A small number of industrial sources in developing countries also make a significant contribution.

[23] The two right panels of Figure 3.2 show emission ratios between POA and BC, and sulfur dioxide and BC. Higher ratios indicate that more aerosol species are co-emitted that could offset direct warming by BC. For BC in snow and sea ice, co-emission of non-absorbing aerosol (*e.g.,* sulfate) does not affect BC forcing, and co-emission of absorbing aerosol (*e.g.,* some POA) adds to the forcing. Not represented in the figure are gaseous species such as carbon monoxide and O_3 precursors, many of which contribute to warming (see Section 10).

[24] Table 3.5 provides numeric values for energy-related emission estimates in Figure 3.2, including additional disaggregation. For an estimate of energy-related BC emissions in the year 2000, we average the GAINS and SPEW totals without flaring, cruise aviation, and international shipping yielding 4430 Gg yr^{-1}. We then add those three sources for a total of 4770 Gg yr^{-1}. Relative uncertainties in BC emissions are taken from the SPEW bottom-up calculations, giving 90% uncertainty bounds of 1220 to 15000 Gg yr^{-1}. A similar estimate for POA gives a central estimate of 15900 Gg yr^{-1} with uncertainty bounds of (8800 to 23800) Gg yr^{-1}.

[25] Table 3.4 provides numeric values for biomass-burning emission estimates in Figure 3.2, including additional disaggregation. For an estimate of all-source, bottom-up emissions in 2000 from open burning, we average the RETRO and GFED climatological values for forests, grasslands and woodlands, yielding approximately 2450 Gg BC yr^{-1}. We add estimated activity-based data (average of SPEW and GAINS) for estimates of agricultural waste burning emissions (310 Gg BC yr^{-1}). The total is 2760 Gg BC yr^{-1}. A parallel estimate for POA gives 29200 Gg POA yr^{-1} from forests, grasses, and woodlands, and 1910 Gg POA yr^{-1} from agricultural waste burning. Bottom-up uncertainty estimates were not available from previous literature and are discussed in Section 3.7.

[26] For energy-related emissions in the background year of 1750, we assume the values of 390 Gg BC yr^{-1} and 1560 Gg POA yr^{-1} given by *Dentener et al.* [2006]. These emissions are entirely from biofuel use. Industrial-era emissions are the difference, 4380 Gg BC yr^{-1} and 14300 Gg POA yr^{-1}. We also assume the *Dentener et al.* [2006] values for background open-burning emissions: 1230 Gg BC yr^{-1} and 12800 Gg POA yr^{-1}. Industrial-era emissions are the difference, 1740 Gg BC yr^{-1} and 18300 Gg POA yr^{-1}.

[27] In the following sections, we briefly review contributions from individual source sectors. Section 3.5 will discuss some reasons for differences between the estimates presented in the figures, as well as other emission estimates.

3.4.1. Diesel engines

[28] On-road diesel engines include diesel cars and trucks, while off-road engines include uses for agriculture, construction, and other heavy equipment. Diesel engines contributed about 20% of global BC emissions in 2000. These sources have the lowest co-emissions of aerosols or aerosol precursors of all the major BC sources. In order to enable use of the most advanced exhaust controls, sulfur must be removed from the diesel fuel during refining. Therefore, in regions with fewer controls, primary particulate matter emission factors are higher, but SO_2 emissions are also higher.

3.4.2. Industrial coal

[29] Industrial coal combustion is estimated to provide about 9% of global emissions, mainly in small boilers, process heat for brick and lime kilns, and coke production for the steel industry. Although coal combustors can be designed to produce little BC, coal can also be highly polluting when burned in simple combustors, which are still present in small industries, particularly in developing countries. Co-emitted SO_2 is estimated from coal sulfur content and exhaust control. The SO_2/BC ratio for industrial coal is much higher than for the other emission categories, where the fuel has little sulfur or more efficient flue-gas controls are in place. Emissions from coal-fired power plants, which emit much less BC because of their better combustion efficiency, are not included here.

3.4.3. Residential solid fuels

[30] Wood, agricultural waste, dung and coal are used for cooking or heating in homes, providing another 25% of BC emissions. Most of the emissions occur in single-family devices, which are often of simple design. When infrastructure and income do not allow access to low-emission residential energy sources such as electricity and natural gas, solid fuels are used extensively for cooking. Otherwise, they are used more often for heating. Coal and, less frequently, wood are also used for heating in multi-family building boilers. The designation 'cooking' in Figure 3.2 refers to regions where wood is primarily used for cooking, even if some heating occurs. Similarly, 'heating' includes all uses in regions where heating is dominant. This sector also includes emissions from both production and consumption of charcoal. The poor combustion and mixing in these simple devices results in relatively high POA:BC ratios, but SO_2 emissions are low except for coal.

3.4.4. Open burning

[31] Open burning of biomass in the location where it is grown is a very large contributor to global BC emissions, with bottom-up estimates predicting that it contributes about 40% of the total. A smaller contribution originates from open burning in agricultural fields, which is often done to clear residues after harvest. This source contributes about 300 Gg yr^{-1} BC and 1500 Gg yr^{-1} OC. In regions like south Asia, this source can contribute about 20% of carbonaceous aerosol emissions [*Venkataraman et al.*, 2006].

[32] Current global emissions estimated from open burning range between 2000 and 11000 Gg yr^{-1} for BC, and between 18000 and 77000 Gg yr^{-1} for OC in average years [*Schultz et al.,* 2008; *Lamarque et al.,* 2010; *van der Werf et al*., 2010]. Most studies fall into the range of 2000 to 6000 Gg yr^{-1} for BC and 20000 to 27000 Gg yr^{-1} for OC. The highest BC and OC emission estimates by *Chin et al.* [2002] resulted from the use of larger emission factors. Table 3.4 compares current estimates of open-burning BC emissions for the periods 1997 to 2006 (GFED 3.1) and 1996-2000 (RETRO) with the climatological values from SPEW. The resulting average of 2560 Gg BC yr^{-1} (including emissions from waste burning as described earlier) agrees well with the mean value of global BC estimates from the review of *Schultz et al.* [2008] after they adjusted the literature estimates to standard emission factors. However, modeling studies that constrain total AOD with satellite observations indicate substantially larger biomass burning emissions of particulate matter (see section 4.5).

[33] Because fuel-air mixing is completely unmanaged in open burning, large quantities of organic matter can escape and average POA:BC ratios are highest of all sectors, although this ratio can vary greatly depending on the burning conditions. If the burning is natural or accidental, vegetation may burn while it is still rooted and standing, thus allowing for some ventilation and oxygen supply. Deliberate burning may involve land clearing before collecting, piling and burning the material, which tends to favor oxygen-poor conditions.

3.4.5. Other emission sources

[34] BC emissions from sources not discussed above are 10-15% of the global total. Significant contributors to this category are listed in Table 3.5. Two of the largest groups are industrial and residential emissions that are not included in one of the preceding categories. In industry, biofuels are responsible for the elevated BC emissions estimated by SPEW. Like coal-burning sources, these small sources are challenging to characterize. About half of the miscellaneous residential emissions come from middle distillate oil, and stationary diesel engines used for distributed power generation are estimated to produce about 85% of that. Charcoal, kerosene and liquefied petroleum gas make up the remainder of residential emissions.

[35] Other BC sources include gasoline engines, shipping, and flaring. Gasoline engines have much lower particulate matter emission rates than diesel engines, so total emissions from gasoline are less than 10% of diesel BC emissions, although gasoline vehicles are more numerous. The contribution of shipping and aircraft to BC mass is quite small, although these sources emit BC into regions or at altitudes that otherwise have low aerosol concentrations. Electricity generation is not considered a large source of BC because the high temperatures and well-managed combustion promote burnout of any BC that is formed. However, BC emission rates from power generation in developing countries are not well known (see Section 3.6.1). Flaring in the oil and gas industry is a poorly understood source both in terms of activity and emissions. Considering data from *Elvidge et al.* [2009], *Johnson et al.* [2011a] and *Johnson and Coderre* [2011], GAINS estimated BC emissions at nearly 4% of the anthropogenic global total with the majority originating in Russia, Nigeria and the Middle East.

3.5. Regional emissions

[36] The level of refinement in current inventories, limited by the availability of data, varies greatly among world regions (Table 3.6). Figure 3.3 presents emission estimates tabulated by region, rather than by source category. Substantial BC emissions occur in all regions, with the largest contributions in regions where open burning is high (Africa and Latin America). Dominant sources of BC emissions from energy-related combustion change with development from residential coal and biomass fuels (60-80%) in Asia and Africa, to on-road and non-road diesel transport (about 70%) in Europe, North and Latin America. Industrial uses of coal are also important in East Asia.

[37] The largest open burning emissions occur in Africa, Latin America and Southeast Asia. Tropical savanna and forest burning contribute about 45% and 40% of global open fire emissions, respectively. Globally, burned area and fire emissions are mostly decoupled because most of the burned

area occurs within savanna ecosystems with relatively low fuel loads and emissions per unit area, while forest lands have less burned area but higher and more variable fuel loads. As a consequence, interannual variability is higher in equatorial Asia than in Africa. Open burning at northern mid- to high-latitudes does not constitute a large fraction of global, annual BC emissions, but the timing and location of Eurasian open burning emissions in particular (*i.e.,* high-latitude spring in Figure 3.4) mean they are optimized to contribute to BC cryosphere climate forcing, which has very high efficacy (Section 7). Figure 3.5 shows the distribution of the major source types by latitude. The Northern Hemisphere contains about 70% of the emissions (*i.e.,* 85% of energy-related emissions and 45% of open-burning emissions).

3.6. Comparison among energy-related emission estimates

[38] Thus far, emission estimates from GAINS and SPEW have provided a perspective on the major sources of global BC emissions. Other estimates of global and regional emissions are summarized in Table 3.7. These differ substantially, by up to factors of three for specific regions. We begin by reviewing global emission estimates. Differences in the totals can usually be ascribed to choices of emission factors or other characteristics within the major source categories, which we discuss individually. We then use this background to discuss differences among Asian emission estimates.

[39] *Penner et al.* [1993] developed one of the first global BC emission estimates based on applying constant global emission factors to broad sectors. *Cooke and Wilson* [1996] were the first to apply emission factors that depend on development level. An updated version of that inventory [*Cooke et al.* [1999], abbreviated as *Cooke99* for the following discussion] is commonly used in atmospheric modeling. Bond *et al.* [2004] discussed the main sources of differences between SPEW and *Cooke99*. As discussed below, the largest differences are for power generation and diesel engines.

3.6.1. Differences in power generation emissions

[40] GAINS and SPEW agree on the magnitude of BC from power generation. However, *Cooke99* has much higher emissions from coal-fired power plants (an increase of 1600 Gg yr^{-1} BC and 2400 Gg yr^{-1} OC above both GAINS and SPEW). This difference resulted from assumptions of very high BC fractions in *Cooke99* while the other estimates relied on existing measurements. New measurements [*Zhang et al.*, 2008a] and subsequent harmonization of emission factors [*Lamarque et al*., 2010] support the use of lower emission factors and values nearer the SPEW and GAINS emissions for this sector. However, there remains a persistent but informal perception [*e.g., Gufran Beig*, personal communication] that BC fractions of particulate matter in developing countries, especially in power plants and industrial installations, could be higher than represented by existing measurements. Even if older, poorly operating power plants have high BC emission factors, there is no evidence that newly installed, modern power plants do. Thus, rapid growth in electricity generation is unlikely to cause sharp increases in BC emissions.

3.6.2. Differences in industrial coal emissions

[41] SPEW estimates of industrial coal emissions are about double those of GAINS. This difference is almost entirely due to assumptions in emission factors and BC fractions for the two major emitting categories, brick kilns and coke ovens. A few particulate matter (PM) measurements were available for brick kilns, but no measurements of total PM from uncaptured coking were available at the time of inventory development. Composition measurements for both sources were estimated based on expert judgment, as no composition measurements were available for either source.

3.6.3. Differences in diesel engine emissions

[42] GAINS and SPEW have similar emissions for year 2000 from on-road and off-road diesel engines, with SPEW being somewhat higher due to different assumptions about emission factors and the fraction of high-emitting vehicles. In previous versions of SPEW [*e.g., Bond et al.*, 2007], diesel emissions were higher than those given here due to different assumptions about the implementation of standards. The *Cooke99* inventory had much higher emissions from diesel engines, resulting from very large assumed emission factors in developing countries that were not based on measurements. Measurements have confirmed higher emission factors in locations with delayed emission standards [*Subramanian et al.,* 2009; *Assamoi and Liousse,* 2010], although no measurements are as high as the assumptions in the *Cooke99* inventory. However, an evaluation of trends in California [*Kirchstetter et al.*, 2008] indicates that emissions prior to regulation could have been higher by a factor of 10, greater than either the emission factors used in SPEW and GAINS, or in any reported measurements.

3.6.4. Differences in residential solid fuel sector

[43] Small-scale residential combustors constitute the largest difference between SPEW and GAINS. Estimates from SPEW are lower by 30% for biofuel used in cooking and all uses of coal, and higher by 35% for biofuel used in heating. The discrepancies in heating biofuel and coal emissions are largely due to activity data. For cooking stoves, activity in SPEW is lower by about 15%, and emission factor choices cause the remainder of the difference. GAINS uses the highest emission factor from fireplace measurements for cooking stoves (about 1.1 g BC [kg fuel]$^{-1}$), while SPEW uses an average of cooking stove measurements (about 0.8 g BC [kg fuel]$^{-1}$). Both are consistent with observed emission factors.

3.6.5. Asian emission inventories

[44] Detailed emission inventories have been developed for the Asian region and for individual countries within Asia. Here, we compare these inventories and identify some reasons for differences. Similar studies are not available in other world regions.

[45] Three emission inventories have been developed for Asia alone. Streets *et al.* [2003b] provided inventories to support modeling during the TRACE-P field campaign [*Jacob et al.,* 2003]. Emission factors in that inventory were an earlier version of those in SPEW [*Bond et al.*, 2004]. Two primary differences were the addition of small industries (brick kilns and coking) in SPEW, and adjustment of emission factors for residential fuel, where BC emission factors were reduced slightly and those for organic matter were greatly reduced. In addition, the TRACE-P inventory relies on some projected energy use because it was developed before year 2000 data became available. *Ohara et al.* [2007] developed an Asian emission inventory and also provided time trends for 1980-

2003. They used a single emission factor for each sector drawn from *Streets et al.* [2003b], except for transportation where they developed a representation based on differing vehicle types. *Klimont et al.* [2009] drew on additional national data collected during the GAINS-Asia project to estimate emissions of BC and OC for the period 1990-2005 and projections to 2030. They developed technology specific factors, although they did not distinguish among some uses (*e.g.,* cooking versus heating), with the result that estimates were about 25% higher estimates than those of *Streets et al.* [2003b], *Ohara et al.* [2007], SPEW, and the current GAINS global model.

[46] For India, central values of BC emissions differ by a factor of about three. The lowest central value [*Reddy and Venkataraman,* 2002a,b; *Venkataraman et al.,* 2005] is from a difference (compared to SPEW) in the residential sector, where the India-only mean emission factor is about 16% lower than the global mean used by *Bond et al.* [2004]. Estimates by *Sahu et al.* [2008] are a factor of three larger, resulting from the use of the high power-plant and diesel emission factors in *Cooke99. Menon et al.* [2010] compared models using both *Sahu et al.* [2008] and *Bond et al.* [2004] estimates. *Parashar et al.* [2005] estimated emissions a factor of two larger than those of *Reddy and Venkataraman*, largely caused by their new measurements of very high emission factors for biofuel (especially dung). Estimates from *Ohara et al.* [2007] and *Streets et al.* [2003b] are based on the same emission factors, so the large difference between them is surprising. Most of the 200-Gg yr^{-1} difference is attributable to biofuels in the residential sector (616 vs 420 Gg yr^{-1}, respectively). Activity data are frequently given in terms of total fuel calorific content rather than mass, and in these units the Ohara and Streets inventories are only 16% different. The difference, therefore, must be caused by differing assumptions in the conversion between fuel calorific content and mass. *Klimont et al.* [2009] used higher emission factors for cooking and national energy use statistics and estimated nearly 30% higher BC than current global GAINS implementation or SPEW, while OC was well within the range of GAINS and SPEW. *Lu et al.* [2011] obtained similar estimates to *Klimont et al.* [2009] and also estimated that BC emissions rose 35% between 2000 and 2010.

[47] For China, regional inventories are in broad agreement with global inventories on magnitudes and sources of BC emissions. *Cao et al.* [2006] developed an emission inventory based on Chinese data and some new emission factors. SPEW and the inventory of *Cao et al.* [2006] are quite similar. The *Streets et al.* [2003b] inventory lacks treatment of small industry. Zhang *et al.* [2009] included small industry, particularly brick and cement kilns, following the approach of *Streets et al*. [2006], and estimated significantly higher total BC emissions from China. Organic matter emissions in *Cao et al.* [2006] are higher than those of the other studies due to the use of different emission factors. *Klimont et al.* [2009] estimates for BC are higher by about 15% than *Streets et al.* [2003b] and global inventories but lower than *Zhang et al.* [2009]. While comparing total emissions for China yields in general fairly good agreement across the studies, there are significant sectoral shifts resulting primarily from uncertainties in coal versus briquette use in the residential sector and assumptions for the brick-making sector. For example, *Zhang et al.* and GAINS use comparable assumptions for coal while *Klimont et al.* [2009] assumes more briquettes, leading to lower emissions from this sector in *Klimont et al.* On the other hand, for brick making both *Zhang et al.* and *Klimont et al.* rely on *Bond et al.* [2004] emission factors and estimate higher emissions than GAINS, which considers anecdotal evidence about the transition in this industry that leads to significantly lower emission factors.

3.7. Major sources of uncertainty in emissions

3.7.1. Energy-related combustion

[48] As discussed in Section 3.6, large differences between emission estimates are attributable to a few choices regarding emission factors made by inventory developers. Some of the diversity is not supported by measurements at emission sources, while other disagreements reflect true uncertainty in knowledge. A bottom-up estimate of uncertainty is about a factor of two using either a simple uncertainty combination for global emissions [*Bond et al.,* 2004] or a Monte Carlo approach for individual countries [*Lu et al.*, 2011].

3.7.1.1. Activity data

[49] For fossil-fuel combustion, activity estimates for many inventories in Table 3.7 have the same source (International Energy Agency (IEA), or United Nations fuel-consumption data), although many inventory developers adjust these data when inconsistencies are found or when finer allocation of activities is required (*e.g.*, road and off-road vehicles or vehicle type). Some national fuel balances contain this level of detail and might be preferred to international statistics, but this would lead to loss of comparability. For several larger countries, regional statistics are also available and using them allows for better spatial resolution; however, there are several consistency issues with the national and international statistics. Finally, some models chose to use datasets specifically developed for particular projects. For example, GAINS often uses national fuel-consumption estimates for most of the European countries, China, India and Pakistan. These may differ from IEA statistics, especially with regard to sectoral allocation. Total fuel consumption can be affected by the use of regional information on the calorific value of fuels.

[50] Consumption of residential solid fuels, especially biofuel, is not well constrained. Biofuel consumption data are frequently drawn from disparate sources. For example, GAINS relies on IEA and national data, while SPEW uses the tabulation of *Fernandes et al.* [2007]. Fuel production and sales are not centralized in this sector, and many fuels are collected by the consumers or by small sellers. Activity data are therefore much more uncertain than for liquid or gaseous fuels or consumption in large installations. Estimates of fuel consumption are often based on per-capita consumption estimates multiplied by the number of people using solid fuels. Comparison of the residential biofuel consumption for the past years in India and China (*Streets and Aunan* [2005], *Venkataraman et al.* [2005], *Ohara et al.*, [2007], and GAINS) shows significant differences, typically ranging within about ±25%.

3.7.1.2. Emission factors

[51] Emission rates of both BC and organic carbon depend on the combustion process, including fuel composition, flame temperature, mixing between fuel and air during combustion and post-combustion treatment of the exhaust. Carbonaceous aerosols can be destroyed if the exhaust is kept hot and well mixed with air. Large, properly operating combustors such as

power plants and some modern installations using biofuel tend to achieve this burnout, resulting in little emitted BC. Mixing between fuel and air before combustion also limits BC formation, so that gasoline engines emit much less BC than do diesel engines. Finally, BC may be removed through end-of-pipe controls that capture fine particles, as it is in particulate filters after diesel engines.

[52] The strong dependence of BC emissions on combustion processes means that the disaggregation of activity to represent combustion quality explicitly is an important component of inventories. The dependence also demands the development of emission factors under realistic operating conditions. Because most sources have several operating modes, it is important to obtain emission factors by measuring during a realistic sequence. This sequence of conditions may be called 'driving cycles' for vehicles, or 'burn cycles' for stoves, small boilers, or open combustion. Although design of existing cycles seeks to represent real-world operation, unrealistic choices of operating conditions may yield emission factors that are poorly representative. For example, very cold conditions or startup phases, which promote poor efficiency and high emissions, may be omitted from vehicle and stove emission testing, or tests may not include the poorest quality fuels.

[53] Uncertainties are particularly acute outside the United States and Europe. A few measurements are becoming available, but the limited number of studies has not dispelled concern that the highest emitters have been missed or significantly underrepresented.

1. Diesel engines. There is a good understanding of on-road emissions from normal vehicles in developed countries, although questions exist about how in-use vehicle emissions compare with those from tests in laboratories. Both averages and ranges of vehicle emissions in developing countries are not well quantified. Compared with on-road engines, there are many fewer measurements of off-road equipment, including engines used for agriculture and construction. A large uncertainty in determining total emissions is the contribution of poorly functioning vehicles with very high emissions, or 'super-emitters.' The fraction of such vehicles and their emission factors are not well known, and these assumptions result in major discrepancies between inventories, because a single super-emitter can produce many times more BC than a properly operating engine with an emission control system. Super-emitters are likely to be more widespread in developing countries, but data on the fraction of vehicles with such high emissions are extremely limited.

2. Industrial solid fuels. Emission estimates from the industrial sector are dominated by small, simple kilns in traditional production processes and old boilers. Activity data and emission factors for these sources are particularly difficult to obtain. Magnitudes and composition of emissions are the most uncertain of any of the major source categories due to lack of measurements.

3. Residential solid fuels. Although the residential sector is highly heterogeneous with regard to the types of fuels and devices used, a relatively small number of emission measurements have been made and most of these are from laboratory rather than in-use measurements. Limited data on emission magnitudes and composition are available to characterize this sector.

3.7.1.3. Summary of uncertainties in energy-related emissions

[54] Major contributors to uncertainty in BC and OC emissions from energy use are: (1) measured particle emission factors obtained under laboratory conditions (*i.e.,* rather than in-use or in-field) for residential combustion, traditional industry, and vehicles with high emissions due to malfunction; (2) speciation of PM from high-emitting technologies into BC and OC; (3) quantification of individual emitters in sectors that contain even a small fraction of highly polluting devices; and (4) amounts of fuel burned in sectors where fuel and output are not formally monitored and tabulated. While most of the estimates tabulated here are given for the year 2000, rapid economic growth in countries with large BC emissions may have caused energy-related BC emissions to increase dramatically over the last decade. The year used for the inventory estimate is important when comparing atmospheric models with observations.

[55] In addition to the factors that affect total emission quantities, the location of emission may be poorly known for sources such as small industry and passenger or freight vehicles. These inaccuracies affect comparisons between measured and modeled concentrations.

3.7.2. Open biomass burning

3.7.2.1. Burned area

[56] Considerable uncertainties remain in the quantification of burned area. Current satellite retrievals cannot detect burn scars much smaller than one square kilometer, and the size of the burned area is sometimes wrongly determined. Active fires can be detected when they are larger than about 0.1 ha, but many fires cannot be observed during their flaming stage because of incomplete coverage of satellite orbits or clouds obscuring the scene. Given the current resolution of satellite instruments that are used for burned area retrievals (typically 0.25 to 1 km^2 at the sub-satellite point and 5 to 10 times larger at swath edges), only burn scars with a size of at least 12 to 40 ha can be detected from space. Field data and satellite retrievals of fire radiative power [*Wooster et al.,* 2005] show that the majority of fires are smaller, particularly in tropical regions [*cf. Schultz and Wooster,* 2008]. Uncertainties arising from the limited spatial resolution of current instruments could be as large as -30% to +40%, but in reality they are smaller due to compensating errors. Validation of individual fire scenes with high-resolution Landsat data indicates that burned areas are probably underestimated by about 10% on average [*M. Wooster, personal communication, 2009*].

3.7.2.2. Fuel load and combustion completeness

[57] Field studies, for example in the savanna regions of South Africa [*Shea et al., 1996*], revealed that fuel loads can easily vary by a factor of three within a region of limited ecosystem diversity. Combustion completeness strongly depends on the weather conditions because bulk fuel, which constitutes a large fraction of fuel mass in wooded ecosystems, burns only when the fuel is sufficiently dry and when it is windy. Uncertainties in vegetation modeling for calculation of available fuel load and combustion completeness are highest in deforestation regions and in regions where peat fires occur [*van*

der Werf et al., 2006] (*e.g.*, Southeast Asia) where problems in modeling the combustion of organic soil layers containing peat leads to an uncertainty of about a factor of five. In some regions, like southern hemisphere Africa, models incorrectly predict seasonality, with peak emissions in bottom-up estimates occurring about 1–2 months earlier than the peak in satellite-detected AOD [*van der Werf,* 2006]. This is attributed to an increase in emissions as the fire season progresses, caused by a shift from grassland fires early in the dry season to woodland fires later in the dry season, associated with different fuel moistures and burning behaviors. Ecosystem modeling frameworks are moving toward capturing such temporal variations. A conservative estimate of the global uncertainty caused by fuel load densities and combustion completeness is a factor of two.

3.7.2.3. Emission factors

[58] As Section 4.5 will show, current models of the atmosphere underestimate absorption aerosol optical depth (AAOD) in Africa and Latin America, which are major biomass burning regions [*Koch et al.*, 2009a]. Some of the extra absorption in Africa could be caused by dust, but an explanation is needed for the underestimate in Latin America. The underestimate could be caused by low biases in burned area or fuel loads (see above), but inverse models [*Arellano et al.*, 2004; *Arellano et al.*, 2006; *Stavrakou and Müller,* 2006] indicate little bias in carbon monoxide (CO) emissions from biomass burning in these regions. The remaining suspects are emission factors or the relationship between emitted mass of BC and optical absorption of the fire plume.

[59] Although biomass burning is a large component of global BC emissions, particulate and BC emission factors for this source are poorly constrained. As discussed in Section 2, measurements of BC depend on the analysis method. These method-dependent biases are more critical for biomass-burning emissions than for other sources, because these emissions pyrolyze and also contain materials that catalyze BC emission. The comprehensive literature review of *Andreae and Merlet* [2001] has become widely used, in particular for the compilation of global inventories [*e.g., van der Werf et al.*, 2006; *Schultz et al.,* 2008]. However, this review included only values based on thermal oxidation techniques and excluded optical absorption measurements. The highest BC emission factor in this tabulation is lower than values inferred from absorption measurements, which have been used in other studies [*Patterson and McMahon*, 1984; *Liousse et al*, 1996; *Chin et al.*, 2002; *Liley et al.,* 2003]. *Martins et al.* [1998a] showed that thermal measurements of BC generally predicted far too little absorption.

[60] Comparisons between chemical and optical measurements would increase confidence in biomass-burning emission factors for BC. A review by *Watson et al.* [2005] showed differences of up to a factor of seven between different BC field measurements and discusses the various uncertainties related to both thermal and optical measurements. In contrast to *Martins et al.* [1998a], thermal measurements did not always yield lower concentration estimates than absorption measurements.

[61] Representativeness of measured emission factors is another concern. Open fires have a high inherent variability. Some emission factors and characteristics are inferred from small, better-controlled fires. The combustion intensity and the burning and airflow characteristics of these smaller fires may differ from those of real fires [*Reid et al.,* 2005]. Oxygen-rich flaming combustion is generally associated with more BC and more heat release, while lower-temperature smoldering fires have higher overall particulate matter emission factors and CO emissions than flaming fires [*Lobert et al.*, 1991; *Ward et al.*, 1992; *Yokelson et al.,* 1997]. If a sample is dominated by emissions from one of these phases, then ratios of BC to total PM, or BC to CO, do not represent the overall emission profile.

[62] The relationship between emitted mass of BC and absorption of the fire plume can be biased because of aging processes. As smoke ages, organic material condenses, but no further BC is created. BC/PM ratios in aged plumes are lower than those in fresh plumes, and single scattering albedos are higher (more scattering relative to absorption). Emission ratios are generally determined in fresh smoke plumes while models are evaluated with data from long-term regional averages, which are mostly of aged aerosol. If the relatively low BC ratios are then applied to fresh plumes, either BC emissions or absorption by BC could be underestimated.

[63] Data are presently insufficient to support firm conclusions about what updates should be made to BC emission rates from open burning of vegetation. However, thermal measurements may under predict absorption, and using regional-average optical properties as constraints could also under predict absorption at the time of emission. This body of evidence suggests that current emission factors from biomass burning might be biased low. Based on the data from *Andreae and Merlet* [2001] we estimate the lower uncertainty of BC emission factors to be a factor of 0.6 multiplied by the central value. Our estimate for the upper bound is a factor of 4.

3.7.2.4. Summary of uncertainties in open burning emissions

[64] The dominant uncertainty term for open burning emissions is the emission factor (error range: factor of 0.6 to 4). Fuel load and combustion completeness are uncertain by about a factor of two, while burned area is probably known within 10% on the global scale, although regional differences can be larger (*cf.,* Supplementary online material of *Schultz et al.* [2008]). Neglecting the independent error estimates from agricultural waste burning and assuming that errors are independent, error propagation yields an uncertainty range of a factor of 0.29 to 5. Based on the emission estimates in Section 3.4, absolute uncertainty ranges are 740 to 12800 Gg yr^{-1} for BC, and 8400 to 144000 Gg yr^{-1} for POA. These ranges are quite asymmetric.

3.8 Trends in BC emissions

[65] *Novakov et al.* [2003], *Ito and Penner* [2005], and *Bond et al.* [2007] all estimate large changes in BC emissions during the industrial era. All of these studies demonstrate that BC emissions are related to, but not directly proportional to fuel consumption. Typically, emission rates become greater as population and economic activity increase, and then decrease as cleaner technology is deployed. The resulting trend is an emission increase followed by a decrease, and is broadly consistent with measurement records downwind of industrializing countries [*McConnell et al.*, 2007].

[66] This discussion has focused primarily on the situation in the year 2000, but historical trends suggest how emissions may have changed since the year 2000 and how they will continue to change (see also Section 12.5). In regions where emission factors decrease faster than fuel consumption is growing, BC emissions and concentrations decline. *Murphy et al.* [2011] observed a 25% decrease across the United States between 1990 and 2004, and *Bahadur et al.* [2011] found a 50% decrease over a similar period in California, a state with more stringent standards. Ice-core measurements in Europe [*Legrand et al.*, 2007] also indicate a decrease in BC deposition since the 1970s. In contrast, when growth is rapid and clean technology has not yet been implemented, BC emissions and concentrations rise. *Lei et al.* [2011] suggests a 30% increase in Chinese BC emissions between 2000 and 2005, and *Lu et al.* [2011] estimate a 50% increase in Asian BC emissions between 2000 and 2010, caused by growth in all source categories. Increasing BC deposition is recorded in Himalayan ice cores [*Ming et al.*, 2008], although more measurements are needed given the high spatial variability in deposition in this region.

[67] Besides increases in fuel use and decreases in emission factors, other trends in fuel use affect net emissions. Cleaner fuels are chosen because of environmental regulations. Households switch to more convenient fuels as income rises, and those fuels tend to be cleaner. Fuels may be adopted for different uses (*e.g.,* energy production from agricultural waste).

[68] Historical records of charcoal deposits and anecdotal evidence suggest a decline of global emissions from open burning between the end of the 19th century and present-day, with strong regional differences [*Moulliot and Field*, 2005; *Power* et al., 2008; *Marlon et al*., 2008]. These changes have been attributed to the expansion of intensive grazing, agriculture and fire management [*Marlon et al*., 2008]. Fire records from North America suggest that fire severity, and hence carbon loss, increased during the last three decades [*Turetsky et al*., 2010]. This is consistent with climate model simulations indicating that fire activity will increase in the future because of increased temperatures and reduced rainfall [*Pechony and Shindell*, 2010; *Liu et al.*, 2010]. However, there have not yet been estimates of BC emissions from future increases in open burning.

3.9. Receptor modeling to evaluate source contributions

[69] Most BC is emitted from sources that are either small and numerous, or large but episodic, so monitoring data for individual sources is not available to validate emission inventories. The quality of emission inventories and the contributions of dominant sources can be determined only by inferences drawn from atmospheric measurements. The use of measured atmospheric chemical composition to deduce the influence of emission source types is generally known as *receptor modeling*. Another type of study that uses the magnitude and spatial distribution of atmospheric constituents to infer emission source strengths is called *inverse modeling*. The latter type of study requires atmospheric measurement networks, which are discussed in Section 4.4. A discussion of inverse modeling results is given in Section 4.5. In this section, we summarize information from receptor studies that have used chemical composition to identify particular source categories.

[70] Receptor methods based on the chemical composition of particles include examining the ratios of target chemical compounds, such as isotope ratios measured in time-averaged aerosol samples [*Gustafsson et al.,* 2009] or in single particles [*Guazzotti et al.,* 2003]. Other approaches use an expanded suite of chemical species to elucidate additional sources, including elemental and ionic composition and organic and elemental carbon [*Watson et al.,* 1994] and additional organic molecular markers [*Schauer et al.,* 1996; *Zheng et al.,* 2002]. A limitation common to all receptor models is the inability to distinguish sources whose emissions have a very similar chemical composition.

[71] Among receptor models, the chemical mass balance model [*Friedlander*, 1973; *Watson et al.,* 1984; *Chow and Watson,* 2002, *Watson et al.,* 2002] and positive matrix factorization [*Paatero,* 1997; *Hopke et al.,* 2010] have seen wide application in air quality assessment. Receptor modeling may also exploit ensembles of atmospheric trajectories [*Ashbaugh et al.,* 1985]. The outcome is the identification of the pollution source types and estimates of the contribution of each source type to the observed concentrations. Elemental carbon (as measured by thermal techniques) is often used as a tracer of certain emission sources. As discussed in Section 2, this measurement may not be equivalent to light-absorbing carbon. However, it will be referred to as BC in this section for congruency with other sections.

3.9.1. Receptor modeling in urban areas

[72] Source apportionment studies have been conducted to determine the sources of particulate matter pollution, usually in urban areas (Table 3.8). The most detailed information exists in the United States, based on measurements from the U.S. Environmental Protection Agency's network of speciation samplers. Source contributions shown are specific to BC, in decreasing order of influence. For United States urban areas, it is possible to separate approximately six to ten major sources of BC, including diesel, gasoline, biomass, residual oil and local traffic. Several other sources also contribute to BC concentrations, depending on the location: steel mills, railroad emissions, and metal processing facilities.

[73] For Europe and other world regions, no separate apportionment of BC has been done. To give an overview of the largest potential BC emitters, reviews [*e.g., Viana et al.,* 2008; *Johnson et al.,* 2011] were used to rank sources that contribute to the mass of particles smaller than 2.5 μm diameter ($PM_{2.5}$). Among these, sources that are BC and OC emitters are shown in the table. Resuspended dust, secondary pollutants like sulfate and nitrate or sea salt could be larger contributors to $PM_{2.5}$ at some locations, but are not included in Table 3.8.

[74] Globally, BC from gasoline combustion is only about 10% that from diesel (Table 3.5), but in the urban atmosphere this source may constitute a significant fraction of particulate emissions. There are considerable problems in separating emissions from diesel and gasoline vehicles. For example, *Shah et al.* [2004] showed that slow-moving and stop-and-go diesel vehicles emit organic and elemental carbon in patterns that are very similar to those of gasoline powered vehicles. Thus, their mass contributions of diesel engines might be mis-allocated to gasoline engines. In a growing number of urban centers, especially in the developing countries like India and

Bangladesh, *Guttikunda and Jawahar* [2011] showed that a significant fraction of BC emissions also originate from the brick kilns surrounding the city administrative boundaries, which consume a mix of coal, agricultural waste, and bunker fuel (in coastal cities).

[75] For European urban areas, the main sources of BC are vehicles, oil or solid-fuel combustion, and industrial and shipping emissions. Emissions from burning of biomass or biofuel were originally reported to be significant only in Denmark and Spain. Later, this source was shown to contribute relatively large fractions in rural and even urban areas [*Szidat et al.,* 2006; *Alfarra et al.,* 2007; *Puxbaum et al.,* 2007] suggesting that this source was not discriminated in the earlier studies.

[76] Information on urban areas in other world regions is largely qualitative, because many studies in these regions did not measure the complete suite of pollutants used for receptor modeling. Furthermore, they often use source profiles that were not locally measured and therefore may be unrepresentative [*Johnson et al.,* 2011]. In Latin America, traffic, oil combustion and small industry, including copper smelters, are important sources of fine particle mass. *Mugica et al.* [2009] attributed 42% of fine particulate matter in Mexico City to vehicles, but they were unable to separate wood burning due to their similarity with diesel sources. In Africa, open burning of biomass and refuse, residential coal combustion and traditional industries (brick making, lead smelters, foundries) are significant contributors. In East Asia, coal burning power plants and industries (cement, brick kilns) are dominant sources followed by traffic and biomass burning. Residential coal burning is a large wintertime contributor. In Southeast Asia, traffic is the dominant source in more urbanized locations while local burning (for cooking and brick making) is important in less urban locations. In South Asia, traffic and burning of refuse and biomass are important sources, followed by industrial sources. Brick kilns are important in some locations, while lumped small industrial sources contribute 10 to 30% of fine particle mass. Overall, where traffic is an important source, an aging motor vehicle fleet containing high emitters is of concern. Coal and biomass combustion for residential cooking and heating and small-scale industrial applications is widespread, likely under poor combustion conditions.

3.9.2. Receptor modeling in continental plumes

[77] Urban studies constrain sources that affect cities, but many emissions, such as residential solid-fuel burning or agricultural use of diesel engines, occur preferentially outside urban areas. Source apportionment studies have been applied to carbonaceous aerosol in the continental plume from South Asia. *Novakov et al.* [2000] suggested that fossil fuel was responsible for 80% of the BC in the continental outflow, while studies in Dhaka [*Salam et al.*, 2003] indicated a negligible contribution of biomass burning in South Asian cities. However, these findings relied on ratios between total carbon and BC that are representative of open biomass burning but not biofuel burning. Studies that do consider differences between emissions from biomass and biofuel estimate an approximately equal contribution of biofuel and fossil fuel [*Stone et al.,* 2007]. In continental outflow, a strong biofuel influence on total carbonaceous particles is indicated by single-particle measurements [74%, *Guazzotti et al.*, 2003] and radiocarbon measurements [66%, *Gustafsson et al*., 2009]. The radiocarbon measurements indicate that between one-half and two-thirds of the BC also result from biofuels. In Indian cities, fossil fuel burning dominates fine particulate matter concentrations, but biofuel is not negligible, according to organic marker studies [*Chowdhury et al.*, 2007]. Fossil fuel and biofuel contribute 20-60% and 7 to 20%, respectively.

3.9.3. Summary of findings from receptor modeling

[78] Results from receptor modeling are in qualitative agreement with major BC sources identified in global or regional emission inventories, with traffic being the largest source in North and Latin America and Europe, and with contributions from residential solid-fuel burning and open burning in Asia and Africa. This broad agreement lends confidence to the identification of the largest BC sources. However, receptor modeling of regional aerosols with specific source markers capable of resolving similar sources is needed before the approach can be extended beyond this qualitative assessment.

4. Constraints on black-carbon atmospheric abundance

4.1. Section summary

[1]

1. Black carbon concentrations, like those of all short-lived species, are variable in space and time and are largest around source regions. Constraints on black carbon abundance are provided by in-situ measurements of BC concentration and by ground- and satellite-based remote sensing of AAOD. AAOD retrievals from satellite remote sensing are nearly global in coverage, but are less quantitative than ground-based data.

2. Ground-based remote sensing provides information on the atmospheric aerosol column burden and optical properties, which is directly relevant to radiative forcing. However, BC AAOD is inferred indirectly from these measurements and therefore is poorly constrained. Aerosol can be sensed only when the sky is cloud-free, absorption sensing has large uncertainties when aerosol loading is low, and the interpretation of BC amount is confounded by the presence of other light-absorbing aerosol in the column.

3. National and global networks of measurements are used to evaluate models that provide estimates of BC surface concentrations (in-situ monitoring) and column AAOD (ground-based remote sensing). Measurements are most sparse in some of the regions with the highest BC loadings: Africa and most of Asia. Measurements from field measurement campaigns, which typically sample only one region over timescales much less than a year, can also be used to test processes within models more comprehensively, but within a limited domain and time.

4. Comparisons with in-situ observations indicate that many models simulate near-surface BC concentrations approximately correctly for North America and East Asia, have a slight high bias in Europe, and have a strong low bias in parts of Asia.

5. On the other hand, many model estimates of column AAOD over continents have a low bias in all regions. In many regions, this underestimate can be explained at least in part by the fact that these models do not account for aerosol internal mixing and, thus, their modeled mass absorption cross section (MAC_{BC}) is too low. However, even if this factor is taken into account, models would still show a low bias in some regions.

6. Comparisons with satellite observations indicate that bottom-up estimates of aerosol emitted from biomass burning are too low by factors of two to four, and emission estimates should be revised upward.

7. Airborne campaigns measuring vertical profiles of BC now allow for comparisons of vertically resolved concentrations away from continents. These measurements suggest that models overpredict BC in remote Pacific regions – on average by a factor of five – and that the overestimate is generally greatest in the upper troposphere. An exception is in the Arctic, where models appear to underpredict upper tropospheric BC. While concentrations in these regions are generally low, the large spatial area and bright underlying surfaces means the contribution of Arctic BC to globally averaged radiative forcing may be significant.

8. These combined results suggest that removal rates in models are an important source of model error. Further, inter-model comparisons indicated that differences between modeled BC concentrations and AAOD can only be attributed in part to differences in assumed emissions; differences in vertical transport and removal rates also play a large role, and MAC_{BC} differs between models.

4.2. Introduction

[2] The impact of BC on climate depends on its atmospheric abundance. Aerosol concentrations vary in space and time, and coverage by observations is insufficient to capture all such variations. Therefore, atmospheric models must be used to determine global concentration fields, and these models can be partially evaluated by comparisons with available observational data. Figure 4.1 shows modeled atmospheric absorption by two absorbing aerosols: BC and dust. The figure shows that BC, like all short-lived species, is most concentrated around source regions. For energy-related combustion, sources and concentrations are largest where population density is highest, as can be seen by comparing the east and west coasts of the United States, or Eastern Asia with Central Asia. Large BC concentrations also occur in and around biomass burning regions, especially South America and central Africa. Continental outflow also contains high concentrations, especially to the east of Asia and the west of Africa.

[3] Section 4.3 presents common measures used to constrain ambient BC concentrations experimentally. In Section 4.4 we discuss how the measurements reviewed in Section 2 are incorporated into networks to detect the spatial and temporal variation of BC concentration. Section 4.5 examines how well global models simulate BC concentration over broad regions, and Section 4.6 compares modeled vertical BC distributions with observations. These evaluations will be used in Section 5 to derive a best estimate of BC direct radiative forcing.

[4] Although BC is not well-mixed throughout the atmosphere, some of it is carried to remote regions. Most energy-related BC emissions occur in the Northern Hemisphere, and BC is found in remote regions there, including in the deep Arctic. In contrast, there is very little BC throughout large remote regions in the Southern Hemisphere.

[5] If all absorption is attributed to BC, then concentrations of BC using measured absorption will be overestimated, especially in dusty regions. Figure 4.1 shows simulated contributions to AAOD by BC and dust.

4.3. Atmospheric absorption and extinction by absorbing species

[6] Section 2.4 discussed measurements of BC mass concentration (with units of g m^{-3}). Another measure of particle abundance, albeit indirect, is AOD, which is the vertically integrated extinction of aerosols in an atmospheric column. Aerosol light extinction and AOD values are given for a specific wavelength; small (sub-micron) aerosols have higher AOD at shorter solar wavelengths. For illustration, if we neglect losses of sunlight to molecular scattering by gases, an aerosol AOD of 1.0 at 550 nm indicates that only 37% [e^{-1}] of the direct solar beam at that wavelength will reach the surface without being scattered or absorbed, if the sun is directly overhead.

[7] Of particular relevance for inferring absorbing aerosol amount is the single-scattering albedo (ω_0), which relates the amount of light scattered to the amount absorbed during an attenuation event (Eqn. 2.2). The value of ω_0 is influenced by microphysical properties (Section 2.4) and by compositional properties, which are quantified by refractive indices. These optical coefficients are usually determined through laboratory or in-situ measurements. The fraction of AOD attributable to absorption, or AAOD, is

$$AAOD = AOD * (1 - \omega_0) \quad (4.1)$$

For any species, the product of mass concentration (with units of g m^{-3}) and mass absorption cross section (MAC) (m^2 g^{-1}) is the absorption coefficient (m^{-1}). AAOD (dimensionless) is the result of integrating absorption coefficient over the entire atmospheric column, and is the quantity shown in Figure 4.1. AAOD is more closely related to BC column abundance than is AOD because BC is responsible for a much larger fraction of total absorption than of total extinction.

[8] As discussed in Section 2, atmospheric concentrations of BC are often inferred from observations of absorption. AAOD measured in the atmosphere is attributable to all light-absorbing aerosols: BC, dust or soil, and light-absorbing organic carbon (brown carbon). If all absorption is attributed to BC, then inferences of BC may be overestimated, especially in dusty regions. The relative contributions of each component to AAOD are required to infer BC column abundance.

[9] Figure 4.1 shows that although the regions most affected by BC and dust are somewhat different, both species make significant contributions to average absorption, and in some regions the contributions are equal. Dust has a much greater total AOD than does BC, but a smaller fraction of that AOD is absorption (*i.e.*, ω_0 is larger), so globally averaged AAOD of BC and dust are of similar magnitudes.

4.4. Observations of atmospheric black carbon concentrations

[10] Monitoring studies provide information about BC concentrations in the atmosphere. These studies incorporate either in-situ observations, in which sampled air is drawn into an instrument for measurement, or remote observations, which measure the intensity of light coming from the atmosphere, and from this infer information on the atmospheric distributions and properties of aerosols. In this section, we outline the contributions of different types of studies to the understanding of BC and other aerosol concentrations and properties (Table 4.1), although we do not provide a comprehensive listing of all studies.

[11] Data gathered from intensive field campaigns or observational networks are subject to the limitations of the measurement techniques used, as discussed in Section 2. Furthermore, when measurements are made at a single point, the measured values may not represent an average of the surrounding area, so comparisons between these point measurements and the average of a large model grid box should be done cautiously [*Vignati et al.*, 2010]. Thus, model simulations of the BC burden are evaluated by comparison with observations, which themselves may be biased. If the bias were known for each observation, or if it were the same for all observations, it might not affect our understanding of BC's life cycle, but this is not the case. Some biases may depend on aerosol age, source type, or location, and these relationships are poorly known.

4.4.1. In-situ monitoring

[12] The in-situ BC measurement techniques described in Section 2, especially thermal-optical measurements on filter samples and optical measurements, have been employed in several intensive field campaigns (Section 4.4.1.1) and in routine monitoring networks (Section 4.4.1.2) at national or continental scales. The uses and limitations of these measurements are described in the following subsections.

4.4.1.1. Intensive field campaigns

[13] Multi-investigator field campaigns have examined the nature of atmospheric aerosol in many world regions. Such campaigns typically take place over the course of a few weeks and provide 'snapshots' of regional aerosol. They often combine measurements from several platforms, beginning with heavily instrumented surface stations but also adding aircraft and shipboard platforms to measure vertical and horizontal distributions in continental plumes. Intensive campaigns provide information about aerosol composition, microphysical properties including scattering and absorption, and reaction rates. Because they incorporate large arrays of measurements, they provide a wealth of information on aerosol and gaseous precursors, and can often be used to evaluate some aspects of emission inventories. This type of observational approach generally has limited temporal and spatial coverage and, alone, does not provide the information required to determine the average influence of BC or other aerosols on climate. The value of this type of effort in the context of evaluating BC concentrations and climate impacts lies in the richness of simultaneous measurements that they provide. These studies provide detailed physical understanding for evaluation and the improvement of the modeling of aerosol processes.

[14] Examples of early field campaigns that studied carbonaceous particles included a mission to the Arctic [*Rosen et al.*, 1984] and the search for the light-absorbing component in the Denver Brown Cloud [*Groblicki et al.*, 1981]. Coordinated campaigns to study aerosol-climate interactions in particular regions began with the Aerosol Characterization Experiments (ACE) series of experiments [*Quinn and Coffman*, 1998; *Raes et al.,* 2000] and these have frequently examined the outflow regions from major source areas [*Russell et al.*, 1999; *Ramanathan et al.*, 2001a; *Mayol-Bracero et al.*, 2002; *Jacob et al.*, 2003; *Huebert et al.*, 2003]. Large field campaigns in more recent years have focused on aerosol evolution and properties in large regions with high aerosol loadings [*Bates et al.*, 2005, *Querol et al.*, 2008, *Zhang et al.*, 2008b]. Equally intensive efforts have examined aerosol in urban areas or heavily source-influenced regions [*Watson et al.*, 2000; *Neususs et al.*, 2002; *Solomon et al.*, 2003; *Cabada et al.*, 2004; *Parrish et al.*, 2009; *Wang et al*., 2010].

[15] Intensive field campaigns have provided information on emissions in addition to aerosol properties. Experiments to evaluate emissions from open biomass burning [*Lindesay et al.*, 1996; *Kaufman et al.*, 1998; *Eck et al.*, 2003] have determined aerosol characteristics and emission ratios. Chemical and transport models have also been used in conjunction with measurements to evaluate regional emission inventories [*Rasch et al.*, 2001; *Dickerson et al.*, 2002; *Carmichael et al.*, 2003;

Minvielle et al., 2004]. The interaction between atmospheric models and campaign measurements can be iterative, as models have also been used to guide aircraft flights to intercept urban and biomass burning plumes.

[16] The long history of intensive measurements now allows for analyses across many campaigns and pollutants. For example, *Clarke and Kapustin* [2010] combined aerosol and trace gas measurements from 11 campaigns to relate anthropogenic aerosol concentrations to concentrations of CCN, AOD, and CO. This type of relationship can be used to test modeled emissions and transport.

[17] One recent campaign relied on a single well-instrumented aircraft performing near-continuous vertical profiling over global scales in remote areas over a period of a few weeks [*Wofsy et al.,* 2011]. The sampling approach of reaching both high northern and southern latitudes was repeated five times in different seasons, so the spatial and temporal coverage is greater than intensive field campaigns. This type of measurement, along with vertical profile measurements in a single location over several years [*Andrews et al.*, 2011], can provide constraints on background aerosol loadings and removal processes.

[18] Intensive field campaigns usually include both in-situ and remote-sensing measurements from multiple surface (either land- or ship-based) platforms and from one or more aircraft, as well as integrating satellite remote sensing measurements. Research aircraft often fly over surface stations and ships, so measurements can be compared between platforms and used to determine vertical profiles of the full aerosol column. This rich set of data allows comparisons of different techniques for measuring BC and other aerosol properties and applications of the same technique in different environments [*e.g., Livingston et al.,* 2000; *Schmid et al.,* 2003; *Doherty et al.,* 2005]. Understanding of the applicability and limitations of each type of measurement is fostered by comparisons between properties measured at the surface, columnar properties measured by satellite-based remote sensing, and vertically resolved information from aircraft measurements [*e.g., Redemann et al.,* 2000; *Magi et al.,* 2003].

4.4.1.2. Long-term in-situ monitoring

[19] Long-term measurements usually combine relatively simple measurement techniques with tens or even hundreds of stations to create a widely spaced network of observations that operate under uniform techniques. Surface sites may be influenced by orography and local sources, although such effects are usually considered when selecting sites. Because network sites are spatially sparse and have relatively simple data products, they do not provide the same level of insight into the fine details of aerosol processes as intensive field campaigns. However, they do provide valuable information on aerosol trends and broad spatial concentration patterns, and these long records contribute strongly to evaluation of the modeling of emissions, transport, and removal.

[20] Table 4.2 lists the major networks contributing information on aerosol absorption and BC concentrations. Continuous in-situ measurements to monitor pollution levels were initiated as early as 1962 [*Novakov and Hansen*, 2004]. The IMPROVE network in the United States [*Malm et al.*, 1994] and the European Monitoring and Evaluation Programme network in Europe [*Kahnert et al.*, 2004] are among the most extensive, and have historically focused on chemical speciation rather than on aerosol properties. While they have achieved broad coverage within their regions, similar coverage is not available in many other world regions, such as South America and Africa. Monitoring stations are being developed throughout Asia [*Oanh et al.,* 2006; *Cao et al.*, 2007; *Ramana and Ramanathan,* 2006; *Marcq et al.*, 2010], although coverage is still poor. Two smaller groups of stations focus on global coverage to monitor aerosol properties relevant to climate in remote locations: those operated by the Climate Monitoring and Diagnostics Laboratory [*Sheridan and Ogren*, 1999] and the Global Atmosphere Watch (presently housed at http://gaw.tropos.de).

[21] As multiple measurement locations are required to evaluate emissions, transport and removal processes in global and regional models, measurements from all of these networks have been used extensively for model evaluation [*Cooke et al.*, 2002; *Park et al.*, 2003; *Solmon et al.*, 2006; *Koch et al.*, 2009a]. Most national networks have rigorous quality control procedures that ensure comparability of their measurements among similar network stations. However, as discussed in Section 2, important differences in sampling or measurement practices may affect comparisons between networks.

4.4.2. Remote sensing

[22] Remote sensing methods measure changes in the amount of sunlight reaching the Earth's surface, or the amount of radiation leaving the Earth's atmosphere, rather than the actual atmospheric BC or aerosol content. Through a process known as *inversion*, the nature and quantity of aerosol is inferred from its observed physical effect on the light. The procedure is also called *retrieval*, because aerosol properties are 'retrieved' from observed changes in radiance. Radiance properties that may be measured include wavelength dependence, angular distribution, and polarization. These can be used to infer the columnar amount of aerosol, the average aerosol size, the presence of non-spherical particles (such as dust) and even estimates of columnar light absorption.

[23] Advantages of remote sensing are the long-term nature of the measurements and the ability to obtain measurements without continuous maintenance. Remote measurements sense column properties of aerosol, rather than concentrations at the surface as are typically quantified by in-situ measurements. Column properties are more directly relevant for quantifying climate impacts. The relationship between surface in-situ observations and column data depends on many factors, including the stability of the boundary layer, the presence of atmospheric layers and measurement conditions that affect in-situ and remote measurements differently. When in-situ measurements are made from an aircraft that profiles the depth of the atmosphere, however, robust comparisons with column-integrated remote sensing measurements are possible. Disadvantages of passive remote sensing include a lack of specificity to individual chemical species and an inability to retrieve the properties of aerosols in distinct layers independently, such as a dust layer overlying a pollution layer.

[24] Information from retrievals may be used to infer the column burdens of chemical species that have distinctive physical or optical characteristics. For example, BC has

stronger absorption and smaller particle sizes than dust, and these properties are used to discriminate between the two absorbing species. However, many assumptions are required for these inferences, resulting in large uncertainties, especially at low optical depths (low concentrations). Furthermore, most remote sensing techniques can obtain valid data only in cloud-free conditions.

4.4.2.1. Ground-based remote sensing

[25] The utility of ground-based remote sensing for constraining BC atmospheric abundance is similar to that of long-term in situ sampling. Networks of measurements can be combined to evaluate model performance, but they do not provide fine-scale or global coverage.

[26] Passive, ground-based remote sensing with upward-looking sun- or sky-photometry can be used to estimate AAOD. AERONET is the largest global network of these photometers [*Holben et al.* 1998; *Dubovik et al.*, 2002]. These instruments use information measured at multiple wavelengths and multiple angles by sun- and sky-photometers [*Dubovik and King*, 2000]. Properties inferred from the radiative inversion include the aerosol size distribution, AOD, and refractive indices at four solar wavelengths; from this, single scatter albedo can be determined. However, for the retrieved refractive indices no distinction is made between fine and coarse mode aerosol. Thus, when both dust and BC are present in an aerosol column, the retrieved imaginary refractive index (which dictates aerosol absorption) does not accurately reflect that of BC alone.

[27] We have calculated values of BC AOD from retrievals of AAOD at AERONET sites and will use these values in Section 5 to produce an scaled estimate of BC direct radiative forcing. The process of extracting BC AAOD from AAOD requires certain assumptions. Limitations in the derivation of AAOD and specifically BC AAOD are discussed next.

[28] First, AAOD data are overestimated in the AERONET Version 2.0 data product. Values of AAOD are based on aerosol extinction optical depth and single-scatter albedo, and single-scatter albedo can only be retrieved reliably for rather polluted conditions. For this reason the AERONET Version 2.0 values of AAOD are published only when AOD is greater than 0.33 at 550 nm. The exclusion of low-AAOD conditions introduces a significant sampling bias that *Reddy et al.* [2005a] estimate to be a factor of two. This issue, and its implication for inferred BC quantities, is explored further in Section 5.5.1 and Appendix B.

[29] Second, not all solar absorption by aerosol is caused by BC; some is due to dust. Dust is less absorbing per mass than BC but its AOD is often much larger. The net effect is that global average dust AAOD is comparable to that of BC AAOD, but of course differently distributed in space and time. Thus, the BC contribution to AAOD needs to be isolated to use AERONET absorption for model evaluation. Dust particles tend to be larger than BC particles, so retrieved size distribution data might be used to attribute absorption by super-micron particles to dust, and absorption by sub-micron particles to BC. Possible contributions to AAOD by organic matter would require a separate treatment.

[30] Third, sample biases may occur because AERONET AAOD retrievals are made only during daylight hours and in cloud-free conditions. Two potential sources of bias oppose each other. Clear conditions can be expected to favor larger concentrations and column burdens of BC because fires are more likely and because scavenging by clouds (*i.e.,* the primary removal mechanism for BC) cannot occur under clear skies. However, solar absorption by BC is enhanced when BC is coated by water, which may be much more likely in the vicinity of clouds: *Jacobson* [2010] estimates solar absorption enhancement to be a factor of 2 to 4, depending on the size of the BC particle. Clear-sky measurements, which will exclude partially cloudy scenes, will likely miss this near-cloud absorption enhancement. To explore sensitivities to these two competing effects, we used the GATOR model [*Jacobson*, 2010], the only aerosol model that treats the full effect of optical focusing on absorption, to compare the AAOD for clear-sky versus all conditions. Although the global mean MAC_{BC} for cloudy conditions (14.4 m^2g^{-1}) is higher than for clear-sky (13.9 m^2g^{-1}) conditions, the global mean burden is greater by 35% for clear sky conditions than for cloudy conditions.

[31] A method to infer BC column mass loading is to determine the volume concentrations of components of aerosol mixtures required to fit the AERONET retrieved total column refractive index. These can then be used, along with assumptions about densities, to determine the column mass of each component, including BC [*Schuster et al.,* 2005]. The BC column mass uncertainty is estimated at -15% to +40%, although the imaginary refractive indices used affect the retrieval and the AAOD. Dust and organic carbon absorb more strongly at near-ultraviolet wavelengths, but this absorption probably does not bias BC column loading results inferred from visible wavelengths [*Schuster et al.,* 2009]. For analyses in this assessment, we use AAOD rather than inferred BC column loadings, as the former requires fewer assumptions.

4.4.2.2. Remote sensing from space

[32] Knowledge of BC concentrations is needed in regions with few or no ground sites, such as over oceans. Remote sensing from space-borne sensors on satellites has near-global coverage and can, therefore, fill observational gaps in ground-based networks. AOD can be inferred from retrievals from satellite data, but the procedure also requires general assumptions regarding environmental properties (*e.g.,* surface reflectance), and aerosol properties [*Torres et al.*, 1998; *Levy et al.*, 2007; *Kahn et al.*, 2010], so that uncertainties are greater than those in ground-based sensing.

[33] All satellite-based aerosol sensors provide information on aerosol distribution. This information is usually spectrally resolved, making general estimates of aerosol size possible. Moderate Resolution Imaging Spectroradiometer (MODIS) sensors have the greatest temporal resolution [*Remer et al.*, 2005]. Additional information on aerosol shape and difficult retrievals over bright surface come from polarization sensing [*e.g.*, POLDER, *Deuzé et al.*, 2001] and multiple views of the same scene [*e.g.*, Multi-angle Imaging Spectro-Radiometer (MISR), *Kahn et al.*, 2009a]. Active remote sensing with a space-borne lidar [CALIPSO, *Winker et al.*, 2010] offers information on aerosol vertical distribution.

[34] Although satellite retrievals may infer the separation between fine and coarse particles, they cannot distinguish BC from other fine mode aerosols like OA or sulfate. This inability to partition aerosol abundance between different aerosol species

greatly limits the ability to infer BC fields from satellite data. The division must be estimated either from the relative magnitude of modeled concentration fields or from ground-based observations. Exceptions that provide data on column aerosol absorption and, therefore, information specific to constraining light-absorbing aerosol are discussed below.

[35] The longest satellite data record on aerosol absorption, dating to 1978, is provided by the TOMS sensor (Total Ozone Mapping Spectrometer, http://jwocky.gsfc.nasa.gov/aerosols/*aerosols_v8.html*). Over the last decade, TOMS-type retrievals have been continued with measurements from OMI (Ozone Measurement Instrument, http://disc.sci.gsfc.nasa.gov/Aura/*data-holdings/OMI*). This instrument senses reflection and its spectral variability in the ultraviolet region (UV) of the solar spectrum [*Torres et al.,* 2002]. Aerosol retrieval at UV wavelengths has two advantages: first, surface contributions to the signal are small, especially over land, and second, small aerosols have stronger signals than at visible wavelengths. On the other hand, in addition to BC, both dust and organic carbon contribute to UV absorption. Thus, the link between column absorption (even in non-dust regions) and BC content is at best general in nature. Another complication is that this UV retrieval has a reduced sensitivity towards the surface, so that BC near the surface (*i.e.,* approximately the lowest kilometer) may not be detected. Therefore, a separate estimate of the vertical distribution of aerosol is an essential element of the retrieval. In the past, the vertical profile of aerosol concentration was prescribed by estimates from global modeling; more recently aerosol profiles inferred from the CALIPSO space-borne lidar have been applied.

[36] The satellite-based MISR instrument [*Kahn et al.*, 2009a] provides another constraint on aerosol absorption. The MISR instrument detects radiance at multiple angles and multiple wavelengths. This additional information is used to constrain uncertainties from surface radiance, and it allows the retrieval to address additional aerosol properties, including estimates of aerosol absorption. The MISR standard retrieval algorithm discriminates among two to four classes of absorbing aerosol, rather than providing exact values of single scattering albedo, when the atmosphere is relatively uniform and cloud-free, and the mid-visible AOD is at least 0.15 or 0.2 [*Chen et al.,* 2008; *Kahn et al.,* 2009c].

4.5. Comparison between modeled and observed BC concentrations

[37] Modern estimates of forcing by individual aerosol species, including BC, have been produced with global chemical transport models (CTMs). Evaluation of BC concentrations in these models is therefore critical in assessing our understanding of climate forcing. A first-order evaluation of these models is accomplished by comparing either simulated aerosol concentrations or simulated optical depths with independent observations. This comparison requires long-term, spatially distributed aerosol measurements, so that observations from nationwide or global networks, such as the ones discussed above, are particularly useful.

[38] Comparisons between models and observations shed light on our understanding of the quantity of BC in the atmosphere, but they often cannot distinguish between various possible causes of model error. For example, a model could underestimate atmospheric concentrations if its emissions are too low or if its removal rates (such as deposition) are too high.

[39] In this section, inferences of BC-AOD from AERONET are compared with modeled concentrations. The left panel of Figure 4.2 shows the AERONET observations and their locations. To avoid the influence of dust, only aerosol less than 1 μm are included, as described in Appendix B. Modeled concentrations from a suite of 15 global models are shown in the middle panels of the figure. The models reported here participated in a model inter-comparison project known as AeroCom (Aerosol Comparisons between Observations and Models [*Kinne et al.,* 2006; *Schulz et al.,* 2006]). Aerosol processes in some of these models have become more detailed in subsequent years; we use this particular collection because it draws on a large number of modeled fields. The fields shown in Figure 4.1a and Figure 4.2 are from the AeroCom 'median model,' for which a median of the local (1°x1° grid resolution) values from all AeroCom models was calculated every month. These median model fields, unlike averages, lose their additivity, but the use of median values excludes the influence of individual outlier models. Figure 4.2 also presents differences in BC-AOD between co-located AERONET and model median values, showing that these models tend to underestimate BC AOD. The regional dependence will be discussed further in Section 5.

[40] *Koch et al.* [2009a] evaluated the AeroCom suite of global models by comparing modeled BC concentrations with observations from both intensive campaigns and long-term in situ measurements. Figure 4.3 summarizes some results from this study. The top portion of Figure 4.3 shows the ratio between observations and modeling for surface concentrations of BC. The figure shows that the median model predicts surface BC concentrations in the North America fairly closely, slightly overestimates BC in Europe, and clearly underestimates it in Asia. The annually averaged difference among models in this suite was about 30% of the median concentration; variations in individual seasons can be greater.

[41] The lower portion of Figure 4.3 shows the observation-to-model ratio for column AAOD measured by AERONET. AERONET data were not separated into contributions from BC and dust, so the figure compares AAOD of the combination. Column AAOD is the product of BC column burden and MAC_{BC}. Because most of the models used in the comparison do not represent internal mixing, the modeled MAC_{BC} (see Section 2.6) and, hence, the AAOD are underestimated. The gray shaded area on this figure indicates the potential magnitude of this bias; that is, ratios lying in the shaded region might be explained by the lack of internal mixing, and ratios above the shaded region require some other explanation. Ratios different than unity, but lying within the shaded area, could also be caused by incorrect emissions or removal rates. Again, there is some agreement for the United States and Europe, and the median model underestimates AAOD over Asia, although not as greatly as for the surface sites. There are also some model underestimates for the rest of the world. In some regions, such as Africa, the poor comparison could be caused by errors in either dust or BC.

[42] The sources of differences between model predictions are not completely understood. In the AeroCom suite, concentrations predicted by the individual models differ by

factors of approximately three (25th to 75th percentile) to five (range excluding outliers) at a given location. *Koch et al.* [2009a] provided sensitivity experiments to explore the sources of this variability by using one model from the suite (GISS, shown as symbols in Figure 4.3). Simulations with different emission inventories are given in red, and concentrations with removal rates increased or decreased by a factor of two are shown as blue squares. Filled symbols indicate base-case results. Varying removal rates and emissions do cause significant variations in a single model, but these uncertainties do not explain most of the inter-model differences. *Textor et al.* [2007] also found that inter-model differences were only partially explained by differences in emission inventories. Large differences in modeled horizontal and vertical transport are largely responsible for the diversity. Once BC is lifted into the free troposphere, removal processes are slower and its atmospheric lifetime may be extended.

[43] The quantity and representativeness of observation sites is fundamentally important in interpreting comparisons between models and measurements. North America and Europe have the best coverage of all long-term measurement sites, followed by Asia. The number of sites is not in proportion to the strength of emissions, and concentrations in regions with large emissions and, therefore, highest aerosol forcing are relatively poorly constrained.

[44] Remote regions with low concentrations also have few measurement sites and hence are also poorly constrained. Although aerosol forcing in these regions is small, their large spatial coverage means that contribution to the global-average forcing may be important. Compared to BC concentrations measured during a field campaign over the remote Pacific Ocean [Figure 4.4; *Schwarz et al.,* 2010], the median model overpredicted remote BC concentrations by a factor of five. Some models, such as the lower quartile of the AeroCom model suite or GATOR [*Jacobson*, 2011], show better comparisons with these remote measurements.

4.5.1. Inverse modeling results

[45] The comparisons between modeled and observed BC concentrations described above are a first step in evaluating model performance. More detailed evaluations have been conducted, usually focusing on inferring the most likely sources of error. The simplest of these compare the temporal or spatial dependence of atmospheric concentrations with that given by models. More complex approaches use a mathematically strict evaluation of sources and sinks using a formulation of Bayes' theorem, which has been demonstrated for CO_2, CO, and aerosols [*e.g., Chevallier et al.,* 2005; *Dubovik et al.*, 2008; *Chevallier et al.,* 2009; *Huneuus et al.*, 2012]. Evaluation methods that use measurements of atmospheric abundance in combination with modeled fields are broadly called *inverse methods*. Inverse modeling of gaseous concentrations on continental scales, particularly CO and oxides of nitrogen (NO_x), can also provide information about emission sources. Although most studies have focused on inferring errors in emission inventories, it should not be forgotten that model processes such as transport and removal rates can also contribute to errors. Here, we summarize the results of inverse modeling studies that have focused on particular regions.

[46] *1. North America.* An inverse model by *Hu et al.* [2009] found that USA emission estimates using data mainly from a rural network (IMPROVE) was about 30 to 35% lower than an estimate that also included urban sites. This implies that, in order to constrain concentrations on continental scales, measurements in high-concentration areas should be included in the measurement network. There are also differences in the thermal evolution methods for measuring BC (Section 2.3) between urban and rural sites in the United States. The former tends to use a transmittance-corrected thermal-optical method, while the latter corrects using reflectance and heats the sample to a lower temperature. Before performing an inverse estimate, these authors had to multiply the transmittance-corrected values by factors ranging from 1.7 to 2.6, depending on the season. The resulting emission estimates were similar to the bottom-up emission estimate in Figure 3.3. On the other hand, an inverse model by *Park et al.* [2003] estimated a BC emission rate of about 750 Gg yr^{-1}, which is about 70% higher than the bottom-up estimate.

[47] *Bhave et al.* [2007] used organic markers to show that USA emission estimates of total aerosol carbon (OC plus BC) from vehicle exhaust and biomass combustion were not biased. They did find a large unexplained source of total aerosol carbon unassociated with combustion, but this would not affect BC totals.

[48] Inverse modeling of carbon monoxide has indicated that inventories overestimate fossil-fuel sources in North America by a factor of three in summer and two in spring [*Miller et al.*, 2008]. *Kopacz et al.* [2010] found a large underestimation especially in winter, ascribing this difference to heating and poor vehicle efficiency at cold temperatures. Although BC model results in the United States do not appear highly biased, these findings indicate that some small sources that could affect BC emissions are not well understood.

[49] *2. Europe. Tsyro et al.* [2007] found that a model based on the IIASA inventory underestimated BC concentrations by about 20%. Significant over- and underestimates of BC were correlated with concentrations of levoglucosan, a tracer of wood smoke, indicating that biofuel or open biomass burning could be responsible for the difference. Modeled concentrations were generally too high in Northern Europe and too low in Southern Europe. Mobile source emissions were thought to be underestimated in Austria and some Eastern European countries.

[50] *3. East Asia. Hakami et al*. [2005] used BC concentrations observed in field campaigns to constrain emission over eastern Asia. They found that the magnitude of the total emission inventory given by *Streets et al.* [2003b] did not change significantly as a result of the assimilation. However, anthropogenic emissions over southeastern China were reduced while those in northeast China and Japan were increased. The increase in the industrialized regions is consistent with the low bias in estimates of CO emissions [*Kasibhatla et al.,* 2002*; Heald et al.*, 2004], which is more strongly associated with the more northern industrialized regions [*Yumimoto and Uno,* 2006]. The observed CO bias has been largely resolved by improving the fraction of small combustors [*Streets et al.*, 2006], as discussed in Section 3.6.4. *Tan et al.* [2004] suggested that particulate carbon emissions in East Asia should increase in order to be consistent with observations, but they did not separate BC and OC nor account

for the formation of secondary organic aerosol, which could increase atmospheric concentrations. Studies that compare ground and aircraft measurements with modeled BC values over the East China Sea estimate an annually averaged BC emission flux of 1920 Gg yr^{-1} [*Kondo et al*., 2011c], close to bottom-up emission estimates estimated for the late 2000s. Inverse modeling of NO_x emissions in East Asia indicates rapid growth in high-temperature sources [*Kurokawa et al.*, 2009], although high-NO_x sources are presently a small part of the East Asian BC inventory.

[51] *4. South Asia.* *Rasch et al.* [2001] estimated that increases of about 10% in sulfate and 20% in carbonaceous aerosols were needed to match satellite observations over South Asia, but this study did not specifically identify biases in BC. *Dickerson et al.* [2002] suggested a BC emission rate of 2000-3000 Gg yr^{-1}, much higher than bottom-up estimates, based on atmospheric ratios of BC and CO that are much higher than is given by bottom-up estimates. *Menon et al.* [2010] also find that modeled concentrations in South Asia are much too low compared with in-situ measurements.

[52] The inverse modeling studies discussed above rely on *in-situ* data from a small number of sites to represent continental-scale concentrations of aerosols. Satellite measurements have much broader spatial coverage and could produce global emission estimates. This approach has been applied in biomass burning regions, where optical depths are large and seasonal. *Freitas et al.* [2005] found that emission estimates derived from observed AOD were larger than bottom-up estimates. *Reid et al.* [2009] estimated that bottom-up emission estimates of biomass burning need to be enhanced by factors of 1.5 to 3. The global emission flux derived for 2006 to 2008 was about 140000 Gg yr^{-1}, as compared with the value of 30000 to 44000 Gg yr^{-1} BC plus POA given in Section 3.4.4, if OA is assumed to be 1.4 times OC. Similarly, *Kaiser et al*. [2011] derived a global average enhancement factor of 3.4 for the OA and BC resulting from biomass burning, summarizing several other top-down studies that recommended emissions two to four times larger than the bottom-up estimates. However, the fraction of the discrepancy attributable to BC is uncertain. Formation of SOA may contribute to the observed OA and particulate matter loading.

[53] In summary, inverse modeling studies have produced inconsistent results for North America, indicating that either BC emissions are estimated well or are too low by 70%. European BC concentrations appear slightly underestimated. East Asian concentrations appear reasonable, especially after the addition of small combustors. Although observations are limited, measurements in South Asia suggest that concentrations are greatly underestimated there. All of the studies described have used single models and await further confirmation. On the other hand, there is a consensus that aerosol concentrations, including BC, may be too low in biomass burning regions. Considering also the likely bias in emission factors (see Section 3.7.2.3), emission values that are greater than bottom-up estimates appear warranted.

4.6. Vertical distribution of BC

[54] As will be discussed in Sections 5 and 6, the vertical distribution of absorbing aerosol affects its forcing. However, dependable in-situ measurements of BC loadings over wide vertical ranges have become available only recently. Vertically resolved measurements below 8 km of the refractory aerosol concentration, which correlates strongly with BC concentration, have been carried out since the 1990s [*Clarke and Kasputin,* 2010]. Remotely piloted airborne sensors have measured optical properties and total aerosol absorption below 3 km [*Corrigan et al.,* 2008].

[55] BC vertical profiles extending through the troposphere have only become available with the development of the SP2 instrument (Section 2.5), which has provided measurements of vertical profiles of BC in very clean air where they were previously unobtainable [*Schwarz et al.,* 2006, *Schwarz et al.,* 2010]. These profiles extend vertically from near the surface to the lower stratosphere, as shown in Figure 4.4. Although BC vertical profiles are quite variable, in polluted regions they generally show a declining BC mass mixing ratio from the surface to about 4 km altitude, and relatively constant values up to well above the tropopause. However, in remote regions influenced by the transport of pollution from source regions, BC loadings tend to peak in the free troposphere or above. BC that has been lifted above the low altitude ranges where aerosol removal is fast due to precipitation is more likely to have a longer lifetime in the atmosphere.

[56] Important BC properties, such as mixing state (Section 2), also change with altitude. One set of vertical profile observations in the tropics indicates that the coatings of BC-containing particles become thicker and more prevalent with increasing altitude between the surface and the lower stratosphere [*Schwarz et al.,* 2008a]. The fraction of coated BC particles and the acquired coating mass depend on both the BC source and the history of the particle and the air it is contained in. Thus, MAC_{BC} (Section 2.7) can be expected to depend on altitude.

4.6.1. Comparison between modeled and observed vertical distributions

[57] *Schwarz et al.* [2010] compared the AeroCom set of models with a global-scale 'snapshot' of SP2 BC measurements from remote locations (Figure 4.4). The AeroCom model ensemble captured the vertical trends of BC concentration in the southern mid to high latitudes, but in northern mid and equatorial latitudes the models underestimated the decrease in concentration with altitude. This comparison in regions far from sources suggests that modeled removal of BC is an important source of model error. However, the aircraft data in this comparison were obtained over a limited time range; in particular, the profile for the northernmost band (60-80ºN) was from a single flight. *Koch et al.* [2009a] also compared BC vertical distributions between AeroCom models and SP2 measurements from several intensive field campaigns, mainly over North America and the Arctic. That comparison indicated that models overestimate mid- and upper-troposphere BC at mid-latitudes, consistent with *Schwarz et al.* [2010], but underestimate BC in the Arctic. This finding of an underestimate in the Arctic relies on a larger data set than *Schwarz et al.* [2010] and, therefore, is more robust. In urban areas, model predictions of column loadings were found by *Schwarz et al.* [2006] to be relatively consistent with observations, but the vertical distribution was not well predicted

[58] Observations of the vertical distribution of AOD have become available in recent years with active remote sensing by the space-borne CALIOP lidar [Winker et al., 2010 (BAMS)], as shown with multi-year averages in Figure 4.5. AOD includes scattering and absorption by BC, dust, and other aerosol types (e.g., sulfates and organics) with sizes greater than 0.1-μm diameter [Omar et al., 2009]. Although chemical speciation is not possible, the data can provide limited inference of aerosol type. Depolarization data can identify non-spherical particles and permit estimates of dust contributions. A comparison of full-column CALIOP AOD in Figure 4.5 to BC and dust AAOD from AeroCom models in Figure 4.1 shows that the respective geographical distributions are very similar. Significant values are found for each parameter in South and East Asia, the Middle East, Africa, and Latin America and extend to North America, Europe and EECCA for BC (Figure 3.1). The sources of BC and all aerosol (excluding dust) have similar source activities or sources in the same regions. A comparison of optical depth values shows that maximum BC + dust AAOD values are a few percent of maximum AOD values. CALIOP AOD is derived with very high vertical (30-60 m) and horizontal (5 km) resolution. The panels in Figure 4.5 show that AOD is confined largely to altitudes below about 4 km. The limited horizontal and vertical distribution of global AOD is due to the short lifetime of the aerosol components. For example, the lifetime of BC is found to be less than 10 d in most global aerosol models (see Table 5.1). Correctly modeling the vertical distribution of AAOD is important for calculations of BC-DRF because total BC absorption depends on cloud location (see Section 5.6.1). Although interpretation of CALIOP data is still undergoing refinement, first comparisons of these data with simulations also indicate that models tend to place aerosol at higher altitudes than is observed [*Koffi et al.,* 2012].

5. Black-carbon direct radiative forcing

5.1. Section summary

[1]

1. Black carbon in the atmosphere reduces the planetary albedo by increasing the absorption of sunlight. The perturbation in the radiative balance resulting from this change is called black-carbon direct radiative forcing (BC-DRF).

2. The best estimate for the BC direct radiative forcing in the industrial-era is +0.43 W m^{-2} with an uncertainty range of +0.17 to +0.68 W m^{-2}. The best estimate of the global annual mean all-source BC-DRF is +0.49 W m^{-2} with an uncertainty of +0.20 to +0.76 W m^{-2}. These values are estimated by scaling all modeled forcing to the observationally constrained estimate of BC-AAOD, and then reducing the estimated forcing by 10% to account for the incorrect vertical distribution of BC. Locally, BC-DRF forcing can be larger, on the order of +5 W m^{-2}, for example, over regions of East and South Asia.

3. All BC-DRF estimates originate with simulations of BC lifecycle and radiative transfer using global models. Model-derived fields, such as aerosol absorption optical depth or BC distributions, are often adjusted to match observations of AAOD or concentration, either by direct scaling or by tuning removal rates.

4. BC radiative forcing can be considered the product of four factors: emissions, lifetime, mass absorption cross section, and radiative forcing per unit absorption optical depth (termed forcing efficiency). Diversity in previous global annual estimates of industrial-era BC-DRF (+0.2 to 0.9 W m^{-2}) is caused by variations in modeling assumptions, as evident in the modeled diversity of these four factors: 6000 to 18000 Gg yr^{-1} for industrial-era BC emissions, 3.8 to 11.4 days for BC lifetime, 4.4 to 13.4 $m^2 g^{-1}$ for mass absorption cross section, and 90 to 270 W m^{-2} per AAOD for forcing efficiency.

5. Emissions, lifetime, and mass absorption cross section - three of the governing factors - combine to produce AAOD, which can be constrained by measurements. Comparison with remote-sensing fields indicates that AAOD from many models appears too low. Applying regionally dependent scale factors to match observations increases globally averaged, industrial-era AAOD by 74%, from 0.00172 to 0.00299. Much, but not all, of the underestimate can be attributed to models not accounting for enhanced absorption due to internal mixing, which would increase AAOD by about 50%.

6. If the remaining model bias is caused by burdens that are too low, then model burdens should be increased by 50-170% in four regions (*i.e.,* South Asia, Southeast Asia, Latin America, and the Pacific region). Models overestimate burdens in Europe, Central Asia, and the Middle East. Modeled burdens in both North America and Africa are approximately correct.

7. If all of the differences in modeled burden were attributed to emissions, total emissions would be 10,100 Gg BC yr^{-1}, or a 31% increase above modeled emissions and a 42% increase above the bottom-up emissions in Chapter 3. Industrial-era emissions would be 8700 Gg BC yr^{-1}. These values are associated with concentrations in approximately the year 2005. We use the latter value as a best estimate of emissions throughout the remainder of this assessment, although poorly modeled aerosol lifetimes could also explain the discrepancies.

8. The uncertainty range of approximately ±60% for the best estimate of industrial-era direct radiative forcing includes approximately equal uncertainties associated with the determination of global BC absorption optical depth (BC-AAOD) and the radiative forcing efficiency per unit BC-AAOD. The asymmetry is caused by reducing the lower bound of the range to account for potential bias in AAOD observations. The estimate of BC-AAOD could be biased high because organic matter may contribute to AAOD, and because clear-sky sampling in the observations may overestimate the average AAOD over all periods.

9. The interpretation of remote-sensing data involves assumptions that affect the amount of absorption and, hence, radiative forcing, that is attributed to BC. Some of these assumptions can result in overestimating BC AAOD by a factor of two, especially dust content and excluding low-AOD conditions. In the estimates presented here, we have accounted for these sources of bias.

10. The altitude of BC in the atmosphere and its location above or below clouds affects its interaction with solar radiation and hence the forcing efficiency. Solar absorption by the BC fraction that lies above low clouds is particularly important and is poorly constrained in models, causing a large uncertainty in forcing efficiency and consequently in calculated radiative forcing. Limited observations suggest that most models overestimate high-altitude BC at tropical and mid-latitudes and, thus, BC forcing. We assume that models have a 10% high bias in radiative forcing due to this mechanism, and reduce the central estimate accordingly.

11. The separation of AAOD into BC and OA contributions has not yet been accomplished. If OA does contribute significantly to absorption at 550 nm, then our estimate of observationally constrained BC radiative forcing would be reduced, but forcing by OA would become less negative or more positive.

5.2. Introduction

[2] Direct radiative forcing by BC refers to the change in the energy balance at the top of the atmosphere due to absorption and scattering of sunlight by BC in the atmosphere. All estimates of BC-DRF are based on the difference between radiative transfer calculations for the atmosphere with present-day BC and with a background level of BC. The BC spatial distribution is generally taken from global models of the BC atmospheric lifecycle, which includes emissions, transport, aging, and removal. As described in Section 1.3, the background level of BC for industrial-era radiative forcing is set by models using year-1750 emissions. For all-source radiative forcing, the background level of BC is zero. Thus, 'industrial-era' in this chapter, when used for any quantity including BC burden, means the difference between modeled quantities with present-day emissions and the same quantities modeled with 1750 emissions.

[3] As with aerosol concentrations, radiative forcing is highly variable in space and time. Global modeling of BC

concentrations [*Liousse et al.*, 1996; *Cooke and Wilson*, 1996] and radiative forcing [*Penner et al.*, 1998] began in the mid-to-late 1990s. Since then, multiple modeling groups have estimated both concentration and radiative forcing fields. An example of modeled direct forcing is illustrated in Figure 5.1, which shows radiative forcing simulated by the Community Atmosphere Model CAM5. As discussed in Section 1.3, any estimated industrial-era forcing depends on the selection of the 'pre-industrial background.' Industrial-era BC-DRF is estimated to be negative in regions such as the eastern United States and the United Kingdom, due to declines in biomass burning since 1750. However, the emission inventories used for the background are associated with considerable uncertainties, especially for open burning. The largest forcing is over the Congo Basin in Africa and southeast China, and Bangladesh, with significant forcing also in the Amazon Basin, over northern India and Indonesia, and off the eastern coasts of South America and Africa where BC is transported over low clouds from distant fires.

[4] To understand the factors that affect radiative forcing in models, it is useful to express the global-mean direct radiative forcing, *DRF,* as the product of four factors [*Schulz et al.,* 2006]:

$$DRF = E\ L\ MAC_{BC}\ AFE \qquad (5.1)$$

where E is the global mean BC emission rate, L is the global mean lifetime of BC governed by removal rates, MAC_{BC} is the global-mean mass absorption cross section discussed in Section 2.7.3.3, and AFE is the global mean absorption forcing efficiency (forcing per aerosol absorption optical depth). This relationship is summarized in Figure 5.2. Three-dimensional models simulate many complex processes that are captured only to first order by the factors in Equation 5.1.

[5] Additional diagnostics shown in Figure 5.2 can be used to compare model results and identify the reasons for differences in simulated radiative forcing. Modeled L can be determined from the ratio of global mean column burden of BC to E, and global average MAC_{BC} is the ratio of the global mean absorption optical depth of BC to the global mean burden. Modeled AFE can be determined from the ratio of the global mean radiative forcing to AAOD, which is the global mean product of E, L, and MAC_{BC}. AAOD, the product of three important factors, is a particularly powerful diagnostic that can be compared with atmospheric measurements and is therefore emphasized in this section. Although AOD can also be used to evaluate modeled aerosol quantities, atmospheric AOD is dominated by scattering and thus has large contributions from other non-absorbing aerosol components.

[6] Table 5.1 summarizes modeled global mean estimates of each term in Equation 5.1 as well as other model diagnostics. Many of these models were used as the basis for IPCC radiative forcing estimates [*Forster et al.,* 2007]. Estimates of industrial-era direct radiative forcing range from +0.2 to +0.9 W m^{-2}. The large diversity is due to different model choices that affect one or more of the factors in Equation 5.1. Emissions of BC range from 5700 to 18000 Gg yr^{-1}. Lifetime ranges from 3.8 to 11.4 days. Global mean MAC_{BC} ranges from 4.3 to 15 m^2g^{-1}. AFE ranges from 91 to 270 W $m^{-2}AAOD^{-1}$ (Table 5.2). Because the correlation among these four factors can be negative [*Schulz et al.*, 2006], and because no model has maximum or minimum values of all four factors, the diversity in the radiative forcing in Table 5.2 (+0.2 to +0.9 W m^{-2}) is much smaller than the diversity estimated by multiplying the minima and maxima of the four factors (+0.05 to +3.7 W m^{-2}). The lower net diversity in simulated DRF is to some extent due to tuning simulations to match observational constraints on BC concentration and AOD. The best estimates of each component are summarized in Sections 5.3 through 5.6 before providing a best estimate of BC-DRF in Section 5.7.

5.3. Emission, lifetime, and burden

[7] As discussed in Section 3, BC emission rates used in estimates of radiative forcing vary regionally and globally [*Haywood and Boucher,* 2000; *Bond et al.,* 2004]. Commonly used values of global industrial-era emissions are 6300 Gg yr^{-1} for AeroCom [*Schulz et al.,* 2006] and 5700 Gg yr^{-1} for the IPCC Fifth Assessment Report (www.ipcc.ch), but emissions as high as 18000 Gg yr^{-1} have been used [*Chin et al.,* 2002].

[8] Column burden is proportional to BC emissions and to modeled lifetime. Lifetime is determined by removal, which is represented differently in each model and varies by location and season. Global average lifetime for BC varies by a factor of nearly three for the models reported in Table 5.1. Removal in precipitation plays a large role in aerosol lifetime [*Ogren and Charlson*, 1983], which is difficult to represent accurately at the coarse resolution of global modeling [*Rasch et al.,* 2000; *Textor et al.,* 2007; *Croft et al.,* 2010]. Differences in dry deposition contribute to uncertainty as well [*Easter et al.*, 2004; *Bauer et al.,* 2008; *Vignati et al.,* 2010]. Because removal processes depend on altitude, aerosol lofting also affects lifetime. For example, *Koch et al*. [2007] showed that lofting of biomass-burning aerosols from South America led to longer lifetimes compared with African emissions. Most developers of aerosol models have applied surface observations of BC concentrations and surface and satellite retrievals of AOD to constrain emissions or the treatment of scavenging, so one would expect the product of emissions and lifetime (burden) to agree broadly with observations [*Vignati et al.,* 2010].

[9] Early models used a limited number of parameters to account for subgrid variability in precipitation and the efficiency with which particles are scavenged. These scavenging treatments used crude parameters that were applied globally. More advanced models treat the coating of BC with hygroscopic material to form particles that are more readily activated to form cloud droplets and scavenged more efficiently. The representation of scavenging affects the magnitude and seasonality of BC concentrations, especially at remote locations [*Croft et al.*, 2005]. Model representation of the BC seasonal cycle in the Arctic improves with more accurate microphysical treatments [*Vignati et al.*, 2010; *Lund and Berntsen,* 2011; *Park et al.*, 2011].

[10] The global mean column burden of BC ranges from 0.11 to 0.53 mg m^{-2} in Table 5.1. The study with the largest radiative forcing estimate [MACR-Assim; *Ramanathan and Carmichael,* 2008] did not calculate a burden, but the BC simulation [*Chin et al.,* 2002] that it relied on for absorption far from AERONET sites [*Chung et al.,* 2005] had a global mean BC column burden of 0.6 mg m^{-2}. Some of the models did not constrain the combination of emissions and lifetime with BC concentration measurements [*Vignati et al.,* 2010], including the model that estimated the largest BC burden [*i.e.,* SPRINTARS, Table 5.2; *Takemura et al.*, 2005]. Some of the

diversity in the column burden of BC in Table 5.1 can be attributed to differences in emissions. Yet many of the estimates used the same BC emission inventory and still yielded BC burdens differing by more than a factor of two (0.16 to 0.38 mg m^{-2}) due to differences in lifetime [*Schulz et al.,* 2006]. As discussed in Section 4.3, most models simulate surface BC concentrations within a factor of two of measurements in most regions, with weak over-predictions in Europe, under-predictions in biomass burning regions, and large under-predictions for eastern and southern Asia [*Koch et al.,* 2009a].

[11] Vertical lofting of BC affects its prospects for wet scavenging and hence its lifetime. Vertical profiles of BC show that simulated concentrations have large biases in the free troposphere [*Koch et al.,* 2009a]. High biases of a factor of 3 to 15 (average 8) are found in tropospheric BC concentrations above the boundary layer at tropical and subtropical latitudes, while most models underestimate the BC concentrations in the Arctic troposphere, on average by a factor of 2.5 [Table 8 of *Koch et al.*, 2009a]. Adjustments to simple scavenging treatments cannot reproduce these observed distributions. Increased removal in tropical regions would reduce the over-prediction at high altitudes there (see Section 4.4) but would enhance the low bias in the Arctic troposphere where abundances may be controlled by scavenging processes [*Garrett et al.*, 2010]. However, improved treatments of scavenging may result in greater fidelity.

5.4. Mass absorption cross section

[12] Section 2.5 discussed measured and modeled MAC of BC and particles that contain BC. Section 2.5 also summarized how mixing of BC with other aerosol components would increase MAC_{BC}, and field measurements have found that BC particles are largely mixed with other components. Since MAC depends on refractive index, water content, particle size and mixing with other aerosol components, measured MAC_{BC} data provide a useful diagnostic check for models when information about each variable is also known.

[13] The global mean MAC_{BC} listed in Table 5.1 ranges from 4.3 to 15 m^2g^{-1}, with the AeroCom median around about 6.5 $m^2 g^{-1}$. Many models have MAC values similar to the *Bond and Bergstrom* [2006] estimate of 7.5 ± 1.2 m^2g^{-1} for freshly emitted, externally mixed BC, and a few others are close to the estimates of about 12.5 m^2g^{-1} for internally mixed aerosol. Two models (LSCE and BCC-AGCM) are much lower than this range. If models that assumed external mixing were excluded or adjusted for the increase in MAC_{BC}, the model average MAC_{BC} and the average estimated DRF would increase [*Jacobson*, 2000; *Myhre et al.,* 2009]. The internally mixed value of MAC_{BC} may be an upper limit on the global mean value because the actual global mean depends on how much of the BC is mixed with other components throughout the atmosphere.

5.5. Scaling of model absorption aerosol optical depth

[14] AAOD is the product of three of the factors that determine BC-DRF (*i.e.,* E, L, and MAC in Equation 5.1), and constraining this product can reduce uncertainty in radiative forcing. In this section, we present an estimate of observationally constrained AAOD that is used to produce scaled forcing estimates in Section 5.7.

[15] Measurements of AAOD are sparsely distributed, and many models underestimate AAOD, as shown in Figure 4.3. In Section 4.4.2.1, we cautioned that both sampling bias and dust absorption could produce a high bias in AERONET AAOD. In the figure in the AAOD comparisons in *Koch et al*. [2009a], AAOD from both observations and models includes contributions from both BC and dust. As a result, either or both BC and dust could be responsible for model discrepancies. However, AAOD comparisons for regions and seasons not affected by dust still show that many models simulate too little absorption in the atmosphere and therefore underestimate BC-DRF.

[16] To obtain an estimate of BC-AAOD constrained more closely by observations, a method was developed to scale modeled BC-AAOD fields using observations from the AERONET ground-based network. Appendix B gives the details and background of this method. Briefly, AERONET retrievals of AAOD were scaled to account for sampling biases, and BC-AAOD was estimated from total aerosol AAOD after accounting for the contribution to AAOD by dust. Biases in the AeroCom median model BC-AAOD were quantified by comparing the AeroCom values and modeled values at the same time and location. Scale factors for these regions and times were determined, and then extended to the regions that lacked observational matches.

[17] The result of the procedure is an increase of the total BC AAOD estimate from 0.00212 before scaling to 0.00339 after scaling, an increase of 60%. Industrial-era BC AAOD increases from 0.00172 before scaling to 0.00299 after scaling, an increase of 74%.

[18] A summary of modeled AAOD values before scaling is presented in Table 5.2 and summarized in Figure 5.3. Industrial-era BC-AAOD for models without any scaling ranges from 0.00111 to 0.00350, with two models giving values above 0.003 and the remainder lying within 30% of the median value. In Figure 5.3, BC-AAOD estimates scaled to observations are also shown for industrial-era sources and for all sources. The figure also shows the difference between industrial-era and all-source BC-AAOD. For scaled fields, all-source AAOD is higher than the industrial-era average by about 13%, but for unscaled model fields, all-source AAOD is 23% higher than industrial-era AAOD.

[19] Error bars in both scaled estimates in Figure 5.3 reflect uncertainty in the spatial distribution of the initial model field. This uncertainty is estimated by applying the full scaling procedure to three additional modeled fields (SPRINTARS, GOCART, and UMI) that were chosen to represent high and low average AAOD. The scaled value of global BC-AAOD ranges from 0.00212 for GOCART to 0.0035 for SPRINTARS, so the highest initial model field results in the lowest scaled value.

[20] The derived AAOD values are very sensitive to assumptions imposed in the use of the AERONET data fields as discussed in Appendix B. To demonstrate this, the all-source AAOD estimate in Figure 5.3 is revised by altering some basic assumptions used in deriving AAOD from AERONET observations. The revised AERONET fields are then used to rescale the AeroCom model fields and a new AeroCom global estimate is calculated. First, the selection of AERONET stations introduces an uncertainty of 30%. When four different

subsets of stations were used for the scaling of all-source AAOD, global averages ranged from 0.00301 to 0.00375. The analysis presented here includes this uncertainty. Second, the AERONET Version 2.0 data exclude low-AOD conditions, so that average AAOD values are biased high. If the AERONET Version 2.0 data are used, estimated AAOD increases by 85%. Third, if all AERONET absorption is ascribed to BC, regardless of particle size, estimated AAOD increases by 150% because significant amounts of absorbing aerosol (*e.g.*, dust) exist outside the fine mode. The scale factors applied here do not suffer from these last two biases because of the method used to interpret the AERONET data. These results indicate that radiative forcing estimates relying on published AERONET data, rather than data scaled for low-AOD conditions and accounting for dust absorption, could be expected to be much greater than those derived in this assessment. These sensitivity calculations highlight the importance of clearly stating assumptions and their consequences when using AERONET observations to scale modeled fields of absorbing aerosol. Uncertainties in this analysis are discussed in Section 5.7.3.

5.5.1. Attribution of low bias in modeled AAOD

[21] Since it is of interest to attribute the model bias in AAOD to individual causes, a limited attempt at such apportionment is provided in this section. Because AAOD is the product of MAC_{BC} and BC burden (see Section 5.2), we assume that the required scaling of AAOD in each region and month derives from errors in modeling one or both factors. Apportionment is considered separately for emissions from open biomass burning and energy-related combustion in the ten regions shown in Figures 3.1 to 3.3. Following the process outlined in Section 5.5, a monthly regional scale factor for AAOD is obtained by taking the ratio between the monthly average of the scaled AAOD over all land in a region and the monthly average AAOD from the AeroCom median model over the same area.

[22] Although it would be of interest to attribute the model bias to a wider variety of causes, including emissions from individual source categories and particular removal processes that affect lifetime, we lack sufficient a priori constraints to perform such a division. We therefore assume that (i) the MAC_{BC} scale factor for all months and regions is 1.5 (*i.e.,* the approximate ratio between the MAC of internally and externally mixed BC) because AeroCom models do not account for internal mixing; (ii) the BC burden scale factors for burning and energy-related sources are equal during each month; and (iii) the burden scale factors can also be applied to emissions without considering lifetime as a potential cause.

[23] The required burden scaling could be caused by emissions, by atmospheric lifetime, or a combination of the two. The scale factors were determined mainly using land-based AERONET observations rather than observations from sites distant from sources, which will be more strongly affected by removal rates, so it is possible that under- or overestimates of emissions are a major factor in the calculated scale factors. The emission rates that would be required to match observations were estimated by applying the monthly scale factors described above to modeled emissions.

[24] The annual averages of modeled emissions for open biomass burning and energy-related combustion sources are shown by region in Table 5.3. Using the monthly emission values comprising these averages, monthly burden (or emission) scale factors are computed for each region. These factors are the ratios of the monthly regional AAOD scale factor and the sum of monthly burning and energy-related emissions. These burden scale factors are subsequently divided by 1.5 to account for the uniform MAC_{BC} scaling. As a final step, the annually averaged burden scale factors for each source and region are calculated separately as the ratios of the annual scaled to unscaled emissions. Table 5.3 also shows the annual scaled totals for energy-related and open-burning emissions and compares them with the bottom-up emission estimates in Chapter 3. This division between energy-related and open-burning scale factors depends on the modeled seasonality of these major source groups, as well as the assumption that monthly scale factors for each group are equal. The scaling of emission totals is more robust than the apportionment of scaling between the two categories.

[25] Figure 5.4 displays the annual scale factors for each region and source group along with the annual fraction of energy-related emissions. The bars for each scale factor show the portions attributable to BC burden (closed) and MAC (open). The magnitude of the burden scale factors indicate whether the unscaled AeroCom median model underestimates or overestimates the burden with a solid bar greater or less than unity, respectively. This analysis suggests that significant burden underestimates, ranging from 45% to 125%, are found in one region dominated by energy-related emissions (South Asia) and in three regions where energy-related and open biomass burning contribute about equally (Southeast Asia, Latin America, and the Pacific region). Burdens are overestimated by more than 20% in Europe and the Middle East; this analysis is consistent with surface observations in Europe (see Figure 4.3), whereas the simple AAOD comparison was not. Modeled burdens in North America, Africa, and EECCA are within 20% of observations. Unlike Figure 4.3, Figure 5.4 does not indicate that BC in Africa is overestimated by AeroCom models, because some of the absorption there is attributed to dust.

5.5.2. Updated estimate of BC emissions

[26] Table 5.3 gives a summary of annual emissions. Three emission estimates are given in the table: modeled emissions, which are an estimate of the median used by AeroCom models; scaled emissions, which are inferred values using the burden scale factors applied to monthly emissions; and current emissions, which are the bottom-up estimates summarized in Section 3. Current emission estimates are different than those used by AeroCom models. Although energy-related emissions are similar, modeled open-burning emissions in AeroCom models were about 35% higher than the most current values.

[27] Scaled estimates for all-source annual emissions are 10100 Gg BC yr^{-1}, a 34% increase over current emission estimates and a 31% increase over modeled values. Because AERONET observations from years 2000 to 2009 were used for scaling, this emission estimate is approximately associated with the year 2005. This simple scaling exercise suggests a 24% increase in energy-related emissions (for a total of 5950 Gg BC yr^{-1}) and an 50% increase in open-burning emissions (to 4150 Gg BC yr^{-1}). The latter value is consistent with other findings that current biomass burning emission estimates should increase,

possibly related to emission factors. Section 3 describes another possible explanation for emission underestimates from energy-related burning. The AERONET observations used for scaling were taken from the mid-2000s, while modeled emissions were from the year 2000. Rapid growth of 30-50% in emissions has been estimated for both South and East Asia over that period [*Lu et al.*, 2011].

[28] Table 5.3 also gives estimates of industrial-era emissions, inferred by subtracting the same assumed pre-industrial emission values mentioned in Section 3. The industrial-era total is 8680 Gg BC yr^{-1}, a 42% increase over current emission estimates and a 38% increase over modeled values. Compared with the estimate of industrial-era emissions in Section 3, the simple scaling exercise suggests a 24% increase in energy-related emissions (for a total of 5560 Gg BC yr^{-1}) and a 50% increase in open-burning emissions (to 4150 Gg BC yr^{-1}).

[29] The industrial-era emission estimate of about 8700 GgC yr^{-1} is the value that would allow models to match observations. However, several caveats should be applied to this value. As discussed above, uncertainties in modeled lifetimes could also contribute to errors in burdens. The MAC scale factor used here is also simplified because it assumes that BC is always internally mixed and, therefore, amplifies absorption at the observation sites. If BC were externally mixed at observation sites, the MAC scale factor would decrease and the burden scale factor would increase. If the appropriate MAC scaling were a 20% increase instead of 50%, all-source emissions would be estimated as 12500 Gg BC yr^{-1}. For an assumed MAC scaling of 80%, the estimate would be 8390 Gg BC yr^{-1}. Observations are sparse in many of the regions with the largest emissions and the largest estimated increases. In the absence of more definitive studies to explain biases in aerosol absorption, the central value is used as a best estimate of industrial-era BC emissions throughout this assessment.

[30] With a 50% increase in MAC and a 38% increase in industrial-era emissions compared with modeled values, global annual industrial-era AAOD might be expected to increase by 100% instead of by 74%. The discrepancy occurs because the largest emission increases occur in two regions (South and Southeast Asia) where modeled aerosol lifetimes are shorter than the global average.

5.6. Forcing efficiency

[31] Radiative effects of BC are estimated by comparing radiative transfer calculations with and without BC emissions, accounting for scattering and absorption by the surface and by gases, clouds and other aerosol components throughout the atmosphere. Aerosol optical properties are important inputs to determine the magnitude and location of aerosol absorption and scattering. However, once the optical depths and single scattering albedo are known, variations in global-average radiative forcing per absorption optical depth are largely driven by environmental variables, especially the reflectivity of the underlying surface. BC aerosol alters the ToA net energy balance much more over a bright reflective surface or cloud layer than above a dark one [*Haywood and Shine,* 1995]. This sensitivity produces a three-fold diversity in the global mean absorption forcing efficiencies (AFE) listed in Table 5.2, with values ranging from 91 to 270 W $m^{-2}AAOD^{-1}$. Figure 5.5 shows the spatial distribution of annually averaged AFE. It tends to be higher for aerosol located over land and stratus clouds, and the highest values occur over snow.

5.6.1. Vertical location of BC

[32] Top-of-atmosphere AFE is enhanced considerably when BC is located over clouds compared with over the dark ocean surface. Thus, some of the diversity in AFE is caused by differences in the BC vertical distribution because elevated BC is more likely to overlie low clouds [*Haywood and Ramaswamy*, 1998]. BC over low clouds increases forcing disproportionately compared with BC in clear skies, while BC under clouds has a decreased contribution [*Zarzycki and Bond*, 2010]. Greater solar flux at high altitudes can also increase forcing by high-altitude BC [*Samset and Myhre*, 2011]. Comparing forcing from models that all use the same emissions, the model with the lowest AFE of 91 W $m^{-2}AAOD^{-1}$ places 14% of the total BC mass above 5 km, and the model that simulates the highest forcing efficiency of 270 W $m^{-2}AAOD^{-1}$ has 37% of its BC above 5 km. *Textor et al.* [2006] find that the fraction of the simulated BC mass above 5 km ranges from 7 to 37% for 16 AeroCom models. Direct forcing can be greatly intensified when aerosol-cloud collocation on sub-grid scales is considered [*Chand et al.*, 2009], and this is not treated in global models or in this estimate.

[33] How realistic are simulated vertical distributions of BC? As discussed in Section 4.5, it has recently become possible to measure the vertical distribution of BC and aerosol in general. These measurements have shown that aerosol models generally simulate too much BC in the upper troposphere, especially at tropical and mid-latitudes [*Schwarz et al.,* 2010]. Models also underestimate the decrease in aerosol extinction with altitude [*Yu et al.,* 2010]. Adjustments to reduce these biases are likely to put more of the BC below rather than above clouds and, hence, reduce estimates of the ToA radiative forcing by BC. Thus, the highest values of AFE shown in Table 5.2 are probably unrealistic. *Zarzycki and Bond* [2010] estimate that radiative forcing would decrease by approximately 15% if a model with an intermediate BC vertical profile was scaled to match measured profiles. *Koffi et al.* [2012] compared AeroCom models and CALIPSO measurements and found that aerosol was too high by about 400 m (range of 50 to 1080 m) in source regions. This finding also suggests a forcing decrease of approximately 15% when combined with the sensitivities given by *Samset and Myhre* [2011].

5.6.2. Horizontal location of BC

[34] Some of the diversity in AFE could also be due to differences in the BC horizontal distribution, particularly with respect to the albedo of the underlying surface or the amount of sunlight at different latitudes. *Kinne et al.* [2006] find the greatest diversity in the simulated BC burden is in polar regions, *Textor et al.* [2006] find that the fraction of BC mass between 80° and 90° N varies greatly in the AeroCom models, and *Shindell et al.* [2008] find that all BC models in their study simulate far too little BC at Barrow and Alert, particularly during winter and early spring.

5.7. All-source and industrial-era direct radiative forcing

[35] Figure 5.6 summarizes the two major determinants of direct radiative forcing—AAOD and AFE—for the model results reported in Tables 5.1 and 5.2. Figure 5.6(a) shows that

modeled radiative forcing has a strong relationship with modeled AAOD. AFE is the ratio between forcing and AAOD, and varies among models. Figure 5.6(b) suggests that AFE can be strongly affected by the amount of BC at high altitudes.

5.7.1. Scaled estimates of BC-DRF

[36] Many of the models with results reported in Tables 5.1 and 5.2 simulate too little AAOD compared to atmospheric observations and, therefore, too little BC-DRF. If modeled values of AFE were trustworthy, then a best estimate of all-source radiative forcing could result from multiplying those values by a best estimate of AAOD for every grid cell and season and averaging over the globe. A map of the increase in radiative forcing obtained by applying this method with the AeroCom median model is shown in Figure 5.7. Because we do not have all the modeled forcing fields to perform this scaling, we capture the diversity in AFE by scaling each of the model-based estimates of industrial-era radiative forcing using the observation-based estimate of industrial-era BC-AAOD, which has a global annual mean of 0.00299. These estimates are only approximate because the scaling ignores regional and seasonal variations. However, this scaling method does improve absorption fields that are too low when models do not include internal mixing or sufficient emissions.

[37] Table 5.2 shows the industrial-era DRF values from each model, scaled by the ratio of the observationally based BC-AAOD to the modeled BC-AAOD. These scaled values range from +0.27 to +0.80 W m^{-2}, with a mean and standard deviation of +0.51 ± 0.11 W m^{-2}. Radiative forcing is reduced for models with initially large BC AAOD such as SPRINTARS and MACR-Assim, and increased for models with initially low BC AAOD such as UMI, UIO-CTM, CAM5, and MPI-HAM. Similarly, this scaling can be used to estimate DRF by all BC sources. Model DRF values scaled to the total BC AAOD of 0.00339 are also listed in Table 5.2. Estimates range from +0.31 to +0.92 W m^{-2}, with a mean and standard deviation of +0.58 ± 0.14 W m^{-2}.

5.7.2. Central estimate of BC-DRF

[38] For a central estimate of BC-DRF, we use an average of the scaled radiative forcing estimates in Table 5.2. However, Section 4.6 showed that most models overpredict BC at high altitudes, leading to an overestimate of BC forcing. We therefore estimate a central value of 15% less than the mean of all estimates to compensate for the tendency of models to place BC too high altitudes and, hence, produce an unrealistically high radiative forcing efficiency, as discussed in Sect. 5.6.1.

[39] With this scaling, the central estimate of global annual DRF by industrial-era BC is +0.43 W m^{-2}. The central estimate of DRF by all-source BC is +0.49 W m^{-2}. These values may be considered an observationally constrained model average.

[40] The modeled forcing discussed above was calculated only at visible wavelengths, except for the work of *Jacobson* [2010]. Aerosols can also have significant effects on infrared radiation, especially in source regions [*Lubin and Simpson*, 1994]. *Reddy et al.* [2005b] estimated infrared forcing by BC as +0.006 W m^{-2}. *Jacobson* [2001] presented a graphical summary in which ToA direct forcing by BC was negligible. We, therefore, assume that the central estimate given above encompasses infrared forcing, even if most models have neglected it.

5.7.3. Uncertainties in BC-DRF

[41] A 90% confidence range for DRF is based on independent uncertainties in the industrial-era BC AAOD and the radiative forcing efficiency, AFE. The final estimate of uncertainty is higher than reflected in the scaled DRF estimates listed in Table 5.2, which do not account for uncertainty in BC AAOD.

[42] The full uncertainty estimate for AAOD is detailed in Appendix B. Uncertainties are caused by the spatial patterns of BC AAOD used in filling gaps between AERONET sites, ambiguity in how the scale factor is defined, the limited number of AERONET sites, clear-sky biases in the BC AAOD, the influence of BC transport from sources to oceanic regions, and the impacts of fine-mode dust and OA on AAOD. The industrial-era BC-AAOD estimate has an additional 18% uncertainty in the estimate of the pre-industrial background. We assume that the overall uncertainty of the AAOD retrieval contributes to the above-mentioned sources of uncertainty, although the degree of this contribution is unknown, and we thus do not account separately for it.

[43] Two factors that could decrease the DRF attributable to BC are the attribution of some AAOD to OA, and a bias caused by retrieving BC-AAOD only under clear-sky conditions. As discussed in Appendix B, we allow these factors to introduce a slightly asymmetric uncertainty. The 90% uncertainty range is (-44%, +38%) for all-source AAOD and (-48%, +42%) for industrial-era AAOD.

[44] The uncertainty in AFE is estimated as 1.6 times the standard deviation of the model AFE values listed in Table 5.2. This uncertainty of 40% is attributable to the vertical location of BC relative to clouds [*Zarzycki and Bond,* 2010], the effect of surface albedo, the temporal covariance of the clouds and BC, and the choice of radiative transfer code (*Boucher et al.,* 1998]. *Schulz et al.* [2006] attributed a variation in total aerosol cloudy-sky radiative forcing of ±0.26 W m^{-2} among 9 AeroCom models mainly to diversity in forcing above clouds. However, this diversity in AFE has not been apportioned to individual sources of uncertainty.

[45] Our final estimate of 90% uncertainty bounds comes from combining the uncertainties in AAOD and the 40% uncertainty in AFE. The global annual DRF by industrial-era BC is estimated to have an asymmetric uncertainty range of +0.17 to +0.68 W m^{-2} about the central estimate of +0.43 W m^{-2}. This range spans all but one scaled estimate listed in Table 5.2. The uncertainty range for all-source BC is +0.20 to +0.76 W m^{-2} about the central estimate of +0.49 W m^{-2}. The relative uncertainty of the total BC-DRF is slightly smaller than that of the industrial-era BC-DRF because the uncertainty of the pre-industrial background plays no role in the total value.

[46] A final uncertainty not estimated here is caused by interpretation of remote-sensing data (*e.g.,* AERONET). Such data sets are subject to periodic revision, and changes in the interpretation would shift the estimate of AAOD and forcing presented here.

5.8. Previous observationally scaled radiative-forcing estimates

[47] *Sato et al.* [2003] and *Ramanathan and Carmichael* [2008] have reported estimates of all-source BC-DRF that are higher than the range given here (+1.0 W m^{-2} and +0.9 W m^{-2},

respectively). *Sato et al.* [2003] used the AERONET Version 2.0 product. As discussed previously (Section 5.5), this product eliminates low-AOD observations, with the result that the average AAOD has a high bias, and any scaling of BC-AAOD using that product are also biased high. Figure 5.3 shows that when the scaled AeroCom median AAOD is rescaled to represent the use of the AERONET Version 2.0 product, the value increases by 85% and is nearly identical to the *Sato et al.* AAOD.

[48] The AFE value given by *Ramanathan and Carmichael* is 155 W $m^{-2}AAOD^{-1}$, similar to the mean of the other estimates in Table 5.2 (171 W $m^{-2}AAOD^{-1}$). The *Ramanathan and Carmichael* DRF estimate was given for all-source BC; if were scaled to our adjusted estimate of all-source AAOD, it would be reduced from +0.90 to +0.53 W m^{-2}. Thus, the fact that this forcing estimate is higher than our best estimate is attributable entirely to the estimate of BC-AAOD, which is 70% greater than our median adjusted estimate from AERONET.

[49] The calculations in the *Ramanathan and Carmichael* study were more complex, and we do not have sufficient information to reproduce them. Some contributing factors for the higher BC-AAOD estimates by *Ramanathan and Carmichael* [2008] could be the reliance on an AOD product from MODIS (Version 4), which has subsequently been reduced by 25% over land [*Levy et al.*, 2007], and the use of a model with relatively high BC-AOD (GOCART) to apportion AOD between BC and dust [*Chung et al.*, 2005]. Dust absorption may also contribute to the estimated BC-AAOD, as evidenced by strong BC direct radiative forcing signals in the dusty regions of Saharan Africa, the Tibetan Plateau, Mexico, and the Southwest United States.

6. Black carbon interactions with clouds

6.1. Section Summary

[1]

1. Black carbon may change cloud cover, emissivity, or brightness in four ways: 1) by changing the vertical temperature structure of the atmosphere (semi-direct effect), 2) by changing the number of liquid cloud droplets (warm cloud indirect effect), 3) by changing phase partitioning and hence precipitation in mixed-phase clouds (glaciation), and 4) by changing ice particle number (cold cloud indirect effect). These effects may cause either positive or negative radiative forcing. Very few model studies isolate the influence of BC on each effect. All aerosol effects on clouds are highly uncertain, and the isolated effects of BC on clouds are even more so.

2. Many of the cloud effects described here may be considered rapid adjustments, either to direct radiative forcing or to the presence of BC. However, all effects can be quantified in units of climate forcing, a practice we continue here for consistency with previous studies and for convenience.

3. In the semi-direct effect, cloud cover can increase or decrease, depending on region and conditions. Some studies examining regional cloud reduction have suggested a positive forcing, but global model studies indicate that the BC semi-direct effect averages -0.13 ± 0.2 W m^{-2} industrial-era forcing if all BC is emitted at the surface. An additional -0.2 W m^{-2} is added to the lower uncertainty range to account for the potential reduction of high-level clouds from biomass-burning BC, making the 90% uncertainty range –0.40 to +0.08 W m^{-2} over the industrial era. Major uncertainties include poorly modeled BC vertical distributions and the fidelity of modeled cloud responses.

4. BC has two competing indirect effects on liquid clouds. First, adding BC increases the aerosol number concentration. If the number of cloud droplets also increased, negative forcing by clouds would increase, but BC-rich particles are inferior cloud-forming particles. Second, BC particles may also serve as sites to collect soluble material, reducing overall cloud droplet number and producing a positive forcing. BC alone is estimated to have an indirect effect of about -0.1 W m^{-2}. Many studies do not separate this effect from the semi-direct effect discussed above, so an isolated estimate is difficult to obtain. Therefore, we estimate the combined industrial-era, liquid-cloud indirect and semi-direct effects of BC alone as -0.2 (with a 90% uncertainty range of -0.52 to +0.05 W m^{-2}).

5. Greater absorption by BC within cloud droplets decreases cloud albedo, heats clouds, and dissipates them. This is a special case of the semi-direct effect that we estimate separately as +0.2 W m^{-2}, with a 90% uncertainty range of -0.1 to +0.7 W m^{-2} over the industrial era. Model results for this effect are very sensitive to the representation of optical properties for the mixed BC and cloud droplet.

6. The liquid-cloud indirect effect is sensitive to BC particle size and to mixing with other particles. Many model studies indicate that particles emitted from biofuel combustion appear to have more negative forcing per emission than do particles from fossil-fuel combustion, possibly because of size or co-emitted POA.

7. The BC mixed-phase indirect effect acts on clouds that are part liquid and part ice. BC may act as ice nuclei (IN) that enhance ice formation and increase ice fall-out. An estimate for this effect is +0.16 ± 0.16 W m^{-2} for industrial-era forcing and 90% uncertainty range, but the magnitude would be reduced for BC mixed with sulfate.

8. In the ice-cloud indirect effect, BC-containing particles act as IN for ice clouds. Greater IN concentrations can increase or decrease the concentrations of ice particles and the lifetime of cirrus clouds, depending on conditions. Cirrus clouds affect both shortwave and longwave radiative fluxes. The cloud cover change and forcing may, therefore, be positive or negative. Two model studies estimate effects of opposite signs: -0.4 and +0.4 W m^{-2}. Laboratory and field observations suggest that both BC concentration and BC's ability to act as an IN are probably less than assumed in these model estimates. We estimate an industrial-era radiative forcing of 0 ± 0.4 W m^{-2} (90% uncertainty range) for this highly uncertain effect, which excludes the effects of aviation.

9. Modeled mixed-phase and ice-cloud indirect effects are sensitive to assumptions about BC's role as IN and to number and mixing state of BC particles in the free and upper troposphere. Ice-cloud effects also depend on the conditions assumed before BC is added, including concentrations of other IN and updraft velocities.

6.2. Introduction

[2] The role of clouds, including their responses to aerosol addition, introduces a large uncertainty in the understanding of total climate forcing and climate response [*Heintzenberg and Charlson,* 2009]. Although BC absorbs light and has positive direct forcing, these effects may be partially offset by poorly known but potentially significant impacts on clouds. The general term 'indirect effects' refers to the suite of radiative forcings that aerosols impose through the modification of cloud properties [*Forster et al.,* 2007; *Denman et al.,* 2007]. Aerosol indirect effects on clouds have been extensively studied, but the influence of BC alone has received less attention, and even the sign of the indirect effect of BC is uncertain. Although BC makes a small contribution to aerosol mass load in the atmosphere, it may play an important role in determining the CCN or IN particle number that in turn alters indirect effects. Aerosol indirect effects and BC's role in the indirect effect differ depending on the cloud phase: liquid, ice or 'mixed' containing both liquid and ice, and these are discussed individually. Furthermore, absorption by BC embedded within cloud droplets is greater than that of BC alone or with coatings.

[3] Figure 6.1 summarizes the mechanisms by which BC can influence clouds. A brief overview is given here before the detailed discussions in the remainder of this section. The first general class of effects involves perturbations to the atmospheric temperature structure, which affect cloud distributions. These mechanisms are commonly termed 'semi-direct effects.' This term is sometimes used to describe evaporation of cloud droplets when absorbing aerosols heat a cloud layer [*Hansen et al.,* 1997; *Ramanathan et al.,* 2001b]. Additional BC radiative effects on clouds have also been

documented whereby cloud cover may be either enhanced or reduced, depending on factors such as its altitude relative to cloud cover [*e.g.*, *Hansen et al.,* 2005; *Johnson et al.,* 2004], aerosol absorption optical depth, and meteorological conditions. BC's semi-direct effects are a rapid adjustment to BC direct radiative forcing, through local warming of the atmosphere. However, some model calculations treat this adjustment as a distinct forcing term. Following these studies, we review semi-direct estimates in forcing units.

[4] Another general category, commonly termed 'indirect effects,' involves changes in concentrations of cloud droplets or ice crystals that alter cloud brightness, emissivity and lifetime, which produce a radiative forcing. This category includes the groups titled 'liquid-cloud effects,' 'mixed-phase cloud effects,' and 'ice-cloud effects' in Figure 6.1. These cloud effects are driven by changes in the number of CCN or IN, aerosols on which cloud droplets or ice particles may form. The process of forming a stable liquid droplet or ice particle is known as activation. In principle, any particle can activate in either liquid or ice clouds. However, when many aerosol types are present, the particles that are easiest to activate do so first and have the greatest potential influence on the resulting number of cloud particles. Microphysical characteristics of a particular type of aerosol are thus very important in determining its cloud effects.

[5] Warm cloud indirect effects include two components. The cloud albedo effect (*i.e.,* the first indirect or Twomey effect [*Twomey*, 1959]) refers to the change in radiation caused by a change in cloud albedo or brightness. Increased CCN lead to more and smaller cloud liquid droplets for a given cloud water content (case LC1 in Figure 6.1). This effect can be observed in ship-track studies [*e.g.*, *Ferek et al.,* 1998]. However, if BC attracts condensing gases that would otherwise form particles, the net result is a decrease in CCN and cloud droplets and is, therefore, a positive radiative forcing (case LC2).

[6] The cloud lifetime effect (LC3, second indirect effect) refers to the fact that in the presence of increased aerosol concentrations, more and smaller cloud droplets form, and these collide less efficiently. While cloud resolving models suggest that this effect could lead to either an increase or decrease in liquid water [*Ackerman et al.,* 2004; *Sandu et al.,* 2008], GCMs generally predict that clouds have longer lifetimes and reflect more solar radiation [*Lohmann and Feichter*, 2005]. In mixed-phase clouds, where temperatures typically fall between 0 and -35ºC, two competing effects have been suggested: first, glaciation, which refers to an increase in either abundance or efficiency of ice nuclei causing more frequent glaciation of supercooled clouds, and second, de-activation. In the glaciation effect, ice crystals grow at the expense of water droplets because of the difference in vapor pressure between water and ice. An increase in IN would enhance this process, causing clouds to precipitate more readily (case MC1 in Figure 6.1) and thereby reducing cloud amount [*Lohmann*, 2002]. However, deactivation occurs when sulfur or secondary organic aerosol coat IN and make them less efficient [*Girard et al.,* 2005] in mixed-phase clouds by changing the mode of freezing from contact to immersion freezing, leading to less sedimentation and more cloud cover [*Storelvmo et al.,* 2008; *Hoose et al.,* 2008] (case MC2 in Figure 6.1).

[7] BC may also affect cirrus clouds that occur at high altitude in the upper troposphere [*Kärcher and Spichtinger*, 2009]. Aerosol particles at these high altitudes have long atmospheric lifetimes and therefore extended opportunities for mixing with other aerosol components. Cirrus clouds are believed to have net positive radiative forcing [*Chen et al.,* 2000]. For sufficiently low optical depth, absorption of infrared radiation and re-emission at colder temperatures dominates scattering of solar radiation, in which case cirrus clouds have positive forcing. As optical depth becomes larger, cloud albedo increases, leading to a net cooling. Efficient IN may either increase or reduce this cloud forcing. Cirrus cloud particles are mostly formed through homogeneous ice nucleation. Even a small number of particles can initiate heterogeneous freezing well below the homogeneous freezing threshold, depleting some of the supersaturated water vapor, partially preventing homogeneous formation of solution droplets and reducing the number of particles [*e.g.*, *Kärcher et al.*, 2006; case IC1 in Figure 6.1]. If high concentrations of IN already exist, heterogeneous freezing dominates the cloud and additional IN increase the number of cloud particles (case IC2 in Figure 6.1).

[8] Some modeling difficulties are common to all of these aerosol-cloud effects. The net effect on radiation is usually inferred by models that perform two sets of simulations: one with and one without perturbed pollution conditions [*Lohmann et al.*, 2010]. In many model studies of indirect effects, impacts on only some cloud types (liquid only, mixed only or ice only) are considered. In other studies, multiple effects are included and are difficult to distinguish. Models use different emission levels, and they produce differing values of direct forcing, so the magnitudes of predicted effects may vary due to these differences. Finally, inter-annual and spatial variability of modeled cloud forcing is large compared with the magnitude of the aerosol-induced changes. Therefore, extracting statistically significant changes is challenging.

[9] While modeling aerosol effects on clouds is difficult, accounting for them is critical because the magnitude of forcing may be similar to or greater than aerosol direct effects. *Denman et al.* [2007] summarized studies ranging from a mean of -1.2 W m^{-2} with a range of -0.2 to -2.3 W m^{-2} for the total effect of all anthropogenic aerosols on climate, including direct forcing, cloud albedo, cloud lifetime, and semi-direct effects. Using a combination of ten models and input from relationships observed by satellite, *Quaas et al.* [2009] estimated the total aerosol effect as -1.5 ± 0.5 W m^{-2}. The global annual mean forcing for just the first indirect effect of all aerosols has been estimated from GCMs with some guidance from satellite observations as -0.7 W m^{-2} with a range between -0.3 and -1.8 W m^{-2} [*Forster et al., 2007*]. Notably, *Lohmann et al.* [2010] showed that estimates of total anthropogenic aerosol effects have become smaller with time.

[10] This assessment focuses on global, annually averaged forcing by semi-direct and indirect effects. However, forcing within a given region may differ significantly from this average. For example, in the Arctic the combined semi-direct and indirect effect of aerosols may produce a much smaller negative forcing than on the global average, or possibly even a positive forcing [*Koch et al.,* 2009b; *Jacobson*, 2010; *Alterskjær et al*., 2010], because of the Arctic's high surface albedo and because changes in cloud emissivity may dominate changes in solar radiative forcing in wintertime there.

[11] In summary, BC may affect clouds by perturbing the atmospheric thermal structure, or by changing liquid cloud droplet number, ice crystal number, or some combination of the two in mixed-phase clouds. The role of BC in each of these cloud effects is presented below: increased absorption by BC inclusions in cloud droplets (Section 6.3); semi-direct effects (Section 6.4); indirect effects on liquid clouds (Section 6.5) and mixed and ice phase clouds (Section 6.6). This is followed by a discussion of uncertainties (Section 6.7). When possible, model results are scaled to be consistent with the forcing or emission assumptions determined in Section 5. All cloud forcings discussed below are industrial-era forcing; all-source forcing is not estimated.

6.3. Black-carbon semi-direct effects on cloud cover

[12] Atmospheric BC absorbs solar radiation, perturbs the temperature structure of the atmosphere and therefore influences the cloud distribution. The first of these effects documented, the original semi-direct effect, is the evaporation and dissolution of clouds by BC suspended near or within clouds [*Hansen et al*., 1997]. Since then, numerous studies have demonstrated this effect, as well as additional mechanisms by which BC either increases or reduces cloud cover. Some of these studies use cloud-scale models, some are observational – typically with focus on a particular region – and some use global models. *Koch and Del Genio* [2010] reviewed many studies on this topic, which are summarized here. The top segment of Figure 6.1 summarizes a framework proposed by *Koch and Del Genio* [2010] to classify previous studies.

[13] Each of the effects shown in the top portion of Figure 6.1 is the result of a rapid adjustment to the initial direct radiative forcing by BC. Following the terminology defined in Section 1, the sum of the direct effect and the semi-direct effect can be interpreted as a single 'adjusted forcing.' However, model studies to date have either calculated the semi-direct effect as an independent forcing; derived a combined forcing for the semi-direct and liquid cloud effects; or report a reduced efficacy for BC direct radiative forcing, attributing this decrease to semi-direct effects. Because semi-direct effects are diverse, all changes other than cloud microphysical changes might be grouped under this label [*e.g., Ghan et al.*, 2012]. For consistency with the existing literature, we also discuss the semi-direct effect here as a cloud forcing term and include the efficacy studies in our estimate of that forcing.

6.3.1. Cloud scale and regional studies

[14] The altitude of BC relative to a cloud or potential cloud layer plays an important role in determining the cloud response. For aerosols embedded near cloud, cloud evaporation is enhanced due to their heating and reduction of relative humidity (Figure 6.1, case SD4). This effect was demonstrated in the large-eddy-simulations (LES) of *Ackerman et al.* [2000] for trade cumulus and *Hill and Dobbie* [2008] and *Johnson et al.* [2004] for marine stratocumulus clouds.

[15] Absorbing aerosols aloft increase atmospheric stability. Increased stability over stratocumulus clouds reduces cloud-top entrainment of overlying dry air, and tends to strengthen the underlying clouds (Figure 6.1, case SD1). LES experiments by *Johnson et al.* [2004] showed that absorbing aerosols above cloud increased cloud cover, because they increased the difference in potential temperature across the inversion, decreased entrainment rate, and caused a shallower, moister boundary layer with higher liquid-water path. The same model had demonstrated cloud reduction when absorbing aerosols were within the cloud layer (Figure 6.1, case SD4). *Brioude et al.* [2009] analyzed satellite cloud observations and modeled biomass-burning tracers for a field study near the coast of California. They found that biomass burning aerosols enhanced cloud cover, especially for high-humidity conditions and for low lower tropospheric stability conditions, when the aerosols increased lower tropospheric stability.

[16] While the stabilizing effect of absorbing aerosols aloft can enhance stratocumulus cloud cover, they may suppress cumulus cloud development (Figure 6.1, case SD2). *Fan et al.* [2008] performed experiments in a cloud-resolving model for the Houston area, and demonstrated that absorbing aerosols aloft decreased the temperature lapse rate, leading to a more stable atmosphere and decreased convection. MODIS observational studies for the Amazon biomass burning season by *Koren et al*. [2004; 2008] also demonstrated cumulus cloud cover reduction due to increased smoke. They argued that smoke plumes stabilized the boundary layer, reducing convective activity and boundary layer cloud formation. The smoke also reduced radiation penetration to the surface, therefore reducing evaporation and atmospheric moisture. *Ten Hoeve et al.* [2011] used satellite data to show that cloud cover increased at low AOD, but decreased at higher AOD.

[17] On the other hand, in some land regions, lofted absorbing aerosols may enhance upper level convection, promoting low-level convergence that could carry moisture from ocean and increase continental clouds (Figure 6.1, case SD3). Monsoon enhancement due to lofted absorbing aerosols was shown in the global model studies of *Lau et al.* [2006], *Randles and Ramaswamy* [2008], and *Chung et al.* [2002]. However, wintertime pollution as observed in the Indian Ocean Experiment reduced the meridional temperature gradient in the global model study of *Ramanathan et al.* [2005] that included coupled ocean response. These SST shifts were found to enhance precipitation over sub-Saharan Africa [*Chung and Ramanathan*, 2006]. Many studies predicting enhanced convergence over land indicate a shift in clouds and precipitation rather than an overall enhancement.

[18] BC below cloud generally promotes convective activity and can enhance cloud cover (Figure 6.1, case SD6). Cloud resolving model studies of *McFarquhar and Wang* [2006] for trade wind cumuli demonstrated that absorbing aerosols placed below cloud promoted vertical motion and increased liquid water path. Similarly, LES experiments of *Feingold et al.* [2005] found that Amazon smoke emitted at the surface could destabilize the surface layer and increase convection and cloud cover. However, smoke at cloud level decreased cloud cover and promoted dissipation in both of these studies.

6.3.2. Global model semi-direct estimates

[19] Consistent with the variety of responses found in regional studies, global model studies also find regional variations and global-average forcing includes positive and negative forcing effects over all regions. Although semi-direct effects cause positive forcing in some regions, most models indicate that the global average is negative. Table 6.1 tabulates the studies discussed here.

[20] *Wang* [2004] performed experiments in the NCAR model, with and without BC. One type of experiment included an ocean temperature response; a second experiment had fixed observed sea-surface temperatures. He found that BC in the experiments with ocean response had enhanced convective activity and cloud cover in the northern branch of the intertropical convergence zone, with a smaller magnitude reduction in clouds and convective activity in the south. The cloud forcing change (*i.e.,* the difference between all-sky and clear-sky radiative flux change due to BC) was -0.16 W m^{-2} at the ToA. However the simulation using observed sea-surface temperatures gave a cloud forcing of -0.06 W m^{-2}. BC semi-direct effects did not cause significant warming in the climate experiments, because the effect was largely a redistribution of cloud cover.

[21] In sensitivity studies of a coupled transient climate model study, *Koch et al.* [2011b, Section 6] showed that removal of BC from 1970 to 2000 would not have caused significant climate cooling. BC removal cooled the atmospheric column, but it also reduced low-level stability and caused a decrease in low-level clouds. Therefore the surface air temperatures were not significantly decreased, probably due to the loss of low-level clouds. *Koch et al.* [2011a] did not isolate the forcing by the semi-direct effect from that of the direct effect, so it is not included in Table 6.1.

[22] *Roeckner et al.* [2006] performed future transient climate simulations in the ECHAM5 model, with one simulation including projected increases for carbonaceous aerosols (37% BC and 25% particulate organic matter). This model included indirect as well as direct and semi-direct effects and did not separately diagnose the individual forcings, so it is not included in Table 6.1. Increased BC in a region caused cooling there, mostly near African biomass burning regions. In these regions, liquid water path and precipitation increased, possibly due to enhanced instability (Figure 6.1, case SD6); the additional cloud cover reduced surface solar radiation and cooled the surface. For this study, the increased organic carbon together with the indirect effects might also contribute to the increased cloud cover.

[23] Some global model studies show reduced high-level clouds from BC, also a cooling effect (Figure 6.1, case SD5). Small-scale models do not capture this effect. *Penner et al.* [2003] found a negligible semi-direct effect for fossil-fuel and biomass burning in the GRANTOUR GCM when all aerosols were injected at the surface. However, when biomass-burning aerosols were injected aloft, they found a net negative semi-direct cloud climate forcing response to carbonaceous aerosols (both BC and organic carbon), mostly due to loss of high-level clouds. In most other studies, BC aerosols were injected at the surface and the response was smaller. *Menon and Del Genio* [2007] also reported a negative semi-direct effect of -0.08 W m^{-2} in their GISS simulations with fixed sea-surface temperature, due to decreased long-wave cloud forcing change and loss of high-level clouds, mostly in biomass burning regions. This study did not specify how the semi-direct effect was calculated nor what was used for emissions in the baseline and forcing scenarios, so it is not included in Table 6.1. *Lohmann and Feichter* [2001] obtained a negative direct plus semi-direct effect of -0.1 W m^{-2} in their ECHAM simulations, also with fixed sea-surface temperatures. However, this value was smaller than the interannual standard deviation. The semi-direct forcing was not isolated, so this study is also not included in Table 6.1.

[24] Some studies report reduced BC radiative forcing 'efficacy' instead of quoting a negative semi-direct forcing. The definition of efficacy is temperature change per forcing relative to that for CO_2, so that efficacy of less than one indicates that a mechanism acts to reduce the positive direct radiative forcing (see Table 1.1). In some cases these studies indicate that either increased low-to-mid level or decreased upper-level cloud changes are responsible for radiative forcing efficacies less than one [*e.g., Roberts and Jones*, 2004; *Hansen et al.,* 2005; *Yoshimori and Broccoli,* 2008]. It is noteworthy that BC radiative forcing efficacy estimates are consistently about 0.6 to 0.8. If we assume that the reduced BC radiative forcing efficacy is entirely due to cloud cover changes, we can infer BC semi-direct forcing estimates for these models. This is justified by the fact that adjusted forcing efficacies for absorbing aerosol are much closer to 1.0, implying that rapid adjustment accounts for most of the small radiative forcing efficacy [*Shine et al.,* 2003*; Hansen et al.*, 2005; *Crook et al., 2011*].

[25] *Roberts and Jones* [2004] found that the radiative forcing efficacy of BC was 0.62, due mostly to reduction of high-altitude clouds. *Hansen et al.* [2005] found BC radiative forcing efficacy of 0.78 for fossil-fuel BC and 0.58 for biomass-burning BC and direct forcing values of +0.49 W m^{-2} and +0.19 W m^{-2}, respectively. If their smaller than 1.0 radiative forcing efficacies are all due to rapid adjustment of clouds, the semi-direct effect forcings are -0.11 and -0.08 W m^{-2}, respectively. *Yoshimori and Broccoli* [2008] had efficacy of 0.59 for direct BC radiative forcing of +0.99 W m^{-2}, giving a maximum semi-direct effect forcing of -0.4 W m^{-2}. *Jones et al.* [2007] report a BC radiative forcing efficacy of 0.71 for BC forcing of +0.39 W m^{-2}, for an inferred semi-direct effect of -0.11 W m^{-2}. *Chung and Seinfeld* [2005] calculated a 0.70 radiative forcing efficacy for 0.33 W m^{-2} forcing, giving a -0.1 W m^{-2} semi-direct effect. These efficacy studies give a range of -0.1 to -0.4 W m^{-2} of inferred semi-direct effect of BC. The range is reduced to -0.07 to -0.17 W m^{-2} when each study is scaled to either direct forcing of +0.43 W m^{-2} (for those studies that reported forcing) or to industrial-era emissions of 8700 Gg yr^{-1}. These scaled estimates are given in Table 6.1.

[26] Our estimate of the BC semi-direct effect for emissions that do not have significant lofting, scaled to 8700 Gg yr^{-1} emissions, is -0.13 ± 0.2 W m^{-2}. The central value is the average of the *Wang* [2004] climate estimate, scaled as described above, the near-zero sum of fossil-fuel and biomass values from *Penner et al.* [2003], and the five efficacy estimates scaled to a BC forcing of +0.43 W m^{-2}. Most of these estimates come from studies that isolate pure BC, but the *Penner et al.* [2003] estimate is for BC and OC. The magnitude of our uncertainty estimate is larger than the standard deviation of the studies, but reflects interannual variability and sensitivity analyses reported by individual studies.

[27] The semi-direct estimate is influenced by the five studies that cast the response in terms of radiative forcing efficacy. These studies may have included other climate responses in addition to changes in cloud amount, so we caution against

comparing this value with pure estimates of the semi-direct effect.

[28] As noted above, *Penner et al.* [2003] also estimated a large negative semi-direct effect when all aerosols from open biomass burning were injected aloft (-0.39 W m^{-2}). This estimate was given for a larger emission rate; scaled to our anthropogenic biomass-burning estimate of 3000 Gg BC yr^{-1}, the additional semi-direct forcing would be -0.2 W m^{-2}, with a 100% uncertainty given by the interannual variability. We do not have estimates of the quantity of biomass burning aerosol that is lofted, so we add this value as an asymmetric uncertainty to the lower bound of the semi-direct forcing. When we estimate forcing by individual source categories (Section 10), this uncertainty for lofted aerosol is attributed entirely to biomass-burning emissions.

[29] The semi-direct effect of absorbing aerosols depends strongly upon the aerosol optical properties. Replacing absorbing with scattering aerosols reduces or even reverses the influence on cloud cover [*e.g., Johnson et al.,* 2004; *Fan et al.,* 2008; *Randles and Ramaswamy,* 2008; *Perlwitz and Miller*, 2010; *Wang,* 2004]. For example, *Perlwitz and Miller* [2010] showed that in GISS model climate simulations, dust caused global mean cloud cover to increase if dust AOD is sufficiently large and absorbing. For weakly absorbing dust, mean cloud cover decreased. *Johnson et al.* [2004] showed that absorbing aerosols above stratocumulus cloud level strongly increase cloud cover, but scattering aerosols cause only a very small increase. Two global model studies found net decreased cloud cover in response to total pollution aerosols, and positive semi-direct effect [*Allen and Sherwood*, 2010; *Lohmann and Feichter*, 2005]. Therefore, apparently only sufficiently absorbing aerosols increase cloud cover.

[30] Although several global models simulate a negative semi-direct effect, the models have substantial uncertainties. First, since cloud enhancement is caused mostly by BC above cloud level, model BC-altitude distributions must be accurate. As discussed in Section 5.6.1, models are especially diverse in their simulated altitude distribution of BC, and measurements to verify vertical distributions are sparse (Section 4.6). Many of the models that simulate negative semi-direct effects overestimate BC at high altitude, when compared with a few available BC measurements over North America [*Koch et al.*, 2009a]. Second, global model cloud schemes may not be able to reproduce the absorbing aerosol-cloud relations captured by cloud-scale models. Small-scale cloud changes, such as cloud layer thickness, cloud-top entrainment, cloud fraction and the tendency to drizzle are affected by the scale of interactions among radiation, turbulence and moist physics on small horizontal and vertical scales. Third is the broader issue of how climate model clouds respond more generally to forcing changes such as GHGs and aerosols. Climate models are diverse in their response to increased CO_2 [*e.g., Soden and Held*, 2006]. It is likely that models would have a similar or greater diversity in response to absorbing aerosols, for which modeling is more challenging.

[31] Model cloud responses to absorbing aerosols have not been compared carefully with cloud-scale model and field studies for specific conditions. The framework presented here, and in greater detail in *Koch and Del Genio* [2010], requires ongoing revision as future studies provide information.

6.3.3 Increased absorption by cloud droplet inclusions

[32] Absorption by BC increases when it is covered with non-absorbing material (Section 2.7.3.2), including water. This increase affects both the amount of atmospheric absorption attributable to BC and the estimated absorption that is collocated with clouds, with both effects possibly leading to positive forcing. The lack of simulated absorption by mixed or cloud-borne BC in most models probably affects the general prediction of the global average semi-direct effect.

[33] Forcing due to altered cloud albedo was first estimated by *Chylek et al.* [1984; 1996] as 1 to 3 W m^{-2} in a simple analysis that assumed fixed volume fractions of BC within cloud droplets. *Chuang et al.* [2002] used a chemical transport model to estimate the positive forcing as +0.07 W m^{-2}, although it was not clear how they determined the fraction of BC within droplets. Models that simulate the dynamics of aerosols and clouds find that only a few percent of the global BC burden is present in cloud droplets [*Jacobson*, 2012; *Ghan et al.*, 2012]. *Stier et al.* [2007] and *Ghan et al.* [2012] estimated direct forcing by BC in droplets as +0.02 W m^{-2} and less than +0.01 W m^{-2}, respectively, using the Bruggeman mixing rule to represent BC-droplet absorption. The dynamic effective medium approximation predicts the greatest absorption increase for wetted particles [*Jacobson*, 2006]; it is consistent with the small number of laboratory studies measuring absorption at high relative humidity (see Section 2.7.1) and results in a direct forcing change of +0.05 to 0.07 W m^{-2}. Another mechanism involves droplet heating by BC and subsequent deactivation of CCN, but this has been shown to be insignificant at appreciable supersaturation levels [*Conant et al.*, 2002].

[34] A potentially greater forcing results from cloud dissipation when cloud-borne BC increases absorption within clouds. The choice of model to represent absorption of BC residing within cloud droplets greatly affects the modeled absorption and, thus, the thermodynamic effect on clouds. In the model with lower absorption described above, cloud absorption caused a small negative semi-direct effect [-0.07 W m^{-2}, *Ghan et al.*, 2012]. However, predicted heating rates within clouds are 2 to 2.3 times greater when the dynamic effective medium approximation is used, compared with a core-shell treatment [*Jacobson*, 2012]. *Jacobson* [2010] found an increase in temperature of +0.31 K for fossil-fuel and biofuel sources when cloud absorption is included versus excluded. With the equilibrium climate-sensitivity of this model (0.6 K $(W\ m^{-2})^{-1}$), this corresponds to a forcing increase of +0.52 W m^{-2} for this effect alone. When scaled to our industrial-era emission rate of 8700 Gg yr^{-1}, this forcing would be +0.7 W m^{-2}. All of these forcing estimates include the small forcing change caused by cloud albedo.

[35] The cloud absorption effect is highly uncertain because there are few measurements of aerosol optical measurements at cloud conditions, or of the relationship between in-cloud aerosol absorption and cloud dissipation. Some of the plausible treatments explored by *Jacobson* [2012] produce lower in-cloud heating rates, so we assign a central estimate of +0.2 W m^{-2} to this effect, with uncertainty bounds of (-0.1, +0.7) W m^{-2}.

6.4. BC indirect effects on liquid clouds

[36] Although aerosol liquid-cloud indirect effects have been extensively studied, only a few studies isolate the influence of

BC alone. Many models have not been equipped with adequate sophistication to simulate aerosol microphysics, including mixing between BC and other aerosol species and the evolution of aerosol size distribution. Earlier model studies had minimal treatment of the aerosol microphysics that are important for capturing the gaseous and aerosol interactions that dominate CCN concentrations and, hence, the BC indirect effect. Below we review earlier literature, discuss the importance of aerosol microphysics, and summarize results from studies that include microphysics.

[37] Two simple global model studies estimated the effect of BC on liquid-cloud indirect effects and found a negative BC indirect effect. *Hansen et al.* [2005] estimated that BC contributed 5% of the aerosol indirect effect in a model study with the net indirect effect magnitude prescribed, and parameterized so that cloud cover and cloud albedo are augmented proportionately to the logarithm of the aerosol number. Aerosol number was derived from aerosol mass and assumed size, and aerosols were externally mixed. *Chuang et al.* [2002] estimated the liquid-cloud effects of carbonaceous aerosols, using a parameterization of cloud droplet number concentration (CDNC or the number of cloud droplets per volume of cloud). CDNC was parameterized based on Köhler theory, but without explicit aerosol microphysics. They estimated that carbonaceous aerosols (mixed BC and organic carbon) from biomass burning and fossil fuels contributed 63% and 28% of the indirect effect, respectively. Sulfate was found to have a smaller effect due to its tendency to mix with other species.

[38] BC could have a substantial influence on the indirect effect due to its potentially large contribution to aerosol number rather than aerosol mass. However, total aerosol particle number does not depend linearly upon BC number. BC also provides a surface upon which volatile inorganic or organic compounds may condense. In the absence of BC, sulfur might preferentially nucleate fresh particles and additional sulfur would condense upon pure sulfate particles. Such particles would generally be better CCN than would a BC-sulfur mixture. In general, larger particles make better CCN or IN, although CCN activity increases when BC is internally mixed with soluble species such as sulfate or OA, while there is evidence that IN activity is optimal for unmixed or pure BC. CCN activation for BC is discussed in Section 2.8, where methodology for applying Köhler theory to a BC-solute mixture is described. Activation depends upon particle size, moles of solute in the particle, and water supersaturation in the environment (see also Figures 2.4 and 2.5). The indirect effect dependence on particle number is also non-linear. Additional particles generally have a greater effect on clouds in clean conditions and relatively less in more polluted environments [*e.g., Lohmann et al.,* 2005; *Hoose et al.,* 2008]. Given these non-linearities, it is difficult to model BC-cloud effects without models that include detailed aerosol microphysical schemes.

[39] Five model studies used aerosol microphysical schemes to look at how BC alters the warm-cloud indirect effect (Table 6.2). These model studies were usually done by comparing a simulation with all aerosols with another simulation in which BC, or BC and OA, have been removed. For consistency, we report all results as the response to the addition of BC. Below, we discuss the forcing changes actually reported by each study. However, each investigation used different changes in emissions, and Table 6.2 shows values scaled to the relevant BC emission rate.

[40] *Kristjansson* [2002] calculated a BC indirect radiative forcing of -0.1 W m^{-2} (5-10 % of the total aerosol indirect effect), with regional values reaching about -0.25 W m^{-2} in more polluted regions where BC was an important component of the accumulation mode aerosols. In some remote oceanic regions the sign was positive because BC reduced aerosol hygroscopicity.

[41] *Chen et al.* [2010a] modeled liquid-cloud indirect effects due to BC and OA reductions. Half of present-day BC and OA from fossil fuel caused -0.13 W m^{-2} indirect forcing, and half of all BC and OA emissions (including biomass-burning emissions) caused -0.31 W m^{-2} indirect forcing. Fossil-fuel BC particles were assumed to have quite small sizes of 25 nm diameter at emission (compare to Section 2.6.2). The indirect effects more than offset the calculated direct effects for fossil fuel and all carbonaceous emissions of +0.07 and +0.12 W m^{-2}, respectively. In the *Chen et al.* model experiments, indirect effects were isolated from semi-direct effects by running the simulation without aerosol-radiation coupling. The authors also estimated the standard deviation of the forcing over multiple years, which was as large or greater than the forcings for 15-year simulations. While the absolute change in BC+OA emissions was larger for biomass emissions and, therefore, one would expect a larger effect, *Chen et al.* also attribute the larger forcing mostly to the larger size of the biomass and biofuel particles as well as to the greater hygroscopicity of the non-fossil-fuel emissions.

[42] *Bauer et al.* [2010] performed three BC reduction experiments. Adding either fossil-fuel BC or fossil-fuel plus biofuel BC decreased CDNC, probably because BC reduces the number of pure sulfate aerosols. The semi-direct effect in these cases was negative (more low-level clouds). The combined warm cloud indirect plus semi-direct effects resulted in positive forcing when fossil-fuel BC only was added, but negative forcing when a mix of biofuel and fossil-fuel BC was added. Adding biofuel emissions apparently produces a larger semi-direct effect, especially at high latitudes of both hemispheres, perhaps due to lofted BC in these regions (Section 5.2). A third experiment tested the combined effect of BC and OA from biofuels only. In this case aerosols caused increased CDNC and cloud cover with a larger negative forcing. The indirect effect was found to depend greatly on assumed particle sizes, with a factor of two decrease or increase in diameter producing a 45% increase and 30% decrease in magnitude, respectively.

[43] *Koch et al.* [2011a] presented a multi-model study of the effects of BC and OA from fossil-fuel and biofuel burning. Six models examined alterations in cloudy-sky fluxes due to the same emission changes. The response to fossil-fuel BC was -0.08 to +0.31 W m^{-2} with an average of +0.08 W m^{-2}, while the response to 50% of biofuel BC and OA ranged from -0.20 to +0.08 W m^{-2} with an average of -0.10 W m^{-2}. Cloud response in this study was diagnosed using the difference in cloudy-sky fluxes between simulations with and without BC, except for one model (GISS, reported separately by *Bauer et al.* [2010] and discussed above). Therefore, these values include not only cloud semi-direct effects and warm-cloud indirect effects but also direct forcing in cloudy skies, which can be more than half of the direct forcing [*Zarzycki and Bond*, 2010]. Removing the

above-cloud direct forcing effect would result in more negative liquid-cloud effect.

[44] Many model studies do not separate microphysical effects from semi-direct effects, although such a division could be useful for comparing across studies that do estimate these effects separately. To isolate liquid-cloud microphysical effects in the *Koch et al.* [2011a] study, we estimated semi-direct and direct forcing in cloudy skies for each model. Adjusted values, scaled to our emission estimates, are summarized in Table 6.2.

[45] *Spracklen et al.* [2011] modeled liquid-cloud effects, comparing CCN against observations. They found that the contribution of carbonaceous aerosols was required to explain observed CCN concentrations. Their estimates of forcing for BC plus OA were -0.23 W m^{-2} for fossil-fuel and biofuel emissions, and -0.34 W m^{-2} for all BC and OA emissions.

[46] *Jacobson* [2010] studied the effects of fossil fuel and biofuel on climate. Fossil-fuel emissions, including BC, OA and primary sulfate, caused a net decrease in liquid cloud cover. Biofuel emissions, including these species as well as co-emitted gaseous species, caused a net increase in liquid cloud cover. In this case the cloud effects include the semi-direct effect, which is reported to be a cloud loss in this model. *Jacobson* [2010] argued that fossil-fuel emissions contain fewer hygroscopic particles and, therefore, do not have significant indirect effect, while the more hygroscopic biofuel particles do affect liquid clouds. This study includes all effects (direct, liquid, mixed, semi-direct, and ice clouds, as well as cryosphere forcing) and they were not separated.

[47] For the studies discussed above, the mean value of the isolated liquid-cloud indirect effect, when scaled to the magnitude of industrial-era BC, from the three studies that modeled all carbonaceous aerosol, is about -0.07 W m^{-2}. These three models give similar forcings when scaled to emissions of 8700 GgC yr^{-1}. We use the model variation from the *Koch et al.* [2011a] study, about 0.2 W m^{-2}, as the total uncertainty in this effect. However, due to the inability of models to distinguish separate mechanisms, we estimate the combined indirect and semi-direct effect, excluding forcing by cloud droplet inclusions, as -0.2 ± 0.3 W m^{-2}, where the uncertainties have been added in quadrature. This value is more robust than the separate estimates. When the asymmetric uncertainty due to lofted biomass emissions is also added, the uncertainty bounds become -0.52 to 0.05 W m^{-2}.

[48] A common result among the models summarized in *Koch et al.* [2011a] is that aerosol emissions from biofuel cause larger indirect effects per mass than do emissions from fossil fuel. Table 6.2 shows how the studies discussed above were scaled for emission rate and, in one case, particle size. Studies that isolate fossil-fuel or diesel emissions suggest a small positive liquid-cloud forcing averaging 0.03 W m^{-2}, while those that isolate biofuel emissions have a small negative forcing averaging -0.03 W m^{-2}. However, studies that examine the two in combination estimate a larger negative forcing that is greater than the near-zero sum. This finding suggests that the liquid-cloud system contains significant nonlinearities so that the total effect is not equal to the sum of the parts. In contrast, *Spracklen et al.* [2011] attribute greater negative forcing to fossil-fuel and biofuel particles compared with open-burning particles.

[49] Biofuel and fossil-fuel emissions are different in four ways that may affect cloud responses. The first is chemical; the ratio of organic to black carbon is larger for biofuel and organic carbon is generally more hygroscopic than BC. However, some models do not explicitly treat the difference in hygroscopicity, so that modeled BC and OA particles are identical. Second, co-emitted aerosol species or precursors also affect the number of particles. For example, altering biofuel sources to remove 1 Gg of BC also removes about 4 Gg of primary OC, so it could reduce primary particle number much more than altering fossil-fuel sources to achieve the same reduction. Third, models assume different emitted particle sizes. Both *Chen et al.* [2010a] and *Bauer et al.* [2010] assumed larger particle size in biofuel emissions than in fossil-fuel emissions. Since particles must grow large enough to act as CCN, biofuel particles are closer to activation than fossil-fuel particles. Conversely, an assumption of smaller diameter yields many more particles for the same mass emission. The modeled indirect effect depends on assumptions about source-specific particle size, number and composition, but such observations are limited. Fourth, cloud response has a regional dependence. Fossil-fuel consumption is more prevalent at temperate latitudes, where cloud types and atmospheric dynamics differ greatly from tropical regions. Few models have conducted experiments that isolate sensitivities to these factors.

6.5. BC indirect effects on mixed-phase and ice clouds

[50] The influence of aerosols on both mixed-phase and ice clouds depends upon whether they can effectively nucleate ice. Typical IN are mineral dust, biological particles and possibly BC. Although coating of BC with sulfate or organic material increases its ability to act as a CCN, coatings might reduce BC's IN activity, although there is less evidence for this change. In order to have an influence on ice particle formation, it is not enough that BC have the capability to serve as IN; it must also be equally or more efficient than other types of aerosols.

6.5.1. Laboratory evidence for BC effectiveness as IN

[51] The mechanisms by which BC can affect ice clouds require that it activate heterogeneously. In general, IN need to be larger than 0.1 μm in order to have ice-active sites [*Marcolli et al.,* 2007]. Such sites can be thought of as imperfections that aid ice nucleation and may result from surface roughness or crevasses. IN activity is thought to be favored for hydrophilic particles, particles with crystallographic structure or with chemical bonds similar to those of water [*Pruppacher and Klett*, 1997]. These requirements mean that dust and crystalline sulfate are good IN and organic carbon or sulfuric acid are poor IN. The IN behavior of BC is open to question. Two parameters are commonly reported to convey the effectiveness of IN. First, the ice nucleation threshold is the supersaturation with respect to ice at which the IN activates (*e.g.*, a threshold of 1.5 means that the particle initiates nucleation of ice crystals at a relative humidity with respect to ice, RH_i, of 150%). Second, the ice-active fraction is the fraction of particles that serve as IN under any conditions.

[52] Figure 6.2 summarizes laboratory studies that have examined IN activity of BC-containing samples as a function of temperature. It includes particles from various sources and with different degrees of aging or processing [*Kärcher et al.,* 2007]. The figure shows the nucleation threshold of each material, and

the dashed (solid) curves indicate the point where supercooled solution droplets (pure water droplets) activate by homogeneous nucleation. In order for BC to compete with solution droplets such as sulfate, it should activate at a lower threshold (*i.e.,* those aerosols that fall below the dashed line in Figure 6.2). Graphite spark-generated aerosol samples (two red areas in Figure 6.2) made efficient heterogeneous IN [*Möhler et al.,* 2005a], but they are probably least chemically similar to atmospheric BC-containing particles. The remainder of the samples lie near the homogeneous nucleation line. Thus, the vast majority of studies suggest that combustion particles from a large number of sources are inefficient ice nuclei [*Kärcher et al.,* 2007].

[53] While some studies suggest that coatings reduce the ice nucleation efficiency of BC [*Möhler et al.,* 2005a; *Crawford et al.,* 2011], others find that they do not significantly alter the IN behaviour of BC [*Friedman et al.,* 2011] or even enhance it [*DeMott et al.,* 1999; *Koehler et al.,* 2009] or that the influence of sulfuric acid coatings depends on the organic matter within the soot [*Crawford et al.,* 2011]. This contrasts with BC CCN activity in liquid clouds, which is always enhanced by coating.

[54] Extensive comparisons of the IN and CCN activity of BC-containing aerosol were reported by *Koehler et al.* [2009], using samples of different hygroscopicity and surface porosity. Larger particles were more ice-active than smaller ones, although the size range investigated was limited. The processes that promote water adsorption facilitated both CCN activation and ice nucleation. At 233K, no combustion aerosol particles nucleated ice better than did aqueous solutions of similarly sized particles. At 216–221K, 1 in 100 particles of oxidized combustion aerosol and 1 in 1000 particles of non-oxidized combustion aerosol and aviation kerosene promoted heterogeneous nucleation of ice. BC particles coated with soluble material behaved like fully soluble particles with the same liquid volume and water activity. This suggests, overall, a limited role for BC in promoting ice nucleation.

[55] Biomass burning emissions, composed of BC and OA, also have limited IN activity, due to inhibition by organic carbon. *DeMott et al.* [2009a] found that biomass-burning aerosol from controlled laboratory burns had the same or lower nucleation activity when compared with liquid solution particles. Aerosol with high OC:BC ratios impeded heterogeneous ice nucleation most strongly. A similar impact has been reported for organic coatings on emissions from propane flames [*Möhler et al.,* 2005b]. At warmer temperatures, significant IN activity of polydisperse samples of small biomass burning particles (number mode diameters 60–140 nm) has been observed only when they have low organic carbon fraction and high water-soluble ion content, associated with flaming fires [*Petters et al.,* 2009]. At warmer temperatures (>240 K), dynamic cloud chamber studies of acetylene combustion emissions suggest no significant IN activity [*DeMott*, 1990], in agreement with the biomass burning aerosol studies.

[56] In contrast, many laboratory studies suggest that mineral dust particles are good to moderate IN as long as they remain uncoated with soluble material [*Kärcher et al*., 2007, Section 4.2 and references therein]. The IN activity of dust particles decreases once coated with soluble material, so that the few processed mineral dust particles reaching the upper troposphere and lower stratosphere (UTLS) are likely those with moderate IN activity [*Wiacek and Peter*, 2009]. Therefore, dust is a major competitor for BC with regard to ice formation. Other competitors include some crystalline inorganic and organic phases within partially soluble aerosols such as ammonium sulfate [*Abbatt et al.,* 2006], oxalic acid [*Zobrist et al.,* 2006], biological particles [*Pratt et al.,* 2009], or mineral dusts with lead [*Cziczo et al.,* 2009].

[57] The laboratory studies summarized in Figure 6.2 employed a wide array of combustion sources and surrogates of BC-containing particles for measurements of IN activity. These studies do not provide fully conclusive information about the behaviour of BC in the atmosphere for two reasons. First, not all studies provide sufficient information to judge their relevance for cloud formation (*i.e.,* ice active fractions and presence of solutes). Second, most studies have not investigated potentially important atmospheric processes that could affect the particles' IN activity, such as surface oxidation or cloud processing. Moreover, a fundamental understanding of the physico-chemical nature of ice nucleation is lacking, although there is some progress in linking source-dependent surface properties of BC-containing aerosol and their ability to adsorb water [*Popovicheva et al.,* 2008].

6.5.2. BC effects on mixed-phase clouds

[58] Clouds with temperatures between 0°C and approximately -35ºC are referred to as mixed-phase clouds because water droplets and ice crystals can co-exist at these temperatures. The water vapor pressure in a mixed-phase cloud lies between water and ice saturation, so the cloud is supersaturated with respect to ice. In these clouds, an increase in IN promotes ice nucleation, and subsequently large ice particles grow in the supersaturated environment. Eventually this cloud will completely turn into an ice cloud (glaciate). This process is called the Bergeron-Findeisen process. As the ice crystals grow in a supersaturated environment, they grow rapidly and start to sediment. The overall effect may be a reduction in cloud cover, causing a positive radiative forcing (Figure 6.1, case MC1). Reduction in IN may cause the opposite effect (case MC2).

6.5.2.1. Mechanisms

[59] Ice formation in mixed-phase clouds occurs by heterogeneous freezing, with the aid of insoluble IN [*Pruppacher and Klett*, 1997]. Heterogeneous freezing can be initiated either by collision of a supercooled cloud droplet and an IN (contact mode), or from within a cloud droplet on an IN that is immersed in it (immersion mode). At relative humidities below 100% with respect to water but above 100% with respect to ice, nucleation of ice directly on bare IN could take place (deposition mode). Based on lidar observations of Saharan dust particles, *Ansmann et al.* [2008] argue that the time available for deposition nucleation may be too short and, hence, is negligible for mixed-phase clouds. Contact nucleation is initiated at higher temperatures than immersion nucleation [*e.g., Shaw et al.,* 2005; *Fornea et al.,* 2009], but it is limited by collision rates, especially for accumulation mode particles that are large enough to serve as IN. Therefore, the immersion mode may be the most important ice-forming mechanism in mixed-phase clouds.

6.5.2.2. Experimental studies

[60] Laboratory and field measurements give conflicting views on the viability of BC as an effective IN. As summarized

above, laboratory results indicate that BC appears to be one of the least efficient IN in the atmosphere, because it nucleates ice at colder temperatures than IN with natural sources such as mineral dust and biological particles. Laboratory studies also suggest that deposition nucleation of ice on most types of BC particles is not important above 243 K and below water saturation [*Dymarska et al.,* 2006]. In contrast, in-situ observations of lower tropospheric mixed phase clouds find an enrichment of BC in ice particle residuals [*Cozic et al.,* 2008; *Targino et al.,* 2009], so there must be some mechanism for BC to enter ice clouds. BC may act as a contact IN at temperatures between 245 and 251 K [*Diehl and Mitra,* 1998; *Fornea et al.,* 2009].

6.5.2.3. Modeling results

[61] Parameterizations have been developed to represent ice formation affected by mineral dust and BC particles in both contact and immersion modes [*Diehl et al.,* 2006; *Phillips et al.,* 2008]. A GCM study using the parameterization of *Diehl et al.* [2006] found that BC did induce a glaciation effect. However, the importance of BC acting as a contact IN, and hence the glaciation effect, decreases in the presence of natural aerosols such as dust that are more efficient IN than BC [*Lohmann and Diehl*, 2006]. The glaciation effect also decreases with increased sulfate coating thickness. The results also depend on the model's parameterization of the Bergeron-Findeisen process. Taking into account all these uncertainties, the glaciation effect of all BC emissions on mixed-phase clouds was estimated as +0.12 and +0.20 W m^{-2} for two different parameterizations [*Lohmann and Hoose*, 2009; see also Table 6.2].

[62] *Storelvmo et al.* [2011] also studied BC impacts on mixed-phase clouds, including the opposing effects of albedo and lifetime. The magnitude and sign of the forcing depended on the ice-active fraction of BC and the parameterization chosen. Forcing became negative when another parameterization [*DeMott et al.,* 2010] was used, but this treatment led to ice crystal sizes that did not agree with observations. When using an intermediate case for ice-active fraction, this study found a forcing of +0.16 ± 0.08 W m^{-2}, which is used in this assessment in calculating our central estimate of the BC effect on mixed-phase clouds.

[63] While other model studies have not produced forcing estimates, they generally agree that BC addition reduces mixed-phase clouds. *Ekman et al.* [2007] studied the influence of BC particles on continental convective clouds using a cloud-resolving model. They found that BC increased heterogeneous ice nucleation, thereby increasing the latent heat release and updraft velocities in the convective plume. As a result, precipitation release was increased and clouds were reduced. One regional climate model study found that externally mixed BC aerosols increase riming and enhance orographic precipitation and cloud loss [*Muhlbauer and Lohmann*, 2009]. In contrast, internally mixed BC aerosols decreased riming rates and orographic precipitation.

[64] Our estimate for mixed-phase cloud indirect effects is +0.16 ± 0.16 W m^{-2} based upon the two estimates of *Lohmann and Hoose* [2009] using different freezing parameterizations, and the estimate of *Storelvmo et al.* [2011]. These estimates are not scaled from the study emission rate to the best estimate of BC emission rate. Forcing does not scale linearly with IN abundance, as shown by the sensitivity experiments in *Storelvmo et al.* [2011].

6.5.3. BC effects on ice-phase clouds

[65] Pure ice-phase clouds (cirrus clouds), which form at temperatures below -35ºC, often reside at high altitude and usually exert positive forcing. As discussed in Section 6.5.1, BC IN activity may either increase or decrease this forcing.

6.5.3.1. Mechanisms

[66] In cirrus clouds, there are no water droplets and therefore no contact nucleation, so nucleation by deposition governs these clouds. In these clouds, the total number of nucleated ice crystals may either increase or decrease depending on temperature, cooling rate, and number of BC particles [*Kärcher et al.,* 2006]. If heterogeneous nucleation dominates unperturbed clouds (especially in slowly cooling air masses), BC could contribute to this nucleation by increasing the number of IN and thereby decrease the mean size of ice crystals. This leads to longer lifetimes of high clouds that exert a net warming effect, resulting in a positive forcing (case IC2, Figure 6.1). At higher cooling rates, adding IN tends to retard or even prevents homogeneous freezing, which decreases the number of ice crystals, resulting in a negative cloud forcing (case IC1, Figure 6.1). In the UTLS, airborne measurements of relative humidity and cirrus indicate that the latter scenario occurs preferentially at the prevailing atmospheric conditions.

[67] Figure 6.3 shows the results of an IN parameterization demonstrating how the total nucleated ice crystal number, n_i, varies with combustion aerosol number, n_s, in the presence of dust IN and liquid background aerosols. Updraft velocities govern the rate at which a developing cloud is cooled, and therefore the formation rate of new ice crystals, so they play an important role in the initial cloud properties. The two panels show different cloud updraft speeds, where the updraft rate increases the cooling rate. For small n_s, where all IN are combustion aerosol (black curves), n_i is determined by homogeneous nucleation and the addition of BC does not affect the ice concentration. As more IN are added, more of them nucleate heterogeneously and take up water. As a result, fewer ice crystals form homogeneously and n_i decreases. (This reduction in ice crystals with IN, corresponding to case IC1 in Figure 6.1, contrasts with liquid clouds where addition of CCN causes increased CDNC.) The resulting larger particles have a shorter atmospheric lifetime, leading to a decrease in cirrus clouds and negative longwave forcing. IN can be added by increasing either combustion particles (n_s) or dust (colored curves). When IN are numerous enough, heterogeneous nucleation dominates the formation of ice crystals, and the suppression of homogeneous nucleation has little effect on the final number. Therefore, the addition of IN causes n_i to increase (case IC2 in Figure 6.1). Under some conditions, formation on n_s could entirely suppress homogeneous freezing.

[68] At small updraft rates (top panel), few ice crystals form and the influence of IN occurs at lower n_s. Large updraft velocities (bottom panel) cause the formation of a large number of ice crystals, since homogeneous freezing dominates ice formation (the number of aerosol droplets is not a limiting factor). In this case, BC is not capable of causing a notable indirect effect. At intermediate updraft velocities, BC depletes the air mass of moisture, causing much fewer (but still more

than BC) background particles to freeze homogenously. This discussion, focused largely on microphysics, addresses only processes that affect the initial ice crystal concentration in single air parcels. This sensitivity study gives a first-order estimate of IN in young clouds, but does not quantify the changes in the cloud as it evolves, and therefore does not reflect global averages.

6.5.3.2. Field evidence for BC acting as IN

[69] Laboratory studies indicate that IN activity of BC is, at best, moderate. Field studies, summarized below, confirm these findings. They indicate that homogeneous freezing is the prevalent ice formation mode [*DeMott et al.,* 2003; *Cziczo et al.,* 2004a]. This is consistent with the ubiquity of high ice supersaturations in cloud free areas of the upper troposphere [*Jensen et al.,* 2001; *Haag et al.,* 2003; *Kahn et al.,* 2009b] and with the fact that total cirrus ice-crystal number densities often far exceed estimated IN concentrations [*Gayet et al*., 2002; *Hoyle et al*., 2005]..

[70] Field measurements using single particle mass spectrometry, electron microscopy, and X-ray emission or particle scattering demonstrate that BC and organic carbon are present in the troposphere and lower stratosphere [*Murphy et al.,* 2007; *Nguyen et al.,* 2008]. Often the predominant particles are composed of organic carbon that originates mainly from surface sources. Even particles that reach the stratosphere may have acquired small amounts of carbon during transport through the upper troposphere. BC's effectiveness as an IN is greatest if it is pure, but, presumably, uncoated BC rarely exists in the UTLS region. Because it is difficult to detect thin coatings on BC, the number of such particles in this region is poorly known.

[71] A constraint that could ascertain whether BC affects ice cloud formation would be direct airborne sampling of particles at high altitudes, along with simultaneous characterization of their chemical composition and measurements of their ice-forming properties. Ice nuclei counters have been employed in several ground-based and airborne measurements [*Rogers et al.,* 1998; *DeMott et al.,* 2003; *Cziczo et al.,* 2004b; *Richardson et al.,* 2007; *Stith et al.,* 2009; *Prenni et al.*, 2009*; Froyd et al.,* 2009]. In qualitative agreement with most laboratory studies, some of these field measurements support the notion that mineral particles can act as IN in cirrus clouds, while BC-containing aerosol is less ice-active, although it often present in ice-nucleating aerosol. However, without adequate characterization of particle composition and properties, field measurements can infer correlations between IN components and heterogeneous ice nucleation but cannot distinguish the processes by which certain particles partition in cirrus ice; therefore, they cannot provide causal links.

[72] This conclusion is particularly true for measurements of cirrus ice crystal residues that show enhancements in insoluble components relative to ambient particles, throughout the troposphere and in aircraft corridors [*Heintzenberg et al.,* 1996; *Ström and Ohlsson*, 1998; *Twohy and Gandrud*, 1998; *Petzold et al.*, 1998; *Twohy and Poellot*, 2005]. Inertial scavenging of BC particles by ice crystals in clouds was found to be more important than ice nucleation in explaining observed BC-to-ice mass ratios at temperatures of 228–248 K [*Baumgardner et al.,* 2008].

[73] Field data sets that measure IN concentrations have not distinguished BC-containing particles from other particles. Such measurements may be viewed as the maximum concentrations of ice-active BC for comparison with models. Measurements over continental areas and in aircraft corridors reveal highly variable IN number concentrations of 0.1–500 L^{-1}, with 60% of data lying in the range 2–20 L^{-1} [*Rogers et al.,* 1998]. Other data sets point to typical background northern hemispheric IN concentrations of 10 to 30 L^{-1} [*DeMott et al.,* 2003; *Haag et al.,* 2003]. Data in the Arctic report lower values (< 1 L^{-1}) with local maxima of 50 L^{-1} [*Prenni et al.,* 2009]. IN concentrations of 100 to 500 L^{-1} are rare and have only been detected locally in dust storms [*DeMott et al.,* 2009b; *Stith et al.,* 2009].

[74] The minimum BC ice active fraction present in lower and mid tropospheric biomass burning plumes required to exert regional impact was estimated to be 10^{-4} or higher [*Petters et al*., 2009]. A comparison of upper tropospheric refractory particle concentrations of about 10,000 L^{-1} [*Minikin et al*., 2003] with inferred IN concentrations of about 10 L^{-1} [*Haag et al.,* 2003] yields a BC ice active fraction of 10^{-3}, when assuming that BC contributed 100% by number to the refractory particles. The latter assumption is likely an overestimate, so the BC ice active fraction in nature was probably smaller.

6.5.3.3. Modeling evidence for BC atmospheric abundance and mixing state

[75] As discussed in Section 2, BC particles are commonly mixed with sulfate or organic carbon within a day. If most BC particles in the UTLS are coated, then BC acting as deposition IN, in which ice forms directly on bare BC, would be rare in the upper troposphere.

[76] Most global models are not well validated in terms of UTLS aerosol speciation and particle number concentrations, in particular for BC [*Koch et al.,* 2009a; *Lohmann and Hoose,* 2009]. Problems in simulating tropospheric BC vertical distribution, mixing state, and other properties are mainly tied to poorly parameterized physical and chemical processes that affect BC lifetime, and, to a smaller degree, to uncertainties in emission inventories [*Textor et al.,* 2007]. One particularly uncertain process is scavenging in ice clouds.

[77] One climate model has specifically compared UTLS aerosol number and mass concentrations with observations [*Aquila et al.*, 2011]. This model tracks the properties and distribution of potential ice nuclei (defined as the sum of dust and BC particles) separately from soluble particles, so that internally and externally mixed BC are explicitly represented. The zonal mean ratio of externally mixed potential IN to the total potential IN number is 0.5–2% throughout most of the free troposphere. These values are much smaller than suggested by observations [*Schwarz et al.,* 2008a], but internally mixed particles are not distinguished as easily by the measurements as they are in the model. Simulated transformation times from external to internal mixtures are predicted to be larger for dust than for BC, implying a larger (but still small) fraction of bare dust particles relative to BC in tropospheric accumulation mode IN. These model results suggest the need for careful examination of observed IN mixing state.

[78] For BC particles (or IN in general) to exert a significant effect on ice formation, their ice nucleation thresholds should

lie well below the homogeneous freezing limit for fully soluble aerosol particles, and the number concentration of the ice active population should be 10 L^{-1} or larger for typical updraft velocities and temperatures in the upper troposphere [*Kärcher et al.,* 2006]. However, as summarized above, BC particles from a wide range of sources do not appear to be potent IN (see Figure 6.2). Therefore, it is realistic to assume an ice nucleation threshold that is close to but below the homogeneous freezing threshold, as was chosen for the simulations in Figure 6.3. While Figure 6.3 explores the effect of BC on IN, the possible range of influence of BC on cirrus properties depend on the details of the ice nucleation rate and other factors that are not included in those simulations.

[79] Resolving moderate impacts of IN, where ice is formed at supersaturations slightly below the homogeneous freezing threshold, and validating IN impacts on cirrus will be very challenging in UTLS in situ measurements, given the present difficulties in measuring relative humidity and cooling rates on the scale of individual clouds. *Kärcher and Ström* [2003] emphasized the crucial role of dynamical forcing in cirrus formation; small uncertainties in estimating cooling rates in cirrus generating cells can easily mask any indirect effect exerted by IN. Furthermore, it is questionable whether the effects of IN on optically thin ice clouds can be unraveled by means of satellite observations [*Chylek et al.,* 2006; *Seifert et al.,* 2007; *Massie et al.,* 2007].

6.5.3.4. Global model studies of BC effects on cirrus

[80] Two model studies have estimated the carbonaceous aerosol effect on ice clouds (Table 6.2). Radiative forcing is the difference between present-day conditions and pre-industrial (background) conditions, and estimates are therefore strongly affected by the nucleation regime in the background atmosphere. If homogeneous nucleation is most common in the pre-industrial atmosphere (left side of Figure 6.3 or an environment with few IN), BC decreases ice particle number and forcing is negative. If heterogeneous nucleation was dominant in the pre-industrial case (toward the upward slope of Figure 6.3 or an environment with more dust), BC increases ice particle number and forcing becomes positive. A predominance of droplets or sulfate particles corresponds to natural conditions with homogeneous nucleation, while predominance of refractory particles like dust would result in heterogeneous domination. The influence of adding IN on ice formation is largely controlled by cloud-scale dynamics, and changes in the dynamic regime since the pre-industrial era are not fully included in this forcing estimate.

[81] *Penner et al.* [2009] used off-line estimates from a CTM aerosol scheme coupled to the NCAR CAM3. They used two parameterizations that allowed for competition between homogeneous and heterogeneous nucleation in an aerosol mass-only and a 3-mode, 2-moment versions of the model. Sulfate droplets were assumed to act as homogeneous freezing agents, BC was assumed to be coated with soluble material and, therefore, to act as immersion IN, and dust was assumed to act as IN in the deposition or condensation mode. For the more sophisticated (3-mode) parameterization, two different ice nucleation schemes gave a radiative forcing from fossil-fuel and biomass burning emissions of -0.3 to -0.4 W m^{-2}. The dominant effect was that heterogeneous IN activity of BC decreased relative humidity with respect to ice, inhibited homogeneous nucleation, decreased the number of ice particles and reduced positive forcing by high-level clouds.

[82] The mass-only version of the aerosol model was applied by *Liu et al.* [2009a] in the NCAR CAM3 global model with a double moment ice microphysical scheme. Adding BC resulted in increased high-level clouds, especially over polar regions but also somewhat over tropical regions. The resulting change in cloud radiative forcing due to BC emitted at the surface was +0.22 W m^{-2} or +0.39 W m^{-2} when critical supersaturations of 1.2 - 1.3 or 1.4, respectively, were assigned to BC. The larger forcing for higher ice nucleation threshold is due to a larger decrease in negative shortwave contribution. The change in sign between this study and the *Penner et al.* [2009] results reflects the large uncertainty in this forcing, stemming from the fact that cirrus clouds affect both shortwave and longwave radiative fluxes, and the change in each is determined by specific cloud properties. The forcing is, therefore, a small number calculated by adding two large numbers of opposing sign, making it very sensitive to changes in the magnitude of either one. Similar uncertainties are seen in the estimation of the climate effects of aviation BC emissions, which are not included here. There are three major differences between this study and *Penner et al.* [2009]. In the pre-industrial atmosphere, homogeneous nucleation dominated in *Penner et al.* [2009] while heterogeneous nucleation dominated background conditions in *Liu et al.* [2009a]. *Liu et al.* used a prognostic treatment of the ice-crystal number concentration including source and sink terms while *Penner et al.* diagnosed ice-crystal number concentration from nucleation. *Liu et al.* [2009a] included climate feedbacks, so that aerosols in the UTLS region tended to enhance relative humidities there; however, they were unable to reproduce the observed supersaturations in the atmosphere, so that the modeled supersaturations were never high enough to allow homogeneous nucleation (see Figure 3 of *Liu et al.* [2007]).

[83] *Jacobson* [2010] included ice-cloud effects in a model of the effect of BC on climate. Ice crystal sizes increased slightly due to BC. He used a temperature-dependent ice-nucleation threshold (Section 6.5.1) that ranged between 1.15 and 1.35, below many of the observations in Figure 6.2. These values are within the range for uncoated spark-generated soot at the lowest temperatures, but below the range of other types of soot. Cloud drop and ice-crystal number were calculated by simultaneously solving the mass balance equations for water vapor, liquid, and ice, considering all aerosol and cloud particle sizes. BC in this model study is a more efficient IN than is observed in the laboratory. In the study, relative humidity increased at high altitudes and in the Arctic, and ice clouds increased due to BC, which are results similar to those in *Liu et al.* [2009a]. Forcing due to this IN mechanism was not isolated, but the direction of ice-cloud changes suggests a positive forcing.

[84] In a global model study by *Hendricks et al.* [2011], a multiple-mode ice microphysical scheme was applied in the ECHAM GCM to simulate IN effects on global cirrus properties. The ice nucleation parameterization by *Kärcher et al.* [2006] was applied to simulate the competition between homogeneous and heterogeneous ice formation. *Hendricks et al.* [2011] assumed that only small fractions of the modeled BC and mineral dust particles (0.25% and 1%, respectively) could act as IN, resulting in IN concentrations on the order of 10 L^{-1} at

cirrus levels. BC and dust-related IN had similar contributions. Heterogeneous nucleation on both types of particles produced significant reductions in the mean cirrus ice particle number concentrations. The effect was most pronounced in the tropics, where the zonal mean annual average ice particle number concentration decreased by up to 20%. Reductions in the mean ice water content, likely resulting from efficient sedimentation and precipitation of large ice particles generated by heterogeneous nucleation, also occurred. This effect led to reductions in the zonal mean, annually averaged, water-vapor mixing ratio of up to 5% at cirrus levels. The BC contribution to these effects was comparable to that related to mineral dust IN only when the assumed ice nucleation threshold is significantly lower than that assumed for dust particles (threshold of 1.2 for BC and 1.3 for mineral dust). When a larger critical value (ice nucleation threshold of 1.40) was assumed for BC, heterogeneous freezing was dominated by mineral dust particles.

[85] Compared to the global model studies by *Liu et al.* [2009a] and *Penner et al.* [2009], *Hendricks et al.* [2011] simulated a much smaller effect of BC on cirrus ice crystal number concentrations. These differences could result from either a smaller availability of active ice nuclei in the *Hendricks et al.* [2011] study or from differences in the representation of relative humidity and cooling rates. Although *Hendricks et al.* [2011] did not discuss the radiative forcings associated with these changes in cirrus cloud properties, the expectation is that they will be correspondingly smaller than those reported by *Liu et al.* [2009a] and *Penner et al.* [2009].

[86] Compared with the measurements discussed in Section 6.4.3.3, the models may overestimate UTLS BC and IN and may, therefore, overestimate the magnitude of the ice-cloud indirect effect. *Liu et al.* [2009a] reported BC concentrations of about 300 to 3000 L^{-1}, which when compared to a few measurements were roughly a factor of two too high. *Penner et al.* [2009] reported reasonable agreement with measurements of IN from one field campaign, but the concentrations exceed those summarized in Section 6.4.3.3 for a more geographically diverse set of regions. IN concentrations in the UTLS region are much smaller in *Liu et al.* [2009a] than in *Penner et al.* [2009].

[87] Our estimate of the BC influence on ice-cloud indirect effects is 0.0 ± 0.4 W m^{-2} based on the average and range of *Liu et al.* [2009a] and *Penner et al.* [2009]. Both models lack fidelity in some aspects, so that there is no clear choice between the two opposing results and the uncertainty range may be more meaningful than the average value. Unlike all other cloud forcings, this estimate has not been scaled to our best estimate of industrial-era BC emission rate. For ice-cloud effects, many factors other than emission rate affect ice-active BC concentrations in the upper troposphere. Most models, including those used in the *Penner et al.* [2009] and *Liu et al.* [2009a] studies, overestimate these concentrations. Therefore, the model results may represent an upper bound on the magnitude of ice-cloud impact.

6.5.3.5. Aircraft impacts on high ice-cloud properties

[88] Aircraft emissions of BC provide an especially potent source of potential ice nuclei [*Kärcher et al.,* 1996; *Schröder et al.,* 1998]. Forcing by aviation emissions is not included in this paper because the location of emission makes aviation a special combustion source, and because these impacts have been reviewed elsewhere [*Lee et al.,* 2009]. We mention these studies here because they may provide additional clues about how BC particles affect cirrus clouds, although BC emitted from aviation may undergo less mixing with tropospheric particles and gases.

[89] Although contrails would form even in the absence of BC emissions, the optical properties of the contrails and cirrus impacts depend on BC emission levels [*Kärcher and Yu,* 2009]. Although contrail formation does not depend on BC and other exhaust species, the optical properties of the contrails and cirrus impacts probably do [*Lee et al.,* 2009]. Water supersaturated conditions during contrail ice formation below approximately 225 K activate even rather hydrophobic BC particles into rapidly freezing water droplets [*Kärcher et al.,* 1996; *Koehler et al.,* 2009]. A decrease in ice cloud particle size for cirrus clouds altered by aircraft may imply that aircraft BC increases the concentration of available IN for these aged contrails or cirrus clouds [*Lee et al.,* 2009]. *Jacobson et al.* [2011] found that an assumption of efficient ice nuclei (*i.e.,* ice nucleation threshold of 1.35 at 185 K) was required for a good match with observed contrail cloud fractions. The model study of *Hendricks et al.* [2005] suggests that aircraft BC increases IN by 10 to 40% in aircraft cruise altitudes in northern midlatitudes. However, the ice nucleating properties of aircraft exhaust for the exact composition and coating of exhaust particles, at the temperature and water vapor conditions in cirrus, remain poorly known. The impact of aircraft BC emissions on cirrus cloud formation in the absence of contrail formation remains very uncertain.

6.6. Comprehensive treatments of BC cloud effects

[90] Although the discussion above has separated effects on individual cloud types, one series of model results [*Jacobson*, 2001; *Jacobson*, 2002; *Jacobson*, 2004; *Jacobson,* 2010] has implemented a progressively more complex treatment of BC that does not separate responses to individual cloud types. Although these studies give shortwave and longwave irradiance changes, those values are not effective forcings because they also include climate responses. Therefore, our comparison is largely based on the reported temperature responses divided by the GHG climate sensitivity of the model [0.6 K $(W\ m^{-2})^{-1}$, *Jacobson*, 2002]. This quotient gives an approximate effective forcing.

[91] *Jacobson* [2004a] included direct forcing, snow forcing, and responses of liquid, mixed, and ice clouds to estimate a temperature increase of +0.27 K for fossil fuel and biofuel emissions. When the effective snow forcing of +0.18 W m^{-2} (see Table 7.1 and Section 8) is subtracted from the total effective forcing, an effective forcing of +0.31 W m^{-2} is obtained. This value is similar to the purely direct-forcing total of +0.34 W m^{-2} expected for the emission rates used in that study and the direct forcing of the model reported earlier [*Jacobson,* 2001]. From this we infer that the balance of positive and negative forcing exerted by liquid, mixed, and ice clouds is near zero, comparable to the values assessed above when ignoring the cloud absorption effect. On the other hand, aerosol from open biomass burning caused a negative temperature change of -0.17 K [*Jacobson*, 2004b].

[92] *Jacobson* [2010] used slightly different emission rates for fossil-fuel and biofuel emission and reported a temperature

change of +0.38 K (*i.e.,* equivalent to about 0.45 W m^{-2} after removing cryosphere forcing) when cloud absorption was ignored, again similar to the emission-based projection of direct aerosol forcing of +0.39 W m^{-2} and indicating a negligible net cloud influence. However, when cloud absorption by BC in droplets was included in the simulation, the temperature change was +0.69 K, an increase of +0.31 K (+0.52 W m^{-2}). This potentially large effect was considered in Section 6.3.1.

6.7. Summary of uncertainties in estimating indirect effects

[93] For all aerosols, there is a much larger relative spread in model estimates of aerosol indirect effects compared with direct effects. For example, the uncertainty estimate for the cloud albedo effect is double that of the aerosol direct effect [*Forster et al.*, 2007].

[94] In addition to aerosol effects on clouds, atmospheric dynamics plays a decisive role in cloud formation, properties, and lifetimes [*Heintzenberg and Charlson,* 2009]. If these dynamical relationships are incorrectly represented in models, the resulting errors could overwhelm the magnitude of aerosol influence. Some studies argue that offsetting mechanisms, or 'buffering,' may reduce the magnitude of perturbations caused by aerosols [*Stevens and Feingold*, 2009].

[95] Global models also suffer from inconsistency between ice microphysics and cloud coverage [*Kärcher and Burkhardt*, 2008], and uncertainties in specifying subgrid-scale vertical velocities, which control the relative roles of IN and liquid particles during cirrus formation [*Kärcher and Ström*, 2003]. These factors may introduce larger uncertainties in determining the indirect effect for cirrus than do assumed variations in the properties of the ice-nucleating aerosols.

[96] From the viewpoint of aerosol-cloud interaction, uncertainties in BC's influence on clouds are of four general types. First, there are process uncertainties regarding the effects of aerosols on clouds generally and of the role of BC more particularly, and modeled aerosol microphysics and cloud responses have not yet been strongly constrained by observations. A current challenge is obtaining sufficient observational information on aerosol number, size, mixing state and chemical composition in various regions and altitudes. To understand how these aerosols affect clouds, cloud-scale measurements determining collocated relative humidity, vertical air motion, and CCN or IN activity and number concentration are important. Many models have only recently represented aerosol microphysics and the coupling to both the vapor phase and cloud microphysics. Including these factors changes the magnitude, and sometimes even the sign, of the reported effects.

[97] Second, only a few model studies have focused on particular types of aerosol-cloud effects, and the influence of BC in those changes. Models frequently lack consistent diagnostics and experimental designs for isolating the effects of particular species or sectors on individual cloud impact mechanisms. This inconsistency causes a lack of comparability among model results that is frequently ignored when such reports are tabulated.

[98] Third, not all cloud types have been included in investigations of aerosol-cloud effects. Modeling of changes in mixed-phase clouds, ice clouds, and increased absorption in cloud droplets is a relatively new research area, with a much small number of studies providing these estimates. Aerosol microphysical effects on convective clouds are poorly known and generally not included in models. For cold ice clouds, GCM cloud schemes do not yet reconcile the physical treatments of fractional coverage, supersaturation and microphysics.

7. Cryosphere changes: Black carbon in snow and ice

7.1. Section summary

[1]

1. Light-absorbing particles in snow can significantly reduce snow albedo. Because of the high albedo of snow, even aerosol with relatively high single scatter albedo (*e.g.,* aerosol with a high OA:BC ratio) causes positive radiative forcing.

2. Small initial snow albedo reductions may have a large adjusted forcing because the resulting warming affects the snow morphology (grain size), snow sublimation rates, and snow melt rates, all of which enhance BC-induced snowpack albedo reductions, leading to an amplification of the radiative forcing. Albedo feedback triggered by this forcing drives a large temperature response (Section 8).

3. The best estimates for all-source and industrial-era adjusted forcing by BC in snow are +0.04 W m^{-2} and +0.035 W m^{-2}, respectively. The all-source estimate is derived by scaling the results of a suite of model studies to achieve consistent estimates of forcing from all present-day sources (fossil-fuel, biofuel and biomass burning). Measurements of the BC content of Arctic snow were also used to adjust two of the model studies' derived forcing for biases in snow BC concentrations. Industrial-era forcing is calculated by scaling by the ratio of industrial-era to all-source BC emissions, accounting for changes 1750 to present day in the fraction of global emissions from fossil-plus-bio-fuel and from open biomass burning which are deposited to snow. Changes in snow and ice cover 1750 to present day are not accounted for. These central estimates also do not account for forcing by BC in sea ice but do account for forcing by snow on sea ice.

4. The bounds for all-source snow BC adjusted forcing are estimated at +0.01 W m^{-2} to +0.09 W m^{-2} and for industrial-era forcing at +0.008 W m^{-2} and +0.078 W m^{-2}. These are based on results of model sensitivity studies applying low and high values of snow cover fraction, rate of snow aging and resulting grain size evolution, scavenging of BC out of the snowpack during melt, and BC emissions, as well as a model estimate of the reduction in radiative forcing by BC caused by the concurrent presence of light-absorbing soil dust. These bounds do not account for uncertainty in how radiative forcing is affected by patchy snow cover, by uncertainties in modeled cloud cover and vegetation cover, or for possible biases in modeled mid-latitude snow BC concentrations.

5. The best estimate for all-source and industrial-era radiative forcing by BC in sea ice are +0.012 W m^{-2} and +0.011 W m^{-2}, respectively. These estimates are derived using Arctic-wide averages for sea ice BC concentration, sea ice area, melt pond fraction, snow cover fraction, and solar irradiance. The bounds on sea ice BC radiative forcing are +0.008 and +0.017 W m^{-2} for all-source forcing and +0.007 and +0.016 W m^{-2} for industrial-era forcing, based on independently calculating negative and positive deviations from the mean given by realistic possible minima and maxima in these factors. These forcings do not account for rapid adjustments that may amplify the initial radiative forcing.

6. Chemical analysis of springtime surface snow samples indicate that most BC and other light-absorbing particles in the North American and Russian Arctic snow and from Greenland are associated with biomass burning. Fossil fuel plays a prominent role in the high-latitude Arctic Ocean and in Greenland in the summertime, but in Greenland concentrations are low. Indirect evidence indicates that pollution may also play a significant role in the Arctic north of Europe, where concentrations are higher.

7. A large fraction of particulate light absorption in Arctic snow (about 30 to 50%) is due to non-BC constituents. Most of the absorption appears to be due to light-absorbing organic carbon from biofuel and agricultural or boreal forest burning. The forcing estimates given above account for only BC. The total radiative forcing by a source which emits both BC and light-absorbing organic carbon is larger than is given by BC forcing alone.

8. In some regions, especially areas with thin and patchy snow cover or mountainous regions, soil dust significantly lowers snow albedo, lessening the influence of BC. Models do not capture these potentially large sources of local dust to the snowpack and, therefore, may be overestimating BC radiative forcing and this is not accounted for here.

9. There is evidence that snow BC concentrations in the Arctic, Europe and N. America were higher in the early and mid 20th century than presently. Also, snow cover is declining with time. Thus, snow BC radiative forcing is likely decreasing in many regions.

10. BC in glacial snow is primarily a concern because of its possible role in altering melt cycles of glaciers in regions that rely on glacial melt to balance the water supply through the seasons. The role of snow BC in glacial melt is still highly uncertain. Few measurements of glacial snow BC content exist, and studies of the impact on glacial snow melt have generally not accounted for the albedo effects of natural impurities (soil dust, algae) in glacial snow and ice.

7.2. Introduction

[2] Light-absorbing particles in snow can significantly reduce snow albedo and increase the amount of absorbed solar radiation because the albedo of pristine snow at visible wavelengths is high and because snow scatters visible radiation very efficiently, producing a large photon path length that amplifies the influence of impurities [Figure 7.1; *Warren and Wiscombe*, 1980b; *Warren*, 1982; *Chylek et al.,* 1983b]. In contrast to atmospheric aerosol radiative forcing, which may be positive or negative depending on the underlying surface albedo and what species are co-emitted with BC, aerosols with a visible-band single scatter albedo less than that of ice grains (about 0.9999+), which includes nearly all species except sulfate sea salt, exert a positive radiative forcing when incorporated into surface layers of optically thick pure snowpacks (Figure 7.2). Thus, even sources with a high OA:BC ratio produce a warming when deposited on snow exposed to sunlight.

[3] Critically, the large climate effects from BC in snow do not come from the initial change in snow albedo but from the rapid adjustments that follow (Figure 7.3). Increased solar heating with lower snow albedo affects the snow aging process, in general causing more rapid growth of the snow effective

grain size through warmer snowpack temperatures. Coarse-grained snow has a lower albedo than fine-grained snow (*GRA* in Figure 7.3), and the reduction in albedo due to BC increases with grain size (*GRB* in Figure 7.3) (see also Figure 7 of *Warren and Wiscombe* [1980b] and Figure 7.1) so the accelerated aging caused by the warmer snowpack further reduces the snowpack albedo, again increasing the amount of absorbed sunlight. The *GRA* and *GRB* feedback processes lead to earlier melt onset. (A competing effect of BC in snow may be to reduce the snowpack temperature gradient, which could slow the rate of snow aging [*Flanner and Zender*, 2006], but this effect has not been studied in-depth). BC accumulates at the surface with snow sublimation, and sublimation may increase or decrease as surface air temperatures increase, depending on ambient humidity changes. This either enhances or decreases surface snow BC concentrations, albedo reduction and warming (*SBC* in Figure 7.3). When melt commences, some of the hydrophobic BC is left at the snow surface [*Conway et al.,* 1996; *Doherty et al.,* 2010, Figure 10], increasing surface snow BC concentrations, further lowering the snow albedo and accelerating melting [*Flanner et al.,* 2007; *MBC* in Figure 7.3]. Climate changes driven by reduced snow and ice albedo may affect atmospheric transport pathways and wet and dry deposition rates, in turn affecting snow BC concentrations, albedo, and climate forcing (see *DAC* in Figure 7.3). The magnitude and direction of the feedback is currently unknown. On the other hand, accelerated melting caused by BC in snow leads to earlier exposure of the underlying surface (vegetation, soil, sea ice, etc.), which has a dramatically lower albedo [about 0.2 for tundra or soil, *Bøggild et al.,* 2010; 0.3-0.6 for sea ice, *Perovich et al.,* 2002] than snow [about 0.8 for new snow; about 0.7 for melting snow; Figure 1 of *Warren and Wiscombe* [1985]] and thereby warms the surface and adjacent atmosphere, a process commonly known as the snow albedo feedback (*SAF* in Figure 7.3). The *SAF* feedback only occurs when melt of seasonal snow uncovers a land or ocean surface; the melting of snow on ice sheets (*e.g.,* on Greenland) or on mountain glaciers reveals an almost equally high albedo sub-layer so the strong albedo feedback is missing. The *SAF* feedback facilitates large temperature changes (Section 8) in response to the BC snow and ice forcing discussed here. BC-induced changes in snow cover occur on a weeks to months time-scale, but the climate system also has a longer-term (months to years) memory for snow cover [*e.g., Dery and Brown,* 2007]. Northern hemisphere albedo feedback is strongest in springtime when the combined effect of snow cover and insolation is maximum and the snowpack is at or near its melt point [*e.g., Hall and Qu,* 2006; *Flanner et al.,* 2011]. Melt onset and local albedo feedback vary with latitude and altitude, however, for example, occurring later in the year on the Greenland plateau and high-elevation mountain areas.

[4] The rapid adjustments *GRB*, *MBC, SBC,* and *DAC* affect the concentrations of BC in the snow (*MBC* and *SBC*) or the change in albedo for a given BC concentration (*GRB*) and constitute 'rapid adjustments' to the initial radiative forcing, as defined in Section 1.3 and Table 1.1. Modeled radiative forcing is the net effect of the initial radiative forcing and these rapid adjustments, which together constitute what we have defined here as the adjusted forcing (Table 1.1). The rapid adjustments *GRA* and *SAF* affect the climate state itself (*i.e.,* the snow cover, *SAF*, and snow grain size, *GRA*), increasing the efficacy of the adjusted forcing. Together the adjusted forcing and high efficacy of that forcing produce an enhanced climate forcing – the effective forcing (see Section 9).

7.3. Modeled forcing

[5] *Warren and Wiscombe* [1985] and *Vogelmann et al.* [1988] originally highlighted the climatic importance of snow albedo reduction by pollutants by examining the potential impacts of a 'nuclear winter' scenario. At around the same time, measurements demonstrated that sufficient BC was already present in snow around the Arctic margin to affect climate [*Clarke and Noone,* 1985; *Warren and Wiscombe,* 1985, Figure 2]. In contrast, concentrations in Antarctica are too small to be climatically important [*Chýlek et al.,* 1987; *Warren and Clarke,* 1990; *Bisiaux et al.,* 2011]. The subject received little attention again until 2004, when *Hansen and Nazarenko* [2004] and *Jacobson* [2004] published model studies on climate forcing by changes to snow and ice albedos. *Hansen and Nazarenko* used the small number of BC-in-snow measurements available at the time to estimate the change in visible-wavelength (λ < 770nm) snow albedo due to BC for the Arctic (2.5%), Greenland (1%) and other snow-covered areas in the northern hemisphere (5%). The authors imposed these snow albedo changes and then calculated the radiative forcing and climate response. Subsequent studies have either followed the model of *Hansen and Nazarenko* [2004] in applying regionally uniform snow albedo changes [*Wang et al.*, 2011]; have scaled albedo changes based on model-derived BC deposition rates [*Hansen et al.,* 2005, 2007; and *Shindell and Faluvegi,* 2009, which used as input the radiative forcing from *Hansen et al.*, 2005]; or have prognostically determined the concentrations of BC in snow [*Jacobson*, 2004; *Flanner et al.,* 2007; *Flanner et al.,* 2009; *Koch et al.,* 2009b; *Rypdal et al.,* 2009a; *Skeie et al.*, 2011], then calculated the change in snow albedo and finally the forcing and climate response. All of these studies (Table 7.1) indicate that BC in snow produces warming both in the Arctic and across the northern hemisphere and that the climate efficacy of BC in snow is about 2 to 4 times that of CO_2, so that BC in snow has larger climatic effects than its small direct radiative forcing would suggest.

[6] These studies have raised interest because they indicate that BC may be playing a significant role in two critical areas: the unexpectedly rapid warming of the Arctic and the retreat of mountain glaciers, particularly in areas such as the Himalaya which has high levels of pollution and where local populations rely heavily on a seasonally balanced hydrologic cycle with glacial melt as a water supply in summer [*Menon et al.,* 2010]. BC in snow may also have contributed to the marked decline in Eurasian springtime snow cover since 1979, which has not been reproduced by models that only account for warming due to GHGs [*Flanner et al.*, 2009]. Accurately modeling these climatic effects requires, first, accurate representation of BC deposition fluxes (*i.e.,* the endpoint of emissions, transport, and deposition along the transport pathway), snow accumulation rates, meltwater scavenging of BC in the snowpack, and snow and sea ice distributions and cloud cover. All of these vary from model to model. Second, climate forcing calculations must account for the feedback processes shown in Figure 7.3, not all of which are included in current studies (Table 7.2).

Finally, the climate response to the radiative forcing and rapid adjustments must be accurately represented (Section 8, Climate Response).

[7] Interpretation across different model studies is complicated by the fact that they differ in terms of which feedbacks are included in each model (Figure 7.3 and Table 7.2) and in that different sources and types of light-absorbing aerosol are used in different models for the baseline and forcing scenarios. Adjusted forcing by BC in the cryosphere was calculated by *Jacobson* [2004] and *Flanner et al.* [2009] using as a baseline a snowpack that included light-absorbing soil dust, which lowers the initial albedo of the snowpack and, therefore, reduces the impact of adding other light-absorbing aerosol (Figure 7.4). None of the other studies in Table 7.2 included the impact of soil dust on snow BC radiative forcing. Some model studies calculated forcing due to fossil-fuel and biofuel (FF+BF) emissions only [*Jacobson*, 2004; *Rypdal*, 2009a; *Skeie et al.*, 2011], but others calculated the effect of all sources: fossil-fuel, biofuel and biomass burning (FF+BF+BB; *Hansen and Nazarenko,* 2004; *Hansen et al.,* 2005, 2007; *Flanner et al.,* 2007, 2009; *Koch et al.,* 2009b]. Finally, while most studies have calculated the total forcing for a given (near present-day) year, *Hansen et al.* [2005, 2007], *Koch et al.* [2009b] and *Skeie et al.* [2011] focused on the change in forcing from pre-industrial to present, defined in these studies as 1880 to 2000, 1890 to 1995 and 1750 to 2000, respectively.

[8] Here the aim is to produce best estimates of the all-source and industrial-era adjusted forcing by BC in the cryosphere and to put uncertainty bounds on that estimate. Some of the sources of uncertainty in this estimate can be quantified using existing measurements and model studies, but for other critical factors the necessary studies do not yet exist to bound the uncertainty. Sections 7.3.1 to 7.3.6 discuss factors that affect snow BC radiative forcing and rapid adjustments that amplify that forcing. Existing measurements of snow BC concentrations are then used to calculate a best-guess estimate of all-source adjusted forcing for snow BC. Model sensitivity studies are used to estimate the possible range of this forcing, based on the uncertainties that can be bounded. Industrial-era forcing is calculated by scaling the all-source forcing by the ratio of industrial-era to all-source BC emissions.

7.3.1. BC concentrations in snow and sea ice and the resulting change in albedo

[9] Studies have used a range of values for present-day and pre-industrial emissions of BC (Table 7.1). Here we use observed snow and ice BC concentrations in the present day to account for biases in the net effects of modeled emissions, transport, wet and dry depositional processes, and post-depositional processes such as snow sublimation and melting. However, no such constraint can be placed on pre-industrial snow and ice concentrations so derived industrial-era forcing relies on quite uncertain estimates of pre-industrial emissions (Section 3) and on modeled BC atmospheric transport, BC deposition rates, snow and ice cover, and climate in 1750.

[10] The change in albedo for a given concentration of BC is a function of snow grain size and of the presence of other impurities, as well as of the effective mass absorption cross section of BC in snow. As with atmospheric BC, this cross section depends on BC mixing state with and the nature of other constituents in the BC-containing particles. In snow, it also depends on whether the BC is incorporated into the snow or on the surface of snow grains. *Warren* [1982] mentioned the possibility of a factor-of-two enhancement of absorption by situating BC particles inside snow grains, citing *Ackerman and Toon's* [1981] computation for BC inside sulfate aerosols. *Chylek et al.* [1983b] then modeled this effect for snow, obtaining a factor-of-two enhancement. *Flanner et al.* [2007; 2009] obtain about a 50% enhancement for their assumptions of the mixing state.

[11] All model studies considered here other than *Hansen and Nazarenko* [2004], *Hansen et al.* [2005; 2007], and *Wang et al.* [2011] determine deposition of BC to surface snow prognostically, accounting for time-dependent emissions, transport, in-atmosphere chemical processing and aging, and wet and dry deposition rates that depend on aerosol hygroscopicity or age. However, the treatment of atmospheric aerosol processes varies considerably from model to model. For example, *Jacobson* [2004] determines BC aging by solving coagulation, condensation, and dissolution among multiple, independent, aerosol size bins and resolves cloud-borne and interstitial BC within these bins, whereas other studies track BC in a single mode and assume fixed BC aging rates, internal mixing times, and in-cloud BC fractions [*e.g., Flanner et al,* 2007, 2009; *Koch et al.,* 2009]. The *DAC* feedback in Figure 7.3 depends on modeled climate changes due to cryosphere BC forcing, as well as how modeled transport and deposition rates depend, for example, on mixing with other constituents, cloud properties, and precipitation patterns. This feedback will not exist at all in models where albedo changes are prescribed. These factors will result in differences in modeled deposition rates of BC to surface snow. Comparisons between modeled and measured surface snow concentrations are discussed in Section 7.4.

[12] Calculated albedo change for a given snow BC concentration is also handled differently across models. The *Jacobson* [2004] study explicitly calculates the change in solar and thermal-IR snow and sea-ice albedo as a function of zenith angle by solving radiative transfer through the atmosphere, snow and ice grains together, by adding a snow or ice layer to the bottom of the atmospheric layers and solving for the upward divided by downward irradiance at the top of the snow layer. The calculation is done for both interstitial BC particles and BC inclusions within snow grains, treated with a core-shell approximation. *Jacobson et al.* [2004] found that the modeled effect of BC on emissivity is small [*Jacobson*, 2004], and IR albedo changes are disregarded in all other model studies. The *Flanner et al.* [2007; 2009] studies explicitly calculate the change in solar snow albedo by solving radiative transfer through multiple layers of snow, based on theory from *Warren and Wiscombe* [1980b] and the two-stream, multiple scattering radiative approximation of *Toon et al.* [1989]. The snow albedo is then added interactively at each time step as a bottom boundary condition to an atmospheric model that accounts for the effects of atmospheric optics (*e.g.,* aerosol, clouds, etc.) on downwelling solar radiation. They treat sulfate-coated and interstitial BC species with coated BC absorbing about 50% more solar radiation per mass of BC. *Koch et al.* [2009b] parameterizes the change in albedo based on the study of *Warren and Wiscombe* [1985], which treated the BC as being

externally mixed with the snow and accounts for absorption enhancement through multiple scattering in the snow. This parameterization provides a spectrally averaged change in albedo, with dependence on snow grain size and BC concentration, but it ignores the zenith-angle and atmospheric optical dependence of the albedo. *Rypdal et al.* [2009a] and *Skeie et al.* [2011] use look-up tables of albedo based on snow grain size and BC concentration; these tables are based on Mie theory and radiative transfer calculations. Radiative transfer calculations are done with a multi-stream model using the discrete ordinate method [*Stamnes*, 1988], where two snow layers have been added below their atmospheric layers. *Hansen and Nazarenko* [2004], *Hansen et al.* [2005; 2007], and *Wang et al.* [2011] impose albedo changes so there is no dependence on BC concentration or other factors.

[13] As with snow, BC concentrations on bare (non snow-covered) sea ice similarly depend on the amount of BC wet and dry deposition to the surface. However, because sea ice is usually snow-covered in the winter to spring season, the BC concentrations in multi-year summer ice are likely a strong function of how much BC resides in the winter and spring snowpack and on how much is retained in the sea ice during melting. A few measurements of sea-ice BC concentrations are available to test models; they indicate that BC in sea ice is comparable to that in snow from the same region [*Doherty et al.,* 2010].

[14] A given concentration of BC produces a larger change in albedo in sea ice than in snow, because the surface of sea ice behaves as large-grained snow. However, sea ice also can contain significant amounts of other light-absorbing impurities, such as sediment, which as discussed below may significantly decrease the forcing by BC. Only three studies in Table 7.1 include radiative forcing by BC in sea ice: *Jacobson* [2004], *Rypdal et al.* [2009a] and *Skeie et al.* [2011]. This may explain, in part, the relatively large forcing per emission of *Jacobson* [2004]. However, forcing by BC in snow on sea ice and by BC in sea ice were not separately diagnosed so it is not possible to know how large a role these forcings played in either study. Below independent estimates are made for forcing by BC in sea ice and its possible upper and lower bounds.

7.3.2. Snow-covered area

[15] Climate forcing by BC in snow is a direct function of the amount of land or ice area covered by snow, so seasonal and sub-gridscale variations in snow cover must be accurately represented. Models allow for fractional snow cover within model gridboxes by employing snow depth dependent parameterizations. The adjusted forcings calculated by *Flanner et al.* [2007] for low and high cases of snow cover are used here to help bound uncertainty in forcing due to errors in fraction of snow covered area.

[16] The allowance for fractional snow coverage within a gridbox might not, however, account for very small-scale snow patchiness, which occurs particularly in areas with low snowfall amounts or broken up sea ice. Melt rates are higher in patchy snow than in uniform snowpacks, and melt rates increase with degree of snow patchiness and exposed area [*Liston,* 1995, 1999, 2004; *Essery,* 1997]. Accounting for this patchiness is expected to have two competing effects: Patchy snow warms and starts to melt more quickly due to local heat advection, and when the snowpack is close to its melt point, the feedbacks enhance the effect of the initial direct forcing most powerfully. On the other hand, patchy snow on land is more likely to be loaded with local soil dust, thereby lowering the 'baseline' snowpack albedo and decreasing the impact of BC (Figure 7.4). It is not known if accurately accounting for these two effects would produce a larger or a smaller radiative effect by BC in snow, so this is an unbounded uncertainty.

7.3.3. Masking by clouds and vegetation

[17] The planetary albedo of cloud-covered areas is relatively insensitive to surface albedo, so cloud cover must be accurately represented. Similarly, BC in snow masked by vegetation contributes little to ToA forcing, so vegetative cover must be accurately represented. Both cloud cover and vegetation are sub-grid-scale features, complicating their representation in models. Model representation of and forcing sensitivity to realistic ranges of cloud cover and vegetation have not been tested, and this is currently an unbounded uncertainty in cryosphere BC adjusted forcing.

7.3.4. Snow grain size

[18] As noted above, snow albedo is highly sensitive to snow grain size. Further, the change in albedo for a given snow BC concentration is greater in larger grained snow than in smaller grained snow (Figure 7.1). Thus, the snowpack BC concentration and snow-grain size must be well constrained down to the penetration depth of sunlight (about 30 cm for a typical snow density of 0.3 g cm^{-3}; *Warren and Wiscombe* [1980a], Figure 13c). 'Grain size' must also be defined consistently: in field measurements, reported values are optical grain sizes, which are proportional to the volume-to-area ratio [*e.g., Grenfell et al.,* 2005] and inversely proportional to the 'specific surface area' (*e.g.*, *Matzl and Schneebeli* [2006]). *Jacobson* [2004] and *Rypdal et al.* [2009a] and *Skeie et al.* [2011] use globally fixed snow-grain radii in their models of 150, 500 and 500 μm, respectively. Grain radii for new snow are less than 150μm, and for old, melting snow they are larger than 500 μm, so the feedbacks that involve grain size (*GRA, GRB* in Figure 7.3) are not captured. The net effect of applying a fixed snow grain size is not known. However, *Flanner et al.* [2007] used a model to determine how a reasonable range in snow aging rate (*i.e.*, the rate of grain size growth) affects the derived annual mean adjusted forcing. These results are used to help bound the possible range of radiative forcings by BC in snow.

7.3.5. Albedo dependence on downwelling radiation

[19] In addition to being a function of snowpack properties, both pure and contaminated snow albedo depend on solar zenith angle and the fraction of direct versus diffuse solar radiation. Models that prescribe solar-zenith-angle-independent albedos may have a bias in clear-sky albedo of several percent for pristine snow [Figure 6 of *Wiscombe and Warren*, 1980], which is of the same magnitude as the albedo perturbation by BC. Direct and diffuse solar radiation must also be accurately represented, in turn requiring accurate representation of cloud cover.

7.3.6. Concentration of BC with sublimation and melting

[20] Precipitation rates and relative humidity in much of the Arctic are low, so in some areas appreciable (up to 30-50% [*Liston and Sturm*, 2004]) surface snow is lost to sublimation.

This process removes snow water but leaves BC and other non-volatile particulate constituents at the snow surface, increasing their concentration. Similarly, variable fractions of BC are left behind at the snow surface with melt, depending on the hygroscopicity of accompanying constituents [*Conway et al.,* 1996]. *Flanner et al.* [2009] apply a 'scavenging efficiency' for BC with melt of 0.2 for hydrophilic BC and 0.03 for hydrophobic BC, based on the *Conway et al.* [1996] study. *Rypdal et al.* [2009a] and *Skeie et al.* [2011] leave all BC at the snow surface as the snow melts, and all other models cited here allow all BC to be washed away with snow melt water. While there is some observational evidence of BC remaining at the surface during melt [*Conway et al.,* 1996; *Xu et al.,* 2006; *Doherty et al.,* 2010], an appropriate BC scavenging ratio remains to be determined. A model sensitivity study which applies a range of melt scavenging efficiencies is used to help bound this source of uncertainty.

7.3.7. Representation of all light absorbing particles in snow

[21] Particulate matter in snow is never pure BC. BC from biomass, biofuel and fossil-fuel burning is accompanied by varying amounts of 'brown' organic carbon. Other sources also produce light-absorbing carbon [*Andreae and Gelencsér,* 2006] and light-absorbing crustal material (*e.g.,* hematite in soil dust). Calculation of BC effects on snow and ice albedo and melt rates must consider *all* light-absorbing constituents in the snow. Glacial snow especially often has high concentrations of locally sourced soil dust and sand that significantly reduce its albedo. While the *Jacobson* [2004] and *Flanner et al.* [2009] studies included soil dust in snow in their baseline calculations, these models don't account for very local sources of coarse-grained (>>10μm) dust and sand, which have an extremely short atmospheric lifetime. Particularly in areas with patchy snow cover, local soil and sand may be present in the snow at high concentrations. This observation was made along the Arctic coast of Siberia (S. Warren and T. Grenfell, personal communication), in Inner Mongolia [*Huang et al.,* 2010] and on summertime Arctic sea ice (B. Light and T. Grenfell, personal communication) during snow and ice sampling surveys. The bias this introduces to modeled forcing cannot currently be bounded. However, the *Flanner et al.* [2009] model can be used to help constrain the impact of including dust deposition to snow. In this model, when dust is included the snow BC radiative forcing is decreased by about 25% for the global mean dust burden of 4.3 ppm calculated in the model. This result is consistent with Figure 7.4, which shows a snow albedo reduction of about 0.006 for a pristine snowpack with 20 ng g^{-1} of BC and an albedo reduction of about 0.005 for a snowpack with 4000 ng g^{-1} of dust and 20 ng g^{-1} of BC. These results indicate that the albedo reduction due to BC is 20% less in the presence of dust.

[22] Importantly, most studies that have measured [*Xu et al.,* 2006; *Ming et al.,* 2009] or estimated [*Yasunari et al.,* 2010; *Castelvecchi,* 2009] BC concentrations for Himalayan glaciers have estimated a significant radiative forcing, but this was by comparing clean (dust- and algae- free) snow to clean snow with BC added. In the Himalayan spring season, when the glacier snow starts to melt and when BC may have its maximum impact, is also when precipitation is at a minimum and when there are large dust events over the Tibetan Plateau and across the Himalaya [*Ming et al.,* 2009; *Marinoni et al.,* 2010]. In addition to being exposed to dust from Central Asia and the Middle East, the south side of the Himalaya can experience significant dust loading from sources in northern India [*Marinoni et al.,* 2010]. Similarly, dust storms from the Sahara can account for a significant fraction of the impurities in Alpine snow [*Thevenon et al.,* 2009; *Haeberli,* 1977], and dust from the Colorado Plateau drives a very large radiative forcing of snowpack in the San Juan Mountains [*Painter et al.,* 2007]. The lower parts of many Himalayan glaciers are entirely hidden by thick debris cover [*Nakawo et al.,* 2000], actually inhibiting melt. Future studies must account for the effects of crustal and other light-absorbing material [*e.g.,* algae; *Jones et al.,* 2001] in mountain glaciers when determining the effects of BC on snow melt.

[23] Measurements from across the Arctic indicate that typically 30 to 50% of sunlight absorbed in the snowpack by impurities is due to constituents other than BC [*Doherty et al.,* 2010]. Either organic matter or soil dust could be responsible, and the spectral absorption measurements can not distinguish them, but chemical analysis of a geographically diverse subset of these Arctic samples indicates that the non-BC light absorbing particulate matter is overwhelmingly light-absorbing OC, not mineral dust [*Hegg et al.,* 2010]. These samples were collected specifically trying to avoid snow that obviously contained significant amounts of soil, dust, or sand, so they may somewhat underrepresent the role of these particles in snow. Regardless, these measurements make it clear that particles other than BC play a significant role in changing snow albedo. While *Flanner et al.* [2007 & 2009] did not include snow OC light absorption in their published forcing calculations, they did test for the effect of OC on snow albedo and found it to be sufficiently small that omitting it would not significantly change their results. If organic matter is in fact a significant source of light absorption in snow, the climate forcing by sources high in OC (*i.e.,* BF and BB) would be larger because of the addition of light-absorbing OC. However, if biomass burning and soil dust emissions are considered a 'natural' source of aerosol, this would mean the natural snowpack has a lower albedo, thus lessening the effect of mitigating anthropogenic sources. On the other hand, mitigating biofuel emissions or any burning which produces light-absorbing OC, or decreasing soil dust emissions would have a larger impact than would be implied by only considering the effect of BC.

[24] These results highlight the importance of determining not only the concentration of snow BC but also light-absorbing OC and soil dust in snow. In addition, while the wavelength dependence of absorption of BC has been studied and is relatively well-constrained to follow λ^{-1}, the wavelength dependence of absorption (or, equivalently, the size distribution and spectrally resolved indices of refraction) for light-absorbing organics and soil dust appear to be quite variable [*e.g., Bond,* 2001; *Kirchstetter et al.,* 2004; *Bergstrom et al.,* 2007; *Sun et al.,* 2007; *Russell et al.,* 2010], making estimates of the impact of OC and dust on light absorption in snow highly uncertain.

7.4. Measurements of BC in snow and comparison with models

[25] As shown in Table 7.1, model studies to date have used a range of assumptions about the sources and quantity of BC

emissions. Similarly, atmospheric transport processes differ from model to model, as do deposition rates. For example for the suite in Table 7.1, the fraction of BC deposited to surface snow by wet (versus dry) deposition ranges from 71% [*Koch et al.,* 2009b] to 98% [*Jacobson*, 2004]. Measurements of snow BC concentrations can be used to test models for the combined influence of all of these factors. Data are available from the Arctic and sub-Arctic, a few mid-latitude locations in the northern hemisphere and the Antarctic. Here we limit model/measurement comparisons to northern hemisphere sites, because concentrations in Antarctic are too small (generally <1 ng g^{-1}; [*Chýlek et al.,* 1987; *Warren and Clarke,* 1990; *Bisiaux et al.*, 2011]) to be important for climate forcing evaluations.

7.4.1. Measurement methods

[26] BC concentrations in snow have been measured using variations of the thermo-optical method [*Chýlek et al.,* 1987; *Cachier and Pertuisot,* 1994; *Lavanchy et al.,* 1999; *Xu et al.,* 2006; *Jenk et al.,* 2006; *Hagler et al.,* 2007a,b; *Legrand et al.,* 2007; *Ming et al.,* 2008; *Forsström et al.,* 2009; *Ming et al.,* 2009; *Thevenon et al.,* 2009; *Xu et al.,* 2009; *Hadley et al.,* 2010] and with an SP2 instrument [*McConnell et al.,* 2007; *McConnell and Edwards,* 2008], both of which are described in Section 2.5. They have also been measured using a third, filter-based method that optically analyzes BC concentrations, used first by *Clarke and Noone* [1985] in the form of the IP Spectrophotometer and later with an improved instrument, the ISSW Spectrophotometer [*Grenfell et al.,* 2011; *Doherty et al.,* 2010]. Using the wavelength-dependence of the measured light absorption it is possible, assuming known BC MAC, to calculate the maximum possible BC concentration, an estimated BC concentration, and the fraction of absorbed solar radiation (integrated 300-750nm) that is due to species other than BC, such as light-absorbing organic carbon and crustal material [*Grenfell et al.,* 2011; *Doherty et al.,* 2010]. Here, modeled values are compared with BC concentrations from the IP and ISSW spectrophotometers, thermo-optical measurements and from the SP2.

7.4.2. Arctic and sub-Arctic snow

[27] Table 7.3 gives measured concentrations of BC in surface snow for various regions of the Arctic. Because the snow-albedo feedback is greatest in spring, most of these measurements were of surface snow in March, April or early May; all are from snow that has not yet experienced melting (and therefore the feedback *MBC* in Figure 7.3) but which may have experienced sublimation (feedback *SBC* in Figure 7.3). These are compared to average surface snow (top 2 cm) concentrations from the *Flanner et al.* [2009] study and to the concentration of BC deposited in snow (via both wet and dry deposition) in the *Koch et al.* [2009b] study. Model average values were calculated using the modeled concentrations from the same month and location (gridbox) as the measurements. In addition, *Skeie et al.* [2011] include a comparison of their modeled snow BC concentrations with measured values reported by *Forsström et al.* [2009] and *Doherty et al.* [2010] for Arctic and sub-Arctic regions. These comparisons are imperfect but allow a first-order check of how well the models are representing BC deposition to the snowpack. The concentrations shown in Table 7.3 produce a change in snow albedo of <5%, which would not be visible to the human eye. In common images of snow visibly darkened by light-absorbing impurities, the impurities are often sand and soil, not BC.

[28] The comparison herein has been limited to two of the six studies which calculated snow BC concentrations (*Flanner et al.*, 2009 and *Koch et al.*, 2009b; Table 7.2) for which modeled snow BC is readily available, and to discussion of the *Skeie et al.* [2011] model and observation comparison. For reference, total, present-day BC emissions from *Flanner et al.* [2009] (7400 Gg yr^{-1}) and *Koch et al.* [2009b] (8200 Gg yr^{-1}) are between the central bottom-up all-source estimate of 7300 Gg yr-1 (Section 3) and the all-source emissions (10100 Gg yr^{-1}) based on a comparison of modeled and measured AAOD (Section 5). The *Hansen et al.* [2005] total present-day BC emissions (11000 Gg yr^{-1}) are larger than either of these estimates. *Jacobson et al.* [2004] total BC emissions are within 5% of the total emissions of *Flanner et al.* [2009], though there is a higher fraction of BB emissions in *Jacobson et al.* than in *Flanner et al.* (44% vs. 35%), and BB emissions are less likely to be deposited to snow [*Flanner et al.,* 2009; *Skeie et al.,* 2011]. The *Rypdal et al.* [2009a] FF+BF emissions are 13% and 18% higher, respectively, than those in *Flanner et al.* [2009] and *Koch et al.* [2009b] studies; *Rypdal et al.* [2009a] did not include BB emissions in their analysis. The *Flanner et al.* [2009] study was specifically run for a representative biomass-burning year and so is a better comparison to measurements than the *Flanner et al.* [2007] study, which explored two extreme (high and low) BB years. Differences in transport and deposition rates also affect the concentration of BC in snow, but this comparison still provides a first-order test of the models. Broad patterns in the observed spatial variability of snow BC concentrations are qualitatively consistent with the model results. Both have higher concentrations of BC in snow over northwestern Russia, Europe and Scandinavia than across the western Arctic and Greenland. However, there are important quantitative differences.

[29] The *Koch et al.* [2009b] modeled values are in agreement with the measured values for Arctic Canada and northern Russia, are biased high in the Arctic Ocean, and are biased low compared to the measurements in all other regions other than Greenland, where they are about a factor of two too high. In contrast, the *Flanner et al.* [2009] model values are somewhat lower than the measured values for northern Russia, Barrow, and sub-Arctic Canada but are higher than the measured values at all other sites. The differences are particularly profound for the Scandinavian sites, where they are 1.6 to 3.4 times the measured concentrations. Notably, these sites also have the highest concentrations and so carry more weight than the other sites at similar latitudes in terms of global radiative forcing. For Greenland, values are shown for both spring (April) and summer (July to August). Only about 25% of the Greenland Ice Sheet is in the 'dry snow zone'; everywhere else some melting occurs during summer. There is a striking increase in Greenland values in the *Flanner et al.* model when moving from spring to summer that is also present in the measurements, but not as pronounced (Table 7.3). Based on the timing and spatial pattern of the increase it appears to be caused by the concentration of BC at the surface with melt, indicating that the *MBC* feedback (Figure 7.3) may be too strong in *Flanner et al.* [2009] study. The timing and extent of melt is clearly critical in this process and needs to be validated against

observations; the limited data presented here are insufficient. Furthermore, improved model treatment may be needed for particle accumulation in perennial snow and ice-sheets, where (in the absence of glacier dynamics) snow either accumulates year after year or is 'capped.'

[30] *Skeie et al.* [2011] prognostically determined snow BC concentrations from all sources (FF+BF+BB) and compared these to measured concentrations. Their forcing was calculated for the FF+BF sources only, but biomass burning only accounted for 4 to 12% of BC in snow north of 65°N. Their comparison with the *Forsström et al.* [2009] measurements indicates that the modeled snow BC concentrations for 2001 to 2008 vary over about the same range as the measured concentrations in 2007 in Ny Ålesund, Svalbard. However, they are much lower than observed concentrations at the Scandinavian sites Pallas, Tromso and Abisko, with underestimates sometimes more than a factor of four and typically at least a factor of two. The exception is in the later spring when the snow starts to melt and in the model all BC consolidates at the snow surface. At this time, modeled surface snow BC concentrations increase by approximately 10-fold. The comparison with the geographically broader snow BC data set of *Doherty et al.* [2010] only includes snow samples that had not yet experienced springtime melt. This comparison shows reasonable agreement for the Canadian and Alaskan Arctic and for Greenland, it indicates a low bias in the model over the Arctic Ocean, and it shows large model underestimates for the Canadian sub-Arctic, across Russia and in Svalbard. Model underestimates vary from about a factor of two (Svalbard) up to a factor of five (Eastern Russia). Notably, this is the region where BC concentrations (and, thus, forcing) are expected to be largest.

7.4.3. Mid-latitude snow measurements

[31] Few measurements of mid-latitude snow exist, despite the fact that the climate impacts of BC in snow at these latitudes may be larger than for Arctic snow because of the combination of higher BC concentrations and higher insolation. *Flanner et al.* [2007] include a comparison of their modeled values for 1998 and 2001 to those measured in the 1980's and 1990's at select mid-latitude sites in North America and Europe (see their Table 2). Modeled concentrations at some sites are about one third to one half the measured values (rural and urban Michigan, USA, and in Lithuania). At other sites they are about equal to the measured values (Cascade mountains in Washington State in the USA and the French Alps in Europe) or are higher by factors of about 1.5 - 7.7 (West Texas and New Mexico in the USA and Halifax, Nova Scotia, in Canada). *Hadley et al.* [2010] measured snow BC concentrations at three remote sites in Northern California and found they were a factor of two to four lower than predicted by *Flanner et al.* [2007] and *Qian* [2009]. The sparseness of these data and the mismatch between the years modeled versus the time of the measurements makes it difficult to draw conclusions.

[32] A snow survey described by *Huang et al.* [2010] provides the possibility of a more robust comparison of mid-latitude snow concentrations. Huang and colleagues sampled snow across north China, reporting concentrations, for example, in northeast China of 600 ± 300 ng g^{-1} at latitudes of 41 to 46°N that decreased to about 40 ng g^{-1} at more northerly latitudes (51°N). These values are based on visual estimates of filter samples; estimates for samples from central and western China were not provided. These samples will be processed with the ISSW Spectrophotometer (described by *Grenfell et al.* [2011] and employed also by *Doherty et al.* [2010]), allowing for comparison with model concentrations.

[33] No other geographically broad data set exists of mid-latitude snow BC concentrations, so it is not possible at this time to bound how well models represent mid-latitude snow BC albedo reductions.

7.4.4. BC in mountain glaciers

[34] BC in mountain snow and glaciers is of concern primarily because of the potential for affecting melt rates and, therefore, the seasonality of and trends in water supplies. The effect of BC in glacial snow differs from BC's effect on seasonal snow because in the former melting does not lead to exposure of the underlying Earth surface, except perhaps at the very margins of the glacier which are anyhow often loaded with light-absorbing soil dust. Thus, the powerful albedo feedback present for seasonal snow (SAF in Figure 7.3) is absent.

[35] Few measurements exist of BC in mountain glaciers, and in most cases they do not permit separation of the role of local versus remote sources, nor are they accompanied by coincident measurements of other light-absorbing impurities. Using a global model to determine snowfall and aerosol deposition to glaciers is particularly difficult because of their small size relative to a model gridbox (Table 7.1), allowing for only one BC concentration per gridbox, regardless of, for example, the dramatic altitude variations in mountainous regions. As discussed above, climate forcing by BC in snow also depends on accurate representation of snow and glacier cover. The coarse resolution of most models makes this representation quite difficult in mountainous areas and in areas with sparse snow cover, such as the Tibetan Plateau (*e.g.,* Figure 2 of *Qian et al.*, 2011).

[36] Ice cores from the European Alps provide historical time series but don't reach present-day and are reflective of glacial ice concentrations, not snow concentrations. Nonetheless, they provide information on the trends in BC deposition to the European Alps and some indication of near-present-day levels. *Jenk et al.* [2006] found a 1900-1940 average BC concentration of 31 ng g^{-1} (range: 9 to 22 ng g^{-1}); *Thevonon et al.* [2009] found a 1950-1980 average of about 20 ng g^{-1}; and *Legrand et al.* [2007] reported concentrations for 1960-1990 of about 10 to 17 ng g^{-1}, with the peak concentrations around 1960 and a decline thereafter. These studies also indicate a shift in the dominant source of BC from biomass burning in the 19th century to coal and later to non-coal fossil fuel. Modeled snow concentrations for present day from *Flanner et al.* [2009] gridboxes corresponding to the measurement sites in these studies range from approximately 115 to 160 ng g^{-1} in January through March, then decline to about 10 to 50 ng g^{-1} in April. Summertime (May-August) concentrations are zero, because all surface snow is assumed to have melted and BC in the glacier itself is not accounted for. In contrast, BC in the deposited snow in the *Koch et al.* [2009b] model increases from about 20 to 25 ng g^{-1} in January to about 50 ng g^{-1} by early summer, much more in line with the measured concentrations in mid-20th century glacial ice.

[37] Analysis by *Xu et al.* [2006] of snow samples taken in 2001 on the Tibetan Plateau and by *Ming et al.* [2009] of samples taken in 2004-2006 from glaciers on the Tibetan Plateau and in northwest China (Xinjiang) yield a median concentration for the surface snow of 29 ng g^{-1} with a large range, from a low of 7 ng g^{-1} to a high of 446 ng g^{-1}. Excluding the latter sample, which was collected from a site where the surrounding rock is rich in coal, the highest surface snow concentration was 107 ng g^{-1}. Overall, concentrations were highest in Xinjiang and in the central Tibetan plateau, with the lower concentrations along the edge of the plateau, particularly along its southern margin. These measurements were made across a range of months, from spring to fall. *Flanner et al.* calculate monthly average concentrations, but in almost all gridboxes in this region there is no snow from June through summer, so the medians and ranges are given for March to May for the suite of gridboxes corresponding to the sample sites in *Xu et al.* [2006] and *Ming et al.* [2009], respectively: March (303 ng g^{-1}; 89 to 462 ng g^{-1}), April (98 ng g^{-1}; 20 to 459 ng g^{-1}), May (14 ng g^{-1}; 14 to 36 ng g^{-1}). Two things are striking: first, model values in early spring are markedly higher than the observed values. Second, model values drop off precipitously moving from spring to early summer, corresponding to the switch from the pre-monsoon to monsoon season. Consistent with this result, *Ram et al.* [2010] and *Marinoni et al.* [2010] found *atmospheric* concentrations of BC in the Himalaya to be much higher in the pre-monsoon period than during the monsoon due to changes in transport and increased scavenging in monsoon precipitation. However, shallow ice cores and snow samples from the Himalaya provide mixed results on snow BC seasonality, with maxima in *summer* at a site on the northeast side of Mt. Everest [*Ming et al.,* 2008] but maxima in *spring* in northwest China [*Ming et al.,* 2009], though these measurements may reflect changes in both deposition and consolidation of surface BC with melt. Notably, the springtime maximum in northwest China was associated with a very heavy dust layer in the snow, so the impact of the BC on snow albedo is moderated.

7.4.5. Trends in Arctic snow BC

[38] While most model studies (*e.g.,* as given in Table 7.1) have focused primarily on the role of BC in recent warming trends, anthropogenic emissions of BC in some regions were much higher in the past and are declining, while in others they are rapidly increasing above historical levels. A small number of ice core records of BC are available to test models' historical representation of BC trends, and atmospheric BC trends for the Arctic can be used as an indicator of likely trends of BC deposition to snow in this region.

[39] Near-surface atmospheric measurements since 1989 at Alert, Ellesmere Island [82°30′N 62°19′W; *Sharma et al.* [2006]; *Gong et al.* [2010]], and since 1998 at Ny Ålesund, Svalbard, Norway [78°55′N 11°56′E; *Hicks and Isaksson* [2006]; *Eleftheriadis et al.* [2009]; *Forsström et al.,* 2009]] also show that Arctic BC concentrations have been declining in recent decades. Ice cores from the Greenland plateau provide insight to longer-term trends. The Greenland cores reflect free-troposphere concentrations of BC and are most strongly influenced by fires and anthropogenic activity in North America [*McConnell et al.,* 2007]. These records indicate that Greenland snow, preceding any human activity, had BC concentrations of about 1.1 to 2.5 ng g^{-1} [*i.e.,* 4-6,000 ybp; *Chýlek et al.,* 1987], or about half the concentrations for the past few decades (1 to 4 ng g^{-1}) [*Cachier and Pertuisot,* 1994; *Chýlek et al.,* 1995; Table 7.3]. Ice core analyses by *McConnell et al.* [2007] and *McConnell and Edwards* [2008] that span the industrial era show that from 1788 to about 1850 Greenland had relatively low concentrations (about 2 ng g^{-1}) of BC associated with biomass or biofuel burning and then a rise occurred to an average of about 10 ng g^{-1} (D4 core) or about 20 ng g^{-1} (ACT2 core), peaking around 1910. After this, BC concentrations declined steadily through the 1940s, finally dropping sharply in 1952 to nearly pre-1850 values. This post-1850 peak in BC was associated with coal burning, with the decline in BC in the mid-1900's associated with air pollution controls, improved combustion and a fuel shift from coal to oil and gas. An ice core on Mt. Logan in the St. Elias range, Yukon, Canada [*Holdsworth et al.,* 1996], shows a similar BC increase starting in the mid-1800's, though these data only extend to about 1950 so it is not possible to determine if there was a subsequent decline. An ice core from the St. Elias range is being analyzed and may help elucidate century-timescale trends on that side of the Arctic (J. McConnell, personal communication).

[40] Notably, the early 20th century peak in BC in the Greenland ice core (about 1890-1950) leads by about 20 years a period of strong positive regional surface-air temperature anomalies from 1920 to 1965 [*e.g.,* see Figure 2 of *Polyakov et al.* [2002]; Figure 3 of *Shindell and Faluvegi* [2009]]. It is expected that the full climate response to a forcing lags the imposed forcing, because of the ocean's heat capacity, for example, so this does not necessarily negate the possibility that the high BC concentrations led to the observed warming. This warming has generally been attributed to solar and natural variability. However *Shindell and Faluvegi* [2009] point out that, in their model, only about half of the early 20th century Arctic (60° to 90°N) temperature rise can be attributed to the combined effects of GHGs, natural forcings and tropospheric O_3. Natural variability is unable to account for the remainder in most models, inferring that a portion of the warming should be interpreted as due to aerosol climate forcing. In a model study of historic aerosol impacts on climate, *Koch et al.* [2011b] calculate a maximum in BC deposition to Arctic snow about 1950 and a peak BC radiative forcing about 1940 to 1970, with declines since then. The peak in radiative forcing correlates well with the Greenland trends of *McConnell et al.* [2007]. *Skeie et al.* [2011] modeled trends in snow BC radiative forcing by fossil-fuel and biofuel sources, reporting forcing relative to year 1750 in the year 1850 and then once per decade from 1900 to 2000. Forcing relative to 1750 is about 0.005 Wm^{-2} in 1850, more than doubles between 1850 and 1900 to about 0.013 Wm^{-2} and increases steadily from 1900 to 1960 to about 0.019 W m^{-2}. After this, forcing varies by about 0.03 W m^{-2} with no apparent trend from 1960 to 2000 [*Skeie et al.,* 2011, Figure 16b]. Thus, this study does not show a forcing peak in the mid-1900's, but it does indicate that snow BC forcing has not appreciably increased since 1960.

[41] In summary, both observations and model studies indicate that BC may in fact have played a significant role in the observed early 20th century Arctic warming. Further, radiative forcing by BC in Arctic snow likely has not increased since the mid-1900's and may instead be declining.

7.4.6. Trends in mountain snow

[42] Several ice core studies from the European Alps provide insight into trends and sources of BC in snow through the industrial era. These data show two features: first, a sharp increase in BC starting in the late 19th century and, second, a transition to fossil fuel as a significant source of BC. At the three locations studied, concentrations increased from the turn of the century to 1940-1950, with peak concentrations of about 15 to 25 ng g^{-1} [*Jenk et al.,* 2006; *Legrand et al.,* 2007; *Thevenon et al.,* 2009]. Only two of the three records extend past 1940 with one showing a slight increasing trend and the other showing a declining trend. These differences may be due to differences in exposure to local pollution sources.

[43] Trends in BC deposition to the Himalaya or Tibetan regions have been measured using ice cores from Mt. Everest [*Ming et al.,* 2008; *Xu et al.,* 2009] and at four other sites on the Tibetan Plateau [*Xu et al.,* 2009] using the thermal-optical method, with records extending about 1952-2004. These records show a great deal of spatial and temporal variability in concentrations, reflecting the variations in source regions and meteorology. Values typically average about 10-40 ng g^{-1}. However, some commonalities are apparent: all but the easternmost site show elevated concentrations from about 1950 (the earliest part of the record) to the early to mid-1970s, which *Xu et al*. attribute to eastern European sources. Concentrations then remain somewhat lower up until about 1990-1995, after which concentrations at most sites indicate increasing but variable concentrations. Thus, unlike the Arctic, it appears that BC radiative forcing may be increasing in the Himalaya.

7.5. Sources of BC to Arctic and Himalayan snow

[44] Currently, there are few sources of pollution within the Arctic itself so almost all BC is transported there from the mid-latitudes. In the winter and spring seasons, when BC deposition to snow is most climatically important, a 'dome' of cold air over the Arctic makes it difficult for air from lower latitudes to enter the Arctic troposphere. Typically, the front formed by this dome reaches to lower latitudes on the Eurasian side of the Arctic than on the North American side, making it easier for Eurasian sources to influence the Arctic troposphere [*Stohl*, 2006]. In order for air masses to cross the polar front, they must originate in cold, dry locations and, typically, follow surfaces of constant potential temperature into the Arctic [*Iversen*, 1984; *Law and Stohl,* 2007]. Thus, air masses originating along the relatively warmer, moister North American and Asian east coasts can not readily enter the Arctic troposphere. While they can be lifted (*e.g.*, in warm conveyor belts) to high altitudes where they can be transported over the Arctic, this pollution is unlikely to be deposited to the snow surface via wet or dry deposition, except on the high Greenland plateau.

[45] A model study by [*Koch and Hansen*, 2005] evaluating regional contributions to the Arctic haze found that Asian sources dominated total atmospheric column aerosol load, but near-surface concentrations were dominated by sources in Europe and Russia. *Stohl* [2006] also found lower tropospheric aerosol sources to be dominated by European and Russian emissions. This was reinforced by a multi-model study of pollutant transport to the Arctic from the source regions of North America, Europe, South Asia and East Asia, which found that the greatest impact on surface-deposited BC in the Arctic comes from European emissions [*Shindell et al.,* 2008]. These results should be viewed with caution, as models appear to have a particularly difficult time predicting Arctic and northern Eurasian tropospheric BC concentrations and atmospheric vertical distributions, due to uncertainties and biases in transport, removal and vertical diffusion mechanisms [*Koch et al.,* 2009a]. Further, the *Shindell et al.* [2008] study did not include northern Eurasia as a source region. However, in the springtime there is extensive agricultural burning in western Russia and there are widespread forest fires across Russia, particularly in the east. The former is clearly an anthropogenic source, and it appears that the latter may be as well: one study has estimated that fully 87% of fires in boreal Russia are man-made [*Mollicone et al.,* 2006]. Given this result, the high latitude of this region (>50 - 70°N) and the tendency of the polar front to drop to lower latitudes on this side of the Arctic, the impact of northern Eurasian biomass burning emissions to Arctic-wide BC (and OC) in snow may be significant.

[46] Indeed, biomass burning appears to be the source of high-concentration plumes observed in the Arctic in recent years, with Russian biomass burning playing a particularly prominent role during the measurements of the International Polar Year (2007-2008) [*Stohl et al.,* 2007; *Warneke et al.,* 2009; *Paris et al.,* 2009; *Jacob et al.,* 2010]. These observations may be more anecdotal than representative, because they are from individual large events [*e.g., Stohl et al.,* 2007] or were made during particularly strong biomass burning years (*e.g.,* 2007-2008) or in sampling locations particularly influenced by biomass versus fossil-fuel burning [*e.g., Warneke et al.,* 2009]. However, chemical analysis of snow samples from 36 sites across the Arctic (Alaska, Canada, Greenland, Russia, and the Arctic Ocean near the north pole) also indicates that the majority (in most cases, >75%) of the BC in surface snow is associated with biomass or biofuel burning [*Hegg et al.,* 2009; *Hegg et al.,* 2010]. Those analyses are from a geographically broad but limited number of samples, all from 2007 to 2009, and they do not yet include samples from the Scandinavian sector of the Arctic, where both models and measurements [*Forsström et al.,* 2009; *Doherty et al.,* 2010] indicate that concentrations are relatively higher and more influenced by fossil-fuel burning than in the rest of the Arctic. These factors may be biasing the conclusions of *Hegg et al.* [2009 and 2010] toward the role of biomass or biofuel emissions in Arctic BC. The model experiments of *Flanner et al.* [2007] attribute 4.5 ng g^{-1} BC in Arctic snow to FF sources, 1.7 ng g^{-1} to BF sources, and 1.9 to 4.7 ng g^{-1} to BB sources, depending on the strength of the boreal fire year, also suggesting a potentially dominant contribution from biomass or biofuel sources. However, *Skeie et al.* [2011] only attribute about 10% of snow BC to biomass burning sources, and *Flanner et al.* [2009] only attribute 25% of present-day snow BC forcing to biomass burning in a "typical" biomass-burning year. Despite the uncertainty, it is important in the context of mitigation decisions to recognize that biomass and biofuel emissions may be a significant source of BC to Arctic snow.

[47] Consistent with Greenland's physical location, the *Shindell et al.* [2008] multi-model study determined that surface-deposited BC in Greenland comes predominantly from North America and Europe in the fall and winter. In the spring,

synoptic systems in Asia loft pollutants to higher altitudes, where they can be transported long distances. Accordingly, they calculated that for the Greenland Ice Sheet – most of which is at high altitudes – BC deposition is most strongly influenced in the spring by East Asian emissions. Chemical analysis of surface snow samples from the Greenland plateau indicate that the BC is largely from biomass or biofuel burning sources in the spring and that fossil-fuel sources dominate in the summer [*Hegg et al.,* 2009, 2010]. In any case, as noted above the Greenland Ice Sheet has very low concentrations of BC in its surface snow (typically <3 ng g^{-1}) and so the radiative forcing by BC in Greenland snow is likely small.

[48] At lower latitudes, sources of BC in snow can be either local or the end-point of long-range transport and can be highly variable not only with season but even within a day, due to the influence of, for example, thermal winds in lifting pollution from populated areas up onto the high mountain glaciers [*Marinoni et al.,* 2010]. In the Himalaya, the south side of the mountains is exposed to pollutants and soil dust from the Indian subcontinent, with some influence from westerly winds from the Middle East, whereas on the north side of the mountains the prevailing exposure is to pollutants from the Middle East [*Xu et al.,* 2009]. However, terrain, meteorological and local sources of BC are sufficiently varied that it is difficult to make generalized statements about the sources of BC to Himalayan snow.

7.6. Estimate of forcing by BC in the cryosphere

7.6.1 Adjusted forcing by BC in snow

[49] Forcing by BC in snow results from the radiative forcing due to the initial albedo reduction when BC is deposited in snow and the rapid adjustment to that forcing through the positive feedbacks *MBC*, *SBC* and *GRB* (Figure 7.3), resulting in the adjusted forcing. Comparable values of forcing by BC in snow are calculated by scaling forcing as derived in model studies to the common base of present-day forcing due to all sources (FF+BF+BB). The *Flanner et al.* [2009] and *Koch et al.* [2009b] modeled adjusted forcings are then scaled based on the biases found in the measurement-model comparison of snow BC concentrations. From these, a representative central estimate is determined. In addition, all studies are normalized to forcing per emission (μW m^{-2} per GgC yr^{-1}) to isolate differences in total emissions from differences in all other model processes that lead to cryosphere BC climate forcing (Table 7.2). For studies that do not report present-day forcing by BC emissions from FF+BF only, the adjusted forcing is calculated by scaling total to FF+BF emissions, in order to provide comparable forcings for what roughly might be considered the minimum 'anthropogenic' BC. Industrial-era (1750 to 2010) forcing is estimated by scaling total present-day forcing based on the ratio of present-day to pre-industrial BC emissions. In scaling by emissions, we use two model studies to account for differences in the amount of biomass burning versus fossil and biofuel emissions that are deposited to snow. Finally, the model sensitivity studies of *Flanner et al.* [2007] and runs from *Flanner et al.* [2009] are used to establish low and high uncertainty forcing bounds based on uncertainties in emissions, rate of snow aging (grain size), the efficiency with which BC is scavenged from surface snow during snow melt, snow cover fraction, the light absorption efficiency of BC, and the reduction in snow BC radiative forcing due to the presence of dust in the snow.

[50] This analysis does not encompass all sources of uncertainty in snow BC adjusted forcing, only those where information is available to set bounds. There are two weaknesses in this approach. First, forcing does not scale linearly with snow BC concentration. This affects both our uncertainty analysis and the scaling of all-source to industrial-era forcing, which is based on scaling by emissions. As with other agents, the forcing increase per unit mass of additional BC decreases with increasing BC amount, as indicated in Figure 3a of *Flanner et al.* [2007]. Second, snow BC concentrations do not scale linearly with global, annual average changes in BC emissions, since the amount of BC deposited in snow from any given source depends on its location and season – *i.e.,* a large increase in sub-Saharan Africa biomass burning has very little effect on BC concentrations in Arctic snow. We attempt to account for this using information from models on the relative role of biomass burning in snow forcing versus its fraction of global, annual emissions. However, there are likely significant but unquantified uncertainties associated with this adjustment, especially for pre-industrial snow BC forcing.

[51] The relative roles of biomass burning, fossil fuel and biofuel in BC cryosphere forcing is a function of their relative emissions, seasonal timing of emissions, and of the fraction of each that are deposited to surface snow and ice. The present-day fraction of emissions due to BB reported in the studies in Table 7.2 range from a low of 30% in a low BB year (2001; *Flanner et al.* [2007]) to a high of 47% in a high BB year (1998; *Flanner et al.* [2007]), with the rest falling in the range 35 to 45% (all other studies in Table 7.1). *Flanner et al.* [2009] attributed 25% of present-day BC-in-snow forcing to biomass burning emissions. However, *Skeie et al.* [2011] attribute only 10% of the present-day BC in snow north of 65°N to BB. In both studies biomass burning is about 35% of global, annual average present-day BC emissions, so this discrepancy must be due to differences in modeled aerosol transport, BC mixing ratios in falling snow, and dry deposition rates from BB versus BF+FF sources, and to feedbacks included in the two models (Table 7.2). Seasonality and non-linearities in forcing per change in snow BC concentration may also be contributing, since *Flanner et al.* [2009] report the fraction of forcing whereas *Skeie et al.* [2011] report the fraction of BC in snow due to BB. The source attribution analyses of *Hegg et al.* [2009; 2010] indicate that both of these studies may be underestimating the fraction of cryosphere forcing by BC from biomass burning. Further, the 35% of total emissions attributed to BB by *Flanner et al.* [2009] and *Skeie et al.* [2011] is at the low end of the range (35-45%) by all studies in Table 7.1. Therefore, the higher value of 25% is selected as the best estimate of the fraction of present-day BC cryosphere forcing due to biomass burning. *Skeie et al.* [2011] also reported that in the year 1750, 20% of snow BC north of 65°N was from biomass burning sources. For consistency with the assumption that present-day cryosphere forcing due to BB is higher than reported by *Skeie et al.*, we estimate that approximately 30% of pre-industrial (*i.e.,* before 1750) forcing by BC in snow was due to BB.

[52] As noted earlier, *Hansen and Nazarenko* [2004] conducted a sensitivity study based on uniformly imposed albedo changes. *Wang et al.* [2011] followed this approach,

applying similar fixed snow-albedo changes within a few broadly defined regions. Thus, there is no basis for applying adjustments for emissions sources or amounts to these two studies' reported forcings. The focus of these studies was understanding the climate response to the imposed albedo change, rather than on accurately modeling the forcing. Therefore, these two studies are not included here in determining the estimate or bounds on BC cryosphere forcing.

[53] *Jacobson* [2004] did not report a forcing value in his study, only the climate response. The adjusted forcing value of 0.06 W m^{-2} for FF+BF emissions shown in Table 7.1 is an estimate provided by M. Z. Jacobson (personal communication). Biomass burning was included in the baseline, with fossil-fuel and biofuel emissions as the forcing agents. All-source adjusted forcing is estimated as 0.08 W m^{-2} using the assumption that 25% of present-day BC cryosphere forcing is due to BB emissions. This all-source forcing is used to calculate forcing per emission, based on the emissions reported by *Jacobson* [2004].

[54] *Hansen et al.* [2005] (whose radiative forcing distribution was used directly by *Shindell and Faluvegi,* 2009]) followed the approach of *Hansen and Nazarenko* [2004] of imposing a snow albedo change, rather than prognostically calculating snow BC concentrations. However, in this updated study they scaled the imposed albedo based on the deposition rates from the study of *Koch* [2001]. *Hansen et al.* [2005] note they use the emissions of *Koch* [2001] in this context, but emission amounts were also not reported by *Koch* [2001]. The FF emissions provided by D. Koch (private communication) for this study were based on global, annual averages from *Penner et al.* [2001] for year 2000, with 1880 emissions approximated as 10% of the year 2000 emissions, and both biomass and biofuel emissions were taken from *Liousse et al.* [1996] (D. Koch, personal communication), resulting in the BC emissions shown in Table 7.1. To get atmospheric abundances, *Hansen et al.* [2005] scaled these BC emissions by a factor of 1.9, so that their global, annual average direct (atmospheric) radiative forcing by BC matched the 1 W m^{-2} given by *Sato et al.* [2003] based on AERONET observations. The model-measurement discrepancy could result from a bias in emissions, deposition rates or BC mass absorption efficiency, so it is not clear how the model might be biased in terms of light absorption by deposited aerosol. It is specified that the "…resulting albedo effect in the region of Arctic sea ice in our present model is only several tenths of 1%, as opposed to the 1.5% spectrally integrated (2.5% visible wavelengths) albedo change assumed by [*Hansen and Nazarenkeo* (2004)]." [*Hansen et al.*, 2005; also, see their Figure 16]. The *Hansen and Nazarenko* [2004] and *Hansen et al.* [2005] studies did not include the feedbacks *MBC*, *SBC* or *GRA* (Table 7.2), so their forcing is a direct radiative forcing due to the initial albedo change alone. This albedo change results in a preindustrial-to-present (1880 to 2000) radiative forcing by BC in snow of 0.08 W m^{-2}, which was later revised down to 0.05 W m^{-2} after correcting for a programming error that caused the modeled albedo change in *Hansen et al.* [2005] to be too high in partially snow-covered land gridboxes and too low for snow on sea ice [*Hansen et al.*, 2007]. In Table 7.1, the present-day adjusted forcings for FF+BF+BB and for FF+BF only are calculated based on the corrected 0.05 W m^{-2} forcing value. Scaling is done by accounting for the change in emissions 1850 to 2000 and by assuming that the fraction of snow BC forcing due to BB is 30% in 1880 and 25% in 2000. Forcing per emission is calculated from this all-source forcing.

[55] The studies of *Flanner et al.* [2007, 2009] calculated present-day adjusted forcing for all emissions sources (FF+BF+BB) as well as calculating forcing for (FF+BF) emissions only, as given in Table 7.1. *Koch et al.* [2009b] report both preindustrial-to-present (1890 to 1995) and present day (1995) adjusted forcing for all sources (FF+BF+BB). Present-day forcing from FF+BF only is calculated by assuming that 75% of present-day forcing is due to these sources.

[56] *Rypdal et al.* [2009a] do not include biomass burning emissions in either their baseline or forcing scenarios, including BC emissions only from fossil-fuel and closed-container biofuel burning. The amount of open- versus closed-container biofuel BC emissions is not sufficiently constrained to apply an adjustment to account for this missing source of BC. Total present-day forcing including biomass burning is calculated by scaling the reported FF+BF forcing, assuming the latter accounts for 75% of total present-day forcing. Forcing per emission is calculated using the sum of the *Rypdal et al.* [2009a] reported FF+BF emissions and the *Flanner et al.* [2009] 'typical year' BB emissions of 2700 GgC yr^{-1}.

[57] *Skeie et al.* [2011], using the same model as *Rypdal et al.* [2009a], reported an industrial-era (1750 to 2000) forcing by FF and BF of only 0.016 W m^{-2}. This gives a forcing per emission for FF+BF of 3.9 μW m^{-2} (GgC yr^{-1})$^{-1}$, which in turn yields FF+BF forcing of 0.018 W m^{-2} for present-day (year 2000) emissions. Assuming 25% of present-day BC cryosphere forcing is due to biomass burning emissions, present-day all-source forcing is 0.024 W m^{-2}. This implies an industrial-era forcing by FF+BF+FF of 0.021 W m^{-2}.

[58] With all studies adjusted to the common metrics of all-source forcing and forcing per emissions, a greater degree of convergence is reached. Total present-day adjusted forcings from the five most recent studies that prognostically calculated forcing span a range of a factor of two (0.024 to 0.050 W m^{-2}). The *Hansen et al.* [2005] and *Jacobson* [2004] forcings are notably higher at 0.07 and 0.08 W m^{-2}, respectively. However, when normalized to forcing per emission, all but the *Jacobson* [2004] study fall in the range of 3 to 7 (μW m^{-2})(GgC yr^{-1})$^{-1}$. If the high biomass-burning year (1998) of *Flanner et al.* [2009] is excluded, this range narrows to 3 to 6 (μW m^{-2})(GgC yr^{-1})$^{-1}$.

[59] The *Jacobson* [2004] study stands out in two regards: it includes forcing by BC in bare (non-snow-covered) sea ice as well as by BC in snow, and it includes UV and blue absorption of certain types of OC in the derived forcing. *Rypdal et al.* [2009a] and *Skeie et al.* [2011] also include forcing by BC in sea ice but otherwise all other studies discussed only include light absorption by BC and only in snow (not sea ice). Other studies include BC in snow on sea ice, but not in the sea ice itself. *Flanner et al.* [2007] excluded light absorption by OC in snow because a sensitivity study indicated that snow forcing from OC was a factor of 200 smaller than BC but acknowledged that modern optical measurements of light-absorbing OC could alter this conclusion. The inclusion of BC in sea ice and OC absorption might explain why the forcing per emission of the *Jacobson* [2004] study is higher than in the other studies. However, the forcing provided is estimated, not

calculated, so it is not possible to know the fraction of forcing due to BC in sea ice versus snow or due to OC versus BC, and it is difficult to know quantitatively how much these factors account for the comparatively high adjusted forcing and forcing per emission of the *Jacobson* [2004] study. The *Rypdal et al.* [2009a] forcing per emission is more in line with that from the other studies, though again it is not known what fraction of this forcing is due to BC in snow versus bare sea ice. On the other hand, forcing per emission in the *Skeie et al.* [2011] study, which also included BC in sea ice, are lower than in the other studies.

[60] The comparison of measured versus modeled snow BC concentrations (Section 7.4) allow us to make a first-order adjustment for biases in the *Flanner et al.* [2009], *Koch et al.* [2009b] and *Skeie et al.* [2011] studies for all-source adjusted forcing. The results of this comparison (Table 7.3) indicate that the *Flanner et al.* [2009] model tends to overestimate snow BC concentrations, particularly in locations with relatively higher concentrations (*e.g.,* Scandinavia). There are also indications that this model may exaggerate the enhancement of surface snow BC concentrations with melt, and therefore feedback process *MBC* (Figure 7.3). The *Koch et al.* [2009b] model, on the other hand, tends to underestimate snow BC concentrations (Table 7.3), and it does not include the *MBC* feedback at all. Some data indicate that this feedback is significant (Dye-3 Greenland samples of *Clarke and Noone* [1985] and work in Norway, Greenland and Alaska [*Doherty et al.,* 2010; *Doherty et al.,* unpublished results]), if perhaps not as large as is given by *Flanner et al.* [2009]. The *Skeie et al.* [2011] comparison indicates that the model tends to underestimate surface snow BC concentrations in many locations by a factor of approximately two to five for cold snow. Once the snow starts to melt the modeled *MBC* feedback leads to large increases in surface snow BC amounts because none of the BC is washed away with the melt water. Based on these data, the all-source adjusted radiative forcing for FF+BF+BB from *Flanner et al.* [2009] is scaled down from 0.047 W m^{-2} to 0.04 W m^{-2}, and the forcing from *Koch et al.* [2009b] is scaled up from 0.03 W m^{-2} to 0.04 W m^{-2}. The *Flanner et al.* [2009] study accounted for dust impurities in the snowpack (which lessens the impact of adding BC) and so should be a more accurate representation of snow BC forcing than is given by *Flanner et al.* [2007]. Applying a correction factor to the all-source forcing derived from the reported *Skeie et al.* [2011] industrial-era FF+BF forcing based on the comparison to observations is somewhat more difficult. The low bias in modeled concentrations, especially in areas where forcing is expected to be greatest, is both large and variable. While forcing is likely biased low by at least a factor of two for cold snow (*i.e.*, winter to early spring), once the surface snow starts to melt it is assumed that all meltwater BC remains at the snow surface, maximizing the *MBC* feedback (Figure 7.3). Thus, adjusted forcing is likely underestimated initially but overestimated once the model snowpack warms to the point of melting. It is unclear what the net effect on adjusted forcing would be of increased cold snow BC concentrations coupled with a more realistic, reduced *MBC* feedback. However, an approximate doubling of the all-source radiative forcing from the *Skeie et al.* [2011] study from 0.024 W m^{-2} is reasonable given the reported large underestimates in snow BC concentrations across much of the Arctic. A comparison of snow BC concentrations is not made for the *Rypdal et al.* [2009a] study, but notably the emissions and forcing are intermediate to the *Flanner et al.* [2009] and *Koch et al.* [2009b] values. With this suite of information, the best estimate of all-source adjusted forcing by BC in snow is estimated to be 0.04 W m^{-2}. This yields a forcing per emission of 5 (μW m^{-2})(GgC yr^{-1})$^{-1}$ for the spatial and temporal emission patterns applied in the models.

[61] Industrial-era adjusted forcing is estimated from the total present-day forcing through scaling by the ratio of industrial era to all-source BC emissions, accounting for changes in the relative fractions of FF+BF versus BB from the industrial era to present day and accounting for differences in the fractions of FF+BF versus BB emissions that are deposited to snow. Caveats in this scaling are that significant uncertainties are associated with the pre-industrial BC emissions, especially from biomass burning; that forcing does not necessarily scale linearly with emissions; and that for forcing by BC in the cryosphere the forcing-per-emission is very sensitive to the season and location of the emissions. Biomass-burning emissions in 1750 were approximately 26% of present-day biomass-burning emissions and industrial-era FF+BF emissions were approximately 6% of present-day emissions (Table 5.3). In present-day, about 25% of the BC-in-snow forcing is due to biomass-burning emissions and 75% to fossil-fuel and biofuel emissions, and in 1750 the split was about 30%/70% (Section 7.6.1). Thus, biomass forcing in 1750 was about 0.003 W m^{-2} (0.04 W m^{-2} × 0.25 × 0.26 x (30/25)) and FF+BF forcing was 0.0017 W m^{-2} (0.04 W m^{-2} × 0.75 × 0.06 x (70/75)), for a total forcing in 1750 of 0.005 W m^{-2}. This yields an industrial-era forcing from all sources of 0.035 W m^{-2}. This forcing is the difference between present-day forcing and forcing in 1750. As noted earlier, snow (and likely sea ice) forcing in the later 1800's and early 1900's may have been greater than in 1750 or present-day.

[62] As noted earlier, it is not possible at this time to account for all known sources of uncertainty in model calculations of the radiative forcing and feedbacks that amplify that forcing as rapid adjustments. However, it is certain that snow BC radiative forcing is greater than zero (Section 7.1; Figure 7.2). Further, it is amplified by the rapid adjustments *GRA*, *SBC* and *MBC* (Section 7.1; Figure 7.3). Thus, the bounds on snow BC forcing are asymmetric about the best estimate.

[63] *Flanner et al.* [2007] calculated ranges of global-mean adjusted forcings resulting from plausible uncertainty bounds of different factors. Ranges of BC emissions produced a forcing range of -46% to +100% of their central estimate; ranges of snow aging (effective grain size): -42% to +58%; ranges of the fraction of BC scavenged from the snowpack with melt: -31% to +8%; ranges of snow cover fraction: -17% to +8%; and ranges of BC mass absorption efficiency -12% to +12%. From these results, uncertainty in three of the factors that directly affect snow BC radiative forcing (emissions or, equivalently, snow BC concentrations; BC absorption efficiency; and snow cover) can be determined, as well as for two of the feedback processes that amplify snow BC radiative forcing (*MBC* and *GRA*; Figure 7.3). Some bounds can also be placed on the uncertainty in BC radiative forcing due to the presence of soil dust using the *Flanner et al.* [2009] study model, where including dust deposition decreased BC adjusted forcing by 20% relative to adding combustion aerosol to a pristine snowpack.

Based on this result, the role of dust in reducing BC forcing is allowed to be as low as 10% or as high as 40%.

[64] The lower (upper) bounds on snow BC adjusted forcing are calculated by adding in quadrature the forcing from low (high) bounds in emissions, rate of snow aging, BC mass absorption efficiency, and snow cover fraction, and using the high (low) bounds in the efficiency of BC scavenging with melt and in the role of dust in reducing snowpack albedo. The resulting lower and upper bounds on the forcing are calculated by subtracting 79% and adding 117% of the central estimate, giving an all-source adjusted forcing uncertainty range of 0.01-0.09 W m^{-2} with a central estimate of 0.04 W m^{-2} and an industrial-era forcing of 0.035 W m^{-2} with a range of 0.008 - 0.078 W m^{-2}. These bounds do not account for uncertainty in how forcing is affected by patchy snow cover or by uncertainties in modeled cloud cover and vegetation cover. They also do not account for possible biases in modeled mid-latitude snow BC concentrations.

7.6.2. Radiative forcing by BC in sea ice

[65] As noted above, both the *Jacobson et al.* [2004] and *Rypdal et al.* [2009a] studies include forcing by BC in bare sea ice in their calculated climate impact of BC in the cryosphere. However, since these studies don't separate forcing by BC in snow versus in sea ice they cannot be used to estimate forcing by BC in sea ice, and the other studies considered don't include forcing by BC in bare sea ice. Therefore, an independent first-order estimate of this forcing is provided here. This estimate only accounts for the direct radiative forcing by BC in sea ice, and does not include feedbacks that may alter sea ice BC concentrations as the ice warms.

[66] After the snow melts in June on Arctic sea ice, the surface then consists of a mixture of puddles ('melt ponds') and drained hummocks. The hummocks have a surface granular layer that resembles coarse-grained snow, with effective grain radii about 2 mm. The BC content of the surface granular layer has been measured in several summer expeditions; it is similar to that of the springtime snow that recently covered it. The median is about 8 ng g^{-1} with estimated bounds of 3 and 15 ng g^{-1} from tables in *Doherty et al.* [2010]. The corresponding broadband albedo reductions under overcast sky (the normal situation in summer) are 0.010 and 0.028, respectively.

[67] The radiative forcing of BC in sea ice is bounded as follows. Only the months June, July, August, and September are considered because the ice is assumed to be completely snow-covered in all other months. (New ice forming in winter is not immediately snow-covered, but it is exposed to very little sunlight in the dark winter.)

1. The upper bound on sea ice area is taken as the average for 1978 to 1987 (Figure 3.1.45 of *Gloersen et al.,* 1992]; the lower bound as that of the extreme summer of 2007 (Table 1 of *Comiso et al.,* 2008]. These estimates of 'ice area' are of ice only; they are smaller than the tabulated 'ice extent' because the extent includes areas of open water within the ice pack.

2. Melt-pond fractions are given in Figure 3 of *Fetterer and Untersteiner* [1998]; 100% uncertainty is assumed to get upper and lower bounds for each month.

3. The average snow depth for each month is given in Figure 13 of *Warren et al.* [1999]; using these data the snow-cover fractions are estimated and an approximately 50% uncertainty assumed to get upper and lower bounds.

4. The year-to-year variability in downward solar irradiance is mainly determined by varying extent and thickness of the widespread stratus clouds covering the Arctic Ocean in summer. The mean monthly values of surface solar irradiance are adopted, as given in Figure 5 of *Fletcher* [1968] and tabulated in Table 1 of *Maykut and Untersteiner* [1971]; 15% is added or subtracted to get upper and lower bounds.

These values are shown in Table 7.4 and used to estimate the lower and upper bounds on all-source radiative forcing by BC in bare sea ice. The uncertainties are combined in quadrature. For example, for June the relative standard deviations for ice area, non-ponded fraction, non-snow-covered fraction, downward solar flux, and albedo reduction are 0.095, 0.02, 0.33, 0.15, and 0.5, respectively, giving a combined relative standard deviation of 0.625. The bounding values for global annual radiative forcing at the surface are 0.008 and 0.017 W m^{-2}. The central estimate is 0.012 W m^{-2}. As for BC in snow, the industrial-era forcing is estimated to be 88% of the all-source forcing (*i.e.*, 0.011 W m^{-2} with bounds of 0.007 and 0.016 W m^{-2}).

8. Climate response to black carbon forcings

8.1. Section summary

[1]

1. The BC direct, in-snow and in-sea-ice radiative forcings and cryosphere forcings cause the troposphere and the top of the cryosphere to warm, which induces further rapid adjustments and climate response in the form of cloud, circulation, surface temperature, snow cover and precipitation changes. BC microphysical effects on clouds also induce adjustments and climate response but models have not yet separated the full climate responses to these complicated and uncertain climate forcing mechanisms and their adjustments (see Section 6).

2. BC direct radiative forcing causes a surface warming that is concentrated in the Northern Hemisphere but may exhibit a different pattern to that of the forcing. In cloud absorption by BC, semi-direct effects and the efficacy of high latitude BC-in-snow and BC-in-sea-ice forcings need to be properly accounted for in the overall climate forcing estimate of BC. This can be done through the concept of the effective forcing, which scales a radiative or adjusted forcing with its climate efficacy.

3. Climate models show that effective forcing and adjusted forcing are equal within their respective uncertainties for most effects other than snow and ice forcing. Further, the inter-model range in effective forcing is smaller than the inter-model range in radiative forcing. These findings indicate that what different models report as the response to radiative forcing in fact contains varying components of the response to rapid adjustments, making adjusted forcing or effective forcing a more meaningful metric for BC's effect on climate. Effective forcings from the BC direct effect ranged from 0.28 to 0.85 Wm^{-2} in a set of climate model studies and corresponding equilibrium temperature changes ranged from 0.1 to 0.7 K.

4. Although models give a wide range of effective forcings, there is only a 2.5-fold range in temperature response per effective forcing. Therefore, differences in processes leading to the adjusted forcing by BC may be responsible for much of the reported difference in global average temperature change.

5. The all-source BC, snow-albedo adjusted forcing (0.01 to 0.09 W m^{-2} globally averaged) drives equilibrium climate warming of 0.05 to 0.20 K in recent climate model studies. Climate response is greatest during local spring and over mid-to-high northern latitudes. The efficacy of this adjusted forcing is much greater than 1 primarily because all radiative energy is deposited directly within the cryosphere, causing earlier melt of snowpack and driving strong albedo feedback. The adjusted-forcing efficacy is estimated to be 3 with a range of 2 to 4.

6. Various studies suggest regional circulation and precipitation changes in response to the BC climate forcing. These changes include a northward shift in the Inter-Tropical Convergence Zone and changes in Asian monsoon systems where concentrations of absorbing aerosols are large.

7. The suggested impact of BC on glacier melting is potentially important but no model studies sufficiently resolve the glacier energy budget, aerosol transport and circulation changes in a region of complex topography to assess the importance of this process.

8.2. Introduction to climate forcing, feedback and response

[2] A climate forcing is a mechanism that induces a change in the climate system. Most climate forcings are radiative forcings, whereby the induced climate change originates from a modification in the radiative budget of the Earth. More specifically, a radiative forcing is defined by the IPCC as the change in ToA net radiation caused by a climate agent, after stratospheric adjustment, but with everything else being held fixed [*Forster et al.,* 2007]. There also exist some rapid adjustments (*e.g.,* some aspects of land use, microphysical effects on precipitation, or the CO_2 physiological forcing). Such forcings do not have an initial radiative driver but after a rapid adjustment lead to a radiative energy change in the climate system. We term radiative forcings and rapid adjustments as 'adjusted forcings' (see Table 1.1). The climate system responds to a radiative imbalance through a complex set of mechanisms (called feedbacks), eventually returning to a near equilibrium state [*Boer and Yu,* 2003; *Soden and Held,* 2006].

[3] Climate models show that the equilibrium global temperature change in response to a climate agent is generally linear in radiative forcing, and the proportionality coefficient between these two quantities, denoted λ, is called the climate sensitivity (unit K $(W\ m^{-2})^{-1}$). Climate models further show that, although the climate sensitivity is model-dependent, it is relatively independent of the climate agent under consideration (within ±20 to 30%, except for snow albedo forcings discussed below). One can define the climate efficacy of a climate agent as the ratio of the climate sensitivity for this climate agent to that for the forcing by CO_2 [*Hansen et al.,* 2005]. Efficacies can be defined for either radiative forcing or adjusted forcing (Table 1.1).

[4] Some studies have shown that climate responses can be categorized into fast feedbacks, also known as rapid adjustments, which respond to forcings on a short timescale (typically days), and slow feedbacks, which are associated with the global surface temperature response and respond on longer timescales [*Gregory et al.,* 2004; *Andrews and Forster,* 2008]. Different climate agents can induce very different rapid adjustments, whereas slow feedbacks appear to be less dependent on the climate agent. BC affects climate in a number of ways, but those discussed in Sections 5 to 7 may all be considered either radiative forcings or rapid adjustments. The direct effect and the snow albedo effect are radiative forcings. The microphysical effects on clouds are partly radiative forcings and partly rapid adjustments. The cloud semi-direct effect cannot easily be dissociated from the direct effect that causes it and should be seen as a rapid adjustment to the direct radiative forcing rather than a separate forcing, although it can be quantified as a change in radiative flux (*i.e.,* a climate forcing). However, in this assessment the semi-direct effect is included in a single liquid-cloud effect (which also includes BC microphysical effects on clouds) because modeling procedures make the two difficult to separate (see Section 6). This calculation also uses the climate efficacy of the direct-effect

radiative forcing to determine the semi-direct effect, assuming the efficacy of the adjusted forcing would be one. Rapid adjustments to the snow-albedo radiative forcing (Figure 7.3) amplify the climate forcing. This amplified forcing produces changes in snow cover that drive a snow-albedo feedback that amplifies the temperature response.

[5] The response of climate to a relatively uniform radiative forcing such as that of long-lived GHGs, although still uncertain, has been studied in many models and aspects of its response pattern are consistent among climate models. The response to more heterogeneous radiative forcings is less well understood and there has been little work in the literature to compare different climate models. Although, there is no direct relationship between the patterns of climate response and the patterns of radiative forcing, except on large scales [*Forster et al.,* 2000]. *Shindell et al.* [2010] performed a multi-model analysis to quantify these scales, using the results of four GCMs. They found that inhomogeneous aerosol forcing caused an impact locally in those GCMs, but the impacts were not confined to those areas and extended quite far in the zonal direction - at least 12000 km - while extending only about 3500 km (or 30° longitude) in the meridional (consistent with transport timescales in the atmosphere). This relationship is illustrated in Figure 8.1, which shows the geographic distributions of BC emissions, burden, direct radiative forcing and surface-temperature response for a particular model. The climate response to a regional radiative forcing, such as that by BC, has a regional and a global component. While the patterns of burden and direct radiative forcing are quite similar, there is no correspondence between the fine-scale patterns of radiative forcing and the surface temperature response. However, both the forcing and the surface temperature response are concentrated in the extratropics of the northern hemisphere.

8.3. Surface temperature response to atmospheric black carbon

8.3.1. Global-mean temperature change

[6] Earlier studies on the climate effect of large injections of smoke and dust aerosols (*i.e.,* so-called nuclear winter) are relevant to understanding forcing by BC. *Cess et al.* [1985] showed that for increasing smoke loadings there is a transition from a surface-troposphere heating induced by the convective coupling of the surface and the troposphere to a surface cooling when this convective coupling breaks down. The climate response to BC may differ from a nuclear winter because the aerosol is more absorbing than smoke and may be concentrated in the lower atmosphere. *Cook and Highwood* [2004], *Hansen et al.* [2005] and *Ban-Weiss* [2011] added BC to different altitude ranges and showed that radiative forcing was not an effective measure of determining the surface temperature response to BC. The efficacy of the radiative forcing term could even change sign. In contrast, the efficacy of the adjusted forcing that accounted for semi-direct effects was much closer to unity [*Shine et al.,* 2003; *Hansen et al.,* 2005; *Crook et al.,* 2011; *Ban-Weiss et al.,* 2011]. The most consistent forcing measure appears to be calculated by allowing tropospheric response but no global mean surface temperature response, either from fixing surface temperature everywhere [*Shine et al.,* 2003] or using a regression method [*Ban-Weiss et al.,* 2011]. *Hansen et al.* [2005] further showed that for BC-in-snow the large efficacy of the high-latitude forcing needs to be properly accounted for (see below). The adjusted forcing implicitly accounts for the variable efficacy of the direct radiative forcing. The adjusted forcing or the effective forcing (*i.e.,* forcing weighted by efficacy (see Table 1.1)) is a more appropriate measure of BC's ultimate effect on global average temperature.

[7] Table 8.1 reports BC radiative forcing, adjusted forcing and effective forcing, and surface-temperature response from various climate models. The different models vary in their experimental designs (*e.g.,* BC alone versus BC and co-emitted species, slab ocean model versus fully coupled ocean-atmosphere model), emission rates, treatment of the effects of BC on climate, and forcing values. Nevertheless, these results show that effective forcing and adjusted forcings from a single model agree to within their respective uncertainties, justifying our approach for calculating the semi-direct effect. It can also be seen that these forcings, when appropriately scaled, are in much better agreement between models. Effective forcings range from 0.28 to 0.85 W m^{-2} and equilibrium temperature changes from BC perturbations range from 0.1 to 0.7 K. Despite a seven-fold range in effective forcing by BC, there is only a 2.5-fold range in temperature response per effective forcing. This finding suggests that differences in rapid adjustments or aerosol processes included in each model may be responsible for much of the difference in global average temperature change.

[8] The climate models clearly differ in their cloud responses. For instance, fossil-fuel BC causes an increase in high-level clouds in the model of *Jacobson* [2010] due to an enhancement of upper-tropospheric water vapor and a decrease in low clouds due to enhanced BC warming, including that within cloud drops and interstitially between cloud drops, as discussed in Section 6.3.3. These experiments, unlike most other studies, considered OA and other co-emitted species, and included the microphysical effects of BC on liquid and ice clouds. The models in Table 8.1 give different temperature responses and adjusted forcings. Some have a more sophisticated treatment of BC optics, some are better documented in their ability to simulate the present-day climate and the historical period, and some simulate better cloud properties than others. There is a smaller range in temperature response per effective or adjusted forcing than in temperature response and in temperature response per radiative forcing. This finding suggests that differences in processes leading to the adjusted forcing by BC may be responsible for a large fraction of the differences in the global mean surface temperature change.

8.3.2. Regional surface temperature change

[9] As discussed in the introduction, the pattern of surface temperature response can be quite different from the pattern of forcing. The temperature response to BC is a combination of regional response and hemispheric response, with polar and land amplification. There is a reasonable agreement among models that the BC warming is concentrated in the Northern Hemisphere with some polar amplification (Figure 8.2). However, there is disagreement on the relative warming of the different continents, with some models showing significant warming over North America and Eurasia while others do not. It is unlikely that the differences in experimental setup and range of BC effects included in the four models presented in Figure 8.2 are sufficient to explain the diversity of results.

Some of the model differences could be due to differences in forcing and climate efficacy (or sign of the semi-direct effect). It is difficult, however, to attribute the differences among the models to a particular process or reason without performing a more comprehensive intercomparison. While some models include more BC forcing mechanisms that have been evaluated at different scales (*e.g.,* GATOR), others have been more thoroughly tested regarding their ability to represent the global historical temperature record and climate variability (*e.g.,* NCAR CAM, GISS, and HadGEM2).

[10] There are few systematic studies of the regional impact of BC aerosols from different regions with the exception of the work by *Shindell and Faluvegi* [2009], who looked at the regional impact of atmospheric BC from four latitudinal bands in the GISS climate model. A summary of their results relevant to BC is shown in Figure 8.3. BC in the 28°N-60°N band is most efficient at inducing warming in the 60°N-90°N band and vice versa. Tropical (28°S to 28°N) BC warms all latitudinal bands, with forcing efficiency increasing in moving from lower to higher latitudes. Finally, it should be noted that atmospheric BC in the 60°N-90°N band cools the surface in that region, possibly because the coupling between the atmosphere and the surface is not strong enough to overwhelm the decrease in solar radiation at the surface induced by BC or because of resulting changes in northward heat transport due to a decreasing latitudinal temperature gradient. These experiments account only for forcing by atmospheric BC; in this same model, when surface forcing from BC deposited to snow and ice is accounted for, the net forcing by BC in the 60°N-90°N latitude band is positive (warming).

[11] It has been further suggested by *Ramanathan and Carmichael* [2008] that absorbing aerosols could have contributed to the observed melting of snowpacks and glaciers in the Himalayan region on the basis that layers of BC aerosol (the so-called atmospheric brown cloud) heat the atmosphere at altitudes up to 3 to 5 km. Evidence for the effectiveness of this mechanism remains elusive. *Menon et al.* [2010] simulate a small decrease in snow and ice cover over the Himalaya associated with the increase in emissions from 1990 to 2000. However their simulations use observed climatological sea-surface temperatures and neglect any response from the ocean. Moreover it is unclear to what extent the precipitation changes in their simulations are statistically significant. *Kuhlmann and Quaas* [2010] used lidar measurements from the CALIPSO satellite to assess the importance of aerosols for atmospheric heating rates. They found that i) in higher layers the shortwave heating was partly balanced by longwave cooling, ii) the contribution of aerosols to atmospheric heating rate over the Tibetan Plateau was relatively small (typically 0.02 K day^{-1}) as compared to neighboring regions (0.2 K day^{-1}), and iii) a large fraction of the aerosol was dust, or at least classified as such by CALIPSO. However, *Kuhlmann and Quaas* did not estimate the impact of the aerosol on the surface energy balance. While it is possible that atmospheric BC aerosols have contributed to the melting of snowpack and glacier in the Himalayan region, appropriate testing of the hypothesis would require robust ensembles of high-resolution simulations with a regional climate model that can resolve the complex atmospheric flow and surface radiative budget over this region.

8.4. Precipitation changes due to black-carbon direct and semi-direct effects

[12] The separation between rapid adjustment and slow feedbacks is particularly useful for examining precipitation responses to forcing. *Andrews et al.* [2010] studied the rapid adjustment associated with a range of climate agents, including BC. They showed that the rapid adjustment in global-mean precipitation correlates negatively with the atmospheric radiative forcing (*i.e.,* the difference between ToA and surface radiative forcing) while the slow response is proportional to the global-mean surface temperature change. Since BC aerosols are responsible for significant atmospheric radiative forcing through absorption of solar radiation, the reduction in precipitation due to the rapid adjustment can dominate over the increase due to the slow feedback. One model showed a global reduction in precipitation of around 0.7% from BC rapid adjustments [*Andrews et al.,* 2010]. This result has been confirmed by *Ming et al.* [2010] who found that the decrease in precipitation due to atmospheric heating could dominate over the increase in precipitation due to surface warming for some vertical distributions of the BC aerosol.

[13] Both *Wang* [2007] and *Jones et al.* [2007] found that BC strengthens the Hadley cell in the Northern Hemisphere but weakens it in the Southern hemisphere. This leads to a northward shift in the Inter Tropical Convergence Zone (ITCZ), which appears to be a robust feature of the climate response to BC also supported by earlier experiments [*Roberts and Jones,* 2004; *Chung and Seinfeld,* 2005].

[14] A number of studies have investigated the regional climate responses to BC in particular regions of the world, generally focusing on precipitation changes. Many of these studies examine Asia because of the large concentrations of absorbing aerosols there. Using the GISS model, *Menon et al.* [2002] simulated a surface warming over most regions in response to absorbing aerosols but a moderate cooling over China. The model also simulates increased precipitation in southern China and over India with a band of decreased precipitation to the south. *Liu et al.* [2009b] obtained different results using the Community Atmosphere Model. They found that sulfate and BC aerosols have the effect of weakening East Asia monsoons in both summer and winter seasons.

[15] *Lau et al.* [2006] used the GEOS GCM with fixed sea surface temperature to show that absorption of solar radiation by dust heats the air on the northern and southern slopes of the Tibetan Plateau, which can then rise and create a positive temperature anomaly in the mid-to-upper troposphere over the Tibetan Plateau. On the southern side, the atmospheric heating is reinforced by anthropogenic emissions of BC over the Indian subcontinent. This can lead to an intensification of the Indian summer monsoon and surface warming over the Tibetan Plateau. While *Lau et al.* found that the effect of BC is important in initiating the monsoon rainfall anomalies over India, it is not enough to produce statistically significant change in the monsoon regime on its own (*i.e.,* without the synergy with dust absorption). Like most of the other earlier studies looking at the regional climate response to BC, this study was performed with an atmosphere-only model, which is a significant limitation because sea surface temperatures are not allowed to respond to the forcing by BC.

[16] *Wang et al.* [2009a] used the NCAR Community Climate Model version 3 (CAM3) coupled to a slab ocean model to investigate the response of the Indian summer monsoon to scattering and absorbing aerosols. They found that absorbing aerosols cause a northward shift in rainfall (both during the onset of the monsoon and averaged over the monsoon period) that is only weakly offset by the effect of scattering aerosols.

[17] *Meehl et al.* [2008] performed a six-member ensemble of 20th-century simulations with a fully coupled ocean-atmosphere climate model, which confirmed some of the earlier results found with atmospheric models coupled to a slab ocean. In their experiments, BC and OA aerosols increase lower tropospheric heating over south Asia and reduce the amount of solar radiation reaching the surface during the dry season, enhancing precipitation over India in the months of March-April-May. With the onset of the monsoon, the reduced surface temperatures in the Bay of Bengal, Arabian Sea, and over India that extend to the Himalaya act to reduce monsoon rainfall over India itself, with some small increases over the Tibetan Plateau. Precipitation over China generally decreases due to the BC effects. Analysis of single ensemble members from the multiple-forcings experiment suggests that the observed increasing precipitation trends over southern China appear to be associated with natural variability connected to surface temperature changes in the northwest Pacific Ocean. *Rotstayn et al.* [2007] suggest that the effects of Asian aerosols on rainfall could be seen in Australia with an increase in cloudiness and rainfall during the period 1951 to 1996, especially in northwestern Australia. *Bollasina et al.* [2011] and *Shindell et al.* [2012] investigated the impact of aerosol forcing on the South Asian monsoon in the GFDL and GISS GCMs, respectively. *Shindell et al*. found distinct perturbations to the South Asian monsoon as well as to precipitation in the Sahel and southern Europe. *Bollasina et al.* found similar changes and suggested that the changes were part of large-scale circulation changes and had fairly little to do with direct local forcing. *Shindell et al* showed that the precipitation responses were in many places similar to those induced by GHGs, but with much greater amplitude per unit forcing.

[18] *Tosca et al.* [2010] also applied the NCAR CAM3 model with a slab ocean model to explore effects of biomass burning emissions over the western equatorial Pacific during intense El Niño episodes, such as the 1997-1998 event. They found that BC and OA emissions from extreme fire years caused sea surface temperature to cool and the atmosphere to warm and that this reduced precipitation by about 10% over greater Indonesia, potentially exacerbating local drought conditions because evapotranspiration reductions were smaller than precipitation changes.

[19] Generally, these studies show that atmospheric heating by BC can have significant effects on precipitation, causing a global reduction via rapid adjustment processes. Model studies have also shown that BC can alter regional precipitation by about 10% and affect circulation patterns such as the monsoon.

8.5. Climate response to the snow albedo effect

[20] BC deposited to snowpack can significantly reduce snow and ice albedo because of the approximately five order-of-magnitude difference in mass absorption cross section between ice and BC, and strong multiple scattering within snow, which enables small mixing ratios of impurities to absorb a disproportionate amount of radiative energy (*e.g., Warren and Wiscombe,* 1980]. BC-induced snow-albedo changes exert a small global-mean forcing through radiative forcing and rapid adjustments (*i.e.,* all-source adjusted forcing range of +0.01 to +0.09 W m^{-2} in Section 7), but models indicate that snow-albedo forcing is unusually effective at warming climate, even when rapid adjustments are accounted for. The high efficacy of the adjusted forcing stems from the following factors:

1. By definition, all of the forcing energy associated with this mechanism is deposited directly within the cryosphere, a component of the Earth System responsible for strong positive feedback [*e.g., Budyko,* 1969] through the snow (and ice) albedo feedback (*SAF* in Figure 7.3). Warming of snow and sea ice by deposited BC exacerbates this feedback mechanism in comparison to forcing mechanisms that distribute energy more evenly throughout the planetary envelope, such as GHG forcing.

2. The mechanism operates mostly at high latitudes, which are uniquely susceptible to surface energy forcings because of stable atmospheric conditions. Smaller lapse rates in high-latitude regions induce shallower mixed layers that permit surface energy forcings to drive larger surface temperature changes. In stratified conditions, the mass of air responding to a surface energy forcing is small, and the energy is not transferred efficiently throughout the system. This condition breaks down with strong warming, however, so that larger forcings have smaller efficacies. It is weaker during summer, when insolation (and therefore radiative forcing via darkening of snow or ice) is greatest [*Forster et al.,* 2000].

3. In some studies, feedbacks driven by changes in snow grain size may also contribute to larger efficacy [*Flanner et al.,* 2007] (*GRA* in Figure 7.3). The reasoning for this result is that BC absorption warms snowpacks so that they age more rapidly, which lowers snow albedo in the near-infrared spectrum. A key uncertainty associated with this process is that snowpack temperature gradient is often a greater controller of snow age than mean temperature [*Flanner and Zender,* 2006], and the influence of absorbing impurities on temperature gradient depends on many factors, including the vertical distribution of impurities and solar absorption, snowpack thermal conductivity, and snowpack-atmosphere coupling.

The relative roles of these three factors are uncertain. *Bellouin and Boucher* [2010] obtained a large climate efficacy in idealized model experiments that do not include the third factor.

[21] Climate response to BC in snow is particularly strong during boreal spring (March-May) over mid- to high-latitudes [*Flanner et al.,* 2009; *Wang et al.*, 2011]. Increasing springtime insolation and widespread snow cover in the Northern Hemisphere drive the greatest radiative forcing during this season, and climate response and efficacy are large when the mechanism induces earlier snow melt, as the contrast in albedo between snow-covered and snow-free surfaces is generally much greater than the reduction in albedo caused by BC. A source of enhanced springtime forcing is the retention of impurities at the snow surface during melt (*MBC* in Figure 7.3; Section 7.3.5). Idealized field studies show that retention of hydrophobic impurities is particularly strong [*Conway et al.,* 1996], but the importance of this effect is largely uncertain and

likely varies considerably with location and type of snowpack. *Koch et al.* [2011b] have suggested that, even absent the *MBC* feedback (Table 7.2), 20% of Arctic warming and snow–ice cover loss is a consequence of the BC albedo effect.

[22] Table 8.2 reports estimates of the BC snow albedo forcing, surface temperature response, and climate efficacy from different model studies. The equilibrium change in global-mean surface temperature ranges from +0.06 to +0.20 K for the trustworthiest experiments. The climate response is more localized than for the BC direct and semi-direct effect with most of the warming over the Arctic region and the Tibetan Plateau and Himalaya. Equilibrium Arctic temperature responses reported from three simulations [*Flanner et al.,* 2007; *Koch et al.,* 2009b] are 0.50, 0.50, and 1.6 K (the latter occurring with strong boreal fire BC emissions in 1998). Climate efficacy for the adjusted forcing is much larger than 1 in all models with most models showing values of 2.0 or more. Based on the spread of adjusted-forcing efficacies given in Table 8.2, the efficacy of the adjusted forcing by BC in the cryosphere is estimated to be 3, with a range of 2 to 4. These same efficacies are also used for BC in sea ice in Section 9 to calculate BC cryosphere effective forcing (Table 1.1).

[23] Most studies of the climate impact of BC in snow have focused on the global, annual impact or on impacts in the Arctic. However, because most of the energy from this forcing directly impacts snowpack temperatures, local impacts may be large, especially where snow melt is relied upon as a water source. Recognizing this, *Qian et al.* [2009] applied the Weather Research and Forecasting (WRF) regional model to study the influence of BC deposition on western North America snowpack. They found the largest response during late winter and early spring, with increased net solar radiation caused by reduced snow cover, and subsequent increases in surface air temperature. Climate changes and deposition of BC on snow were both largest over the central Rockies and southern Alberta, where shifts in regional stream flow were also found. An experiment with doubling of regional BC emissions showed a much greater-than-linear climate response in this region. *Qian et al.* [2011] used a global model to look at the influence of BC and dust on the Tibetan Plateau snowpack with a specific focus on the impacts on the Asian hydrological cycle and monsoon climate. In this study, BC and dust in snow were found to produce 5 to 25 W m^{-2} adjusted forcing during spring, reducing spring snowpack over the Tibetan Plateau more than does warming by anthropogenic CO_2 and atmospheric BC. However, *Qian et al.* acknowledge that the global model used grossly overpredicts snow cover in this region (their Figure 2) and, therefore, likely also forcing by BC and dust in snow. These studies highlight the possible strong regional impacts of BC in snow, but also emphasize the need for studies that can account for the large variations in terrain, snow cover and BC deposition, especially in mountainous terrain.

8.6. Detection and attribution of climate change due to black carbon

[24] As Sections 8.3 to 8.5 have outlined there is evidence of regional climate responses to BC that is manifest in observations. In particular, there is some evidence for a BC effect on: 1) regional temperature and precipitation changes [*e.g., Menon et al.,* 2010], 2) Arctic temperatures and snow-ice cover [*e.g.*, *Flanner et al.,* 2009*; Koch et al.,* 2011b], 3) monsoon and other circulation changes [*e.g.*, *Rotstayn et al.,* 2007*; Bollasina et al.,* 2011*; Shindell et al.,* 2012] and 4) Himalayan and North American snow and ice cover [*Qian et al.,* 2009*; Qian et al.,* 2011]. However, it should be noted that none of these studies formally attribute changes to BC in a statistically rigorous sense.

[25] It is desirable to find a confirmation of the model results on the climate response to BC in the observational climate records. Methods have been developed to detect and attribute climate change to particular climate agents by regressing the spatial and temporal patterns of climate change simulated by the models against the observed patterns. Scaling factors that maximize the fit to the observations provide a measure of whether a particular forcing is detected, by testing the hypothesis that the scaling factors are consistent with a value of zero. When a particular combination of forcings is detected, the scale factors can be used to reconstruct the contribution of each individual forcing to temperature change. Detection and attribution methods have established that the anthropogenic "…greenhouse gas forcing has very likely caused most of the observed global warming over the last 50 years." [*Hegerl et al.,* 2007] The cooling due to sulfate aerosols could also be detected. However, it proves to be more difficult to detect the warming effect due to BC.

[26] *Jones et al.* [2005] included fossil-fuel BC in a detection and attribution analysis with GHG and sulfate aerosols. While the introduction of BC did not affect the attribution of the warming to GHGs, it was not possible to detect the pattern due to BC because it was too similar to the cooling pattern of sulfate aerosols. The influence of carbonaceous aerosols (BC and OA from fossil-fuel and biomass burning sources) was detected by *Nagashima et al.* [2006] in the mid part of the 20th century. However the relative contribution from BC cannot be deduced from this study.

[27] *Jones et al.* [2011] revisited their earlier work using an ensemble of HadGEM1 model simulations that include different combinations of the GHGs, sulfate aerosols, BC, and natural radiative forcings. They used their detection and attribution method to examine the climate influence of BC from fossil-fuel and biofuel sources. The BC forcing included the direct and semi-direct effect but not the snow albedo effect. The climate response to BC was obtained as the difference between a simulation with all forcings and a simulation with all forcings except that from BC. BC was found to have a detectable contribution to the warming over the period 1950-1999 but not over the period 1900-1999 or 1957-2006. The attributed climate change due to BC was 0.41 K(century)$^{-1}$ (range 0.20 to 0.60 K(century)$^{-1}$) for the period 1950-1999. This corresponds to a warming of about 0.20 K (range 0.10 to 0.30 K) for the 50-year period. Global warming by industrial-era BC would be about twice as large because 1950 emissions of BC were about half of present-day emissions. Moreover, any committed warming would add only slightly to the equilibrium climate response. Accounting for the snow albedo effect would possibly improve the detection and narrow the uncertainties in the scale factors but would not necessarily result in a larger contribution of BC to the observed warming because the scale factor can compensate for the missing warming in the climate simulations. For the period 1957-2006, the attributed climate

change due to BC –not statistically significant– is 0.10 K(century) $^{-1}$ (range -0.03 to 0.21 K(century) $^{-1}$). Failure to detect the climate response to BC over this period can be due to the discontinuities introduced in the simulations by merging the historical emission inventories until 2000 with the SRES emission projections after 2000.

[28] In conclusion it can be said that the global warming due to BC can be detected in the observational temperature record but the detection remains very sensitive to the modeling assumptions. The deduced contribution of BC to the observed warming is comparable to that obtained from models alone but it is not accurate enough to constrain further the various estimates obtained from the models so far. Inclusion of the pattern of warming due to the snow albedo effect and regression of the simulated patterns against both the observed surface and vertical temperature change patterns could contribute to a better detection of the BC signal.

8.7. Conclusions

[29] Figure 8.4 summarizes our knowledge on the effects of BC on climate. There is some agreement among models that BC mostly warms the northern hemisphere and causes a northward shift in the Intertropical Convergence Zone. Other changes in precipitation are likely, especially the Asian monsoon systems as these regions experience large burdens of BC. However, there is no agreement among models on the patterns of rainfall changes in these regions. Darkening of snow and ice surfaces by BC is associated with enhanced melting and an amplification of the surface temperature response in these regions. Finally, the climate response to the indirect effect of BC on liquid and ice clouds has not been studied in isolation of the direct and semi-direct effects and remains largely unknown.

9. Synthesis of black-carbon climate effects

9.1. Section summary

[1]

1. The industrial-era (1750 to 2005) climate forcing of BC is made up of components from its direct radiative forcing, its effect on cloud microphysics, rapid adjustments to its atmospheric heating, and the effect of BC deposited on snow and sea-ice.

2. Employing radiative forcing alone is inadequate for assessing the climate role of BC. In particular, semi-direct effects and the efficacy of high-latitude forcing terms need to be properly accounted for.

3. The level of scientific understanding of these components is generally assessed as low or very low, making their uncertainty bounds difficult to characterize accurately. It is also difficult to quantify how errors in individual terms are correlated to those in other terms – this makes errors difficult to combine.

4. With these caveats the industrial-era effective climate forcing of BC is assessed to be +0.77 W m^{-2} with a 90% uncertainty range of +0.06 to 1.53 W m^{-2}, allowing for the correlation of emission uncertainty. This climate forcing has a larger uncertainty range and is likely greater than the radiative forcing from the BC direct effect (+0.43 W m^{-2} with a 90% uncertainty range of +0.17 to +0.68 W m^{-2}).

5. In addition to the direct radiative forcing of BC, adding the positive climate forcings from cloud-droplet inclusions, BC-in-snow and BC-in sea ice increases the median forcing estimate. Semi-direct and liquid-cloud effects add negative climate forcing, and cloud absorption and mixed-cloud changes add positive climate forcing. The net effect of BC cloud effects is estimated to be positive. Adding cloud effects, accounting for both the semi-direct effect and the efficacy of BC-in-snow and BC-in-sea-ice, all make the total BC climate forcing estimate considerably more uncertain than its direct radiative forcing.

6. The components of this effective climate forcing are: direct radiative forcing (+0.43 W m^{-2} with a 90% uncertainty range of +0.17 to 0.68 W m^{-2}); cloud, cloud droplet inclusions, and semi-direct effects (+0.17 W m^{-2} with a 90% uncertainty range of -0.45 to 0.86 W m^{-2}); and BC-in-snow and BC-on-ice (+0.14 W m^{-2} with a 90% uncertainty range +0.04 to +0.34 W m^{-2}). See Table 0.1 for a further breakdown of forcing components.

9.2. Introduction

[2] Earlier sections have discussed emissions of BC, the mechanisms by which BC affects the Earth's radiative balance and BC's various effects on climate. Here we synthesize these discussions to provide best estimates and uncertainty bounds for the role of BC in the current climate using the metric of globally averaged climate forcing. Section 8 pointed out that regional changes and especially changes to the hydrological cycle are how we experience climate change, and that such impacts are not necessarily represented by global forcing metrics. Nonetheless, in this assessment we have chosen to use a global forcing metric as it is more comparable across mechanisms and better constrained than other choices.

9.3. Global climate forcing definition

[3] We are ultimately interested in quantifying the impact of BC emissions on the Earth's climate. The definition of radiative forcing employed in IPCC reports [*Forster et al.,* 2007] is the change in net energy (down minus up) at the tropopause since 1750 due to a given mechanism or climate forcing agent, after allowing stratospheric temperatures to adjust to radiative equilibrium. As discussed in Section 1.3, we retain this definition of forcing relative to a base year, but use the term 'industrial-era forcing' to indicate that the forcing is based on time rather than wholly attributable to anthropogenic activity. The net global climate response to BC (encompassing direct, snow, sea-ice and cloud effects) is also very different from the response to other forcing agents such as the long-lived GHGs (Section 8). BC emissions affect clouds, snow and sea ice (see Sections 6 and 7). In IPCC reports, some of these effects are classified as part of the cloud albedo effect or represented separately as BC snow albedo forcing, while others are considered part of the climate response. For BC in snow, snowpack evolution, grain size growth, melting, and consolidation of BC combine to yield a rapid adjustment to the forcing. We implicitly include both the rapid adjustment of the snowpack and different global response to BC snow albedo changes by accounting for the efficacy of BC snow albedo change in our climate forcing estimate, employing the concept of 'effective forcing' discussed next.

[4] The notion of effective forcing means that the radiative forcing is scaled by an efficacy which incorporates the relative strengths of climate feedbacks. This effective forcing is then more representative of the actual radiative impacts of BC [*e.g.*, *Hansen et al.*, 2005; also see Table 1.1 and 8.1]. Alternatively, forcings can be calculated from fixed sea-surface temperature experiments or regression techniques [*Hansen et al.*, 2005, *Andrews et al.,* 2010]. In practice, diverse forcing definitions are used in the different studies we assess and care is required when comparing reported forcings (see Section 8 and Table 8.1). For example, the separation of BC forcing into direct, cloud-albedo forcing and semi-direct forcing is not straightforward (see Section 6). In this assessment we have been particularly careful to include all relevant terms when assessing the total climate forcing from BC without double counting (see Section 1).

9.4. BC global climate forcing components and uncertainties

[5] In this section, we summarize the best estimates of individual climate forcing components for global BC emissions in 2005, compared to 1750. These values are shown in Figure 9.1 along with 90% uncertainty range estimates. The combined climate forcings represent the known direct and indirect (cloud, snow and ice) radiative forcings from BC changes plus all known rapid adjustments of clouds and the snowpack (Section 7.4). They also capture the high efficacy of high-latitude snow and ice forcings. The sum of these terms represents the effective forcing of BC. Table 9.1 summarizes each of the terms evaluated, describes their relation to the forcing definitions described in Section 1, explains how the uncertainty range was determined, and identifies where in this assessment

the radiative forcing is estimated in detail. It also presents our general level of scientific understanding, which, following IPCC terminology [*Forster et al.*, 2007], is based on an assessment of the nature of assumptions involved, the uncertainties prevailing about the processes that govern the forcing, and the resulting confidence in the numerical value of the estimate. The following sections review these choices.

9.4.1. BC direct forcing

[6] The best estimate and range of the direct BC radiative forcing arises from scaled AeroCom model results to observations from AERONET sites (see Section 5). The uncertainty range comes from a 40% uncertainty in both AOD and normalized forcing, due to uncertainties in the underlying reflectivity of the surface and atmosphere, particularly the presence of clouds below BC (Section 5.7). Our assessment of the direct radiative forcing from BC is a +0.43 W m^{-2} best estimate with a 90% uncertainty range of +0.17 W m^{-2} to 0.68 W m^{-2}. Fossil-fuel BC emission contributes approximately +0.16 W m^{-2}, biofuel +0.12 W m^{-2}, and open burning +0.15 W m^{-2} (see Section 10). Figure 9.1 also presents the pre-industrial background plus industrial-era direct forcing from BC. This is comprised of emissions from all anthropogenic and natural sources. This all-source forcing is evaluated to be +0.49 W m^{-2} with a 90% uncertainty range of +0.20 to +0.76 W m^{-2}.

9.4.2. BC cloud indirect effects

[7] BC effects on clouds, discussed in Section 6, are particularly poorly constrained for at least four reasons. First, there are process uncertainties regarding the microphysical effects of aerosols on clouds generally and of the role of BC more particularly. Second, only a few model studies with appropriate diagnostics have focused on the role of BC on these cloud effects. Third, modeled aerosol microphysics and cloud responses have not yet been closely constrained by observations. Fourth, the magnitude of aerosol-induced cloud changes is small compared to the spatial and inter-annual variability in modeled cloud forcing, so quantifying changes due to aerosol forcing is difficult. Our best attempt at assessing likely ranges for these cloud effects is discussed below.

9.4.2.1. Liquid cloud and semi direct effects

[8] The semi-direct effect follows from the in-situ heating of the atmosphere from the direct radiative forcing of BC. Heating causes several observed and modeled effects on cloud properties and their distribution, via changes in atmospheric stability and regional circulation. These cloud modifications or 'rapid adjustments' can be quantified in W m^{-2}. There is good agreement in models that realistic distributions of BC have a semi-direct effect that yields a negative forcing. Our best estimate of the semi-direct effect (-0.13 ± 0.2 W m^{-2}) is based on two modeling studies that explicitly calculate the forcing and on five model studies that calculated a reduced radiative-forcing efficacy of BC direct forcing. The reduced efficacy was interpreted as being an adjustment in cloud distributions resulting from BC direct forcing and, therefore, a semi-direct forcing. Semi-direct effects are more properly associated with the 'rapid adjustment' component of the direct radiative forcing term. Yet, for consistency with how the cloud indirect effects are estimated in climate models, this forcing is combined with the warm liquid-cloud forcing estimate.

[9] Climate forcing due to changes in warm liquid clouds occurs principally from changes in cloud microphysics. Uncertainty results from lack of constraint on particle size, number and composition. A small amount of BC may reduce CCN by suppressing new particle formation. BC with co-emitted OA make more and better CCN, causing increased cloud albedo and an overall negative radiative forcing. This estimate is based on a limited number of microphysical models that have isolated the effect caused by BC.

[10] BC also causes additional rapid adjustments to cloud, inducing both semi-direct and cloud lifetime changes. These semi-direct and lifetime effects are also included in the estimate of the warm liquid-cloud climate forcing, as the models used to estimate this effect have not separated the microphysical component. The main uncertainty arises from the fact that lifetime effects are inferred from total anthropogenic aerosol studies and the impact of BC aerosol on cloud lifetime has not yet been isolated. The climate forcing for the BC effect on liquid cloud including rapid adjustment and semi-direct effects is assessed to be -0.2 W m^{-2} with a 90% uncertainty range of -0.52 to +0.05 W m^{-2}.

9.4.2.2. BC inclusion in cloud drops

[11] BC, when present in cloud drops, changes their absorption characteristics and increases absorption within a cloud. A small number of studies have assessed this radiative forcing and have explored assumptions about the optical properties of mixed particles and their shape. Uncertainties arise due to different optical representations of the BC and droplet combination, which affects in-cloud heating rates. This effect is estimated separately from other semi-direct effects. The industrial-era climate forcing for the effect of BC inclusion in cloud drops is assessed to be +0.2 W m^{-2} with a 90% uncertainty range of -0.1 W m^{-2} to +0.7 W m^{-2}.

9.4.2.3. Mixed-phase cloud effect

[12] Climate forcing through changes in mixed-phase clouds is a mixture of radiative forcing and rapid adjustments. BC acts as an ice nucleus and can thereby produce increased glaciation rates, changes in precipitation, and changes in lifetime (Section 6.6.2). The forcing estimate is based on a range of three studies employing anthropogenic BC emissions that has been scaled to total BC emissions in year 2005. Confidence in this forcing value and range is very low as the physical processes are not properly understood. Major uncertainties are that this estimate is based largely on a single model and does not have any observational constraint. The climate forcing for the BC effect on mixed phase cloud is assessed to be +0.16 W m^{-2} with a 90% uncertainty range of +0.0 to +0.32 W m^{-2}.

9.4.2.4. Ice cloud effect

[13] BC may affect ice clouds via two mechanisms. First, BC could increase the number of ice particles, which can lead to increased cloud amounts and positive forcing. Second, it can lead to increased numbers of supercooled solution droplets, thereby reducing the atmospheric relative humidity and cloud cover, and resulting in negative cloud forcing. Both these effects are seen in modeling studies. Our estimate of the BC influence on ice-cloud is based on two modeling approaches that lead to forcings of different signs for total BC emissions. This climate forcing term is also a mixture of radiative forcing and rapid adjustment. The same two modeling approaches

estimate the effect of aviation BC alone on ice cloud to be between -0.16 W m^{-2} to +0.26 W m^{-2}. BC emissions from aviation are a very small fraction of direct forcing, yet have a much larger effect on ice clouds than emissions at the surface. Because aviation is so different from most BC emissions, and because it is assessed separately elsewhere [*Lee et al.*, 2010], we do not include its forcing in Figure 9.1. The climate forcing for the BC effect on ice-cloud is assessed to be 0.0 W m^{-2} with a 90% uncertainty range of -0.4 to +0.4 W m^{-2}.

9.4.3. BC in snow and cryosphere changes

[14] The BC snow forcing estimates arise from changes in snowpack reflectivity and rapid adjustments to that forcing, constituting an adjusted forcing. The best estimate and range is based on a number of model results adjusted based on comparisons to observations of Arctic snow BC concentrations (Section 7.4 and 7.6.1). The lower (upper) bounds on snowpack BC forcing are calculated by adding in quadrature the forcing from low (high) bounds in emissions, rate of snow aging, BC mass absorption efficiency, and snow cover fraction, and using the high (low) bounds in the efficiency of BC scavenging with melt and in the role of dust in reducing snowpack albedo. The range in forcing does not account for uncertainty in the patchiness of snow cover or uncertainties in modeled cloud cover and vegetation cover. It also does not account for possible biases in modeled mid-latitude snow BC concentrations.

[15] The climate forcing for snowpack shown on Figure 9.1 scales the adjusted forcing by an efficacy of 3 (2 to 4 range) to give an forcing that accounts for both rapid adjustments in the snowpack, the strong impact of this forcing on near-surface temperature and the strong snow-albedo feedback (see Section 8). The industrial-era effective forcing for BC in snow is assessed to be +0.11 W m^{-2} with a 90% uncertainty range of +0.016 to +0.31 W m^{-2}. The all-source effective forcing is assessed to be +0.12 W m^{-2} with a 90% uncertainty range of +0.02 to +0.36 W m^{-2}.

9.4.4. BC in sea ice

[16] Radiative forcing by BC on summertime sea ice after snow has melted (bare sea ice) is assessed separately and only includes forcing by the direct change in ice albedo with the inclusion of BC. Most model studies to date have not included this forcing by BC on bare sea ice, and those that have do not separately diagnose this forcing term. While snow BC radiative forcing is dominant in the spring, bare sea ice forcing arises due to the enhanced absorption of sunlight in June-July-August-September in the Arctic Ocean. The radiative forcing bounds presented in Section 7 are based on estimates of sea ice coverage, melt-pond area, area of sea ice covered in snow, sea ice grain size, cloud cover and average solar irradiance (Section 7.6.2). The climate forcing in Figure 9.1 scales the direct radiative forcing of sea ice by an efficacy of 3 (2 to 4 range). Currently, no modeling study has explicitly calculated this efficacy for BC in sea ice. We use the same efficacy as for BC on snow effects, as both forcing types will produce similar rapid adjustments and, as with snow, forcing by BC in sea ice directly warms the sea ice and leads to ice melt and, thus, an albedo feedback. The industrial-era effective forcing for BC in sea ice is assessed to be +0.033 W m^{-2} with a 90% uncertainty range of +0.014 to +0.064 W m^{-2}. The all-source effective forcing is estimated to be +0.036 W m^{-2} with a 90% uncertainty range of +0.016 to +0.068 W m^{-2}.

9.4.5. Net effect of BC and co-emitted species

[17] It is important to remember that BC is not emitted in isolation. Co-emitted aerosol species such as organic matter, sulfate, and O_3 precursors also affect climate, and many mitigation actions could affect all of these species. Thus, 'climate forcing by BC' is a useful paradigm for exploring physical effects, but it is not a practical one: this forcing could neither be measured individually nor removed from the aerosol mix through mitigation actions.

[18] The lower two bars in Figure 9.1 demonstrate how the total climate forcing by BC (top bar), compares with the total climate forcing from the mix of BC and its co-emitted species (bottom bar). These combined forcing values require estimates of climate forcing by non-BC species, and Section 10 describes how we estimate and combine these values based on previous literature. These additional climate-forcing terms are introduced in Figure 9.1 to remind the reader of the close coupling between BC and co-emitted species. The remainder of this section continues the discussion of BC alone, and Section 10 will explore the question of co-emitted species in more depth.

9.5. Uncertainties in BC global climate forcings

[19] Uncertainties in BC global climate forcings arise from many potential sources as discussed below. Except as noted, we have assumed that diversity in model results already reflects these uncertainties.

9.5.1. Atmospheric burden, emissions, and rate of deposition

[20] Concentrations of BC in the atmosphere and in snow are affected by emissions, lifetime and removal rates. The range of lifetime estimates is largely due to uncertainties in wet deposition, leading to uncertain concentrations in both the atmosphere and cryosphere. Uncertainties in deposition rates appear to lead to large errors in the atmospheric burden in remote areas (Section 4). In the Arctic, variations in wet deposition strongly affect atmospheric BC concentrations [*Garrett et al.*, 2010] and wet deposition rates directly affect surface snow and ice concentrations. However, our atmospheric direct forcing estimate is constrained by observations (Section 5). Larger modeled emission rates would give a larger burden, a different correction to observations, and very little change in forcing. A similar argument applies to atmospheric lifetime, although observational constraints are less stringent over oceans. In-situ observations of surface snow concentrations have similarly been used to adjust for apparent biases in modeled surface snow concentrations (Section 7), though this adjustment fails to account for interannual variability in snow concentrations.

[21] Large uncertainties in atmospheric burden estimates may result from interpretation of observations. In some of the observations of absorption optical depth, dust cannot be distinguished from BC, which can lead to an overestimate of BC concentrations (Section 4). Also important for direct radiative forcing and cloud effects is the atmospheric vertical distribution of BC. Vertical distribution varies between models and can lead to factor of two differences in direct forcing (Section 5). Uncertainties in BC distribution, especially aloft, may cause large changes in cloud effects that are affected by

BC concentration (Section 6). Although recent observations can help constrain this uncertainty range for the direct forcing, this has not been possible for the cloud effect terms, where this uncertainty is assumed to be captured by the range of model forcing results (Section 6).

9.5.2. Selection of pre-industrial emissions

[22] Industrial-era BC forcing depends on the magnitude and distribution of pre-industrial emissions and on atmospheric aerosol transport pathways and deposition rates in the pre-industrial climate. Forcing by BC in the cryosphere further depends on the distribution of snow and ice cover in 1750. Shifts in the latitudinal distribution of emissions will affect BC atmospheric lifetimes, forcing efficiency, proximity to clouds, and deposition to surface snow and ice. Pre-industrial open burning emissions are particularly uncertain, and changes in assumptions about both the magnitude and location of these emissions might significantly change the estimate of pre-industrial forcing. Presently, the largest open-burning emissions are in sub-tropical Africa and South America and are largely anthropogenic (Section 3). In contrast, in 1750 there was likely significant open burning from land-clearing activities at northern mid-latitudes.

9.5.3. Scaling to emission rate or atmospheric burden

[23] We assume in this work that the components of BC forcing generally scale with global emissions or atmospheric burdens. This is reasonably valid for direct forcing. For cloud and cryosphere forcing (see Sections 6 and 7), this scaling may be valid for small deviations from the modeled state, but it has not been properly evaluated for many of the effects considered here. In particular this linear scaling may not hold over highly polluted regions or for large estimated changes. For cryosphere BC forcing, changes in the latitudinal distribution of BC emissions between pre-industrial and present-day makes scaling by emissions to estimate pre-industrial forcing particularly uncertain. This is accounted for using modelled estimates of the fraction of total emissions from biomass burning deposited to snow in 1750 versus in present-day.

[24] Emissions of co-emitted species and other aerosol, such as dust, also affect direct forcing, cloud forcing and snow and ice forcing by BC. Uncertainties in the regional pattern of emission are also important for global forcing, as BC emitted in different regions can give different climate forcing per emission due to longer atmospheric lifetime, snow deposition, or above-cloud fraction.

9.5.4. Dependence on atmospheric and surface state

[25] Climate forcing estimates depend on latitude, background clouds, surface albedo and aerosol, especially the relative vertical distributions of clouds and BC. Underlying surface reflectivity, particularly from distributions of snow and ice, are important both for BC snow forcing and accurate determination of the direct effect. For BC in snow we use uncertainties from one model study to derive the bounds in present-day forcing, which include uncertainty in snow cover. For BC in sea ice, bounds are calculated based on a range in sea ice cover, snow cover on sea ice, melt ponds on sea ice, and cloud cover. Changes in snow and ice cover from pre-industrial to present-day are not accounted for in the industrial-era estimates of BC cryosphere forcing (Section 7). For the other terms, uncertainty due to atmospheric state has not been explicitly estimated, but it is assumed to be captured by the range of model results employed.

9.6. Total forcing estimates and comparison with previous work

[26] The total effective forcing value and uncertainty in Figure 9.1 are estimated by combining the estimates and uncertainties of the individual forcing terms. The construction of this error is shown in Figure 9.2, which shows the error analysis for individual terms (top panel), the role of semi-direct effects and efficacy (middle panel) and the aggregate climate forcing terms (bottom panel). To combine errors we make a number of assumptions, outlined below.

1. We assume that the total effective forcing of BC is represented by the sum of individual forcing terms. Efficacies are explicitly included in the individual bars for the BC-on-snow and BC-on-sea-ice terms, but not explicitly included for the other terms (see center panel of Figure 9.2). Our summation, therefore, assumes that the efficacy of the combination of the direct radiative forcing terms and the adjusted forcing from the cloud effects and semi direct effects would be equal to one and, therefore, comparable to the effective snow and sea-ice forcings. This implies that all rapid adjustment effects are accounted for and the resulting geographical pattern of forcing would not be that different to an equivalent forcing from CO_2 to make a material difference to the efficacy.

2. To account for covariance between errors in component terms, we assume that emission uncertainties provide the only commonality between the uncertainties of each term. We also assume that emission uncertainty has a negligible effect on the cloud forcing uncertainty, as the large uncertainties are caused by differences in model processes. Emission uncertainty accounts for 50% of the relative uncertainty in direct forcing (Section 5) and 32% of the relative uncertainty in snow and sea-ice effective forcing (Section 7). This leads to a 0.16 correlation between the direct forcing and the snow and sea ice terms, and a correlation of 0.1 between the snow and sea-ice terms themselves.

3. We assume that uncertainties, shown by whiskers on the contributing forcings in Figure 9.1, represent a 90% (5%-95%) uncertainty range and construct the probability distribution functions (PDFs) in Figure 9.2 accordingly. The uncertainty of the total effective forcing also assumes that the distribution of probability within a given range is formed from combining either normal or log-normal distributions. Symmetric normal distributions are used for the mixed-phase cloud, ice-cloud and cloud-droplet inclusion effects. Asymmetric normal distributions are used for the direct effect and the liquid-cloud and semi-direct effects. Asymmetric log-normal distributions are used for the BC-in-snow and the BC-in-sea-ice effects.

[27] Using these assumptions a Monte Carlo model was run one million times to produce the estimate of climate forcing. The random number sequences generated are used to choose a point to sample in the forcing range, based on a fraction of the area under the probability distribution curve. The forcing value defined by the fractional area is then chosen to represent the forcing for that mechanism during the given iteration. Correlated errors are allowed for by making the appropriate

fraction of the random numbers generated match between the direct forcing and the snow and sea ice terms. To generate correlated errors a subset of the same random number sequences are used for the correlated forcing terms. For example, 10% of the random number sequence for snow and sea-ice identically match, giving their million-point forcing series a correlation of 0.1. The PDFs for the different climate-forcing terms are shown in Figure 9.2. Using this methodology the individual forcing terms can be combined to estimate the overall error represented by the total effective forcing error bar in Figure 9.1 and the pdf (black line) shown in the bottom panel of Figure 9.2.

[28] The IPCC Fourth Assessment Report report only considered radiative forcing of BC and did not consider its total climate forcing [*Forster et al.*, 2007]. IPCC estimated a 1750-to-2005 fossil-fuel BC direct radiative forcing of +0.2 ± 0.15 W m^{-2}, comparable to our direct-forcing estimate of BC from fossil fuel of only +0.16 W m^{-2}. IPCC did not explicitly evaluate the direct forcing of other sources of BC, including biofuel. Nevertheless, Table 2.13 of *Forster et al.* [2007] lists the direct radiative forcing values for 'anthropogenic' BC as obtained from published studies and AeroCom models, which together yield an average of +0.34 W m^{-2} (+0.09 to +0.59 W m^{-2} range). This value is smaller than the best estimate found here of +0.43 W m^{-2} (+0.17 to +0.68 W m^{-2} range). The evolution of forcing estimates between the IPCC tabulation and the present assessment is explained as follows.

1. Some of the studies in the IPCC tabulation used relatively larger emission estimates. Forcing adjusted to a common bottom-up emission inventory is reflected in the AeroCom average of +0.27 W m^{-2}.

2. AAOD and, hence, forcing, increases by about 50% when the change in MAC_{BC} due to internal mixing is considered, giving +0.41 W m^{-2}.

3. The apparent BC burden in the atmosphere is greater than that in the models. The adjustment required to match industrial-era observations, even after the consideration of increased MAC_{BC}, is an additional 16%, giving +0.48 W m^{-2}. This value is similar to the +0.51 average in Table 5.2, but not identical, because additional models are included.

4. The estimated model-average forcing was decreased by 15% to account for the fact that models place BC too high in the atmosphere, giving a total of +0.43 W m^{-2}.

5. The higher value of forcing presented here comes from applying AERONET observational constraints, and is supported by observations of increased MAC_{BC} and underestimated atmospheric absorption. Therefore, our estimate is more robust than the purely model-based estimate in IPCC.

[29] The estimate of all-source (*i.e.,* 1750 background plus industrial-era) direct radiative forcing of +0.49 W m^{-2} with a range of +0.20 to +0.76 W m^{-2} is smaller than estimates of around +1.0 W m^{-2} suggested by *Sato et al.* [2003] because we avoided bias in deriving BC AAOD from AERONET observations (see Section 5.8). Our estimate is also smaller than the +0.9 W m^{-2} given by *Ramanathan and Carmichael* [2008] because our estimate of BC AAOD is lower for reasons that are not clear.

[30] The principal results from our uncertainty analysis are:

1. Considering only radiative forcings ignores the changes imposed by rapid adjustments. For BC, all effects need to be considered to get a true representation of the climate forcing. These additional effects are demonstrated in the middle panel of Figure 9.2, where accounting for many semi-direct effects leads to a more-negative liquid-cloud climate forcing, and accounting for the higher efficacy of BC-in-snow and BC-in-ice leads to a more positive forcing. These adjustments also significantly increase the uncertainty in their respective climate forcings. These uncertainties, along with the uncertain ice cloud forcing, lead to the overall rather large uncertainty in the total effective BC climate forcing.

2. The globally averaged, industrial-era, total effective forcing from BC is +0.77 W m^{-2} with a 90% uncertainty range of +0.06 to +1.53 W m^{-2}. This distribution gives a 6% chance that the net effect of BC in isolation is actually a cooling effect (negative climate forcing), rather than a warming, when all cloud effects are considered. It is, therefore, very likely (96% chance) that BC leads to an overall positive forcing and climate warming.

3. The radiative forcing from the BC direct effect is +0.43 W m^{-2}, with a 90% uncertainty range of +0.17 to +0.68 Wm^{-2}.

4. While there are large uncertainties in the role of BC effects on clouds, the best estimate of their combined net effect, including the semi-direct effect and cloud droplet inclusions, is +0.17 W m^{-2} with a 90 % uncertainty range of -0.45 to +0.86 W m^{-2}. Therefore, studies without any cloud indirect effects may have a negative bias in forcing. Model studies agree that semi-direct and liquid-cloud estimates are negative, while only a few studies have examined how BC affects mixed-phase clouds, predicting positive forcing. As the two effects are nearly equal in magnitude but opposite in sign, the positive net cloud forcing arises from the poorly understood role of cloud droplet inclusions and suffers from lack of confirmation. Finally, only one group has estimated the BC forcing effect for ice clouds, indicating that the magnitude could be relatively large but the sign is unknown.

5. The combined BC on snow and BC on sea-ice effective forcing over the industrial era is estimated to be +0.14 W m^{-2} with a 90 % uncertainty range of +0.04 to +0.34 W m^{-2}. The effects of BC on snow and ice is unequivocally a net positive forcing, so any study of BC climate forcing that does not include those effects is biased towards a smaller warming effect.

[31] Our assessment is that the overall climate warming for BC is more positive and more uncertain than that from the direct radiative forcing alone (*i.e.,* comparing red and black pdfs in the bottom panel of Figure 9.2). The more positive climate forcing compared to the BC direct radiative forcing comes from incorporating the BC snow and sea-ice effective forcings. Introducing additional cloud forcing terms increase both the median and spread of climate forcing. The total, direct radiative forcing from BC of +0.43 W m^{-2} (90% uncertainty range of +0.17 to +0.68 W m^{-2}) can be compared to the total effective BC forcing of +0.77 W m^{-2} (90% uncertainty range of +0.06 to +1.53 W m^{-2}).

[32] Caution needs to be applied when considering total, global-average forcing as the sole metric when considering the

impact of BC emissions on climate change. The climate forcing of BC, and all aerosols, is much more regionally variable than for long-lived GHGs and this metric does not relate to expected precipitation changes (see Section 8). These factors may affect the consideration of how BC would be included in climate mitigation strategies (see Section 12).

10. Net climate forcing by black-carbon-rich source categories

10.1. Section summary

[1]

1. The net climate forcing of emissions from BC-rich source categories or individual source types depends on the effects of co-emitted species, such as organic carbon, sulfate, and gaseous constituents in addition to all effects of BC.

2. We use previously developed forcing-per-emission values to provide a comprehensive estimate of forcing from BC-rich source emissions. As for BC, large uncertainties are introduced in estimating cloud effects of co-emitted aerosols and aerosol precursors.

3. Attribution of direct forcing and cryosphere changes to emitting sources is relatively straightforward. For these effects, net forcing is positive for all BC-rich source categories.

4. Attribution of cloud changes to emitting sources is uncertain because effects on cloud droplets are non-linear and complex. When this indirect forcing contribution is included, using a simple linear proportionality to emission rate, net climate forcing becomes neutral to negative for all source categories except diesel engines.

5. Source categories are often heterogeneous. Individual sources within each category have different profiles of chemical emission components and may have relatively more positive or more negative forcing than the category average might indicate.

6. Our best estimate of the net climate forcing by all emissions from BC-rich sources is -0.08 W m^{-2} with 90% uncertainty bounds of (-1.24, +0.81) W m^{-2}. This total would be near zero (*i.e.,* less than 0.01 W m^{-2}), with a range of (-0.62, +0.57 W m^{-2}) if open burning emissions, which emit high levels of organic matter, were excluded.

7. For most of these source categories, short-lived species have substantial forcing in the first year after emission, and this forcing is significant in comparison with forcing by emissions of all species over longer time scales. When climate forcing by all co-emitted species is integrated over 100 years, the magnitude of integrated forcing by short-lived species from each source category ranges from 5-60% of forcing by longer-lived species, including CH_4 and CO_2. The sign of short-lived species can be either positive, enhancing GHG warming, or negative.

8. Integrating net forcing by aerosols, O_3, CH_4, and CO_2 masks complex spatial patterns in forcing that differ over time. Climate forcing through effects on the CH_4 system tends to offset some of the effects of short-lived species. For diesel engines, longer-term negative forcing via NO_x offsets short-lived positive forcing; for biofuel sources, longer-term positive forcing via organic gases offsets short-lived negative forcing that is largely attributable to cloud effects.

10.2. Introduction

[2] Until this point, we have focused entirely on how BC affects radiative and climate forcing. However, BC is never emitted in isolation. Changes in source magnitudes affect all emitted species, whether those changes are deliberately chosen for mitigation, or occur without intention. Estimates of climate changes caused by BC forcing alone were summarized in the previous section, but those values do not reflect the net climate effect of altering sources whose emissions contain high concentrations of BC (*i.e.,* BC-rich sources).

[3] In this section, we estimate the net climate forcing of emissions from BC-rich sources, considering the major emitted species. Some species that make minor contributions to mass have been ignored. In order to provide total climate forcing by these sources, estimates of forcing by other species that are co-emitted with BC are also required. As in the presentation for BC, we require consideration of all effects. However, this assessment does not include recommendations for climate forcing by other species and we rely mainly on previous published summaries for these values. Therefore, the resulting quantification should be viewed cautiously. Although accounting for forcing by co-emitted species is fraught with uncertainty, ignoring these effects may convey a mistaken impression about the magnitude or even the sign of net climate forcing by BC-rich sources.

[4] We first discuss the approach to estimating net forcing values for a particular source activity. In Section 10.2, we describe methods to estimate forcing-per-emission values for each co-emitted species. Then, in Section 10.3, we estimate the net climate effect of the BC-rich source categories summarized in Section 3. These categories are aggregates of many individual source types, such as certain types of diesel engines or cooking stoves, whose emission component profile may differ from that of the aggregate category. Estimates of forcing for a few of these individual sources will be summarized in Section 10.4. In these first sections, we present only forcing by short-lived species (*i.e.,* those with lifetimes less than one year). This near-immediate forcing is attributable primarily to aerosols, their precursors, and emitted O_3 precursors. In Section 10.5, this forcing in the very short term is compared with GHG forcing on decadal scales.

10.3. Approach to estimating forcing from BC-rich source categories

[5] Determining the net change in effective climate forcing per change in emission or per change in activity is the goal of this section. This quantitative measure may be thought of as the slope of a curve representing forcing versus activity, at present-day conditions. A fully comprehensive measure would aggregate all effects caused by all emitted pollutants from a particular source. Previous work on this topic has estimated the influence of a particular source either by summarizing direct forcing by all pollutants [*Fuglestvedt et al.*, 2010], or by examining the influence of all pollutants from source sectors with a model that represents multiple climate mechanisms [*Jacobson,* 2004; *Unger et al.* 2010].

[6] Missing in these progressive studies are systematic methods for incorporating scientific uncertainties, for incorporating findings from other studies that may differ, or for altering findings as knowledge advances. Here, we present the foundations of such a framework. Its essential elements are expert recommendations of the following for each chemical species emitted from a source:

1. Emission factors for a source activity;

2. Central values and uncertainties for the radiative forcings, obtained for a defined emission rate;

3. Central values and uncertainties for rapid adjustments, fast enough to be considered as part of an effective forcing, normalized to a defined emission rate.

[7] We begin with a source activity that emits *I* pollutants. Each pollutant may have *J* effects that are best expressed as radiative forcing values, and *K* effects that are expressed as rapid adjustments. To a first approximation, total climate forcing *CF* (in W m^{-2}) by a particular source activity is

$$CF = \sum_{i=1}^{I} EF_i \left(\sum_{j=1}^{J} rforc_{i,j} + \sum_{k=1}^{K} fresp_{i,k} \right) \quad (10.1)$$

where *FC* is fuel consumption by the activity in kg s^{-1}, and EF_i is the emission factor of pollutant *i* (kg pollutant (kg fuel)$^{-1}$). The bracket contains forcing terms: $RF_{i,j}$ is the change in radiative forcing, for effect *j* and species *i*, per emission rate of species *i* emitted ((W m^{-2}) (kg s^{-1})$^{-1}$), and $RA_{i,k}$ is the rapid adjustment for effect *k* and species *i* given in the same units. Each effect must be carefully distributed among the summations to avoid double counting. Further, this calculation assumes that forcings are additive. Although slight variants of the units given here are used in this section, the principle remains the same.

[8] Ideally the value $rforc_{i,j}$ would be determined as:

$$rforc_{i,j} = \left. \frac{\partial f_j}{\partial e_i} \right|_{PD} \quad (10.2)$$

where f_j is the forcing via mechanism *j*, e_i is the emission of species *i*, the notation *PD* indicates present-day, and the partial derivative indicates that no other effects are operating and all other species are held constant. The same is true for the rapid adjustments. In practice, models usually provide total forcing or anthropogenic forcing, not partial derivatives. The assumption of linearity with respect to emission rate is adequate for many of the effects discussed here, but it breaks down for cloud microphysical forcings, as noted in the last section. Incremental changes in emissions are more realistic than removal or addition of entire source categories or pollutant categories. Model studies examining smaller emission changes may clarify whether total forcing divided by emission rate produces reasonable estimates for $rforc_{i,j}$ or $fresp_{,j}$.

[9] Two other challenges in applying Equation 10.1 above are interactions between species that affect forcing nonlinearly [*Stier et al.*, 2006b], and dependence of forcing on the region of emission [*Berntsen et al.*, 2006; *Naik et al.*, 2007; see Section 11]. We acknowledge that further development of Equation 10.1 should provide a method to account for these dependences. For the analysis here, we use total forcing divided by emission to approximate $rforc_{i,j}$ and $fresp_{i,j}$ for BC and all co-emitted species.

10.4. Climate forcing per emission for co-emitted aerosols and precursors

[10] Earlier sections of this assessment examined climate forcing by BC only. As discussed previously, we rely mainly on previous published summaries and analyses for forcing values of co-emitted species and have not evaluated the rigor of these estimates. Table 10.1 summarizes the basis for our best estimates of forcing per emission for sulfate and organic matter, for all effects that were previously given for BC, and the values used are given in Appendix C (Table C.1). The following sub-sections give more detail about the values chosen.

10.4.1. Direct effect for co-emitted aerosol and precursors

[11] Table 10.2 summarizes global mean estimates of direct radiative forcing and radiative forcing per emission for primary organic aerosol (POA) from a variety of studies. With little absorption, POA leads to a negative radiative forcing. Radiative forcing by total anthropogenic POA varies widely, from -0.06 to -0.49 W m^{-2}, with the smallest estimate coming from the study with one of the largest emissions. Consequently, the relative diversity in the radiative forcing per unit emission is even greater, with values ranging from -0.8 to -7.4 (μW m^{-2})(Gg yr^{-1})$^{-1}$. This diversity is largely due to uncertainty in the radiative forcing per unit mass, which varies from -24 to -198 W m^{-2} g^{-1}. Differences in radiative forcing per unit mass are more likely caused by assumptions about water uptake or optical properties than by differences in its vertical distribution, as most modeling studies do not represent absorption by OA. For radiative forcing by POA from fossil-fuel combustion, estimates of radiative forcing vary from -0.01 to -0.09 W m^{-2}, and the forcing per unit emission varies from -0.4 to -19 (μW m^{-2})(Gg yr^{-1})$^{-1}$, which is somewhat larger than that for total POA. A best estimate for POA radiative forcing per mass emitted with 90% uncertainty bounds is -4 ± 3 μW m^{-2} (Gg yr^{-1})$^{-1}$, with greater magnitudes for POA from fossil-fuel combustion (-9 ± 9). With our increased estimate of 42000 Gg yr^{-1} (see Section 10.5), this gives a POA radiative forcing of -0.20 W m^{-2}.

[12] Forcing by light-absorbing organic carbon, known as brown carbon, has not been explicitly considered here, although some of the models listed in Table 10.2 assume a small amount of absorption. *Park et al.* [2010] estimated that brown carbon over East Asia had positive forcing about 15% as great as BC. No global model has yet isolated forcing by this material, although *Jacobson et al.* [2001] assumed absorption for some OA and estimated smaller negative forcing did than other models. Furthermore, if brown carbon contributes to atmospheric absorption and positive forcing, its contribution should be removed from the estimate of BC AAOD based on observations. A fraction of our BC forcing estimate may in fact be attributable to brown carbon.

[13] The most recent IPCC report provides a best estimate of -0.4 ± 0.2 W m^{-2} for direct radiative forcing by anthropogenic sulfate [*Forster et al.*, 2007]. Assuming the AeroCom estimate of 109,000 Gg S yr^{-1} [*Dentener et al.*, 2006], this translates to a range of -3.7 ± 1.8 (μW m^{-2})(Gg yr^{-1})$^{-1}$ for radiative forcing per mass of S emitted.

10.4.2. Liquid cloud effect for co-emitted aerosol and precursors

[14] The effect of co-emitted aerosol on liquid clouds has large uncertainties, both because estimates of the total liquid-cloud radiative forcing of anthropogenic aerosol vary widely, and because studies that isolate the contributions of individual pollutants or sources are scarce. (Exceptions are *Jacobson* [2002] and *Bauer et al.* [2010].) We adopt a preliminary approach to estimating changes in liquid-cloud forcing due to

co-emitted species, which we describe first before listing several cautions.

[15] Our preliminary estimate of cloud climate forcing assumes that: (1) the total liquid-cloud effect has a central value of -1.25 W m^{-2} for both albedo and lifetime effects and a range of -2.9 to -0.3 W m^{-2}, as summarized by *Isaksen et al.* [2009]; (2) this effect can, to first order, be apportioned among individual species; (3) the liquid-cloud change in the studies contributing to the estimate is attributable to submicron species that are considered anthropogenic: BC, organic matter, and sulfate; and (4) except for BC, the cloud effect may be apportioned by mass. The latter assumption is approximately justified if particle size is the dominant factor determining the number of CCN, because organic matter and sulfate have similar size distributions. The apportionment by mass may produce a negative bias in forcing by organic matter, as its lower solubility has not been considered in the apportionment.

[16] Details of the liquid-cloud estimate are given in Appendix C (Table C.2 and C.3). We estimate sulfate liquid-cloud forcing as -0.81 W m^{-2}, with an uncertainty range of -1.80 to -0.30 W m^{-2}. Liquid-cloud forcing attributable to organic matter is estimated as -0.38 W m^{-2} with an uncertainty range of -0.84 to -0.14 W m^{-2}. These estimates are then divided by AeroCom anthropogenic emission rates of 109000 Gg yr^{-1} for S and 30000 Gg yr^{-1} for organic matter [*Dentener et al.*, 2006] to obtain values of forcing-per-emission. Individual studies to determine liquid-cloud forcing may have used different emission rates, but an in-depth examination is beyond the scope of this assessment. This method of apportioning the forcing by burden, and scaling the species-specific forcing by emission, implicitly accounts for the conversion of SO_2 to sulfate.

[17] Our treatment of liquid-cloud effects deserves several caveats. We caution that the liquid-cloud estimate for SO_2 and POA has not undergone a thorough examination as have the effects of BC. We have chosen to present a more realistic but less rigorous picture for total forcing by sources that are BC-rich, rather than a physically unrealistic depiction that evaluates BC alone. No modeling studies have examined the validity of apportioning total liquid-cloud effects among individual species.

[18] The relationship between cloud forcing, CCN, and emissions is not expected to be linear. Cloud forcing is more sensitive to increased particle concentration in a cleaner atmosphere, as demonstrated for global averages by *Boucher and Pham* [2002]. This is consistent with inferences of low indirect effect over land [*Ruckstuhl et al.*, 2010]. Therefore, our linear apportionment could overestimate the impact of the small fraction of total particle mass attributable to BC-rich sources.

[19] Studies disagree on the importance of primary particles, and the relationship between cloud forcing and the emission of primary particles such as BC or POA may not even be monotonic. One study indicates that primary particles play a larger role in cloud formation than other particles [*Adams and Seinfeld*, 2003], while others find that primary emissions suppress nucleation [*Bauer et al.*, 2010], and therefore have a much lower influence on CCN than would be expected in the absence of gas-particle interactions [*Merikanto et al.*, 2009].

[20] The discussion above indicates that the linear apportionment used here is a zero-order estimate. Yet, present understanding is insufficient to support a different apportionment. Although there is some evidence that forcing-per-emission values may be overestimated, models that account for microphysical interactions [*Bauer et al.*, 2010; *Koch et al.*, 2011a] have indicated greater forcing-per-emission of POA via liquid-cloud changes than our central value. The uncertainties given here reflect only the uncertainty in the magnitude of the indirect effect, not the uncertainty in apportionment, or regional differences in cloud behavior.

10.4.3. Other cloud effects for co-emitted aerosol and precursors

[21] Other cloud effects (*i.e.,* mixed-phase, ice-cloud and semi-direct effects) considered for BC are assumed negligible for sulfate and organic matter. These two species may influence water condensation and ice nucleation activity if they are emitted with BC (see Sections 2.8 and 6.6). This is particularly relevant for cold ice clouds, where BC particles do not become water droplets prior to ice formation. In this case, it is not possible to separate or scale cloud effects from the amount of co-emitted species. Two GCM studies [*Hoose et al.*, 2008; *Storelvmo et al.*, 2008] suggest that sulfate coating decreases the ability of mineral dust to act as IN. This increases the lifetime of supercooled water clouds, producing negative forcing. These effects have not yet been quantified and are not included here.

[22] Current understanding indicates that aerosols with minimal light absorption have little effect on semi-direct forcing. All such changes are caused by light absorption that heats the atmosphere at various vertical locations (see Figure 6.1). We also do not include the effects of other absorbing material within cloud droplets, although absorbing OA may also contribute to enhanced cloud-droplet absorption [*Jacobson*, 2012].

10.4.4. Snow albedo forcing for co-emitted aerosol

[23] *Doherty et al.* [2010] found that the light-absorbing aerosol in Arctic snow and sea ice had a strong wavelength dependence, and inferred from this the amount of light absorption due to BC versus other species, specifically brown carbon, mineral dust and soil dust. They reported that 40% of the spectrally weighted light absorption in snow and sea ice is due to these non-BC constituents. Only a small fraction of this absorption is due to mineral and soil dust, so we estimate global snow and sea-ice forcing by organic matter from combustion as 20% that of BC. We then scale this value to emissions of organic matter to produce an effective forcing per emission of 0.9 μW m^{-2} (Gg yr^{-1})$^{-1}$ with a range of 0 - 3.0, assuming an efficacy with a central value of 3 and an upper bound of 4. POA from solid-fuel combustion is known to absorb light, while other organic matter is not. Therefore, this forcing was applied only to POA emitted from solid fuel: biofuel, coal, and open biomass burning.

10.4.5. Forcing by co-emitted gaseous species

[24] Short-lived, co-emitted gaseous species considered here include carbon monoxide (CO), volatile organic compounds (VOCs), and NO_x. These species produce indirect forcing by interacting with tropospheric O_3 and CH_4 and, for NO_x, by producing nitrate. *Fuglestvedt et al.* [2010] summarized studies on radiative forcing by these compounds for the development of metrics. They did not provide recommendations for central values of forcing per emission, but a later study [*Uherek et al.*, 2010] used their summary to provide GWP values. We inferred

a best estimate of forcing per emission using studies cited by *Fuglestvedt et al.* [2010], as shown in Appendix C (Table C.4). For each species, forcing is separated by mechanism, as suggested by *Shindell et al.* [2005]. All species increase O_3, representing a positive forcing that occurs within the first year. NO_x increases nitrate aerosol, giving a negative first-year forcing. These species also alter the lifetime of CH_4, causing forcing that lasts a few decades. CO and VOCs cause a positive forcing, while NO_x causes a negative forcing.

[25] Studies cited in *Fuglestvedt et al.* [2010] gave forcing values for the effects of NO_x emissions on CH_4 and tropospheric O_3 abundances but not for nitrate aerosol resulting from NO_x emission. We estimated a value of forcing per emission by nitrate by assuming that the nitrate forcing summarized by *Forster et al.* [2007] had the same emission base as that for O_3 from NO_x. This method is legitimate for short-lived species, such as nitrate and O_3 caused by emissions of NO_x or volatile organic compounds. (Present-day forcing values for long-lived species result from all historical emissions that remain in the atmosphere, and cannot be used to estimate forcing per emission.) While *Forster et al.* [2007] attributed all nitrate forcing to NO_x emissions, *Unger et al.* [2010] reported that sectors with substantial ammonia emissions also affect nitrate forcing. The nonlinearity of ammonium, sulfate, nitrate, and NO_x chemistry means that changes in nitrate forcing are difficult to attribute to particular sectors. We assign only 44% of the total nitrate forcing to NO_x emissions, based on the ratio of NO_x-related to total nitrate forcing reported by *Unger et al.* [2010].

10.4.6. Climate forcing by secondary organic aerosol

[26] Estimating the climate impact of sources using POA alone ignores the complex evolution of organic aerosol throughout the atmosphere. Emitted precursors lead to formation of substantial quantities of SOA [*de Gouw and Jimenez,* 2009]. Oxygenated organic aerosol, thought to be equivalent to SOA, is found wherever measurements are made [*Zhang et al.*, 2007]. SOA yields from diesel engines and wood stoves were estimated to be small in comparison to POA emissions [*Chan et al.*, 2009]. However, observed SOA appears to be much more prevalent than could be explained by models that treat identified SOA precursor molecules [*Robinson et al.*, 2007]. For that reason, mechanisms that account for SOA production have been proposed, using the fraction of emitted vapors with low volatility as inputs [*Donahue et al.*, 2006].

[27] SOA associated with individual sources has not been resolved in climate models. Direct forcing is often provided for POA alone [*Schulz et al.*, 2006], and models of cloud forcing have usually not distinguished POA versus SOA burdens. Simulations by *O'Donnell et al.* [2011] gave a direct effect due to SOA of -0.29 W m^{-2} and an indirect effect of +0.20 W m^{-2}. In this model, which did not include the volatility representation of SOA formation, 90% of the SOA burden came from biogenic sources.

[28] POA:BC ratios may underestimate the total atmospheric OA attributable to each source. Nevertheless, in this analysis, we neglect direct and indirect forcing by SOA. The single estimate of net SOA forcing given above is small, and the chain that relates precursor emissions to concentrations and global forcing is presently limited. We acknowledge, however, that this omission could be a source of bias.

10.5. Net climate forcing by BC-rich source categories

[29] Using the values developed in the previous section, total climate forcing by BC-rich source categories can be estimated. Forcing per emission for each effect in W m^{-2} (Tg yr^{-1})$^{-1}$ is multiplied by total emissions, yielding units of W m^{-2}. Forcings by each species emitted within each category are then summed to provide total forcing. Annual emissions of BC, POA, SO_2, CO, non-methane volatile organic compounds (NMVOCs), and NO_x from each source category were summarized from the GAINS database for the year 2000 for energy-related emissions. Open burning estimates come from the RETRO database. Emissions were adjusted to reflect the observationally based scale factors given in Section 5.7, so that energy-related emissions were scaled by factors of 0.9 to 1.7, depending on the category, and open-burning estimates were increased by a factor of 1.4 to 1.7. Emission rates used are given in Appendix C (Table C.5). For energy-related burning, we have assumed that the most uncertain factor is levels of activity with relatively high emission rates, and have adjusted those emissions associated with incomplete combustion (BC, POA, CO, NMVOC) with the scale factors used for BC. For open biomass burning, we assume that the cause of the uncertainty could be the low bias in emission factors of BC alone (see Section 3.7.2.3) and adjust only the BC emissions. Only the effects of POA are included here; some of the gaseous NMVOCs from these sources could form SOA after emission, adding to aerosol-driven forcing mechanisms. This possibility is discussed in Section 10.5.6.

[30] Figure 10.1 shows forcing by short-lived emissions in the BC-rich source categories summarized in Figure 3.2. These categories comprise 99% of the BC emissions, and the effective climate forcing includes all aerosol direct, indirect, and snow effects. We also include forcing changes caused by the interaction of CO, VOCs and NO_x with tropospheric O_3. These effects capture most of the forcing that occurs in the first year after emission.

[31] The forcing shown in Figure 10.1 is similar to that shown by *Forster et al.* [2007] because it is the value that would be observed if year-2000 emission rates continued indefinitely. It differs from IPCC figures because forcing is grouped by source category instead of by species, and because it gives effective forcing values instead of direct forcing. The species chosen for this figure exert their forcing entirely within the first year after emission. Other emitted species or effects that act over longer time scales will be discussed in Section 10.7. We have not included effective forcing due to vegetation changes [*Collins et al.*, 2010].

[32] The top bar in Figure 10.1 shows the forcing components that can be attributed to emissions with high confidence: direct forcing by aerosol and gases, effective cryosphere forcing, and cloud response to aerosol absorption. Attribution of liquid-cloud forcing to individual aerosol species or to particular sources is not well developed. We therefore segregate these forcing terms in the second (middle) bar, for which we have less confidence in attribution. Also included in this low-confidence bar is the negative forcing due to nitrate aerosol. The bottom bar shows estimated net forcing by each emission

source, or the combination of high-confidence and low-confidence components.

[33] Uncertainties in aerosol forcing only, as discussed throughout this assessment for BC and in earlier sections for other aerosol species, are reflected in Figure 10.1. Uncertainties in emission factors and gaseous forcing are also important and are not represented here. A bar centered on the zero line means that forcing has equal probability of being positive or negative; a bar that barely crosses the zero line means that there is a slight uncertainty that the forcing has a different sign than the central estimate. In combining uncertainties, most of the effects are assumed to be independent. However, the best estimates and uncertainties for the effects of individual aerosol species on liquid clouds were derived by a simple subtraction. These cloud uncertainties are assumed to be fully correlated with each other.

[34] As the top bars in Figure 10.1 demonstrate, the net effect of direct and cryosphere forcing by aerosols and gases is positive with high confidence for many source categories. Inclusion of cloud forcing components (middle bar for each source) makes forcing more negative and increases uncertainty, especially when sources have comparatively large emissions of other aerosols or precursors. Cloud forcing also increases uncertainty in the sign of net forcings (lowest bar for each source). This simple apportionment is subject to several uncertainties, as detailed in Section 10.5.6.

[35] Positive and negative forcing components and sources of uncertainty differ among source categories, as discussed in more detail below. We also compare the values in Figure 10.1 with the few studies that have examined the total impact of economic sectors. This comparison must be interpreted in light of the fact that BC-rich source categories differ from total sectors.

10.5.1. Diesel engines

[36] Forcing that can be easily attributed to diesel emissions is positive with high confidence. Both cloud and nitrate forcing reduce the net forcing and increase uncertainty.

[37] BC is a large fraction of aerosol emissions from both on-road and off-road diesel engines. The relative impact of organic matter is low, and negative forcing in the high-confidence category comes primarily from the semi-direct effect. In the low-confidence group, negative cloud forcing, attributable to sulfur, approximately cancels the net positive cloud forcing by BC. This impact is greater in regions where low-sulfur fuel has not been mandated.

[38] In *Unger et al.* [2010], total cloud effects (including semi-direct effects) from all on-road engines are strongly positive and greater than one-half the direct BC forcing. *Bauer et al.* [2010] find that diesel emissions give positive cloud forcing equal to the direct forcing, but this study did not include sulfur emissions. *Jacobson* [2010] found a net decrease in cloud optical depth attributable to total fossil-fuel BC, OA, and sulfur, although his study included only primary sulfur and aerosol components in order to examine the effect of end-of-pipe particulate controls. The effects of sulfur co-emitted with diesel engines have not been examined.

[39] Negative forcing by nitrate is also substantial in comparison with other forcing mechanisms, in agreement with *Unger et al.* [2010]. Neither *Bauer et al.* [2010] nor *Jacobson* [2010] considered changes in NO_x emissions.

10.5.2. Industrial coal

[40] Like diesel engines, industrial coal emissions (mostly from small industry) have a relatively large BC component and a small POA component. These emissions also include substantial sulfur, which causes negative forcing for both direct and cloud categories. These strong negative forcings agree with the results of *Unger et al.* [2010].

10.5.3. Residential solid fuel

[41] Forcings that are easily attributable to residential biofuel (top bar) are also strongly positive. Although POA-to-BC ratios are higher than for diesel engines, negative direct forcing by POA counteracts only about 20% of the BC direct forcing. This negative forcing would be greater if secondary organic aerosol was included here, but it still would not cancel BC forcing. In addition, absorption by OA deposited on snow and changes in tropospheric O_3 due to carbon monoxide and VOC add to positive forcing.

[42] Because these sources also emit POA, however, large negative forcing due to liquid-cloud interactions is predicted and introduces very large uncertainty. With our simple apportionment, these cloud changes are sufficient to make the net forcing negative. NO_x emissions are low for these sources, so NO_x effects on either O_3 or nitrate forcing play very little role.

[43] A critical question is whether the cloud response due to residential solid fuels offsets the strong positive direct forcing. Models tend to agree that cloud interactions add some negative forcing for these sources, but they disagree on the magnitude. *Unger et al.* [2010] report a positive indirect effect, citing the portion of the semi-direct effect that burns off clouds, but without using aerosol microphysics. *Bauer et al.* [2010] included aerosol microphysics in the same GCM used by *Unger et al.* and found net negative cloud forcing three times greater than the positive direct forcing by BC. *Jacobson* [2010] shows increased cloud optical depth due to biofuel emissions (including gases), but also finds a positive ToA forcing and a warming, suggesting that the cloud changes do not overwhelm the direct forcing. This study also includes ionic components of biofuel emissions that affect water uptake and climate response.

[44] Residential coal emits more BC compared to POA than do residential biofuels. The sulfur-to-BC ratio is much higher than for residential biofuels, and much lower than for industrial coal. This category has net positive direct forcing mainly attributable to BC, and net negative cloud forcing mainly caused by sulfur. The result, with very low certainty, is a slight net positive forcing.

10.5.4. Open biomass burning

[45] All three categories of open biomass burning emissions contain large POA fractions. As with residential solid fuel, the direct forcing by POA emissions does not fully counteract BC forcing, and forcing via O_3 has a substantial positive contribution. Once again, POA interaction with clouds is responsible for the large negative forcing, and large uncertainties. *Unger et al.* [2010] agree that cloud changes are large and negative. They also simulate a small negative nitrate forcing and a much larger POA direct forcing than calculated here.

10.5.5. Summary of BC-rich source categories

[46] For almost all source categories, net forcing that is easily attributable to individual species (*i.e.,* without clouds and nitrate) is positive with high confidence; that is, the lower limit of uncertainty is well above zero. Categories that emit relatively large quantities of sulfur are exceptions.

[47] The inclusion of forcing via clouds and nitrate makes the estimated impact of each category more negative and greatly increases the uncertainty. The origins of this negative, uncertain forcing differ among source categories. Sulfate effects on clouds are the primary cause for both residential and industrial coal. For diesel engines, the possible negative forcing comes from nitrate and cloud interactions with sulfate. Interactions between organic matter and clouds are the main source of uncertainty for residential biofuel and open biomass burning.

[48] Confidence in positive net forcing is highest for categories with relatively small quantities of co-emitted aerosols or precursors, such as diesel engines. Except for industrial coal, other energy-related combustion sources have a high probability of producing either positive or negative forcing. These source categories are quite heterogeneous, as will be discussed further in Section 10.6, so that individual emitters may still have net positive forcing.

10.5.6. Cumulative sum of forcing by BC-rich source categories

[49] Figure 10.2 demonstrates the fact that BC forcing results from an aggregate of multiple sources by presenting the cumulative sum of source-category forcing from top to bottom. For example, the values listed for 'Industrial coal' are the forcing by industrial coal, on-road diesel and off-road diesel. This figure shows probability density functions for effective forcing by BC alone (red line), for direct forcing by BC and all co-emitted species including organic matter and sulfate (purple line), and by all these species plus the forcing due to cloud changes (blue line). The highest point of each curve is the most likely value. The curve labeled 'Other BC sources' is the sum of all categories in Figure 10.1 and matches total forcing in Figure 9.1. In addition, Figure 10.2 includes forcing by emissions from two other source groups that emit large quantities of aerosols or precursors, but little BC (less than 1% of the global total).

[50] Figure 10.2 repeats some messages that appear in Figure 10.1. The best estimate of BC-only forcing is positive with high confidence, even when cloud forcing is considered. The best estimate of direct and snow forcing by BC and co-emitted species is also positive. However, when cloud forcing is considered, the best estimate of first-year forcing from many categories is close to neutral or negative because of co-emitted species. The figure also emphasizes the important distinctions between source categories. About half the BC forcing in the aerosol mixture (red line in Figure 10.2) comes from diesel engines, industrial coal, and residential solid fuels (first six categories). These are accompanied by negative direct and cloud forcings that result in climate forcing that is close to neutral (blue line in Figure 10.2). The remaining BC forcing comes from open burning, and it is accompanied by larger negative forcing. The thick black line separates BC-rich sources from others. The cumulative sum of forcing for the sources above that line is -0.08 W m^{-2} with 90% uncertainty bounds of (-1.24, +0.81 W m^{-2}). This total corresponds to the bars in Figure 9.1, which indicate the net climate effect of BC and co-emitted species. The total of all BC-rich sources excluding open biomass burning (*i.e.,* energy-related sources) is +0.004 W m^{-2} (-0.62, +0.57 W m^{-2}).

[51] The bottom two source categories in Figure 10.2 are power generation and a conglomeration of other low-BC sources. These categories emit very low BC amounts but are rich in sulfur and organic matter, and produce most (65%) of the net negative aerosol forcing. Including these two categories, total forcing by aerosols, short-lived gases, and cloud changes is -0.86 W m^{-2} with 90% uncertainty bounds of (-2.7, +0.39 W m^{-2}). Thus, most of the net negative aerosol forcing is confined to categories that are not BC-rich sources. The central value compares well with forcing estimated using an energy-balance approach and relying on observations [*Murphy et al.*, 2009]. However, our forcing estimate, which draws on ranges of modeled values, has much greater uncertainty bounds both above and below the central estimate than does the forcing estimate based on observations. It is possible that the broad uncertainty range from indirect effects is overstated.

10.6. Climate forcing by selected sources

[52] Figure 10.1 presents the total magnitude of forcing by sources in each category, emphasizing the sources with largest activities. These aggregated source categories are not homogeneous, but are made up of individual sources with different chemical emission profiles and rates. In Figure 10.3, we show forcing by individual sources that are contained within the major emitting categories. To do so, we obtain values for climate forcing per mass of fuel burned by multiplying emission factors (given in Table C.5), in mass of pollutant per mass of fuel burned, by the same forcing-per-emission values used for Figure 10.1 (see Table C.1 and C.4). Figure 10.3 shows effective forcing per source activity, or quantity of fuel burned, emphasizing the difference in emission rates within categories. Sources with higher emission factors for a particular pollutant—usually those with the poorest combustion—have larger climate forcing per fuel burned. These sources are often easier or less expensive to mitigate (see Section 12). This presentation contrasts with Figure 10.1, which accentuates categories with large total emissions.

[53] The units of forcing in Figure 10.3 differ from those in Figure 10.1 and the standard treatment by IPCC because continuous emissions are not assumed. Instead, the forcing caused by consuming one kg of fuel is integrated over time to give units of (μW m^{-2} yr) (Gg fuel burned)$^{-1}$. This difference is necessary because individual sources are unlikely to continue in perpetuity. However, the species or effects included in this figure have short atmospheric lifetimes, and this forcing occurs entirely during the first year after emission. For this reason, the values in this figure would be the same whether they represented continuous forcing for constant emissions, with units of μW m^{-2} (Gg fuel yr^{-1})$^{-1}$, or integrated forcing from finite consumption, with units of μW m^{-2} yr (Gg fuel)$^{-1}$. Likewise, the values in Figure 10.1 could represent integrated emissions from the year 2000, with units of W m^{-2} yr.

[54] As in Figure 10.1, the top bar for each source includes direct forcing by aerosol and gases, cryosphere forcing, and

cloud response to aerosol absorption. Other cloud responses and nitrate forcing are given in the middle bar, and the bottom bar shows the total of the two. Uncertainties are calculated in the same manner as for Figure 10.1 and, again, uncertainties in emission factors are not represented. Similar to the message in Figure 10.1, the sum of direct, cryosphere and semi-direct forcing by many source types is estimated to be positive. Cloud and nitrate forcing reduce the positive forcing and increase the possibility that the net forcing is negative.

[55] On-road diesel engines are a mix of low-emitting (controlled) engines using low-sulfur fuel and higher-emitting engines implemented in regions with limited regulations. The latter typically use fuel with higher sulfur content. Off-road diesel engines are presently more similar to the high-emitting engines.

[56] As in the category graph in Figure 10.1, direct and cloud forcing by sulfur are large for both residential and industrial coal sources. Industrial boilers have net negative forcing, but the high BC emission rates more than balance the negative forcing by sulfur for brick kilns and coal cooking stoves. This forcing is highly dependent on coal sulfur content. For example, the brick kiln emissions used in Figure 10.3 were measured in India, where sulfur content is low. The same source in a region with high-sulfur coal might have a different net forcing.

[57] Wood used in many heating stoves (*i.e.,* conventional wood stoves) produces a higher POA:BC ratio than wood for cooking (*i.e.,* mud cooking stoves), while larger heating technologies (*i.e.,* 'wood boiler') have low POA:BC ratios. This difference is apparent in Figure 10.3, which indicates a lower cloud impact from cooking with wood and a near-zero forcing. On the other hand, cooking stove emissions suggest net positive forcing, although the uncertainty is high. For cooking stoves, emission factors were taken from in-field measurements on this specific type of stoves. Its net positive forcing contrasts with the net negative value for the entire source category given in Figure 10.1. This difference results from the choice of emission factors within the GAINS model (see Section 3.6.3). Emission factors specific to individual technologies need to be chosen carefully when sources, rather than categories, are scrutinized closely to determine the net effect on forcing.

[58] Profiles of field and forest burning are similar to the category graphs, with important contributions to direct forcing from organic matter and gases, and a net negative forcing due to cloud interactions with POA.

[59] The values in Figure 10.3 represent the total climate impact of particular sources. They do not reflect the change caused by mitigation actions, which would be the difference between the current climate impact and the impact of the chosen alternative.

10.7. Comparison with forcing on longer time scales

[60] It is important to consider contributions to climate change beyond the first year after emission. Forcing results both from direct emissions of GHGs (*e.g.,* CO_2 and CH_4) and from short-lived air pollutants interacting with CH_4. While CH_4 is considered a shorter-lived pollutant in some discussions, its forcing is not contained solely within the first year after emissions as are the forcings of the other constituents discussed earlier in this chapter. Common practice is to integrate these forcings over 100 years after emission, and these integrated forcings are shown in Figure 10.4 as bars. Figure 10.4a shows the longer-lived forcings for year 2000 emissions within each source category in Figure 10.1, and Figure 10.4b shows the total forcing per mass of fuel burned for each individual source in Figure 10.3. For biofuel and open biomass burning, the contribution of CO_2 may not be treated as forcing in traditional GHG accounting, if the biomass consumed is regrown. Only combustion emissions are shown here, so, for example, refrigerants emitted from vehicles are not included.

[61] Figure 10.4 also shows the estimated forcing from Figures 10.1 and 10.3 for comparison (red circles). Because no forcing is exerted by these species or effects after the first year, the 100-year integral is identical to the values already given. The two types of forcing in the figure are distinct: one acts during the first year ('first-year forcing') and one requires longer integration times ('longer-term forcing'). These two groups form a mutually exclusive and collectively exhaustive set of forcing impacts by combustion emissions. Although forcing by CH_4 during the first year after emission is about 10% of its integrated forcing, we classify this as longer-term forcing because of the need for integration.

[62] First-year forcing by BC-rich source categories is substantial but not dominant, with absolute values ranging from 5 - 60% of the integrated long-term forcing. Furthermore, first-year values that appear small in comparison with long-term forcings are usually the small net of two larger values with opposing signs. Thus, emissions from these sources can immediately produce climate forcing that is significant in comparison with the long-term forcing, even if the latter is integrated over 100 years. Regardless of whether any of these sources are chosen for mitigation to reduce climate forcing, changes in these emitters will affect the radiation budget substantially in the near future.

[63] Of particular note are the opposing effects of first-year forcing and longer-term effects on the CH_4 system for two major source categories. For both on-and off-road diesel engines, the best estimate of first-year forcing is positive, although the uncertainty is high. However, this forcing is countered by the negative forcing after the first year, caused by NO_x emissions that reduce CH_4 concentrations. The opposite effect is seen in another large source, biofuel used for cooking. Its first-year forcing is estimated to be nearly neutral, largely due to the cancellation of cloud and direct forcing. The interaction of short-lived pollutants with the CH_4 budget opposes this negative forcing, and the best estimate of biofuel emission impact is a slightly positive forcing from aerosol, O_3 and CH_4 interactions. For both of these large BC-rich source categories, the net forcing by aerosols, O_3 and CH_4 is deceptively small, masking large offsetting terms that may occur during different decades.

10.8. Cautions regarding net forcing estimates

[64] The values given here represent our best estimate of the global response to worldwide source categories, based on current knowledge. Nevertheless, they should be interpreted in light of the cautions below.

10.8.1 Forcing dependence on emitting region is not captured

[65] In developing the figures in this section, we applied globally averaged values of forcing per unit of emission. Some values of forcing per emission depend on the emitting region. The climate forcing per emission of short-lived pollutants depends on the region (and timing) of emission. Thus, the summed climate forcing of all species for a source category emitting in a particular region (or season) may have a different magnitude than the global average, or even a different sign. Atmospheric forcing per emission of BC may vary by about 50% [*Rypdal et al.*, 2009a], and cryosphere forcing is quite dependent on emitting region [*Reddy and Boucher*, 2007; *Shindell et al.*, 2008]. *Bond et al.* [2011] showed that direct radiative forcing by BC and OA is positive in any region when the OA-to-BC ratio was less than 12:1, but when cryosphere forcing was considered for regions near ice, even sources with an OA-to-BC ratio of 30:1 could have positive forcing.

[66] Forcing per emission by gases is also regionally dependent, especially for NO_x, for which values of forcing-per-emission vary by an order of magnitude between the tropics and higher latitudes [*Wild et al.*, 2001].

10.8.2 Regional impacts are not well captured by global averages

[67] As discussed at the end of Section 9, the presentation here measures impact in terms of globally averaged, ToA climate forcing. Globally averaged forcing does not reflect the strong regional impacts of short-lived climate forcers. Forcing that appears small in the global average may be significant over a smaller area and near zero over the rest of the globe. Such regional forcing may induce climate responses different than those of long-lived, well-mixed climate forcers (see Chapter 8).

[68] ToA climate forcing does not reflect some societally relevant changes, such as shifts in precipitation. Forcing that is zero at the top of the atmosphere but alters the distribution of radiation within the atmosphere may still have significant impacts.

10.8.3. Large uncertainties remain in deriving and apportioning cloud impacts

[69] Uncertainty about the sign of forcing is most directly attributable to the uncertainty in cloud forcing by co-emitted species and to lack of knowledge about the magnitude of the total indirect effect itself. This large uncertainty is not unique to BC-rich sources, but reflects the existing state of knowledge regarding clouds. In this analysis, we have included an estimate of cloud impacts because direct forcing alone may give a misleading impression of net impact in terms of both certainty and sign of effect.

[70] Estimates of warm-cloud forcing have become less negative over time as constraints from satellite measurements are applied to models [*Lohmann et al.*, 2010]. If the best estimate of warm-cloud microphysical interactions is later revised to be less negative, estimates of net first-year forcing will become more positive for transportation and solid-fuel sources, and less negative for open-burning and sulfur-rich sources.

[71] Negative forcing is ascribed to semi-direct effects of BC, but model responses may depend on BC overlying clouds, an assumption that is questionable in light of observations. If estimates of this effect were weakened (becoming less negative), forcing by all BC sources would also become less negative or more positive.

[72] Enhanced absorption within clouds is highly uncertain. If the forcing attributable to such absorption is as great as that estimated by *Jacobson* [2010], forcing by all BC-rich sources would become strongly positive. Forcing by sources that emit light-absorbing OA or OA precursors, such as biofuel and open biomass burning, would also have greater effects. This potentially large effect is included within our uncertainty bounds, but our central estimate has been more conservative.

[73] The net effect of BC and co-emitted species on mixed-phase and ice clouds depends on the fraction of BC that is ice-active. If BC is found to be ice-active in the upper troposphere, then the estimate of BC effects on ice clouds may warrant increased positive forcing estimates. On the other hand, if coatings or co-emitted species cause less ice nucleation, then mixed-phase cloud forcings may become more positive.

[74] Forcing by all cloud effects may depend strongly on the region of emission, on co-emissions, or on the environment in which emissions occur, but no study has examined such differences. A more robust treatment would involve examining each individual source with a model that includes all effects described in this assessment, and that also has the ability to examine sensitivity to critical model inputs.

10.8.4. Climate forcing by additional co-emitted species may affect totals

[75] Although forcing by SOA is not included here, it is known to be a large fraction of the atmospheric aerosol. If SOA has a small negative forcing, as some models predict, and if BC-rich sources emit large quantities of SOA precursors, then net forcing estimates will become more negative.

[76] Ionic species such as magnesium and calcium are small fractions of emitted mass and were not included in this analysis. These species are included in biofuel simulations by *Jacobson* [2010], but their effects have not been isolated.

10.8.5. Constraints on emissions of BC and co-emitted species are limited

[77] Total emission estimates are acknowledged to contain uncertainty, and those used for Figures 10.1 and 10.2 are determined by scaling modeled atmospheric concentrations to observations. This analysis is hampered because the regions in which the greatest scaling occurs have few observations. We acknowledge that this scaling treatment is subject to many assumptions. At least one other estimate incorporating observations [*Ramanathan and Carmichael*, 2008] has estimated a greater atmospheric burden of BC.

[78] These results also rely on our assumption that BC and other products of incomplete combustion scale equally. If BC alone should be increased to match atmospheric absorption—perhaps due to poor measurements of BC mass at the point of emission—then all categories in Figure 10.1 would have greater positive forcing. On the other hand, if larger increases in particulate matter are required to match satellite observations—perhaps due to formation of secondary organic aerosol—then negative forcing in some categories would increase.

11. Emission metrics for black carbon

11.1 Section summary

[1]

1. The purpose of an emission metric like the Global Warming potential (GWP) or the Global Temperature Change Potential (GTP) is to put future climate impacts of unit emissions of compounds with different lifetimes and radiative efficiencies on a common scale. Such metrics are useful not only in legally binding agreements, but also in assessments of net climate impact of different mitigation options affecting emissions of many compounds.

2. Physically based metrics like the GWP and the GTP for BC emissions can be calculated from estimates of global annual mean climate forcing normalized to BC emissions. For the GTP additional information about the response times of the climate system are needed.

3. Based on the total effective BC forcing as given in Section 9, the $GWP_{20\text{-}yr}$, $GWP_{100\text{-}yr}$ and $GWP_{500\text{-}yr}$ for BC are 2800, 800 and 240, respectively. The $GTP_{20\text{-}yr}$, $GTP_{50\text{-}yr}$ and $GTP_{100\text{-}yr}$ estimates are 820, 140 and 110, respectively. Uncertainties are (-100, +105) % for the GWPs and (-115, +145%) for the GTPs.

4. The GWP and GTP metrics vary with the region where BC is emitted by about ±30% based on the results from two studies.

5. The GWP and GTP metric values (which are all relative to CO_2) increase with decreasing time horizon due to the short lifetime of BC. The choice of time horizon is a value judgment related to the overall target of the climate policy being considered.

6. Current climate policies seem to move in the direction of achieving some temperature target. Under such an approach, the time horizon is initially long and the value of a short-lived forcer such as BC is small but grows as the temperature target is approached. A stricter temperature target implies the value of BC grows faster as the temperature target is approached.

7. BC is not well mixed, unlike most GHGs, because of its short lifetime. Additionally, BC interacts differently with the climate system in several ways. These differences between BC and the GHGs, as well as the different natures of the short-term and long-term climate problem, raise questions about the appropriate use of any metric that attempts to place BC and GHGs on a common scale.

8. Co-emission effects, discussed in Section 10, are not captured by BC metrics presented here but can be calculated in a similar approach.

11.2. Introduction

[2] The United Nations Framework Convention on Climate Change [UNFCCC, 1992, article 3] carried strong statements about the need for comprehensive (*i.e.,* across all components and sectors) measures that are also cost effective. To achieve this goal, climate policies may target not only CO_2 but also other compounds leading to warming of the system. To facilitate the evaluation of multiple species, a measure that puts climate impacts of emissions of different compounds on a common scale, or a *metric*, is needed [*IPCC*, 1990; *Kandlikar*, 1996; *Fuglestvedt et al.,* 2003; *Forster et al.,* 2007]. In this context, climate impacts are understood as all future impacts imposed from the time of the emission. Since BC has such a short lifetime compared to the long-lived GHGs, the length of time over which future impacts are evaluated (*e.g.,* through the choice of a time horizon in the common metric, the GWP, or through a discount rate) strongly influences the metric value. This is an inevitable challenge in constructing metrics as it fundamentally involves value judgments with respect to how one treats short-term versus long-term climate impacts [*e.g., O'Neill,* 2000; *IPCC*, 2009].

[3] Reductions are often presented in terms of total 'CO_2-equivalent' emissions. Based on a metric value M_{BC} for BC and the emissions of EM_{BC} of BC, CO_2-equivalent emissions that can be compared with similarly calculated emissions of other species, are calculated through

$$EM_{CO_2eq} = EM_{BC} \cdot M_{BC} \qquad (11.1)$$

[4] This CO_2-equivalent value means that emitting EM_{BC} kg of BC would have the same effect (in terms of the impact parameter used in the metric definition) as emitting $EM_{CO2\text{-}eq}$ kg of CO_2 at the same time. In a multi-component climate agreement, such as the Kyoto Protocol, a set of metric values are decided for each component included in the agreement. The overall commitments are given in terms of reductions in total CO_2-equivalent emissions, summed up over the all components included in the agreement, and it is then up to each party to the agreement to decide the composition of the total mitigation, depending on the costs of reducing the individual components. An alternative to this 'basket' approach would be to agree on commitments for individual components. The role of a metric would then be to provide guidance with respect to how much emissions of one component should be reduced relative to another component, involving the same value judgments discussed above. So-called 'multi-basket' approaches have also been proposed [*Fuglestvedt et al.,* 2000; *Rypdal et al.,* 2005; *Jackson*, 2009], where components with similar lifetimes are lumped in separate baskets. Again metrics can be used to help determine the targets for each basket.

[5] The use of metrics is not restricted to legal agreements, but is also very useful for comparing different policies or technological options [*e.g., Jacobson,* 2002] or in assessments of different economic sectors [*e.g., Fuglestvedt et al.,* 2008; *Boucher and Reddy*, 2008; *Berntsen and Fuglestvedt,* 2008].

[6] Metrics have been defined both in terms of physical and economic impacts on climate [*Kandlikar*, 1996; *Fuglestvedt et al.,* 2003; *Forster et al.,* 2007]. We limit the discussion here to physical metrics, especially those metrics that have already been used in climate change policy. Metrics based on economics are extensions of physical metrics and the extension is of a more generic nature, not particularly related to BC. Metrics based on economics can be designed to allow for cost-benefit optimization by taking damage cost functions into account [*Tol et al.,* 2008]. Different metric concepts can be defined to serve specific policies such as those with a long-term temperature target (*e.g.,* the maximum 2ºC as agreed upon in the Copenhagen accords of the Conference of Parties-15 (COP-15) meeting [*Manne and Richels,* 2001]).

[7] Using Equation (11.1) to derive a value of CO_2-equivalent emissions does not ensure that all aspects of climate change are equivalent to those from actual CO_2 emissions, in particular for a very short-lived compound like BC. Equivalence is only obtained with respect to the physical impact chosen in calculating the metric [*O'Neill,* 2000]. Different combinations of compounds with equal total CO_2-equivalent emissions, for example, do not provide equivalence with respect to regional climate impacts or the temporal development of climate change. Although these latter impacts are the key end points of concern, they are farther down the causal chain and, thus, are more difficult to capture with simplified and policy-friendly metrics.

11.3. The GWP and GTP metrics

[8] Two purely physically based metrics, the GWP and the GTP, have been established in the literature. The absolute GWP (AGWP) is defined as the integrated radiative forcing of a unit-mass pulse emission over a time horizon H. The AGWP for a component *i* with an atmospheric lifetime of τ_i and specific radiative forcing of A_i (forcing per unit burden change, W m^{-2} kg^{-1}) can be calculated as:

$$AGWP_i(H) \equiv \int_{t=0}^{H} RF(t)dt = \int_{t=0}^{H} A_i \exp(-t/\tau_i)dt = A_i\tau_i(1-\exp(-H/\tau_i)) \approx A_i\tau_i \quad (11.2)$$

For all forcing mechanisms involving BC, $\tau_i << H$. The product A_i τ_i (W m^{-2} (kg $yr^{-1})^{-1}$) is the specific normalized radiative forcing at steady state for a continuous unit emission. These values can be derived from model simulations that calculate the annual mean RF for a given emission, such as the values tabulated in Appendix C.

[9] The generic definition of the absolute GTP (AGTP) can be given as

$$AGTP_i(H) = \int_0^H RF_i(t) \cdot R(H-t)dt \quad (11.3)$$

where an impulse-response function for the climate system *R(H-t)* gives the surface temperature response at time *H* due to a radiative forcing at time *t* [*Shine et al.,* 2005; *Fuglestvedt et al.,* 2010]. For both the GWP and the GTP the metric values are obtained by dividing the AGWPs and AGTPs by the corresponding AGWP or AGTP values for the reference gas CO_2. The AGWP values for CO_2 for 20, 100 and 500 years time horizon of $2.47 \cdot 10^{-14}$, $8.69 \cdot 10^{-14}$ and $28.6 \cdot 10^{-14}$ W m^{-2} yr (kg $CO_2)^{-1}$ are used to calculate the GWPs [*Forster et al.*, 2007]. The AGTP values for CO_2 used here [*Fuglestvedt et al.*, 2010] are $6.8 \cdot 10^{-16}$, $5.8 \cdot 10^{-16}$ and $5.1 \cdot 10^{-16}$ K (kg $CO_2)^{-1}$ for 20, 50 and 100 year time horizons. The GTP is commonly referred to as an *end-point* metric since Equation (11.3) gives the global mean temperature response at time H.

[10] The Kyoto Protocol regulates a basket of six gases, or groups of gases, that are primarily long-lived GHGs. The global warming potential with a 100-year time horizon was chosen as the metric for use in this legal agreement. Metrics are most commonly defined for pulse emissions, since comparisons of future scenarios can readily be carried out by regarding each emission trajectory as a series of pulse emissions [*Berntsen and Fuglestvedt*, 2008]. A special case of a future scenario is constant sustained emissions. *Hansen et al.* [2007] used an alternative GWP defined as change in forcing per change in emission. *Jacobson* [2010] calculated a STRE (Surface Temperature Response per unit Emission) emission index that is defined for sustained emissions, but with a non-standard response function for CO_2.

11.4. Calculations of metric values for BC

[11] Based on Equations (11.2) and (11.3) above, metric values for BC emissions including all relevant processes can be calculated (*i.e.*, the processes summarized in Section 9) when the specific normalized radiative forcings and the impulse-response function are given. Here we have used the impulse response function from *Boucher and Reddy* [2008]. The detailed method for calculating the AGTPs is given in *Fuglestvedt et al.* [2010]. Using the estimates for global radiative forcing given in Section 9 (Figure 9.1) and the estimated industrial-era emissions of BC of 8700 Gg yr^{-1} (Section 5), the GTP and GWP values for direct BC forcing as well as for the total effective BC forcing were derived as shown in Figure 11.1. Due to the short lifetime of all BC forcing mechanisms, the annual mean product A_i τ_i can be accurately estimated as the ratio between the annual mean climate forcings (Figure 9.1) and the annual emissions.

[12] Figure 11.1 gives global GWP values for the standard 100-year time horizon, as well as values for 20 and 500 years, and GTP values for 20, 50 and 100 years. Since the lifetime for all RF mechanisms discussed in Section 9 are much shorter than any of the time horizons chosen, each mechanism has the same relative contribution to either GWP or GTP. It should be noted that the values for GWP_{100} and GTP_{20} are about equal, which is a robust finding in general for short-lived climate forcers [*Fuglestvedt et al.,* 2010].

11.5. Uncertainties

[13] Relative uncertainties in metric values are assumed to be the same as those given in Section 9 for total forcing. Normalization of the observationally constrained radiative forcing by uncertain annual emissions could in principle change the uncertainty range of the normalized forcing, either increasing or decreasing the uncertainty. Since the RF estimates are commonly based on combinations of model results and measurements, rigorous propagation of uncertainty is difficult to determine. Although uncertainties in the metric values are of little practical use in formal agreements or trading schemes, where only the central estimates of the metrics are used, they become important when the metric values are used as a first-order assessment of the net effects of different mitigation options. For GTPs, the uncertainties are much larger than for GWPs due to uncertainties in the climate sensitivity and, hence, the temporal response of the climate system. For GTPs in Figure 11.1, a factor of 2 uncertainty in the impulse response function is included based on the result of *Fuglestvedt et al.* [2010] for GTP_{50} of BC.

[14] Uncertainties in the values of metrics can be classified as structural or scientific. Structural uncertainties refer to the consequences of using different types of metrics for a given

application, or to choices about key aspects of a metric such as its time horizon and whether discounting is applied. Scientific uncertainties refer to the range of values that can be calculated for a given metric due to incomplete knowledge of the important aspects of the climate or economic system that relate some anthropogenic emission to climate impacts, damages, or mitigation costs [*IPCC*, 2009]. In previous sections of this paper we present the scientific uncertainties based on the uncertainties for each of the forcing mechanisms for BC as presented in Sections 5, 6 and 7, and illustrated in Figure 9.1. The structural uncertainties, which can be very large, are demonstrated by presenting numerical values for different metrics (GWP and GTP) and for a range of time horizons. For the selected metrics presented in Figure 11.1, the range is between 110 and 2800 for the central estimates for GTP_{100} and GWP_{20} respectively.

11.6. Shortcomings of global metrics

[15] Differences between BC and the long-lived GHGs may not be well captured by globally averaged metrics. Because BC absorbs incoming shortwave radiation, BC in the atmosphere causes surface dimming and changes the vertical temperature profile differently than the long-lived GHGs. The various hydrological impacts caused by the dimming from BC are not captured in metrics that are based on global radiative forcing or global mean surface temperature change.

[16] Another issue for BC and other short-lived climate forcers is that metric values for global impact (global mean climate forcing for the GWP and global mean temperature for the GTP) depend on the region of the emissions and also on the timing of the emissions due to the short lifetime of BC. Since there have been no studies of the radiative forcing due to emissions during different seasons, metric values cannot be differentiated according to when the emission takes place. Two studies have calculated normalized radiative forcings or GWPs for the direct effect and the snow albedo effect for regional emissions [*Rypdal et al.,* 2009a; *Bond et al.,* 2011]. They both find a regional variability of ±30-40% for the direct effect, with the largest forcings typically found for emissions from regions located at low latitudes since there is more solar radiation available. For the snow albedo effect the regional variation is much larger with higher values for high latitude regions where the emitted BC is more likely to be deposited on snow surfaces. The snow albedo effect ranges from practically zero for emissions in the tropics to values that reach 30 to 60 % of the direct effect for emissions in Russia and the former Soviet Union [*Rypdal et al.* [2009a] and *Bond et al.* [2011], respectively], not including an enhanced efficacy factor for the snow albedo effect. Since there is a certain cancellation effect depending on the latitude of the emissions (*i.e.,* high direct forcing occurs with low snow-albedo forcing and vice versa) the total of the two mechanisms shows less regional dependence.

[17] In addition to the potential for different global impacts resulting from BC emitted in different regions, the impact on climate in a given region may depend on where the radiative forcing occurs [*Shindell and Faluvegi,* 2009]. So far there has only been one GCM study on this topic, but if it proves to be a robust finding, the choice of location for emission reductions will not be completely flexible [*Sarofim*, 2010].

11.7. Choice of time horizon

[18] The choice of time horizon for either the GWP or GTP metric is essentially a value judgement, conceptually related to discounting future costs of the impacts of climate change. As discussed by several authors [*Aaheim et al.,* 2006; *Bradford*, 2001; *Johansson et al.,* 2006; *Manne and Richels,* 2001; *Shine et al.,* 2007], for a cost-effective policy that sets a long-term limit on the allowed change in global temperatures [*e.g., COP-15*, 2009], the relative importance of different emissions (*i.e.,* the metric values) will depend on how far into the future that threshold is likely to be reached. Thus, if the global temperature continues to increase, the metric values of short-lived components will increase as global temperatures get closer to the temperature constraint. If such a dynamic time-horizon is incorporated in legally binding agreements or trading schemes, it becomes important for the stakeholders to know not only the metric values at the time of the investment in new technology to reduce emissions, but to have information about the potential change of the metric values over the lifetime of the investment due to shortening of the time horizon as global temperatures get closer to the temperature constraint. Once a threshold is set (*e.g.*, as the 2°C threshold agreed upon in the Copenhagen Accord [*COP-15*, 2009]) it is possible to estimate, with uncertainties, what is the relevant timeframe and how the metric values will evolve over time [*e.g., Manne and Richels,* 2001]. This information can be communicated to decision makers, so that it is taken into account when there are investments in new long-lasting equipment (*e.g.,* power-plants that will be in operation for 40–50 years).

[19] There has been some concern that a policy that increases the focus on short-lived climate forcers like BC would reduce the focus on reduction of CO_2 and other long lived GHGs, with possible severe irreversible long-term climate effects. An assessment by the U.S. National Academy of Sciences went so far as stating that CO_2 emission mitigation and short-term forcing emission mitigation are "…separate control knobs that affect entirely distinct aspects of the Earth's climate, and should not be viewed as substituting for one another" [*NRC*, 2011]. If a metric with a dynamic time-horizon is applied to all climate forcers in a cost-effective framework with a long-term temperature constraint (*e.g.,* in accordance with the Copenhagen accords [*COP-15*, 2009]), it can be shown that within this framework short- and long-lived climate forcers can be treated in a common framework and that an increased mitigation of BC does not displace additional CO_2 mitigation [*Berntsen et al.,* 2010]. This is because in a cost-effective framework increased mitigation of BC is only consistent with a higher metric value for BC, which is equivalent to a shorter time horizon. In this framework the only political decision that can shorten the time horizon is to lower the acceptable temperature threshold. The key to this argument is that with a lower threshold the total CO_2-equivalent emissions must be reduced significantly more. Due to the dominant role of CO_2 this means that even if the relative reductions of BC are enhanced, the absolute CO_2 reductions must also be greater if the temperature threshold is decreased [*Berntsen et al.,* 2010].

11.8. Towards metrics for the net effect of mitigation options

[20] As shown in Section 10 and further discussed in Section 12, any mitigation strategy targeting BC reductions will inevitably also change emissions of other species that affect climate. Metrics are suitable tools to make first-order estimates of the net effect of all emission changes [*Berntsen et al.,* 2006; *Boucher and Reddy,* 2008]. Using pre-calculated metrics for all the relevant species allows for much quicker assessments. Simulating the broader climate effects, including end-point risks and impacts, requires earth system models which include full coupling between chemistry, radiation, dynamics, clouds, vegetation, etc. However, even if such an earth system model is applied, the question of how to weigh responses occurring at different times in the future remains.

[21] Section 10 presented the net effect of short-lived emissions from individual source categories. This analysis required estimates of normalized radiative forcing for individual species (Appendix C), largely drawing on the comprehensive review of *Fuglestvedt et al.* [2010] but also including the cloud forcing attributable to aerosols and precursors. Although this section presents metric values only for BC, GWPs and GTPs can be derived for the other species by dividing by the appropriate value of AGWP or AGTP for CO_2.

12. Mitigation analysis for BC-rich sources

12.1. Section summary

[1]

1. Prioritization of BC mitigation options is informed by science questions such as the magnitude of BC emissions by sector and region (Section 3), net climate forcing by categories including co-emissions (Section 10), impacts on the Arctic (Section 7), and direct effects on precipitation (Section 8.4). In addition, information on technical and financial feasibility, costs and benefits of mitigation, policy design, and implementation feasibility also inform mitigation options. The major sources of BC are presently in different stages of evolution with regard to technical and programmatic feasibility for near-term mitigation actions.

2. Regardless of net climate forcing or other climatic effects, all BC mitigation options bring health benefits through reduced particulate matter exposure.

3. The quality of cost estimates of BC mitigation vary, ranging from robust estimates, for example, for diesel retrofits in industrialized countries to poor estimates for sources such as improved brick kilns in developing countries or open burning.

4. Diesel engine sources of BC appear to offer the best mitigation potential to reduce near-term climate forcing. In developed countries, retrofitting older diesel vehicles and engines is a key mitigation strategy; in developing countries, transitioning a growing vehicle fleet to a cleaner fleet will be important.

5. Mitigating emissions from residential solid fuels may yield a reduction in net positive forcing, especially when the longer-term effects on the methane budget are considered. The net effect remains uncertain because of uncertain knowledge regarding the impacts of co-emitted species on clouds. Furthermore, for biomass use, technology and programs to accomplish mitigation are still emerging.

6. The net effect of small industrial sources depends on the sulfur content of individual sources, and the feasibility of mitigation is in the emerging phase. Net climate benefits may be possible from individual source types with low sulfur emissions when technology is available.

7. Estimation, and especially monetization, of the benefits of BC mitigation is a nascent field. CO_2-equivalency metrics serve as a first-order guide to estimating the climate benefits of BC mitigation but do not capture all potential objectives.

8. Unlike long-lived GHGs, the location, and in some cases timing, of BC emissions may change the climate forcing effect compared to the global average. For example, BC sources that affect the Arctic or other regions with extensive snow and ice cover may offer mitigation potential to reduce climate forcing for those regions. Such regionally specific benefits have not yet been quantified.

9. Mitigation considerations are ideally informed by how emissions are projected to change over time based on existing policies, so that emphasis is placed on sources whose emissions are expected to grow or remain significant.

12.2. Mitigation framework for comprehensive evaluation

[2] The introduction to this assessment describes a potential role for BC in climate mitigation. Because BC has a short atmospheric lifetime, changes in source activity affect radiative forcing within a few weeks and, therefore, actions that reduce emissions from BC-rich sources could contribute to managing the trajectory of climate forcing. Until this point, this assessment has focused wholly on climate-related physical science, addressing the question of the magnitudes of the diverse range of BC sources and the associated components of climate forcings from BC and co-emitted species. We have treated comprehensively the suite of climate forcings of BC rather than limiting the analysis to direct forcing (Section 9). In presenting mitigation actions in this section, a comprehensive view is also taken by considering factors beyond climate science: first, feasibility in technical and policy-related terms; second, health co-benefits from BC mitigation; and third, an economic assessment of whether benefits of mitigation are commensurate with costs. A detailed investigation of these additional factors is beyond the scope of this assessment. More in-depth analysis of the potential for BC mitigation can be found in reports such as *UNEP/WMO* [2011a; b], *Arctic Council Task Force on Short-Lived Climate Forcers* [2011] and *EPA* [2012].

[3] In considering the mitigation of a climate-forcing agent, several principal aspects are involved as illustrated in Figure 12.1. In the case of BC and co-emitted species, *scientific understanding* addresses what is known about the environmental and health effects of BC emissions and their accumulation in the atmosphere. The net impact of mitigation actions is proportional to the reduction in these effects. For climate, this net impact depends critically on understanding how actions affect both BC and co-emitted species.

[4] Mitigation is generally accomplished with alternatives that provide the same service or function with lower environmental impacts or by reducing the level of service. *Technical feasibility* refers to the availability of these workable alternatives. Even with scientific understanding and technical feasibility in hand, successful mitigation actions further depend on institutional and policy frameworks that can facilitate widespread implementation of mitigation options. This *programmatic feasibility* refers to the existence of an effective framework, which increases confidence that significant emission reductions could be achieved over a known time frame.

[5] The evolution of each of these principal aspects can be divided into four stages as illustrated in Figure 12.1. Scientific understanding moves from recognition of an effect (*nascent* stage), to simple estimation that may rely heavily on expert judgment (*emerging* stage). When increased attention to emission sources motivates more sophisticated quantification, advanced models and observations are applied (*solidifying* stage). When multiple estimates are available for the effects, the community can move toward consensus regarding their magnitude and importance (*mature* stage). The goal of this assessment has been moving the understanding of physical science toward the solidifying and mature stages with regard to climate effects.

[6] Evolution or growth of knowledge also occurs with regard to technical feasibility. This evolution often occurs separately from, but parallel to, the development of scientific understanding. It also has a nascent stage, where technical solutions are first envisioned. The emerging stage consists of initial, limited efforts to provide technical solutions and delivery programs. Not until the solidifying stage does the increased attention to environmental or health effects demand effective solutions, so that formal research, development, and evaluation approach completion. Resources are invariably required to support this leap in capacity. Finally, at the mature stage, the most promising technical mitigation options have been identified that can be produced at the scales required and with well known costs and benefits. A similar evolution occurs in programmatic feasibility beginning with experimental interventions. Specialized programs then emerge that lead to pilot programs and finally to policies and institutions that can facilitate and implement mitigation plans at regional, national or even international scales.

[7] The major sources of BC are presently in different stages with regard to technical and programmatic feasibility. This disparity does not diminish the importance of any source, but it does mean that the near-term feasibility of mobilizing mitigation activities differs among source categories. Section 12.4 gives a brief review of what is known about technical and policy-related feasibility for each of the major BC-rich source categories.

12.3. Costs and benefits of mitigation

[8] Mitigation actions generally have both benefits and costs. If the benefits exceed the costs then the action is generally considered desirable by policymakers. On the other hand, if the costs exceed the benefits, then the action is generally not considered desirable. Formally, a policy is considered acceptable if the marginal benefit of the next unit of reductions equals the marginal costs of that unit of reductions, and the current net benefits resulting from that action are greater than zero.

[9] One step in a cost-benefit analysis is to determine the cost of mitigation. If the benefits of mitigation have been valued in monetary terms, then a cost-benefit approach is possible, but when benefits are difficult or impossible to estimate, the approach of cost effectiveness is often used. Cost effectiveness does not attempt to equate cost and benefits, but rather to identify the least-cost method of reaching a given goal, or most effective use of a given quantity of resources. The goal still requires a metric for comparison; often this is the total quantity of pollutants reduced, or in more sophisticated analyses the reduction in physical impacts or damages associated with lower emissions. For example, cost effectiveness can be calculated based on cost per Mg BC reduced, per Mg CO_2 equivalent (see Section 11), or per degree of global mean temperature reduction. In the case of a cost-benefit analysis, the cost can be compared to the monetized benefits (where feasible for health, climate, or both) of mitigation. Because cost is an important part of such analyses, it will be discussed in the next section. Although earlier sections presented emissions in terms of Gg per year, costs are usually tabulated in terms of Mg reductions (1 Gg = 1000 Mg).

[10] The engineering costs of a reduction measure can include capital costs, installation or adoption costs, and fixed or variable operating costs such as changes in fuel demand, future maintenance needs, or labor demands. Estimating the reductions could involve calculating the expected difference in emissions between the baseline and a new projection or using an approximation of calculating the annual reductions multiplied by the expected lifetime of the project.

12.3.1 Health benefits

[11] BC is one component of particulate matter that can have adverse effects on human health [*Pope et al.,* 2009]. The location of the emission source affects exposure and, hence, the magnitude of health benefit that can come from mitigating that source. To date, public health agencies have not addressed the health effects of BC specifically; rather, the health effects of BC have generally been considered to be associated with the health effects that have been linked to $PM_{2.5}$. As a result, the mitigation literature has traditionally focused on PM rather than explicitly on the BC component. Presently, there is a growing literature on efforts to isolate the specific health effects of BC exposure. As with climate forcing, however, mitigation affects all emissions from a source, so that effects of BC alone may not be a good estimate of potential benefits from mitigation.

[12] Short-term exposure to $PM_{2.5}$ is likely causally associated with mortality from cardiopulmonary diseases, hospitalization and emergency department visits for cardiopulmonary diseases, increased respiratory symptoms, decreased lung function, and physiological changes or biomarkers for cardiac changes [*EPA,* 2009a]. Long-term exposure to $PM_{2.5}$ is likely causally associated with mortality from cardiopulmonary diseases and lung cancer, and effects on the respiratory system such as decreased lung function or the development of chronic respiratory disease [*EPA,* 2009a]. Epidemiological evidence explicitly linking BC to such health effects is limited [*Smith et al.,* 2009], and simply assigning a fraction of $PM_{2.5}$ health effects to the portion of $PM_{2.5}$ made up by BC is not common, as there are known differential toxicities among PM components, uncertainties about how different mixtures of particulate materials may change toxicity, as well as heterogeneity in the exposure of a population to different PM components. Several studies [*Jannsen et al.*, 2011; *Ostro et al.,* 2010; *Smith et al.,* 2010; *Bell et al.,* 2009; *Brunekreef et al.,* 2009, *Cooke et al.,* 2007] describe attempts to differentiate health outcomes among specific components or sources of $PM_{2.5}$.

[13] A study by *Fann et al.* [2009] monetized, on a US dollar per Mg basis (USD Mg^{-1}), the health benefits of reducing carbonaceous particulate material by assuming a differentiated proximity of the receptor populations to sources of carbonaceous PM versus other PM components. *Fann et al.* estimated the health benefits of reducing carbonaceous PM to be on the order of 72 thousand to 2.8 million USD Mg^{-1} in the USA. *UNEP/WMO* [2011a; b] and *Shindell et al.* [2012] assessed the global health benefits of implementing a number of BC measures and found a reduction in annual premature deaths due to outdoor air pollution of 2.3 million (+2.2/-1.6) persons over 30 years of age in 2030. Using a country-specific value of a statistical life, these studies determined a monetized benefit of this mortality reduction of USD 5.1 trillion (+4.7/-3.6). Residential solid-fuel sources of BC also produce high indoor

exposures whose effects have been monetized [*Mehta and Shahpar*, 2004].

12.3.2. Valuing climate benefits of BC mitigation

[14] While earlier sections in this assessment discussed climate impact, no value was placed on the reduction of these impacts for use in a cost-benefit assessment. With regard to climate change, the term 'benefits' refers to the avoided risks and impacts (see Figure 8.4) associated with less climate change that would be the result of decreased BC emissions. No direct monetization of the benefits of BC reductions for climate change has yet been reported in the literature.

[15] One possible approach to valuation is using metrics (for example, GWP, see Section 11) to convert BC emissions into estimates of CO_2-equivalent emissions. BC mitigation estimates in these CO_2-equivalent units would then represent first-order, proxy measures for the climate benefits of BC mitigation actions. Furthermore, the CO_2-equivalent metric also provides a first-order approximation for how the BC mitigation measures compare to other CO_2 and GHG mitigation options. Using the GWP estimates presented in Figure 11.1 (GWP_{100} = 800), costs of BC mitigation options expressed as USD per tonne of CO_2-equivalent emissions could be compared to consider their competitiveness alongside a range of current monetized per-tonne CO_2 emission estimates. Higher (or lower) CO_2 prices, and a higher (or lower) GWP for BC, would imply more (or fewer) BC mitigation options would be considered to be cost-effective for climate purposes (not accounting for the health benefits described in the previous section).

[16] Monetizing climate benefits of CO_2 reduction is even more uncertain than estimation of health benefits. Impacts of CO_2 emissions are felt globally, over long time periods, are difficult to quantify, and affect a large number of health, economic and environmental systems. Despite these uncertainties, there have been a number of attempts to quantify and monetize these impacts in USD $(Mg\ CO_2)^{-1}$ (equivalent to USD $(tonne CO_2)^{-1}$) units (referred to as the social cost of CO_2). A meta-analysis of the literature found a median value for the social cost of CO_2 of 47 USD $(MgC)^{-1}$ under one set of assumptions, with a wide uncertainty range [*Tol,* 2007]. A recent U.S. Department of Energy rule presented a range of values from 17 to 238 USD $(MgC)^{-1}$ for the year 2010 (Table IV.19 of DOE, 2010). The few existing policies to date that have resulted in a CO_2 market price can provide another means of gauging acceptable monetization values, as these policies implicitly assigned a value to the reduction of emissions; however, such prices are determined much differently than the analytical approach described above. One example is the European Union Emission Trading Scheme, where European Union Allowance futures prices ranged from about 30 to 90 USD $(MgC)^{-1}$ during 2011 [see www.theice.com].

[17] It may be feasible to use CO_2-equivalent emissions of BC and the social cost of CO_2 to approximate a monetization of the climate benefits of BC reductions. Along with monetized estimates of the health benefits, this valuation would enable comparison of the net benefits of a BC reduction measure to the net costs of that measure. For example, *UNEP/WMO* [2011b] and *Shindell et al.* [2012] found a net present climate benefit of USD 225 billion (+118/-212) from the reduction of BC in the year 2030 due to the implementation of several BC measures. However, there are many caveats about using the social cost of CO_2 in such an analysis. Most estimates of the social cost of CO_2 come from evaluating impacts that occur decades in the future. Some estimates of the social cost of carbon even show near-term benefits from slight warming which are outweighed by the larger negative impacts from more extreme warming in the future. In contrast, BC has a very short lifetime. Therefore, both impacts of CO_2 and the resulting valuation should differ from those of BC.

[18] Additionally, several BC impacts are not captured in a globally averaged, climate-forcing based metric. Depending on the location of emission, sources may affect snow- and ice-dominated regions such as the Arctic. They may also affect climate in ways not represented by global-average climate forcing. Some of these issues are outlined in Sections 7 and 8, but targeted scientific studies have not yet supported quantification of these additional factors. Therefore, these inquiries are in the emerging phase.

12.4. Technical and programmatic feasibility for individual BC-rich source categories

[19] We briefly review here key mitigation options for each of the major emission source categories, and discuss the mitigation potential for each source with regard to the key factors presented above. The potential for reducing climate forcing presented here is largely based on the global results for emission and forcing categories shown in Figs. 3.2, 3.3, 10.1, and 10.3. The latter two show the role of co-emissions in producing climate forcings, specifically from POA, SO_2, CO, NMVOC, and NO_x. Forcing by POA and SO_2 is negative, and thereby offsets some direct forcing from BC. Positive forcing due to O_3 production by NO_x is balanced by negative forcing due to nitrate production, with additional longer term cooling due to methane destruction. The result is a net cooling effect that is temporally and spatially complex. A key caveat is that the analysis in Sections 3 and 10 reflect the contribution of all emissions from a given source sector, whereas a mitigation technology may not reduce all of those emissions proportionally.

[20] To date, almost no policies have specifically sought to reduce BC. Most related policies have addressed the more aggregated particulate matter, of which BC is a component, for purposes of improving local air quality and public health. There is therefore a significant amount of literature on the potential and costs of PM emission reductions, but much less literature focused on mitigation options addressing BC specifically.

[21] Many of the mitigation options for PM are identical for BC, but this is not always the case. While a number of studies estimate the costs of mitigating PM, mitigation measures often affect primary PM emissions in a different manner than they affect secondary PM precursor emissions, and sometimes lead to differing reductions of the components of primary PM such as POA and BC. Therefore, mitigation analyses that explicitly determine effects on BC emissions are important. Furthermore, reductions in PM have typically been sought in areas of high concentration, mainly urban areas, and are most easily developed for sources for which end-of-pipe mitigation options are available, such as power plants, vehicles and some industrial processes. Research into mitigation for sources that are more rural in nature is just beginning, especially for those sources that are predominantly located in developing countries, and

many of these sources may be important for climate change considerations.

12.4.1. Diesel engines

[22] Mitigating BC emissions from on-road and off-road diesel sources appears to offer the best potential to reduce net forcing because the net climate forcing is positive and larger than found for other principal source categories. These off-road sources include agricultural, construction and other land-based mobile equipment. From these sources, more than the others in Figure 3.2, the emission ratio of BC:POA is higher, which reduces the magnitude of negative aerosol forcing terms relative to the direct positive forcing. Longer-term forcing by effects of NO_x on the methane budget is negative, but the integrated value is less than the central estimate of first-year forcing. The net impact of mitigation options depends on whether NO_x emissions are reduced in addition to particles.

[23] Reductions in mobile-source emissions have been pursued since the 1960s, and technology to reduce emissions from diesel engines is mature. Programs to implement this technology differ by region and type of engine use.

1. In industrialized countries such as the USA, European Union, and Japan, PM emission standards effectively control BC emissions from most new diesel vehicles. Diesel emissions in these countries will decrease even in the absence of further standard tightening as older vehicles are retired and replaced with the cleaner new vehicles. In these countries, further mitigation of BC from diesel engines is available mainly from retrofits and accelerated vehicle retirement.

2. In some developing countries, higher-emitting vehicles are still being sold. Accelerating implementation of advanced emission standards in these countries would lead to reductions of BC.

3. Even in countries with on-road vehicle emission standards, some unregulated or poorly controlled sources remain. For example, regulations may not cover some stationary diesel engines or off-road sources, and better inspection and maintenance programs could address poorly maintained, high-emitting vehicles.

4. Finally, work still remains to determine the most effective ways to apply existing technology to marine and other off-road engines.

[24] The costs of a diesel retrofit for a heavy duty truck ranging from 5,000 to 17,000 USD per vehicle have been reported [*Schrooten et al.,* 2006; *CARB,* 2009], and in some locations (such as the USA, and particularly California) there have been investments of hundreds of millions of dollars in such retrofits. A diesel particulate filter reduces more BC when installed on a large truck than on a small truck if all else is equal, while older vehicles are more polluting per mile but have a shorter remaining lifetime. Therefore, the cost-effectiveness of a diesel retrofit will depend on both the type and age of a vehicle. *Sarofim et al.* [2010] analyzed the potential of diesel retrofits for on-road vehicles to reduce BC emissions in the USA; the study focused on diesel engines that do not meet the more rigorous particulate emission standards that were introduced in the USA in 2007. The study found that costs ranged from 36 thousand USD $(Mg)^{-1}$ to 318 thousand USD $(Mg)^{-1}$ BC abated, depending on the age and type of vehicle being retrofitted. The study did not address high emitters or any abatement options besides retrofits. *UNEP* [2011] reported comparable costs for heavy-duty diesel vehicles (*i.e.,* 120 to 200 thousand USD per Mg BC). Installation of filters in new diesel vehicles costs less than retrofitting older vehicles [*EPA*, 2012].

[25] Most developing countries have not yet implemented strict emission standards, and in many cases their fuels are still too sulfur rich to be compatible with diesel particulate filters. Diesel particulate filters can be used with low sulfur fuel (50 ppm) but are more effective when the sulfur content is even lower [*Blumberg et al.,* 2003]. Diesel oxidation catalysts, which can be used to reduce PM emissions even with fuel compositions of several-hundred-ppm sulfur, are ineffective at controlling BC. Some projections [*e.g., Streets*, 2007] reflect the possibility that BC emissions could continue to grow in the transport sector in these regions absent policy interventions, given projected growth in vehicle fleets. *Shindell et al.* [2011] found climate benefits in 2030 as a result of applying European emission standards for diesel vehicles in India and Latin America, with health benefits resulting from the tighter standards in all regions. However, reductions of organic carbon and sulfates make the net climate effect less clear or even lead to warming in some other developing countries such as China.

[26] Non-retrofit reduction options also exist. Reduction of idling through regulation, education, electrification of rest stops, and other means has been explored by the *EPA* [2009b]. Improved inspection and maintenance, accelerated vehicle retirement, improved efficiency, smart transport algorithms to plan shipping routes, and shifting transport modes to rails, can also lead to decreased emissions. These abatement possibilities may generate fuel savings, as well as GHG reductions. Biodiesel use may also lead to lower particulate emissions [*EPA*, 2002].

[27] Diesel retrofits are a good example of how mitigation options do not always reduce all POA species proportionally. Diesel oxidation catalysts reduce OC emissions but offer little BC mitigation benefit [*Shah et al.,* 2007], whereas diesel particulate filters reduce BC with equal or greater effectiveness to other PM components. Diesel particulate filters are also a case where mitigation of some pollutants (BC and POA) may lead to changes in emissions of other pollutants such as an increased NO_2 to NO ratio leading to the potential for higher local O_3 concentrations [*Millstein and Harley,* 2010] or a possible fuel penalty resulting from increased back pressure. As with any end-of-pipe abatement technology, the net climate effect of the installation of a diesel particulate filter will be different from the net effect of the diesel category overall because a filter does not reduce all pollutants equally.

[28] Technical mitigation of diesel engines is in the mature stage for end-of-pipe control, but may have reached only the solidifying stage for retrofit programs. In addition, programs that promote mitigation are in a wide range of phases in less-industrialized countries.

12.4.2. Industry

[29] Figure 10.1 shows that industrial sources as a whole produce substantial negative direct and indirect climate forcings from co-emissions, especially sulfur. However, industrial sources are quite heterogeneous, and the aggregated value in Figure 10.1 masks the fact that individual source profiles have

more positive or more negative forcing. For example, the Bull's trench brick kiln shown in Figure 10.3, which is an Indian brick kiln using low-sulfur coal, may have positive forcing. Other industrial coal combustion activities discussed in Section 3 include small boilers, process heat for brick and lime kilns, and coke production for the steel industry. Knowledge regarding this source category is in an emerging state. Data availability for both activity and emission factors for these sources are poor; estimates of emission magnitudes and composition sometimes have no measurement support.

[30] Extensive work has addressed emission reductions from industrial and manufacturing sources, but these measures may not apply to installations such as brick kilns or coke ovens, which are widespread in developing countries and almost completely absent in developed countries. Likewise, although technical and programmatic feasibility is in advanced stages in industrialized countries, it is still in emerging stages in the developing countries where most BC emissions occur.

[31] Lower-emitting technology and controls exist for both brick kilns [*Heierli and Maithel,* 2008] and coke ovens [*Polenski and McMichael*, 2002; *EPA*, 2008]. These alternatives usually require complete replacement of the installation with more modern technology and thus require large capital outlays (at least 25,000 USD for a more energy efficient technology identified by *Heierli and Maithel* [2008]). To the extent that lower-emitting technologies emit less BC per unit fuel, they would be more beneficial for climate purposes than technologies that strictly improve efficiency (and would therefore reduce BC or sulfur per unit output in equal proportions).

[32] *Rypdal et al.* [2009a] found that industrial source abatement makes up a significant fraction of the least expensive abatement options globally based on extrapolating GAINS model cost curves to the developing world. *Rypdal et al.* did not consider fuel switching as a mitigation option, which is especially important for emissions in reductions of residential combustion. *Streets* [2007] found that East Asia was a source of potential industrial reductions of BC emissions, but that existing regulations have already captured a large portion of those reductions in other regions.

[33] In some regions, both coke ovens and brick kilns are being phased out due to developing government action. The fraction of coke produced by traditional or beehive ovens in China has declined after the 1990s, and several South Asian countries have introduced regulations to limit brick kiln operation near urban areas. Improved kilns could also improve efficiency for charcoal production and thereby reduce emissions in Kenya [*Bailis,* 2009]. Potential for addressing these sources could be large. Replacement of a single industrial source would reduce larger quantities of emissions than a replacement of a residential or mobile source and, thus, transaction costs could be lower.

12.4.3. Residential solid fuel: Heating

[34] As shown in Figures 3.2 and 3.3, wood for heating purposes is a significant source in northern regions such as Europe, North America, and central Asia [see also *Arctic Council Task Force*, 2011]. Figure 10.1 shows little to no potential for reducing global climate forcing from conventional wood stoves by targeting BC emissions because co-emitted species contribute a substantial negative climate forcing, and the net effect of emissions from the residential heating category is uncertain in sign. Like industrial sources, this sector is also heterogeneous. Figure 10.3 shows that wood boilers specifically offer potential to reduce positive forcing associated with BC emissions. Further, the potential for mitigating climate forcing might be greater in certain regions such as the Arctic. *Quinn et al.* [2011] states that OA co-emitted with BC is unlikely to offset positive climate forcing due to BC when emissions reach the Arctic. Over snow and ice covered surfaces, even OA may exert a positive forcing. Furthermore, as noted in Section 6.2, the net aerosol indirect and semi-direct effects in the Arctic may lead to a smaller negative forcing or even positive forcing compared with the global average. *UNEP/WMO* [2011a; b] explored the effect of widespread adoption of pellet stoves and boilers in industrialized countries as well as use of coal briquettes in China, Russia and Eastern Europe, and found that the combination resulted in 0.05°C of avoided warming globally and 0.1°C of avoided warming in the Arctic by 2040.

[35] Wood stoves serving single-family homes can be used as the primary source of heat or as a supplement to conventional heating systems. Stove emissions can be reduced through changes in the stove technology or changes in the nature of the fuel. In the USA, emission limits have been in place for new stoves since 1988. Three major categories of stoves meet modern particulate emission standards: non-catalytic, catalytic, or pellet stoves. Non-catalytic stoves include baffles and secondary combustion chambers for emission reductions whereas catalytic stoves reduce emissions through the use of metals that increase oxidation rates. Catalytic stoves are slightly cleaner and more efficient, but are more expensive and require more maintenance and upkeep. Pellet stoves are designed to burn pellets of sawdust, wood, or other biomass materials. In Europe, several countries (*e.g.*, Nordic countries, Germany, Sweden, and Austria) have introduced voluntary eco-labeling of stoves with standards for efficiency and emissions. Some countries (*e.g.,* Austria, Sweden, Norway, Denmark, Germany) also issue national emission standards for small residential installations; the most comprehensive at this time is German law from 2010 (*Federal Law Gazette*, 2010). Finally, the European Commission Renewable Directive (2009/28/EC) set combustion efficiency standards while the Ecodesign Directive (2009/125/EC) is being extended to include small residential combustion of solid fuels. These developments mean that the technical feasibility of alternatives is in the mature phase, although programmatic feasibility for widespread implementation may vary considerably by country. While pellet stoves are cleaner than many other options, they may not be cost-effective for users who harvest their own wood for fuel. Prices for these kinds of stoves range from 1000 to 3000 USD; one estimate suggests that the cost-effectiveness of reductions for replacement of a wood stove ranges from 130 USD $(\text{Mg PM})^{-1}$ for a non-catalytic stove to almost 1000 USD $(\text{Mg PM})^{-1}$ for a pellet stove [*Houck and Eagle*, 2006]. Few studies have examined the relative BC to POA ratios for each of these technologies and, therefore, the net climate effect of switching to a less polluting technology may differ from the net climatic impact of the entire category.

[36] Larger boilers for multi-family homes may also be wood-fired, and such installations are found in several European countries. These boilers can range from 150 kW up to 1 MW in size. Little information is available about the quantities and technologies used in these installations. Cyclones are sometimes used to reduce PM emissions in older installations, but more advanced controls would be required for effective removal of submicron particles, including BC. Newly build installations are often efficient, low-emission pellet, chip, or sawdust boilers.

12.4.4. Residential solid fuel: Cooking

[37] Figure 10.1 shows a net negative forcing from biofuel cooking based on emission factors within the GAINS model due mainly to co-emissions of organic matter. In contrast, Figure 10.3 shows a net positive forcing from residential cooking stoves based on in-field measurements, demonstrating that careful scrutiny of specific technologies may be necessary to have confidence in the net effect of mitigation choices. For wood use, changes in the methane budget due to direct methane and CO emissions add positive forcing in the long-term. Mitigation options that reduce all products of incomplete combustion have the potential to reduce long-term forcing even if first-year forcing is uncertain.

[38] Residential solid fuel is used for cooking primarily in developing countries, and consists of wood, agricultural residues, dung, charcoal, and coal. Improved household energy solutions have been sought for several years. In the early 1980s, forest depletion was the main reason for concern. More recently, in addition to forest depletion, concern is also driven by high PM exposures resulting from indoor solid-fuel use; these exposures lead to severe respiratory ailments and premature deaths numbering in the millions [*Smith et al.,* 2004]. These activities have largely taken place in the context of development programs without the large-scale investment in environmental measurement or engineering solutions that characterizes the move toward mature technology development.

[39] Stove improvements and fuel switching are the main solutions to reduce environmental and health impacts of household energy use. Early programs that focused on stove efficiency did not always improve air quality [*Smith et al.,* 2007], implying that they had little effect on BC. Since that time, stove improvements have included insulating combustion chambers, adding chimneys, and managing air-fuel mixing before and after combustion [*Bryden et al*., 2006]. Chimneys can reduce indoor air pollution and improve combustion by adding draft through the chamber, although some of the reduction in indoor pollution is accomplished by shifting the particulate matter outside [*Johnson et al.*, 2006]. Improved stove design has resulted from the advent of emission testing by non-governmental organizations [*MacCarty et al.*, 2010], and efforts to promote mass manufacture are also occurring. More advanced combustion technology coupled with a broader understanding of the field has resulted in renewed interest [*World Bank*, 2011]. Nevertheless, understanding of in-use efficiency and emissions as compared with laboratory performance is still limited [*Roden et al.,* 2009; *Johnson et al.,* 2006; *Johnson et al.,* 2008; *Christian et al.,* 2010], with in-use emissions typically higher than those measured in laboratory settings. While enhancing efficiency of these stoves decreases total emissions, field measurements indicate that particulate emission per unit fuel is reduced by only up to 50% [*Roden et al.,* 2009]. Much of the emission reduction may be POA rather than BC, so that not all mitigation options may reduce total climate forcing.

[40] Air flow management in stoves and cleaner fuels may be required to reduce emissions further. The former can be accomplished either with fans that introduce secondary air or with gasification stoves, which separate fuel devolatilization and combustion. Both fan stoves [*Jetter and Kariher*, 2009] and gasification stoves [*Mukunda et al.*, 2010] show very good emission performance in laboratory settings, but they are rare enough in the field that in-use performance is not well characterized. Stoves without chimneys are in the 10-20 USD range, while those with chimneys require more material, individual installation and presently range from 40-100 USD. Gasifier stoves are typically 50-100 USD.

[41] Emissions from residential cooking are greatly reduced when the users switch to modern fuels such as liquefied petroleum gas, kerosene, or electricity [*Smith et al.*, 2000a; b]. Cleaner fuels can also be provided by processing solid fuels and producing briquettes, pellets, and charcoal made from either wood or agricultural waste. Some programs deliver both stove and fuel [*Zhi et al.*, 2009], because performance depends on the combination of the two. However, emissions from fuel production in addition to end-use must be considered in the calculation of climate impact [*Bailis et al.*, 2005].

[42] Implementation of cookstove replacement programs is challenging. Stoves that do not offer affordable, reliable operation that meets the specific need of the main user are not suitable replacements. Historical programs in China had some success in delivering better wood stoves with chimneys [*Smith et al.,* 2007, *Sinton et al.,* 2004] but a large, long-standing national program in India may not have affected emissions. These are examples of the importance of addressing implementation feasibility alongside cost and environmental attributes. Most recently, the Global Alliance for Clean Cookstoves was launched as a public-private initiative to address public health and climate change by "…creating a thriving global market for clean and efficient household cooking solutions." Technical and programmatic feasibility for this source category is in the emerging phase.

12.4.5. Open burning

[43] Figures 10.1 and 10.3 show either near-zero or net negative forcing estimates for current baseline emissions from agricultural burning, forest burning and grassland burning. The negative climate forcing from co-emitted POA is substantial for each category, even offsetting the long-term positive forcing caused by effects on the methane budget. These sources, therefore, are not good candidates for mitigation actions. The exception here, as with residential heating, is if some burning sources affect the Arctic or other snow- and ice-dominated areas [Section 7; *Quinn et al.*, 2011].

[44] Work on open burning reduction for BC mitigation is moving from the nascent to the emerging phase of analysis in Figure 12.1. For open burning sources the preliminary nature of the analysis, resistance to changing management practices, and difficulties in quantifying reductions may present barriers to implementing mitigation options.

[45] *Sarofim et al.* [2010] analyzed biomass burning abatement potential in the USA by considering mitigation options such as using propane burners on stacked crop residues, backing fires, conservation tillage, soil incorporation, central processing sites, and a number of forestry prescribed-burn mitigation options [derived from *Ottmar et al.,* 2001; *EPA,* 1992, 2005; *Massey,* 1997; *WRAP,* 2002; *USDA,* 2005]. Some of the options are estimated to have negative costs: mainly conservation tillage for agriculture [*Massey,* 1997], but also mechanical removal of small trees followed by use of the biomass as feedstock for electricity generation facilities [*USDA,* 2005]. The remaining options for reducing BC emissions for less than 40 thousand USD $(Mg)^{-1}$ all relate to adoption of practices to reduce emissions from prescribed burning of forests or grasslands. While this analysis serves as a representative example of how to develop mitigation cost estimates for open burning, extension of this analysis to regions outside the USA is only appropriate for regions with similar properties in terms of managed forests, grasslands, and agricultural practices.

12.4.6. Other sources

[46] Marine shipping contributes about 2% of global BC emissions, but may constitute a larger fraction of direct BC emissions in remote regions. In particular, the Arctic is a sensitive region with few other direct sources of BC emissions, where the high surface albedo due to snow and ice cover will reduce the cooling by co-emissions, and where there is potential for increased ship routes in the future as sea-ice recedes (though the reduction of sea-ice cover will also lead to a reduced albedo and, therefore, a smaller BC impact over time). If sulfate emissions from ships are controlled for non-climate reasons, the BC-to-sulfate ratio will increase and increase the probability that mitigation would have net climate benefits. For example, new regulations of the United Nations International Maritime Organization will require sulfur content in fuel for marine vessels to be reduced to 0.5% by 2020 [*Winebrake et al.,* 2009], and some proposed and existing Emission Control Areas currently have stricter standards than the global standard of 4.5%. However, the fact that most BC emissions from ships occur over low-albedo surfaces in regions where hydrological impacts are less critical means that mitigation of emissions globally is less likely to have climate benefits.

[47] There is interest in better quantifying BC emissions from oil and gas flaring but the work in this area is still preliminary [*Arctic Council Task Force*, 2011]. As shown in Table 3.4, there are a number of other smaller BC sources such as power generation and gasoline engines that have traditionally not been a major target of BC mitigation analysis. However, there have been some exceptions – *Shindell et al.* [2011] show that BC reductions are a key contributor to net cooling resulting from tighter gasoline vehicle standards. There has also been occasional interest in the impacts of BC emissions from aviation despite being less than 1% of global emissions. However, due in part to the altitude of the emissions [*Hendricks et al.,* 2005; *Koch et al.,* 2005] there is little BC mitigation data available for these sources.

12.5. International perspective on BC reductions in aggregate

[48] In addition to understanding the BC mitigation opportunities and potential for each individual source, as briefly provided above, we present here a more macro perspective for evaluating BC mitigation.

12.5.1. Projected future emissions

[49] Mitigation considerations are informed by how emissions are projected to change over time. Future emission drivers include economic development, implementation of air quality policies, technological changes, fuel consumption, land-use change, and behavioral changes. When using projections to prioritize mitigation, it is important to differentiate between those projections which are solely based on existing policies and drivers, and those that make projections based on a presumption of future regulations due to, for example, an assumption that a richer society will demand cleaner air. For projections based on existing regulations, sectors where emissions are expected to grow over time or remain significant are of more importance than those where emissions are expected to decline – however, for projections which include assumptions about future policies, it is important not to discount mitigation actions that are assumed but not yet implemented. A few studies have looked at future BC projections: *Streets et al.* [2004], *Streets* [2007], *Streets et al.* [2011], *Cofala et al.* [2007], and *Rypdal et al.* [2009a] globally; *Klimont et al.* [2009] in Asia; *Sarofim et al.* [2010] and *EPA* [2012] in the USA, *Rypdal et al.* [2009b] in the USA, European Union, and China; and *Walsh* [2008] for the global transport sector. Using the RAINS (Regional Air Pollution Information and Simulation) model, *Cofala et al.* [2007] estimated a 17% reduction of global anthropogenic BC emissions by 2030 relative to present, mainly due to reductions in the mobile sector (diesel particulate controls) and the domestic sector (less coal use and replacement of traditional stoves). *Streets* [2007] also shows global reductions in BC emissions of 9 to 34% by 2030 relative to present, and highlights some regions and sectors where projected emissions may increase under some scenarios over that time period. The changes depend on assumptions about growth, technology development, and environmental policy creation and enforcement. The growth regions and sectors include residential emissions in Africa, open biomass burning emissions in South America, and transportation emissions in the developing world. Projections by *Streets et al.* [2011] show similar regional differentiation in future trends but with less overall global BC emissions decline by 2030. In these projections, decreases between 2005 and 2030 in Northeast Asia, Southeast Asia, the Pacific, North America and Europe due to further air pollution legislation result in slight net global decreases despite increases in most other regions. It has also been suggested that retreat of Arctic sea ice may increase marine shipping in the Arctic [*Granier et al.*, 2006; *Corbett et al.,* 2010], which might lead to increased emissions in a region with higher sensitivity to carbonaceous emissions due to snow albedo effects.

[50] Because of the short atmospheric lifetime of BC, the timescale of projections most pertinent to mitigation decisions are those on timescales similar to the lifetime of infrastructure investments (*i.e.,* two to three decades). Nevertheless, for a long-term perspective, it is also instructive to view how BC and co-emissions of POA are projected within the models that have traditionally been used to produce long-term (*i.e.,* out to year 2100 or even beyond) GHG emission scenarios. Long-term emission scenarios have been developed for the climate

projections of the forthcoming IPCC Fifth Assessment Report (www.ipcc.ch), scheduled for publication in 2013. These emission scenarios are referred to as 'Representative Concentration Pathways' and based on scenarios from four modeling teams (available at http://www.iiasa.ac.at/web-apps/tnt/RcpDb). These pathways are named according to their 2100 radiative forcing level as reported by the individual modeling teams (the four range from 2.6 to 8.5 W m^{-2}). The radiative forcing estimates are based on the forcing of GHGs and other forcing agents, including BC and OC. The Representative Concentration Pathways do not represent specific futures with respect to climate policy action (or no action). Any differences can be attributed in part to differences between models and scenario assumptions (scientific, economic, and technological). Across the four modeling scenarios, projected patterns of global BC emissions are similar: emissions after 2010 decrease steadily, reaching about half of 2010 emissions by the end of the century (Figure 12.2) [*RCP Database*, 2009]. Sectorally, there are more differences: global emissions in each major sector increase in at least one model out to 2020, and one model shows an increase in global open burning emissions even out to 2030. Regionally, several scenarios show emission growth in Asia (especially transport) and the Middle East and Africa regions (residential and commercial). Organic carbon emissions show a somewhat less consistent pattern, where, depending on the modeling team or scenario, emissions are projected to remain relatively steady or decline more gradually throughout the century. The economic models that produce these scenarios treat emissions in aggregate and lack engineering details, especially after 2030. Therefore, the projection of declining BC and POA emissions is not based on specific policies or technology shifts, but on the assumption that cleaner fuels are used and emission factors decline as income increases.

12.5.2. Comprehensive international assessments of BC mitigation actions

[51] Few studies have examined the potential for BC mitigation across multiple emission sources and across multiple regions within a common economic modeling framework. Simple analyses include those of *Bond and Sun* [2005], *Montgomery et al.* [2009], and *Kandlikar et al.* [2009], who assessed costs and benefits of a few BC mitigation options. Diesel engine retrofits and replacements, cookstove replacements, and super-emitting vehicles are analyzed in all three studies, in addition to gasoline engine and industrial kiln upgrades in a subset of the studies. All three studies identified cookstoves as having the most promising cost-benefit characteristics, whether to achieve climate benefits alone or both climate and health benefits. These studies considered neither the counteracting role of co-emitted aerosols and precursors on indirect effects, nor the additional longer-term positive forcing by co-emitted gases, which could change the results of the analysis.

[52] Analyses by *UNEP/WMO* [2011a; b] and *Rypdal et al.* [2009a] assessed future mitigation strategies to reduce the climate impact of BC and POA from contained combustion. *Rypdal et al.* [2009a] developed cost curves for each of 12 major world regions to describe the technical mitigation potential and costs of reducing BC, as well as co-emitted OC. The cost curves for Europe were generated by the RAINS model, while extrapolations were made for other regions due to lack of detailed region-specific data on technology availability and costs. Because of this extrapolation, the analysis excluded viable alternatives for some sources, especially those for which knowledge is still emerging or is in the early stages of solidifying. For example, small industrial sources and cooking stoves are not widely used in Europe, so replacement technologies were not present in RAINS. Fuel switching was not considered as an option either. These omissions mean that some BC mitigation opportunities are not captured by the analysis. Under these assumptions, in the year 2030, 418 Gg of BC yr^{-1} could be reduced for 4 billion USD annually, 775 Gg for 30 billion USD, and 1200 Gg for 126 billion USD. In comparison, the *Rypdal et al.* study projected that 4400 Gg BC will be emitted in 2030 under current legislation.

[53] While mitigation in the transport sector dominated the suite of feasible reductions in 2030 in the *Rypdal et al.* [2009a] analysis, emission reductions from industrial process activities (such as coke ovens in China and brick kilns in India) are less expensive and, therefore, made up the majority of the first quartile of emissions reductions, as ranked by cost effectiveness.

[54] *UNEP WMO* [2011a; 2011b] identified several BC mitigation measures that could produce a net global-mean cooling effect. Measures were initially chosen from the GAINS database using one specific value of GWP from the literature. The opportunities identified included tightening of diesel emission standards (*i.e.,* including use of particle filters), brick kiln and coke oven modernization, cookstove improvements, use of efficient pellet stoves for residential heating as well as substitution of coal by coal briquettes, and reduction of agricultural waste burning. Impacts and uncertainties of the selected measures were then evaluated in more detail. The ultimate analysis of temperature impacts was based on modeling the change in radiative forcing when the mitigation measures were applied in two climate models. The percentage of industrial-era forcing reductions achieved by the measures was scaled by a best estimate and central range of industrial-era forcings. Thus, as in this assessment, modeled BC-DRF was increased based on the models' underestimate of BC AAOD relative to observational constraints.

[55] Total effective BC forcing is generally similar between this assessment [+0.6 W m^{-2}, with uncertainty range of (-0.62, +0.63) W m^{-2}] and the UNEP/WMO Assessment [0.60, (-0.6, +0.4) W m^{-2}]. Specific components of BC forcing are slightly different, but large uncertainties are attributed to indirect effects in both reports.

[56] Greater differences between the two assessments are attributable to the treatment of co-emitted POA, especially its indirect effect. The present assessment attributed indirect forcing to different aerosol species based on total atmospheric mass. Given the lack of constraints from the literature and the lower solubility of OA, the UNEP/WMO Assessment instead attributed indirect effects entirely to sulfate. The total net forcing from co-emitted POA is much smaller in the UNEP/WMO assessment, so that climate benefits of measures tend to be larger than those estimated here. Both assessments stress the uncertainty in attribution of aerosol indirect effects to individual species, and both include large ranges in assessed climate impact.

[57] In the UNEP/WMO Assessment, BC measures were grouped into 'technical' and 'regulatory' groups. The technical group included primarily diesel measures and the emission reductions produced net cooling, as also suggested here. The regulatory group of measures had impacts whose range encompassed zero, as also found here.

[58] *Shindell et al.* [2012] used the same emission scenarios described above along with detailed climate modeling, and found global mean temperature impacts consistent with the simplified estimates in the UNEP/WMO Assessment. In that model, the combined indirect and semi-direct aerosol forcings resulting from the measures were negative and, hence, augmented rather than offset the reductions in BC-DRF. In addition to radiative forcing and global mean climate response, both the UNEP/WMO Assessment and *Shindell et al.* [2012] estimated the impacts of the mitigation measures on health, crop yields, and Arctic temperatures, with large regional precipitation shifts attributed to BC in the climate modeling study.

12.6. Policy delivery mechanisms

[59] At the international level, there are forums and agreements where BC mitigation strategies could be addressed. The eight-nation Arctic Council is currently exploring mitigation opportunities for BC, and the Convention on Long-Range Transboundary Air Pollution is exploring the question of how BC could be addressed within its current structure. Some have voiced interest in introducing BC into the United Nations Framework Convention on Climate Change. In 2012, six nations announced the Climate and Clean Air Coalition to Reduce Short-Lived Climate Pollutants. Barriers include questions about addressing both long-lived GHGs and short-lived forcers such as BC in a common framework (see Section 11), and concerns about the consequences of de-emphasizing the importance of long-lived GHGs.

[60] Even if international agreement occurs to move forward with BC reductions, implementation must take place within individual countries. Existing air quality policies may offer the means to deliver near-term mitigation strategies for BC in developed countries and, where such policy frameworks exist, in developing countries where most growth in BC emissions is expected to occur. For example, existing vehicle emission standards for new vehicles, and scrappage and retrofit programs may provide a means of implementing additional BC mitigation in the transportation sector. Other sources may require additional infrastructure for implementation on a large scale, such as reductions of residential cooking emissions in remote areas of developing countries. Some important BC emission sources, such as remote open burning, currently lack a policy or program infrastructure even if PM emissions are already addressed. The portfolio of regulations, policies, and programs capable of delivering BC mitigation varies by country, and in some cases could even vary within a country where some air-quality or land-use policies are administered at sub-national levels.

12.7. Synthesis of considerations for identifying important mitigation options

[61] Table 12.1 provides a matrix that presents multiple criteria discussed in this section, and evaluated elsewhere in this assessment, to help identify important mitigation strategies. It summarizes the level of understanding for the following key considerations for identifying promising mitigation opportunities for BC: the magnitude of the emission source (and thus a first-order indication of technical mitigation potential), the potential to reduce net climate forcing, the potential to benefit sensitive regions such as the Arctic, the availability of technologies and management practices, the costs of these strategies, potential health benefits, and implementation feasibility. Not all of the factors for all emission sources can currently be quantified with uniform, or even robust, levels of understanding. The 'level of understanding' evaluations in this table are intended to be illustrative and are informed both by quantitative analysis from previous sections of this assessment and by qualitative judgment for some of the non-science factors briefly discussed in this section.

[62] There is considerable variation across BC sources regarding the potential to reduce globally averaged positive climate forcing, with many broad emission categories such as residential coal burning, field burning and forest burning offering at best uncertain potential in this regard. If some of these sources preferentially reduce climate forcing in the Arctic or other snow- and ice-dominated regions, they may provide climate benefits that are not reflected in Figure 10.3. With regard to technical feasibility, there are known emission mitigation options for most BC sources. However, there is variation in the degree to which these mitigation options are characterized with regard to impacts on BC and co-emissions and costs. Programmatic feasibility also varies. Some emission sources are already associated with a policy infrastructure to deliver mitigation practices at large scale (*e.g.,* diesel sources), whereas other sources (*e.g.,* forest burning) are less amenable to near-term policy intervention.

[63] While health effects are not evaluated in this report, there is always the potential to obtain some degree of health benefits by mitigating BC emissions. Emissions that preferentially occur in populated areas have large health impacts, while emissions that occur indoors expose fewer people, but at higher concentrations. The lowest health impacts occur for outdoor emissions that occur at low population density. *UNEP WMO* [2011a; b] provide detailed evaluations of health impacts from outdoor air.

[64] Diesel sources of BC appear to offer the most promising mitigation opportunities in terms of near-term forcing and maturity of technology and delivery programs, although some options, such as diesel retrofits, can be costly. Mitigating emissions from residential solid fuels may yield a reduction in net positive forcing, especially when the longer-term effects on the methane budget are considered. The net effect remains uncertain because of uncertain knowledge regarding the impacts of co-emitted species on clouds. Furthermore, the evolution of feasibility is still in the emerging phase for these sources. The net effect of small industrial sources depends greatly on the sulfur content of individual sources, and the feasibility of mitigation is in the emerging phase. Individual source types that have low sulfur emissions and for which alternative technology is available could offer net climate benefits.

Acknowledgments

[65] This assessment is a contribution of the IGBP-IGAC/WCRP-SPARC Atmospheric Chemistry and Climate Initiative (AC&C). The authors acknowledge financial and technical support from the International Global Atmospheric Chemistry (IGAC) project (http://igac.jisao.washington.edu/index.php), C. Koblinsky of the Climate Program Office of the National Oceanic and Atmospheric Administration (NOAA), H. Maring of the Radiation Sciences Program of the National Aeronautic and Space Administration (NASA), Rose Kendall of CSC, and Beth Tully of Tully Graphics. IGAC funding for this project is via the Joint Institute for the Study of the Atmosphere and Ocean (JISAO) under NOAA Cooperative Agreement NA10OAR4320148, Contribution No. 2035. The authors wish to thank the AeroCom modeling community and the AERONET data providers for their great help in providing basic data sets, further analyzed here. We also thank N. Riemer of the University of Illinois for particle-resolved simulation results in Figure 2.5, N. Mahowald of Cornell University for dust fields in Figure 4.1, and D. M. Winker of NASA for providing the CALIPSO data in Figure 4.5. A. Heil is thanked for providing information on biomass fuel loads and M. O. Andreae for providing updates of his biomass burning emission factor compilation. E. Baum, J. Bachmann, R. Minjares, K. Ram, V. Ramanathan, and D. Zaelke are thanked for reading and providing comments that improved the document. Piers Forster acknowledges support from a Royal Society Wolfson Research Merit award. O. Boucher and N. Bellouin were supported by the Joint DECC/Defra Met Office Hadley Centre Climate Programme (GA01101). S. Ghan was supported by the U.S. Department of Energy (DOE), Office of Science, Scientific Discovery through Advanced Computing (SciDAC) program, and the DOE Decadal and Regional Climate Prediction using Earth System Models (EaSM) program. The Pacific Northwest National Laboratory is operated for the DOE by Battelle Memorial Institute under contract DE-AC06-76RLO 1830. Y. Kondo was supported by the Ministry of Education, Culture, Sports, Science, and Technology (MEXT), strategic international cooperative program of Japan Science and Technology Agency (JST), and the global environment research fund of the Japanese Ministry of the Environment (A-1101). For P. K. Quinn's work, this is NOAA PMEL contribution no. 3786. M. Schulz received funding support through the EUCAARI project (EU-FP6 Contract 34684). M. Z. Jacobson received funding from the U.S. National Science Foundation. J. W. Kaiser was supported by the European Union Seventh Research Framework Programme (MACC project, contract number 218793). S. G. Warren acknowledges support from U.S. NSF grant ARC-06-12636. The views expressed in this paper are those of the authors and do not necessarily reflect the views or policies of the U.S. Environmental Protection Agency.

Appendix A. Author contributions

The development of this assessment required a large, diverse group of dedicated authors. They synthesized multiple topics in the individual sections and interlinked the topics throughout. Each section required lead-author commitment equivalent to the production of a typical journal paper. The publication of this assessment in a peer-reviewed journal necessitates a single lead author, thereby precluding the chapter lead authors from receiving the lead-author credit normally accorded for this level of effort. The table below acknowledges the principal contributions of each author in an attempt to further recognize their substantial investment in this assessment. The role of coordinating lead authors was shared by T. C. Bond, S. J. Doherty, D. W. Fahey, and P. M. Forster.

Table A.1. Author principal contributions

Section – topic	Lead authors	Contributing authors
1 – Introduction	T. C. Bond	
2 – Measurements and microphysics	P. K. Quinn Y. Kondo	S. Ghan U. Lohmann J. P. Schwarz
3 – Emissions	C. Venkataraman M. G. Schultz	T. C. Bond S. K. Guttikunda P. K. Hopke J. W. Kaiser Z. Klimont
4 – Constraints on abundance	S. Kinne T. C. Bond	M. Schulz
5 – Direct radiative forcing	S. Ghan M. Schulz S. Kinne H. Zhang	
6 – Cloud effects	D. Koch B. Kärcher	T. Storelvmo U. Lohmann
7 – Cryosphere changes	S. J. Doherty M. G. Flanner	S. G. Warren O. Boucher
8 – Climate response	O. Boucher P. M. Forster	N. Bellouin D. Koch M. G. Flanner S. J. Doherty M. Z. Jacobson D. Shindell C. S. Zender
9 – Synthesis	P. M. Forster D. W. Fahey	
10 – Net climate forcing	T. C. Bond	
11 – Metrics	T. Berntsen	
12 – Mitigation context	B. J. DeAngelo M. C. Sarofim S. Zhang	

Appendix B. Using sky-photometer aerosol absorption optical depth retrievals to constrain black carbon models

B.1. Background and methods

[1] Aerosol column absorption optical depth (AAOD) associated with BC is a key factor controlling model estimates of BC-DRF. The diversity in modeled AAOD is one of the major factors contributing to diversity in estimates of BC-DRF. To reduce BC-DRF uncertainty, we use retrievals from a global network of ground-based sun-/sky-radiance observations (AERONET) to constrain the BC-AAOD simulated by models. AAOD measurements cover complete annual cycles at 171 land sites distributed worldwide, and further incomplete annual cycles are available from 249 sites. By applying further assumptions, detailed below, values of BC column absorption (BC-AAOD) can be extracted from the AERONET retrievals. These values can be compared to those simulated by models at the same location and time, and regional scale factors for BC-AAOD can be determined from the ratio of observed/simulated BC-AAOD. These scale factors are used in this assessment to reduce the bias in models used to determine BC-DRF.

[2] Sun and sky radiance observations [*Dubovik and King,* 2000] in the mid-visible range allow inference of the aerosol column absorption in terms of the AAOD (= AOD × [1-ω_0]) from retrievals of AOD and single scattering albedo (ω_0) at 550nm. Regular retrievals for cloud-free conditions with identical instrumentation at many AERONET locations [*Holben et al.,* 1998] provide extensive coverage over continents and islands. However, the retrievals of ω_0 are less certain at low AOD [*Dubovik et al.,* 2000]. This led to the removal of absorption data for low AOD cases in the official AERONET Version 2.0 product. This filter introduces a positive bias for local statistics of AAOD because only cases with high AOD are counted. To remove this AAOD bias, missing refractive index data in the Version 2.0 data product have been recovered from the lower quality Version 1.5 data product, so that now low AOD cases are included as well. This procedure adds noise to the retrieved AAOD data set, but is expected to reduce the sampling bias (*O. Dubovik*, personal communication). However, a small positive sampling bias may still exist, because negative ω_0 is excluded from the data set. The retrieved AAOD is similar to that from an alternative procedure in which ω_0 is retrieved only from high-AOD observations at each station and applied to all AOD values at that station, thus maximizing the use of Version 2.0 data.

[3] In the mid-visible solar spectral region, non-BC contributions to absorption are mainly from relatively coarse dust particles. To separate BC-AAOD from total AAOD, we assume that BC controls the mid-visible absorption of small (*i.e.,* 'fine-mode') aerosol particles. This implies that any mid-visible absorption by organic matter, brown carbon or small sized dust is attributed to BC, while ignoring BC absorption contributions if BC is attached, for example, to large dust particles. This separation by size is possible because the AERONET inversion method provides detailed size distribution data. Thus, we truncate the AERONET derived size-distributions at 1-µm diameter and assume that the retrieved imaginary part of the refractive index applies to these small sizes. The retrieval is strictly valid only for the entire size-distribution. This assumption of using the retrieved refractive index for the small particle fraction may be violated if the dust absorption dominates the retrieved refractive index. Since coarse particles are often less absorbing than the fine particles, the BC-AAOD could be underestimated with this method especially in regions where dust dominates the overall absorption of the particle population. On the other hand, BC-AAOD could be overestimated if some absorption is caused by organic matter.

[4] If AERONET stations provided global uniform high-resolution coverage for ocean as well as marine locations, the AERONET BC-AAOD retrievals could be directly used to constrain model simulations. However, Figure 4.2 shows that, although there are hundreds of AERONET stations distributed across the Earth, coverage is limited to land, and is far from homogeneous over land. Additional assumptions are required to fill in the gaps between the AERONET station locations.

[5] To fill in the gaps between stations we use spatial distributions of BC-AAOD from AeroCom simulations [*Kinne et al.,* 2006]. Median values of the set of 15 AeroCom models are used for each month and each 1°x1° latitude-longitude grid cell. The model ensemble median is, henceforth, referred to as the AeroCom median. The AeroCom BC-AAOD is estimated from the BC-AOD saved for each model. Based on Mie theory and the assumption of the same BC size distribution (*i.e.,* lognormal with 0.065-µm number mode radius and geometric standard deviation of 1.7) and refractive index (1.7, 0.7*i*) for all models, we use an ω_0 of 0.64 for BC to convert from BC-AOD to BC-AAOD. To compare AeroCom models that estimate only industrial-era AAOD with AERONET observations of total AAOD, we rely on one AeroCom model (LOA) to provide the industrial-era fraction of BC (*i.e.,* (all-source BC-AAOD - pre-industrial BC-AAOD) / (all-source BC-AAOD)), thus estimating a pre-industrial background AAOD of 0.0004. Using global mean values for both the industrial-era and all-source BC-AAOD this ratio in the LOA model is 0.80, but the ratio among model grid boxes (1°x1°) varies widely, from near zero in regions with large natural emissions to 97% in regions with large anthropogenic emissions. Modeled values without any scaling are 0.00172 for industrial era AAOD and 0.00212 for all-source AAOD.

[6] The AeroCom BC-AAOD values do not agree with the AERONET retrievals, so the distribution from AeroCom requires scaling to agree with the AERONET retrievals at the station locations. Scale factors are applied on a regional basis because errors in emissions or BC scavenging vary spatially, producing different biases. In each region (Table B.1), all AERONET data available for a given month are combined, and from this data set a characteristic regional value is calculated using the 3-PDF mean. The 3-PDF mean is defined as the average of the 25, 50 and 75 percentile values of the probability distribution (PDF) and is chosen instead of the mean to avoid the impacts of extreme outliers. The same quantity is determined for the AeroCom median field at the locations of AERONET observations. The 3-PDF mean ratios of AERONET to AeroCom then define the regional (monthly) scale factors.

[7] Table B.1 lists annual mean characteristic values of BC-AAOD for each region from the AERONET retrievals and from the AeroCom BC-AAOD at the same month and locations as

retrievals at AERONET sites within each region. The ratios of the characteristic values (AERONET / AeroCom), also listed in Table B.1, define regional scale factors that can be applied to the AeroCom BC-AAOD within each region to compensate for regional AeroCom biases. According to Table B.1 the ratios are larger than 1 for all regions, but vary widely from region to region (*e.g.,* 1.11 to 3.37 for annual means) and from month to month (*e.g.,* 0.7 to 6.0). The global annual mean of the resulting scaled AeroCom BC-AAOD is 0.00339, which is smaller than the values listed in Table B.1 for AERONET locations only. The table lists BC-AAOD at AERONET sites, where AAOD is higher than the global average, so the global mean after scaling is smaller than the average of the values in the table.

[8] After scaling to AERONET observations, all-source AAOD is 0.00339, and industrial-era AAOD is 0.00299, assuming the same pre-industrial background AAOD. The global average all-source BC-AAOD increases by 60%, and the industrial-era BC-AAOD increases by 74%. These percentage increases depend on the value of ω_0 assumed in deriving BC-AAOD from BC-AOD fields, but the absolute BC-AAOD value does not. If a more-absorbing aerosol (*i.e.,* lower ω_0) had been chosen, the unscaled model AAOD would be greater, the final AAOD would be identical, and the percentage increase would be lower.

B.2. Uncertainties

[9] Table B.2 summarizes estimates of eight sources of uncertainty in BC-AAOD and how each is estimated. We assume the eight factors contributing to uncertainty are uncorrelated, so that they can be added in quadrature. Two of the uncertainties are asymmetric. The lower and upper uncertainties for all-source BC-AAOD are estimated to be -44% and +38%, respectively. For industrial-era BC-AAOD, the uncertainties are -48% and +42%, respectively.

1. Impact of model spatial pattern. The regional monthly BC-AAOD scale factors are based on existing data-pairs (AeroCom/Aeronet) for that region and month. The derived scale factor is then applied to all data-points of the reference model in that region and month. However, spatial distributions can vary significantly among models, which introduces uncertainty. To quantify this uncertainty, the analysis was performed after replacing the AeroCom median field with fields from three individual models. This resulted in the following scaled all-source BC-AAOD values: AeroCom median model: 0.00339; SPRINTARS: 0.00318; GOCART: 0.00211; and IMPACT: 0.00354. From this we derive a 29% uncertainty due to the model spatial pattern.

2. Characteristic value. The BC-AAOD scale factors for each month and region are based on characteristic values at the AERONET sites. In this study the characteristic value is defined by the 3-PDF mean. Other statistical calculations lead to the following all-source BC-AAOD values: 3-PDF: 0.00339; median value: 0.00315; mean: 0.00388; 7 percentiles between 10%-90% averaged: 0.0336; interquartile range of values between 25% and 75% percentiles averaged: 0.00305; interpercentile range of values between 10% and 90% percentiles averaged: 0.00308. From this we derive a 16% uncertainty due to the statistical derivation of the characteristic values.

3. Limited AERONET sites and sampling. To quantify the influence of the limited number of AERONET sites used, sub-samples were used to re-estimate the scale factors. Using half of all available AERONET sites in four different ways produced the following global all-source scaled AeroCom BC-AAOD values: 0.00324; 0.00338; 0.00375; and 0.00301. From this we derive a 13% uncertainty due to the limited AERONET network coverage.

4. Clear-sky bias of AERONET. A related sampling uncertainty is that AERONET data are acquired only during times of direct sunlight whereas model simulated BC-AAOD values refer to all times. Under clear-sky conditions, BC emissions from open fires may be greater, BC removal by precipitation is suppressed, and aerosol dilution may be smaller in the anti-cyclonic weather systems that are associated with clear skies. The associated biases are estimated with models because AERONET retrievals are not possible under cloudy conditions. Estimates based on sampling from the GATOR aerosol model suggest that globally the clear-sky BC-AAOD is 20% larger than BC-AAOD values sampled at all times. However, a much smaller clear-sky BC-AAOD bias, < 5%, was found from AAOD simulated at AERONET sites by four AeroCom models. Model values on days with AERONET AAOD retrievals were compared to values on all days. *Zhang and Reid* [2009] also find a small clear-sky bias, albeit for AOD rather than BC-AAOD. Our best estimate of this asymmetric uncertainty is -5% ± 5%. The effect on radiative forcing could be different than the effect on AAOD depending on the location of BC relative to clouds, but we have not accounted for this uncertainty.

5. Transport in unsampled regions. In defining the 12 regions we have neglected the influence of BC transport from sources to oceanic regions. To address this deficiency we extended some regions with large BC sources downwind partway across the oceans. This increased the global mean BC-AAOD by 10%. We estimate this uncertainty to be 5%.

6. Dust impact on fine-mode AAOD. It is important that dust contributions to the AAOD are not counted as BC-AAOD. The most natural discrimination is separation by particle size. The 1-μm diameter threshold is justified above. Still, dust aerosol can be present in smaller sizes. This can introduce a small bias when linking fine mode AAOD to BC. We estimate this uncertainty to be 10%.

7. Organic matter impact on fine-mode AAOD. To extract the AAOD associated with BC, it was assumed that, after contributions of larger (dust) aerosol sizes to absorption are removed, the remaining absorption by small particles can be attributed to BC. However, there are also other absorbers among small particles like organic aerosol (*i.e.,* OA), which is usually co-emitted with BC. Initial tests with AeroCom median AOD maps for OA and BC and a plausible OA mid-visible imaginary part of the refractive index of 0.005 yielding a co-albedo of 0.027 suggest that 20% of the AAOD of small particles could be attributable to OA. Such an attribution would reduce the BC AAOD. An asymmetric uncertainty of -10% ± 10% is applied to account for this possibility. There are presently insufficient data to apportion direct radiative forcing between BC and OA, and we have not reduced the best estimate of BC DRF for that reason.

Furthermore, we have not attributed this forcing to absorbing OA forcing which would be underestimated if BC DRF was decreased without making a complementary increase to OA. Estimates of forcing per emission developed in Section 10 may be reasonably accurate, as long as both BC and OA are emitted from the same source.

8. Pre-industrial contribution to BC. Compared with all-source BC, industrial-era BC has an additional uncertainty because the preindustrial background is unknown. We assume a 50% uncertainty in the absolute magnitude of background AAOD, leading to an 18% uncertainty in the pre-industrial total.

Table B.1. Comparison of BC-AAOD from the AeroCom median model and AERONET retrievals in selected regions [a]

Region	# pairs	AeroCom AAOD	AERONET AAOD	Ratio	Min factor Max factor
North America	140-220	0.0028	0.0042	1.53	x 1.3 (SON) x 1.9 (JJA)
South America	80-110	0.0049	0.0092	1.87	x 1.2 (JJA) x 3.3 (SON)
Middle East	20-35	0.0110	0.0134	1.22	x 0.6 (JJA) x 1.2 (SON)
Africa	70-110	0.0114	0.0188	1.65	x 1.0 (DJF) x 1.9 (SON)
Europe	90-120	0.0059	0.0069	1.17	x 0.9 (JJA) x 1.8 (DJF)
EECCA	40-60	0.0084	0.0094	1.11	x 0.6 (JJA) x 1.9 (DJF)
South Asia	15-20	0.0101	0.0340	3.37	x 1.1 (JJA) x 5.1 (DJF)
East Asia	30-60	0.0101	0.0230	2.27	x 1.2 (MAM) x 2.0 (JJA)
Southeast Asia	25-30	0.0081	0.0211	2.62	x 2.3 (JJA) x 5.3 (MAM)
Pacific	35-40	0.0024	0.0049	2.02	x 0.8 (JJA) x 3.7 (DJF)
Polar land	0-6				
All oceans	160-210	0.0042	0.0064	1.52	x 1.5 (JJA) x 2.0 (DJF)

[a] Annual averages of monthly characteristic (3-PDF mean) values of BC-AAOD. The ratios of AERONET to AeroCom AAOD are also shown. The reliability of these ratios depends on the number of matching points (column 2), which varies not only by region but also with season. Also indicated are the seasons with the smallest and largest ratios or scale factors. DJF = December, January, February; MAM = March, April, and May; JJA = June, July, and August; SON = September, October and November.

Table B.2. Uncertainties for AeroCom scaled BC-AAOD based on AERONET observations [a]

#	Uncertainty source	Methodology	Uncertainty [b]
1	Impact of model spatial pattern	Comparison of 4 AeroCom models	± 29 %
2	Characteristic value	PDF statistics	± 16 %
3	Limited AERONET sampling	Subsample AERONET sites	± 13 %
4	Clear-sky bias of AERONET	Use modeling subsamples	(-10, 0)%
5	Transport into unsampled regions	Extension of large BC source regions	± 10 %
6	Dust impact on fine-mode AAOD	Estimate of small size composition	± 10 %
7	Organic matter impact on fine AAOD	Estimated absorption of model organic matter	(-20, 0)%
8	BC-AAOD industrial-era component	Assumed uncertainty in background	± 15 %
	All-source AAOD (#1-7)		(-44, 38) %
	Industrial-era AAOD (#1-8)		(-48, 42) %

[a] Uncertainties added in quadrature.

[b] Values in brackets indicate low and high values of asymmetric uncertainties.

Appendix C. Data supporting co-emitted species forcings in Section 10

Table C.1. Estimates of forcing per emission for aerosol species and precursor SO_2, grouped by effect category [a]

Effect	Central	Low	High
BC atmosphere [b]	49.1	19.4	77.6
BC snow and sea ice	16.3	5.4	39.4
BC clouds [c]	18.3	-48.4	99.1
POA atmosphere			
Fossil fuel	-8.6	-17.0	-0.1
Biofuel and open biomass	-4.2	-7.1	-1.2
POA snow [d]	0.9	0.0	3.0
POA clouds	-12.8	-28.4	-4.7
SO_2 atmosphere	-3.7	-5.5	-1.8
SO_2 clouds	-7.5	-16.5	-2.8

[a] Units are ($\mu W\ m^{-2}$) ($Gg\ yr^{-1}$)$^{-1}$. Effects correspond to those shown in Figures 10.1 and 10.2.

[b] Includes direct forcing.

[c] Includes all effects in liquid (including semi-direct and cloud absorption), mixed-phase, and ice clouds.

[d] Applied to biofuel and open biomass only.

Table C.2. Determination of fraction used to apportion indirect effect

	Sulfate	Organic matter
Total industrial-era burden ($mg\ m^{-2}$) [a]	2.12	1.32
Industrial-era burden, considering associated species ($mg\ m^{-2}$) [b]	2.83	1.32
Fraction used in apportionment	0.68	0.32

[a] From *Schulz et al.* [2006].

[b] Scaling for sulfate accounts for the mass ratio of $(NH_4)_2SO_4$ to that of $SO_4^{=}$.

Table C.3. Estimates of liquid-cloud indirect effect for sulfate and organic matter [a]

Effect	Central	Low	High
Total liquid-cloud effect [b]			
Cloud albedo effect	-0.9	-1.4	-0.3
Cloud lifetime effect	-0.35	-1.5	0
Sum [c]	-1.25	-2.9	-0.3
BC liquid-cloud effect [d]			
This assessment	-0.08	-0.36	0.20
Scaled to cloud study emission rate	-0.06	-0.26	0.14
Sulfate and POA liquid-cloud effect [e]			
Remaining	-1.19	-2.64	-0.44
Sulfate (68%)	-0.81	-1.80	-0.30
Organic matter (32%)	-0.38	-0.84	-0.14

[a] All values given are forcings in W m^{-2}.

[b] From *Isaksen et al.* [2009]. These values do not include semi-direct effects.

[c] Sum of total liquid-cloud effect, minus scaled BC effect.

[d] Emission rate assumed here is 8700 Gg yr^{-1}, but most cloud studies would have used a different emission rate, therefore estimating a different impact for BC. We assumed that the most common rate was the anthropogenic net given in *Dentener et al.* [2006] of 6100 Gg yr^{-1}.

[e] Fractions for apportionment are from Table C.2.

Table C.4. Estimates of forcing per emission for co-emitted gaseous species [a]

Forcing and $GWP_{100\text{-yr}}$	CO	NMVOCs	NO_x (as N)	CH_4
Forcings (mW m^{-2}) (Gg yr^{-1})$^{-1}$				
via short-lived O_3	0.09 [b]	0.21 [c]	2.8 [d]	-
via CH_4	0.15 [b]	0.18 [c]	-3.8 [d]	2.2 [b,e]
via nitrate	0	0	-2.0 [f]	-
Total	0.24	0.39	-3.2	
$GWP_{100\text{-yr}}$ (dimensionless)	2.8	4.54	-38	

[a] Short-lived O_3 and nitrate forcings are included in first-year forcing shown in Figures 10.1, 10.2 and 10.3. Longer-lived CH_4 forcing is shown in integrated forcing in Figure 10.4.

[b] Calculations begin with the $GWP_{100\text{-yr}}$ from *Fuglestvedt et al.* [2010] based on an average of the two models reported in Berntsen et al. [2005]. Multiplied by 100-year integral of CO_2 forcing of (0.0086 mW m^{-2}) (Gg yr^{-1})$^{-1}$. Separation of CO into O_3 and CH_4 mechanisms was taken from *Shindell et al.* [2005].

[c] Six VOCs from *Collins et al.* [2002] with weighting recommended by *Fuglestvedt* [2010].

[d] *Wild et al.* [2001] global average.

[e] Although CH_4 does affect short-lived O_3, the resulting forcing is assumed to be included in its total GWP and is subsumed in longer-term forcing. While not precisely accurate for representing first-year forcing, this allocation makes a very small difference.

[f] Calculation begins with total nitrate forcing as given in *Forster et al.* [2007], multiplied by 0.44 to account for the fact that NO_x produces only a fraction of nitrate forcing, with the remainder attributable to ammonia emissions (see text). Forcing-per-emission values are obtained by assuming the same N emission base as the forcing for O_3 attributed to NO_x in *Forster et al.* [2007], so that the ratio between the forcing-per-emission values is the same as the ratio between the forcing values.

Table C.5. Emission rates used for Figures 10.1, 10.2, and 10.4(a) [a]

Category	BC	POA	SO_2 (as S)	CO	CH_4	NMVOC	NO_x (as N)	CO_2
On-road	1030	700	1500	27000	400	2800	6300	1477
Off-road	500	400	900	4000	0	1700	2400	567
Industry	490	900	9900	29000	0	300	1100	2516
Wood/cook	2240	14000	1100	200000	9400	47000	500	4213
Wood/heat	150	600	100	5000	400	1800	0	227
Coal	540	700	2500	19000	100	800	100	1215
Ag fields	360	1200	100	19000	2300	2900	100	414
Forests	1140	10100	900	120000	7300	8600	1100	2349
Savannas	1540	10600	900	150000	5300	7800	2600	5278
Other rich	660	2300	3300	314000	1800	39700	7500	5762
Power	20	0	50100	2000	0	700	6300	7328
Other low	100	300	22500	51000	244500	19300	3900	5092
Industrial-era total	8770	41800	93800	940000	271500	133400	31900	36438

[a] All emissions are in Gg yr^{-1} except CO_2, which is in Tg. Values are developed beginning with year 2000 emissions given by GAINS (see Table 3.5) and RETRO, scaled to inferred BC emission rates in each region using the scale factors given in Section 5.

Table C.6. Emission factors in (g kg^{-1}) used to develop Figure 10.3 and 10.4(b)

Emission source	BC	POA	SO_2	CO	CH_4	NMVOC	NO_x	CO_2
Euro II heavy-duty vehicle [a]	0.47	0.1	0.9	7	0.2	1.4	35.3	3087
Pre-regulation truck [a]	2.39	1.3	11.9	11	0.4	3.0	11.2	3087
Bull's Trench brick kiln [b]	2.44	0.1	10.5	41	1.5	0.3	0.0	2182
Industrial coal boiler [c]	0.01	0.0	5.2	5	0.4	0.7	2.1	1947
Mud cooking stove [d]	0.80	5.7	0.3	67	5.6	2.7	1.0	1833
Conventional wood stove [e]	0.36	3.9	0.2	130	15.0	23.6	2.8	1833
Wood boiler [f]	1.09	1.5	0.3	105	9.0	14.0	1.2	1833
Coal cooking stove [g]	0.58	0.8	0.2	166	0.9	0.5	2.2	2130
Field burning [h]	0.69	4.6	0.4	92	2.7	7.0	1.2	1833
Forest burning [h]	0.56	11.2	1.0	107	4.7	5.7	1.4	1833

[a] GAINS implementation of COPERT4 emission factors [*Ntziachristos and Samaras,* 2009].

[b] *Greentech* [2011], except CH_4 and NMVOC values which were not measured. For those gases, one-half of *Zhang et al.* [2000] values for coal stoves were used, assumed to scale approximately with CO emissions.

[c] *Wang et al.* [2009b]

[d] *Roden et al.* [2009] in-field data for BC, POA, and CO; *Smith et al.* [2000a; b] for other gases.

[e] *McDonald et al.* [2000], except SO_2, CH_4 and NMVOC from *EPA* [1996].

[f] *Johansson et al.* [2004]; *Rau* [1989].

[g] *Zhang et al.* [2000]; *Zhi et al.* [2008].

[h] *Andreae and Merlet* [2001], except CO_2 from carbon balance.

Supplemental Information

Table S.1. Country groups corresponding to regions in Figure 3.1

North America
Canada
St. Pierre & Miquelon
United States of America

Latin America
Mexico
Antigua/Barbuda
Argentina
Aruba
Bahamas
Barbados
Belize
Bermuda
Bolivia
Brazil
Cayman Island
Chile
Colombia
Costa Rica
Cuba
Dominica
Dominican Republic
Ecuador
El Salvador
Falkland Islands
French Guiana
Grenada
Guadeloupe
Guatemala
Guyana
Haiti
Honduras
Jamaica
Martinique
Mexico
Netherlands Antilles
Nicaragua
Other Latin America
Panama
Paraguay
Peru
St. Kitts & Nevis
St. Lucia
St. Vincent & Grenadines
Suriname
Trinidad & Tobago
Turks & Caicos Islands
U.S. Virgin Islands
Uruguay
Venezuela

Middle East
Bahrain
Cyprus
Iran
Iraq
Israel
Jordan
Kuwait
Lebanon
Oman
Qatar
Saudi Arabia
Syrian Arab Republic
United Arab Emirates
Yemen

Africa
Algeria
Angola
Benin
Botswana
Burkina Faso
Burundi
Cameroon
Cape Verde
Central African Republic
Chad
Comoros
Congo
Cote d'Ivoire
Dem. Republic Congo
Djibouti
Egypt
Equatorial Guinea
Eritrea
Ethiopia
Gabon
Gambia
Ghana
Guinea
Guinea Bissau
Kenya
Lesotho
Liberia
Libya
Madagascar
Malawi
Mali
Mauritania
Mauritius
Morocco
Mozambique
Namibia
Niger
Nigeria
Other Africa
Reunion
Rwanda-Urundi
Sao Tome & Principe
Senegal
Seychelles
Sierra Leone
Somalia
South Africa
St. Helena
Sudan
Swaziland
Tanzania
Togo
Tunisia
Uganda
Western Sahara
Zambia
Zimbabwe

Europe
Albania
Austria
Belgium
Bosnia-Herzegovina
Bulgaria
Croatia
Cyprus
Czech Republic
Denmark
Estonia
Faeroe Islands
Finland
France
Germany
Gibraltar
Greece
Greenland
Hungary
Iceland
Ireland
Italy
Latvia
Liechtenstein
Lithuania
Luxembourg
Macedonia
Malta
Monaco
Netherlands
Norway
Poland
Portugal
Romania
Serbia and Montenegro
Slovak Republic
Slovenia
Spain
Sweden
Switzerland
Turkey
United Kingdom

Eastern Europe, Caucasus and Central Asia (EECCA)
Armenia
Azerbaijan
Belarus
Georgia
Kazakhstan
Kyrgyzstan
Moldova
Russian Federation
Tajikistan
Turkmenistan
Ukraine
Uzbekistan

South Asia
Afghanistan
Bangladesh
Bhutan
India
Maldives
Nepal
Pakistan
Sri Lanka

East Asia
China
Korea, North
Korea, South
Macau
Mongolia
Taiwan

Southeast Asia
Brunei Darussalam
Cambodia
Laos
Malaysia
Myanmar
Philippines
Singapore
Vietnam
Thailand

Pacific
American Samoa
Australia
Cook Islands
Fiji
French Polynesia
Guam
Japan
Kiribati
Marshall Islands
Micronesia
Nauru
New Caledonia
New Zealand
Niue
Pacific Islands
Papua New Guinea
Samoa
Solomon Islands
Tonga
Vanuatu
Wake Island

References

Aaheim, H. A., J. S. Fuglestvedt, and O. Godal (2006), Costs savings of a flexible multi-gas climate policy, *Energ. J.*, *S13*, 485-502.

Abbatt, J. P. D., S. Benz, D. J. Cziczo, Z. Kanji, U. Lohmann, and O. Mohler (2006), Solid ammonium sulfate aerosols as ice nuclei: A pathway for cirrus cloud formation, *Science*, *313* (5794), 1770-1773, doi: 10.1126/science.1129726.

Abdul-Razzak, H., and S. J. Ghan (2000), A parameterization of aerosol activation 2. Multiple aerosol types *J. Geophys. Res.*, *105* (D5), 6837-6844, doi: 10.1029/1999JD901161.

Abel, S. J., J. M. Haywood, E. J. Highwood, J. Li, and P. R. Buseck (2003), Evolution of biomass burning aerosol properties from an agricultural fire in southern Africa, *Geophys. Res. Lett.*, *30* (15), doi: 10.1029/2003GL017342.

Abu-Allaban, M., A. W. Gertler, and D. H. Lowenthal (2002), A preliminary apportionment of the sources of ambient PM_{10}, $PM_{2.5}$, and VOCs in Cairo, *Atmos. Environ.*, *36* (35), 5549-5557, doi: 10.1016/S1352-2310(02)00662-3.

Ackerman, T. P., and O. B. Toon (1981), Absorption of visible radiation in atmosphere containing mixtures of absorbing and nonabsorbing particles, *Appl. Opt.*, *20* (20), 3661-3667, doi: 10.1364/AO.20.003661.

Ackerman, A. S., O. B. Toon, D. E. Stevens, A. J. Heymsfield, V. Ramanathan, and E. J. Welton (2000), Reduction of tropical cloudiness by soot, *Science*, *288* (5468), 1042-1047, doi: 10.1126/science.288.5468.1042.

Ackerman, A. S., M. P. Kirkpatrick, D. E. Stevens, and O. B. Toon (2004), The impact of humidity above stratiform clouds on indirect aerosol climate forcing, *Nature*, *432* (7020), 1014-1017, doi: 10.1038/nature03174.

Adachi, K., S. H. Chung, and P. R. Buseck (2010), Shapes of soot aerosol particles and implications for their effects on climate, *J. Geophys. Res.*, *115* (D15206), doi: 10.1029/2009JD012868.

Adams, P. J., and J. H. Seinfeld (2003), Disproportionate impact of particulate emissions on global cloud condensation nuclei concentrations, *Geophys. Res. Lett.*, *30* (5), 1239, doi: 10.1029/2002GL016303.

Alfaro, S. C., S. Lafon, J. L. Rajot, P. Formenti, A. Gaudichet, and M. Maille (2004), Iron oxides and light absorption by pure desert dust: An experimental study, *J. Geophys. Res.*, *109* (D08208), doi: 10.1029/2003JD004374.

Alfarra, M. R., A. S. H. Prevot, S. Szidat, J. Sandradewi, S. Weimer, V. A. Lanz, D. Schreiber, M. Mohr, and U. Baltensperger (2007), Identification of the mass spectral signature of organic aerosols from wood burning emissions, *Environ. Sci. Technol.*, *41* (16), 5770-5777, doi: 10.1021/es062289b.

Allen, R. J., and S. C. Sherwood (2010), Aerosol-cloud semi-direct effect and land-sea temperature contrast in a GCM, *Geophys. Res. Lett.*, *37* (L07702), doi: 10.1029/2010GL042759.

Alterskjær, K., J. E. Kristjánsson, and C. Hoose (2010), Do anthropogenic aerosols enhance or suppress the surface cloud forcing in the Arctic?, *J. Geophys. Res.*, *115*, D22204, doi: 10.1029/2010JD014015.

Amann, M., I. Bertok, J. Borken-Kleefeld, J. Cofala, C. Heyes, L. Hoglund-Isaksson, Z. Kilmont, B. Nguyen, M. Posch, P. Fafaj, R. Sandler, W. Schopp, F. Wagner, and W. Winiwarter (2011), Cost-effective control of air quality and greenhouses gases in Europe: Modeling and policy applications, *Environ. Modell. Softw.*, *26* (12), 1489-1501, doi: 10.1016/j.envsoft.2011.07.012.

Andreae, M. O., and P. Merlet (2001), Emission of trace gases and aerosols from biomass burning, *Global Biogeochem. Cycles*, *15* (4), 955-966, doi: 10.1029/2000GB001382.

Andreae, M. O., and A. Gelencser (2006), Black carbon or brown carbon? The nature of light-absorbing carbonaceous aerosols, *Atmos. Chem. Phys.*, *6*, 3131-3148, doi: 10.5194/acp-6-3131-2006.

Andrews, T., and P. M. Forster (2008), CO_2 forcing induces semi-direct effects with consequences for climate feedback interpretations, *Geophys. Res. Lett.*, *35* (L04), 802, doi: 10.1029/2007GL032273.

Andrews, T., P. M. Forster, O. Boucher, N. Bellouin, and A. Jones (2010), Precipitation, radiative forcing and global temperature change, *Geophys. Res. Lett.*, *37* (L14701), 701, doi: 10.1029/2010GL043991.

Andrews, E., P. J. Sheridan, and J. A. Ogren (2011), Seasonal differences in the vertical profiles of aerosol optical properties over rural Oklahoma, *Atmos. Chem. Phys.*, *11*, 10661-10676, doi: 10.5194/acp-11-10661-2011.

Ansmann, A., M. Tesche, D. Althausen, D. Müller, P. Seifert, V. Freudenthaler, B. Heese, M. Wiegner, G. Pisani, P. Knippertz, and O. Dubovik (2008), Influence of Saharan dust on cloud glaciation in southern Morocco during the Saharan Mineral Dust Experiment, *J. Geophys. Res.*, *113, D04210*, doi: 10.1029/2007JD008785.

Aoki, T., H. Motoyoshi, Y. Kodama, T. J. Yasunari, S. Konosuke, and H. Kobayashi (2006), Atmospheric aerosol deposition on snow surfaces and its effect on albedo, *Scientific Online Letters on the Atmosphere (SOLA)*, *2*, 13-16, doi: 10.2151/sola.2006—004.

Aquila, V., J. Hendricks, A. Lauer, N. Riemer, H. Vogel, D. Baumgardner, A. Minikin, A. Petzold, J. P. Schwarz, J. R. Spackman, B. Weinzierl, M. Righi, and M. Dall'Amico (2011), MADE-in: A new aerosol microphysics submodel for global simulation of insoluble particles and their mixing state, *Geosci. Model Dev.*, *4*, 325-355, doi: 10.5194/gmd-4-325-2011.

Arctic Council (2011), An Assessment of Emissions and Mitigation Options for Black Carbon for the Arctic Council, 173 pp., Arctic Council Task Force on Short-Lived Climate Forcers, Arctic Council.

Arellano, A. F., P. S. Kasibhatla, L. Giglio, G. R. van der Werf, and J. T. Randerson (2004), Top-down estimates of global CO sources using MOPITT measurements, *Geophys. Res. Lett.*, *31* (1), L01104, doi: 10.1029/2003GL018609.

Arellano, A. F., P. S. Kasibhatla, L. Giglio, G. R. van der Werf, J. T. Randerson, and G. J. Collatz (2006), Time-dependent inversion estimates of global biomass-burning CO emissions using Measurement of Pollution in the Troposphere (MOPITT) measurements, *J. Geophys. Res.*, *111* (D9), 303, doi: 10.1029/2005JD006613.

Arnott, W. P., H. Moosmuller, and C. F. Rogers (1997), Photoacoustic spectrometer for measuring light absorption by aerosol: instrument description, *Atmos. Environ.*, *33* (17), 2845-2852.

Ashbaugh, L. L., W. C. Malm, and W. Z. Sadeh (1985), A residence time probability analysis of sulfur concentrations at Grand-Canyon-National-Park, *Atmos. Environ.*, *19* (8), 1263-1270.

Assamoi, E. M., and C. Liousse (2010), A new inventory for two-wheel vehicle emissions in West Africa for 2002, *Atmos. Environ.*, *44* (32), 3985-3996, doi: 10.1016/j.atmosenv.2010.06.048.

Bahadur, R., Y. Feng, L. M. Russell, and V. Ramanathan (2011), Impact of California's air pollution laws on black carbon and their implications for direct radiative forcing, *Atmos. Environ.*, *45*, 1162-1167, doi: 10.1016/j.atmosenv.2010.10.054.

Bailis, R., M. Ezzati, and D. M. Kammen (2005), Mortality and greenhouse gas impacts of biomass and petroleum energy futures in Africa, *Science*, *308* (5718), 98-103, doi:

10.1126/science.1106881.
Bailis, R. (2009), Modeling climate change mitigation from alternative methods of charcoal production in Kenya, *Biomass Bioenerg.*, *33* (11), 1491-1502, doi: 10.1016/j.biombioe.2009.07.001.
Banta, J. R., J. R. McConnell, R. Edwards, and J. P. Engelbrecht (2008), Delineation of carbonate dust, aluminous dust, and sea salt deposition in a Greenland glaciochemical array using positive matrix factorization, *Geochem. Geophys. Geosyst.*, *9* (7), Q07013, doi: 10.1029/2007GC001908.
Ban-Weiss, G. A., L. Cao, G. Bala, and K. Caldeira (2011), Dependence of climate forcing and response on the altitude of black carbon aerosols, *Climate Dyn.*, *38*, 897-911, doi: 10.1007/s00382-011-1052-y.
Bates, T. S., P. K. Quinn, D. J. Coffman, J. E. Johnson, and A. M. Middlebrook (2005), Dominance of organic aerosols in the marine boundary layer over the Gulf of Maine during NEAQS 2002 and their role in aerosol light scattering, *J. Geophys. Res.*, *110* (D18), 202, doi: 10.1029/2005JD005797.
Battye, W., K. Boyer, and T. G. Pace (2002), Methods for improving global inventories of black carbon and organic carbon particulates, Report No. 68-D-98-046, prepared for U.S. Environmental Protection Agency, Research Triangle Park, NC, by EC/R Inc., Chapel Hill, NC.
Bauer, S. E., D. L. Wright, D. Koch, E. R. Lewis, R. McGraw, L. S. Chang, S. E. Schwartz, and R. Ruedy (2008), MATRIX (Multiconfiguration Aerosol TRacker of mIXing state): An aerosol microphysical module for global atmospheric models, *Atmos. Chem. Phys.*, *8* (20), 6003-6035, doi: 10.5194/acp-8-6003-2008.
Bauer, S. E., S. Menon, D. Koch, T. C. Bond, and K. Tsigaridis (2010), A global modeling study on carbonaceous aerosol microphysical characteristics and radiative forcing, *Atmos. Chem. Phys.*, *10*, 4543-4592, doi: 10.5194/acpd-10-4543-2010.
Baumgardner, D., R. Subramanian, C. Twohy, J. Stith, and G. Kok (2008), Scavenging of black carbon by ice crystals over the northern Pacific, *Geophys. Res. Lett.*, *35* (L22815), doi: 10.1029/2008GL035764.
Bell, M. L., K. Ebisu, R. D. Peng, J. M. Samet, and F. Dominici (2009), Hospital admissions and chemical composition of fine particle air pollution, *Am. J. Resp. Crit. Care*, *179* (12), 1115-1120, doi: 10.1164/rccm.200808-1240OC.
Bellouin, N., and O. Boucher (2010), Climate response and efficacy of snow forcing in the HadGEM2-AML climate model, *Hadley Centre Technical Note*, No. 82, 8 pp., Met Office, United Kingdom.
Bergstrom, R. W. (1973), Extinction and absorption coefficients of the atmospheric aerosol as a function of particle size, *Contrib. Atmos. Phys.*, *46*, 223-234.
Bergstrom, R. W., P. B. Russell, and P. Hignett (2002), Wavelength dependence of the absorption of black carbon particles: predictions and results from the TARFOX experiment and implications for the aerosol single scattering albedo, *J. Atmos. Sci.*, *59* (3), 567-577.
Bergstrom, R. W., P. Pilewskie, P. B. Russell, J. Redemann, T. C. Bond, P. K. Quinn, and B. Sierau (2007), Spectral absorption properties of atmospheric aerosols, *Atmos. Chem. Phys.*, *7* (23), 5937-5943, doi: 10.5194/acp-7-5937-2007.
Berntsen, T. K., J. S. Fuglestvedt, M. M. Joshi, K. P. Shine, N. Stuber, M. Ponater, R. Sausen, D. A. Hauglustaine, and L. Li (2005), Response of climate to regional emissions of ozone precursors: sensitivities and warming potentials, *Tellus B*, *57* (4), 283-304, doi: 10.1111/j.1600-0889.2005.00152.x.
Berntsen, T., J. Fuglestvedt, G. Myhre, F. Stordal, and T. F. Berglen (2006), Abatement of greenhouse gases: does location matter?, *J. Climate*, *74*, 377-411.
Berntsen, T., and J. S. Fuglestvedt (2008), Global temperature responses to current emissions from the transport sectors, *P. Natl. Acad. Sci. USA*, *105 (49)*, 19254-19159.
Berntsen, T. K., K. Tanaka, and J. S. Fuglestvedt (2010), Does black carbon abatement hamper CO_2 abatement?, *Climatic Change Lett.*, *103*, 627-633, doi: 10.1007/s10584-010-9941-3.
Bhave, P. V., G. A. Pouliot, and M. Zheng (2007), Diagnostic model evaluation for carbonaceous PM2.5 using organic markers measured in the southeastern US, *Environ. Sci. Technol.*, *41* (5), 1577-1583, doi: 10.1021/es061785x.
Birch, M. E., and R. A. Cary (1996), Elemental carbon-based method for monitoring occupational exposures to particulate diesel exhaust, *Aerosol Sci. Technol.*, *25*, 221-241.
Bisiaux, M. M., R. Edwards, J. R. McConnell, M. A. J. Curran, T. D. Van Ommen, A. M. Smith, T. A. Neumann, D. R. Pasteris, J. E. Penner, and K. Taylor (2011), Large scale changes in 20th century black carbon deposition to Antarctica, *Atmos. Chem. Phys. Discuss.*, *11*, 27815-27831, doi: 10.5194/acpd-11-27815-2011, 2011.
Blumberg, K., M. P. Walsh, and C. Pera (2003), Low-Sulfur Gasoline and Diesel: The Key to Lower Vehicle Emissions, prepared for the International Council on Clean Transportation. (http://www.walshcarlines.com/mpwdocs.html), edited.
Boer, G. J., and B. Yu (2003), Climate sensitivity and response, *Climate Dyn.*, *20* (4), 415-429, doi: 10.1007/s00382-002-0283-3.
Bøggild, C. E., R. E. Brandt, K. J. Brown, and S. G. Warren (2010), The ablation zone in northeast Greenland: ice types, albedos and impurities, *J. Glaciol.*, *56*, 101-113, doi: 10.3189/002214310791190776.
Bollasina, M. A., Y. Ming, and V. Ramaswamy (2011), Anthropogenic Aerosols and the Weakening of the South Asian Summer Monsoon, *Science*, *334* (6055), 502-505, doi: 10.1126/science.1204994.
Bonasoni, P., P. Laj, A. Marinoni, M. Sprenger, F. Angelini, J. Arduini, U. Bonafe, F. Calzolari, T. Colombo, S. Decesari, C. Di Biagio, A. G. di Sarra, F. Evangelisti, R. Duchi, M. C. Facchini, S. Fuzzi, G. P. Gobbi, M. Maione, A. Panday, F. Roccato, K. Sellegri, H. Venzac, G. P. Verza, P. Villani, E. Vuillermoz, and P. Cristofanelli (2010), Atmospheric Brown Clouds in the Himalayas: first two years of continuous observations at the Nepal Climate Observatory-Pyramid (5079 m), *Atmos. Chem. Phys.*, *10* (15), 7515-7531, doi: 10.5194/acp-10-7515-2010.
Bond, T. C., T. L. Anderson, and D. Campbell (1999), Calibration and intercomparison of filter-based measurements of visible light absorption by aerosols, *Aerosol Sci. Technol.*, *30*, 582-600.
Bond, T. C. (2001), Spectral dependence of visible light absorption by carbonaceous particles emitted from coal combustion, *Geophys. Res. Lett.*, *28* (21), 4075-4078.
Bond, T. C., D. G. Streets, K. F. Yarber, S. M. Nelson, J. H. Woo, and Z. Klimont (2004), A technology-based global inventory of black and organic carbon emissions from combustion, *J. Geophys. Res.*, *109* (D14), 203, doi: 10.1029/2003JD003697.
Bond, T. C., and H. Sun (2005), Can reducing black carbon emissions counteract global warming?, *Environ. Sci. Technol.*, *39* (16), 5921-5926, doi: doi: 10.1021/es0480421.
Bond, T. C., and R. W. Bergstrom (2006), Light absorption by carbonaceous particles: an investigative review, *Aerosol Sci. Technol.*, *40* (1), 27-67.
Bond, T. C., G. Habib, and R. W. Bergstrom (2006), Limitations in the enhancement of visible light absorption due to mixing state, *J. Geophys. Res.*, *111* (D20), 211, doi: 10.1029/2006JD007315.
Bond, T. C., E. Bhardwaj, R. Dong, R. Jogani, S. K. Jung, C. Roden, D. G. Streets, and N. M. Trautmann (2007), Historical emissions of black and organic carbon aerosol from energy-

related combustion, 1850-2000, *Global Biogeochem. Cycles*, *21* (2), doi: 10.1029/2006GB002840.

Bond, T. C., C. Zarzycki, M. G. Flanner, and D. M. Koch (2011), Quantifying immediate radiative forcing by black carbon and organic matter with the Specific Forcing Pulse, *Atmos. Chem. Phys.*, *11* (4), 1505-1525, doi: 10.5194/acp-11-1505-2011.

Boucher, O., S. E. Schwartz, T. P. Ackerman, T. L. Anderson, B. Bergstrom, B. Bonnel, P. Chylek, A. Dahlback, Y. Fouquart, Q. Fu, R. N. Halthore, J. M. Haywood, T. Iversen, S. Kato, S. Kinne, A. Kirkevag, K. R. Knapp, A. Lacis, I. Laszlo, M. I. Mishchenko, S. Nemesure, V. Ramaswamy, D. L. Roberts, P. Russell, M. E. Schlesinger, G. L. Stephens, R. Wagener, M. Wang, J. Wong, and F. Yang (1998), Intercomparison of models representing direct shortwave radiative forcing by sulfate aerosols, *J. Geophys. Res.*, *103* (D14), 16979-16998.

Boucher, O., and M. Pham (2002), History of sulfate aerosol radiative forcings, *Geophys. Res. Lett.*, *29* (9), 1308, doi: 10.1029/2001GL014048.

Boucher, O., and M. S. Reddy (2008), Climate trade-off between black carbon and carbon dioxide emissions, *Energ. Policy*, *36*, 193-200.

Bradford, D. F. (2001), Global change - Time, money and tradeoffs, *Nature*, *410* (6829), 649-650, doi: 10.1038/35070707.

Brem, B. T., F. C. M. Gonzalez, S. R. Meyers, T. C. Bond, and M. J. Rood (2012), Laboratory-Measured Optical Properties of Inorganic and Organic Aerosols at Relative Humidities up to 95%, *Aerosol Sci. Technol.*, *46* (2), 178-190, doi: 10.1080/02786826.2011.617794.

Brioude, J., O. R. Cooper, G. Feingold, M. Trainer, S. R. Freitas, D. Kowal, J. K. Ayers, E. Prins, P. Minnis, S. A. McKeen, G. J. Frost, and E. Y. Hsie (2009), Effect of biomass burning on marine stratocumulus clouds off the California coast, *Atmos. Chem. Phys.*, *9* (22), 8841-8856.

Brunekreef, B., R. Beelen, G. Hoek, L. Schouten, S. Bausch-Goldbohm, P. Fischer, B. Armstrong, E. Hughes, M. Jerrett, and P. van den Brandt (2009), Effects of long-term exposure to traffic-related air pollution on respiratory and cardiovascular mortality in the Netherlands: The NLCS-AIR study, *Research Report*, 139, Health Effects Institute, Boston, MA.

Bryden, M., D. Still, P. Scott, G. Hoffa, D. Ogle, R. Bailis, and K. Goyer (2006), Design principles for wood burning cook stoves, EPA-402-K-05-004, Aprovecho Research Center.

Budyko, M. I. (1969), The effect of solar radiation variations on the climate of the Earth, *Tellus*, *21* (5), 611-619.

Bueno, P. A., D. K. Havey, G. W. Mulholland, J. T. Hodges, K. A. Gillis, R. R. Dickerson, and M. R. Zachariah (2011), Photoacoustic measurements of amplification of the absorption cross section for coated soot aerosols, *Aerosol Sci. Technol.*, *45*, 1217-1230, doi: 10.1080/02786826.2011.587477.

Cabada, J. C., S. Rees, S. Takahama, A. Khlystov, S. N. Pandis, C. I. Davidson, and A. L. Robinson (2004), Mass size distributions and size resolved chemical composition of fine particulate matter at the Pittsburgh supersite, *Atmos. Environ.*, *38* (20), 3127-3141, doi: 10.1016/j.atmosenv.2004.03.004.

Cachier, H., and M. H. Pertuisot (1994), Particulate carbon in Arctic ice, *Analusis*, *22* (7), M34-M37.

Cao, J. J., F. Wu, J. C. Chow, S. C. Lee, Y. Li, S. W. Chen, Z. S. An, K. K. Fung, J. G. Watson, C. S. Zhu, and S. X. Liu (2005), Characterization and source apportionment of atmospheric organic and elemental carbon during fall and winter of 2003 in Xi'an, China, *Atmos. Chem. Phys.*, *5*, 3127-3137.

Cao, G. L., X. Y. Zhang, and F. C. Zheng (2006), Inventory of black carbon and organic carbon emissions from China, *Atmos. Environ.*, *40* (34), 6516-6527, doi: 10.1016/j.atmosenv.2006.05.070.

Cao, J. J., S. C. Lee, J. C. Chow, J. G. Watson, K. F. Ho, R. J. Zhang, Z. D. Jin, Z. X. Shen, G. C. Chen, Y. M. Kang, S. C. Zou, L. Z. Zhang, S. H. Qi, M. H. Dai, Y. Cheng, and K. Hu (2007), Spatial and seasonal distributions of carbonaceous aerosols over China, *J. Geophys. Res.*, *112* (D22s11), doi: 10.1029/2006JD008205.

Cappa, C. D., D. A. Lack, J. B. Burkholder, and A. R. Ravishankara (2008), Bias in filter-based aerosol light absorption measurements due to organic aerosol loading: Evidence from laboratory measurements, *Aerosol Sci. Technol.*, *42* (12), 1022-1032, doi: 10.1080/02786820802389285.

CARB (2009), Technical Support Document: Proposed Regulation for In-use On-road Diesel Vehicles, 303, Table XIII-301 pg. 175 pp., California Air Resources Board, Sacramento, CA.

Carmichael, G. R., Y. Tang, G. Kurata, I. Uno, D. G. Streets, N. Thongboonchoo, J.-H. Woo, S. Guttikunda, A. White, T. Wang, D. R. Blake, E. Atlas, A. Fried, B. Potter, M. A. Avery, G. W. Sachse, S. T. Sandholm, Y. Kondo, R. W. Talbot, A. Bandy, D. Thorton, and A. D. Clarke (2003), Evaluating regional emission estimates using the TRACE-P observations, *J. Geophys. Res.*, *108* (D21), 8810, doi: 10.1029/2002JD003116.

Castelvecchi, D. (2009), Subcontinental smut: Is soot the culprit behind melting himalayan glaciers?, *Sci. Amer.*, *December 15*, http://www.scientificamerican.com/article.cfm?id=subcontinental-smut-himalayas.

Cess, R. D., G. L. Potter, S. J. Ghan, and W. L. Gates (1985), The climatic effects of large injections of atmospheric smoke and dust - a study of climate feedback mechanisms with one-dimensional and 3-dimensional climate models, *J. Geophys. Res.*, *90* (D7), 2937-2950.

Chan, A. W. H., K. E. Kautzman, P. S. Chhabra, J. D. Surratt, M. N. Chan, J. D. Crounse, A. Kurten, P. O. Wennberg, R. C. Flagan, and J. H. Seinfeld (2009), Secondary organic aerosol formation from photooxidation of naphthalene and alkylnaphthalenes: implications for oxidation of intermediate volatility organic compounds (IVOCs), *Atmos. Chem. Phys.*, *9*, 3049-3060, doi: 10.5194/acp-9-3049-2009.

Chand, D., R. Wood, T. L. Anderson, S. K. Satheesh, and R. J. Charlson (2009), Satellite-derived direct radiative effect of aerosols dependent on cloud cover, *Nature Geosci.*, *2* (3), 181-184, doi: 10.1038/ngeo437.

Charalampopoulos, T. T., H. Chang, and B. Stagg (1989), The effects of temperature and composition on the complex refractive-index of flame soot, *Fuel*, *68* (9), 1173-1179.

Chen, T., W. B. Rossow, and Y. C. Zhang (2000), Radiative effects of cloud-type variations, *J. Climate*, *13*, 264-286, doi: 10.1175/1520-0442(2000)013<0264:REOCTV>2.0.CO;2.

Chen, W. T., R. A. Kahn, D. Nelson, K. Yau, and J. H. Seinfeld (2008), Sensitivity of multiangle imaging to the optical and microphysical properties of biomass burning aerosols, *J. Geophys. Res.*, *113* (D10), 203, doi: 10.1029/2007JD009414.

Chen, W. T., Y. H. Lee, P. J. Adams, A. Nenes, and J. H. Seinfeld (2010a), Will black carbon mitigation dampen aerosol indirect forcing?, *Geophys. Res. Lett.*, *37* (L09801), doi: 10.1029/2010GL042886.

Chen, L. W. A., J. G. Watson, J. C. Chow, D. W. DuBois, and L. Herschberger (2010b), Chemical mass balance source apportionment for combined PM2.5 measurements from U. S. non-urban and urban long-term networks, *Atmos. Environ.*, *44* (38), 4908-4918, doi: 10.1016/j.atmosenv.2010.08.030.

Chevallier, F., M. Fisher, P. Peylin, S. Serrar, P. Bousquet, F. M. Breon, A. Chedin, and P. Ciais (2005), Inferring CO_2 sources and sinks from satellite observations: Method and application to TOVS data, *J. Geophys. Res.*, *110* (D24), 309, doi: 10.1029/2005JD006390.

Chevallier, F., A. Fortems, P. Bousquet, I. Pison, S. Szopa, M. Devaux, and D. A. Hauglustaine (2009), African CO emissions between years 2000 and 2006 as estimated from MOPITT observations, *Biogeosciences*, *6* (1), 103-111.

Chin, M., P. Ginoux, S. Kinne, O. Torres, B. N. Holben, B. N. Duncan, R. V. Martin, J. A. Logan, A. Higurashi, and T. Nakajima (2002), Tropospheric aerosol optical thickness from the GOCART model and comparisons with satellite and Sun photometer measurements, *J. Atmos. Sci.*, *59* (3), 461-483.

Chin, M., T. Diehl, O. Dubovik, T. F. Eck, B. N. Holben, A. Sinyuk, and D. G. Streets (2009), Light absorption by pollution, dust, and biomass burning aerosols: A global model study and evaluation with AERONET measurements, *Ann. Geophys.*, *27* (9), 3439-3464, doi: 10.5194/angeo-27-3439-2009.

Chow, J. C., J. G. Watson, L. C. Pritchett, W. R. Pierson, C. A. Frazier, and R. G. Purcell (1993), The DRI thermal/optical reflectance carbon analysis system: Description, evaluation and applications in U.S. air quality studies, *Atmos. Environ.*, *27A* (8), 1185-1201, doi: 10.1016/0960-1686(93)90245-T.

Chow, J. C., J. G. Watson, D. Crow, D. H. Lowenthal, and T. Merrifield (2001), Comparison of IMPROVE and NIOSH Carbon Measurements, *Aerosol Sci. Technol.*, *34* (1), 23-34.

Chow, J. C., and J. G. Watson (2002), Review of PM2.5 and PM10 apportionment for fossil fuel combustion and other sources by the chemical mass balance receptor model, *Energy & Fuels*, *16* (2), 222-260, doi: 10.1021/Ef0101715.

Chow, J. C., J. G. Watson, L.-W. A. Chen, W. P. Arnott, and H. Moosmüller (2004), Equivalence of elemental carbon by thermal/optical reflectance and transmittance with different temperature protocols, *Environ. Sci. Technol.*, *38*, 4414-4422.

Chowdhury, Z., M. Zheng, J. J. Schauer, R. J. Sheesley, L. G. Salmon, G. R. Cass, and A. G. Russell (2007), Speciation of ambient fine organic carbon particles and source apportionment of PM2.5 in Indian cities, *J. Geophys. Res.*, *112* (D15), doi: D15303, doi:10.1029/2007JD008386.

Christian, T. J., R. J. Yokelson, B. Cardenas, L. T. Molina, G. Engling, and S. C. Hsu (2010), Trace gas and particle emissions from domestic and industrial biofuel use and garbage burning in central Mexico, *Atmos. Chem. Phys.*, *10* (2), 565-584.

Chuang, C. C., J. E. Penner, J. M. Prospero, K. E. Grant, G. H. Rau, and K. Kawamoto (2002), Cloud susceptibility and the first aerosol indirect forcing: Sensitivity to black carbon and aerosol concentrations, *J. Geophys. Res.*, *107* (D21), 4564, doi: 10.1029/2000JD000215.

Chung, C. E., V. Ramanathan, and J. T. Kiehl (2002), Effects of the south Asian absorbing haze on the northeast monsoon and surface-air heat exchange, *J. Climate*, *15* (17), 2462-2476.

Chung, S. H., and J. H. Seinfeld (2002), Global distribution and climate forcing of carbonaceous aerosols, *J. Geophys. Res.*, *107*, doi: 10.1029/2001JD001397.

Chung, C. E., V. Ramanathan, D. Kim, and I. A. Podgorny (2005), Global anthropogenic aerosol direct forcing derived from satellite and ground-based observations, *J. Geophys. Res.*, *110* (D24), 207, doi: 10.1029/2005JD006356.

Chung, S. H., and J. H. Seinfeld (2005), Climate response of direct radiative forcing of anthropogenic black carbon, *J. Geophys. Res.*, *110* (D11), 102, doi: 10.1029/2004JD005441.

Chung, C. E., and V. Ramanathan (2006), Weakening of North Indian SST gradients and the monsoon rainfall in India and the Sahel, *J. Climate*, *19* (10), 2036-2045.

Chylek, P., V. Ramaswamy, A. Ashkin, and J. M. Dziedzic (1983a), Simultaneous determination of refractive-index and size of spherical dielectric particles from light-scattering data, *Appl. Opt.*, *22* (15), 2302-2307, doi: 10.1364/AO.22.002302.

Chylek, P., V. Ramaswamy, and V. Srivastava (1983b), Albedo of soot-contaminated snow, *J. Geophys. Res.*, *88* (C15), 10837-10843, doi: 10.1029/JC088iC15p10837.

Chylek, P., V. Ramaswamy, and R. J. Cheng (1984), Effect of Graphitic Carbon on the Albedo of Clouds, *J. Atmos. Sci.*, *41* (21), 3076-3084, doi: 10.1175/1520-0469(1984)041<3076:EOGCOT>2.0.CO;2.

Chylek, P., V. Srivastava, L. Cahenzli, R. G. Pinnick, R. L. Dod, T. Novakov, T. L. Cook, and B. D. Hinds (1987), Aerosol and graphitic carbon content of snow, *Journal of Geophysical Research*, *92* (D8), 9801-9809, doi: 10.1029/JD092iD08p0980.

Chylek, P., B. Johnson, P. A. Damiano, K. C. Taylor, and P. Clement (1995), Biomass burning record and black carbon in the GISP2 Ice Core, *Geophys. Res. Lett.*, *22* (2), 89-92, doi: 10.1029/94GL02841.

Chylek, P., G. B. Lesins, G. Videen, J. G. D. Wong, R. G. Pinnick, D. Ngo, and J. D. Klett (1996), Black carbon and absorption of solar radiation by clouds, *J. Geophys. Res.*, *101* (D18), 23365-23371, doi: 10.1029/96JD01901.

Chylek, P., M. K. Dubey, U. Lohmann, V. Ramanathan, Y. J. Kaufman, G. Lesins, J. Hudson, G. Altmann, and S. Olsen (2006), Aerosol indirect effect over the Indian Ocean, *Geophys. Res. Lett.*, *33* (L06806), doi: 10.1029/2005GL025397.

Clarke, A. D., and K. J. Noone (1985), Soot in the Arctic snowpack - A cause for perturbations in radiative transfer, *Atmos. Environ.*, *19* (12), 2045-2053, doi: 10.1016/0004-6981(85)90113-1.

Clarke, A. D., Y. Shinozuka, V. N. Kapustin, S. Howell, B. Huebert, S. Doherty, T. Anderson, D. Covert, J. Anderson, X. Hua, K. G. Moore II, C. McNaughton, G. Carmichael, and R. Weber (2004), Size distributions and mixtures of dust and black carbon aerosol in Asian outflow: Physiochemistry and optical properties, *J. Geophys. Res.*, *109* (D15S09), doi: 10.1029/2003JD004378.

Clarke, A., C. McNaughton, V. Kapustin, Y. Shinozuka, S. Howell, J. Dibb, J. Zhou, B. Anderson, V. Brekhovskikh, H. Turner, and M. Pinkerton (2007), Biomass burning and pollution aerosol over North America: Organic components and their influence on spectral optical properties and humidification response, *J. Geophys. Res.*, *112* (D12s18), doi: 10.1029/2006JD007777.

Clarke, A., and V. Kapustin (2010), Hemispheric aerosol vertical profiles: Anthropogenic impacts on optical depth and cloud nuclei, *Science*, *329* (5998), 1488-1492, doi: 10.1126/science.1188838.

Cofala, J., M. Amann, Z. Klimont, K. Kupiainen, and L. Hoglund-Isaksson (2007), Scenarios of global anthropogenic emissions of air pollutants and methane until 2030, *Atmos. Environ.*, *41* (38), 8486-8499, doi: 10.1016/j.atmosenv.2007.07.010.

Collins, W. D., P. J. Rasch, B. A. Boville, J. J. Hack, J. R. McCaa, D. L. Williamson, B. P. Briegleb, C. M. Bitz, S.-J. Lin, and M. Zhang (2006), The formulation and atmospheric simulation of the Community Atmosphere Model Version 3 (CAM3), *J. Climate*, *19*, 2144-2161, doi: 10.1175/JCL13760.1.

Collins, W. J., R. G. Derwent, C. E. Johnson, and D. S. Stevenson (2002), The oxidation of organic compounds in the troposphere and their global warming potentials *Climatic Change*, *52* (4), 453-479, doi: 10.1023/A:1014221225434.

Collins, W. J., S. Sitch, and O. Boucher (2010), How vegetation impacts affect climate metrics for ozone precursors, *J. Geophys. Res.*, *115* (D23308), doi: 10.1029/2010JD014187.

Comiso, J. C., C. L. Parkinson, R. Gersten, and L. Stock (2008), Accelerated decline in the Arctic sea ice cover, *Geophys. Res. Lett.*, *35* (1), 703, doi: 10.1029/2007GL031972.

Conant, W. C., A. A. Nenes, and J. H. Seinfeld (2002), Black carbon radiative heating effects on cloud microphysics and implications for the aerosol indirect effect - 1. Extended Kohler theory, *J. Geophys. Res.*, *107*, 4604, doi: 10.1029/2002jd002094.

Conway, H., A. Gades, and C. F. Raymond (1996), Albedo of dirty snow during conditions of melt, *Water Resour. Res.*, *32* (6), 1713-1718.

Cook, J., and E. J. Highwood (2004), Climate response to tropospheric absorbing aerosols in an intermediate general-circulation model, *Quart J. Roy. Meteor. Soc.*, *130* (596), 175-191, doi: 10.1256/qj.03.64.

Cooke, W. F., and J. J. N. Wilson (1996), A global black carbon aerosol model, *J. Geophys. Res.*, *101* (D14), 19395-19409.

Cooke, W. F., C. Liousse, H. Cachier, and J. Feichter (1999), Construction of a 1° x 1° fossil fuel emission data set for carbonaceous aerosol and implementation and radiative impact in the ECHAM4 model, *J. Geophys. Res.*, *104* (D18), 22137-22162.

Cooke, W. F., V. Ramaswamy, and P. Kasibhatla (2002), A general circulation model study of the global carbonaceous aerosol distribution, *J. Geophys. Res.*, *107* (D16), doi: 10.1029/2001JD001274.

Cooke, R. M., A. M. Wilson, J. T. Tuomisto, O. Morales, M. Tainio, and J. S. Evans (2007), A probabilistic characterization of the relationship between fine particulate matter and mortality: Elicitation of European experts, *Environ. Sci. Technol.*, *41* (18), 6598-6605, doi: 10.1021/es0714078.

COP-15 (2009), COP-15, Copenhagen Accord, Report of the Conference of the Parties on its fifteenth session, held in Copenhagen from 7 to 19 December 2009. Addendum. Part Two: Action taken by the Conference of the Parties at its fifteenth session, United Nations Framework Convention on Climate Change, http://unfccc.int/meetings/copenhagen_dec_2009/items/5262.php2009, 2009.

Corbett, J. J., D. A. Lack, J. J. Winebrake, S. Harder, J. A. Silberman, and M. Gold (2010), Arctic shipping emissions inventories and future scenarios, *Atmos. Chem. Phys. Discuss*, *10*, 10271-10311, doi: 10.5194/acpd-10-10271-2010.

Corrigan, C. E., G. C. Roberts, M. V. Ramana, D. Kim, and V. Ramanathan (2008), Capturing vertical profiles of aerosols and black carbon over the Indian Ocean using autonomous unmanned aerial vehicles, *Atmos. Chem. Phys.*, *8* (3), 737-747.

Cozic, J., S. Mertes, B. Verheggen, D. J. Cziczo, S. J. Gallavardin, S. Walter, U. Baltensperger, and E. Weingartner (2008), Black carbon enrichment in atmospheric ice particle residuals observed in lower tropospheric mixed phase clouds, *J. Geophys. Res.*, *113* (D15), 209, doi: 10.1029/2007JD009266.

Crawford, I., O. Mohler, M. Schnaiter, H. Saathoff, D. Liu, G. McMeeking, C. Linke, M. Flynn, K. N. Bower, P. J. Connolly, M. W. Gallagher, and H. Coe (2011), Studies of propane flame soot acting as heterogeneous ice nuclei in conjuntion with single particle soot photometer measurements., *Atmos. Chem. Phys.*, *11* (18), 9549-9561, doi: 10.5194/acp-11-9549-2011.

Croft, B., U. Lohmann, and K. von Salzen (2005), Black carbon ageing in the Canadian Centre for Climate modeling and analysis atmospheric general circulation model, *Atmos. Chem. Phys.*, *5*, 1931-1949, doi: 10.5194/acp-5-1931-2005.

Croft, B., U. Lohmann, R. V. Martin, P. Stier, S. Wurzler, J. Feichter, C. Hoose, U. Heikkila, A. van Donkelaar, and S. Ferrachat (2010), Influences of in-cloud aerosol scavenging parameterizations on aerosol concentrations and wet deposition in ECHAM5-HAM, *Atmos. Chem. Phys.*, *10* (4), 1511-1543, doi: 10.5194/acp-10-1511-2010.

Crook, J. A., P. M. Forster, and N. Stuber (2011), Spatial patterns of modeled climate feedback and contributions to temperature response and polar amplification, *J. Climate*, *24*, 3575-3592, doi: 10.1175/2011JCLI3863.1

Cross, E. S., T. B. Onasch, A. Ahern, W. Wrobel, J. G. Slowik, J. Olfert, D. A. Lack, P. Massoli, C. D. Cappa, J. P. Schwarz, J. R. Spackman, D. W. Fahey, A. Sedlacek, A. Trimborn, J. T. Jayne, A. Freedman, L. R. Williams, N. L. Ng, C. Mazzolen, M. Dubey, B. Brem, G. Kok, R. Subramanian, S. Freitag, A. Clarke, D. Thornhill, L. C. Marr, C. E. Kolb, D. R. Worsnop, and P. Davidovits (2010), Soot Particle Studies—Instrument Inter-Comparison—Project Overview, *Aerosol Sci. Technol.*, *44* (8), 592-611, doi: 10.1080/02786826.2010.482113.

Cziczo, D. J., P. J. DeMott, S. D. Brooks, A. J. Prenni, D. S. Thomson, D. Baumgardner, J. C. Wilson, S. M. Kreidenweis, and D. M. Murphy (2004a), Observations of organic species and atmospheric ice formation, *Geophys. Res. Lett.*, *31* (12), 116, doi: 10.1029/2004GL019822.

Cziczo, D. J., D. M. Murphy, P. K. Hudson, and D. S. Thomson (2004b), Single particle measurements of the chemical composition of cirrus ice residue during CRYSTAL-FACE, *J. Geophys. Res.*, *109* (D4), 201, doi: 10.1029/2003JD004032.

Cziczo, D. J., O. Stetzer, A. Worringen, M. Ebert, S. Weinbruch, M. Kamphus, S. J. Gallavardin, J. Curtius, S. Borrmann, K. D. Froyd, S. Mertes, O. Mohler, and U. Lohmann (2009), Inadvertent climate modification due to anthropogenic lead, *Nature Geosci.*, *2* (5), 333-336, doi: 10.1038/ngeo499.

Darby, D. A., L. H. Burckle, and D. L. Clark (1974), Airborn dust on Arctic pack ice, its composition and fallout rate, *Earth Planet Sc Lett*, *24* (2), 166-172.

De Angelis, M., J. P. Steffensen, M. Legrand, H. Clausen, and C. Hammer (1997), Primary aerosol (sea salt and soil dust) deposited in Greenland ice during the last climatic cycle: Comparison with east Antarctic records, *J. Geophys. Res.*, *102* (C12), 26681-26698.

de Gouw, J. A., and J. L. Jimenez (2009), Organic aerosols in the Earth's atmosphere, *Environ. Sci. Technol.*, *43*, 7614-7618, doi: 10.1021/es9006004.

DeMott, P. J. (1990), An exploratory-study of ice nucleation by soot aerosols, *J. Appl. Meteorol.*, *29* (10), 1072-1079.

DeMott, P. J., Y. Chen, S. M. Kreidenweis, D. C. Rogers, and D. E. Sherman (1999), Ice formation by black carbon particles, *Geophys. Res. Lett.*, *26*, 2429-2432, doi: 10.1029/1999GL900580.

DeMott, P. J., D. J. Cziczo, A. J. Prenni, D. M. Murphy, S. M. Kreidenweis, D. S. Thomson, R. Borys, and D. C. Rogers (2003), Measurements of the concentration and composition of nuclei for cirrus formation, *P. Natl. Acad. Sci. USA*, *100* (25), 14655-14660, doi: 10.1073/pnas.2532677100.

DeMott, P. J., M. D. Petters, A. J. Prenni, C. M. Carrico, S. M. Kreidenweis, J. L. Collett, and H. Moosmuller (2009a), Ice nucleation behavior of biomass combustion particles at cirrus temperatures, *J. Geophys. Res.*, *114* (D16), 205, doi: 10.1029/2009JD012036.

DeMott, P. J., K. Sassen, M. R. Poellot, D. Baumgardner, D. C. Rogers, S. D. Brooks, A. J. Prenni, and S. M. Kreidenweis (2009b), African dust aerosols as atmospheric ice nuclei, *Geophys. Res. Lett.*, *36* (L07), 808, doi: 10.1029/2009GL037639.

DeMott, P. J., A. J. Prenni, Z. Liu, S. M. Kreidenweis, M. D. Petters, C. H. Twohy, M. S. Richardson, T. Eidhammer, and D. C. Rogers (2010), Predicting global atmospheric ice nuclei distributions and their impact on climate, *P. Natl. Acad. Sci. USA*, *107*, 11,217-211,222, doi: 10.1073/pnas.0910818107.

Denman, K. L., G. Brasseur, A. Chidthaisong, P. Ciais, P. M. Cox, R. E. Dickinson, D. Hauglustaine, C. Heinze, E. Holland, D. Jacob, U. Lohmann, S. Ramachandran, P. L. da Silva Dias, S. C. Wofsy, and X. Zhang (2007), Couplings between changes in the climate system and biogeochemistry, in *Climate change 2007: The physical science basis*, edited by S. Solomon, D. Qin, M. Manning, Z. Chen, M. Marquis, K. B. Averyt, M. Tigor and H. L. Miller, 129-234 pp., Cambridge University Press, Cambridge,

UK.

Dentener, F., S. Kinne, T. Bond, O. Boucher, J. Cofala, S. Generoso, P. Ginoux, S. Gong, J. J. Hoelzemann, A. Ito, L. Marelli, J. E. Penner, J.-P. Putaud, C. Textor, M. Schulz, G. R. v. d. Werf, and J. Wilson (2006), Emissions of primary aerosol and precursor gases in the years 2000 and 1750: prescribed data-sets for AeroCom, *Atmos. Chem. Phys.*, *6*, 4321-4344.

Déry, S. J., and R. D. Brown (2007), Recent northern hemisphere snow cover extent trends and implications for the snow-albedo feedback, *Geophys. Res. Lett.*, *34* (22), L22504, doi: 10.1029/2007GL031474.

Deuzé, J. L., F. M. Bréon, C. Devaux, P. Goloub, M. Herman, B. Lafrance, F. Maignan, A. Marchand, F. Nadal, G. Perry, and D. Tanré (2001), Remote sensing of aerosol over land surfaces from POLDER/ADEOS-1 polarized measurements, *J. Geophys. Res.*, *106*, 4913-4926, doi: 10.1029/2000JD900364.

Deville, R. E. L., N. Riemer, and M. West (2011), Weighted Flow Algorithms (WFA) for stochastic particle coagulation, *J. Comput. Phys.*, *230* (23), 8427-8451, doi: 10.1016/j.jcp.2011.07.027.

Dickerson, R. R., M. O. Andreae, T. Campos, O. L. Mayol-Bracero, C. Neusuess, and D. G. Streets (2002), Analysis of black carbon and carbon monoxide observed over the Indian Ocean: Implications for emissions and photochemistry, *J. Geophys. Res.*, *107* (D19), 8017, doi: 10.1029/2001JD000501.

Diehl, K., and S. K. Mitra (1998), A laboratory study of the effects of a kerosene-burner exhaust on ice nucleation and the evaporation rate of ice crystals, *Atmos. Environ.*, *32* (18), 3145-3151.

Diehl, K., M. Simmel, and S. Wurzler (2006), Numerical sensitivity studies on the impact of aerosol properties and drop freezing modes on the glaciation, microphysics, and dynamics of clouds, *J. Geophys. Res.*, *111* (D07), 202, doi: 10.1029/2005JD005884.

Doherty, S. J., P. K. Quinn, A. Jefferson, C. M. Carrico, T. L. Anderson, and D. Hegg (2005), A comparison and summary of aerosol optical properties as observed in situ from aircraft, ship, and land during ACE-Asia, *J. Geophys. Res.*, *110* (D4), 201, doi: 10.1029/2004JD004964.

Doherty, S. J., S. G. Warren, T. C. Grenfell, A. D. Clarke, and R. E. Brandt (2010), Light-absorbing impurities in Arctic snow, *Atmos. Chem. Phys.*, *10* (23), 11647-11680, doi: 10.5194/acp-10-11647-2010.

Donahue, N. M., A. L. Robinson, C. O. Stanier, and S. N. Pandis (2006), Coupled partitioning, dilution, and chemical aging of semivolatile organics, *Environ. Sci. Technol.*, *40* (8), 2635-2643, doi: 10.1021/es052297c.

Dubovik, O., and M. D. King (2000), A flexible inversion algorithm for retrieval of aerosol optical properties from Sun and sky radiance measurements, *J. Geophys. Res.*, *105* (D16), 20673-20696.

Dubovik, O., A. Smirnov, B. N. Holben, M. D. King, Y. J. Kaufman, T. F. Eck, and I. Slutsker (2000), Accuracy assessment of aerosol optical properties retrieved from Aerosol Robotic Network (AERONET) Sun and sky radiance measurements, *J. Geophys. Res.*, *105* (D8), 9791-9806.

Dubovik, O., B. Holben, T. F. Eck, A. Smirnov, Y. J. Kaufman, M. D. King, D. Tanre, and I. Slutsker (2002), Variability of absorption and optical properties of key aerosol types observed in worldwide locations, *J. Atmos. Sci.*, *59* (3), 590-608.

Dubovik, O., T. Lapyonok, Y. J. Kaufman, M. Chin, P. Ginoux, R. A. Kahn, and A. Sinyuk (2008), Retrieving global aerosol sources from satellites using inverse modeling, *Atmos. Chem. Phys.*, *8* (2), 209-250.

Dymarska, M., B. J. Murray, L. M. Sun, M. L. Eastwood, D. A. Knopf, and A. K. Bertram (2006), Deposition ice nucleation on soot at temperatures relevant for the lower troposphere, *J. Geophys. Res.*, *111* (D04), 204, doi: 10.1029/2005JD006627.

Easter, R. C., S. J. Ghan, Y. Zhang, R. D. Saylor, E. G. Chapman, N. S. Laulainen, H. Abdul-Razzak, L. R. Leung, X. D. Bian, and R. A. Zaveri (2004), MIRAGE: Model description and evaluation of aerosols and trace gases, *J. Geophys. Res.*, *109* (D20), 210, doi: 10.1029/2004JD004571.

Eck, T. F., B. N. Holben, D. E. Ward, M. M. Mukelabai, O. Dubovik, A. Smirnov, J. S. Schafer, N. C. Hsu, S. J. Piketh, A. Queface, J. Le Roux, R. J. Swap, and I. Slutsker (2003), Variability of biomass burning aerosol optical characteristics in southern Africa during the SAFARI 2000 dry season campaign and a comparison of single scattering albedo estimates from radiometric measurements, *J. Geophys. Res.*, *108* (D13), 8477, doi: 10.1029/2002JD002321.

Ekman, A. M. L., A. Engstrom, and C. Wang (2007), The effect of aerosol composition and concentration on the development and anvil properties of a continental deep convective cloud, *Quart J. Roy. Meteor. Soc.*, *133* (627), 1439-1452, doi: 10.1002/qj.108.

Eleftheriadis, K., S. Vratolis, and S. Nyeki (2009), Aerosol black carbon in the European Arctic: Measurements at Zeppelin station, Ny-Ålesund, Svalbard from 1998-2007, *Geophys. Res. Lett.*, *36* (2), 809, doi: DOI: 10.1029/2008GL035741.

Elvidge, C. D., K. Baugh, B. Tuttle, D. Ziskin, T. Ghoshet, M. Zhizhin, and D. Pack (2009), Improving satellite data estimation of gas flaring volumes: Year two final report to the GGFR.

Engelbrecht, J. P., L. Swanepoel, J. C. Chow, J. G. Watson, and R. T. Egami (2002), The comparison of source contributions from residential coal and low-smoke fuels, using CMB modeling, *Environ. Sci. Technol.*, *5* (2), 157-167.

EPA (1992), Particulate matter best available control measure technical guidance documents for prescribed burning and fugitive dust, U. S. Environmental Protection Agency, Research Triangle Park, NC.

EPA (1996), Compilation of Air Pollution Emission Factors, Vol. 1, Stationary Point and Area Sources, AP42, Fifth Edition, U.S. Environmental Protection Agency, Washington, DC.

EPA (2002), A Comprehensive Analysis of Biodiesel Impacts on Exhaust Emissions, U. S. Environmental Protection Agency, Draft Technical Report, Ann Arbor, MI.

EPA (2005), AirControlNET Version 4.1 Documentation Report, Prepared by E.H. Pechan & Associates Inc., Springfield, VA.

EPA (2008), Emission Factor Documentation for AP-42: Section 12.2, Coke Production. Finalized by RTI International for U.S. Environmental Protection Agency., Research Triangle Park, NC.

EPA (2009a), Integrated Science Assessment for Particulate Matter, U. S. Environmental Protection Agency, Washington, DC.

EPA (2009b), Available from http://www.epa.gov/ne/eco/diesel/idling.html.

EPA (2012), Report to Congress on Black Carbon, US Environmental Protection Agency, Washington, DC, in preparation.

Essery, R. (1997), Modelling fluxes of momentum, sensible heat and latent heat over heterogeneous snow cover, *Quart J. Roy. Meteor. Soc.*, *123* (543), 1867-1883.

Etyemezian, V., M. Tesfaye, A. Yimer, J. C. Chow, D. Mesfin, T. Nega, G. Nikolich, J. G. Watson, and M. Wondmagegn (2005), Results from a pilot-scale air quality study in Addis Ababa, Ethiopia, *Atmos. Environ.*, *39* (40), 7849-7860, doi: 10.1016/j.atmosenv.2005.08.033.

Fan, J. W., R. Y. Zhang, W. K. Tao, and K. I. Mohr (2008), Effects of aerosol optical properties on deep convective clouds and radiative forcing, *J. Geophys. Res.*, *113* (D08), 209, doi: 10.1029/2007JD009257.

Fann, N., C. Fulcher, and B. Hubbell (2009), The influence of

location, source, and emission type in estimates of the human health benefits of reducing a ton of air pollution, *Air Quality, Atmosphere & Health*, *2* (3), doi: 10.1007/s11869-009-0044-0.

Federal Law Gazette (2010, First Regulation implementing the Federal Pollution Control Act, Ordinance on small and medium-sized combustion plants - 1.BimSchV, 26 January 2010, Federal Law Gazette, Part I, No. 4, Bonn, 2010.

Feingold, G., H. L. Jiang, and J. Y. Harrington (2005), On smoke suppression of clouds in Amazonia, *Geophys. Res. Lett.*, *32* (2), 804, doi: 10.1029/2004GL021369.

Ferek, R. J., D. A. Hegg, P. V. Hobbs, P. Durkee, and K. Nielsen (1998), Measurements of ship-induced tracks in clouds off the Washington coast, *J. Geophys. Res.*, *103* (D18), 23199-23206.

Fernandes, S. D., N. M. Trautmann, and D. G. Streets (2007), Global biofuel use, 1850-2000, *Global Biogeochem. Cycles*, *21* (2), doi: 10.1029/2006GB002836.

Fetterer, F., and N. Untersteiner (1998), Observations of melt ponds on Arctic sea ice, *J. Geophys. Res.*, *103* (C11), 24821-24835, doi: 10.1029/98JC02034.

Fialho, P., M. C. Freitas, F. Barata, B. Vieira, A. D. A. Hansen, and R. E. Honrath (2006), The Aethalometer calibration and determination of iron concentration in dust aerosols, *J. Aerosol. Sci.*, *37* (11), 1497-1506, doi: 10.1016/j.jaerosci.2006.03.002.

Flanner, M. G., and C. S. Zender (2006), Linking snowpack microphysics and albedo evolution, *J. Geophys. Res.*, *111* (D12), 208, doi: 10.1029/2005JD006834.

Flanner, M. G., C. S. Zender, J. T. Randerson, and P. J. Rasch (2007), Present-day climate forcing and response from black carbon in snow, *J. Geophys. Res.*, *112* (D11), 202, doi: 10.1029/2006JD008003.

Flanner, M. G., C. S. Zender, P. G. Hess, N. M. Mahowald, T. H. Painter, V. Ramanathan, and P. J. Rasch (2009), Springtime warming and reduced snow cover from carbonaceous particles, *Atmos. Chem. Phys.*, *9* (7), 2481-2497.

Flanner, M. G., K. M. Shell, M. Barlage, D. K. Perovich, and M. A. Tschudi (2011), Radiative forcing and albedo feedback from the Northern Hemisphere cryosphere between 1979 and 2008, *Nature Geosci.*, *4*, 151-155, doi: 10.1038/ngeo1062.

Fletcher, J. O. (1968), The influence of the Arctic pack ice on climate, *Meteor. Monogr.*, *8* (30), 93-99.

Fornea, A. P., S. D. Brooks, J. B. Dooley, and A. Saha (2009), Heterogeneous freezing of ice on atmospheric aerosols containing ash, soot, and soil, *J. Geophys. Res.*, *114*, doi: D13201, 10.1029/2009jd011958.

Forsström, S., J. Ström, C. A. Pedersen, E. Isaksson, and S. Gerland (2009), Elemental carbon distribution in Svalbard snow, *J. Geophys. Res.*, *114* (D19), 112, doi: 10.1029/2008JD011480.

Forster, P. M., M. Blackburn, R. Glover, and K. P. Shine (2000), An examination of climate sensitivity for idealised climate change experiments in an intermediate general circulation model, *Climate Dyn.*, *16* (10-11), 833-849.

Forster, P., V. Ramaswamy, P. Artaxo, T. Berntsen, R. Betts, D. W. Fahey, J. Haywood, J. Lean, D. C. Lowe, G. Myhre, J. Nganga, R. Prinn, G. Raga, M. Schulz , and R. Van Dorland (2007), Changes in atmospheric constituents and in radiative forcing, in *Climate Change 2007: The Physical Science Basis. Contribution of Working Group I to the Fourth Assessment Report of the Intergovernmental Panel on Climate Change* edited by S. Solomon, D. Qin, M. Manning, Z. Chen, M. Marquis, K. B. Averyt, M. Tignor and H. L. Miller Cambridge University Press, New York.

Freitas, S. R., K. M. Longo, M. Diasb, P. L. S. Diasb, R. Chatfield, E. Prins, P. Artaxo, G. A. Grell, and F. S. Recuero (2005), Monitoring the transport of biomass burning emissions in South America, *Environ. Fluid Mech.*, *5* (1-2), 135-167.

Friedlander, S. K. (1973), Chemical element balances and identification of air-pollution sources, *Environ. Sci. Technol.*, *7* (3), 235-240.

Friedman, B., G. Kulkarni, J. Beránek, A. Zelenyuk, J. A. Thornton, and D. J. Cziczo (2011), Ice nucleation and droplet formation by bare and coated soot particles, *J. Geophys. Res.*, *116* (D17203), doi: 10.1029/2011JD015999.

Froyd, K. D., D. M. Murphy, T. J. Sanford, D. S. Thomson, J. C. Wilson, L. Pfister, and L. Lait (2009), Aerosol composition of the tropical upper troposphere, *Atmos. Chem. Phys.*, *9* (13), 4363-4385.

Fuglestvedt, J. S., T. Berntsen, O. Godal, and T. Skodvin (2000), Climate implications of GWP based reductions in greenhouse gas emissions, *Geophys. Res. Lett.*, *27*, 409-412.

Fuglestvedt, J. S., T. K. Berntsen, O. Godal, R. Sausen, K. P. Shine, and T. Skodvin (2003), Metrics of climate change: assessing radiative forcing and emission indices, *Climatic Change*, *58* (3), 267-331.

Fuglestvedt, J. S., T. Berntsen, G. Myhre, K. Rypdal, and R. B. Skeie (2008), Climate forcing from the Transport Sectors, *P. Natl. Acad. Sci. USA*, *105 (2)*, 454-458.

Fuglestvedt, J. S., K. P. Shine, T. Berntsen, J. Cook, D. S. Lee, A. Stenke, R. B. Skeie, G. J. M. Velders, and I. A. Waitz (2010), Transport impacts on atmosphere and climate: Metrics, *Atmos. Environ.*, *44* (37), 4648-4677, doi: 10.1016/j.atmosenv.2009.04.044.

Fuller, K. A. (1995), Scattering and absorption cross sections of compounded spheres. III. Spheres containing arbitrarily located spherical inhomogeneities, *J. Opt. Soc. Am. A*, *12* (5), 893-904, doi: 10.1364/JOSA.A.12.000893.

Fuller, K. A., W. C. Malm, and S. M. Kreidenweis (1999), Effects of mixing on extinction by carbonaceous particles, *J. Geophys. Res.*, *104* (D13), 15941-15954.

Garrett, T. J., C. Zhao, and P. C. Novelli (2010), Assessing the relative contributions of transport efficiency and scavenging to seasonal variability in Arctic aerosol, *Tellus B*, *62* (3), 190-196, doi: 10.1111/j.1600-0889.2010.00453.x.

Gayet, J. F., F. Auriol, A. Minikin, J. Strom, M. Seifert, R. Krejci, A. Petzold, G. Febvre, and U. Schumann (2002), Quantitative measurement of the microphysical and optical properties of cirrus clouds with four different in situ probes: Evidence of small ice crystals, *Geophys. Res. Lett.*, *29* (24), 2230, doi: 10.1029/2001GL014342.

Ghan, S. J., G. Guzman, and H. Abdul-Razzak (1998), Competition between sea salt and sulfate particles as cloud condensation nuclei, *J. Atmos. Sci.*, *55* (22), 3340-3347, doi: 10.1175/1520-0469(19980055<3340:CBSSAS>2.0.CO;2.

Ghan, S. J., X. Liu, R. C. Easter, R. Zaveri, P. J. Rasch, and J.-H. Yoon (2012), Toward a minimal representation of aerosol direct, semi-direct and indirect effects: Comparative decomposition of aerosol direct, semi-direct and indirect effects, *J. Climate*, *in press*.

Giglio, L., T. Loboda, D. P. Roy, B. Quayle, and C. O. Justice (2009), An active-fire based burned area mapping algorithm for the MODIS sensor, *Remote Sens. Environ.*, *113* (2), 408-420, doi: 10.1016/j.rse.2008.10.006.

Gildemeister, A. E., P. K. Hopke, and E. Kim (2007), Sources of fine urban particulate matter in Detroit, MI, *Chemosphere*, *69* (7), 1064-1074, doi: 10.1016/j.chemosphere.2007.04.027.

Girard, E., J. P. Blanchet, and Y. Dubois (2005), Effects of Arctic sulphuric acid aerosols on wintertime low-level atmospheric ice crystals, humidity and temperature at Alert, Nunavut, *Atmos. Res.*, *73* (1-2), 131-148, doi: 10.1016/j.atmosres.2004.08.002.

Gloersen, P., W. J. Campbell, D. J. Cavalieri, J. C. Comiso, and C. L. Parkinson (1992), Arctic and Antarctic sea-ice, 1978-1987:

Satellite passive-microwave observations and analysis *NASA Publication*, SP-511, 290 pp., NASA, Washington, DC.

Goldammer, J. G., and B.Seibert (1990), in *Fire in the tropical biota. Ecosystem processes and global challenges* edited by J. G. Goldammer, 11-31 pp., Springer-Verlag, Berlin-Heidelberg-New York.

Gong, S. L., T. L. Zhao, S. Sharma, D. Toom-Sauntry, D. Lavoue, X. B. Zhang, R. Leaitch, and L. A. Barrie (2010), Identification of trends and inter-annual variability of sulphate and black carbon in the Canadian High Arctic: 1981 to 2007, *J. Geophys. Res.*, *115*, D07305, doi: 10.1029/2009JD012943.

Gotschi, T., M. E. Hazenkamp-Von Arxb, J. Heinrich, R. Bono, P. Burney, B. Forsberg, D. Jarvis, J. Maldonado, D. Norback, W. B. Stern, J. Sunyer, K. Toren, G. Verlato, S. Villani, and N. Kunzli (2005), Elemental composition and reflectance of ambient fine particles at 21 European locations, *Atmos. Environ.*, *39* (32), 5947-5958, doi: 10.1016/j.atmonsenv.2005.06.049.

Graber, E. R., and Y. Rudich (2006), Atmospheric HULIS: How humic-like are they? A comprehensive and critical review, *Atmos. Chem. Phys.*, *6*, 729-753.

Grahame, T. J., and R. B. Schlesinger (2007), Health effects of airborne particulate matter: Do we know enough to consider regulating specific particle types or sources?, *Inhal. Toxicol.*, *19* (6-7), 457-481, doi: doi:10.1080/08958370701382220.

Granier, C., U. Niemeier, J. H. Jungclaus, L. Emmons, P. Hess, J. F. Lamarque, S. Walters, and G. P. Brasseur (2006), Ozone pollution from future ship traffic in the Arctic northern passages, *Geophys. Res. Lett.*, *33* (13), 807 doi: 10.1029/2006GL026180.

Greentech (2011), Monitoring of brick kilns and strategies for cleaner brick production in India, Shakti Sustainable Energy, Greentech Knowledge Solutions, New Delhi, India.

Gregory, J. M., W. J. Ingram, M. A. Palmer, G. S. Jones, P. A. Stott, R. B. Thorpe, J. A. Lowe, T. C. Johns, and K. D. Williams (2004), A new method for diagnosing radiative forcing and climate sensitivity, *Geophys. Res. Lett.*, *31* (3), 205, doi: 10.1029/2003GL018747.

Grenfell, T. C., S. P. Neshyba, and S. G. Warren (2005), Representation of a nonspherical ice particle by a collection of independent spheres for scattering and absorption of radiation: 3. Hollow columns and plates, *J. Geophys. Res.*, *110* (D17), 203, doi: 10.1029/2005JD005811.

Grenfell, T. C., S. J. Doherty, A. D. Clarke, and S. G. Warren (2011), Light absorption by particulate impurities in snow and ice determined by spectrophotometric analysis of filters, *Appl. Opt.*, *50*, 2037-2048.

Groblicki, P. J., G. T. Wolff, and R. J. Countess (1981), Visibility-reducing species in the Denver "brown cloud"-- I. Relationships between extinction and chemical composition, *Atmos. Environ.*, *15* (12), 2473-2484.

Guazzotti, S. A., D. T. Suess, K. R. Coffee, P. K. Quinn, T. S. Bates, A. Wisthaler, A. Hansel, W. P. Ball, R. R. Dickerson, C. Neusüss, P. J. Crutzen, and K. A. Prather (2003), Characterization of carbonaceous aerosols outflow from India and Arabia: Biomass/biofuel burning and fossil fuel combustion, *J. Geophys. Res.*, *108* (D15), 4485.

Gundel, L. A., R. L. Dod, H. Rosen, and T. Novakov (1984), The relationship between optical attenuation and black carbon concentration for ambient and source particles, *Sci. Total Environ.*, *36*, 197-202.

Gustafsson, O., M. Krusa, Z. Zencak, R. J. Sheesley, L. Granat, E. Engstrom, P. S. Praveen, P. S. P. Rao, C. Leck, and H. Rodhe (2009), Brown clouds over South Asia: Biomass or fossil fuel combustion?, *Science*, *323* (5913), 495-498, doi: 10.1126/science.1164857.

Guttikunda, S. K., and P. Jawahar (2011), Urban Air Pollution Analysis in India, UrbanEmissions.Info (Ed.), SIM-air Working Paper Series , New Delhi, India.

Haag, W., B. Karcher, J. Strom, A. Minikin, U. Lohmann, J. Ovarlez, and A. Stohl (2003), Freezing thresholds and cirrus cloud formation mechanisms inferred from in situ measurements of relative humidity, *Atmos. Chem. Phys.*, *3*, 1791-1806.

Hadley, O. L., C. E. Corrigan, T. W. Kirchstetter, S. S. Cliff, and V. Ramanathan (2010), Measured black carbon deposition on the Sierra Nevada snow pack and implication for snow pack retreat, *Atmos. Chem. Phys. Discuss.*, *10* (4), 10463-10485, doi: 10.5194/acpd-10-10463-2010.

Haeberli, W. (1977), Sahara dust in the Alps - - A short review, *Z. Gletscher. Glazialgeol.*, *13*, 206-208.

Hagler, G. S. W., M. H. Bergin, E. A. Smith, and J. E. Dibb (2007a), A summer time series of particulate carbon in the air and snow at Summit, Greenland, *J. Geophys. Res.*, *112* (D21), 309, doi: 10.1029/2007JD008993.

Hagler, G. S. W., M. H. Bergin, E. A. Smith, J. E. Dibb, C. Anderson, and E. J. Steig (2007b), Particulate and water-soluble carbon measured in recent snow at Summit, Greenland, *Geophys. Res. Lett.*, *34* (16), L16505, doi: 10.1029/2007GL030110.

Hakami, A., D. K. Henze, J. H. Seinfeld, T. Chai, Y. Tang, G. R. Carmichael, and A. Sandu (2005), Adjoint inverse modeling of black carbon during the Asian Pacific Regional Aerosol Characterization Experiment, *J. Geophys. Res.*, *110* (D14), 301, doi: 10.11029/12004JD005671.

Hall, A., and X. Qu (2006), Using the current seasonal cycle to constrain snow albedo feedback in future climate change, *Geophys. Res. Lett.*, *33* (3), L03502, doi: 10.1029/2005GL025127.

Hansen, A. D. A., H. Rosen, and T. Novakov (1982), Real-time measurement of the absorption coefficient of aerosol particles, *Appl. Opt.*, *21* (17), 3060-3062.

Hansen, J., M. Sato, and R. Ruedy (1997), Radiative forcing and climate response, *J. Geophys. Res.*, *102* (D6), 6831-6864.

Hansen, J. E., M. Sato, R. Ruedy, A. Lacis, and V. Oinas (2000), Global warming in the twenty-first century: An alternative scenario, *P. Natl. Acad. Sci. USA*, *97* (18), 9875-9880.

Hansen, J., and L. Nazarenko (2004), Soot climate forcing via snow and ice albedos, *P. Natl. Acad. Sci. USA*, *101* (2), 423-428, doi: 10.1073/pnas.2237157100.

Hansen, J., M. Sato, R. Ruedy, L. Nazarenko, A. Lacis, G. A. Schmidt, G. Russell, I. Aleinov, M. Bauer, S. Bauer, N. Bell, B. Cairns, V. Canuto, M. Chandler, Y. Cheng, A. Del Genio, G. Faluvegi, E. Fleming, A. Friend, T. Hall, C. Jackman, M. Kelley, N. Kiang, D. Koch, J. Lean, J. Lerner, K. Lo, S. Menon, R. Miller, P. Minnis, T. Novakov, V. Oinas, J. Perlwitz, J. Perlwitz, D. Rind, A. Romanou, D. Shindell, P. Stone, S. Sun, N. Tausnev, D. Thresher, B. Wielicki, T. Wong, M. Yao, and S. Zhang (2005), Efficacy of climate forcings, *J. Geophys. Res.*, *110* (D18), D18104, doi: 10.1029/2005JD005776.

Hansen, J., M. Sato, P. Kharecha, G. Russell, D. W. Lea, and M. Siddall (2007), Climate change and trace gases, *Philos. Trans. R. Soc. A-Math. Phys. Eng. Sci.*, *365* (1856), 1925-1954, doi: 10.1098/rsta.2007.2052.

Haywood, J. M., and K. P. Shine (1995), The effect of anthropogenic sulfate and soot aerosol on the clear sky planetary radiation budget, *Geophys. Res. Lett.*, *22* (5), 603-606.

Haywood, J. M., and V. Ramaswamy (1998), Global sensitivity studies of the direct radiative forcing due to anthropogenic sulfate and black carbon aerosols, *J. Geophys. Res.*, *103* (D6), 6043-6058.

Haywood, J., and O. Boucher (2000), Estimates of the direct and indirect radiative forcing due to tropospheric aerosols: A review, *Rev. Geophys.*, *38* (4), 513-543.

Hazenkamp-von Arx, M. E., T. Gotschi, U. Ackermann-Liebrich, R. Bono, P. Burney, J. Cyrys, D. Jarvis, L. Lillienberg, C. Luczynska, J. A. Maldonado, A. Jaen, R. de Marco, Y. H. Mi, L. Modig, L. Bayer-Oglesby, F. Payo, A. Soon, J. Sunyer, S. Villani, J. Weyler, and N. Kunzli (2004), PM2.5 and NO_2 assessment in 21 European study centres of ECRHS II: Annual means and seasonal differences, *Atmos. Environ.*, *38* (13), 1943-1953, doi: 10.1016/j.atmosenv.2004.01.016.

Heald, C. L., D. J. Jacob, D. B. A. Jones, P. I. Palmer, J. A. Logan, D. G. Streets, G. W. Sachse, J. C. Gille, R. N. Hoffman, and T. Nehrkorn (2004), Comparative inverse analysis of satellite (MOPITT) and aircraft (TRACE-P) observations to estimate Asian sources of carbon monoxide, *J. Geophys. Res.*, *109* (D23), 306, doi: 10.1029/2004JD005185.

Heald, C. L., and D. V. Spracklen (2009), Atmospheric budget of primary biological aerosol particles from fungal spores, *Geophys. Res. Lett.*, *36, L09806*, doi: 10.1029/2009GL037493.

Hegerl, G. C., F. W. Zwiers, P. Braconnot, N. P. Gillett, Y. Luo, J. A. Marengo Orsini, N. Nicholls, J. E. Penner, and P. A. Stott (2007), Understanding and attributing climate change, in *Climate change 2007: The physical science basis*, edited by S. Solomon, D. Qin, M. Manning, Z. Chen, M. Marquis, K. B. Averyt, M. Tigor and H. L. Miller, 129-234 pp., Cambridge University Press, Cambridge, UK.

Hegg, D. A., S. G. Warren, T. C. Grenfell, S. J. Doherty, T. V. Larson, and A. D. Clarke (2009), Source attribution of black carbon in Arctic snow, *Environ Sci Technol*, *43* (11), 4016-4021.

Hegg, D. A., S. G. Warren, T. C. Grenfell, S. J. Doherty, and A. D. Clarke (2010), Sources of light-absorbing aerosol in Arctic snow and their seasonal variation, *Atmos. Chem. Phys.*, *10*, 10923-10938, doi: 10.5194/acp-10-10923-2010.

Heidenreich, R. D., W. M. Hess, and L. L. Ban (1968), A test object and criteria for high resolution electron microscopy, *J. Appl. Crystallogr.*, *1* (1-19).

Heierli, U., and S. Maithel (2008), Brick by brick: The Herculean task of cleaning up the Asian brick industry, edited by P. Osborn, Swiss Agency for Development and Cooperation (SDC), Natural Resources and Environment Division, Berne, Switzerland.

Heintzenberg, J., K. Okada, and J. Strom (1996), On the composition of non-volatile material in upper tropospheric aerosols and cirrus crystals, *Atmos. Res.*, *41* (1), 81-88.

Heintzenberg, J., and R. J. Charlson (Eds.) (2009), Clouds in the Perturbed Climate System: Their Relationship to Energy Balance, Atmospheric Dynamics, and Precipitation. Strüngmann Forum Report, Volume 2, ISBN-10: 0-262-01287-1, The MIT Press, Cambridge, MA.

Heller, W. (1965), Remarks on refractive index mixture rules, *J. Phys. Chem.*, *69*, 1123-1129.

Hendricks, J., B. Karcher, U. Lohmann, and M. Ponater (2005), Do aircraft black carbon emissions affect cirrus clouds on the global scale?, *Geophys. Res. Lett.*, *32*, L12814, doi: 10.1029/2005GL022740.

Hendricks, J., B. Kärcher, and U. Lohmann (2011), Effects of ice nuclei on cirrus clouds in a global climate model, *J. Geophys. Res.*, *116*, D18206, doi: 10.1029/2010JD015302.

Hess, W. M., and C. R. Herd (1993), Microstructure, morphology, and general physical properties, in *Carbon Black*, edited by J.-B. Donnet, R. C. Bansal and M.-J. Wang, Marcel Dekker, New York.

Hess, M., P. Koepke, and I. Schult (1998), Optical properties of aerosols and clouds: the software package OPAC, *Bull. Amer. Meteorol. Soc.*, *79* (5), 831-844.

Hicks, S., and E. Isaksson (2006), Assessing source areas of pollutants from studies of fly ash, charcoal, and pollen from Svalbard snow and ice, *J. Geophys. Res.*, *111* (D2), D02113, doi: 10.1029/2005JD006167.

Hien, P. D., V. T. Bac, and N. T. H. Thinh (2004), PMF receptor modelling of fine and coarse PM10 in air masses governing monsoon conditions in Hanoi, northern Vietnam, *Atmos. Environ.*, *38* (2), 189-201, doi: 10.1016/j.atmosenv.2003.09.064.

Higuchi, K., and A. Nagoshi (1977), Effect of particulate matter in surface snow layers on the albedo of perennial snow patches, *Isotopes and Impurities in Snow and Ice, IAHS*, Publ. No. 118, 95-97 pp., International Association of Hydrological Sciences, Washington, DC.

Hill, A. A., and S. Dobbie (2008), The impact of aerosols on non-precipitating marine stratocumulus. II: The semi-direct effect, *Quart J. Roy. Meteor. Soc.*, *134* (634), 1155-1165, doi: 10.1002/qj.277.

Holben, B. N., T. F. Eck, I. Slutsker, D. Tanre, J. P. Buis, A. Setzer, E. Vermote, J. A. Reagan, Y. J. Kaufman, T. Nakajima, F. Lavenu, I. Jankowiak, and A. Smirnov (1998), AERONET - A federated instrument network and data archive for aerosol characterization, *Remote Sens. Environ.*, *66*, 1-16.

Holdsworth, G., K. Higuchi, G. A. Zielinski, P. A. Mayewski, M. Wahlen, B. Deck, P. Chylek, B. Johnson, and P. Damiano (1996), Historical biomass burning: Late 19th century pioneer agriculture revolution in northern hemisphere ice core data and its atmospheric interpretation, *J. Geophys. Res.*, *101* (D18), 23317-23334, doi: 10.1029/96JD01158.

Hoose, C., U. Lohmann, R. Erdin, and I. Tegen (2008), The global influence of dust mineralogical composition on heterogeneous ice nucleation in mixed-phase clouds, *Environ. Res. Lett.*, *3* (2), 5003, doi: 10.1088/1748-9326/3/2/025003.

Hopke, P. K. (2010), The Application of Receptor Modeling to Air Quality Data, Pollution Atmosphérique, *Special Issue*, 91-109.

Horvath, H. (1997), Systematic deviations of light absorption measurements by filter transmission methods, *J. Aerosol Sci.*, *28*, S55-S56.

Houck, J. E., and B. N. Eagle (2006), Control Analysis and Documentation for Residential Wood Combustion in the MANE-VU Region, OMNI Environmental Services.

Houthuijs, D., O. Breugelmans, G. Hoek, E. Vaskovi, E. Mihalikova, J. S. Pastuszka, V. Jirik, S. Sachelarescu, D. Lolova, K. Meliefste, E. Uzunova, C. Marinescu, J. Volf, F. de Leeuw, H. van de Wiel, T. Fletcher, E. Lebret, and B. Brunekreef (2001), PM10 and PM2.5 concentrations in Central and Eastern Europe: results from the Cesar study, *Atmos. Environ.*, *35* (15), 2757-2771.

Hoyle, C. R., B. P. Luo, and T. Peter (2005), The origin of high ice crystal number densities in cirrus clouds, *J. Atmos. Sci.*, *62* (7), 2568-2579.

Hu, Y. T., S. L. Napelenok, M. T. Odman, and A. G. Russell (2009), Sensitivity of inverse estimation of 2004 elemental carbon emissions inventory in the United States to the choice of observational networks, *Geophys. Res. Lett.*, *36* (L15), 806, doi: 10.1029/2009GL039655.

Huang, J., Q. Fu, W. Zhang, X. Wang, R. Zhang, H. Ye, and S. G. Warren (2011), Dust and black carbon in seasonal snow across northern China, *Bull. Am. Meteor. Soc.*, *92*, 175-781.

Huebert, B. J., T. S. Bates, P. B. Russell, G. Shi, Y. J. Kim, K. Kawamura, G. Carmichael, and T. Nakajima (2003), An overview of ACE-Asia: strategies for quantifying the relationships between Asian aerosols and their climatic impacts, *J. Geophys. Res.*, *108* (D23), 8633, doi: 10.1029/2003JD003550.

Huneeus, N., F. Chevallier, and O. Boucher (2012), Estimating aerosol emissions by assimilating observed aerosol optical depth in a global aerosol model, *Atmos. Chem. Phys. Discuss.*, *12,* 3075-3130, doi: 10.5194/acpd-12-3075-2012.

Huntzicker, J. J., R. L. Johnson, J. J. Shah, and R. A. Cary (1982),

Analysis of organic and elemental carbon in ambient aerosols by a thermal-optical method, in *Particulate Carbon: Atmospheric Life Cycle*, edited by G. T. Wolff and R. L. Klimisch, 79-88 pp., Plenum Press, New York.

Ichoku, C., and Y. J. Kaufman (2005), A method to derive smoke emission rates from MODIS fire radiative energy measurements, *IEEE Trans. Geosci. Remote Sens.*, *43* (11), 2636-2649.

IPCC (1990), Intergovernmental Panel on Climate Change (IPCC): The Scientific Assessment, UNEP/WMO, Cambridge, UK.

IPCC (2007), Climate Change 2007: The Physical Science Basis. Contribution of Working Group I to the Fourth Assessment, Report of the Intergovernmental Panel on Climate Change, 996 pp., Cambridge University Press, Cambridge, UK, and New York, NY, USA.

IPCC (2009), IPCC Expert Meeting on the Science of Alternative Metrics Meeting Report, 82 pp., Grand Hotel, Oslo, Norway.

Isaksen, I. S. A., C. Granier, G. Myhre, T. K. Berntsen, S. B. Dalsoren, M. Gauss, Z. Klimont, R. Benestad, P. Bousquet, W. Collins, T. Cox, V. Eyring, D. Fowler, S. Fuzzi, P. Jockel, P. Laj, U. Lohmann, M. Maione, P. Monks, A. S. H. Prevot, F. Raes, A. Richter, B. Rognerud, M. Schulz, D. Shindell, D. S. Stevenson, T. Storelvmo, W. C. Wang, M. van Weele, M. Wild, and D. Wuebbles (2009), Atmospheric composition change: Climate-Chemistry interactions, *Atmos. Environ.*, *43* (33), 5138-5192, doi: 10.1016/j.atmosenv.2009.08.003.

Ito, A., and J. Penner (2005), Historical emissions of carbonaceous aerosols from biomass and fossil fuel burning for the period 1870-2000, *Global Biogeochem. Cycles*, *19* (2), doi: 10.1029/2004GB002374.

Jackson, S. C. (2009), Parallel pursuit of near-term and long-term climate mitigation *Science*, *326* (5952), 526-527, doi: 10.1126/science.1177042.

Jacob, D. J., J. H. Crawford, M. M. Kleb, V. S. Connors, R. J. Bendura, J. L. Raper, G. W. Sachse, J. C. Gille, L. Emmons, and C. L. Heald (2003), Transport and Chemical Evolution over the Pacific (TRACE-P) aircraft mission: Design, execution, and first results, *J. Geophys. Res.*, *108* (D20), 1-19, doi: 10.1029/2002JD003276.

Jacob, D. J., J. H. Crawford, H. Maring, A. D. Clarke, J. E. Dibb, L. K. Emmons, R. A. Ferrare, C. A. Hostetler, P. B. Russell, H. B. Singh, A. M. Thompson, G. E. Shaw, E. McCauley, J. R. Pederson, and J. A. Fisher (2010), The Arctic Research of the Composition of the Troposphere from Aircraft and Satellites (ARCTAS) mission: Design, execution, and first results, *Atmos Chem Phys*, *10* (11), 5191-5212, doi: 10.5194/acp-10-5191-2010.

Jacobson, M. Z. (2000), A physically-based treatment of elemental carbon optics: Implications for global direct forcing of aerosols, *Geophys. Res. Lett.*, *27* (2), 217-220.

Jacobson, M. Z. (2001a), Strong radiative heating due to the mixing state of black carbon in atmospheric aerosols, *Nature*, *409*, 695-697.

Jacobson, M. Z. (2001b), Global direct radiative forcing due to multicomponent anthropgenic and natural aerosols, *J. Geophys. Res.*, *106*, 1551-1568, doi: 10.1029/2000JD900514.

Jacobson, M. Z. (2002), Control of fossil-fuel particulate black carbon and organic matter, possibly the most effective method of slowing global warming, *J. Geophys. Res.*, *107 (D19)*, 4410, doi: 10.1029/2001JD001376.

Jacobson, M. Z. (2004), Climate response of fossil fuel and biofuel soot, accounting for soot's feedback to snow and sea ice albedo and emissivity, *J. Geophys. Res.*, *109* (D21), D21201, doi: 10.1029/2004JD004945.

Jacobson, M. Z. (2006), Effects of externally-through-internally-mixed soot inclusions within clouds and precipitation on global climate, *J. Phys. Chem. A*, *110* (21), 6860-6873, doi: 10.1021/jp056391r.

Jacobson, M. Z. (2010), Short-term effects of controlling fossil-fuel soot, biofuel soot and gases, and methane on climate, Arctic ice, and air pollution health, *J. Geophys. Res.*, *115*, doi: D14209, doi:10.1029/2009JD013795.

Jacobson, M. Z., J. T. Wilkerson, A. D. Naiman, and S. K. Lele (2011), The effects of aircraft on climate and pollution. Part I: Numerical methods for treating the subgrid evolution of discrete size- and composition-resolved contrails from all commercial flights worldwide, *J. Comput. Phys.*, *230*, 5115-5132, doi: 10.1016/j.jcp.2011.03.031.

Jacobson, M. Z. (2012), Investigating cloud absorption effects: Global absorption properties of black carbon, tar balls, and soil dust in clouds and aerosols, *J. Geophys. Res.*, *in press*, doi: 10.1029/2011JD017218.

Janssen, N. A., G. Hoek, M. Simic-Lawson, P. Fischer, L. van Bree, H. ten Brink, M. Keuken, R. W. Atkinson, H. R. Anderson, B. Brunekreef, and F. R. Cassee (2011), Black Carbon as an Additional Indicator of the Adverse Health Effects of Airborne Particles Compared with PM_{10} and $PM_{2.5}$, *Environ. Health Perspect.*, *119*, 1691-1699, doi: 10.1289/ehp.1003369.

Janzen, J. (1979), The refractive index of carbon black, *J. Colloid Interf. Sci.*, *69* (3), 436-447.

Janzen, J. (1980), Extinction of light by highly nonspherical strongly absorbing colloidal particles - spectrophotometric determination of volume distributions for carbon-blacks, *Appl. Opt.*, *19* (17), 2977-2985, doi: 10.1364/AO.19.002977.

Jenk, T. M., S. Szidat, M. Schwikowski, H. W. Gäggeler, S. Brütsch, L. Wacker, H. A. Synal, and M. Saurer (2006), Radiocarbon analysis in an Alpine ice core: Record of anthropogenic and biogenic contributions to carbonaceous aerosols in the past (1650-1940), *Atmos. Chem. Phys.*, *6* (12), 5381-5390, doi: 10.5194/acp-6-5381-2006.

Jensen, E. J., O. B. Toon, S. A. Vay, J. Ovarlez, R. May, T. P. Bui, C. H. Twohy, B. W. Gandrud, R. F. Pueschel, and U. Schumann (2001), Prevalence of ice-supersaturated regions in the upper troposphere: Implications for optically thin ice cloud formation, *J. Geophys. Res.*, *106* (D15), 17253-17266.

Jetter, J. J., and P. Kariher (2009), Solid-fuel household cook stoves: Characterization of performance and emissions, *Biomass Bioenerg.*, *33*, 294-305, doi: 10.1016/j.biombioe.2008.05.014.

Johansson, D. J. A., U. M. Persson, and C. Azar (2006), The cost of using global warming potentials: Analysing the trade off between CO_2, CH^4 and N_2O, *Climatic Change*, *77* (3-4), 291-309, doi: 10.1007/s10584-006-9054-x.

Johansson, L. S., B. Leckner, L. Gustavsson, D. Cooper, C. Tullin, and A. Potter (2004), Emission characteristics of modern and old-type residential boilers fired with wood logs and wood pellets, *Atmos. Environ.*, *38* (25), 4183-4195, doi: 10.1016/j.atmosenv.2004.04.020.

Johnson, B. T., K. P. Shine, and P. M. Forster (2004), The semi-direct aerosol effect: Impact of absorbing aerosols on marine stratocumulus, *Quart J. Roy. Meteor. Soc.*, *130* (599), 1407-1422, doi: 10.1256/qj.03.61.

Johnson, K. S., B. de Foy, B. Zuberi, L. T. Molina, M. J. Molina, Y. Xie, A. Laskin, and V. Shutthanandan (2006), Aerosol composition and source apportionment in the Mexico City Metropolitan Area with PIXE/PESA/STIM and multivariate analysis, *Atmos. Chem. Phys.*, *6*, 4591-4600.

Johnson, M., R. Edwards, C. A. Frenk, and O. Masera (2008), In-field greenhouse gas emissions from cookstoves in rural Mexican households, *Atmos. Environ.*, *42* (6), 1206-1222, doi: 10.1016/j.atmosenv.2007.10.034.

Johnson, M. R., and A. R. Coderre (2011), An analysis of flaring and venting activity in the Alberta upsteam oil and gas industry,

J. Air Waste Manage. Assoc., *61* (2), 190-200, doi: 10.3155/1047-3289.61.2.190.

Johnson, M. R., R. W. Devillers, and K. A. Thomson (2011a), Quantitative field measurement of soot emission from a large gas flare using Sky-LOSA, *Environ. Sci. Technol.*, *45* (1), 345-350, doi: 10.1021/es102230y.

Johnson, T. M., S. Guttikunda, G. J. Wells, P. Artaxo, T. C. Bond, A. G. Russell, J. G. Watson, and J. West (2011b), Tools for Improving Air Quality Management: A Review of Top-down Source Apportionment Techniques and Their Application in Developing Countries, ESMAP Publication Series, The World Bank, Washington, DC, USA.

Jones, H. G., J. W. Pomeroy, D. A. Walker, and R. W. Hoham (Eds.) (2001), *Snow Ecology*, 398 pp., Cambridge University Press.

Jones, G. S., A. Jones, D. L. Roberts, P. A. Stott, and K. D. Williams (2005), Sensitivity of global-scale climate change attribution results to inclusion of fossil fuel black carbon aerosol, *Geophys. Res. Lett.*, *32* (14), 701, doi: 10.1029/2005GL023370.

Jones, A., J. M. Haywood, and O. Boucher (2007), Aerosol forcing, climate response and climate sensitivity in the Hadley Centre climate model, *J. Geophys. Res.*, *112* (D20), 211, doi: 10.1029/2007JD008688.

Jones, G. S., N. Christidis, and P. A. Stott (2011), Detecting the influence of fossil fuel and bio-fuel black carbon aerosols on near surface temperature changes, *Atmos. Chem. Phys.*, *11*, 799-816, doi: 10.5194/acpd-11-799-2011.

Kahn, R. A., D. L. Nelson, M. J. Garay, R. C. Levy, M. A. Bull, D. J. Diner, J. V. Martonchik, S. R. Paradise, E. G. Hansen, and L. A. Remer (2009a), MISR aerosol product attributes and statistical comparisons with MODIS, *IEEE Trans. Geosci. Remote Sens.*, *47* (12), 4095-4114, doi: 10.1109/tgrs.2009.2023115.

Kahn, B. H., A. Gettelman, E. J. Fetzer, A. Eldering, and C. K. Liang (2009b), Cloudy and clear-sky relative humidity in the upper troposphere observed by the A-train, *J. Geophys. Res.*, *114* (D00h02), doi: 10.1029/2009JD011738.

Kahn, R., A. Petzold, M. Wendisch, E. Bierwirth, T. Dinter, M. Esselborn, M. Fiebig, B. Heese, P. Knippertz, D. Muller, A. Schladitz, and A. Von Hoyningen-Huene (2009c), Desert dust aerosol air mass mapping in the western Sahara, using particle properties derived from space-based multi-angle imaging, *Tellus B*, *61* (1), 239-251, doi: 10.1111/j.1600-0889.2008.00398.x.

Kahn, R. A., B. J. Gaitley, M. J. Garay, D. J. Diner, T. F. Eck, A. Smirnov, and B. N. Holben (2010), Multiangle Imaging SpectroRadiometer global aerosol product assessment by comparison with the Aerosol Robotic Network, *J. Geophys. Res.*, *115*, D23209, doi: 10.1029/2010JD014601.

Kahnert, M., M. Lazaridis, S. Tsyro, and K. Torseth (2004), Requirements for developing a regional monitoring capacity for aerosols in Europe within EMEP, *J. Environ. Monit.*, *6* (7), 646-655, doi: 10.1039/b315136k.

Kahnert, M. (2010), On the discrepancy between modeled and measured mass absorption cross sections of light absorbing carbon aerosols, *Aerosol Sci. Technol.*, *44* (6), 453-460, doi: 10.1080/02786821003733834.

Kaiser, J. W., Suttie, M., Flemming, J., Morcrette, J.-J., Boucher, O., and Schultz, M. G. (2009), Global real-time fire emission estimates based on space-borne fire radiative power observations, *AIP Conf. Proc.*, *1100*, 645-648, doi: 10.1063/1.3117069.

Kaiser, J. W., A. Heil, M. O. Andreae, A. Benedetti, N. Chubarova, L. Jones, J.-J. Morcrette, M. Razinger, M. G. Schultz, M. Suttie, and G. R. van der Werf (2011), Biomass burning emissions estimated with a global fire assimilation system based on observed fire radiative power, *Biogeosciences Discuss.*, *8* (4), 7339-7398.

Kandlikar, M. (1996), Indices for comparing greenhouse gas emissions: Integrating science and economics, *Energ. Econ.*, *18*, 265-281.

Kandlikar, M., C. Reynolds, and A. Grieshop (2009), A perspective paper on black carbon mitigation as a response to climate change, *Report prepared for the Copenhagen Consensus on Climate*, Copenhagen Consensus Center, Frederiksberg, Denmark.

Kärcher, B., T. Peter, U. M. Biermann, and U. Schumann (1996), The initial composition of jet condensation trails, *J. Atmos. Sci.*, *53* (21), 3066-3083.

Kärcher, B., and J. Strom (2003), The roles of dynamical variability and aerosols in cirrus cloud formation, *Atmos. Chem. Phys.*, *3*, 823-838, doi: 10.5194/acp-3-823-2003.

Kärcher, B., J. Hendricks, and U. Lohmann (2006), Physically based parameterization of cirrus cloud formation for use in global atmospheric models, *J. Geophys. Res.*, *111* (D1), 205, doi: 10.1029/2005JD006219.

Kärcher, B., O. Mohler, P. J. DeMott, S. Pechtl, and F. Yu (2007), Insights into the role of soot aerosols in cirrus cloud formation, *Atmos. Chem. Phys.*, *7* (16), 4203-4227.

Kärcher, B., and U. Burkhardt (2008), A cirrus cloud scheme for general circulation models, *Q. J. R. Meteorol. Soc.*, *134*, 1439-1461, doi: 10.1002/qj.301.

Kärcher, B., and P. Spichtinger (2009), Cloud-controlling factors of cirrus, in *Clouds in the perturbed climate system: Their relationship to energy balance, atmospheric dynamics, and precipitation*, edited by J. Heintzenberg and R. J. Charlson, 235-268 pp., MIT Press, Cambridge, MA.

Kärcher, B., and F. Yu (2009), Role of aircraft soot emissions in contrail formation, *Geophys. Res. Lett.*, *36* (L01804), doi: 10.1029/2008GL036649.

Kasibhatla, P., A. Arellano, J. A. Logan, P. I. Palmer, and P. Novelli (2002), Top-down estimate of a large source of atmospheric carbon monoxide associated with fuel combustion in Asia, *Geophys. Res. Lett.*, *29* (19), doi: 10.1029/2002GL015581.

Kasischke, E. S., and N. H. F. French (1995), Locating and estimating the areal extent of wildfires in Alaskan boreal forests using multiple-season AVHRR NDVI composite data, *Remote Sens. Environ.*, *51* (2), 263-275.

Kaufman, Y. J., P. V. Hobbs, V. W. J. H. Kirchhoff, P. Artaxo, L. A. Remer, B. N. Holben, M. D. King, D. E. Ward, E. M. Prins, K. M. Longo, L. F. Mattos, C. A. Nobre, J. D. Spinhirne, Q. Ji, A. M. Thompson, J. F. Gleason, S. A. Christopher, and S.-C. Tsay (1998), Smoke, clouds, and radiation-- Brazil (SCAR-B) experiment, *J. Geophys. Res.*, *103* (D24), 31783-31808.

Keene, W. C., R. M. Lobert, P. J. Crutzen, J. R. Maben, D. H. Scharffe, T. Landmann, C. Hely, and C. Brain (2006), Emissions of major gaseous and particulate species during experimental burns of southern African biomass, *J. Geophys. Res.*, *111* (D4), 301, doi: 10.1029/2005JD006319.

Khalizov, A. F., H. X. Xue, L. Wang, J. Zheng, and R. Y. Zhang (2009), Enhanced light absorption and scattering by carbon soot aerosol internally mixed with sulfuric acid, *J. Phys. Chem. A*, *113*, 1066-1074, doi: 10.1021/jp807531n.

Kim, E., and P. K. Hopke (2007), Source identifications of airborne fine particles using positive matrix factorization and US environmental protection agency positive matrix factorization, *J. Air Waste Manage. Assoc.*, *57* (7), 811-819, doi: 10.3155/1047-3289.57.7.811.

Kim, D., C. Wang, A. M. L. Ekman, M. C. Barth, and P. J. Rasch (2008), Distribution and direct radiative forcing of carbonaceous and sulfate aerosols in an interactive size-resolving aerosol-climate model, *J. Geophys. Res.*, *113* (D16), 309, doi:

10.1029/2007JD009756.

Kinne, S., M. Schulz, C. Textor, S. Guibert, Y. Balkanski, S. E. Bauer, T. Berntsen, T. F. Berglen, O. Boucher, M. Chin, W. Collins, F. Dentener, T. Diehl, R. Easter, J. Feichter, D. Fillmore, S. Ghan, P. Ginoux, S. Gong, A. Grini, J. E. Hendricks, M. Herzog, L. Horowitz, L. Isaksen, T. Iversen, A. Kirkavag, S. Kloster, D. Koch, J. E. Kristjansson, M. Krol, A. Lauer, J. F. Lamarque, G. Lesins, X. Liu, U. Lohmann, V. Montanaro, G. Myhre, J. E. Penner, G. Pitari, S. Reddy, O. Seland, P. Stier, T. Takemura, and X. Tie (2006), An AeroCom initial assessment - optical properties in aerosol component modules of global models, *Atmos. Chem. Phys.*, *6*, 1815-1834.

Kirchstetter, T. W., T. Novakov, and P. V. Hobbs (2004), Evidence that the spectral dependence of light absorption by aerosols is affected by organic carbon, *J. Geophys. Res.*, *109* (D21), D21208, doi: 10.1029/2004JD004999.

Kirchstetter, T. W., J. Aguiar, S. Tonse, and T. Novakov (2008), Black carbon concentrations and diesel vehicle emission factors derived from coefficient of haze measurements in California: 1967-2003, *Atmos. Environ.*, *42*, 480-491.

Kirkevag, A., and T. Iversen (2002), Global direct radiative forcing by process-parameterized aerosol optical properties, *J. Geophys. Res.*, *107* (D20), 4433, doi: 10.1029/2001JD000886.

Klimont, Z., J. Cofala, J. Xing, W. Wei, C. Zhang, S. Wang, K. J., P. Bhandari, R. Mathura, P. Purohit, P. Rafaj, A. Chambers, M. Amann, and J. Hao (2009), Projections of SO_2, NO_x, and carbonaceous aerosol emissions in Asia, *Tellus B*, *61* (4), 602-617, doi: 10.1111/j.1600-0889.2009.00428.x.

Knox, A., G. J. Evans, J. R. Brook, X. Yao, C. H. Jeong, K. J. Godri, K. Sabaliauskas, and J. G. Slowik (2009), Mass absorption cross-section of ambient black carbon aerosol in relation to chemical age, *Aerosol Sci. Technol.*, *43* (6), 522-532, doi: 10.1080/02786820902777207.

Koch, D. (2001), Transport and direct radiative forcing of carbonaceous and sulfate aerosols in the GISS GCM, *J. Geophys. Res.*, *106* (D17), 20311-20332.

Koch, D., and J. Hansen (2005), Distant origins of Arctic black carbon: A Goddard Institute for Space Studies ModelE experiment, *J. Geophys. Res.*, *110* (D4), 204, doi: 10.1029/2004JD005296.

Koch, D., T. C. Bond, D. Streets, N. Unger, and G. R. van der Werf (2007), Global impacts of aerosols from particular source regions and sectors, *J. Geophys. Res.*, *112* (D02205), doi: 10.1029/2005JD007024.

Koch, D., M. Schulz, S. Kinne, C. McNaughton, J. R. Spackman, Y. Balkanski, S. Bauer, T. Berntsen, T. C. Bond, O. Boucher, M. Chin, A. Clarke, N. De Luca, F. Dentener, T. Diehl, O. Dubovik, R. Easter, D. W. Fahey, J. Feichter, D. Fillmore, S. Freitag, S. Ghan, P. Ginoux, S. Gong, L. Horowitz, T. Iversen, A. Kirkevag, Z. Klimont, Y. Kondo, M. Krol, X. Liu, R. Miller, V. Montanaro, N. Moteki, G. Myhre, J. E. Penner, J. Perlwitz, G. Pitari, S. Reddy, L. Sahu, H. Sakamoto, G. Schuster, J. P. Schwarz, O. Seland, P. Stier, N. Takegawa, T. Takemura, C. Textor, J. A. van Aardenne, and Y. Zhao (2009a), Evaluation of black carbon estimations in global aerosol models, *Atmos. Chem. Phys.*, *9* (22), 9001-9026.

Koch, D., S. Menon, A. Del Genio, R. Ruedy, I. Alienov, and G. A. Schmidt (2009b), Distinguishing aerosol impacts on climate over the past century, *J. Climate*, *22* (10), 2659-2677, doi: 10.1175/2008jcli2573.1.

Koch, D., and A. D. Del Genio (2010), Black carbon semi-direct effects on cloud cover: review and synthesis, *Atmos. Chem. Phys.*, *10* (16), 7685-7696, doi: 10.5194/acp-10-7685-2010.

Koch, D., Y. Balkanski, S. E. Bauer, R. C. Easter, S. Ferrachat, S. J. Ghan, C. Hoose, T. Iversen, A. Kirkevag, J. E. Kristjansson, X. Liu, U. Lohmann, S. Menon, J. Quaas, M. Schulz, O. Seland, T. Takemura, and N. Yan (2011a), Soot microphysical effects on liquid clouds, a multi-model investigation, *Atmos. Chem. Phys.*, *11* (3), 1051-1064, doi: 10.5194/acp-11-1051-2011.

Koch, D., S. Bauer, A. Del Genio, G. Faluvegi, J. R. McConnell, S. Menon, R. L. Miller, D. Rind, R. Ruedy, G. A. Schmidt, and D. Shindell (2011b), Coupled aerosol-chemistry-climate twentieth century transient model investigation: Trends in short-lived species and climate responses, *J. Climate*, *24*, 2693-2714, doi: 10.1175/2011JCL13582.1.

K□hler, K. A., P. J. DeMott, S. M. Kreidenweis, O. B. Popovicheva, M. D. Petters, C. M. Carrico, E. D. Kireeva, T. D. Khokhlova, and N. K. Shonija (2009), Cloud condensation nuclei and ice nucleation activity of hydrophobic and hydrophilic soot particles, *Phys. Chem. Chem. Phys.*, *11* (36), 7906-7920, doi: 10.1039/b905334b.

Koffi, B., M. Schulz, F.-M. Breon, J. Griesfeller, Y. Balkanski, S. Bauer, T. Berntsen, M. Chin, W. D. Collins, F. Dentener, T. Diehl, R. Easter, S. Ghan, P. Giroux, S. Gong, L. W. Horowitz, T. Iversen, A. Kirkevåg, D. Koch, M. Kroll, G. Myhre, P. Stier, T. Takemura, and D. Winker (2012), Application of CALIOP layer product to evaluate the vertical distribution of aerosols estimated by global models: Part 1. AeroCom phase I results, *J. Geophys. Res.*, submitted.

Kondo, Y., L. Sahu, M. Kuwata, Y. Miyazaki, N. Takegawa, N. Moteki, J. Imaru, S. Han, T. Nakayama, N. T. K. Oanh, M. Hu, Y. J. Kim, and K. Kita (2009), Stabilization of the mass absorption cross section of black carbon for filter-based absorption photometry by the use of a heated inlet, *Aerosol Sci. Technol.*, *43* (8), 741-756, doi: 10.1080/02786820902889879.

Kondo, Y., L. Sahu, N. Moteki, F. Khan, N. Takegawa, X. Liu, M. Koike, and T. Miyakawa (2011a), Consistency and traceability of black carbon measurements made by laser-induced incandescence, thermal-optical transmittance, and filter-based photo-absorption techniques, *Aerosol Sci. Technol.*, *45* (2), 295-312, doi: 10.1080/02786826.2010.533215.

Kondo, Y., H. Matsui, N. Moteki, L. Sahu, N. Takegawa, M. Kajino, Y. Zhao, M. J. Cubison, J. L. Jimenez, S. Vay, G. S. Diskin, B. Anderson, A. Wisthaler, T. Mikoviny, H. E. Fuelberg, D. R. Blake, G. Huey, A. J. Weinheimer, D. J. Knapp, and W. H. Brune (2011b), Emissions of black carbon, organic, and inorganic aerosols from biomass burning in North America and Asia in 2008, *J. Geophys. Res.*, *116*, D08204, doi: 10.1029/2010JD015152.

Kondo, Y., N. Oshima, M. Kajino, R. Mikami, N. Moteki, N. Takegawa, R. L. Verma, Y. Kajii, S. Kato, and A. Takami (2011c), Emissions of black carbon in East Asia estimated from observations at a remote site in the East China Sea, *J. Geophys. Res.*, *116, D16201*, doi: 10.1029/2011JD015637.

Koop, T., B. P. Luo, A. Tsias, and T. Peter (2000), Water activity as the determinant for homogeneous ice nucleation in aqueous solutions, *Nature*, *406* (6796), 611-614.

Koopmans, A., and J. Koppejan (1997), Agricultural and forest residues: generation, utilization and availability, in *Regional Consultation on Modern Applications of Biomass Energy, FAO*, edited, Kuala Lumpur.

Kopacz, M., D. J. Jacob, J. A. Fisher, J. A. Logan, L. Zhang, I. A. Megretskaia, R. M. Yantosca, K. Singh, D. K. Henze, J. P. Burrows, M. Buchwitz, I. Khlystova, W. W. McMillan, J. C. Gille, D. P. Edwards, A. Eldering, V. Thouret, and P. Nedelec (2010), Global estimates of CO sources with high resolution by adjoint inversion of multiple satellite datasets (MOPITT, AIRS, SCIAMACHY, TES), *Atmos. Chem. Phys.*, *10* (3), 855-876.

Koren, I., Y. J. Kaufman, L. A. Remer, and J. V. Martins (2004), Measurement of the effect of Amazon smoke on inhibition of

cloud formation, *Science*, *303* (5662), 1342-1345.

Koren, I., J. V. Martins, L. A. Remer, and H. Afargan (2008), Smoke invigoration versus inhibition of clouds over the Amazon, *Science*, *321* (5891), 946-949, doi: 10.1126/science.1159185.

Kristjansson, J. E. (2002), Studies of the aerosol indirect effect from sulfate and black carbon aerosols, *J. Geophys. Res.*, *107* (D15), 4246, doi: 10.1029/2001JD000887.

Kuhlmann, J., and J. Quaas (2010), How can aerosols affect the Asian summer monsoon? Assessment during three consecutive pre-monsoon seasons from CALIPSO satellite data, *Atmos. Chem. Phys.*, *10* (10), 4673-4688, doi: 10.5194/acp-10-4673-2010.

Kupiainen, K., and Z. Klimont (2007), Primary emissions of fine carbonaceous particles in Europe, *Atmos. Environ.*, *41*, 2156-2170, doi:10.1016/j.atmosenv.2006.10.066.

Kurokawa, J., K. Yumimoto, I. Uno, and T. Ohara (2009), Adjoint inverse modeling of NO_x emissions over eastern China using satellite observations of NO_2 vertical column densities, *Atmos. Environ.*, *43* (11), 1878-1887, doi: 10.1016/j.atmosenv.2008.12.030.

Kuwata, M., Y. Kondo, M. Mochida, N. Takegawa, and K. Kawamura (2007), Dependence of CCN activity of less volatile particles on the amount of coating observed in Tokyo, *J. Geophys. Res.*, *112* (D11207), doi: 10.1029/2006JD007758.

Kuwata, M., Y. Kondo, and N. Takegawa (2009), Critical condensed mass for activiation of black carbon as cloud condensation nuclei in Tokyo, *J. Geophys. Res.*, *114* (D20202), doi: 10.1029/2009JD012086.

Laborde, M., P. Mertes, P. Zieger, J. Dommen, U. Baltensperger, and M. Gysel (2012), Sensitivity of the Single Particle Soot Photometer to different black carbon types, *Atmos. Meas. Tech. Discuss.*, *5*, 663-690, doi: 10.5194/amtd-5-663-2012.

Lack, D. A., E. R. Lovejoy, T. Baynard, A. Pettersson, and A. R. Ravishankara (2006), Aerosol absorption measurement using photoacoustic spectroscopy: Sensitivity, calibration, and uncertainty developments, *Aerosol Sci. Technol.*, *40* (9), 697-708, doi: 10.1080/02786820600803917.

Lack, D. A., C. D. Cappa, D. S. Covert, T. Baynard, P. Massoli, B. Sierau, T. S. Bates, P. K. Quinn, E. R. Lovejoy, and A. R. Ravishankara (2008), Bias in filter-based aerosol light absorption measurements due to organic aerosol loading: evidence from ambient measurements, *Aerosol Sci. Technol.*, *42* (12), 1033-1041.

Lack, D. A., C. D. Cappa, E. S. Cross, P. Massoli, A. T. Ahern, P. Davidovits, and T. B. Onasch (2009), Absorption enhancement of coated absorbing aerosols: Validation of the photo-acoustic technique for measuring the enhancement, *Aerosol Sci. Technol.*, *43* (10), 1006-1012, doi: 10.1080/02786820903117932.

Lack, D. A., and C. D. Cappa (2010), Impact of brown and clear carbon on light absorption enhancement, single scatter albedo and absorption wavelength dependence of black carbon, *Atmos. Chem. Phys.*, *10* (9), 4207-4220, doi: 10.5194/acp-10-4207-2010.

Lall, A. A., and S. K. Friedlander (2006), On-line measurement of ultrafine aggregate surface area and volume distributions by electrical mobility analysis: I. Theoretical analysis, *J. Aerosol. Sci.*, *37* (3), 260-271, doi: 10.1016/j.jaerosci.2005.05.021.

Lamarque, J. F., T. C. Bond, V. Eyring, C. Granier, A. Heil, Z. Klimont, D. Lee, C. Liousse, A. Mieville, B. Owen, M. G. Schultz, D. Shindell, S. J. Smith, E. Stehfest, J. Van Aardenne, O. R. Cooper, M. Kainuma, N. Mahowald, J. R. McConnell, V. Naik, K. Riahi, and D. P. van Vuuren (2010), Historical (1850-2000) gridded anthropogenic and biomass burning emissions of reactive gases and aerosols: methodology and application, *Atmos. Chem. Phys.*, *10* (15), 7017-7039, doi: 10.5194/acp-10-7017-2010.

Lau, K. M., M. K. Kim, and K. M. Kim (2006), Asian summer monsoon anomalies induced by aerosol direct forcing: the role of the Tibetan Plateau, *Climate Dyn.*, *26* (7-8), 855-864, doi: 10.1007/s00382-006-0114-z.

Lavanchy, V. M. H., H. W. Gäggeler, U. Schotterer, M. Schwikowski, and U. Baltensperger (1999), Historical record of carbonaceous particle concentrations from a European high-alpine glacier (Colle Gnifetti, Switzerland), *J. Geophys. Res.*, *104* (D17), 21227-21236, doi: 10.1029/1999JD900408.

Law, K. S., and A. Stohl (2007), Arctic air pollution: Origins and impacts, *Science*, *315* (5818), 1537-1540, doi: 10.1126/science.1137695.

Lee, K. B., M. W. Thring, and J. M. Beér (1962), On the rate of combustion of soot in a laminar soot flame, *Combustion and Flame*, *6*, 137-145.

Lee, S. H., D. M. Murphy, D. S. Thomson, and A. M. Middlebrook (2002), Chemical components of single particles measured with Particle Analysis by Laser Mass Spectrometry (PALMS) during the Atlanta SuperSite Project: Focus on organic/sulfate, lead, soot, and mineral particles, *J. Geophys. Res.*, *107* (D1-D2), 4003, doi: 10.1029/2000JD000011.

Lee, D. S., D. W. Fahey, P. M. Forster, R. C. N. Wit, L. L. Lim, B. Owen, and R. Sausen (2009), Aviation and global climate change in the 21st century, *Atmospheric Environment*, *43* (22-23), 3520-3537, doi: 10.1016/j.atmosenv.2009.04.024.

Lee, D. S., G. Pitari, V. Grewe, K. Gierens, J. E. Penner, A. Petzold, M. J. Prather, U. Schumann, A. Bais, T. Berntsen, D. Iachetti, L. L. Lim, and R. Sausen (2010), Transport impacts on atmosphere and climate: Aviation, *Atmos. Environ.*, *44* (37), 4678-4734, doi: 10.1016/j.atmosenv.2009.06.005.

Lefohn, A. S., J. D. Husar, and R. B. Husar (1999), Estimating historical anthropogenic global sulfur emission patterns for the period 1850-1990, *Atmos. Environ.*, *33* (21), 3435-3444.

Legrand, M., S. Preunkert, M. Schock, M. Cerqueira, A. Kasper-Giebl, J. Afonso, C. Pio, A. Gelencsér, and I. Dombrowski-Etchevers (2007), Major 20th century changes of carbonaceous aerosol components (EC, WinOC, DOC, HULIS, carboxylic acids, and cellulose) derived from Alpine ice cores, *J. Geophys. Res.*, *112* (D23), D23S11, doi: 10.1029/2006JD008080.

Lei, Y., Q. Zhang, K. B. He, and D. G. Streets (2011), Primary anthropogenic aerosol emission trends for China, 1990–2005, *Atmos. Chem. Phys.*, *11*, 931-954, doi: 10.5194/acp-11-931-2011.

Levy, R. C., L. A. Remer, S. Mattoo, E. F. Vermote, and Y. J. Kaufman (2007), Second-generating operational algorithm: Retrieval of aerosol properties over land from inversion of Moderate Resolution Imaging Spectroradiometer spectral reflectance, *J. Geophys. Res.*, *112*, D13211, doi: 10.1029/2006JD007811.

Lewis, K., W. P. Arnott, H. Moosmuller, and C. E. Wold (2008), Strong spectral variation of biomass smoke light absorption and single scattering albedo observed with a novel dual-wavelength photoacoustic instrument, *J. Geophys. Res.*, *113* (D16203), doi: 10.1029/2007JD009699.

Li, J., M. Posfai, P. V. Hobbs, and P. R. Buseck (2003), Individual aerosol particles from biomass burning in southern Africa: 2, Compositions and aging of inorganic particles, *J. Geophys. Res.*, *108* (D13), 8484, doi: 10.1029/2002JD002310.

Liley, J. B., D. Baumgardner, Y. Kondo, K. Kita, B. R. Blake, M. Koike, T. Machida, N. Takegawa, S. Kawakami, T. Shirai, and T. Ogawa (2003), Black carbon in aerosol during BIBLE B, *J. Geophys. Res.*, *108* (D3), doi: 10.1029/2001JD000845.

Lin, C.-I., M. Baker, and R. J. Charlson (1973), Absorption coefficient of atmospheric aerosol: a method for measurement, *Appl. Opt.*, *12* (6), 1356-1363.

Lindesay, J. A., M. O. Andreae, J. G. Goldammer, G. Harris, H. J.

Annegarn, M. Garstang, R. J. Scholes, and B. W. vanWilgen (1996), International geosphere-biosphere programme international global atmospheric chemistry SAFARI-92 field experiment: Background and overview, *J. Geophys. Res.*, *101* (D19), 23521-23530.

Liousse, C., J. E. Penner, C. Chuang, J. J. Walton, H. Eddleman, and H. Cachier (1996), A global three-dimensional model study of carbonaceous aerosols, *J. Geophys. Res.*, *101* (D14), 19411-19432.

Liston, G. E. (1995), Local advection of momentum, heat, and moisture during the melt of patchy snow covers, *J. Appl. Meteorol.*, *34* (7), 1705-1715.

Liston, G. E. (1999), Interrelationships among snow distribution, snowmelt, and snow cover depletion: Implications for atmospheric, hydrologic, and ecologic modeling, *J. Appl. Meteorol.*, *38* (10), 1474-1487.

Liston, G. E. (2004), Representing subgrid snow cover heterogeneities in regional and global models, *J. Climate*, *17* (6), 1381-1397.

Liston, G. E., and M. Sturm (2004), The role of winter sublimation in the Arctic moisture budget, *Nordic Hydrology*, *35* (4-5), 325-334.

Liu, X., J. E. Penner, S. J. Ghan, and M. Wang (2007), Inclusion of Ice Microphysics in the NCAR Community Atmospheric Model Version 3 (CAM3), *J. Climate*, *20*, 4526-4547, doi: 10.1175/JCL14264.1.

Liu, X. H., J. E. Penner, and M. H. Wang (2009a), Influence of anthropogenic sulfate and black carbon on upper tropospheric clouds in the NCAR CAM3 model coupled to the IMPACT global aerosol model, *J. Geophys. Res.*, *114* (D03), 204, doi: 10.1029/2008JD010492.

Liu, Y., J. R. Sun, and B. Yang (2009b), The effects of black carbon and sulphate aerosols in China regions on East Asia monsoons, *Tellus B*, *61* (4), 642-656, doi: 10.1111/j.1600-0889.2009.00427.x.

Liu, Y. Q., J. Stanturf, and S. Goodrick (2010), Trends in global wildfire potential in a changing climate, *Forest Ecol. Manag.*, *259*, 685-697, doi: 10.1016/j.foreco.2009.09.002.

Liu, X., R. C. Easter, S. J. Ghan, R. Zaveri, P. Rasch, J.-F. Lamarque, A. Gettelman, H. Morrison, F. Vitt, A. Conley, S. Park, R. Neale, C. Hannay, A. Eckman, P. Hess, N. Mahowald, W. Collins, M. Iacono, C. Bretherton, M. Flanner, and D. Mitchell (2011), Toward a minimal representation of aerosol direct and indirect effects: Model description and evaluation, *Geosci. Model Dev. Discuss*, *4*, 3485-3598, doi: 10.5194/gmdd-4-3485-2011.

Livingston, J. M., V. N. Kapustin, B. Schmid, P. B. Russell, P. K. Quinn, T. S. Bates, P. A. Durkee, P. J. Smith, V. Freudenthaler, M. Wiegner, D. S. Covert, S. Gasso, D. Hegg, D. R. Collins, R. C. Flagan, J. H. Seinfeld, V. Vitale, and C. Tomasi (2000), Shipboard sunphotometer measurements of aerosol optical depth spectra and columnar water vapor during ACE-2, and comparison with selected land, ship, aircraft, and satellite measurements, *Tellus B*, *52* (2), 594-619.

Lobert, J. M., D. H. Scharffe, W.-M. Hao, T. A. Kuhlbusch, R. Seuwen, P. Warneck, and P. J. Crutzen (1991), Experimental evaluation of biomass burning emissions: nitrogen and carbon containing compounds, in *Global biomass burning: Atmospheric, climatic, and biospheric implications*, edited by J. S. Levine, Massachussetts Institute of Technology.

Lohmann, U. (2002), A glaciation indirect aerosol effect caused by soot aerosols, *Geophys. Res. Lett.*, *29* (4), 1052, doi: 10.1029/2001GL014357.

Lohmann, U., and J. Feichter (2001), Can the direct and semi-direct aerosol effect compete with the indirect effect on a global scale?, *Geophys. Res. Lett.*, *28* (1), 159-161, doi: 10.1029/2000GL012051.

Lohmann, U., and J. Feichter (2005), Global indirect aerosol effects: A review, *Atmos. Chem. Phys.*, *5*, 715-737.

Lohmann, U., and K. Diehl (2006), Sensitivity studies of the importance of dust ice nuclei for the indirect aerosol effect on stratiform mixed-phase clouds, *J. Atmos. Sci.*, *63* (3), 968-982.

Lohmann, U., P. Stier, C. Hoose, S. Ferrachat, S. Kloster, E. Roeckner, and J. Zhang (2007), Cloud microphysics and aerosol indirect effects in the global climate model ECHAM5-HAM, *Atmos. Chem. Phys.*, *7* (13), 3425-3446.

Lohmann, U., and C. Hoose (2009), Sensitivity studies of different aerosol indirect effects in mixed-phase clouds, *Atmos. Chem. Phys.*, *9* (22), 8917-8934.

Lohmann, U., L. Rotstayn, T. Storelvmo, A. Jones, S. Menon, J. Quaas, A. M. L. Ekman, D. Koch, and R. Ruedy (2010), Total aerosol effect: radiative forcing or radiative flux perturbation?, *Atmos. Chem. Phys.*, *10* (7), 3235-3246, doi: 10.5194/acp-11-931-2011.

Lu, Z., Q. Zhang, and D. G. Streets (2011), Sulfur dioxide and primary carbonaceous aerosol emissions in China and India, 1996-2010, *Atmos. Chem. Phys.*, *11*, 9839-9864, doi: 10.5194/acp-11-9839-2011.

Lubin, D., and A. S. Simpson (1994), The longwave emission signature of urban pollution: Radiometric FTIR measurement, *Geophys. Res. Lett.*, *21* (1), 37-40, doi: 10.1029/93GL03374.

Lund, M. T., and T. Berntsen (2011), Parameterization of black carbon aging in the OsloCTM2 and implications for regional transport to the Arctic, *Atmos. Chem. Phys. Discussions*, *11*, 32499-32534, doi: 10.5194/acpd-11-32499-2011.

Luo, C., N. Mahowald, and J. d. Corral (2003), Sensitivity study of meteorological parameters on mineral aerosol mobilization, transport and distribution, *J. Geophys. Res.*, *108* (D15), 4447, doi: 10.1029/2003JD0003483.

MacCarty, N., D. Still, and D. Ogle (2010), Fuel use and emissions performance on fifty cooking stoves in the laboratory and related benchmarks of performance, *Energ. Sust. Dev.*, *14*, 161-171.

Mack, M. C., M. S. Bret-Harte, T. N. Hollingsworth, R. R. Jandt, E. A. G. Schuur, G. R. Shaver, and D. L. Verbyla (2011), Carbon loss from an unprecedented Arctic tundra wildfire, *Nature*, *475* (7357), 489-492.

Magi, B. I., P. V. Hobbs, B. Schmid, and J. Redemann (2003), Vertical profiles of light scattering, light absorption, and single scattering albedo during the dry, biomass burning season in southern Africa and comparisons of in situ and remote sensing measurements of aerosol optical depths, *J. Geophys. Res.*, *108* (D13), 8504, doi: 10.1029/2002JD002361.

Mahowald, N. M., D. R. Muhs, S. Levis, P. J. Rasch, M. Yoshioka, C. S. Zender, and C. Luo (2006), Change in atmospheric mineral aerosols in response to climate: Last glacial period, preindustrial, modern, and doubled carbon dioxide climates, *J. Geophys. Res.*, *111* (D10202), doi: 10.1029/2005JD006653.

Malm, W. C., J. F. Sisler, D. Huffman, R. A. Eldred, and T. A. Cahill (1994), Spatial and seasonal trends in particle concentration and optical extinction in the United States, *J. Geophys. Res.*, *99* (D1), 1347-1370.

Manne, A. S., and R. G. Richels (2001), An alternative approach to establishing trade-offs among greenhouse gases, *Nature*, *410* (6829), 675-677.

Manoli, E., D. Voutsa, and C. Samara (2002), Chemical characterization and source identification/apportionment of fine and coarse air particles in Thessaloniki, Greece, *Atmos. Environ.*, *36* (6), 949-961.

Marcolli, C., S. Gedamke, T. Peter, and B. Zobrist (2007), Efficiency of immersion mode ice nucleation on surrogates of

mineral dust, *Atmos. Chem. Phys.*, *7* (19), 5081-5091, doi: 10.5194/acp-7-5081-2007.

Marcq, S., P. Laj, J. C. Roger, P. Villani, K. Sellegri, P. Bonasoni, A. Marinoni, P. Cristofanelli, G. P. Verza, and M. Bergin (2010), Aerosol optical properties and radiative forcing in the high Himalaya based on measurements at the Nepal Climate Observatory-Pyramid site (5079 m a.s.l.), *Atmos. Chem. Phys.*, *10* (13), 5859-5872, doi: 10.5194/acp-10-5859-2010.

Marinoni, A., P. Cristofanelli, P. Laj, R. Duchi, F. Calzolari, S. Decesari, K. Sellegri, E. Vuillermoz, G. P. Verza, P. Villani, and P. Bonasoni (2010), Aerosol mass and black carbon concentrations, two year-round observations at NCO-P (5079 m, Southern Himalayas), *Atmos. Chem. Phys. Discuss.*, *10* (3), 8379-8413, doi: 10.5194/acpd-10-8379-2010.

Marlon, J. R., P. J. Bartlein, C. Carcaillet, D. G. Gavin, S. P. Harrison, P. E. Higuera, F. Joos, M. J. Power, and I. C. Prentice (2008), Climate and human influences on global biomass burning over the past two millennia, *Nature Geoscience*, *1*, 697-702, doi: 10.1038/ngeo313.

Martins, J. V., P. Artaxo, C. Liousse, J. S. Reid, P. V. Hobbs, and Y. Kaufman (1998a), Effects of black carbon content, particle size, and mixing on light absorption by aerosol from biomass burning in Brazil, *J. Geophys. Res.*, *103* (D24), 32041-32050.

Martins, J. V., P. V. Hobbs, R. E. Weiss, and P. Artaxo (1998b), Sphericity and morphology of smoke particles from biomass burning in Brazil, *J. Geophys. Res.*, *103* (D24), 32051-32057.

Massey, R. (1997), No-tillage and conservation tillage: Economic considerations, University of Missouri Extension Publication G355, University of Missouri, Columbia, MO.

Massie, S. T., A. Heymsfield, C. Schmitt, D. Muller, and P. Seifert (2007), Aerosol indirect effects as a function of cloud top pressure, *J. Geophys. Res.*, *112* (D6), 202, doi: 10.1029/2006JD007383.

Matzl, M., and M. Schneebeli (2006), Measuring specific surface area of snow by near infrared photography, *J. Glaciol.*, *52*, 558-564.

Maykut, G. A., and N. Untersteiner (1971), Some results from a time-dependent thermodynamic model of sea ice, *J. Geophys. Res.*, *76* (6), 1550-1575, doi: 10.1029/JC076i006p01550.

Mayol-Bracero, O. L., R. Gabriel, M. O. Andreae, T. W. Kirchstetter, T. Novakov, J. Ogren, P. Sheridan, and D. G. Streets (2002), Carbonaceous aerosols over the Indian Ocean during the Indian Ocean Experiment (INDOEX): Chemical characterization, optical properties, and probable sources, *J. Geophys. Res.*, *107* (D19), 8030.

McConnell, J. R., R. Edwards, G. L. Kok, M. G. Flanner, C. S. Zender, E. S. Saltzman, J. R. Banta, D. R. Pasteris, M. M. Carter, and J. D. W. Kahl (2007), 20th-century industrial black carbon emissions altered Arctic climate forcing, *Science*, *317* (5843), 1381-1384, doi: 10.1126/science.1144856.

McConnell, J. R., and R. Edwards (2008), Coal burning leaves toxic heavy metal legacy in the Arctic, *P. Natl. Acad. Sci. USA*, *105* (34), 12140-12144, doi: 10.1073/pnas.0803564105.

McDonald, J. D., B. Zielinska, E. M. Fujita, J. C. Sagebiel, J. C. Chow, and J. G. Watson (2000), Fine particle and gaseous emission rates from residential wood combustion, *Environ. Sci. Technol.*, *34*, 2080-2091.

McFarquhar, G. M., and H. L. Wang (2006), Effects of aerosols on trade wind cumuli over the Indian Ocean: Model simulations, *Quart J. Roy. Meteor. Soc.*, *132* (616), 821-843, doi: 10.1256/qj.04.179.

Medalia, A. I., and F. A. Heckman (1969), Morphology of aggregates-- II. Size and shape factors of carbon black aggregates from electron microscopy, *Carbon*, *7*, 569-582.

Medalia, A. I., and L. W. Richards (1972), Tinting strength of carbon black, *J. Colloid Interf. Sci.*, *40* (2), 233-252.

Meehl, G. A., J. M. Arblaster, and W. D. Collins (2008), Effects of black carbon aerosols on the Indian monsoon, *J. Climate*, *21* (12), 2869-2882, doi: 10.1175/2007jcli1777.1.

Mehta, S., and C. Shahpar (2004), The health benefits of interventions to reduce indoor air pollution from solid fuel use: a cost-effectiveness analysis, *Energy for Sustainable Development*, *8* (3), doi: 10.1016/S0973-0826(08)60466-4.

Menon, S., J. Hansen, L. Nazarenko, and Y. F. Luo (2002), Climate effects of black carbon aerosols in China and India, *Science*, *297* (5590), 2250-2253.

Menon, S., and A. D. Genio (2007), Evaluating the impacts of carbonaceous aerosols on clouds and climate, in *Human-Induced Climate Change: An Interdisciplinary Assessment* edited by M. E. Schlesinger, H. Kheshgi, J. B. Smith, F. C. D. L. Chesnaye, J. M. Reilly, T. Wilson and C. Kolstad, 34-48 pp., Cambridge University Press.

Menon, S., D. Koch, G. Beig, S. Sahu, J. Fasullo, and D. Orlikowski (2010), Black carbon aerosols and the third polar ice cap, *Atmos. Chem. Phys.*, *10* (10), 4559-4571, doi: 10.5194/acp-10-4559-2010.

Merikanto, J., D. V. Spracklen, G. W. Mann, S. J. Pickering, and K. S. Carslaw (2009), Impact of nucleation on global CCN, *Atmos. Chem. Phys.*, *9* (21), 8601-8616.

Mikhailov, E. F., S. S. Vlasenko, I. A. Podgorny, V. Ramanathan, and C. E. Corrigan (2006), Optical properties of soot-water drop agglomerates: An experimental study, *J. Geophys. Res.*, *111* (D07209), doi: 10.1029/2005JD006389.

Miller, R. L., I. Tegen, and J. Perlwitz (2004), Surface radiative forcing by soil dust aerosols and the hydrologic cycle, *J. Geophys. Res.*, *109* (D4), 203, doi: 10.1029/2003JD004085.

Miller, S. M., D. M. Matross, A. E. Andrews, D. B. Millet, M. Longo, E. W. Gottlieb, A. I. Hirsch, C. Gerbig, J. C. Lin, B. C. Daube, R. C. Hudman, P. L. S. Dias, V. Y. Chow, and S. C. Wofsy (2008), Sources of carbon monoxide and formaldehyde in North America determined from high-resolution atmospheric data, *Atmos. Chem. Phys.*, *8* (24), 7673-7696.

Millstein, D. E., and R. A. Harley (2010), Effects of retrofitting emission control systems on in-use heavy diesel vehicles, *Environ. Sci. Technol.*, *44* (13), 5042-5048, doi: 10.1021/es1006669.

Ming, Y., V. Ramaswamy, P. A. Ginoux, and L. H. Horowitz (2005), Direct radiative forcing of anthropogenic organic aerosol *J. Geophys. Res.*, *110*, D20208, doi: 10.1029/2004JD005573.

Ming, J., H. Cachier, C. Xiao, D. Qin, S. Kang, S. Hou, and J. Xu (2008), Black carbon record based on a shallow Himalayan ice core and its climatic implications, *Atmos. Chem. Phys.*, *8* (5), 1343-1352, doi: 10.5194/acp-8-1343-2008.

Ming, J., C. Xiao, H. Cachier, D. Qin, X. Qin, Z. Li, and J. Pu (2009), Black Carbon (BC) in the snow of glaciers in west China and its potential effects on albedos, *Atmos. Res.*, *92* (1), 114-123.

Ming, Y., V. Ramaswamy, and G. Persad (2010), Two opposing effects of absorbing aerosols on global-mean precipitation, *Geophys. Res. Lett.*, *37* (L13), 701, doi: 10.1029/2010GL042895.

Minikin, A., A. Petzold, J. Strom, R. Krejci, M. Seifert, P. van Velthoven, H. Schlager, and U. Schumann (2003), Aircraft observations of the upper tropospheric fine particle aerosol in the Northern and Southern Hemispheres at midlatitudes, *Geophys. Res. Lett.*, *30* (10), 1503, doi: 10.1029/2002GL016458.

Minvielle, F., G. Cautenet, M. O. Andreae, F. Lasserre, G. Foret, S. Cautenet, J. F. Leon, O. L. Mayol-Bracero, R. Gabriel, P. Chazette, and R. Roca (2004), Modelling the transport of aerosols during INDOEX 1999 and comparison with experimental data - 1: carbonaceous aerosol distribution, *Atmos. Environ.*, *38* (12), 1811-1822, doi:

10.1016/j.atmosenv.2003.07.017.

Moffet, R. C., and K. A. Prather (2009), In-situ measurements of the mixing state and optical properties of soot with implications for radiative forcing estimates, *P. Natl. Acad. Sci. USA*, *106* (29), 11872-11877.

Möhler, S., S. Büttner, C. Linke, M. Schnaiter, H. Saathoff, O. Stetzer, R. Wagner, M. Krämer, A. Mangold, V. Ebert, and U. Schurath (2005a), Effect of sulfuric acid coating on heterogeneous ice nucleation by soot aerosol particles, *J. Geophys. Res.*, *110*, D11210, doi: 10.1029/2004JD005169.

Möhler, O., C. Linke, H. Saathoff, M. Schnaiter, R. Wagner, A. Mangold, M. Kramer, and U. Schurath (2005b), Ice nucleation on flame soot aerosol of different organic carbon content, *Meteor. Z.*, *14* (4), 477-484, doi: 10.1127/0941-2948/2005/0055.

Molina, M., D. Zaelke, K. M. Sarma, S. O. Andersen, V. Ramanathan, and D. Kaniaru (2009), Reducing abrupt climate change risk using the Montreal Protocol and other regulatory actions to complement cuts in CO_2 emissions, *P. Natl. Acad. Sci. USA*, *106* (49), 20616-20621, doi:10.1073/pnas.0902568106.

Mollicone, D., H. D. Eva, and F. Achard (2006), Human role in Russian wild fires, *Nature*, *440* (7083), 436-437, doi: 10.1038/440436a.

Montgomery, W. D., R. E. Baron, and S. D. Tuladhar (2009), An analysis of black carbon mitigation as a response to climate change, Report prepared for the Copenhagen Consensus on Climate, Copenhagen Consensus Center, Frederiksberg, Denmark.

Moosmüller, H., W. P. Arnott, C. F. Rogers, J. L. Bowen, J. A. Gillies, W. R. Pierson, J. F. Collins, T. D. Durbin, and J. M. Norbeck (2001), Time-resolved characterization of diesel particulate emissions. 2. Instruments for elemental and organic carbon measurements, *Environ. Sci. Technol.*, *35* (10), 1935-1942.

Morrison, H., and A. Gettelman (2008), A new two-moment bulk stratiform cloud microphysics scheme in the community atmosphere model, version 3 (CAM3). Part I: Description and numerical tests *J. Climate*, *21* (15), 3642-3659, doi: 10.1175/2008JCL12105.1.

Moss, R. H., J. A. Edmonds, K. A. Hibbard, M. R. Manning, S. K. Rose, D. P. v. Vuuren, T. R. Carter, S. Emori, M. Kainuma, T. Kram, G. A. Meehl, J. F. B. Mitchell, N. Nakicenovic, K. Riahi, S. J. Smith, R. J. Stouffer, A. M. Thomson, J. P. Weyant, and T. J. Wilbanks (2010), The next generation of scenarios for climate change research and assessment, *Nature*, *463*, 747-756, doi: 10.1038/nature08823.

Moteki, N., and Y. Kondo (2007), Effects of mixing state on black carbon measurements by laser-induced incandescence, *Aerosol Sci. Technol.*, *41* (4), 398-417, doi: 10.1080/02786820701199728.

Moteki, N., and Y. Kondo (2010), Dependence of laser-induced incandescence on physical properties of black carbon aerosols: Measurements and theoretical interpretation, *Aerosol Sci. Technol.*, *44* (8), 663-675, doi: 10.1080/02786826.2010.484450.

Moteki, N., Y. Kondo, Y. Miyazaki, N. Takegawa, Y. Komazaki, G. Kurata, T. Shirai, D. R. Blake, T. Miyakawa, and M. Koike (2007), Evolution of mixing state of black carbon particles: Aircraft measurements over the western Pacific in March 2004, *Geophys. Res. Lett.*, *34* (L11803), doi: 10.1029/2006GL028943.

Moteki, N., Y. Kondo, and S. Nakamura (2010), Method to measure refractive indices of small nonspherical particles: Application to black carbon particles, *J. Aerosol. Sci.*, *41* (5), 513-521, doi: 10.1016/J.JAEROSCI.2010.02.013.

Moulliot, F., and C. B. Field (2005), Fire history and the global carbon budget: a 1°×1° fire history reconstruction for the 20th century, *Global Change Biology*, *11*, 398-420, doi: 10.1111/j.1365-2486.2005.00920.x.

Mugica, V., E. Ortiz, L. Molina, A. De Vizcaya-Ruiz, A. Nebot, R. Quintana, J. Aguilar, and E. Alcantara (2009), PM composition and source reconciliation in Mexico City, *Atmos. Environ.*, *43* (32), 5068-5074, doi: 10.1016/j.atmosenv.2009.06.051.

Muhlbauer, A., and U. Lohmann (2009), Sensitivity studies of aerosol-cloud interactions in mixed-phase orographic precipitation, *J. Atmos. Sci.*, *66* (9), 2517-2538, doi: 10.1175/2009jas3001.1.

Mukunda, H. S., S. Dasappa, P. J. Paul, N. K. S. Rajan, M. Yagnaraman, D. R. Kumar, and M. Deogaonkar (2010), Gasifier stoves - science, technology and field outreach, *Curr. Sci.*, *98* (5), 627-638.

Mullins, J., and A. Williams (1987), The optical properties of soot: a comparison between experimental and theoretical values, *Fuel*, *66*, 277-280.

Murphy, D. M., and T. Koop (2005), Review of the vapour pressures of ice and supercooled water for atmospheric applications, *Quart J. Roy. Meteor. Soc.*, *131* (608), 1539-1565, doi: 10.1256/qj.04.94.

Murphy, D. M., D. J. Cziczo, P. K. Hudson, and D. S. Thomson (2007), Carbonaceous material in aerosol particles in the lower stratosphere and tropopause region, *J. Geophys. Res.*, *112* (D4), 203, doi: 10.1029/2006JD007297.

Murphy, D. M., S. Solomon, R. W. Portmann, K. H. Rosenlof, P. M. Forster, and T. Wong (2009), An observationally based energy balance for the Earth since 1950, *J. Geophys. Res.*, *114* (D17), 107, doi: 10.1029/2009JD012105.

Murphy, D. M., J. C. Chow, E. M. Leibensperger, W. C. Malm, M. Pitchford, B. A. Schichtel, J. G. Watson, and W. H. White (2011), Decreases in elemental carbon and fine particle mass in the United States, *Atmos. Chem. Phys.*, *11*, 4679-4686, doi: 10.5194/acp-11-4679-2011.

Myhre, G., T. F. Berglen, M. Johnsrud, C. R. Hoyle, T. K. Berntsen, S. A. Christopher, D. W. Fahey, I. S. A. Isaksen, T. A. Jones, R. A. Kahn, N. Loeb, P. Quinn, L. Remer, J. P. Schwarz, and K. E. Yttri (2009), Modelled radiative forcing of the direct aerosol effect with multi-observation evaluation, *Atmos. Chem. Phys.*, *9*, 1365-1392.

Naeher, L. P., M. Brauer, M. Lipsett, J. T. Zelikoff, C. D. Simpson, J. Q. Koenig, and K. R. Smith (2007), Woodsmoke health effects: A review, *Inhal. Toxicol.*, *19* (1), 67-106.

Nagashima, T., H. Shiogama, T. Yokohata, T. Takemura, S. A. Crooks, and T. Nozawa (2006), Effect of carbonaceous aerosols on surface temperature in the mid twentieth century, *Geophys. Res. Lett.*, *33* (4), 702, doi: 10.1029/2005GL024887.

Naik, V., D. L. Mauzerall, L. W. Horowitz, M. D. Schwarzkopf, V. Ramaswamy, and M. Oppenheimer (2007), On the sensitivity of radiative forcing from biomass burning aerosols and ozone to emission location, *Geophys. Res. Lett.*, *34* (3), doi: L03818, doi:10.1029/2006GL028149.

Nakawo, M., C. F. Raymond, and A. Fountain (Eds.) (2000), *Debris-covered glaciers*, 288 pp.

Nenes, A., and J. H. Seinfeld (2003), Parameterization of cloud droplet formation in global climate models, *J. Geophys. Res.*, *108* (D14), doi: 10.1029/2002JD002911.

Neususs, C., H. Wex, W. Birmili, A. Wiedensohler, C. Koziar, B. Busch, E. Bruggemann, T. Gnauk, M. Ebert, and D. S. Covert (2002), Characterization and parameterization of atmospheric particle number-, mass-, and chemical-size distributions in central Europe during LACE 98 and MINT, *J. Geophys. Res.*, *107* (D21), 8127, doi: 10.1029/2001JD000514.

Nguyen, H. N., B. G. Martinsson, J. B. Wagner, E. Carlemalm, M. Ebert, S. Weinbruch, C. A. M. Brenninkmeijer, J. Heintzenberg, M. Hermann, T. Schuck, P. F. J. van Velthoven, and A. Zahn

(2008), Chemical composition and morphology of individual aerosol particles from a CARIBIC flight at 10 km altitude between 50 degrees N and 30 degrees S, *J. Geophys. Res.*, *113* (D23), 209, doi: 10.1029/2008JD009956.

Novakov, T., and C. E. Corrigan (1995), Thermal characterization of biomass smoke particles, *Microchim. Acta*, *119*, 157-166.

Novakov, T., M. O. Andreae, R. Gabriel, T. W. Kirchstetter, O. L. Mayol-Bracero, and V. Ramanathan (2000), Origin of carbonaceous aerosols over the tropical Indian Ocean: Biomass burning or fossil fuels?, *Geophys. Res. Lett.*, *27* (24), 4061-4064.

Novakov, T., V. Ramanathan, J. E. Hansen, T. W. Kirchstetter, M. Sato, J. E. Sinton, and J. A. Satahye (2003), Large historical changes of fossil-fuel black carbon aerosols, *Geophys. Res. Lett.*, *30* (6), 1324, doi: 10.1029/2002GL016345.

Novakov, T., and J. E. Hansen (2004), Black carbon emissions in the United Kingdom during the past four decades: an empirical analysis, *Atmos. Environ.*, *38* (25), 4155-4163.

NRC (2011), National Research Council. Climate Stabilization Targets: Emissions, Concentrations, and Impacts over Decades to Millennia, The National Academies Press, Washington, DC.

Oanh, N. T. K., N. Upadhyaya, Y. H. Zhuang, Z. P. Hao, D. V. S. Murthy, P. Lestari, J. T. Villarin, K. Chengchua, H. X. Co, N. T. Dung, and E. S. Lindgren (2006), Particulate air pollution in six Asian cities: Spatial and temporal distributions, and associated sources, *Atmos. Environ.*, *40* (18), 3367-3380, doi: 10.1016/j.atmosenv.2006.01.050.

O'Donnell, D., K. Tsigaridis, and J. Feichter (2011), Estimating the direct and indirect effects of secondary organic aerosols using ECHAM5-HAM, *Atmos. Chem. Phys.*, *11*, 8635-8659, doi: 10.519/acp-11-8635-2011.

Ogren, J. A., and R. J. Charlson (1983), Elemental carbon in the atmosphere: cycle and lifetime, *Tellus*, *35B*, 241-254.

Ohara, T., H. Akimoto, J. Kurokawa, N. Horii, K. Yamaji, X. Yan, and T. Hayasaka (2007), An Asian emission inventory of anthropogenic emission sources for the period 1980-2020, *Atmos. Chem. Phys.*, *7* (16), 4419-4444.

Omar, A. H., D. M. Winker, M. A. Vaughan, Y. Hu, C. R. Trepte, R. A. Ferrare, K.-P. Lee, C. A. Hostetler, C. Kittaka, R. R. Rogers, R. E. Kuehn, and Z. Liu (2009), The CALIPSO Automated Aerosol Classification and Lidar Ratio Selection Algorithm, *J. Atmos. Oceanic Technol.*, *26*, 1994–2014, doi: 10.1175/2009JTECHA1231.1.

O'Neill, B. C. (2000), The jury is still out on global warming potentials, *Clim. Change*, *44* (427-443).

Ostro, B., M. Lipsett, P. Reynolds, D. Goldberg, A. Hertz, C. Garcia, K. D. Henderson, and L. Bernstein (2010), Long-term exposure to constituents of fine particulate air pollution and mortality: Results from the California teachers study, *Environ. Health Perspect.*, *118* (3), 363-369, doi: 10.1289/ehp.0901181.

Ottmar, R. D., J. L. Peterson, B. Leenhouts, and J. E. Core (2001), Smoke management: techniques to reduce or redistribute emissions. In: Smoke management guide for prescribed and wildland fire: 2001 Edition, National Wildfire Coordination Group.

Paatero, P. (1997), Least squares formulation of robust non-negative factor analysis, *Chemometr. Intell. Lab.*, *37* (1), 23-35.

Painter, T. H., A. P. Barrett, C. C. Landry, J. C. Neff, M. P. Cassidy, C. R. Lawrence, K. E. McBride, and G. L. Farmer (2007), Impact of disturbed desert soils on duration of mountain snow cover, *Geophys. Res. Lett.*, *34* (12), 502, doi: 10.1029/2007GL030284.

Parashar, D. C., R. Gadi, T. K. Mandal, and A. P. Mitra (2005), Carbonaceous aerosol emissions from India, *Atmos. Environ.*, *39* (40), 7861-7871, doi: 10.1016/j.atmosenv.2005.08.034.

Paris, J. D., A. Stohl, P. Nédélec, M. Y. Arshinov, M. V. Panchenko, V. P. Shmargunov, K. S. Law, B. D. Belan, and P. Ciais (2009), Wildfire smoke in the Siberian Arctic in summer: source characterization and plume evolution from airborne measurements, *Atmos. Chem. Phys.*, *9* (23), 9315-9327, doi: 10.5194/acp-9-9315-2009.

Park, K., D. B. Kittelson, M. R. Zachariah, and P. H. McMurry (2004), Measurement of inherent material density of nanoparticle agglomerates, *J. Nanopart. Res.*, *6* (267-272).

Park, R. J., D. J. Jacob, M. Chin, and R. V. Martin (2003), Sources of carbonaceous aerosols over the United States and implications for natural visibility, *J. Geophys. Res.*, *108* (D12), 4355, doi: 10.1029/2002JD003190.

Park, R. J., M. J. Kim, J. I. Jeong, D. Youn, and S. Kim (2010), A contribution of brown carbon aerosol to the aerosol light absorption and its radiative forcing in East Asia, *Atmos. Environ.*, *44* (11), 1414-1421, doi: 10.1016/j.atmosenv.2010.01.042.

Park, S. H., S. L. Gong, V. S. Bouchet, W. Gong, P. A. Makar, M. D. Moran, C. A. Stroud, and J. Zhang (2011), Effects of black carbon aging on air quality predictions and direct radiative forcing estimation, *Tellus B*, *63*, 1026-1039, doi: 10.1111/j.1600-0889.2011.00558.x.

Parrish, D. D., D. T. Allen, T. S. Bates, M. Estes, F. C. Fehsenfeld, G. Feingold, R. Ferrare, R. M. Hardesty, J. F. Meagher, J. W. Nielsen-Gammon, R. B. Pierce, T. B. Ryerson, J. H. Seinfeld, and E. J. Williams (2009), Overview of the second texas air quality study (TexAQS II) and the gulf of mexico atmospheric composition and climate study (GoMACCS), *J. Geophys. Res.*, *114* (D00f13), doi: 10.1029/2009JD011842.

Patterson, E. M., and C. K. McMahon (1984), Absorption characteristics of forest fire particulate matter, *Atmos. Environ.*, *18* (11), 2541-2551.

Pechony, O., and D. T. Shindell (2010), Driving forces of global wildfires over the past millennium and the forthcoming century, *P. Natl. Acad. Sci. USA*, *107* (45), 19167-19170, doi: 10.1073/pnas.1003669107.

Penner, J. E., H. Eddleman, and T. Novakov (1993), Towards the development of a global inventory for black carbon emissions, *Atmos. Environ.*, *27A* (8), 1277-1295.

Penner, J. E., C. C. Chuang, and K. Grant (1998), Climate forcing by carbonaceous and sulfate aerosols, *Climate Dyn.*, *14* (12), 839-851.

Penner, J. E., M. Andreae, H. Annegarn, L. Barrie, J. Feichter, D. Hegg, A. Jayaraman, R. Leaitch, D. Murphy, J. Nganga, and G. Pitari (2001), Aerosols: Their direct and indirect effects, in IPCC, 2001: Climate Change 2001: The Scientific Basis. Contribution of Working Group I to the Third Assessment Report of the Intergovernmental Panel on Climate Change, 289-348 pp., Cambridge University Press, Cambridge, United Kingdom and New York, NY, USA.

Penner, J. E., S. Y. Zhang, and C. C. Chuang (2003), Soot and smoke aerosol may not warm climate, *J. Geophys. Res.*, *108* (D21), 4657, doi: 10.1029/2003JD003409.

Penner, J. E., Y. Chen, M. Wang, and X. Liu (2009), Possible influence of anthropogenic aerosols on cirrus clouds and anthropogenic forcing, *Atmos. Chem. Phys.*, *9* (3), 879-896.

Perlwitz, J., and R. L. Miller (2010), Cloud cover increase with increasing aerosol absorptivity: A counterexample to the conventional semidirect aerosol effect, *J. Geophys. Res.*, *115* (D08), 203, doi: 10.1029/2009JD012637.

Perovich, D. K., T. C. Grenfell, B. Light, and P. V. Hobbs (2002), Seasonal evolution of the albedo of multiyear Arctic sea ice, *J. Geophys. Res.*, *107* (C10), 8044, doi: 10.1029/2000JC000438.

Petters, M. D., M. T. Parsons, A. J. Prenni, P. J. DeMott, S. M.

Kreidenweis, C. M. Carrico, A. P. Sullivan, G. R. McMeeking, E. Levin, C. E. Wold, J. L. Collett, and H. Moosmuller (2009), Ice nuclei emissions from biomass burning, *J. Geophys. Res.*, *114* (D07), 209, doi: 10.1029/2008JD011532.

Petzold, A., J. Strom, S. Ohlsson, and F. P. Schroder (1998), Elemental composition and morphology of ice-crystal residual particles in cirrus clouds and contrails, *Atmos. Res.*, *49* (1), 21-34.

Petzold, A., H. Schloesser, P. J. Sheridan, W. P. Arnott, J. A. Ogren, and A. Virkkula (2005a), Evaluation of multiangle absorption photometry for measuring aerosol light absorption, *Aerosol Sci. Technol.*, *39*, 40-51.

Petzold, A., M. Gysel, X. Vancassel, R. Hitzenberger, H. Puxbaum, S. Vrochticky, E. Weingartner, U. Baltensperger, and P. Mirabel (2005b), On the effects of organic matter and sulphur-containing compounds on the CCN activation of combustion particles, *Atmos. Chem. Phys.*, *5*, 3187-3203.

Philippin, S., A. Wiedensohler, and F. Stratmann (2004), Measurements of non-volatile fractions of pollution aerosols with an eight-tube volatility tandem differential mobility analyzer (VTDMA-8), *J. Aerosol. Sci.*, *35* (2), 185-203, doi: 10.1016/j.jaerosci.2003.07.004.

Phillips, V. T. J., P. J. DeMott, and C. Andronache (2008), An empirical parameterization of heterogeneous ice nucleation for multiple chemical species of aerosol, *J. Atmos. Sci.*, *65* (9), 2757-2783, doi: 10.1175/2007jas2546.1.

Polenske, K. R., and F. C. McMichael (2002), A Chinese cokemaking process-flow model for energy and environmental analyses, *Energ. Policy*, *30* (10), 865-883, doi: 10.1016/S0301-4215(01)00147-1.

Polyakov, I. V., G. V. Alekseev, R. V. Bekryaev, U. Bhatt, R. L. Colony, M. A. Johnson, V. P. Karklin, A. P. Makshtas, D. Walsh, and A. V. Yulin (2002), Observationally based assessment of polar amplification of global warming, *Geophys. Res. Lett.*, *29* (18), 1878, doi: 10.1029/2001GL011111.

Pope, C. A., M. Ezzati, and D. W. Dockery (2009), Fine-particulate air pollution and life expectancy in the united states, *N. Engl. J. Med.*, *360* (4), 376-386.

Popovicheva, O., N. M. Persiantseva, N. K. Shonija, P. Demott, K. Koehler, M. Petters, S. Kreidenweis, V. Tishkova, B. Demirdjian, and J. Suzanne (2008), Water interaction with hydrophobic and hydrophilic soot particles, *Phys. Chem. Chem. Phys.*, *10*, 2332-2344, doi: 10.1039/B718944N.

Pósfai, M., J. R. Anderson, P. R. Buseck, and H. Sievering (1999), Soot and sulfate particles in the remote marine troposphere, *J. Geophys. Res.*, *104* (D17), 21685-21693.

Pósfai, M., R. Simonics, J. Li, P. V. Hobbs, and P. R. Buseck (2003), Individual aerosol particles from biomass burning in southern Africa: 1. Compositions and size distributions of carbonaceous particles, *J. Geophys. Res.*, *108* (D13), 8483, doi: 10.1029/2002JD002291.

Power, M. J., J. Marlon, N. Ortiz, P. J. Bartlein, S. P. Harrison, F. E. Mayle, A. Ballouche, R. H. W. Bradshaw, C. Carcaillet, C. Cordova, S. Mooney, P. I. Moreno, I. C. Prentice, K. Thonicke, W. Tinner, C. Whitlock, Y. Zhang, Y. Zhao, A. A. Ali, R. S. Anderson, R. Beer, H. Behling, C. Briles, K. J. Brown, A. Brunelle, M. Bush, P. Camill, G. Q. Chu, J. Clark, D. Colombaroli, S. Connor, A.-L. Daniau, M. Daniels, J. Dodson, E. Doughty, M. E. Edwards, W. Finsinger, D. Foster, J. Frechette, M.-J. Gaillard, D. G. Gavin, E. Gobet, S. Haberle, D. J. Hallett, P. Higuera, G. Hope, S. Horn, J. Inoue, P. Kaltenrieder, L. Kennedy, Z. C. Kong, C. Larsen, C. J. Long, J. Lynch, E. A. Lynch, M. McGlone, S. Meeks, S. Mensing, G. Meyer, T. Minckley, J. Mohr, D. M. Nelson, J. New, R. Newnham, R. Noti, W. Oswald, J. Pierce, P. J. H. Richard, C. Rowe, M. F. S. Goni, B. N. Shuman, H. Takahara, J. Toney, C. Turney, D. H. Urrego-Sanchez, C. Umbanhowar, M. Vandergoes, B. Vanniere, E. Vescovi, M. Walsh, X. Wang, N. Williams, J. Wilmshurst, and J. H. Zhang (2008), Changes in fire regimes since the Last Glacial Maximum: An assessment based on a global synthesis and analysis of charcoal data, *Climate Dyn.*, *30*, 887-907, doi: 10.1007/s00382-007-0334-x.

Pratt, K. A., P. J. DeMott, J. R. French, Z. Wang, D. L. Westphal, A. J. Heymsfield, C. H. Twohy, A. J. Prenni, and K. A. Prather (2009), In situ detection of biological particles in cloud ice-crystals, *Nature Geosci.*, *2* (6), 397-400, doi: 10.1038/ngeo521.

Prenni, A. J., P. J. Demott, D. C. Rogers, S. M. Kreidenweis, G. M. McFarquhar, G. Zhang, and M. R. Poellot (2009), Ice nuclei characteristics from M-PACE and their relation to ice formation in clouds, *Tellus B*, *61* (2), 436-448, doi: 10.1111/j.1600-0889.2009.00415.x.

Pruppacher, H. R., and J. D. Klett (1997), *Microphysics of clouds and precipitation*, 954 pp., Kluwer Academic Publishers, Dordrecht, The Netherlands.

Puxbaum, H., A. Caseiro, A. Sanchez-Ochoa, A. Kasper-Giebl, M. Claeys, A. Gelencser, M. Legrand, S. Preunkert, and C. Pio (2007), Levoglucosan levels at background sites in Europe for assessing the impact of biomass combustion on the European aerosol background, *J. Geophys. Res.*, *112* (D23s05), doi: 10.1029/2006JD008114.

Qian, Y., W. I. Gustafson, L. R. Leung, and S. J. Ghan (2009), Effects of soot-induced snow albedo change on snowpack and hydrological cycle in western United States based on Weather Research and Forecasting chemistry and regional climate simulations, *J. Geophys. Res.*, *114* (D03), 108, doi: 10.1029/2008JD011039.

Qian, Y., M. G. Flanner, L. R. Leung, and W. Wang (2011), Sensitivity studies of the impacts of Tibetan Plateau snowpack pollution on the Asian hydrologic cycle and monsoon climate, *Atmos. Chem. Phys.*, *11*, 1929-1948, doi: 10.5194/acp-11-1929-2011.

Quaas, J., Y. Ming, S. Menon, T. Takemura, M. Wang, J. E. Penner, A. Gettelman, U. Lohmann, N. Bellouin, O. Boucher, A. M. Sayer, G. E. Thomas, A. McComiskey, G. Feingold, C. Hoose, J. E. Kristjansson, X. Liu, Y. Balkanski, L. J. Donner, P. A. Ginoux, P. Stier, B. Grandey, J. Feichter, I. Sednev, S. E. Bauer, D. Koch, R. G. Grainger, A. Kirkevag, T. Iversen, O. Seland, R. Easter, S. J. Ghan, P. J. Rasch, H. Morrison, J. F. Lamarque, M. J. Iacono, S. Kinne, and M. Schulz (2009), Aerosol indirect effects - general circulation model intercomparison and evaluation with satellite data, *Atmos. Chem. Phys.*, *9* (22), 8697-8717.

Querol, X., J. Pey, M. C. Minguillon, N. Perez, A. Alastuey, M. Viana, T. Moreno, R. M. Bernabe, S. Blanco, B. Cardenas, E. Vega, G. Sosa, S. Escalona, H. Ruiz, and B. Artinano (2008), PM speciation and sources in Mexico during the MILAGRO-2006 Campaign, *Atmos. Chem. Phys.*, *8* (1), 111-128.

Quinn, P. K., and D. J. Coffman (1998), Local closure during the First Aerosol Characterization Experiment (ACE1): Aerosol mass concentration and scattering and backscattering coefficients, *J. Geophys. Res.*, *103* (D13), 16575-16596.

Quinn, P. K., and T. S. Bates (2005), Regional aerosol properties: Comparisons of boundary layer measurements from ACE 1, ACE 2, aerosols99, INDOEX, ACE asia, TARFOX, and NEAQS, *J. Geophys. Res.*, *110* (D14), 202, doi: 10.1029/2004JD004755.

Quinn, P. K., T. S. Bates, E. Baum, N. Doubleday, A. M. Fiore, M. Flanner, A. Fridlind, T. J. Garrett, D. Koch, S. Menon, D. Shindell, A. Stohl, and S. G. Warren (2008), Short-lived pollutants in the Arctic: their climate impact and possible mitigation strategies, *Atmos. Chem. Phys.*, *8*, 1723-1725.

Quinn, P. K., A. Stohl, A. Arneth, T. Berntsen, J. F. Burkhart, J.

Christensen, M. Flanner, K. Kupiainen, H. Lihavainen, M. Shepherd, V. Shevchenko, H. Skov, and V. Vestreng (2011), The impact of black carbon on Arctic Climate, 128 pp., Arctic Monitoring and Assessment Programme (AMAP), Oslo, Norway.

Raes, F., T. Bates, F. McGovern, and M. Van Liedekerke (2000), The 2nd aerosol characterization experiment (ACE-2): General overview and main results, *Tellus B*, *52* (2), 111-125.

Ram, K., M. M. Sarin, and P. Hegde (2010), Long-term record of aerosol optical properties and chemical composition from a high-altitude site (Manora Peak) in Central Himalaya, *Atmos. Chem. Phys.*, *10* (23), 11791-11803, doi: 10.5194/acp-10-11791-2010.

Ramana, M. V., and V. Ramanathan (2006), Abrupt transition from natural to anthropogenic aerosol radiative forcing: Observations at the ABC-Maldives Climate Observatory, *J. Geophys. Res.*, *111* (D20), doi: 10.1029/2006JD007063.

Ramanathan, V., P. J. Crutzen, J. Lelieveld, A. P. Mitra, D. Althausen, J. Anderson, M. O. Andreae, W. Cantrell, G. R. Cass, C. E. Chung, A. D. Clarke, J. A. Coakley, W. D. Collins, W. C. Conant, F. Dulac, J. Heintzenberg, A. J. Heymsfield, B. Holben, S. Howell, J. Hudson, A. Jayaraman, J. T. Kiehl, T. N. Krishnamurti, D. Lubin, G. McFarquhar, T. Novakov, J. A. Ogren, I. A. Podgorny, K. Prather, K. Priestley, J. M. Prospero, P. K. Quinn, K. Rajeev, P. Rasch, S. Rupert, R. Sadourny, S. K. Satheesh, G. E. Shaw, P. Sheridan, and F. P. J. Valero (2001a), Indian ocean experiment: An integrated analysis of the climate forcing and effects of the great Indo-Asian haze, *J. Geophys. Res.*, *106* (D22), 28371-28398, doi: 10.1029/2001JD900133.

Ramanathan, V., P. J. Crutzen, J. T. Kiehl, and D. Rosenfeld (2001b), Atmosphere - Aerosols, climate, and the hydrological cycle, *Science*, *294* (5549), 2119-2124.

Ramanathan, V., C. Chung, D. Kim, T. Bettge, L. Buja, J. T. Kiehl, W. M. Washington, Q. Fu, D. R. Sikka, and M. Wild (2005), Atmospheric brown clouds: Impacts on South Asian climate and hydrological cycle, *P. Natl. Acad. Sci. USA*, *102* (15), 5326-5333, doi: 10.1073/pnas.0500656102.

Ramanathan, V., F. Li, M. V. Ramana, P. S. Praveen, D. Kim, C. E. Corrigan, H. Nguyen, E. A. Stone, J. J. Schauer, G. R. Carmichael, B. Adhikary, and S. C. Yoon (2007), Atmospheric brown clouds: Hemispherical and regional variations in long-range transport, absorption, and radiative forcing, *J. Geophys. Res.*, *112, D22S21*, doi: 10.1029/2006JD008124.

Ramanathan, V., and G. Carmichael (2008), Global and regional climate changes due to black carbon, *Nature Geosci.*, *1* (4), 221-227, doi: 10.1038/NGEO156.

Ramanathan, V., and Y. Y. Xu (2010), The Copenhagen Accord for limiting global warming: Criteria, constraints, and available avenues, *P. Natl. Acad. Sci. USA*, *107* (18), 8055-8062, doi: doi:10.1073/pnas.1002293107.

Randles, C. A., and V. Ramaswamy (2008), Absorbing aerosols over Asia: A Geophysical Fluid Dynamics Laboratory general circulation model sensitivity study of model response to aerosol optical depth and aerosol absorption, *J. Geophys. Res.*, *113* (D21), 203, doi: 10.1029/2008JD010140.

Rasch, P. J., J. Feichter, K. Law, N. Mahowald, J. Penner, C. Benkovitz, C. Genthon, C. Giannakopoulos, P. Kasibhatla, D. Koch, H. Levy, T. Maki, M. Prather, D. L. Roberts, G.-J. Roelofs, D. Stevenson, Z. Stockwell, S. Taguchi, M. Kritz, M. Chipperfield, D. Baldocchi, P. McMurry, L. Barrie, Y. Balkanski, R. Chatfield, E. Kjellstrom, M. Lawrence, H. N. Lee, J. Lelieveld, K. J. Noone, J. Seinfeld, G. Stenchikov, S. Schwartz, C. Walcek, and D. Williamson (2000), A comparison of scavenging and deposition processes in global models: results from the WCRP Cambridge Workshop of 1995, *Tellus*, *52B*, 1025-1056.

Rasch, P. J., W. D. Collins, and B. E. Eaton (2001), Understanding the Indian Ocean Experiment (INDOEX) aerosol distributions with an aerosol assimilation, *J. Geophys. Res.*, *106* (D7), 7337-7355.

Rau, J. A. (1989), Composition and size distribution of residential wood smoke particles, *Aerosol Sci. Technol.*, *10* (1), 181-192, doi: 10.1080/02786828908959233.

RCP Database (2009), Representative Concentration Pathways (RCP) Database (Version 2.0), International Institute for Applied Systems Analysis (IIASA), http://www.iiasa.ac.at/web-apps/tnt/RcpDb/dsd?Action=htmlpage&page=about., edited.

Reddy, M. S., and C. Venkataraman (2002a), Inventory of aerosol and sulphur dioxide emissions from India: Part I - fossil fuel combustion, *Atmos. Environ.*, *36*, 677-697.

Reddy, M. S., and C. Venkataraman (2002b), Inventory of aerosol and sulphur dioxide emissions from India, Part II - biomass combustion, *Atmos. Environ.*, *36* (4), 699-712, doi: 10.1016.S1352-2310(01)00464-2.

Reddy, M. S., O. Boucher, N. Bellouin, M. Schulz, Y. Balkanski, J. L. Dufresne, and M. Pham (2005a), Estimates of global multicomponent aerosol optical depth and direct radiative perturbation in the Laboratoire de Meteorologie Dynamique general circulation model, *J. Geophys. Res.*, *110, D10s16*, doi: 10.1029/2004jd004757.

Reddy, M. S., O. Boucher, Y. Balkanski, and M. Schulz (2005b), Aerosol optical depths and direct radiative perturbations by species and source type, *Geophys. Res. Lett.*, *32* (12), 803, doi: 10.1029/2004GL021743.

Reddy, M. S., and O. Boucher (2007), Climate impact of black carbon emitted from energy consumption in the world's regions, *Geophys. Res. Lett.*, *34*, L11802.

Redemann, J., R. P. Turco, K. N. Liou, P. B. Russell, R. W. Bergstrom, B. Schmid, J. M. Livingston, P. V. Hobbs, W. S. Hartley, S. Ismail, R. A. Ferrare, and E. V. Browell (2000), Retrieving the vertical structure of the effective aerosol complex index of refraction from a combination of aerosol in situ and remote sensing measurements during TARFOX, *J. Geophys. Res.*, *105* (D8), 9949-9970.

Reff, A., P. V. Bhave, H. Simon, T. G. Pace, G. A. Pouliot, J. D. Mobley, and M. Houyoux (2009), Emissions inventory of $PM_{2.5}$ trace elements across the United States, *Environ. Sci. Technol.*, *43* (15), 5790-5796, doi: 10.1021/es802930x.

Reid, J. S., P. V. Hobbs, C. Liousse, J. v. Martins, R. E. Weiss, and T. F. Eck (1998), Comparisons of techniques for measuring shortwave absorption and black carbon content of aerosols from biomass burning in Brazil, *J. Geophys. Res.*, *103* (D24), 32031-32040.

Reid, J. S., R. Koppmann, T. F. Eck, and D. P. Eleuterio (2005), A review of biomass burning emissions part II: intensive physical properties of biomass burning particles, *Atmos. Chem. Phys.*, *5*, 799-825.

Reid, J. S., E. J. Hyer, E. M. Prins, D. L. Westphal, J. L. Zhang, J. Wang, S. A. Christopher, C. A. Curtis, C. C. Schmidt, D. P. Eleuterio, K. A. Richardson, and J. P. Hoffman (2009), Global monitoring and forecasting of biomass-burning smoke: Description of and lessons from the fire locating and modeling of burning emissions (FLAMBE) program, *IEEE J. Sel. Top. Appl. Earth Observ. Remote Sens.*, *2* (3), 144-162, doi: 10.1109/jstars.2009.2027443.

Remer, L. A., Y. J. Kaufman, D. Tanre, S. Mattoo, D. A. Chu, J. V. Martins, R. R. Li, C. Ichoku, R. C. Levy, R. G. Kleidman, T. F. Eck, E. Vermote, and B. N. Holben (2005), The MODIS aerosol algorithm, products, and validation, *J. Atmos. Sci.*, *62* (4), 947-973.

Richardson, M. S., P. J. DeMott, S. M. Kreidenweis, D. J. Cziczo, E. J. Dunlea, J. L. Jimenez, D. S. Thomson, L. L. Ashbaugh, R.

D. Borys, D. L. Westphal, G. S. Casuccio, and T. L. Lersch (2007), Measurements of heterogeneous ice nuclei in the western United States in springtime and their relation to aerosol characteristics, *J. Geophys. Res.*, *112* (D2), 209, doi: 10.1029/2006JD007500.

Riemer, N., M. West, R. A. Zaveri, and R. C. Easter (2009), Simulating the evolution of soot mixing state with a particle-resolved aerosol model, *J. Geophys. Res.*, *114* (D9), 202, doi: 10.1029/2008JD011073.

Roberts, D. L., and A. Jones (2004), Climate sensitivity to black carbon aerosol from fossil fuel combustion, *J. Geophys. Res.*, *109* (D16), 202, doi: 10.1029/2004JD004676.

Robinson, A. L., N. M. Donahue, M. K. Shrivastava, E. A. Weitkamp, A. M. Sage, A. P. Grieshop, T. E. Lane, J. R. Pierce, and S. N. Pandis (2007), Rethinking organic aerosols: semivolatile emissions and photochemical aging, *Science*, *315*, 1259-1262, doi: 10.1126/science.1133061.

Roden, C. A., T. C. Bond, S. Conway, A. B. S. Pinel, N. MacCarty, and D. Still (2009), Laboratory and field investigations of particulate and carbon monoxide emissions from traditional and improved cookstoves, *Atmos. Environ.*, *43* (6), 1170-1181, doi: 10.1016/j.atmosenv.2008.05.041.

Roeckner, E., P. Stier, J. Feichter, S. Kloster, M. Esch, and I. Fischer-Bruns (2006), Impact of carbonaceous aerosol emissions on regional climate change, *Climate Dyn.*, *27* (6), 553-571, doi: 10.1007/s00382-006-0147-3.

Rogers, D. C., P. J. DeMott, S. M. Kreidenweis, and Y. L. Chen (1998), Measurements of ice nucleating aerosols during SUCCESS, *Geophys. Res. Lett.*, *25* (9), 1383-1386.

Rosen, H., A. D. A. Hansen, L. Gundel, and T. Novakov (1978), Identification of the optically absorbing component in urban aerosols, *Appl. Opt.*, *17* (24), 3859-3861.

Rosen, H., A. D. A. Hansen, and T. Novakov (1984), Role of graphitic carbon particles in radiative transfer in the Arctic haze, *Sci. Total Environ.*, *36* (JUN), 103-110.

Rotstayn, L. D., W. J. Cai, M. R. Dix, G. D. Farquhar, Y. Feng, P. Ginoux, M. Herzog, A. Ito, J. E. Penner, M. L. Roderick, and M. H. Wang (2007), Have Australian rainfall and cloudiness increased due to the remote effects of Asian anthropogenic aerosols?, *J. Geophys. Res.*, *112* (D9), 202, doi: 10.1029/2006JD007712.

Rotstayn, L. D., M. D. Keywood, B. W. Forgan, A. J. Gabric, I. E. Galbally, J. L. Gras, A. K. Luhar, G. H. McTainsh, R. M. Mitchell, and S. A. Young (2009), Possible impacts of anthropogenic and natural aerosols on Australian climate: A review, *Int. J. Climatol.*, *29*, 461-479, doi: 10.1002/joc.1729.

Roy, D. P., P. E. Lewis, and C. O. Justice (2002), Burned area mapping using multi-temporal moderate spatial resolution data - a bi-directional reflectance model-based expectation approach, *Remote Sens. Environ.*, *83* (1-2), 263-286.

Ruckstuhl, C., J. R. Norris, and R. Philipona (2010), Is there evidence for an aerosol indirect effect during the recent aerosol optical depth decline in Europe?, *J. Geophys. Res.*, *115*, doi: D04204, doi:10.1029/2009JD012867.

Russell, P. B., P. V. Hobbs, and L. L. Stowe (1999), Aerosol properties and radiative effects in the United States East Coast haze plume: An overview of the Tropospheric Aerosol Radiative Forcing Observational Experiment (TARFOX), *J. Geophys. Res.*, *104* (D2), 2213-2222.

Russell, L. (2003), Aerosol organic-mass-to-organic-carbon ratios, *Environ. Sci. Technol.*, *37*, 2982-2987.

Russell, P. B., R. W. Bergstrom, Y. Shinozuka, A. D. Clarke, P. F. DeCarlo, J. L. Jimenez, J. M. Livingston, J. Redemann, O. Dubovik, and A. Strawa (2010), Absorption Angstrom Exponent in AERONET and related data as an indicator of aerosol composition, *Atmos. Chem. Phys.*, *10* (3), 1155-1169, doi: 10.5194/acp-10-1155-2010.

Rypdal, K., F. Stordal, J. S. Fuglestvedt, and T. Berntsen (2005), Introducing top-down methods in assessing compliance with the Kyoto Protocol, *Climate Policy*, *5 (4)*, 393-405.

Rypdal, K., N. Rive, T. K. Berntsen, Z. Klimont, T. K. Mideksa, G. Myhre, and R. B. Skeie (2009a), Costs and global impacts of black carbon abatement strategies, *Tellus B*, *61* (4), 625-641, doi: 10.1111/j.1600-0889.2009.00430.x.

Rypdal, K., N. Rive, T. Berntsen, H. Fagerli, Z. Klimont, T. K. Mideksa, and J. S. Fuglestvedt (2009b), Climate and air quality-driven scenarios of ozone and aerosol precursor abatement, *Environ. Sci. Policy*, *12* (7), 855-869, doi: 10.1016/j.envsci.2009.08.002.

Sahu, S. K., G. Beig, and C. Sharma (2008), Decadal growth of black carbon emissions in India, *Geophys. Res. Lett.*, *35* (2), doi: 10.1029/2007GL032333.

Sakurai, H., K. Park, P. H. McMurry, D. D. Zarling, D. B. Kittelson, and P. J. Ziemann (2003), Size-dependent mixing characteristics of volatile and nonvolatile components in diesel exhaust aerosols, *Environ. Sci. Technol.*, *37*, 5487-5495.

Salam, A., H. Bauer, K. Kassin, S. M. Ullah, and H. Puxbaum (2003), Aerosol chemical characteristics of a mega-city in Southeast Asia (Dhaka-Bangladesh), *Atmos. Environ.*, *37* (18), 2517-2528, doi: 10.1016/s1352-2310(03)00135-3.

Samset, B. H., and G. Myhre (2011), Vertical dependence of black carbon, sulphate and biomass burning aerosol radiative forcing, *Geophys. Res. Lett.*, *38, L24802*, doi: 10.1029/2011GL049697.

Sandu, I., J. L. Brenguier, O. Geoffroy, O. Thouron, and V. Masson (2008), Aerosol impacts on the diurnal cycle of marine stratocumulus, *J. Atmos. Sci.*, *65* (8), 2705-2718, doi: 10.1175/2008jas2451.1.

Sarofim, M., B. DeAngelo, R. Beach, K. Weitz, M. Bahner, and A. Zapata (2010), Marginal abatement curves for U.S. black carbon emissions, *J. Integr. Environ. Sci.*, *7* (S1), 279-288, doi: 10.1080/19438151003774455.

Sato, M., J. Hansen, D. Koch, A. Lacis, R. Ruedy, O. Dubovik, B. Holben, M. Chin, and T. Novakov (2003), Global atmospheric black carbon inferred from AERONET, *P. Natl. Acad. Sci. USA*, *100* (11), 6319-6324, doi: 10.1073/PNAS.0731897100.

Schauer, J. J., W. F. Rogge, L. M. Hildemann, M. A. Mazurek, and G. R. Cass (1996), Source apportionment of airborne particulate matter using organic compounds as tracers, *Atmos. Environ.*, *30* (22), 3837-3855.

Schmid, H., L. Laskus, H. J. Abraham, U. Baltensperger, V. Lavanchy, M. Bizjak, P. Burba, H. Cachier, D. Crow, J. Chow, T. Gnauk, A. Even, H. M. t. Brink, K.-P. Giesen, R. Hitzenberger, C. Huegelin, W. Maenhaut, C. Pio, A. Carvalho, J.-P. Putaud, D. Toom-Sauntry, and H. Puxbaum (2001), Results of the "carbon conference" international aerosol carbon round robin test stage I, *Atmos. Environ.*, *35*, 2111-2121.

Schmid, B., J. Redemann, P. B. Russell, P. V. Hobbs, D. L. Hlavka, M. J. McGill, B. N. Holben, E. J. Welton, J. R. Campbell, O. Torres, R. A. Kahn, D. J. Diner, M. C. Helmlinger, D. A. Chu, C. Robles-Gonzalez, and G. de Leeuw (2003), Coordinated airborne, spaceborne, and ground-based measurements of massive thick aerosol layers during the dry season in southern Africa, *J. Geophys. Res.*, *108* (D13), 8496, doi: 10.1029/2002JD002297.

Schnaiter, M., H. Horvath, O. Möhler, K.-H. Naumann, H. Saathoff, and O. Schock (2003), UV-VIS-NIR spectral optical properties of soot and soot-containing aerosols, *J. Aerosol Sci.*, *34*, 1421-1444, doi: 10.1016/S0021-8502(03)00361-6.

Schnaiter, M., C. Linke, O. Möhler, K.-H. Naumann, H. Saathoff, R. Wagner, U. Schurath, and B. Wehner (2005), Absorption amplification of black carbon internally mixed with secondary

organic aerosol, *J. Geophys. Res.*, *110* (D19), 204, doi: 10.1029/2005JD006046.

Schröder, F. P., B. Karcher, A. Petzold, R. Baumann, R. Busen, C. Hoell, and U. Schumann (1998), Ultrafine aerosol particles in aircraft plumes: In situ observations, *Geophys. Res. Lett.*, *25* (15), 2789-2792.

Schrooten, L., I. De Vlieger, F. Lefebre, and R. Torfs (2006), Costs and benefits of an enhanced reduction policy of particulate matter exhaust emissions from road traffic in Flanders, *Atmos. Environ.*, *40* (5), 904-912, doi: 10.1016/j.atmosenv.2005.10.013.

Schultz, M. G., A. Heil, J. J. Hoelzemann, A. Spessa, K. Thonicke, J. G. Goldammer, A. C. Held, J. M. C. Pereira, and M. van het Bolscher (2008), Global wildland fire emissions from 1960 to 2000, *Global Biogeochem. Cycles*, *22* (2), doi: 10.1029/2007GB003031.

Schultz, M. G., and M. Wooster (2008), Evaluation of a fire radiative power product derived from METEOSAT 8/9 and identification of operational user needs, FREEVAL final report, Band/Volume 23, Darmstadt, Germany.

Schulz, M., C. Textor, S. Kinne, Y. Balkanski, S. Bauer, T. Berntsen, T. Berglen, O. Boucher, F. Dentener, S. Guibert, I. S. A. Isaksen, T. Iversen, D. Koch, A. Kirkevag, X. Liu, V. Montanaro, G. Myhre, J. E. Penner, G. Pitari, S. Reddy, O. Seland, P. Stier, and T. Takemura (2006), Radiative forcing by aerosols as derived from the AeroCom present-day and pre-industrial simulations, *Atmos. Chem. Phys.*, *6*, 5225-5246, doi: 10.5194/acp-6-5225-2006.

Schuster, G. L., O. Dubovik, B. N. Holben, and E. E. Clothiaux (2005), Inferring black carbon content and specific absorption from Aerosol Robotic Network (AERONET) aerosol retrievals, *J. Geophys. Res.*, *110*, D10S17, doi: 10.1029/2004JD004548.

Schuster, G. L., B. Lin, and O. Dubovik (2009), Remote sensing of aerosol water uptake, *Geophys. Res. Lett.*, *36* (L03), 814, doi: 10.1029/2008GL036576.

Schwarz, J. P., R. S. Gao, D. W. Fahey, D. S. Thomson, L. A. Watts, J. C. Wilson, J. M. Reeves, M. Darbeheshti, D. G. Baumgardner, G. L. Kok, S. H. Chung, M. Schulz, J. Hendricks, A. Lauer, B. Karcher, J. G. Slowik, K. H. Rosenlof, T. L. Thompson, A. O. Langford, M. Loewenstein, and K. C. Aikin (2006), Single-particle measurements of midlatitude black carbon and light-scattering aerosols from the boundary layer to the lower stratosphere, *J. Geophys. Res.*, *111* (D16), 207, doi: 10.1029/2006JD007076.

Schwarz, J. P., J. R. Spackman, D. W. Fahey, R. S. Gao, U. Lohmann, P. Stier, L. A. Watts, D. S. Thomson, D. A. Lack, L. Pfister, M. J. Mahoney, D. Baumgardner, J. C. Wilson, and J. M. Reeves (2008a), Coatings and their enhancement of black carbon light absorption in the tropical atmosphere, *J. Geophys. Res.*, *113* (D3), 203, doi: 10.1029/2007JD009042.

Schwarz, J. P., R. S. Gao, J. R. Spackman, L. A. Watts, D. S. Thomson, D. W. Fahey, T. B. Ryerson, J. Peischl, J. S. Holloway, M. Trainer, G. J. Frost, T. Baynard, D. A. Lack, J. A. de Gouw, C. Warneke, and L. A. Del Negro (2008b), Measurement of the mixing state, mass, and optical size of individual black carbon particles in urban and biomass burning emissions, *Geophys. Res. Lett.*, *35* (13), 810, doi: 10.1029/2008GL033968.

Schwarz, J. P., J. R. Spackman, R. S. Gao, L. A. Watts, P. Stier, M. Schulz, S. M. Davis, S. C. Wofsy, and D. W. Fahey (2010), Global-scale black carbon profiles observed in the remote atmosphere and compared to models, *Geophys. Res. Lett.*, *37* (L18), 812, doi: 10.1029/2010GL044372.

Seifert, P., A. Ansmann, D. Mueller, U. Wandinger, D. Althausen, A. J. Heymsfield, S. T. Massie, and C. Schmitt (2007), Cirrus optical properties observed with lidar, radiosonde, and satellite over the tropical Indian Ocean during the aerosol-polluted northeast and clean maritime southwest monsoon, *J. Geophys. Res.*, *112* (D17), 205, doi: 10.1029/2006JD008352.

Shah, S. D., D. R. Cocker, J. W. Miller, and J. M. Norbeck (2004), Emission rates of particulate matter and elemental and organic carbon from in-use diesel engines, *Environ. Sci. Technol.*, *38*, 2544-2550.

Shah, S. D., D. R. Cocker, K. C. Johnson, J. M. Lee, B. L. Soriano, and J. W. Miller (2007), Reduction of particulate matter emissions from diesel backup generators equipped with four different exhaust aftertreatment devices, *Environ. Sci. Technol.*, *41* (14), 5070-5076, doi: 10.1021/es0614161.

Sharma, S., J. R. Brook, H. Cachier, J. Chow, A. Gaudenzi, and G. Lu (2002), Light absorption and thermal measurements of black carbon in different regions of Canada, *J. Geophys. Res.*, *107* (D24), 4771, doi: 10.1029/2002JD002496.

Sharma, S., E. Andrews, L. A. Barrie, J. A. Ogren, and D. Lavoué (2006), Variations and sources of the equivalent black carbon in the high Arctic revealed by long-term observations at Alert and Barrow: 1989-2003, *J. Geophys. Res.*, *111*, D14208, doi: 10.1029/2005JD006581.

Shaw, R. A., A. J. Durant, and Y. Mi (2005), Heterogeneous surface crystallization observed in undercooled water, *J. Phys. Chem. B*, *109* (20), 9865-9868, doi: 10.1021/jp0506336.

Shea, R. W., B. W. Shea, J. B. Kauffman, D. E. Ward, C. I. Haskins, and M. C. Scholes (1996), Fuel biomass and combustion factors associated with fires in savanna ecosystems of South Africa and Zambia, *J. Geophys. Res.*, *101* (D19), 23551-23568, doi: 10.1029/95JD02047.

Sheesley, R. J., J. J. Schauer, and M. L. Orf (2010), Assessing the Impact of Industrial Source Emissions on Atmospheric Carbonaceous Aerosol Concentrations Using Routine Monitoring Networks, *J. Air Waste Manage. Assoc.*, *60* (2), 149-155, doi: 10.3155/1047-3289.60.2.149.

Sheridan, P. J., and J. A. Ogren (1999), Observations of the vertical and regional variability of aerosol optical properties over central and eastern North America, *J. Geophys. Res.*, *104* (D14), 16793-16805.

Shindell, D. T., G. Faluvegi, N. Bell, and G. A. Schmidt (2005), An emissions-based view of climate forcing by methane and tropospheric ozone, *Geophys. Res. Lett.*, *32*, L04803.

Shindell, D. T., M. Chin, F. Dentener, R. M. Doherty, G. Faluvegi, A. M. Fiore, P. Hess, D. M. Koch, I. A. MacKenzie, M. G. Sanderson, M. G. Schultz, M. Schulz, D. S. Stevenson, H. Teich, C. Textor, O. Wild, D. J. Bergmann, I. Bey, H. Bian, C. Cuvelier, B. N. Duncan, G. Folberth, L. W. Horowitz, J. Jonson, J. W. Kaminski, E. Marmer, R. Park, K. J. Pringle, S. Schroeder, S. Szopa, T. Takemura, G. Zeng, T. J. Keating, and A. Zuber (2008), A multi-model assessment of pollution transport to the Arctic, *Atmos. Chem. Phys.*, *8* (17), 5353-5372.

Shindell, D., and G. Faluvegi (2009), Climate response to regional radiative forcing during the twentieth century, *Nature Geosci.*, *2* (4), 294-300, doi: 10.1038/ngeo473.

Shindell, D., M. Schulz, Y. Ming, T. Takemura, G. Faluvegi, and V. Ramaswamy (2010), Spatial scales of climate response to inhomogeneous radiative forcing, *J. Geophys. Res.*, *115* (D19110), doi: 10.1029/2010jd014108.

Shindell, D., G. Faluvegi, M. Walsh, S. C. Anenberg, R. V. Dingenen, N. Z. Muller, J. Austin, D. Koch, and G. Milly (2011), Climate, health, agricultural and economic impacts of tighter vehicle-emission standards, *Nature Climate Change*, *1*, 59-66, doi: 10.1038/nclimate1066.

Shindell, D., J. C. I. Kuylenstierna, E. Vignati, R. van Dingenen, M. Amann, Z. Klimont, S. C. Anenberg, N. Muller, G. Janssens-Maenhout, F. Raes, J. Schwartz, G. Faluvegi, L. Pozzoli, K. Kupiainen, L. Höglund-Isaksson, L. Emberson, D. Streets, V.

Ramanathan, K. Hicks, N. T. K. Oanh, G. Milly, M. Williams, V. Demkine, and D. Fowler (2012), Simultaneously Mitigating Near-Term Climate Change and Improving Human Health and Food Security, *Science*, *335* (6065), 183-189, doi: 10.1126/science.1210026.

Shine, K. P., J. Cook, E. J. Highwood, and M. M. Joshi (2003), An alternative to radiative forcing for estimating the relative importance of climate change mechanisms, *Geophys. Res. Lett.*, *30* (20), 2047, doi: 10.1029/2003GL018141.

Shine, K. P., J. S. Fuglestvedt, K. Hailemariam, and N. Stuber (2005), Alternatives to the global warming potential for comparing climate impacts of emissions of greenhouse gases, *Climatic Change*, *68*, 281-302.

Shine, K. P., T. K. Berntsen, J. S. Fuglestvedt, R. B. Skeie, and N. Stuber (2007), Comparing the climate effect of emissions of short- and long-lived climate agents, *Philos. Trans. R. Soc. A-Math. Phys. Eng. Sci.*, *365* (1856), 1903-1914, doi: 10.1098/rsta.2007.2050.

Shiraiwa, M., Y. Kondo, N. Moteki, N. Takegawa, Y. Miyazaki, and D. R. Blake (2007), Evolution of mixing state of black carbon in polluted air from Tokyo, *Geophys. Res. Lett.*, *34*, L16803, doi: 10.1029/2007GL029819.

Shiraiwa, M., Y. Kondo, N. Moteki, N. Takegawa, L. K. Sahu, A. Takami, S. Hatakeyama, S. Yonemura, and D. R. Blake (2008), Radiative impact of mixing state of black carbon aerosol in Asian outflow, *J. Geophys. Res.*, *113*, doi: D24210, 10.1029/2008JD010546.

Shiraiwa, M., Y. Kondo, T. Iwamoto, and K. Kita (2010), Amplification of light absorption of black carbon by organic coating, *Aerosol Sci. Technol.*, *44* (1), 46-54, doi: 10.1080/02786820903357686.

Simon, M., S. Plummer, F. Fierens, J. J. Hoelzemann, and O. Arino (2004), Burnt area detection at global scale using ATSR-2: The GLOBSCAR products and their qualification, *J. Geophys. Res.*, *109* (D14), doi: 10.1029/2003JD003622.

Sinton, J. E., K. R. Smith, J. W. Peabody, L. Yaping, Z. Xiliang, R. Edwards, and G. Quan (2004), An assessment of programs to promote improved household stoves in China, *Energy for Sustainable Development*, *8* (3), 33-52.

Skeie, R. B., T. Berntsen, G. Myhre, C. A. Pedersen, J. Ström, S. Gerland, and J. A. Ogren (2011), Black carbon in the atmosphere and snow, from pre-industrial times until present, *Atmos. Chem. Phys.*, *11*, 6809-6836, doi: 10.5194/acp-11-6809-2011.

Slowik, J. G., K. Stainken, P. Davidovits, L. R. Williams, J. T. Jayne, C. E. Kolb, D. R. Worsnop, Y. Rudich, P. F. DeCarlo, and J. L. Jimenez (2004), Particle morphology and density characterization by combined mobility and aerodynamic diameter measurements. Part 2: application to combustion-generated soot aerosols as a function of fuel equivalence ratio, *Aerosol Sci. Technol.*, *38*, 1206-1222.

Slowik, J. G., E. S. Cross, J. H. Han, P. Davidovits, T. B. Onasch, J. T. Jayne, L. R. Williams, M. R. Canagaratna, D. R. Worsnop, R. K. Chakrabarty, H. Moosmuller, W. P. Arnott, J. P. Schwarz, R. S. Gao, D. W. Fahey, G. L. Kok, and A. Petzold (2007), An inter-comparison of instruments measuring black carbon content of soot particles, *Aerosol Sci. Technol.*, *41* (3), 295-314, doi: 10.1080/02786820701197078.

Smith, K. R., R. Uma, V. V. N. Kishore, K. Lata, V. Joshi, J. Zhang, R. A. Rasmussen, and K. A. Khalil (2000a), Greenhouse gases from small-scale combustion devices in developing countries: household stoves in India, EPA-600/R-00-052, Environmental Protection Agency, Research Triangle Park, NC.

Smith, K. R., R. Uma, V. V. N. Kishore, J. Zhang, V. Joshi, and M. A. K. Khalil (2000b), Greenhouse implications of household stoves: An analysis for India, *Ann. Rev. Energy Environ.*, *25*, 741-763.

Smith, K. R., S. Mehta, and M. Maeusezahl-Feuz (2004), Indoor smoke from household solid fuels, 1435-1493 pp., World Health Organization, Geneva, Switzerland.

Smith, K. R., K. Dutta, C. Chengappa, P. P. S. Gusain, O. Masera, V. Berrueta, R. Edwards, R. Bailis, and K. N. Shields (2007), Monitoring and evaluation of improved biomass cookstove programs for indoor air quality and stove performance: conclusions from the Household Energy and Health Project, *Energy for Sustainable Development*, *11* (2), 5-18.

Smith, K. R., M. Jerrett, H. R. Anderson, R. T. Burnett, V. Stone, R. Derwent, R. W. Atkinson, A. Cohen, S. B. Shonkoff, D. Krewski, C. A. Pope, M. J. Thun, and G. Thurston (2009), Health and climate change 5 public health benefits of strategies to reduce greenhouse-gas emissions: Health implications of short-lived greenhouse pollutants, *Lancet*, *374* (9707), 2091-2103, doi: 10.1016/s0140-6736(09)61716-5.

Smith, K. R., J. P. McCracken, L. Thompson, R. Edwards, K. N. Shields, E. Canuz, and N. Bruce (2010), Personal child and mother carbon monoxide exposures and kitchen levels: Methods and results from a randomized trial of woodfired chimney cookstoves in Guatemala (RESPIRE), *J. Expo. Sci. Env. Epid.*, *20* (5), 406-416, doi: doi:10.1038/jes.2010.30.

Soden, B. J., and I. M. Held (2006), An assessment of climate feedbacks in coupled ocean-atmosphere models, *J. Climate*, *19* (23), 3354-3360, doi: 10.1175/JCLI3799.1.

Sofiev, M., R. Vankevich, M. Lotjonen, M. Prank, V. Petukhov, T. Ermakova, J. Kosk- inen, and J. Kukkonen (2009), An operational system for the assimilation of the satellite information on wild-land fires for the needs of air quality modelling and forecasting, *Atmos. Chem. Phys.*, *9* (18), 6833-6847.

Soja, A. J., W. R. Cofer, H. H. Shugart, A. I. Sukhinin, P. W. Stackhouse, D. J. McRae, and S. G. Conard (2004), Estimating fire emissions and disparities in boreal Siberia (1998-2002), *J. Geophys. Res.*, *109* (D14s06), doi: 10.1029/2004JD004570.

Sokolov, A. P. (2006), Does model sensitivity to changes in CO_2 provide a measure of sensitivity to other forcings?, *J. Climate*, *19*, 3294-3306, doi: 10.1175/JCL13791.1.

Solmon, F., F. Giorgi, and C. Liousse (2006), Aerosol modelling for regional climate studies: application to anthropogenic particles and evaluation over a European/African domain, *Tellus B*, *58* (1), 51-72, doi: 10.1111/j.1600-0889.2005.00155.x.

Solomon, P. A., W. Chameides, R. Weber, A. Middlebrook, C. S. Kiang, A. G. Russell, A. Butler, B. Turpin, D. Mikel, R. Scheffe, E. Cowling, E. Edgerton, J. St John, J. Jansen, P. McMurry, S. Hering, and T. Bahadori (2003), Overview of the 1999 Atlanta supersite project, *J. Geophys. Res.*, *108* (D7), 8413, doi: 10.1029/2001JD001458.

Song, Y., Y. H. Zhang, S. D. Xie, L. M. Zeng, M. Zheng, L. G. Salmon, M. Shao, and S. Slanina (2006), Source apportionment of PM2.5 in Beijing by positive matrix factorization, *Atmos. Environ.*, *40* (8), 1526-1537, doi: 10.1016/j.atmosenv.2005.10.039.

Spracklen, D. V., K. S. Carslaw, U. Poschl, A. Rap, and P. M. Forster (2011), Global cloud condensation nuclei influenced by carbonaceous combustion aerosol, *Atmos. Chem. Phys.*, *11* (17), 9067-9087, doi: 10.5194/acp-11-9067-2011.

Stamnes, K., S. C. Tsay, W. Wiscombe, and K. Jayaweera (1988), Numerically stable algorithm for discrete-ordinate-method radiative-transfer in multiple-scattering and emitting layered media, *Appl. Opt.*, *27*, 2502-2509.

Stavrakou, T., and J. F. Müller (2006), Grid-based versus big region approach for inverting CO emissions using Measurement of Pollution in the Troposphere (MOPITT) data, *J. Geophys.*

Res., *111* (D15), 304, doi: 10.1029/2005JD006896.

Stevens, B., and G. Feingold (2009), Untangling aerosol effects on clouds and precipitation in a buffered system, *Nature*, *461* (7264), 607-613, doi: 10.1038/nature08281.

Stier, P., J. Feichter, S. Kinne, S. Kloster, E. Vignati, J. Wilson, L. Ganzeveld, I. Tegen, M. Werner, Y. Balkanski, M. Schulz, O. Boucher, A. Minikin, and A. Petzold (2005), The aerosol-climate model ECHAM5-HAM, *Atmos. Chem. Phys.*, *5*, 1125-1156.

Stier, P., J. H. Seinfeld, S. Kinne, J. Feichter, and O. Boucher (2006a), Impact of nonabsorbing anthropogenic aerosols on clear-sky atmospheric absorption, *J. Geophys. Res.*, *111* (D18), doi: D18201,10.1029/2006JD007147.

Stier, P., J. Feichter, S. Kloster, E. Vignati, and J. Wilson (2006b), Emission-induced nonlinearities in the global aerosol system: results from the ECHAM4-HAM aerosol-climate model, *J. Climate*, *19*, 3845-3862.

Stier, P., J. H. Seinfeld, S. Kinne, and O. Boucher (2007), Aerosol absorption and radiative forcing, *Atmos. Chem. Phys.*, *7*, 5237-5261.

Stith, J. L., V. Ramanathan, W. A. Cooper, G. C. Roberts, P. J. DeMott, G. Carmichael, C. D. Hatch, B. Adhikary, C. H. Twohy, D. C. Rogers, D. Baumgardner, A. J. Prenni, T. Campos, R. Gao, J. Anderson, and Y. Feng (2009), An overview of aircraft observations from the Pacific Dust Experiment campaign, *J. Geophys. Res.*, *114* (D05), 207, doi: 10.1029/2008JD010924.

Stocks, B. J., J. A. Mason, J. B. Todd, E. M. Bosch, B. M. Wotton, B. D. Amiro, M. D. Flannigan, K. G. Hirsch, K. A. Logan, D. L. Martell, and W. R. Skinner (2002), Large forest fires in Canada, 1959-1997, *J. Geophys. Res.*, *108* (D1), doi: 10.1029/2001JD000484.

Stohl, A. (2006), Characteristics of atmospheric transport into the Arctic troposphere, *J. Geophys. Res.*, *111* (D11), D11306, doi: 10.1029/2005JD006888.

Stohl, A., T. Berg, J. F. Burkhart, A. M. Fjæraa, C. Forster, A. Herber, Ø. Hov, C. Lunder, W. W. McMillan, S. Oltmans, M. Shiobara, D. Simpson, S. Solberg, K. Stebel, J. Ström, K. Tørseth, R. Treffeisen, K. Virkkunen, and K. E. Yttri (2007), Arctic smoke and ash; record high air pollution levels in the European Arctic due to agricultural fires in Eastern Europe in spring 2006, *Atmos. Chem. Phys.*, *7* (2), 511-534, doi: 10.5194/acp-7-511-2007.

Stone, E. A., G. C. Lough, J. J. Schauer, P. S. Praveen, C. E. Corrigan, and V. Ramanathan (2007), Understanding the origin of black carbon in the atmospheric brown cloud over the Indian Ocean, *J. Geophys. Res.*, *112* (D22), D22s23, doi: 10.1029/2006JD008118.

Storelvmo, T., J. E. Kristjansson, and U. Lohmann (2008), Aerosol influence on mixed-phase clouds in CAM-Oslo, *J. Atmos. Sci.*, *65* (10), 3214-3230, doi: 10.1175/2008jas2430.1.

Storelvmo, T., C. Hoose, and P. Eriksson (2011), Global modeling of mixed-phase clouds: The albedo and lifetime effects of aerosols, *J. Geophys. Res.*, *116*, D05207, doi: 10.1029/2010JD014724.

Streets, D. G., K. F. Yarber, J. H. Woo, and G. R. Carmichael (2003a), Biomass burning in Asia: Annual and seasonal estimates and atmospheric emissions, *Global Biogeochem. Cycles*, *17* (4), 1099, doi: 10.1029/2003gb002040.

Streets, D. G., T. C. Bond, G. R. Carmichael, S. D. Fernandes, Q. Fu, D. He, Z. Klimont, S. M. Nelson, N. Y. Tsai, M. Q. Wang, J.-H. Woo, and K. F. Yarber (2003b), An inventory of gaseous and primary aerosol emissions in Asia in the year 2000, *J. Geophys. Res.*, *108* (D21), 8809, doi: 10.1029/2002JD003093.

Streets, D. G., T. C. Bond, T. Lee, and C. Jang (2004), On the future of carbonaceous aerosol emissions, *J. Geophys. Res.*, *109* (D24), doi: 10.1029/2004JD004902.

Streets, D. G., and K. Aunan (2005), The importance of China's household sector for the black carbon emissions, *Geophys. Res. Lett.*, *32*, 1-4.

Streets, D. G., Q. Zhang, L. Wang, K. He, J. Hao, Y. Wu, Y. Tang, and G. R. Carmichael (2006), Revisiting China's CO emissions after the Transport and Chemical Evolution over the Pacific (TRACE-P) mission: Synthesis of inventories, atmospheric modeling, and observations, *J. Geophys. Res.*, *111* (D14), 306, doi: 10.1029/2006JD007118.

Streets, D. G. (2007), Dissecting future aerosol emissions: Warming tendencies and mitigation opportunities, *Climatic Change*, *81* (3-4), 313-330, doi: 10.1007/s10584-006-9112-8.

Streets, D. G., F. Yan, M. Chin, T. Diehl, N. Mahowald, M. Schultz, M. Wild, Y. Wu, and C. Yu (2009), Anthropogenic and natural contributions to regional trends in aerosol optical depth, 1980-2006, *J. Geophys. Res.*, *114*, doi: 10.1029/2008JD011624.

Streets, D., H. Akimoto, P. Artaxo, Z. Klimont, K. Kupiainen, G. Janssens-Maenhout, and H. Vallack (2011), Black Carbon and tropospheric ozone precursors: Driver, emissions and trends, in *Integrated Assessment of Black Carbon and Tropospheric Ozone*, edited, 282 p., United Nations Environment Programme, Nairobi, Kenya, and World Meteorological Organization, Geneva, Switzerland.

Str□m, J., and S. Ohlsson (1998), In situ measurements of enhanced crystal number densities in cirrus clouds caused by aircraft exhaust, *J. Geophys. Res.*, *103* (D10), 11355-11361.

Subramanian, R., A. Y. Khlystov, and A. L. Robinson (2006), Effect of peak inert-mode temperature on elemental carbon measured using thermal-optical analysis, *Aerosol Sci. Technol.*, *40* (10), 763-780, doi: 10.1080/02786820600714403.

Subramanian, R., T. C. Bond, W. Thiansathit, N. T. K. Oanh, K. G. Duleep, I. Paw-armart, and E. Winijkul (2009), Source characterization to support quantification of co-benefits: a piggyback study in Bangkok, Thailand, *Environ. Sci. Technol.*, *43*, 4213-4218.

Sun, H., L. Biedermann, and T. C. Bond (2007), Color of brown carbon: A model for ultraviolet and visible light absorption by organic carbon aerosol, *Geophys. Res. Lett.*, *34* (17), L17813, doi: 10.1029/2007GL029797.

Szidat, S., T. M. Jenk, H. A. Synal, M. Kalberer, L. Wacker, I. Hajdas, A. Kasper-Giebl, and U. Baltensperger (2006), Contributions of fossil fuel, biomass-burning, and biogenic emissions to carbonaceous aerosols in Zurich as traced by C-14, *J. Geophys. Res.*, *111*, D07206, doi: 10.1029/2005JD006590.

Takemura, T., T. Nozawa, S. Emori, T. Y. Nakajima, and T. Nakajima (2005), Simulation of climate response to aerosol direct and indirect effects with aerosol transport-radiation model, *J. Geophys. Res.*, *110* (D2), 202, doi: 10.1029/2004JD005029.

Tan, Q., W. L. Chameides, D. Streets, T. Wang, J. Xu, M. Bergin, and J. Woo (2004), An evaluation of TRACE-P emission inventories from China using a regional model and chemical measurements, *J. Geophys. Res.*, *109, D22305*, doi: 10.1029/2004JD005071.

Targino, A. C., H. Coe, J. Cozic, J. Crosier, I. Crawford, K. Bower, M. Flynn, M. Gallagher, J. Allan, B. Verheggen, E. Weingartner, U. Baltensperger, and T. Choularton (2009), Influence of particle chemical composition on the phase of cold clouds at a high-alpine site in Switzerland, *J. Geophys. Res.*, *114* (D18), 206, doi: 10.1029/2008JD011365.

Ten Hoeve, J. E., L. A. Remer, and M. Z. Jacobson (2011), Microphysical and radiative effects of aerosols on warm clouds during the Amazon biomass burning season as observed by MODIS: Impacts of water vapor and land cover, *Atmos. Chem. Phys.*, *11*, 3021-3036, doi: 10.5194/acp-11-3021-2011.

Textor, C., M. Schulz, S. Guibert, S. Kinne, Y. Balkanski, S. Bauer,

T. Berntsen, T. Berglen, O. Boucher, M. Chin, F. Dentener, T. Diehl, R. Easter, H. Feichter, D. Fillmore, S. Ghan, P. Ginoux, S. Gong, A. Grini, J. Hendricks, L. Horowitz, P. Huang, I. Isaksen, T. Iversen, S. Kloster, D. Koch, A. Kirkevåg, J. E. Kristjansson, M. Krol, A. Lauer, J. F. Lamarque, X. Liu, V. Montanaro, G. Myhre, J. Penner, G. Pitari, S. Reddy, Ø. Seland, P. Stier, T. Takemura, and X. Tie (2006), Analysis and quantification of the diversities of aerosol life cycles within AeroCom, *Atmos. Chem. Phys.*, *6*, 1777-1813.

Textor, C., M. Schulz, S. Guibert, S. Kinne, Y. Balkanski, S. Bauer, T. Berntsen, T. Berglen, O. Boucher, M. Chin, F. Dentener, T. Diehl, J. Feichter, D. Fillmore, P. Ginoux, S. Gong, A. Grini, J. Hendricks, L. Horowitz, P. Huang, I. S. A. Isaksen, T. Iversen, S. Kloster, D. Koch, A. Kirkevag, J. E. Kristjansson, M. Krol, A. Lauer, J. F. Lamarque, X. Liu, V. Montanaro, G. Myhre, J. E. Penner, G. Pitari, M. S. Reddy, O. Seland, P. Stier, T. Takemura, and X. Tie (2007), The effect of harmonized emissions on aerosol properties in global models - an AeroCom experiment, *Atmos. Chem. Phys.*, *7* (17), 4489-4501.

Thevenon, F., F. S. Anselmetti, S. M. Bernasconi, and M. Schwikowski (2009), Mineral dust and elemental black carbon records from an Alpine ice core (Colle Gnifetti glacier) over the last millennium, *J. Geophys. Res.*, *114* (D17), 102, doi: 10.1029/2008JD011490.

Thompson, L. G., S. Hastenrath, and B. Morales-Arnao (1979), Climatic ice core records from the tropical Quelccaya ice cap, *Science*, *203* (4386), 1240-1243.

Tol, R. S. J., K. Berntsen, B. C. O'Neill, J. S. Fuglestvedt, K. P. Shine, Y. Balkanski, and L. Makra (2008), Metrics for agregating the climate effect of different emissions: A unifying framework, ESRI Working Paper 257, The Economic and Social Research Institute, Dublin, Ireland.

Toon, O. B., C. P. McKay, T. P. Ackerman, and K. Santhanam (1989), Rapid calculation of radiative heating rates and photodissociation rates in Inhomogeneous multiple scattering atmospheres, *J. Geophys. Res.*, *94* (D13), 16287-16301, doi: 10.1029/JD094iD13p16287.

Torres, O., P. K. Bhartia, J. R. Herman, and Z. Ahmad (1998), Derivation of aerosol properties from satellite measurements of backscattered ultraviolet radiation: Theoretical basis, *J. Geophys. Res.*, *103*, 17099-17110, doi: 10.1029/98JD00900.

Torres, O., P. K. Bhartia, J. R. Herman, A. Sinyuk, P. Ginoux, and B. Holben (2002), A long-term record of aerosol optical depth from TOMS observations and comparison to AERONET measurements, *J. Atmos. Sci.*, *59* (3), 398-413.

Tosca, M. G., J. T. Randerson, C. S. Zender, M. G. Flanner, and P. J. Rasch (2010), Do biomass burning aerosols intensify drought in equatorial Asia during El Nino?, *Atmos. Chem. Phys.*, *10* (8), 3515-3528.

Tsyro, S., D. Simpson, L. Tarrason, Z. Klimont, K. Kupiainen, C. Pio, and K. E. Yttri (2007), Modeling of elemental carbon over Europe, *J. Geophys. Res.*, *112* (D23s19), doi: 10.1029/2006JD008164.

Turetsky, M. R., E. S. Kane, J. W. Harden, R. D. Ottmar, K. L. Manies, E. Hoy, and E. S. Kasischke (2010), Recent acceleration of biomass burning and carbon losses in Alaskan forests and peatlands, *Nature Geosci.*, *4*, 27-31, doi: 10.1038/ngeo1027.

Turpin, B. J., R. A. Cary, and J. J. Huntzicker (1990), An *in situ*, time-resolved analyzer for aerosol organic and elemental carbon, *Aerosol Sci. Technol.*, *12*, 161-171.

Twohy, C. H., and B. W. Gandrud (1998), Electron microscope analysis of residual particles from aircraft contrails, *Geophys. Res. Lett.*, *25* (9), 1359-1362.

Twohy, C. H., and M. R. Poellot (2005), Chemical characteristics of ice residual nuclei in anvil cirrus clouds: evidence for homogeneous and heterogeneous ice formation, *Atmos. Chem. Phys.*, *5*, 2289-2297.

Twohy, C. H., P. J. DeMott, D. A. Pratt, R. Subramanian, G. L. Kok, S. M. Murphy, T. Lersch, A. J. Heymsfield, Z. E. Wang, K. A. Prather, and J. H. Seinfeld (2010), Relationships of biomass-burning aersols to ice in orographic wave clouds, *J. Atmos. Sci.*, *67* (8), 2437-2450, doi: 10.1175/2010JAS3310.1.

Twomey, S. A. (1959), The nuclei of natural cloud formation part II: The supersaturation in natural clouds and the variation of cloud droplet concentrations, *Geofis. Pura. Appl*, *43*, 227-242.

Uherek, E., T. Halenka, J. Borken-Kleefeld, Y. Balkanski, T. Berntsen, C. Borrego, M. Gauss, P. Hoor, K. Juda-Rezler, J. Lelieveld, D. Melas, K. Rypdal, and S. Schmid (2010), Transport impacts on atmosphere and climate: Land transport, *Atmos. Environ.*, *44* (37), 4772-4816, doi: 10.1016/j.atmosenv.2010.01.002.

UNECE (1999), Protocol to the 1979 Convention on Long-Range Transboundary Air Pollution to abate acidification, eutrophication and ground-level ozone. Adopted in Gothenburg, Swede, on 30 November, 1999. http://www.unece.org/env/lrtap/multi_h1.html.

UNECE (2011), Options for revising the 1999 Gothenburg Protocol to Abate Acidification, Eutrophication and Ground-level Ozone. ECE/EB.AIR/2011/8 revised at the 29th session of the Executive Body of the LRTAP Convention; http://www.unece.org/fileadmin/DAM/env/documents/2011/eb/ebbureau/ece.eb.air.2011.8.-REVISED_1612am_AK.doc.

UNEP (2011), Near-term Climate Protection and Clean Air Benefits: Actions for Controlling Short-Lived Climate Forcers, 78 pp., United Nations Environment Programme, Nairobi, Kenya.

UNEP/WMO (2011a), Integrated Assessment of Black Carbon and Tropospheric Ozone: Summary for Decision Makers, 38 pp., United Nations Environment Programme, Nairobi, Kenya, and World Meteorological Organization, Geneva, Switzerland.

UNEP/WMO (2011b), Integrated Assessment of Black Carbon and Tropospheric Ozone, 282 pp., United Nations Environment Programme, Nairobi, Kenya, and World Meteorological Organization, Geneva, Switzerland.

UNFCCC (1992), United Nations Framework Convention on Climate Change, 24 pp., United Nations.

Unger, N., T. C. Bond, J. S. Wang, D. M. Koch, S. Menon, D. T. Shindell, and S. Bauer (2010), Attribution of climate forcing to economic sectors, *P. Natl. Acad. Sci. USA*, *107* (8), 3382-3387, doi: 10.1073/pnas.0906548107.

USDA (2005), A strategic assessment of forest biomass and fuel reduction treatments in Western states, *Gen. Tech. Rep.*, RMRS-GTR-149, U.S. Department of Agriculture, Forest Service, Rocky Mountain Research Station.

van Aardenne, J. A., F. J. Dentener, J. G. J. Olivier, C. G. M. K. Goldewijk, and J. Lelieveld (2001), A 1°×1° resolution data set of historical anthropogenic trace gas emissions for the period 1890–1990, *Global Biogeochem. Cycles*, *15* (4), 909-928, doi: 10.1029/2000gb001265.

van der Werf, G. R., J. T. Randerson, L. Giglio, G. J. Collatz, P. S. Kasibhatla, and A. F. Arellano Jr (2006), Interannual variability in global biomass burning emissions from 1997 to 2004, *Atmos. Chem. Phys.*, *6* (11), 3423-3441, doi: 10.5194/acp-6-3423-2006.

van der Werf, G. R., J. T. Randerson, L. Giglio, G. J. Collatz, M. Mu, P. S. Kasibhatla, D. C. Morton, R. S. DeFries, Y. Jin, and T. T. van Leeuwen (2010), Global fire emissions and the contribution of deforestation, savanna, forest, agricultural, and peat fires (1997–2009), *ACP*, *10*, 11707-11735.

Van Dingenen, R., F. Raes, J. P. Putaud, U. Baltensperger, A. Charron, M. C. Facchini, S. Decesari, S. Fuzzi, R. Gehrig, H. C. Hansson, R. M. Harrison, C. Huglin, A. M. Jones, P. Laj, G.

Lorbeer, W. Maenhaut, F. Palmgren, X. Querol, S. Rodriguez, J. Schneider, H. ten Brink, P. Tunved, K. Torseth, B. Wehner, E. Weingartner, A. Wiedensohler, and P. Wahlin (2004), A European aerosol phenomenology-1: physical characteristics of particulate matter at kerbside, urban, rural and background sites in Europe, *Atmos. Environ.*, *38* (16), 2561-2577, doi: 10.1016/j.atmosenv.2004.01.040.

Van-Hulle, P., M. Talbaut, M. Weill, and A. Coppalle (2002), Inversion method and experiment to determine the soot refractive index: application to turbulent diffusion flames, *Meas. Sci. Technol.*, *13* (3), 375-382.

Venkataraman, C., G. Habib, A. Eiguren-Fernandez, A. H. Miguel, and S. K. Friedlander (2005), Residential biofuels in south Asia: Carbonaceous aerosol emissions and climate impacts, *Science*, *307*, 1454-1456.

Venkataraman, C., G. Habib, D. Kadamba, M. Shrivastava, J. F. Leon, B. Crouzille, O. Boucher, and D. G. Streets (2006), Emissions from open biomass burning in India: Integrating the inventory approach with high-resolution Moderate Resolution Imaging Spectroradiometer (MODIS) active-fire and land cover data, *Global Biogeochem. Cycles*, *20* (Gb2013), doi: 10.1029/2005gb002547.

Viana, M., T. A. J. Kuhlbusch, X. Querol, A. Alastuey, R. M. Harrison, P. K. Hopke, W. Winiwarter, A. Vallius, S. Szidat, A. S. H. Prevot, C. Hueglin, H. Bloemen, P. Wahlin, R. Vecchi, A. I. Miranda, A. Kasper-Giebl, W. Maenhaut, and R. Hitzenberger (2008), Source apportionment of particulate matter in Europe: A review of methods and results, *J. Aerosol. Sci.*, *39* (10), 827-849, doi: 10.1016/j.jaerosci.2008.05.007.

Vignati, E., J. Wilson, and P. Stier (2004), M7: An efficient size-resolved aerosol microphysics module for large-scale aerosol transport models, *J. Geophys. Res.*, *109* (D22), doi: D22202, 10.1029/2003JD004485.

Vignati, E., M. Karl, M. Krol, J. Wilson, P. Stier, and F. Cavalli (2010), Sources of uncertainties in modelling black carbon at the global scale, *Atmos. Chem. Phys.*, *10* (6), 2595-2611.

Virkkula, A., N. C. Ahlquist, D. S. Covert, W. P. Arnott, P. J. Sheridan, P. K. Quinn, and D. J. Coffman (2005), Modification, calibration and a field test of an instrument for measuring light absorption by particles, *Aerosol Sci. Technol.*, *39*, 68-83.

Vogelmann, A. M., A. Robock, and R. G. Ellingson (1988), Effects of dirty snow in nuclear winter simulations, *J. Geophys. Res.*, *93* (D5), 5319-5332.

Walsh, M. P. (2008), Ancillary benefits for climate change mitigation and air pollution control in the world's motor vehicle fleets, *Annual Review of Public Health*, *29*, 1-9, doi: 10.1146/annurev.publhealth.29.091307.183257.

Wang, C. (2004), A modeling study on the climate impacts of black carbon aerosols, *J. Geophys. Res.*, *109* (D3), 106, doi: 10.1029/2003JD004084.

Wang, C. (2007), Impact of direct radiative forcing of black carbon aerosols on tropical convective precipitation, *Geophys. Res. Lett.*, *34* (5), 709, doi: 10.1029/2006GL028416.

Wang, C., D. Kim, A. M. L. Ekman, M. C. Barth, and P. J. Rasch (2009a), Impact of anthropogenic aerosols on Indian summer monsoon, *Geophys. Res. Lett.*, *36* (L21), 704, doi: 10.1029/2009GL040114.

Wang, S., X. Zhao, X. Li, W. Wei, and J. Hao (2009b), Emission characteristics of fine particles from grate firing boilers (in Chinese), *Environ. Sci.*, *30* (4), 963-968.

Wang, S. X., M. Zhao, J. Xing, Y. Wu, Y. Zhou, Y. Lei, K. B. He, L. X. Fu, and J. M. Hao (2010), Quantifying the air pollutants emission reduction during the 2008 Olympic games in Beijing, *Environ. Sci. Technol.*, *44* (7), 2490-2496, doi: 10.1021/es9028167.

Wang, Z. L., H. Zhang, and X. S. Shen (2011), Radiative forcing and climate response due to black carbon in snow and ice, *Adv. Atmos. Sci.*, *28* (6), 1336-1344, doi: 10.1007/s00376-011-0117-5.

Ward, D. E., R. A. Susott, J. B. Kauffman, R. E. Babbitt, D. L. Cummings, B. Dias, B. N. Holben, Y. J. Kaufman, R. A. Rasmussen, and A. W. Setzer (1992), Smoke and fire characteristics for cerrado and deforestation burns in Brazil – BASE-B experiment, *J. Geophys. Res.*, *97* (D13), 14601-14619.

Warneke, C., R. Bahreini, J. Brioude, C. A. Brock, J. A. de Gouw, D. W. Fahey, K. D. Froyd, J. S. Holloway, A. Middlebrook, L. Miller, S. Montzka, D. M. Murphy, J. Peischl, T. B. Ryerson, J. P. Schwarz, J. R. Spackman, and P. Veres (2009), Biomass burning in Siberia and Kazakhstan as an important source for haze over the Alaskan Arctic in April 2008, *Geophys. Res. Lett.*, *36* (2), L02813, doi: 10.1029/2008GL036194.

Warren, S. G., and W. J. Wiscombe (1980), A model for the spectral albedo of snow. II: Snow containing atmospheric aerosols, *J. Atmos. Sci.*, *37* (12), 2734-2745.

Warren, S. G. (1982), Optical-properties of snow, *Rev. Geophys.*, *20* (1), 67-89.

Warren, S. G., and W. J. Wiscombe (1985), Dirty snow after nuclear-war, *Nature*, *313* (6002), 467-470.

Warren, S. G., and A. D. Clarke (1990), Soot in the atmosphere and snow surface of Antarctica, *J. Geophys. Res.*, *95* (D2), 1811-1816.

Warren, S. G., I. G. Rigor, N. Untersteiner, V. F. Radionov, N. N. Bryazgin, Y. I. Aleksandrov, and R. Colony (1999), Snow depth on Arctic sea ice, *J. Climate*, *12* (6), 1814-1829.

Watson, J. G., J. A. Cooper, and J. J. Huntzicker (1984), The effective variance weighting for least-squares calculations applied to the mass balance receptor model, *Atmos. Environ.*, *18* (7), 1347-1355.

Watson, J. G., J. C. Chow, D. H. Lowenthal, L. C. Pritchett, C. A. Frazier, G. R. Neuroth, and R. Robbins (1994), Differences in the carbon composition of source profiles for diesel-powered and gasoline-powered vehicles, *Atmos. Environ.*, *28* (15), 2493-2505.

Watson, J. G., J. C. Chow, J. L. Bowen, D. H. Lowenthal, S. Hering, P. Ouchida, and W. Oslund (2000), Air quality measurements from the Fresno Supersite, *J. Air Waste Manage. Assoc.*, *50* (8), 1321-1334.

Watson, J. G., J. C. Chow, D. H. Lowenthal, N. F. Robinson, C. F. Cahill, and D. L. Blumenthal (2002), Simulating changes in source profiles from coal-fired power stations: Use in chemical mass balance of PM2.5 in the Mount Zirkel Wilderness, *Energy & Fuels*, *16* (2), 311-324, doi: 10.1021/Ef010202w.

Watson, J. G., J. C. Chow, and L.-W. A. Chen (2005), Summary of organic and elemental carbon/black carbon analysis methods and intercomparisons, *Aerosol Air Qual. Res.*, *5* (1), 65-102.

Watson, J. G., L. W. A. Chen, J. C. Chow, P. Doraiswamy, and D. H. Lowenthal (2008), Source apportionment: Findings from the US Supersites program, *J. Air Waste Manage. Assoc.*, *58* (2), 265-288, doi: 10.3155/1047-3289.58.2.265.

Weingartner, E., H. Saathof, M. Schnaiter, N. Streit, B. Bitnar, and U. Baltensperger (2003), Absorption of light by soot particles: determination of the absorption coefficient by means of aethalometers, *J. Aerosol. Sci.*, *34*, 1445-1463.

Wiacek, A., and T. Peter (2009), On the availability of uncoated mineral dust ice nuclei in cold cloud regions, *Geophys. Res. Lett.*, *36* (L17), 801, doi: 10.1029/2009GL039429.

Wild, O., M. J. Prather, and H. Akimoto (2001), Indirect long-term global radiative cooling from NO_x emissions, *Geophys. Res. Lett.*, *28* (9), 1719-1722.

Winebrake, J. J., J. J. Corbett, E. H. Green, A. Lauer, and V. Eyring (2009), Mitigating the health impacts of pollution from oceangoing shipping: An assessment of low-sulfur fuel mandates,

Environ. Sci. Technol., *43* (13), 4776-4782, doi: 10.1021/es803224q.

Winker, D. M., J. Pelon, J. A. Coakley, S. A. Ackerman, R. J. Charlson, P. R. Colarco, P. Flamant, Q. Fu, R. M. Hoff, C. Kittaka, T. L. Kubar, H. Le Treut, M. P. McCormick, G. Megie, L. Poole, K. Powell, C. Trepte, M. A. Vaughan, and B. A. Wielicki (2010), The Calipso mission A Global 3D view of aerosols and clouds, *Bull. Amer. Meteorol. Soc.*, *91* (9), 1211-1229, doi: 10.1175/2010bams3009.1.

Wiscombe, W. J., and S. G. Warren (1980), A model for the spectral albedo of snow. I: Pure snow, *J. Atmos. Sci.*, *37*, 2712-2733.

Wofsy, S. C., and H. S. T. C. M. T. S. Team (2011), HIAPER Pole-to-Pole Observations (HIPPO): fine-grained, global-scale measurements of climatically important atmospheric gases and aerosols, *Philos. Trans. R. Soc. A-Math. Phys. Eng. Sci.*, *369* (1943), 2073-2086, doi: 10.1098/rsta.2010.0313.

Wonaschuetz, A., R. Hitzenberger, H. Bauer, P. Pouresmaeil, B. Klatzer, A. Caseiro, and H. Puxbaum (2009), Application of the intergrating sphere method to separate the contributions of brown and black carbon in atmospheric aerosols, *Environ. Sci. Technol.*, *43* (4), 1141-1146, doi: 10.1021/es8008503.

Wooster, M. J., G. Roberts, G. L. W. Perry, and Y. J. Kaufman (2005), Retrieval of biomass combustion rates and totals from fire radiative power observations: FRP derivation and calibration relationships between biomass consumption and fire radiative energy release, *J. Geophys. Res.*, *110* (D24), 311, doi: 10.1029/2005JD006318.

World Bank (2011), Household Cookstoves, Environment, Health and Climate Change: A New look at an Old Problem, The International Bank for Reconstruction and Development/The World Bank, Washington, DC.

WRAP (2002), Non-burning management alternatives on agricultural lands in the western United States, Volume II: Non-burning management alternatives and implementation plan strategies, Western Air Regional Partnership, Prepared by Eastern Research Group, Inc. (ERG) , Sacramento, CA.

Xu, B., T. Yao, X. Liu, and N. Wang (2006), Elemental and organic carbon measurements with a two-step heatinggas chromatography system in snow samples from the Tibetan Plateau, *Ann. Glaciol.*, *43*, 257-262, doi: 10.3189/172756406781812122.

Xu, B., J. Cao, J. Hansen, T. Yao, D. R. Joswia, N. Wang, G. Wu, M. Wang, H. Zhao, W. Yang, X. Liu, and J. He (2009), Black soot and the survival of Tibetan glaciers, *P. Natl. Acad. Sci. USA*, *106* (52), 22114-22118, doi: 10.1073/pnas.0910444106.

Yang, M., S. G. Howell, J. Zhuang, and B. J. Huebert (2009), Attribution of aerosol light absorption to black carbon, brown carbon, and dust in China - interpretations of atmospheric measurements during EAST-AIRE, *Atmos. Chem. Phys.*, *9* (6), 2035-2050, doi: 10.5194/acp-9-2035-2009.

Yasunari, T. J., P. Bonasoni, P. Laj, K. Fujita, E. Vuillermoz, A. Marinoni, P. Cristofanelli, R. Duchi, G. Tartari, and K. M. Lau (2010), Estimated impact of black carbon deposition during pre-monsoon season from Nepal Climate Observatory - Pyramid data and snow albedo changes over Himalayan glaciers, *Atmos. Chem. Phys.*, *10* (14), 6603-6615, doi: 10.5194/acp-10-6603-2010.

Yokelson, R. J., R. Susott, D. E. Ward, J. Reardon, and D. W. T. Griffith (1997), Emissions from smoldering combustion of biomass measured by open-path Fourier transform infrared spectroscopy, *J. Geophys. Res.*, *102* (D15), 18865-18877.

Yoshimori, M., and A. J. Broccoli (2008), Equilibrium response of an atmosphere-mixed layer ocean model to different radiative forcing agents: Global and zonal mean response, *J. Climate*, *21* (17), 4399-4423, doi: 10.1175/2008jcli2172.1.

Yoshioka, M., N. Mahowald, A. Conley, W. Collins, D. Fillmore, C. Zender, and D. Coleman (2007), Impact of desert dust radiative forcing on Sahel precipitation: Relative importance of dust compared to sea surface temperature variations, vegetation changes and greenhouse gas warming, *J. Climate*, *20*, 1445-1467, doi: 10.1175/JCL14056.1.

Yu, H., M. Chin, D. M. Winker, A. H. Omar, Z. Liu, C. Kittaka, and T. Diehl (2010), Global view of aerosol vertical distributions from CALIPSO lidar measurements and GOCART simulations: Regional and seasonal variations, *J. Geophys. Res.*, doi: 10.1029/2009JD013364.

Yumimoto, K., and I. Uno (2006), Adjoint inverse modeling of CO emissions over Eastern Asia using four-dimensional variational data assimilation, *Atmos. Environ.*, *40* (35), 6836-6845, doi: 10.1016/j.atmosenv.2006.05.042.

Zarzycki, C. M., and T. C. Bond (2010), How much can the vertical distribution of black carbon affect its global direct radiative forcing?, *Geophys. Res. Lett.*, *37*, doi: L20807, doi:10.1029/2010GL044555.

Zhang, H., Z.-L. Wang, Z.-Z. Wang, Q.-X. Liu, S. Gong, X.-Y. Zhang, Z.-P. Shen, P. Lu, X.-D. Wei, H.-Z. Che, and L. Li (2011), Simulation of direct radiative forcing of aerosols and their effects on East Asian climate using an interactive AGCM-aerosol coupled system, *Clim. Dyn.*, doi: 10.1007/s00382-011-1131-0.

Zhang, J., K. R. Smith, Y. Ma, S. Ye, F. Jiang, W. Qi, P. Liu, M. A. K. Khalil, R. A. Rasmussen, and S. A.Thorneloe (2000), Greenhouse gases and other airborne pollutants from household stoves in China: A database for emission factors, *Atmos. Environ.*, *34*, 4537-4549.

Zhang, J., and J. S. Reid (2009), An analysis of clear sky and contextual biases using an operational over ocean MODIS aerosol product, *Geophys. Res. Lett.*, *36*, L15824, doi: 10.1029/2009GL038723.

Zhang, Q., J. L. Jimenez, M. R. Canagaratna, J. D. Allan, H. Coe, I. Ulbrich, M. R. Alfarra, A. Takami, A. M. Middlebrook, Y. L. Sun, K. Dzepina, E. Dunlea, K. Docherty, P. F. DeCarlo, D. Salcedo, T. Onasch, J. T. Jayne, T. Miyoshi, A. Shimono, S. Hatakeyama, N. Takegawa, Y. Kondo, J. Schneider, F. Drewnick, S. Borrmann, S. Weimer, K. Demerjian, P. Williams, K. Bower, R. Bahreini, L. Cottrell, R. J. Griffin, J. Rautiainen, J. Y. Sun, Y. M. Zhang, and D. R. Worsnop (2007), Ubiquity and dominance of oxygenated species in organic aerosols in anthropogenically-influenced Northern Hemisphere midlatitudes, *Geophys. Res. Lett.*, *34* (L13801), doi: 10.1029/2007gl029979.

Zhang, Q., D. G. Streets, G. R. Carmichael, K. B. He, H. Huo, A. Kannari, Z. Klimont, I. S. Park, S. Reddy, J. S. Fu, D. Chen, L. Duan, Y. Lei, L. T. Wang, and Z. L. Yao (2009), Asian emissions in 2006 for the NASA INTEX-B mission, *Atmos. Chem. Phys.*, *9* (14), 5131-5153, doi: 10.5194/acp-9-5131-2009.

Zhang, Y. X., J. J. Schauer, Y. Zhang, L. Zeng, Y. Wei, Y. Liu, and M. Shao (2008a), Characteristics of particulate carbon emissions from real-world Chinese coal combustion, *Environ. Sci. Technol.*, *42*, 5068-5073.

Zhang, Y. H., M. Hu, L. J. Zhong, A. Wiedensohler, S. C. Liu, M. O. Andreae, W. Wang, and S. J. Fan (2008b), Regional integrated experiments on air quality over Pearl River Delta 2004 (PRIDE-PRD2004): Overview, *Atmos. Environ.*, *42* (25), 6157-6173, doi: 10.1016/j.atmosenv.2008.03.025.

Zheng, M., G. R. Cass, J. J. Schauer, and E. S. Edgerton (2002), Source apportionment of PM2.5 in the southeastern United States using solvent-extractable organic compounds as tracers, *Environ. Sci. Technol.*, *36* (11), 2361-2371, doi: 10.1021/es011275x.

Zheng, M., L. G. Salmon, J. J. Schauer, L. M. Zeng, C. S. Kiang, Y.

H. Zhang, and G. R. Cass (2005), Seasonal trends in PM2.5 source contributions in Beijing, China, *Atmos. Environ.*, *39* (22), 3967-3976, doi: 10.1016/j.atmosenv.2005.03.036.

Zhi, G., Y. Chen, Y. Feng, S. Xiong, J. Li, G. Zhang, G. Sheng, and J. Fu (2008), Emission characteristics of carbonaceous particles from various residential coal-stoves in China, *Environ. Sci. Technol.*, *42* (9), 3310-3315, doi: 10.1021/es702247q.

Zhi, G. R., C. H. Peng, Y. J. Chen, D. Y. Liu, G. Y. Sheng, and J. M. Fu (2009), Deployment of coal briquettes and improved stoves: Possibly an option for both environment and climate, *Environ. Sci. Technol.*, *43*, 5586-5591, doi: 10.1021/es802955d.

Zhou, L., P. K. Hopke, and W. X. Zhao (2009), Source Apportionment of Airborne Particulate Matter for the Speciation Trends Network Site in Cleveland, OH, *J. Air Waste Manage. Assoc.*, *59* (3), 321-331, doi: 10.3155/1047-3289.s9.3.321.

Zobrist, B., C. Marcolli, T. Koop, B. P. Luo, D. M. Murphy, U. Lohmann, A. A. Zardini, U. K. Krieger, T. Corti, D. J. Cziczo, S. Fueglistaler, P. K. Hudson, D. S. Thomson, and T. Peter (2006), Oxalic acid as a heterogeneous ice nucleus in the upper troposphere and its indirect aerosol effect, *Atmos. Chem. Phys.*, *6* (10), 3115-3129, doi: 10.5194/acp-6-3115-2006.

Table R.1. Acronyms and abbreviations

Acronym	Definition
AAOD	aerosol absorption optical depth
AeroCom	Aerosol Comparison between Observations and Models
AERONET	Aerosol Robotic NETwork
AGTP	absolute global temperature change potential
AGWP	absolute global warming potential
AOD	aerosol optical depth
BB	biomass burning
BC-DRF	black-carbon direct radiative forcing
CALIPSO	Cloud Aerosol Lidar and Infrared Pathfinder Satellite Observations
CAM	Community Atmosphere Model
CAM3	Community Atmosphere Model3
CAM5	Community Atmosphere Model5
CAM-Oslo	Community Atmosphere Model-Oslo
CTM	chemical transport model
DRF	direct radiative forcing
ECHAM	European Centre HAmburg Model
EECCA	Eastern Europe, Caucasus and Central Asia
FF	fossil fuel
GAINS	Greenhouse Gas and Air Pollution Interactions and Synergies
GATOR	Gas, Aerosol, TranspOrt, Radiation model
GATOR-GCMOM	Gas, Aerosol, TranspOrt, Radiation - General Circulation, Mesoscale, and Ocean Model
GCM	global climate model
GHG	greenhouse gas
GISS	Goddard Institute for Space Studies
GOCART	Goddard Chemistry Aerosol Radiation and Transport model
GRA	albedo reduction via growth of snow grains with accelerating snow aging
GRB	increase in albedo reduction for a given BC concentration in coarse grained vs. fine-grained snow
GTP	global temperature change potential
GWP	global warming potential
HadGEM	Hadley Centre Global Environmental Model
HIPS	Hybrid Integrating Plate System
IE	indirect effect
IEA	International Energy Agency
IIE	ice cloud indirect effect
IMPACT	Lawrence Livermore National Laboratory (LLNL) Integrated Massively Parallel Atmospheric (IMPACT) Model
IMPROVE	Interagency Monitoring of Protected Visual Environments
IN	ice nuclei
IPCC	Intergovernmental Panel on Climate Change
ISSW	Integrating Sphere Sandwich Spectrophotometer
LES	large-eddy simulation
lidar	light detection and ranging
LOSU	level of scientific understanding
LSCE	Laboratoire des Sciences du Climat et de l'Environnement
MAC	mass absorption cross section
MBC	Increase in surface snow BC concentration via enhanced surface snow melt and retention of BC
MIE	mixed-phase cloud indirect effect
MISR	Multi-angle Imaging Spectroradiometer
MODIS	Moderate Resolution Imaging Spectroradiometer
MPI-HAM	Max Planck Institute-Meterology, Hamburg
MSC	mass scattering cross-section
NASA	National Aeronautics and Space Administration
NCAR	National Center for Atmospheric Research
OMI	Ozone Measurement Instrument
OPAC	Optical Properties of Aerosols and Clouds
PAS	photoacoustic spectrometer
ppm	part per million
PSAP	Particle Soot Absorption Photometer
RAINS	Regional Air Pollution Information and Simulation model
RETRO	Reanalysis of the TROposphere over the last 40 years
RF	radiative forcing
SAF	snow albedo feedback
SBC	change in surface snow BC concentration via change in sublimation
SPEW	Speciated Pollutant Emissions Wizard
SPRINTARS	
SP2	Single Particle Soot Photometer
SST	sea-surface temperature
ToA	top of the atmosphere
TRACE-P	Transport and Chemical Evolution over the Pacific

UIO-CTM	University of Oslo CCM
UMI	University of Michigan
USSR	Union of Soviet Socialist Republics
UTLS	upper-tropsphere-lower-stratosphere
UV	ultraviolet
WIE	warm cloud indirect effect
W	watt
WRF	Weather Research and Forecasting model

Table R.2. Chemical definitions

Chemical	Definition
BC	black carbon
CH_4	methane
CO	carbon monoxide
CO_2	carbon dioxide
EC	elemental carbon
Mg CO_2	megragram carbon dioxide
NMVOC	non-methane volatile organic compounds
NO	nitric oxide
NO_2	nitrogen dioxide
NO_x	sum of nitric oxide and nitrogen dioxide
OC	organic carbon
OM	organic matter
O_3	ozone
PM	particulate matter
$PM_{2.5}$	particulate matter less than 2.5 micron in diameter
POM	particulate organic matter
rBC	refractory black carbon
S	sulfur
SO_2	sulfur dioxide
VOC	volatile organic compounds

Table 0.1. Black carbon climate forcing terms, evaluated for industrial era (1750 - 2005) unless otherwise stated

Climate forcing term	Forcing components	Forcing (W m^{-2}) (90% uncertainty range)
Black carbon direct effect	Atmosphere absorption and scattering	+0.43 (+0.17 to +0.68)
Direct radiative forcing split	Fossil fuel sources	+0.17
	Bio fuel sources	+0.12
	Open burning sources	+0.15
Black carbon cloud semi-direct and indirect effects	Combined liquid cloud and semi-direct effect	-0.2 (-0.52 to -0.05)
	Black carbon in cloud drops	+0.2 (-0.1 to +0.7)
	Mixed phase cloud	+0.16 (+0.0 to +0.32)
	Ice clouds	0.0 (-0.4 to +0.4)
	Combined cloud and semi-direct effects	+0.17 (-0.45 to +0.86)
Black carbon snow and sea-ice effects	Snowpack effective forcing	+0.11 (+0.016 to +0.31)
	Sea-ice effective forcing	+0.033 (+0.014 to +0.064)
	Combined surface forcing terms	+0.14 (+0.04 to 0.34)
Total effective forcings	Black carbon only	+0.77 (-0.06 to +1.53)
	Black carbon + co-emitted species:	
	All sources	-0.08 (-1.24 to +0.81)
	Excluding open burning	+0.004 (-0.62 to +0.57)
All source (includes pre-industrial) forcings	Direct radiative forcing	+0.49 (+0.20 to +0.76)
	Snow pack effective forcing	+0.12 (+0.02 to +0.36)
	Sea-ice effective forcing	+0.036 (+0.016 to +0.068)

Table 1.1. Definition of climate forcing and response terms

Forcing term	Definition	Model calculation
Climate forcing	Generic term encompassing all forcing types below, quantifying a perturbation to the Earth's energy balance in W m^{-2}	
Radiative forcing (RF)	RF is the change in the net vertical irradiance at the tropopause caused by a particular constituent. Usually RF is computed after allowing for stratospheric temperatures to readjust to radiative equilibrium, but with all tropospheric properties held fixed at their unperturbed values. Radiative forcing without stratospheric adjustment is called instantaneous.	Difference between simulations: 1) with radiative effect of the constituent change 2) without radiative effect of constituent change Held constant: All other tropospheric quantities, including cloud
Rapid adjustment	Globally averaged flux change from the adjustment of the troposphere and land-surface to a radiative forcing, whilst holding the globally averaged surface temperature constant.[a] Energy balance perturbations arise from temperature, cloud and constituent changes in the troposphere, and from land-surface temperature and moisture changes. These changes occur within one year after a forcing is applied, usually within a few days but up to a season in the case of snow pack changes. For BC the rapid adjustment to the direct effect is also called the "semi-direct effect". The radiative forcing plus the rapid adjustment gives the "adjusted forcing" (see below).	Difference between models: 1) with radiative effect of constituent change and changes in cloud and land-surface temperature 2) with radiative effect of constituent change and no tropospheric response Held constant: global mean surface temperature [a]
Adjusted forcing	Flux perturbation from a given mechanism, allowing for changes in the stratosphere, troposphere and land surface, but not the global mean surface temperature. This is the sum of a radiative forcing plus its rapid adjustment.	Difference between models: 1) with atmospheric constituent change and full atmospheric response 2) without atmospheric constituent change Held constant: global mean surface temperature response [a]
Effective radiative forcing	A radiative forcing or adjusted forcing multiplied by its efficacy (see below) to give a climate forcing that is comparable to an equivalent climate forcing from carbon dioxide changes. Effective radiative forcing includes rapid adjustments, and it also accounts for differences in globally averaged responses due to latitudinal dependence of forcing.	The efficacy is calculated for the constituent of interest in a climate model (see below). This is then multiplied by the associated radiative forcing or adjusted forcing to give the effective forcing. [b]

Table 1.1. Definition of climate forcing and response terms (cont'd)

Response term	Definition	Model calculation
Climate response	Large scale long-term changes in temperature, snow and ice cover and rainfall caused by a specific forcing mechanism. One of the most important climate responses is that of equilibrium globally averaged surface temperature (ΔT).	Diagnostics from a global atmospheric climate model, either coupled to a mixed layer ocean for equilibrium experiments or a full ocean model for transient experiments
Climate sensitivity (λ)	Equilibrium globally averaged surface warming per W m^{-2} of forcing (F), either radiative forcing or adjusted forcing. $\lambda = \Delta T/F$.	Computed from the climate response and radiative forcing diagnostics of a equilibrium climate model integration (see above)
Efficacy (E)	Ratio of the climate sensitivity for a given forcing agent (λ_i) to the climate sensitivity for CO_2 changes (*i.e.*, $E_i = \lambda_i / \lambda_{CO2}$). Efficacy can then be used to define an effective forcing ($= E_i F_i$), where F_i can either be radiative forcing or the adjusted forcing.	Computed from equilibrium climate model experiments with the constituent of interest, compared these with equivalent climate model diagnostics for a $2xCO_2$ experiment. Global mean equilibrium temperature and radiative forcing diagnostics are needed.
Climate impact	Regional or local changes in weather and or climate indicators such as heat waves and storms that impact human livelihoods.	Diagnosed from a climate model integration

[a] The adjusted forcing can be computed in different ways. Either regression can be used to determine the forcing at zero global temperature change or a fixed SST model forcing can be modified to account for a change in land-temperatures, after *Hansen et al.* 2005, to give an estimate of the zero global surface T response forcing. The semi-direct effect is computed as the difference between the whole atmosphere adjusted forcing and the radiative forcing when the aerosol direct effect is included. The adjusted forcing for the cryosphere terms employs a different methodology (see Section7.2.)

[b] For all changes apart from the snow and sea ice terms we assume that this effective forcing is the same as the adjusted forcing. This is justified from *Hansen at al.* (2005) and *Shine et al.* (2003) who showed that for most forcings the rapid adjustment accounted for the non-unity efficacy of the radiative forcing terms. However, for snow and sea ice changes this is not the case. Their forcings directly influence surface snow and ice and, because they occur at high latitudes, the resulting heating is confined to the near surface. These forcings accelerate snow and ice melt, leading to a strong positive surface albedo feedback. These feedbacks lead to a very high efficacy that their associated rapid adjustments do not account for. Hence, the snow-pack forcings are scaled to account for its enhanced climate response to give an effective forcing.

Table 2.1. Techniques for measuring BC mass, method-defined terminology for BC, and sources of systematic biases

Technique	Common name	Common instruments	Suggested name	Sources of bias	Direction of bias [a]
Optical absorption	BC	Aethalometer; Particle Soot Absorption Photometer (PSAP);	Equivalent BC (BC + other absorbing material)	Change in MAC with aerosol aging [b]	+, -
		Multi-Angle Absorption Photometer		Presence of light-absorbing organic carbon (filter-based only)	+
		(MAAP)		Presence of other absorbers (dust, organic carbon) [c]	+
Optical absorption with heated inlet	BC	Continuous Soot Monitoring System (COSMOS)	Equivalent BC	Charring of low volatility organic species	+
Thermal-heating and optical absorption	Elemental carbon (EC)	Thermal Optical Reflectance (TOR); Thermal Optical Transmittance (TOT)	Apparent elemental carbon (EC_a)	Failure to accurately correct for charred organic carbon;	+
				Catalytic oxidation of BC in presence of metals or metal oxides;	-
				Absorption by charred material affects split between OC and EC [d]	-
				Detection of less-volatile organic carbon	+
Continuous-laser induced incandescence	BC or Refractory BC (rBC)	Single Particle Soot Photometer (SP2)	Refractory BC (rBC)	Lack of detection of small particles [e]	-

[a] (+) = BC measured too high; (-) = BC measured too low.

[b] If calibrated with fresh, unmixed BC, measurement overestimates BC mass after mixing with non-absorbing species and increase in absorption.

[c] Depends on wavelength; measurements around 630 nm often are unaffected unless dust concentrations are high.

[d] More extreme for transmission-based monitoring of charring.

[e] Particles with mass below about 80 fg, corresponding to a spherical particle of about 80 nm diameter.

Table 3.1. Recommended grade levels for inventories of energy-related emissions

Level	Activity data	Emission factors
Low	National fuel use for each fuel and sector or commodity	Sectoral averages *Low-*: Global average *Low+*: Regionally-specific average
Medium	National fuel use for each fuel and sector or commodity, apportioned by technology	Specific to each technology and fuel *Medium-:* Some extrapolation from other countries *Medium+*: Full participation of country in specifying activity
High	Country tabulations of technology divided by substantially different emission characteristics; identification of major individual point sources	Measured at each installation or closely matched to emitting technology, including control

Table 3.2. Recommended grade levels for inventories of open-burning emissions

Level	Forest, grassland, or woodland burned area	Fuel load (FL) and combustion completeness (CC)	Emission factors	Agricultural waste
Low	Global satellite product	Aggregated ecosystem-dependent estimates at grid cell level	Default (3 ecosystem average values)	Global data compilations of burned mass
Medium-	Satellite product, plus fire hot spot data and retrieval uncertainty assessment	Ecosystem-dependent estimates at fire pixel level , FL and CC highly aggregated (< 12 ecosystem classes)	3 ecosystem average values with adjustments for peat soils	Bottom-up inventory using regional-scale information
Medium+	Satellite product, plus fire hot spot data and retrieval uncertainty assessment	Finer aggregation of FL and CC	3 ecosystem average values with adjustments for peat soils	
High	High-resolution (spatial and temporal) satellite product or complete aerial surveillance, fire hot spot and fire radiative power;	Information on available fuel load and combustion parameters at tree stand level	Ecosystem based emission factors with adjustments dependent on fire behaviour (at least 12 global ecosystem classes)	Cross-validation of satellite-derived and bottom-up estimates for agricultural waste burning emissions

Table 3.3. Best-estimate values for BC and POA emissions in year 2000 [a] (Gg yr^{-1})

	BC	BC range	POA	POA range
All sources				
Energy-related	4770	1220 to 15000	15900	8800 to 23800
Open burning	2760	800 to 13800	31100	9000 to 156000
Total All-source	7530	2020 to 28800	47000	17800 to 179000
1750 Background				
Energy-related	390		1560	
Open burning	1020		12800	
Total background	1410		14360	
Industrial-era				
Energy-related	4380		14300	
Open burning	1740		18300	
Total Industrial era	6120		32600	

[a] Energy-related emissions are from year 2000; open-burning emissions are a climatological average of years around year 2000.

Table 3.4. Central estimates of all-source global black-carbon emissions from open biomass burning (Gg yr^{-1})

	Inventory					
	GFED [a]		RETRO [b]	RETRO [c]	GAINS	SPEW
	2000	clim.	2000	clim.	2000	clim. [d]
Grassland and woodland fires [e]						
Grassland and open savanna	820	850	310	290		
Woodland	330	350	1220	1220		
Total grassland and woodland	1150	1200	1530	1510		1710
Forest fires						
Deforestation and degradation	230	440	n.s.	n.s.		
Forest (excluding deforestation and degradation)	300	370	n.s.	n.s.		
Peat	2	130	n.s.	n.s.		
Total forest fires	530	940	830	1240		1240
Agricultural waste burning [f]	50	60	n.e.	n.e.	290	330
Grand total	1730	2200	2370	2750		3280

[a] Version 3.1 from http://www.falw.vu/~gwerf/GFED/GFED3/tables/emis_BC_absolute.txt; clim.: mean climatological values from 1997 to 2006.

[b] n.s. = not specified; n.e. = not estimated.

[c] clim.: mean climatological values for 1996 to 2000.

[d] SPEW totals provide a climatological average rather than representing any particular year.

[e] GFED and RETRO have different classifications of grasslands and woodlands.

[f] GFED agricultural waste burning is inferred from remote-sensing data and includes only large fires, while GAINS and SPEW are based on activity estimates.

Table 3.5. Bottom-up central estimates of all-source global black carbon emissions from energy-related combustion in the year 2000 (Gg yr^{-1}) [a]

	Inventory	
Source	SPEW	GAINS
Diesel engines		
On-road diesel engines	840	780
Off-road diesel engines	480	370
Total diesel	1320	1150
Industrial coal		
All coal in industry	740	340
Total industrial coal	740	340
Residential solid fuel		
Wood, cooking regions	1000	1580
Other biofuel, cooking regions	290	310
All biofuel, heating regions	260	200
Coal, cooking and heating	330	420
Total residential solid fuel	1880	2510
Other sources		
Non-coal industry, including biofuel	170	30
On-road gasoline engines	110	80
Residential, including diesel generation	100	170
Aviation	20	1 [b]
Shipping	100	40 [c]
Flaring	- [d]	260
All other BC-rich sources	70	20
Power plants [e]	20	20
Other low-BC sources [e]	- [d]	60
Total other sources	590	690
Grand total	4510	4690

[a] Data are based on year-2000 energy data and technology. Totals do not match exactly due to rounding.

[b] Includes only landing and takeoff (no cruise) emissions.

[c] Does not include international shipping.

[d] Not estimated.

[e] Considered to be low-BC sources.

Table 3.6. Black carbon emission inventory grades

Region	Energy-use		Open burning
	Urban	Rural	
North America	High	High	Medium+
Latin America	Medium+	Low	Low
Europe	High	High	Medium+
Former USSR	Low	Low	Medium-
Middle East	Low	Low	Low
Pacific	Low	Low	Low
Africa	Low	Low	Medium-
East Asia	High	Medium+	Medium-
South Asia	Medium+	Low	Low
Southeast Asia	Low	Low	Low

[a] Highest possible inventory grades based on current available disaggregation of activity and emission data for different world regions. Grades defined in Table 3.1 and 3.2.

Table 3.7. Bottom-up estimates of all-source global and regional BC and OC emission rates from energy-related sources (fossil fuel and biofuel combustion) [a]

Source	Emission rate (Gg yr^{-1}) BC	OC [b]	Inventory level [c]	Year of estimate
Global				
GAINS [*Cofala et al.,* 2007] [d]	4700	12300	Med-/+	2000
SPEW [*Bond et al.,* 2007] [d]	4530	8700	Med-	2000
Cooke et al. [1999]	6100 [e]	16000 [e]	Low+	1984
Penner et al. [1993]	12600	-	Low-	1980
India				
Reddy and Venkataraman [2002a,b]	400	1150	High/ Med	2000
Sahu et al. [2008]	1300	-	Low+	2001
Parashar et al. [2005]	900 [f]	2300 [f]	Low+	1995
Ohara et al. [2007]	800	3300	Low+/Med-	2000
Streets et al. [2003b]	600	2800	Med-	2000
Klimont et al. [2009]	750	1600	Med+	2000
Lu et al. [2011]	680	1700	Med+	2000
	920	2200		2010
GAINS	580	1900	Med+	2000
SPEW	500	1600	Med-	2000
China				
Cao et al. [2006]	1500	4200		2000
Streets et al. [2003b]	1000	3400	Med-	2000
Zhang et al. [2009]	1600	2800	Med+	2001
	1800	3200	Med+	2006
Klimont et al. [2009]	1200	2800	Med+	2000
Lu et al. [2011]	1200	2400	Med+	2000
	1700	3400		2010
GAINS	1100	3500	Med+	2000
SPEW	1200	2800	Med-	2000
United States				
Reff et al. [2009]	440	960	High	2000
Battye et al. [2002]	430	-	High	1999
SPEW	350	500	Med-	2000
GAINS	260	370	Med-	2000

[a] Subsets of global inventories are given under each country for comparison. All emission rate values are rounded.

[b] Because most inventories report OC emission rates rather than POA, OC values are given here.

[c] See Table 3.6 for definitions of inventory levels.

[d] GAINS and SPEW emission factors and technology divisions have been updated since the original publications describing the methodology.

[e] Paper includes fossil fuel emissions only (5100 Gg yr^{-1} BC, 7000 Gg yr^{-1} OC). For comparability with other global estimates, we added biofuel emissions from *Liousse et al.* [1996]; the two inventories are often used together. Bulk BC emissions (rather than only submicron emissions) are estimated to be 6400 Gg yr^{-1}.

[f] Average of range: 400-1400 for BC, 1200-3300 for OC.

Table 3.8. Major sources contributing to urban BC (USA) and PM2.5 (other world regions) [a,b]

Region	Sources	Cities	Sample references
North America	TR, IN, SA, RE	Anchorage, Atlanta, Baltimore, Buffalo, Burlington, Camden, Chester, Chicago, Cleveland, Detroit, Dover, Elizabeth, Indianapolis, Los Angeles, New Brunswick, New York City, Portland, Rochester, San Jose, San Diego, Seattle, St Louis, Wilmington	*Chen et al.* [2010b]; *Sheesley et al.* [2010]; *Zhou et al.* [2009]; *Watson et al.* [2008]; *Gildemeister et al.* [2007]; *Kim and Hopke* [2007]
Latin America	TR, IN, RE	Mexico City, Santiago, Sao Paolo	*Johnson et al.* [2006]; *Johnson et al.* [2011b]
Europe	TR, IN, SA	Areao, A Coruña, Ballinasloe, Birkenes, Skrealaden, Coimbra, Lisbon, L'Hospitalet, Milan, Gent, Waasmunster, Amsterdam, Dublin, Cork, Birmingham, Duisburg, Erfurt, Helsinki, Dresden, Huelva	*Viana et al.* [2008]; *van Dingenen et al.* [2004]; *Hazenkamp-von Arx et al.* [2004]; *Manoli et al.* [2002]; *Götschi et al.* [2005]; *Houthuijs et al.* [2001]
Africa	OB, RE, IN, TR	Cairo, Oalabotjha, Addis Ababa (qualitative)	*Abu-Allaban et al.* [2002]; *Engelbrecht et al.* [2002]; *Etyemezian et al.* [2005]
East Asia	IN, RE, TR	Shanghai (TC), Beijing, Xi'an	*Song et al.* [2006]; *Zheng et al.* [2005]; *Cao et al.* [2005]
South Asia	TR, IN, OB, RE	Delhi, Mumbai, Kolkata, Chandigarh, Hyderabad, Dhaka, Rajshahi	*Chowdhury et al.* [2007]; *Johnson et al.* [2011b]
Southeast Asia	TR, IN, RE	Bangkok, Hanoi, Bandung, Manila	*Hien et al.* [2004]

[a] Estimated from receptor modeling, in order of decreasing importance. TR= transport (vehicle exhaust including gasoline and diesel); IN = industry including coal and oil and biomass burning; coal burning power plants; RE = residential energy; OB = open burning of biomass and refuse; SA = secondary aerosols; O = Others.

[b] In receptor modeling, quantity assessed is usually elemental carbon from thermal-optical analysis rather than BC. Here, the major sources of both substances are assumed to be the same.

Table 4.1. Observations that contribute to the understanding of black-carbon distributions

Type of monitoring	Spatial coverage	Major contributions
Intensive field campaigns	Single point, surface or aircraft	In-depth examination of aerosol properties and transformation processes
In-situ monitoring (includes networks)	Single point, surface	Long-term average aerosol concentrations, properties, and fluctuations in remote or urban locations
Ground-based remote sensing (includes networks)	Single point, column	Long-term averages and fluctuations of aerosol optical depth and inferences about other optical properties, often with unattended operation
Space-based remote sensing	Global coverage, column	Global coverage of aerosol optical depth, with limited information on properties

Table 4.2. Largest global or regional ground-based observational networks providing long-term measurement information on aerosol absorption or black-carbon concentrations

Network	Location and # of sites	Dates	Products	Comments (Reference or URL)
AERONET	World 400+	1996 - present	AAOD (column)	AOD*(1-SSA), less accuracy at lower AOD (http://aeronet.gsfc.nasa.gov/)
IMPROVE	US 100+	1985 - present	Absorption coefficient, EC measurement (ground)	(http://vista.cira.colostate.edu/improve/)
EMEP	Europe 70	1989-present	PM (ground)	(http://www.emep.int/)
EUSAAR	Europe 10	2007-present	Absorption coefficient (ground)	(http://www.eusaar.net/)
ABC	10	2004-present	Absorption coefficient, EC	*Ramanathan et al.* [2007] *Bonasoni et al.* [2010]
CMDL	7+ cooperative	1994-present	Absorption coefficient	http://www.esrl.noaa.gov/gmd/aero/net/index.html
AIRPET	Asia 6	2001-2004+	BC by reflectance, $PM_{2.5}$	*Oanh et al.* [2006]
CARIBIC	1 container (Lufthansa)	2005-present	Absorption (in-situ)	(http://www.caribic-atmospheric.com)

Table 5.1. Global industrial-era or all-source black-carbon mass-related properties as simulated by several models [a]

Model	Reference	EMI [b]	Lifetime [c]	Load above 5 km [d]	Ind-era fraction BC AOD [e]	Load [f]	Mixing [g]	MAC [h]	BC AAOD [i]
		Tg yr^{-1}	d	%	%	mg m^{-2}		m^2 g^{-1}	*1000
AeroCom models									
GISS	*Schulz et al.* [2006]	6.3	7.2	21.2	80	0.24	Ext	8.4	1.83
LOA	*Schulz et al.* [2006]	6.3	7.3	19.1	80	0.25	Ext	8.0	1.98
LSCE	*Schulz et al.* [2006]	6.3	7.5	40.6	73	0.25	Ext	4.4	1.11
MPI-HAM	*Schulz et al.* [2006]	6.3	4.9	6.1		0.16	Int	7.7	1.23
SPRINTARS	*Schulz et al.* [2006]	6.3	10.6	19.1	78	0.37	Ext	9.8	3.50
UIO-CTM	*Schulz et al.* [2006]	6.3	5.5	14.5	88	0.19	Ext	7.2	1.34
UIO-GCM	*Schulz et al.* [2006]	6.3	5.5	32.7	89	0.19	Int	10.5	1.95
UMI	*Schulz et al.* [2006]	6.3	5.8	17.5	79	0.19	Ext	6.8	1.29
Other models									
BCC_AGCM [k]	*Zhang et al.* [2011]	7.7	3.31	16		0.14	Ext	4.3	0.60
CAM3 ECA	*Kim et al.* [2008]	14.4	3.75			0.29	Ext	10.6	3.06
CAM5 3-mode	*Ghan et al.* [2012]	5.7	3.6		68	0.11	Int	15.0	1.65
GATOR [k]	*Jacobson* [2010]	4.7	5.9			0.25	Int	14	3.11
GISS-GCM II	*Chung and Seinfeld* [2002]	11.5	6.4		91	0.39	Ext		
		11.5	6.4		91	0.39	Int	7.8	3.01 [j]
GOCART [k]	*Textor et al.* [2006]	13.9	7.16	32		0.53	Ext	8.1	4.1
MACR-Assim [k]	*Ramanathan and Carmichael* [2008]	13.9 [l]					n/a		5.8 [m]
UIO-CTM	*Myhre et al.* [2009]	6.3	5.5		91	0.19	Ext	7.3	1.39 [j]
		6.3	5.5		91	0.19	Int		

[a] AeroCom models UMI-SPRINTARS represent difference between present day and preindustrial simulations: AeroCom experiments B and PRE.

[b] EMI= Emissions. For comparison to emission totals in the rest of the document, 1 Tg = 1000 Gg.

[c] Lifetime computed from load and emissions.

[d] Load above 5 km refers to the fraction of BC mass above 5 km altitude (from *Textor et al.*, 2006).

[e] Ind-era fraction BC AOD: Industrial-era fraction of BC aerosol optical depth.

[f] Load is global area weighted column mass of BC.

[g] Int = Treatment or explicit assumption of internal mixing; Ext = External mixing, or no explicit treatment of internal mixing, even if a relatively high value of MAC was uniformly applied to all aerosol.

[h] MAC: mass absorption coefficient due to BC.

[i] Absorption aerosol optical depth due to industrial-era BC, except for MACR-Assim, GOCART, GATOR and BCC_AGCM, which use all-source BC.

[j] Inferred from column burden of BC and MAC_{BC} given for pure BC. This calculation cannot be done for internal mixtures, as MAC_{BC} depends on the aerosol composition.

[k] All-source BC is reported for these models rather than the industrial-era component.

[l] Emissions in underlying GOCART model, but modified through assimilation.

[m] C.E. Chung, personal communication [2010], and *Chung et al.* [2005].

n/a = not applicable

Table 5.2. Global averages of aerosol absorption optical depth (AAOD) industrial-era (ind.-era) or all-source BC direct radiative-forcing (DRF) measures as simulated in several models. [a]

	Model values				Normalized values		Scaled BC-DRF	
Model	BC quantity	BC AAOD [b]	BC-DRF TOA [c]	BC-Atm RF [d]	AFE [e]	Normalized DRF [f]	Ind.-era TOA [g]	All-source TOA [h]
Units		*1000	W m^{-2}	W m^{-2}	W m^{-2}/ AAOD	W g^{-1}	W m^{-2}	W m^{-2}
AeroCom models								
GISS	Ind. era	1.83	0.22		120	920	0.36	0.41
LOA	Ind. era	1.98	0.32		159	1280	0.48	0.55
LSCE	Ind. era	1.11	0.30	0.85	270	1200	0.81	0.92
MPI-HAM	Ind. era	1.23	0.20		165	1250	0.49	0.55
SPRINTARS	Ind. era	3.50	0.32	1.00	91	870	0.27	0.31
UIO-CTM	Ind. era	1.34	0.22		164	1160	0.49	0.56
UIO-GCM	Ind. era	1.95	0.36		184	1900	0.55	0.63
UMI	Ind. era	1.29	0.25	0.89	194	1320	0.58	0.66
Other models								
BCC-AGCM	All	0.60	0.10		166	710	0.50	0.55
CAM3 ECA	Ind. era	3.06	0.57	1.57	186	1970	0.56	0.63
CAM5 3-mode	Ind. era	1.65	0.30		182	2730	0.54	0.62
GATOR	All	3.11	0.55		177	1830	0.53	0.60
GISS-GCM II ext	Ind. era	3.01	0.51		170	1310	0.51	0.58
GISS-GCM II int	Ind. era		0.79			2030		
GOCART	All	4.1						
MACR-Assim	All	5.80	0.90	2.6	155		0.46	0.53
UIO-CTM ext	Ind. era	1.30	0.26		187	1370	0.56	0.63
UIO-CTM int	"		0.33			1740		
Average ± 1σ							0.51 ± 0.11 [i]	0.58 ± 0.13 [i]

[a] All model values are those reported by the listed model for either industrial-era (Ind. era) or all-source (All) BC emissions. See Table 5.1 for references associated with each model.

[b] BC AAOD: Absorption optical depth due to modeled BC, either industrial era or all-source emissions.

[c] BC-DRF TOA: Top of atmosphere all-source (MACR-Assim and GOCART) or industrial-era (all other models) shortwave radiative forcing from unscaled AeroCom models.

[d] BC-DRF-Atm: Atmospheric radiative forcing of column due to modeled BC.

[e] AFE: Normalized radiative forcing per unit absorption aerosol optical depth.

[f] Normalized DRF: Direct radiative forcing normalized to BC column load (g).

[g] Industrial-era BC-DRF TOA scaled: Top-of-atmosphere industrial-era shortwave radiative forcing after scaling to 2.63 x 10^{-3} industrial-era absorption optical depth.

[h] All-source BC-DRF TOA adjusted: Top-of-atmosphere all-source shortwave radiative forcing by BC after scaling to 3.2 x 10^{-3} all-source absorption optical depth.

[i] Final central estimate of direct forcing is 15% lower than these values to account for BC vertical distribution (Section 5.7.2)

Table 5.3. Modeled, scaled, and current bottom-up annual BC emissions by region in Gg yr^{-1}

	Energy-related emissions			Open biomass emissions			Total emissions	
Region	Modeled [a]	Scaled [b]	Current [c]	Modeled [d]	Scaled [b]	Current [c]	Scaled [b]	Current [c]
North America	340	300	330	80	100	40	400	370
Latin America	400	600	360	590	900	720	1500	1080
Middle East	80	50	140	0	0	0	50	140
Africa	500	500	680	1520	1400	1140	1900	1820
Europe	450	400	470	10	10	10	410	480
EECCA	270	200	310	280	200	120	400	430
South Asia	610	1200	670	20	30	40	1230	710
East Asia	1440	1700	1310	10	10	50	1710	1360
Southeast Asia	380	800	400	400	1100	460	1900	860
Pacific	130	200	120	190	400	170	600	290
All-source	4600	5950	4790	3100	4150	2750	10100	7540
Pre-industrial	390	390	390	1030	1030	1030	1420	1420
Industrial-era	4210	5560	4400	2070	3120	1720	8680	6120

[a] Based on SPEW emissions, which were used in many AeroCom models.

[b] Modeled regional emissions adjusted by burden scale factors as described in Section 5.5.1.

[c] As reported in Tables 3.4 and 3.5, and Figures 3.2 and 3.3, for comparison with the initial and scaled modeled values given here. Current energy-related emissions are a composite of SPEW and GAINS as described in Section 3. Current biomass burning emissions given here are from RETRO only and do not match the central estimate for that reason. Biomass burning estimates have decreased substantially since the initial AeroCom exercise.

[d] Based on GFED 2.0 emission fields, reported as the source of open-burning emissions for AeroCom models [*Dentener et al.*, 2006]. Regions scaled identically to total emission rate reported for AeroCom exercise.

[e] Pre-industrial emissions estimated by *Dentener et al.* [2006], and assumed to be constant to estimate industrial-era forcing.

Table 6.1. Studies used to estimate values of the semi-direct effect

Study	Reported semi-direct effect (W m^{-2})	Adjustment type (Value used in study) [a]	Adjusted Effect (W m^{-2})
Semi-direct effect calculated directly			
Wang [2004]	-0.16	EM (14 Tg yr^{-1})	-0.10
Penner et al. [2003]	-0.01, surface emissions	EM (12.2 Tg yr^{-1})	-0.01
	-0.39, lofted BB emissions	EM (BB) (5.6 Tg yr^{-1})	-0.20
Semi-direct effect inferred from efficacy [b]			
Yoshimori and Broccoli [2007]	-0.40	DRF (+0.99 W m^{-2})	-0.18
Hansen et al. [2005]	-0.08	DRF (+0.19 W m^{-2})	-0.18
Hansen et al. [2005]	-0.11	DRF (+0.49 W m^{-2})	-0.09
Jones et al. [2007]	-0.11	DRF (+0.39 W m^{-2})	-0.12
Chung and Seinfeld [2005]	-0.1	DRF (+0.33 W m^{-2})	-0.13

[a] Adjustments: EM = scaled from BC emissions used in study to our estimate of BC emissions (8.6 Tg yr^{-1} or 3 Tg yr^{-1} for biomass); DRF = scaled from BC direct forcing found in study to direct forcing of +0.43 W m^{-2}; BB = biomass burning. For comparison to emission values in the remainder of the document, 1 Tg = 1000 Gg.

[b] Reported effect = DRF x (1 - efficacy).

Table 6.2. Studies that provide indirect effect estimates

Study	Reported indirect effect (W m^{-2})	Emissions changed in study; (BC/OC (Tg yr^{-1})) [a]	Adjusted IE for BC (W m^{-2}); adjustment method [b]	Effects [c]; diagnostic method [d]
Liquid clouds (microphysics and lifetime)				
Kristjansson [2002]	-0.1	100% BC; 12.4/0	ALL: -0.07 EM	WIE, SD (DE); M1
Chen et al. [2010a]	-0.13 ± 0.33	50% FF BC+OC; 1.5/2.2	FF: -0.08 EM, SZ	WIE; M1
	-0.31 ± 0.33	50% ALL BC+OC; 3.9/30	ALL: -0.08 EM	
Bauer et al. [2010]	+0.05	100% FF BC [f]; 3.0/0	FF: +0.11; EM, SD	WIE, SD (DE); M1
	-0.12	50% FF+BF BC; 2.3/0	BF: -0.05; EM, SD	
	-0.2	100% BF BC+OC; 1.6/6.4	FF+BF: -0.19; EM, SD	
Koch et al. [2011b] [e]	-0.08 to +0.31	100% FF BC [f]; 3.0/0	FF: +0.03 (-0.09 to +0.15); EM, SD, DE	WIE, SD, DE; M3
	-0.2 to +0.08	100% BF BC+OC; 1.6/6.4	BF: -0.05 (-0.06 to +0.01); EM, SD, DE	
Spracklen et al. [2011]	-0.23	100% FF+BF BC+OC	FF+BF: -0.08 EM	WIE
	-0.34	100% ALL BC+OC	ALL: -0.06 EM	
Storelvmo et al. [2012]	-0.01	100% FF	ALL: -0.01	WIE
Mixed-phase clouds				
Lohmann and Hoose [2009]	+0.12	Process changed, not emission; 6.3/0	ALL: +0.12; None	MIE (WIE, SD); M2
	+0.2		ALL: +0.2; None	
Storelvmo et al. [2011]	+0.16 ± 0.08	100% BC; 6.3/0	ALL: +0.16; None	MIE (WIE, SD); M2
Ice clouds				
Penner et al. [2009]	-0.3, -0.4	100% BC+OC; 13.5/97	ALL: -0.27; EM	IIE; M1
Liu et al. [2009a]	+0.22, +0.39	100% BC+OC; 13.5/97	ALL: +0.24; EM	IIE, SD (WIE, DE); M3
All effects, including direct and cryosphere				
Jacobson [2010] [g, h]	+0.47	100% FF BC+OC; 3.2/2.4	FF: +0.47	WIE, SD, DE, MIE, IIE, CRY, CLIM
	+0.68	100% FF+BF BC+OC, BF gases	FF+BF: +0.68	

Table 6.2 Footnotes

[a] FF = fossil fuel, BF = biofuel, BB = biomass burning; ALL = FF + BF + BB. When a percentage reduction is given, it refers to all-source emissions. For comparison to emission values in the remainder of the document, 1 Tg = 1000 Gg.

[b] Adjustments: EM = scaled from mass of emissions used in study to our estimate of BC emissions (FF 3.8, BF 1.8, OB 3.0, ALL 8.6 Tg yr^{-1}); SD = estimate of semi-direct effect deducted assuming -30% of direct forcing; DE = estimate of direct effect in cloudy skies removed by assuming 65% of direct forcing; SZ = adjusted from particle size used in study to 100-nm diameter using dependence reported by *Bauer et al.* [2010].

[c] WIE = warm cloud indirect effect, MIE = mixed-phase cloud indirect effect, IIE = ice cloud indirect effect, DE = direct effect, SD = semi-direct effect, CRY = cryosphere, CLIM = climate response. Effects in parentheses are included in the simulations but did not affect the indirect effect diagnostic and, therefore, are not included in the values in the 'Reported indirect effect' column.

[d] M1 = Change in TOA cloud forcing with and without BC; M2 = Difference between model runs with and without mixed-phase indirect effects; the two estimates use different parameterizations for the Bergeron-Findeisen process; M3 = Change in cloud forcing with and without BC+OC.

[e] Values exclude those from the GISS model, which are reported separately in *Bauer et al.* [2010].

[f] Simulations were also done with reductions of 50% BC + OC emitted from diesel. The results were very similar to those for fossil-fuel BC emissions.

[g] This study included a simulation with biofuel and biomass emissions removed. Emissions of short-lived and long-lived GHGs emitted from BF and BB were also removed, so the results are not comparable with the aerosol-only effects summarized here.

[h] Effective forcing values from this study were not separated by mechanism, so the total forcing is discussed in Section 9.

Table 7.1 Model studies used to derive the climate forcing of black carbon on snow and ice [a]

	Hansen and Nazarenko [2004]	*Jacobson* [2004]	*Hansen et al.* [2005; 2007] [b] *Shindell and Faluvegi* [2009]	*Flanner et al.* [2007]	*Flanner et al.* [2009]	*Koch et al.* [2009b]	*Rypdal et al.* [2009a]
Emissions *year* and global, annual BC emissions used to derive forcing (GgC yr^{-1})	n/a	FF+BF: 3920 BB: 3140 Total: 7060	Year *1880, 2000*: FF: 500, 5700 BF: 500, 1000 BB: 2300, 4600 Total *1880, 2000*: 3300, 11300	Year *1996* FF + BF: 4700 Year *1998* [c] BB: 4100 Year *2001* BB: 2000 Total *1998*, *2001*: 8800, 6700	Year *1996* FF + BF: 4700 Year *2002* BB [d]: 2700 Total: 7400	Year *1890*, *1995*: FF + BF: 1800, 4500 BB: 2200, 3700 Total *1890*, *1995*: 4000, 8200	FF + contained BF burning: 5300
Emission inventories used	n/a	Early version of *Bond et al.* [2004] [e] for year *1996*	FF: *Penner et al.* [2001] (via D. Koch, pers. comm.) BB and BF: *Liousse et al.* [1996]	*Bond et al.* [2004] + GFEDv2 [*van der Werf et al.*, 2006] for open burn	*Bond et al.* [2004] + GFEDv2 [*van der Werf et al.*, 2006] for open burn	BB: GFEDv1; Pre-indust. FF: *Lefohn et al.* [1999] BF: *van Aardenne et al.* [2001] [f]; Present day FF + BF: *Bond et al.* [2004]	*Cofala et al.* [2007]
Gridbox size (latitude x longitude)	4°x5°	4°x5°	4°x5°	2.8°x2.8°	2.8°x2.8°	4°x5°	1°x1°
BC forcing medium [g]	n/a	SN_L, SN_I, SI	SN_L, SN_I	SN_L, SN_I	SN_L, SN_I	SN_L, SN_I	SN_L, SN_I, SI
Present-day adjusted forcing for FF+BF only (W m^{-2})	n/a	0.06 [h]	{0.05}	**0.043**	**0.037**	{0.02}	**0.03** [i]
Pre-industrial-to-present (*years*) adjusted forcing for FF+BF+BB	n/a	n/a	(*1880-2000*) *Hansen et al.* [2005; 2007] **0.08; 0.05**	n/a	n/a	(*1890-1995*) **0.01**	n/a
Present-day adjusted forcing, for FF+BF+BB (W m^{-2})	0.16	{0.08}	{0.07}	**0.054** (*1998*) **0.049** (*2001*)	**0.047**	**0.03**	{0.04}
Climate forcing per emission (μW m^{-2}) (GgC yr^{-1})$^{-1}$ for all-source forcing	n/a	{11}	{6}	6 (*1998* BB), 7 (*2001* BB)	6	4	{5} [j]

Table 7.1 Model studies used to derive the climate forcing of black carbon on snow and ice [a] (cont'd)

	Skeie et al. [2011] [k]	*Wang et al.* [2011]
Emissions *year* and global, annual BC emissions used to derive forcing (GgC yr^{-1})	Year *1750, 2000*: FF+BF: 0400, 4500 BB: 1000, 2600 Total *1750, 2000*: 1400, 7100	n/a
Emission inventories used	FF+BF: *Bond et al.* [2007] BB: *Lamarque et al.* [2010]	n/a
Gridbox size (latitude x longitude)	1°x1°	2.8°x2.8°
BC forcing medium [g]	SN_L, SN_I, SI	n/a
Present-day adjusted forcing for FF + BF only (W m^{-2})	{0.018}	n/a
Pre-industrial-to-present (*years*) adjusted forcing for FF + BF + BB	(*1750-2000*) {0.021}	n/a
Present-day adjusted forcing, for FF + BF + BB (W m^{-2})	{0.024}	**0.042** [l]
Climate forcing per emission (μW m^{-2}) (GgC yr^{-1})$^{-1}$ for all-source forcing	{3}	n/a

Table 7.1 Footnotes

[a] 'Climate forcing' here refers to radiative forcing plus the rapid adjustments to that forcing (Table 7.2), producing the adjusted forcing as defined in Table 1.1. However, as shown in Table 7.2, studies included different rapid adjustments; for the *Rypdal et al.* [2009a], *Skeie et al.* [2011] and *Wang et al.* [2011] studies, no rapid adjustments were included so the climate forcing equals the radiative forcing. Shown are the model BC emission sources and strengths (global, annual average; FF = fossil fuel; BF = biofuel; BB = biomass burning), model gridbox size, and the global, annual average, adjusted forcing for FF + BF only and for FF + BF + BB. The global, annual average forcing per emissions for FF + BF + BB is also given. Values that are either directly reported in the studies or which can be calculated from reported values are given in bold face. Values shown in {brackets} are estimates based on scaling the reported values, as described in Section 7.6.1.

[b] *Hansen et al.* [2007] revised down the total snow BC forcing given by *Hansen et al.* [2005] after correcting a programming error. Both sets of data are given here.

[c] *Flanner et al.* [2007] provided calculations for high (1998) and low (2001) biomass burning years.

[d] *Flanner et al.* [2009] selected 2002 biomass burning emissions because this is a "typical" boreal fire year (versus the "high" and "low" cases selected for *Flanner et al.* [2007].

[e] *Jacobson* [2004] used an "early version" of the *Bond et al.* [2004] inventory for submicron BC emissions, where FF+BF ~20% lower (global, annual average) than was ultimately given in *Bond et al.* [2004]. However, *Jacobson* [2004] also included super-micron BC emissions, set at 25% of the mass of sub-micron emissions, so the total BC emissions were, in terms of mass, close to those of *Bond et al.* [2004], though the differing size distributions affect deposition rates and therefore spatial distribution of deposited BC. *Bond et al.* [2004] annual biomass burning emissions were used to determine monthly emissions by scaling using the monthly inventory of *Cooke and Wilson* [1996].

[f] Pre-industrial (1890) BF emissions comes from taking *van Aardenne et al.* [2001] SO_2 biofuel emissions and calculating BC+OC BF emissions using the ratios of SO_2:BC and SO_2:OC in 1990 from *van Aardenne* (SO_2) and *Bond et al.* [2004] (BC and OC).

[g] Forcing by BC in snow on land (SN_L), BC in snow on sea ice (SN_I) and BC in bare (non-snow-covered) sea ice (SI).

[h] Estimated value provided via personal communication (M. Z. Jacobson). Radiative forcing was not reported in *Jacobson* [2004].

[i] *Rypdal et al.* [2009a] BF includes only energy-related biofuel burning.

[j] *Rypdal et al.* [2009a] did not include biomass burning emissions, so here we have used the *Flanner et al.* [2009] 2.7 TgC yr^{-1} for BB emissions, and have scaled the *Rypdal et al.* (FF + contained BF) forcing linearly to get a forcing for FF + BF + BB.

[k] *Skeie et al.* [2011] include BB aerosols in their model, but forcing is calculated for FF + BF emissions only and all reported forcings are relative to base year 1750.

[l] *Wang et al.* [2011] is surface forcing; ToA forcing was not reported but would be lower than the surface forcing because of the effect of atmospheric transmission.

n/a = not applicable

Table 7.2. Indirect effects and feedback processes induced by black carbon in snow in model studies which produce rapid adjustments to the radiative forcing (*GRB*, *MBC* and *SBC*) or which increase the efficacy of snow BC forcing (*GRA* and *SAF*). [a]

Process in model studies	*Hansen and Nazarenko* [2004]; *Hansen et al.* [2005]; *Wang et al.* [2011]	*Jacobson* [2004]	*Flanner et al.* [2007; 2009]	*Koch et al.* [2009b]	*Rypdal et al.* [2009b], *Skeie et al.* [2011]
Indirect effects and feedbacks driving the climate impact of BC in snow	SAF	SBC, DAC, SAF	GRA, GRB, MBC, SBC, DAC, SAF	GRA, GRB, SBC, DAC, SAF	MBC
Not included	GRA, GRB, MBC, SBC, DAC	GRA, GRB, MBC		MBC	GRA, GRB, SBC, DAC, SAF

[a] Process in model studies that influence the calculation of radiative forcing in various studies, where the processes are as shown in Figure 7.3 and described in the text. For the MBC process, where hydrophobic soot is left at the snow surface during melt, *Flanner et al.* [2007; 2009] allow for a fraction of the BC to consolidate at the snow surface; *Rypdal et al.* [2009b] leave all BC at the surface when melt commences; and all other models allow the BC to be washed away with the melt water. *Jacobson* [2004] and *Rypdal et al.* [2009b] used a fixed snow grain radius (150μm and 500μm, respectively) so snow grain size does not change with climate. *Jacobson* [2004] also allows dry-deposited BC to "fall" through the snowpack at a rate of 9mm/day, and both *Jacobson* [2004] and *Flanner et al.* [2007; 2009] include frost deposition to the snow surface, which results in a decrease in snow BC concentration. Both of these effects are small and are not included here or in Figure 7.3.

The abbreviations are snow albedo feedback (SAF); albedo reduction via growth of snow grains with accelerated snow aging (GRA); increase in albedo reduction for a given BC concentration in coarse grained vs. fine-grained snow (GRB; see Figure 7.1); increase in surface snow BC concentration via enhanced sublimation (SBC); increase in surface snow BC concentration via enhanced surface snow melt (MBC), and changes in deposition resulting from climate changes due to snow and ice BC climate forcing (DAC).

Table 7.3. Arctic surface snow measurements of BC compared with model results [a]

Region	# sites	Sampling period	Measured EC, BC (ng g^{-1})	*Flanner et al.* [2009] BC (ng g^{-1})	*Koch et al.* [2009b] BC (ng g^{-1})	Ratio Flanner: Measured	Ratio Koch: Measured	References for measurements
Greenland (~63°-81°N)	12	April Jul +Aug	Apr: 3±1 Jul+Aug: cold snow: 2±1 melting snow:16±5	April: 5±1 May: 7±4 June: 13±7 July: 29±18 Aug: 27±30	April: 6±6 May: 4±2 June: 5±2 July: 5±3 Aug: 4±2	April: 1.3 Jul/Aug: 14 (cold snow) 1.8 (melting snow)	April: 1.6 Jul/Aug: 2.3 (cold snow)	*Chýlek et al.*, 1987; *Cachier and Pertuisot*, 1994; *Chýlek et al.,* 1995; *Hagler et al.,* 2007a ,b; *McConnell et al.,* 2007; *Doherty et al.*, 2010.
Arctic Ocean (~84°-90°N)	5	April	5±3	7±1	11.8±1.2			*Doherty et al.*, 2010.
Arctic Canada, (~66°-77°N)	25	April-May	8±3	13±8	8.4±2.3	1.5	1.0	*Doherty et al.*, 2010.
Sub-Arctic Canada, (~63.5°-67.5°N)	27	March-April	14±9	11±3	7.6±3.3	0.8	0.6	*Doherty et al.*, 2010.
Barrow, Alaska (~71.3°N)	1	March-April	9	5	5.8	0.6	0.6	*Doherty et al.*, 2010.
Svalbard, Norway (~79°N)	10	Mar-May	Mar:10±20 Apr: 9±8 May: 10	Mar: 17 Apr: 14 May: 16	Mar: 7.6 Apr: 4.9 May: 9.2	1.6	0.7	*Forsström et al.,* 2009 [b]; *Doherty et al.*, 2010.
Tromso, Norway (~69.7°N)	1	March-May	21±12	78	7.6	3.4	0.3	*Doherty et al.*, 2010.
Abisko, Sweden (~68.3°N)	1	March-April	31	76	7.8	2.4	0.3	*Clarke and Noone*, 1985
Northern Russia (~62°-74.5°N)	9	March-May	18±28	17±14	17.2±13.2	0.9	1.0	*Doherty et al.*, 2010.

[a] Arctic surface snow EC (thermo-optical (T.O.) or SP-2 method) or estimated BC (IP or ISSW Spectrophotometer) from measurements versus in models. Where more than ten measurements are available, a median and standard deviation are given. The model values are calculated from monthly averages of the model gridboxes that contain the sample sites. Monthly averages for Greenland are shown explicitly because of the large change in concentration in the *Flanner et al.* [2009] study moving from spring to summer.

[b] Excludes *Forsström et al.* [2009] data from Linnébreen because of contamination by local sources.

Table 7.4. Factors affecting albedo reduction by BC in bare sea ice [a]

Factors	June	July	August	September
Arctic ice area (10^{12} m^2)	9.6, 11.4	6.7, 10.0	4.4, 8.0	3.8, 7.5
Area not covered by melt ponds (fraction)	0.95, 1.00	0.7, 0.9	0.85, 0.95	1.0
Area not snow-covered (fraction)	0.4, 0.8	0.8, 0.95	0.8, 1.0	0.1, 0.7
Downward solar flux at surface (W m^{-2})	260, 360	190, 250	120, 170	50, 70
Energy absorbed by BC in sea ice (10^{18} J $month^{-1}$)	94 ± 59	63 ± 36	32 ± 20	7 ± 6
Energy absorbed by BC in sea ice during one Arctic summer (10^{18} J)	196 ± 72			
Global annual radiative forcing (W m^{-2})	0.008 - 0.017			

[a] Lower and upper bounds are shown for each quantity.

Table 8.1. Summary of results for black carbon in climate models [a]

Study	Processes included	Emissions [b] (Tg BC yr^{-1})	Radiative forcing (W m^{-2})	Adjusted forcing (W m^{-2})	Effective forcing (W m^{-2})	Equilibrium temperature response (K)	Notes
Roberts and Jones [2004]	Direct and semi-direct effects	20.24 (x4)	0.78 (x4)		0.48 (x4)	0.44 (x4)	HadSM4. Fossil-fuel BC emissions were quadrupled to increase signal to noise.
Wang [2004]	Direct and semi-direct effects	14	0.35	0.14 ± 0.3		0.07	NCAR CCM3 with slab ocean model from CCM3.6.6. CO_2 climate sensitivity not known.
Hansen et al. [2005]	Direct and semi-direct effects	Not specified	1.03 (x6) BB 0.96 (x2) FF	0.71 ± 0.17 (x6) 0.5 ± 0.1 (x2)	0.76 (x6) 0.59 (x2)	0.27 (x6) 0.35 (x2)	GISS model E. BB = Biomass burning BC only. Experiment E2BCBx6 (biomass burning BC emissions were multiplied by 6) and E2BCIx2 (industrial BC emissions were doubled).
Chung and Seinfeld [2005]	Direct and semi-direct effects	7.9	0.33 (Ext) 0.60 (Int)		0.47 (Ext) 0.85 (Int)	0.20 (Ext) 0.37 (Int)	GISS model II-prime with external (Ext) and internal (Int) mixtures
Sokolov [2006]	Direct and semi-direct effects			2.36 (x10)	3.0 (x10)	1.76 (x10)	Earth System Model of Intermediate Complexity. The change in BC has been multiplied by 10.
Jones et al. [2007]	Direct and semi-direct effects. External mixture.	7.9 (year 2000) versus 0.6 (year 1860)	0.45	0.39 ± 0.09	0.28	0.28	Improved version of HadGEM1 coupled to a mixed-layer ocean. Direct and semi-direct effects only. Fossil-fuel BC only.
Jacobson [2010]	Direct (external + internal mixtures), BC inclusion in cloud droplets, snow albedo effect, semi-direct and all cloud effects.	3.18 FS [c] 7.92 FSBSG [c]			0.47 [d] 0.78 [d]	0.49 0.71	Forcing is an estimate based on an earlier version of the model. CO_2 climate sensitivity 0.6 K $(W\ m^{-2})^{-1}$.

[a] Adjusted forcing includes radiative forcing and rapid adjustments to that forcing quantified as a top-of-atmosphere (TOA) flux change; effective forcing is either radiative or adjusted forcing multiplied by its efficacy (Table 1.1). Multipliers in brackets refer to the scalings of the BC effect used in integrations to generate a statistically significant response in the climate models.

[b] FF = fossil-fuel BC; FS = fossil-fuel BC + POA; BB = biomass burning BC; FSBSG = fossil-fuel and biofuel BC + POA.

[c] Co-emitted POA is included for FS, and all aerosols and gases for FSBSG.

[d] Top-of-atmosphere irradiance changes that include climate response and, thus, are not true effective forcings.

Table 8.2. Summary of climate model studies focusing on the snow albedo effect [a]

Study	Forcing [b] ($W\ m^{-2}$)	Equilibrium Temperature Response (K)	Climate Sensitivity ($KW^{-1}m^2$)	Climate Efficacy (%)	Note
Hansen and Nazarenko [2004]	0.16	0.24	1.5	212	Idealized snow albedo decrease (2.5% in Arctic, 1% in Greenland, and 5% in Northern Hemisphere land snow)
Jacobson [2004]		0.06 [c]			GATOR GCMM Range 0.03-0.11 K
Hansen et al. [2005]	0.082	0.065		171	GISS model E
Flanner et al. [2007]	0.054 [e]	0.15		452 [d]	1998 central estimate. NCAR CAM3
Flanner et al. [2007]	0.049 [e]	0.10		329 [d]	2001 central estimate. NCAR CAM3
Flanner et al. [2007]	0.043 [e]				Fossil-fuel and biofuel BC only
Flanner et al. [2007]	0.033 [e]				Fossil-fuel BC only
Flanner et al. [2009]	0.057	0.08	1.4	231 [f]	Experiment PI4 (pre-industrial climate with fossil and biofuel BC only) NCAR CAM3.1
Koch et al. [2009b]	0.01	0.18			GISS model E. RF is estimated as difference in fluxes from experiments with fixed SST and is not a good approximation.
Bellouin and Boucher [2010]	0.28	0.72	2.6	260	Idealized experiment with HadGEM2-AML. The radiative forcing is for an ad-hoc decrease in the land snow albedo of 0.05.
Wang et al. [2011]	0.042[g]	0.071 [h]			Idealized snow albedo decrease (2.5% in Arctic, 1% in Greenland, and 5% in Northern Hemisphere land snow)

[a] Specifics of the forcing calculations for all but the *Bellouin and Boucher* [2010] study can be found in Table 7.1. *Bellouin and Boucher* [2010] were specifically looking at climate response, so this study is excluded from Table 7.1.

[b] *Bellouin and Boucher* [2010], *Hansen and Nazarenko* [2004] and *Hansen et al.* [2005] forcings are radiative forcings. All other studies included rapid adjustments in the forcings and so are adjusted forcings.

[c] Not equilibrium temperature but 10-yr average (including spin up).

[d] Results from *Flanner et al.* [2007] show a large range of climate efficacies which could be due to noise.

[e] TOA forcing is estimated as Fa = 0.91 Fs,snow. CO_2 climate sensitivity is estimated to be 2.47 / 3.58 = 0.69 $KW^{-1}m^2$.

[f] CO_2 climate sensitivity in *Flanner et al.* [2009] is estimated as 0.89/(5.35ln(380/289)) = 0.89/1.46 = 0.61 $KW^{-1}m^2$.

[g] Surface forcing, Fs.

[h] Temperature response is not equilibrium temperature but a 10-yr average, with 1 year spin up. Equilibrium temperature response is not reported so climate sensitivity and climate efficacy are not given.

Table 8.3. Description of the model and experimental set-up for Figure 8.2 [a]

Model	Experimental design	BC sources and state of mixture	Effects included	References
GATOR	Present-day emissions vs no emissions; 'quasi-equilibrium' climate response using last 10-yr average from 15-yr experiment; full ocean model	FF + BF (BC + POA + other co-emitted species); Evolution from external to internal mixture	Direct; semi-direct; cloud indirect; BC inclusion in water drops and ice crystals; snow albedo effects	*Jacobson* [2010]
GISS	80% of present-day emissions; Equilibrium climate response; full ocean model	80% of FF + BF (only BC); External mixture	Direct; semi-direct; cloud indirect; snow-albedo effects	*Koch and Hansen* [2005]; *Shindell and Faluvegi* [2009].
NCAR CAM3.1	Present-day emissions vs. no emissions; equilibrium climate response; slab ocean model	FF + BF (BC + POA); External mixture	Direct; semi-direct; snow albedo effects (and indirect effects)	*Collins et al.* [2006]; *Flanner et al.* [2009]
HadGEM2	Present-day vs. pre-industrial emissions; equilibrium climate response; slab ocean model	FF (only BC); External mixture	Direct; semi-direct	*Jones et al.* [2007]

[a] Refer to Section 7 for a more detailed description of snow-albedo effect.

Table 9.1. Black-carbon climate forcing terms, uncertainties, and level of scientific understanding (LOSU) [a]

Climate forcing term	Climate forcing type	Section	Basis for best estimate and uncertainty range	Scientific understanding basis	LOSU
Direct Effect	Radiative forcing from absorption and scattering	5.7	Accounts for uncertainty in optical depth and radiative forcing efficiency. Range comes from model results constrained by ground-based observations.	Well-understood processes and good knowledge of radiative forcing in clear skies. General emission estimates and background clouds are relatively poorly known. Uncertainty remains in reasons for biases in models, compared to observations.	Med
Liquid cloud effect	An adjusted forcing made up from the radiative forcing from microphysical cloud -albedo BC-driven changes, including cloud lifetime and semi-direct (rapid adjustment) effects.	6.4	Range from several model results with different approaches	Microphysical processes well understood. Limited studies have isolated BC effects. Different modeling approaches make separation of semi-direct effects difficult.	Low
Semi-direct effect	Rapid adjustment associated with dynamical cloud changes driven by the BC direct effect	6.3	Range from two model studies and from average efficacy estimates. Implicitly included in liquid cloud forcing estimate.	Basic mechanisms observed and well modeled with good understanding of major processes. More complex fast responses in cloud are poorly constrained.	Low
BC in cloud droplets	Adjusted forcing from changes to cloud droplet absorption characteristics	6.3.3	Based on three studies, exploring different radiative transfer approaches	Uncertainty in the optical properties of mixed particles and the relative size of inclusions; uncertainty in rapid adjustment component.	Very low
Mixed phase cloud effect	Adjusted forcing from cloud albedo and emissivity BC-driven changes.	6.5.2	Range of three model studies	Competing physical mechanisms only partly understood and poorly quantified. Lack of observations.	Very low
Ice cloud effect	Adjusted forcing from cloud albedo and emissivity BC-driven changes.	6.5.3	Two model results highlight different mechanisms to give a wide range of estimated forcing, aviation effects currently excluded.	Plausible physical mechanisms partly understood. Observed aviation BC effects on ice clouds.	Very low
BC snowpack effect	The effective forcing of BC-driven snow-albedo changes, including BC in snow that is on sea ice. Includes rapid adjustments to the snow layer.	7.6.1	Model results constrained by observations, accounting for uncertainty in emission, BC aging, BC consolidation at the surface with melt, snow cover fraction and mass absorption efficiency.	Derived from a combination of snow reflectivity change and snowpack-surface feedbacks. Failure to adequately account for local dust or soil contributions to snowpack albedo and errors in model snowpack climatology may lead to bias.	Med
BC sea-ice effect	The effective forcing from albedo changes from BC on bare summer sea ice; does not include rapid adjustments to the snow layer.	7.6.2	An estimate derived from known physics, observations of BC in Arctic sea ice, and estimates of cloud, snow, ice and melt pond areas.	Poorly quantified snow cover estimates for sea-ice and poor knowledge of stratus cloud distribution. Not yet diagnosed in models.	Low

[a] All forcings are assumed to be over the industrial era (1750-2000). For the direct effect and snow and ice effects, the all-source forcings (*i.e.,* from all anthropogenic and natural forcings) are also included.

Table 10.1. Basis for estimates of climate forcing by co-emitted species

Climate forcing term	Forcing type	Section where discussed	Basis for best estimate and uncertainty range	LOSU [a]
Direct Effect	Radiative forcing	10.4.1	Multiple-model ensemble of forcing by sulfate and organic matter; some constraint of overall aerosol effect with observations	High
Liquid cloud effect	Adjusted forcing	10.4.2	Subtract BC liquid-cloud effect from total liquid-cloud effect; partition remainder among atmospheric mass (see Text)	Low
Semi direct effect	Rapid adjustment	10.4.3	Possible small absorption by OA ignored; other co-emitted species do not absorb light. No changes in thermal structure induced.	High
Mixed phase cloud effect	Adjusted forcing	10.4.3	Assumed no effect	Very low
Ice cloud effect	Adjusted forcing	10.4.3	Assumed no effect because OA and sulfate are not good ice nuclei	Very low
Snowpack effect	Effective forcing [b]	10.4.4	Many have no light absorption; therefore no changes in snow albedo. OA estimated based on measured fraction of absorption due to non-BC constituents.	High (sulfate) Medium (OA)
Sea-ice effect	Effective forcing	10.4.4	Many have no light absorption; therefore no changes in snow albedo. OA estimated based on measured fraction of absorption due to non-BC constituents.	High (sulfate) Medium (OA)
Gaseous species	Radiative forcing	10.4.5	Forcing per emission from review paper; regional differences not considered	Medium

[a] LOSU = Level of scientific understanding.

[b] Effective forcing is the sum of radiative forcing and rapid adjustment.

Table 10.2. Model results used to determine direct forcing per emission for organic matter [a]

Model	Reference	Emission ($TgC\ yr^{-1}$)		Load ($mg\ m^{-2}$)	Radiative Forcing ($W\ m^{-2}$)		NRFmass ($W\ g^{-1}$)	RF per Emission $(W\ m^{-2})(Tg\ yr^{-1})^{-1}$	
		Total POA	FF POA	Total POA	Total POA	FF POA	Total POA	Total POA	FF POA
AeroCom models									
GISS	*Schulz et al.* [2006]	32.5	3.2	1.22	-0.14	-0.03	-115	-0.0043	-0.009
LOA	*Schulz et al.* [2006]	32.5	3.2	1.41	-0.16	-0.04	-113	-0.0049	-0.012
LSCE	*Schulz et al.* [2006]	32.5	3.2	1.50	-0.17	-0.04	-113	-0.0052	-0.012
MPI-HAM	*Schulz et al.* [2006]	32.5	3.2	1.0	-0.10	-0.03	-100	-0.0031	-0.009
SPRINTARS	*Schulz et al.* [2006]	32.5	3.2	1.84	-0.10	-0.01	-54	-0.0031	-0.003
UMI	*Schulz et al.* [2006]	32.5	3.2	1.16	-0.23	-0.06	-198	-0.0071	-0.019
UIO-CTM	*Schulz et al.* [2006]	32.5	3.2	1.12	-0.16	-0.04	-143	-0.0049	-0.012
UIO-GCM	*Schulz et al.* [2006]	32.5	3.2	0.88	-0.06	-0.02	-68	-0.0018	-0.006
Other models									
CAM3	*Bond et al.* [2011]	30	---	---	-0.12	---	---	-0.0040	---
CAM3 ECA	*Kim et al.* [2008]	54.4	---	1.49	-0.19	---	-128	-0.0035	---
GATORG	*Jacobson* [2001b]	73	28	2.55	-0.06	-0.01	-24	-0.0008	-0.0004
LOA	*Reddy et al.* [2005]	90	7.0	2.33	-0.25	-0.02	-107	-0.0028	-0.003
MOZART	*Ming et al.* [2005]	46	10.1	2.33	-0.34	-0.09	-146	-0.0074	-0.009
SPRINTARS	*Takemura et al.* [2005]	88	14.7	---	-0.49	---	---	-0.0056	---

[a] Global mean emissions of anthropogenic primary organic aerosol (POA) and POA from fossil fuel combustion (FFPOA), mean column burden (load) of POA, mean radiative forcing by total and FFPOA, mean radiative forcing normalized by mean burden (NRFmass), and radiative forcing normalized by emissions. For comparison to emission values in the remainder of the document, 1 Tg = 1000 Gg.

Table 12.1. Evaluation of criteria for mitigation of BC emission sources [a]

	Criteria						
Emission Source	Source magnitude [b]	Global climate forcing [c]	Arctic climate forcing [d]	Mitigation technologies or practices [e]	Mitigation cost effectiveness [f]	Health benefit [g]	Implementation [h]
On-road diesel	H	H	H	H	H	H	H
Off-road diesel	M	M	M	H	M	H	H
Industrial coal	M	L	L	M	M-L	H	M
Biofuel cooking	H	H-L	L	M	M	H	L
Biofuel heating	L	M-L	H	M	M	H	M-L
Residential coal	L	L	M	M	M	H	M
Agricultural field burning	L	M-L	M	M-L	M	H-M	M-L
Forest burning	H	L	H-M	M-L	H-L	H-L	L
Grass and woodland burning	H	L	L	M-L	H-L	H-L	L

[a] This table presents a qualitative evaluation of several criteria for a range of emission sources that may inform priorities for BC mitigation actions. The first two columns represent criteria for which comprehensive, quantitative analysis is available from previous sections of this assessment. Indicators designate criteria potential as high (H), medium (M) or low (L).

[b] Sources with greater magnitude are considered to have greater technical mitigation potential. See Section 3.

[c] Potential to reduce globally averaged climate forcing, based on best estimates from Section 10. The range reflects inclusion of effects on methane. 'High' reflects likely warming effect globally, 'Medium' reflects uncertainty regarding global effect, and 'Low' reflects likely cooling effect globally.

[d] Potential to reduce Arctic climate forcing, reflecting near-Arctic sources of emissions and albedo effects. See Section 7.

[e] Availability and characterization of mitigation technologies or practices. See Section 12.

[f] Magnitude of mitigation costs per unit of BC reduced. See Section 12.

[g] Potential to provide health benefits, reflecting likely population exposure. See Section 12 for brief discussion.

[h] Potential for near-term implementation at large scales. See Section 12 for brief discussion.

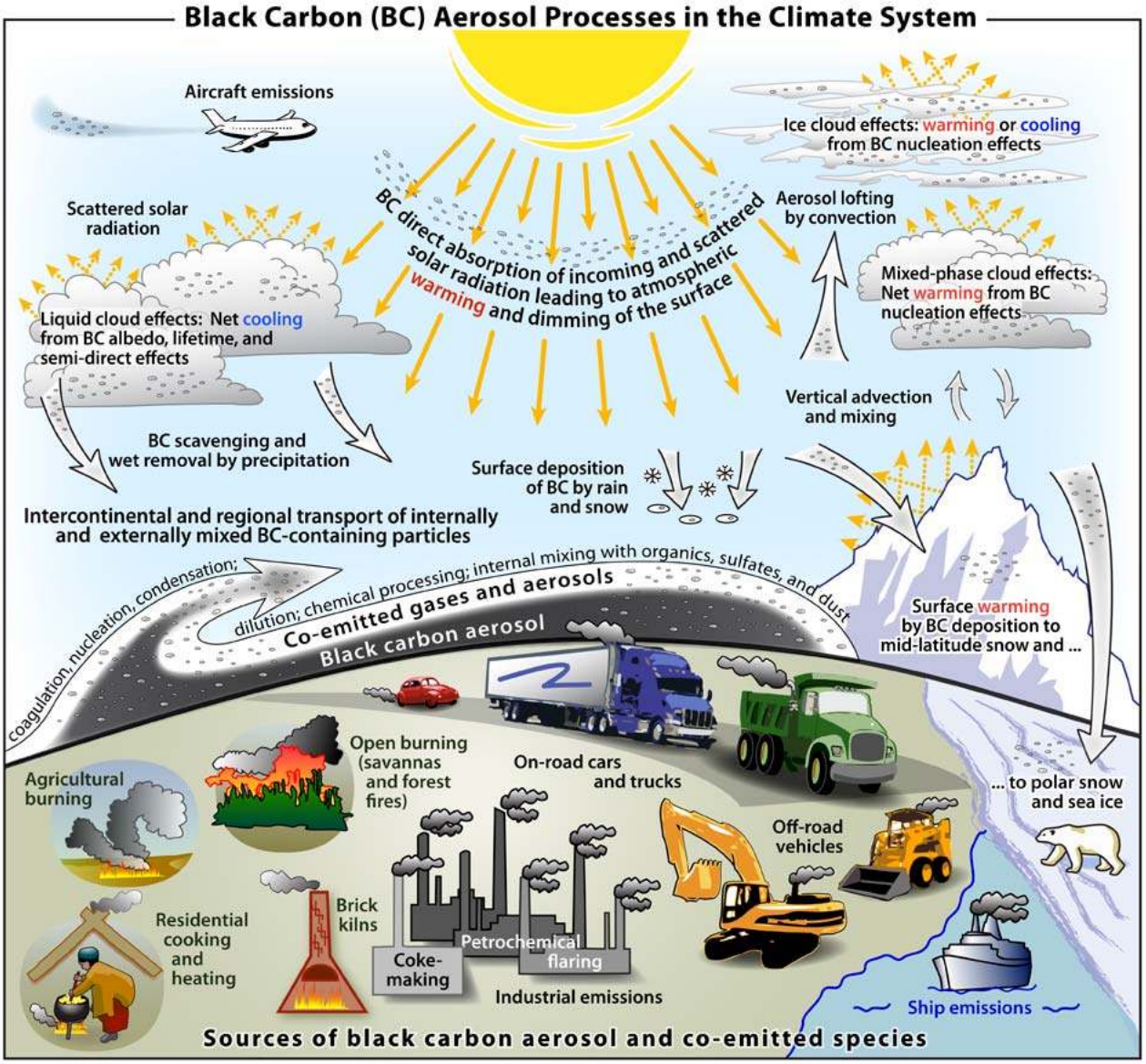

Figure 1.1. Schematic overview of the primary black-carbon emission sources and the processes that control the distribution of black carbon in the atmosphere and determine its role in the climate system.

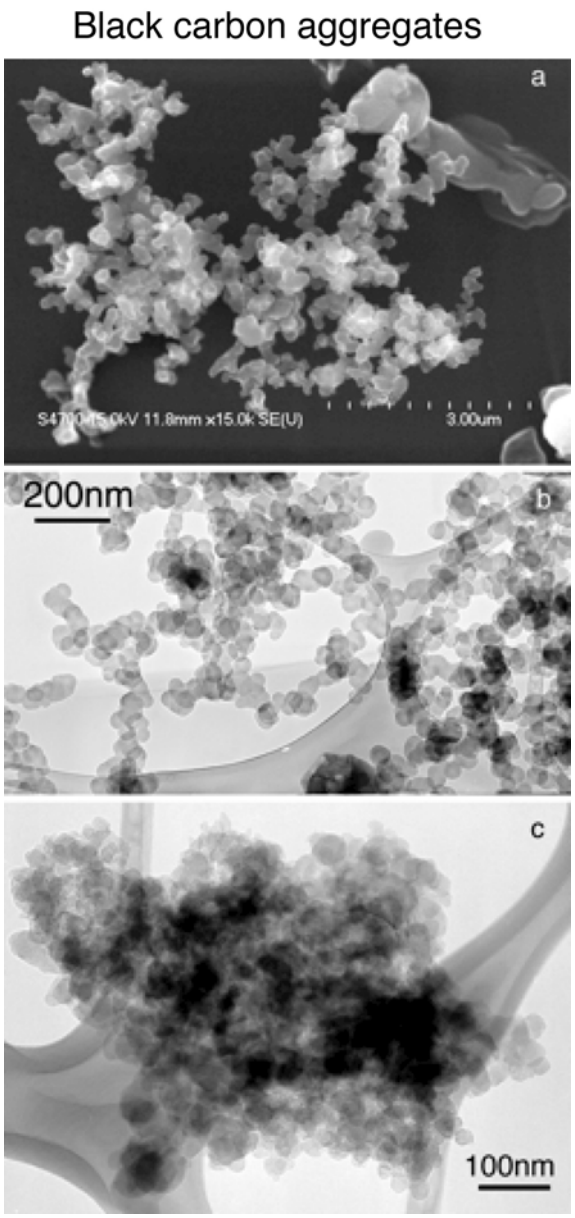

Figure 2.1. (a) Scanning electron microscope image of BC aggregates in young smoke from the Madikwe Game Reserve fire, South Africa, on 20 August 2000; (b) transmission electron microscope (TEM) image of chain-like BC aggregates in flaming smoke from the dambo fire near Kaoma, Zambia, on 5 September 2000; (c) TEM image of a compact BC aggregate in regional haze near Skukuza, South Africa, on 22 August 2000 [*Li et al.,* 2003). (Reproduced with permission of the American Geophysical Union).

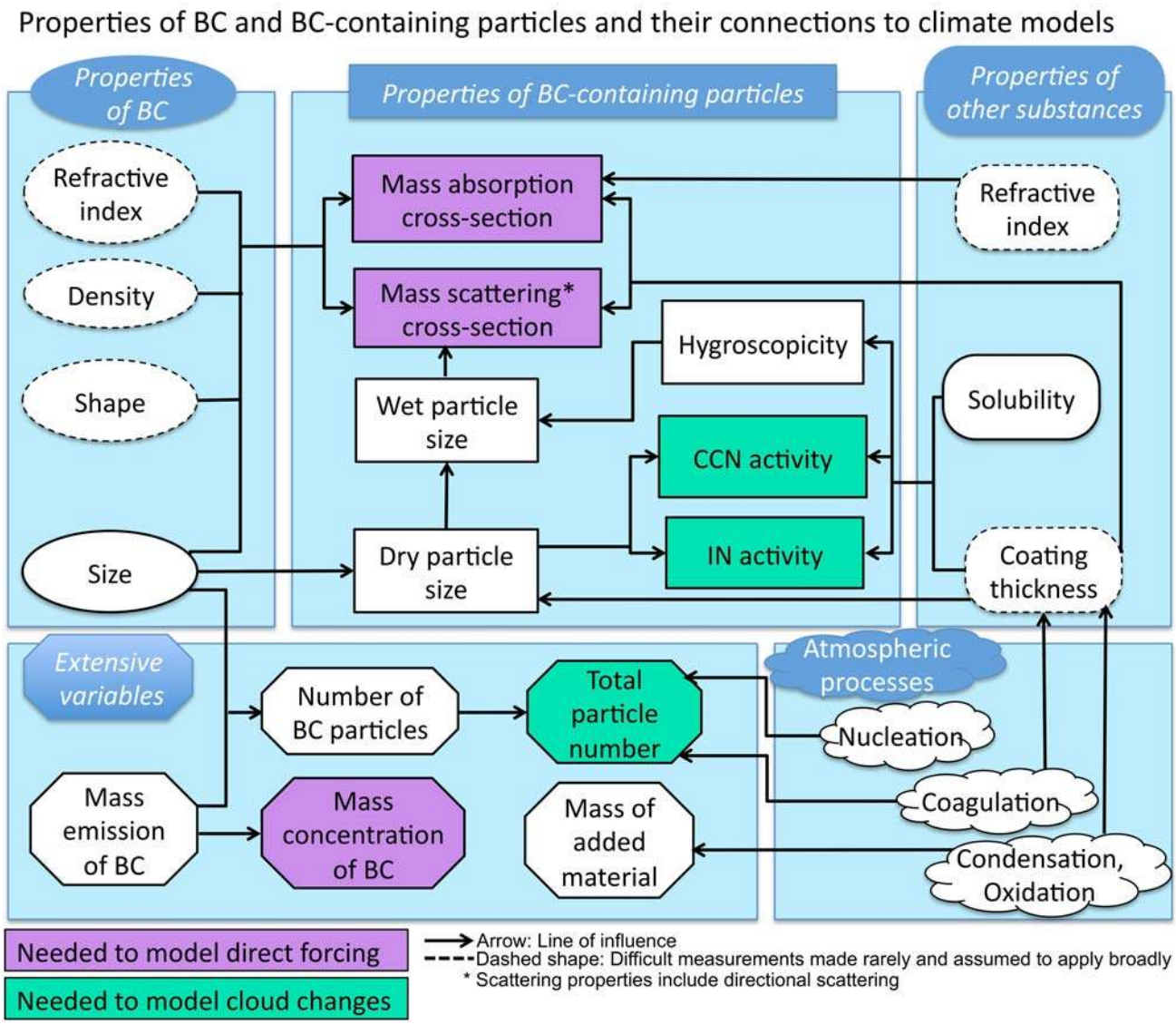

Figure 2.2. Schematic of the connections between properties of BC and BC-containing particles. A combination of these properties determines the contribution of BC and BC-containing particles to climate forcing. The properties depend on those of other substances produced in the atmosphere or co-emitted with BC, and on atmospheric processes such as nucleation and condensation. Mass and number of BC and BC-containing particles (extensive variables) depend, in part, on particle properties that affect the lifecycle of BC (not represented here).

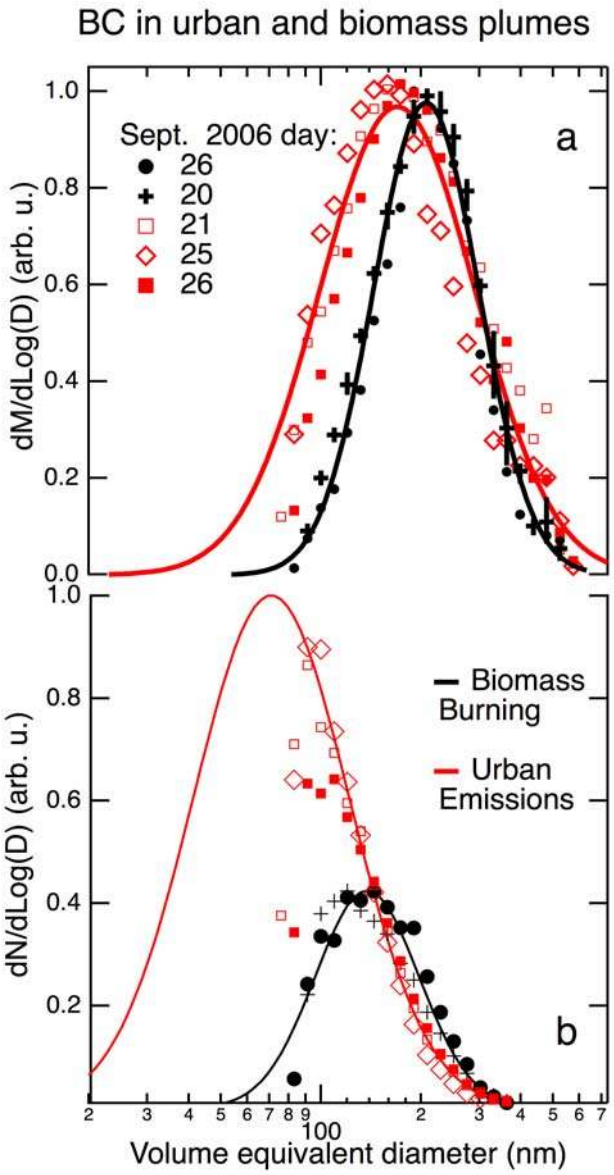

Figure 2.3. Mass and number size distributions of BC particles observed in three fresh urban (red) and two fresh biomass burning (black) plumes as identified in the legend. The measurements are made on board an aircraft using an in situ, single-particle detection instrument (SP2). The variable coatings on the BC particles is not shown. The observed mass (a) and number (b) amounts are plotted as symbols versus volume equivalent diameter based on assuming a spherical particle shape. The mass distributions are normalized to the same peak value. The observations are fit by a lognormal function between 90-600 nm (solid lines). The number distribution fits are those consistent with the fit to the respective mass distribution and are scaled to represent the same BC mass. From *Schwarz et al.* [2008b].

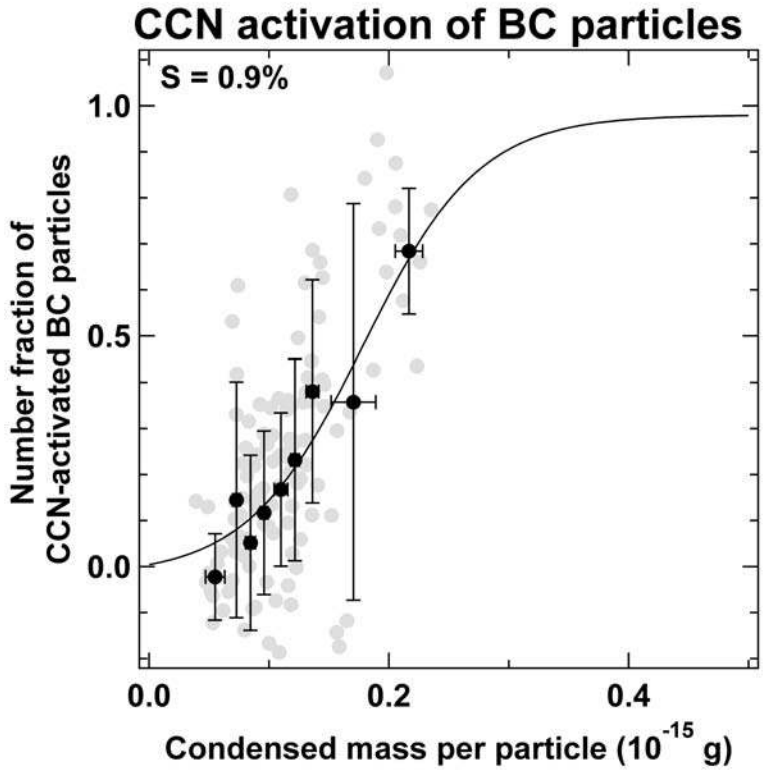

Figure 2.4. The number fraction of CCN-active BC particles versus mass of coating material for supersaturation of 0.9%. The data represent the response of 100-nm BC particles sampled in Tokyo in April 2007. The black points with 1-σ error bars are averages of the individual runs shown as gray data points. The solid curve is a sigmoidal fit to the averaged data points. A sigmoidal function is used because the ordinate should fall in the region between 0 and 1 by definition, although some deviations are apparent likely due to the measurement errors as well as some deviations from the assumptions employed for the calculation. Adapted from Figure 11 of *Kuwata et al.* [2009].

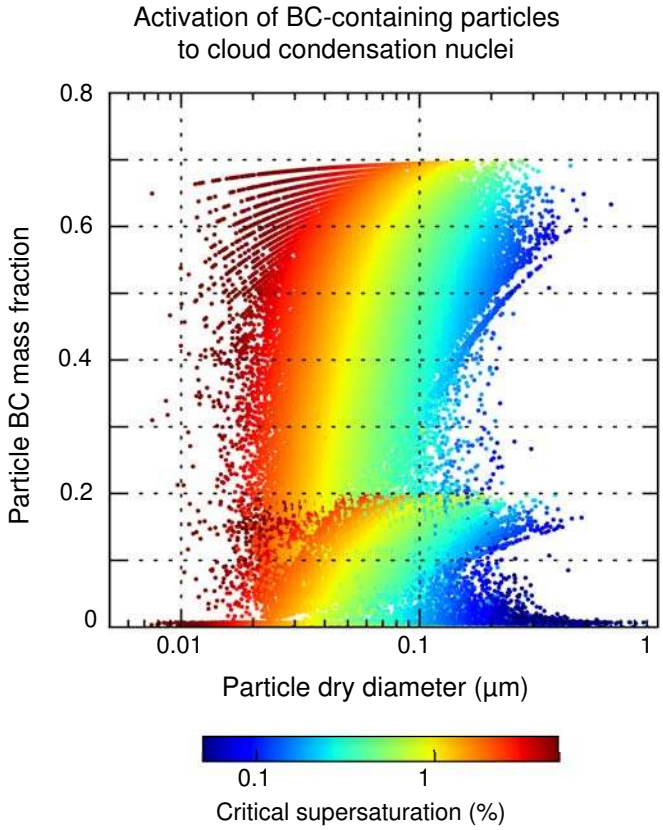

Figure 2.5. Critical supersaturation required to activate particles of varying size and BC content into cloud condensation nuclei. Higher supersaturation values mean that particles are less likely to become cloud droplets. Results are from a particle-resolved model that simulates coagulation and condensation in ambient air onto individual particles. The two branches show aged particles from diesel exhaust (70% BC) and gasoline exhaust (20% BC), assuming that Köhler theory describes activation. Particle diameter has the greatest effect on activation, with BC content inhibiting activation to a lesser extent. Figure is based on simulations published in *Deville et al.* [2011].

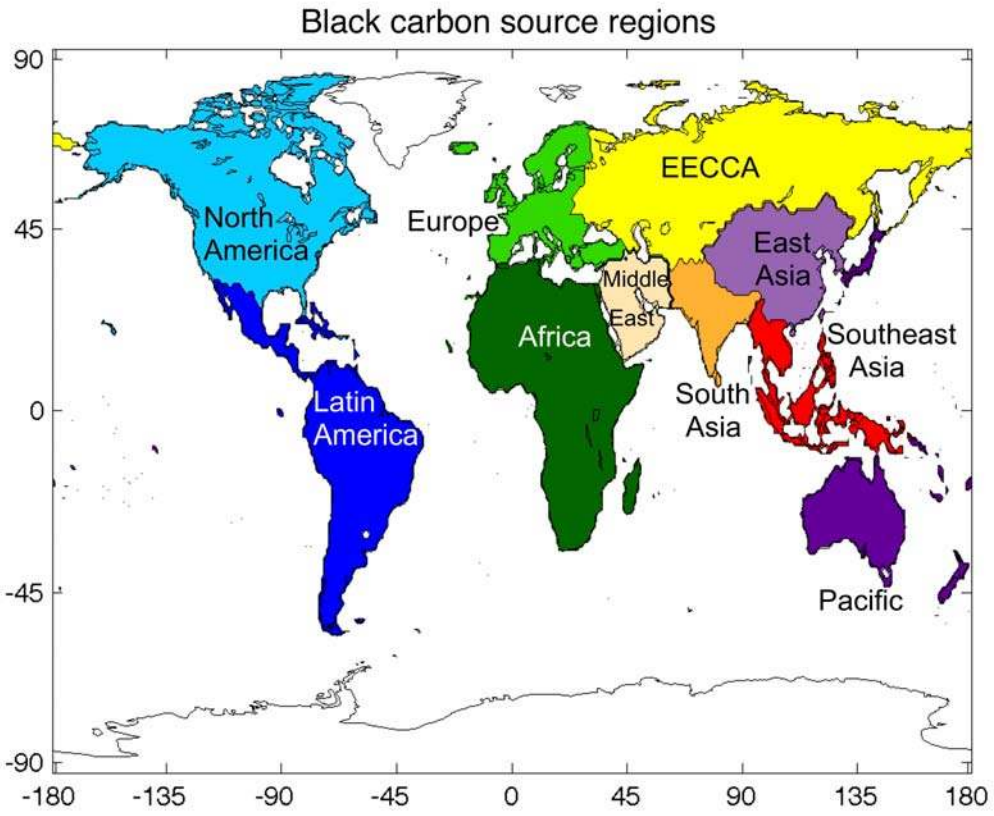

Figure 3.1. Regions (country groups) used for summarizing emissions and concentrations in this assessment. EECCA = Eastern Europe, Caucasus and Central Asia. The regional country groups are listed in Table S.1.

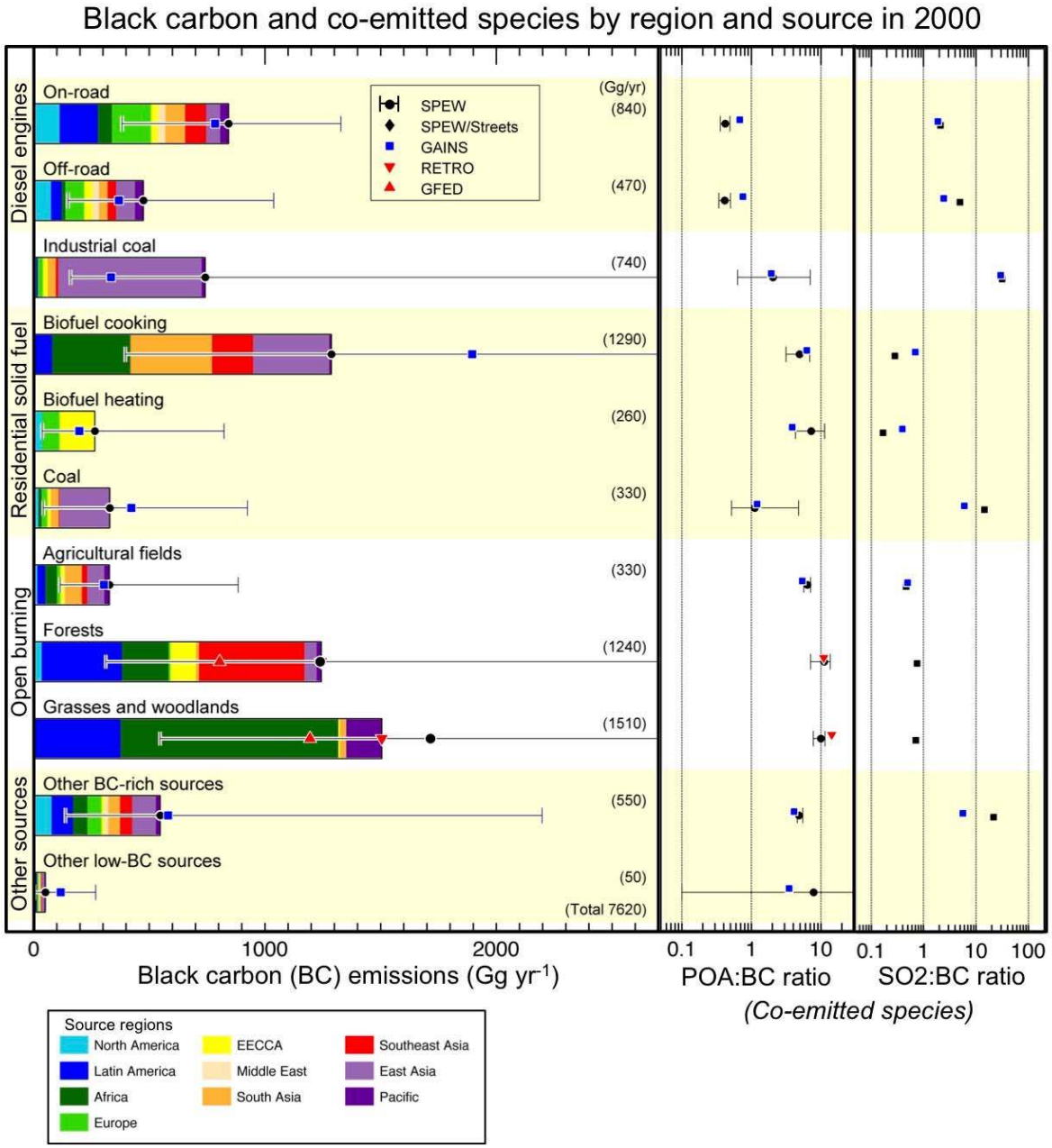

Figure 3.2. Emission rates of BC in the year 2000 by source category, and ratios of co-emitted aerosols (*e.g.,* primary organic aerosol, POA) and aerosol precursors (*e.g.,* SO_2) to BC. For reference, it is often assumed that the ratio of OA to primary organic carbon (OC) varies from 1.1 to 1.4, depending on the source (Section 2.2.2). SPEW emissions are shown as colored bars and are described by *Lamarque et al.* [2010]. GAINS estimates are from *UNEP/WMO* [2011a; b] and RETRO emissions for open burning are described by *Schultz et al.* [2008]. Sulfur emissions from *Streets et al.* [2009] were used for ratios to SPEW.

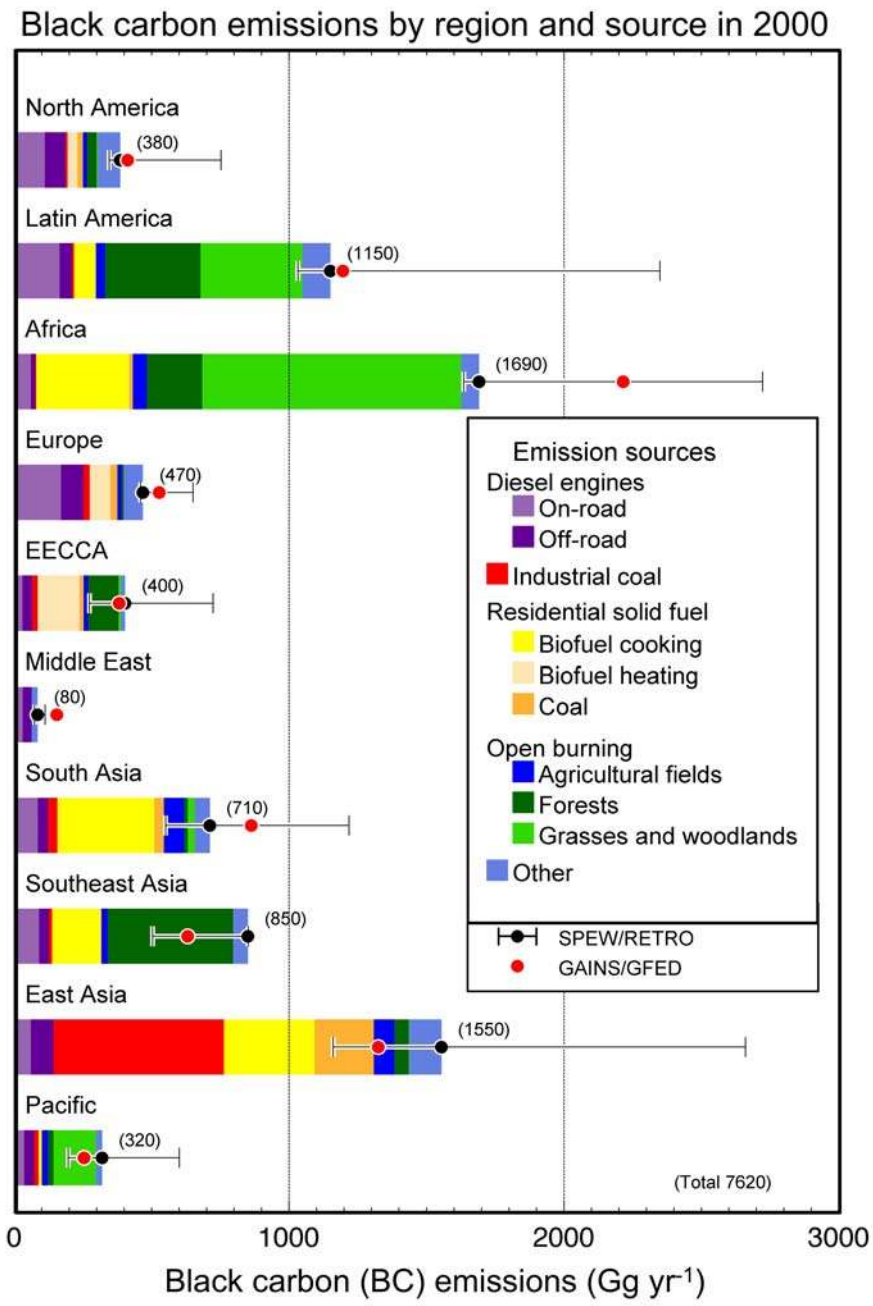

Figure 3.3. Emission rates of BC in the year 2000 by region, indicating major source categories in each region. SPEW, GAINS and RETRO emission data are the same as in Figure 3.2.

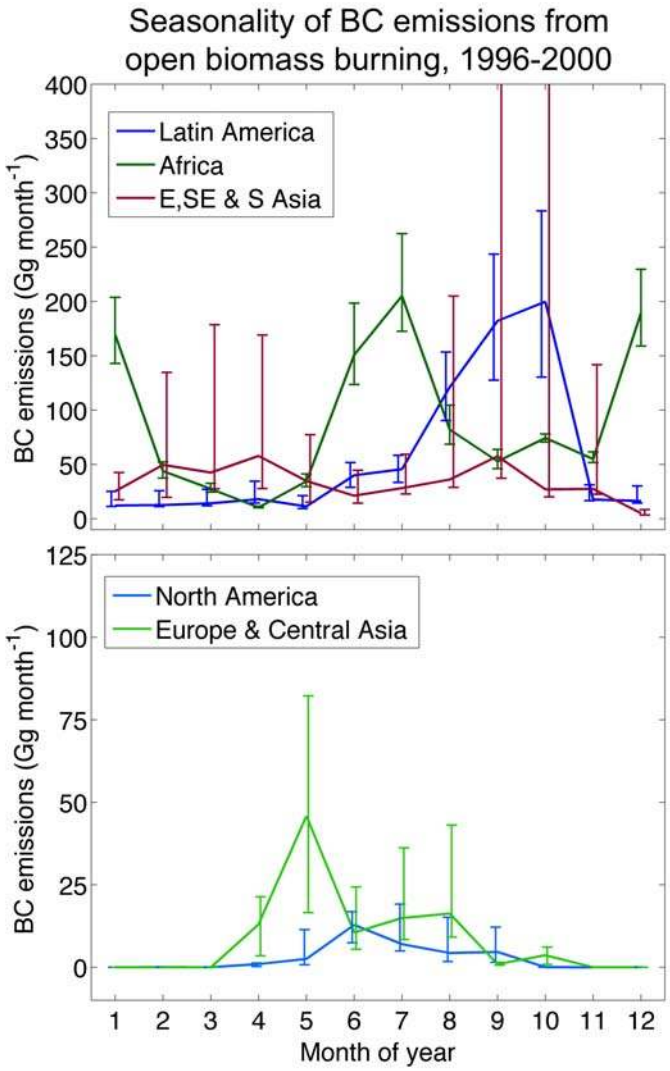

Figure 3.4. Seasonality of BC emissions from forest, grassland and woodland burning. Average monthly emissions estimated by RETRO for the period 1996-2000 are shown [*Schultz et al*., 2008]. Error bars indicate minima and maxima during each period. Regions correspond to those in Figure 3.1. Africa, which includes the small Middle East emissions, has two burning seasons because the equator bisects it. The group of East, Southeast and South Asia (E, SE & S Asia) includes emissions from Oceania. The very large error bars in that region results from the very high-fire season in 1997. Note the different vertical scales in the two panels.

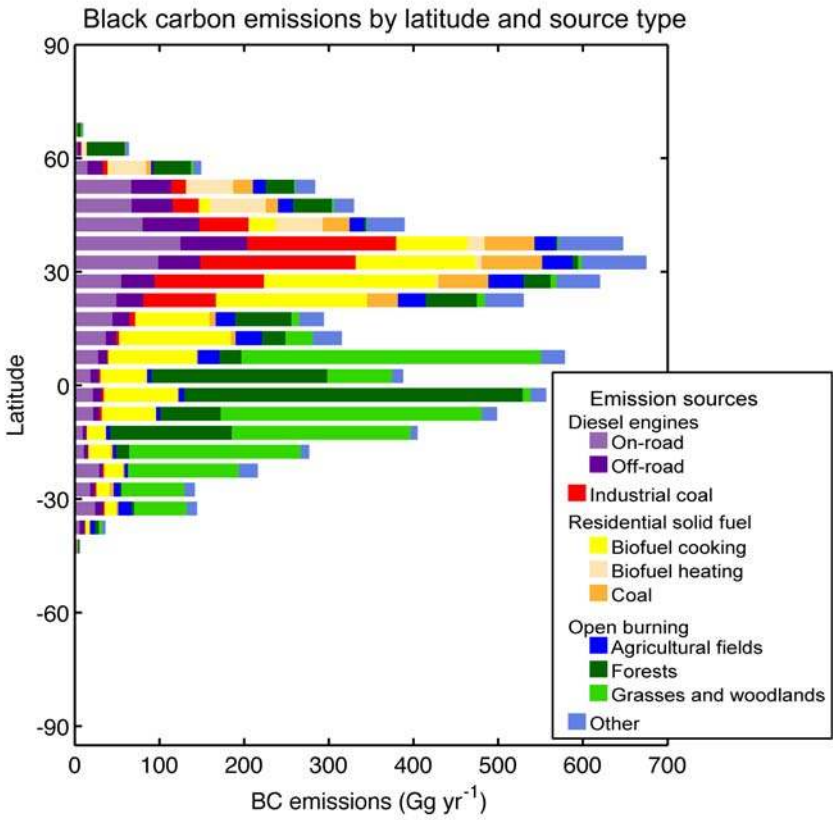

Figure 3.5. Latitude plot of the data shown in Figures 3.2 and 3.3 using 5° latitude bins.

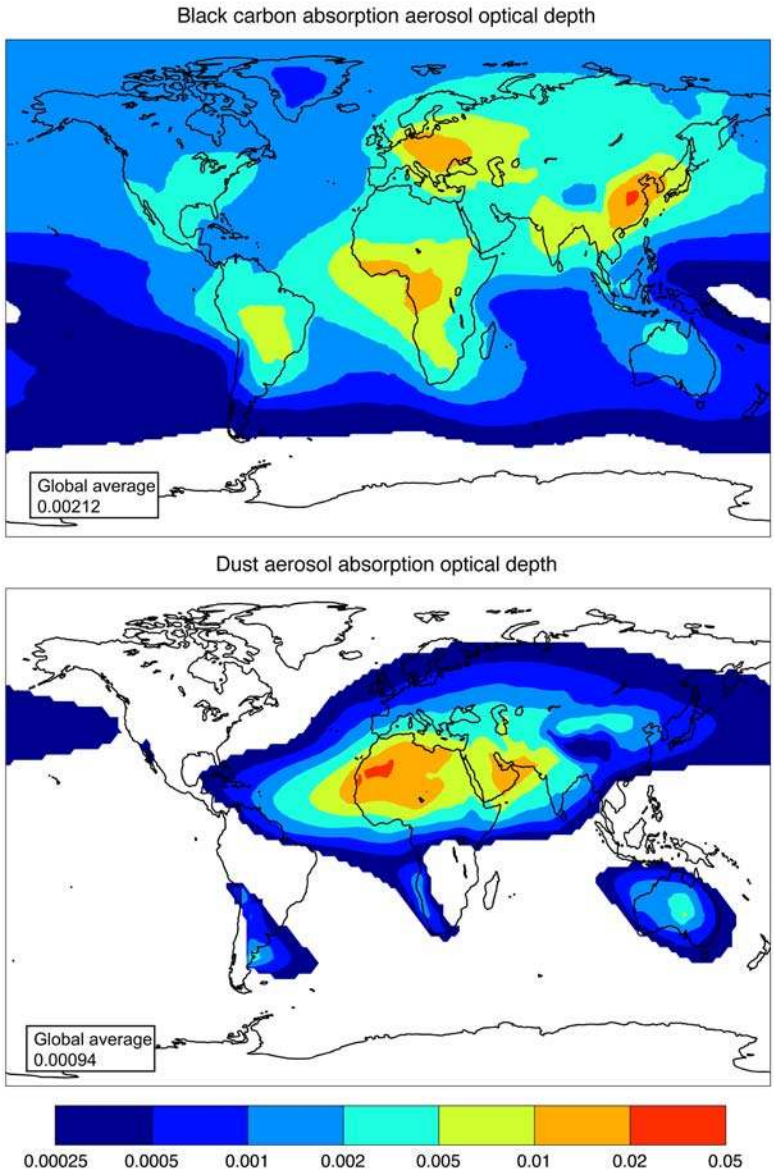

Figure 4.1. Aerosol absorption optical depth (AAOD) attributable to BC and dust. BC-AAOD fields are from the AeroCom median model fields [*Schulz et al.,* 2006] of all-source BC, including AAOD that would have been present before the pre-industrial era. Dust distribution is from *Luo et al.* [2003], with AAOD calculated from particle size in *Mahowald et al.* [2006] and optical properties in *Yoshioka et al.* [2007]. BC AAOD, after scaling to match observations, is about 65% greater than the value shown here (see Section 5.5) and would have a different spatial distribution. Values in the legend are global average values.

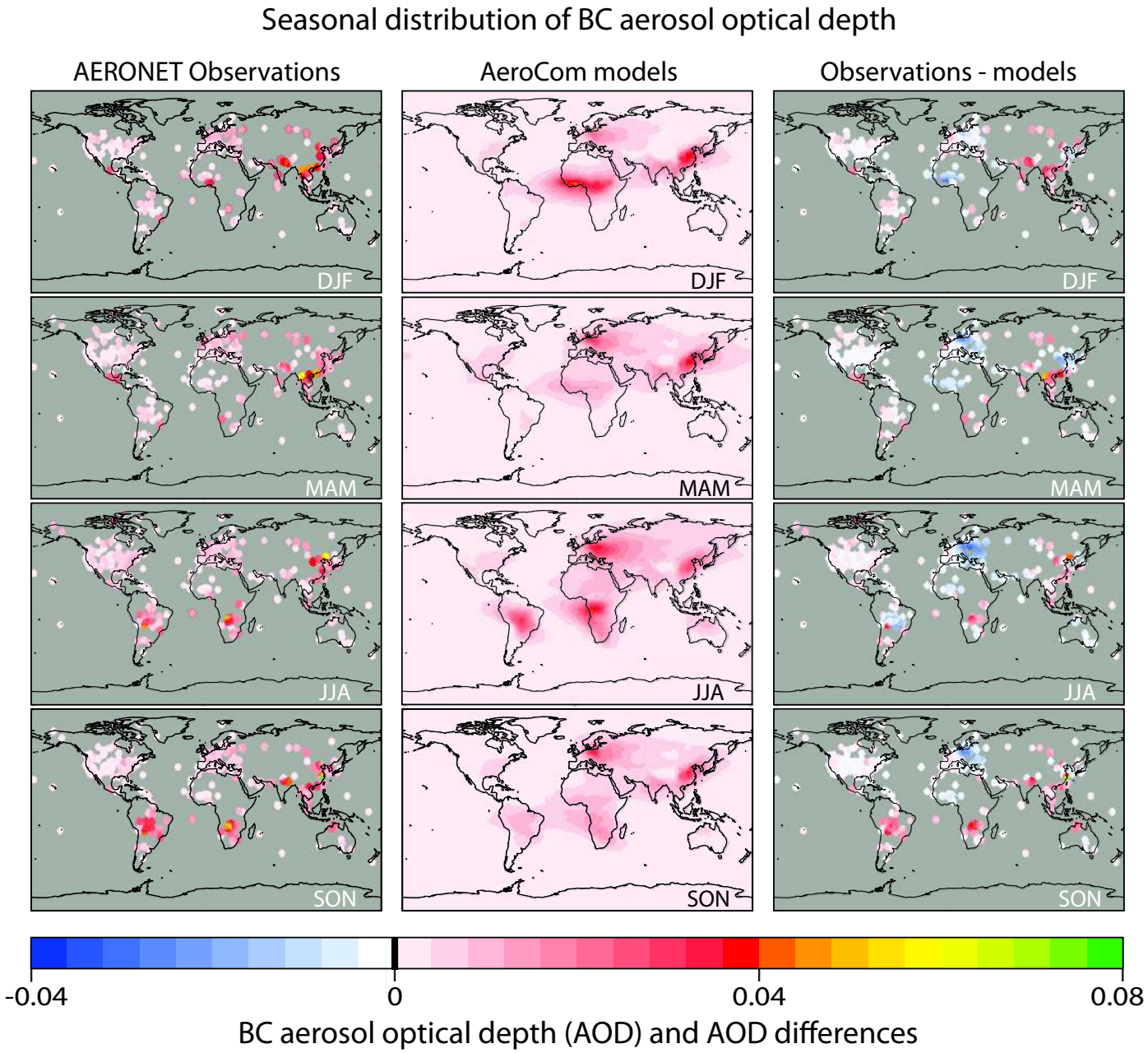

Figure 4.2. Seasonal aerosol optical depth (AOD) due to BC from observations and models. The left-panels show seasonal averages for BC-AOD at AERONET sites, as they were derived from sky-inversion data that were sampled during the last decade. Note the symbol size is increased for legibility. The middle panels show seasonal BC-AOD median maps of AeroCom models (listed in Table 5.1) for year 2000 conditions. The right panels shows local differences for BC-AOD values between AERONET observational data (left column) and AeroCom modeling efforts (middle column), illustrating model deficiencies in BC-global modeling.

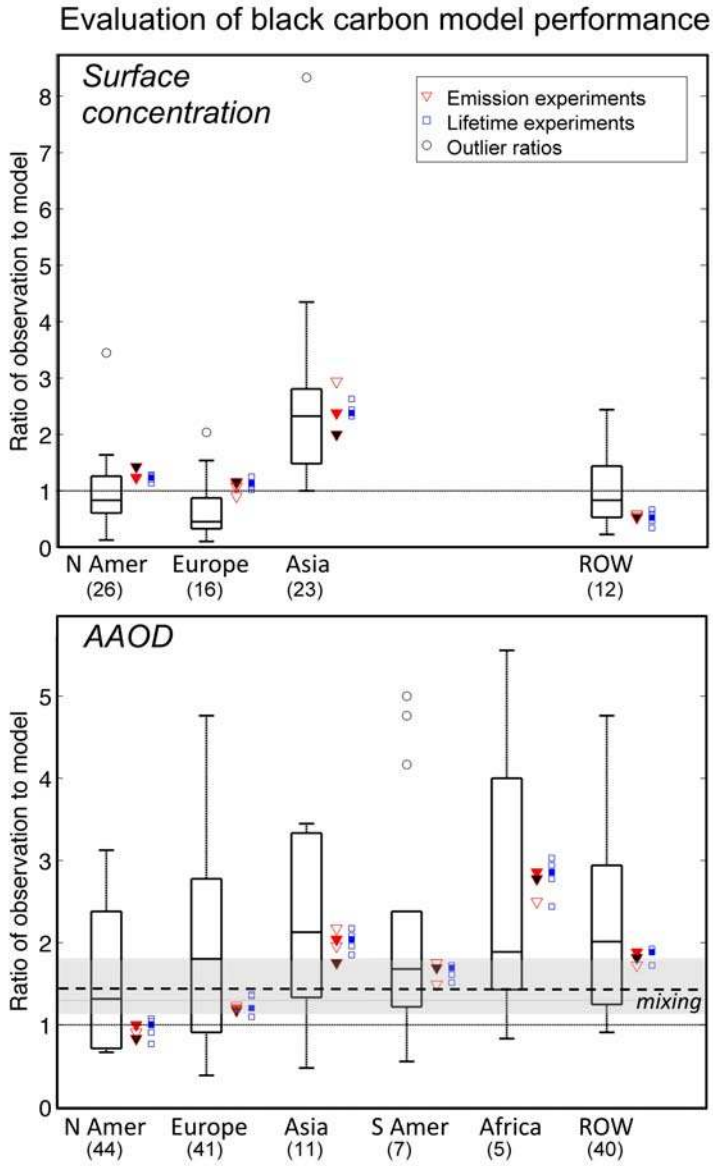

Figure 4.3. Evaluation of model performance and model sensitivities for simulating BC concentrations in surface air (top panel) and AAOD (bottom panel) for specific regions and the rest of the world (ROW). Box plots show ratios between observations and models (*i.e.*, the factor by which modeled values are multiplied to obtain observed values). AAOD is derived using AERONET and modeled AAOD. The middle bar in each box shows the median model value. Box boundaries show 25th and 75th percentiles. Data points outside 1.5 times the interquartile distance from the box are marked as outliers; otherwise, they are included in the whiskers. Models that do not represent BC internal mixing are expected to underestimate AAOD (see Section 2.7), and the magnitude of this underestimate is shown as a light shaded area in the bottom panel. Symbols show sensitivity experiments using different emission databases (red triangles) and removal rates (blue squares) in a single model (GISS) with the base case shown as filled symbols. For emission experiments, SPEW is shown with red fill and GAINS with black fill; unfilled symbols show results using two other emission databases. The number of surface observations (top) or AERONET stations (bottom) is shown below each region name. Data from *Koch et al.* [2009a].

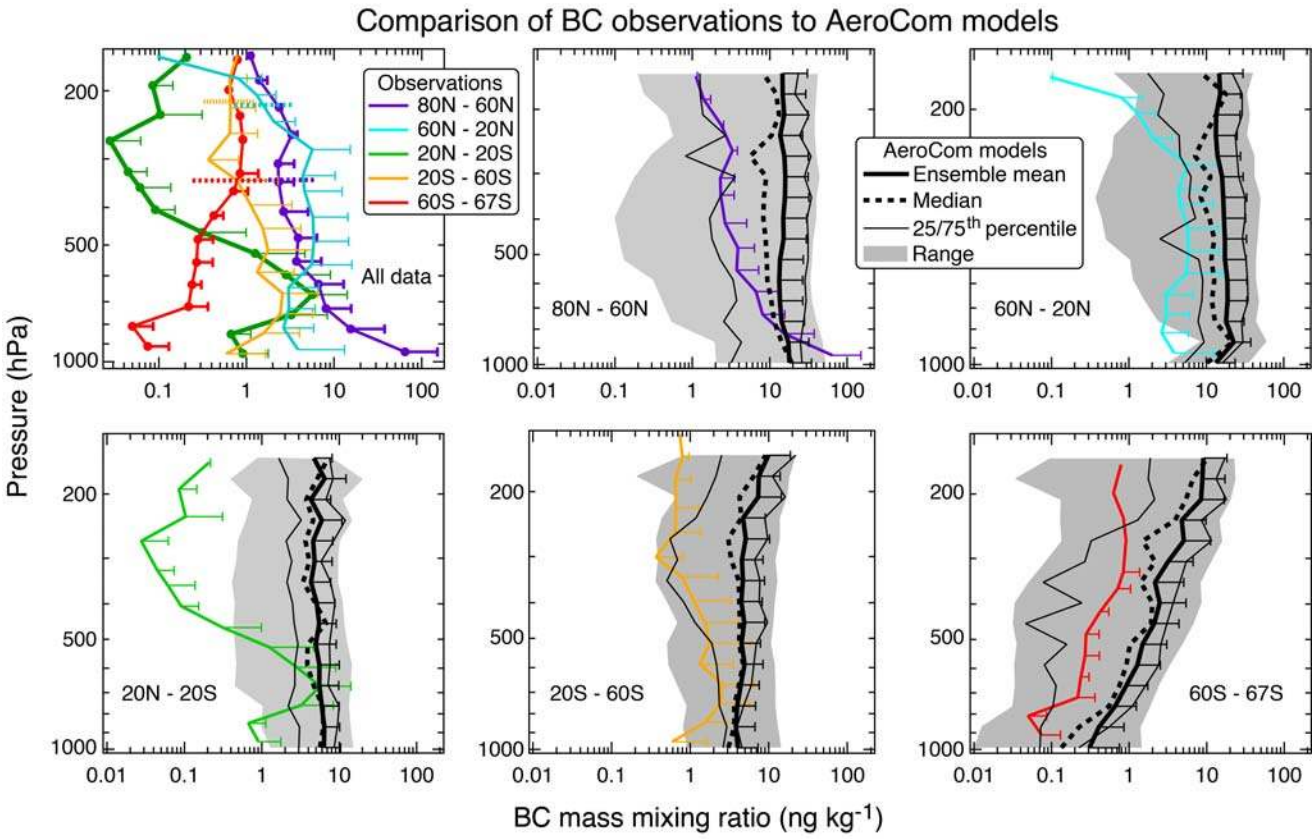

Figure 4.4. Airborne, in situ measurements of BC made in the remote Pacific Ocean between 80°N and 67°S in January 2009 using an SP2 instrument. Upper left panel: average measured BC mass concentrations observed in five latitude bands with whiskers representing atmospheric variability. In the additional panels, colored lines repeat the observed average profiles and include the range of BC mass mixing ratios from the AeroCom model suite. The legend explains lines and shading used to represent model results. The whiskers are numerically symmetric about the average values but are omitted on the left side to simplify the presentation on a log-scale. Adapted from *Schwarz et al.* [2010].

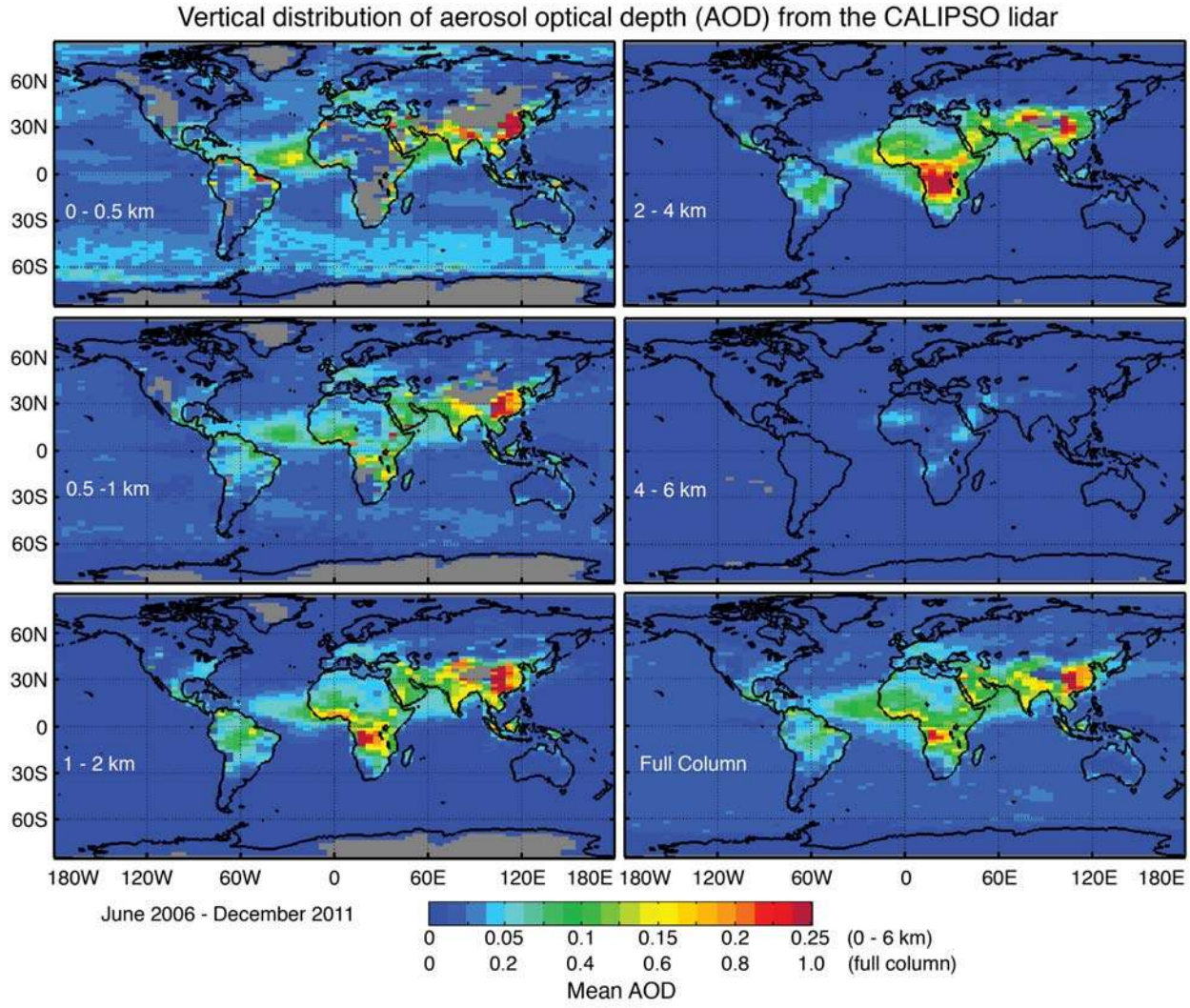

Figure 4.5. Multi-year averages of the global vertical distribution of mid-visible (532 nm), AOD from the Cloud-Aerosol Lidar with Orthogonal Polarization (CALIOP) spaceborne lidar on the NASA CALIPSO satellite. The panel colors show average AOD derived from CALIOP observations from June 2006 to December 2011 (Version 3) for specific altitude intervals referenced to sea level (see legends). The color bar has separate scales for the 0 to 6-km and full-column data panels as indicated. The full-column AOD is shown in the bottom right panel. The gray shading indicates 'no observations' usually because of elevated land surfaces. CALIOP statistics were provided by D. Winker of NASA Langley Research Center (Hampton, VA, USA).

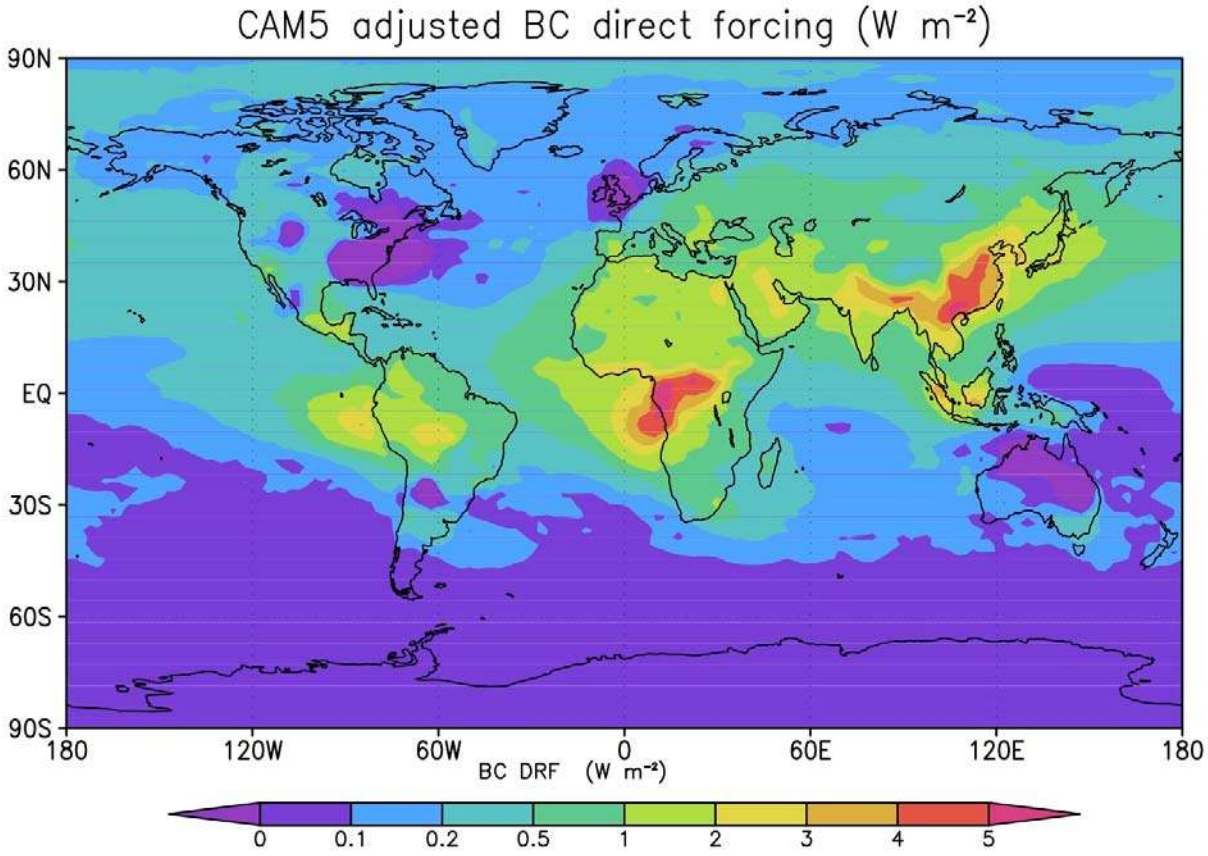

Figure 5.1. Annual mean direct radiative forcing by BC from 1850 to present day, as estimated by the CAM5 AeroCom model and adjusted according to the global annual mean bias of about 1.6, similar to the scaling of BC AAOD derived in the comparison with Aeronet observations (see Table 5.2 and Section 5.7.1). Forcing is negative in regions where biomass or fossil fuel (*e.g.*, coal) emissions were large in 1850. Year 1750 emissions from these regions would be lower, so the total forcing would be more positive. Based on *Liu et al.* [2012] and *Ghan et al.* [2012].

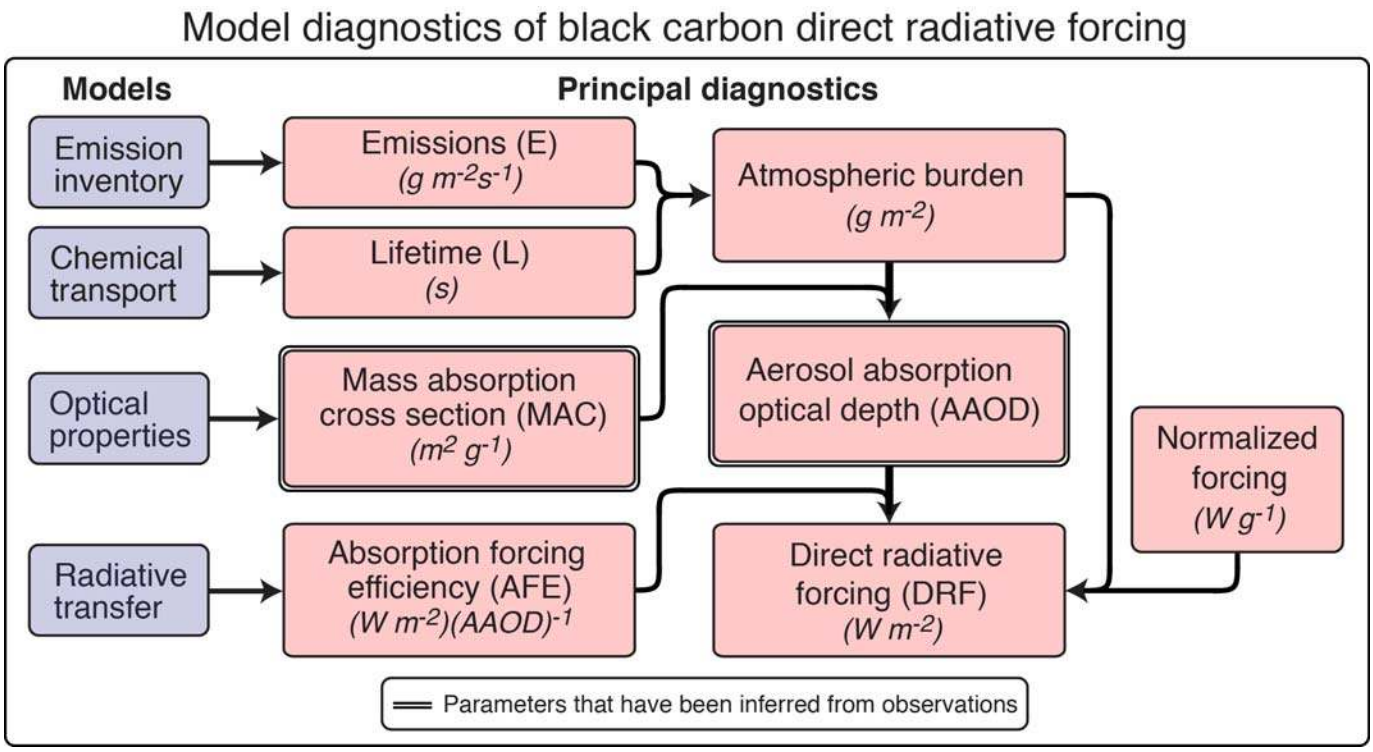

Figure 5.2. Schematic showing the relationships between principal diagnostics of models used to simulate BC direct radiative forcing (DRF) and the role of models in deriving these diagnostics. The arrows show which diagnostics can be multiplied to yield another diagnostic. The schematic expands upon Equation 5.1 which expresses DRF as a product of factors DRF = E L MAC_{BC} AFE. The diagnostics shown within double lines can be directly inferred from observations.

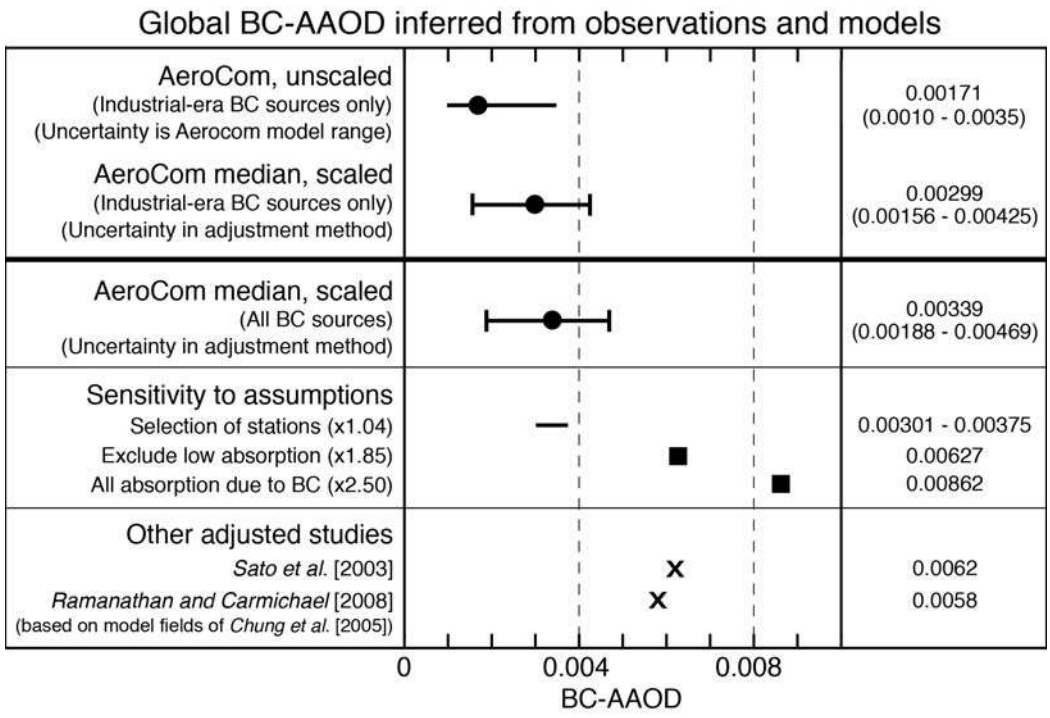

Figure 5.3. Summary of the sensitivity of global BC-AAOD derived from AeroCom models. The scaling of AeroCom BC-AAOD values is based on AERONET observations following the method in Appendix B and discussed in Section 5.4. Separate unscaled and scaled AeroCom model values are shown in Table 5.2. Data points (circles) are AeroCom median values. Ranges are shown with lines and uncertainty with whiskers. The sensitivity of scaled all-source BC-AAOD to key assumptions in using the AERONET observations is shown for three cases (see text). Two other model study results are shown at the bottom for reference. Central estimates, value ranges and uncertainty ranges are shown in the right-hand column.

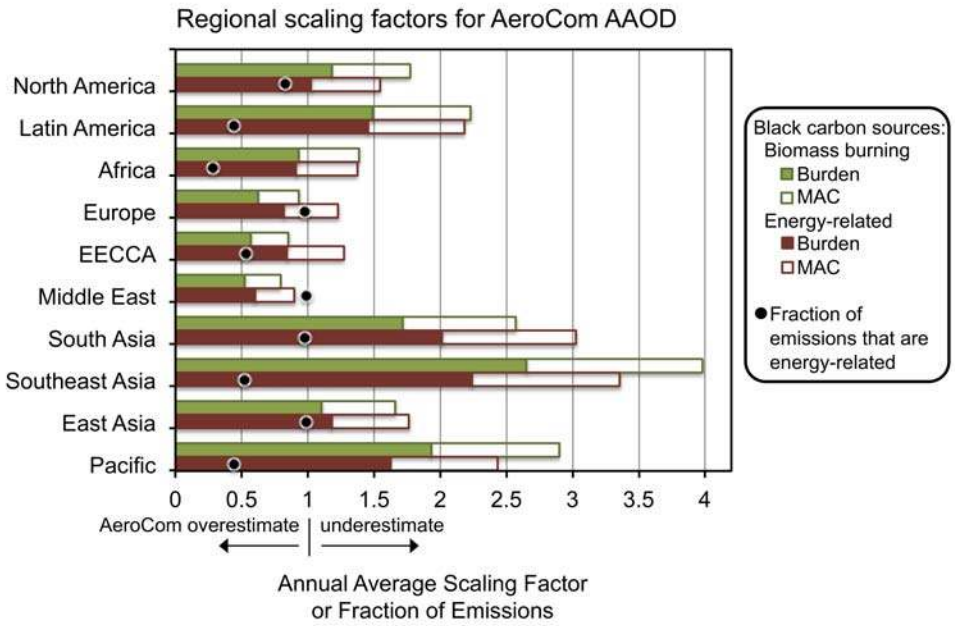

Figure 5.4. Summary of regional scaling factors required for AeroCom median model values to match observed AERONET aerosol absorption optical depth (AAOD). The regions are shown in Figure 3.1. Scaling factors are effective annual averages apportioned between open biomass burning and energy related burning. Each annual average is an average of monthly scaling factors in each region and includes a prescribed MAC scaling for all months and regions of 1.5 (open bar), the approximate ratio between the MAC of internally and externally mixed BC. Also shown are the fractions of emissions due to energy-related combustion in each region.

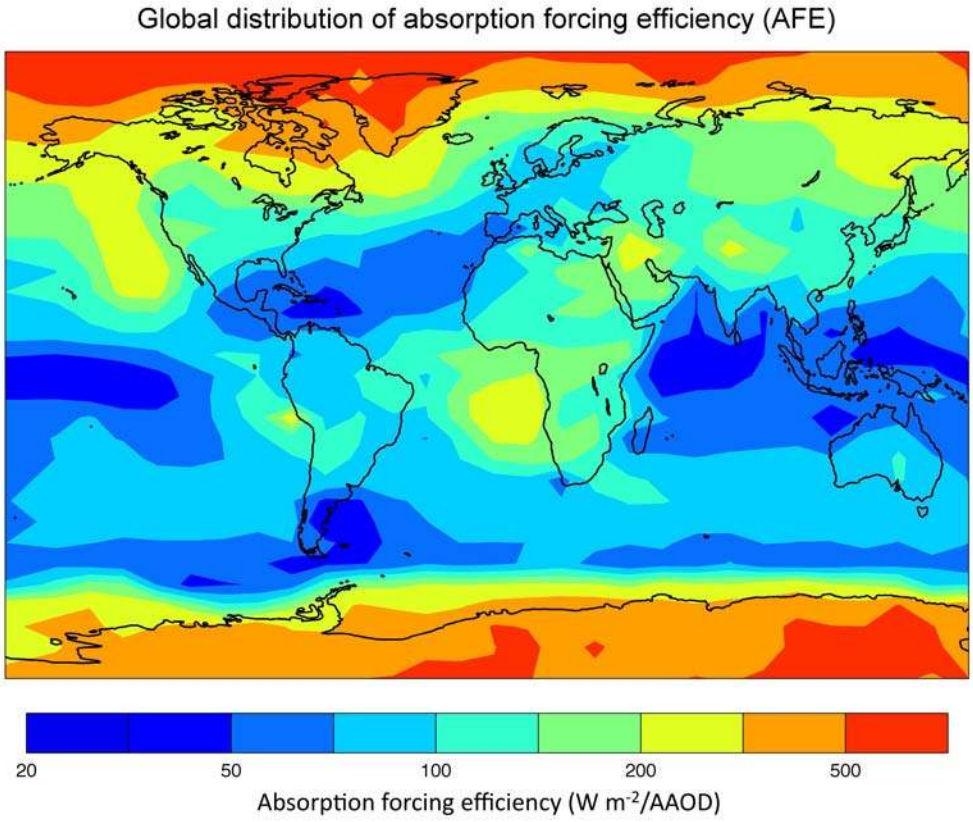

Figure 5.5. Global distribution of absorption forcing efficiency (AFE) defined as direct radiative forcing divided by aerosol absorption optical depth (AAOD). Both forcing and AAOD used are AeroCom median values as described in Section 4.3.

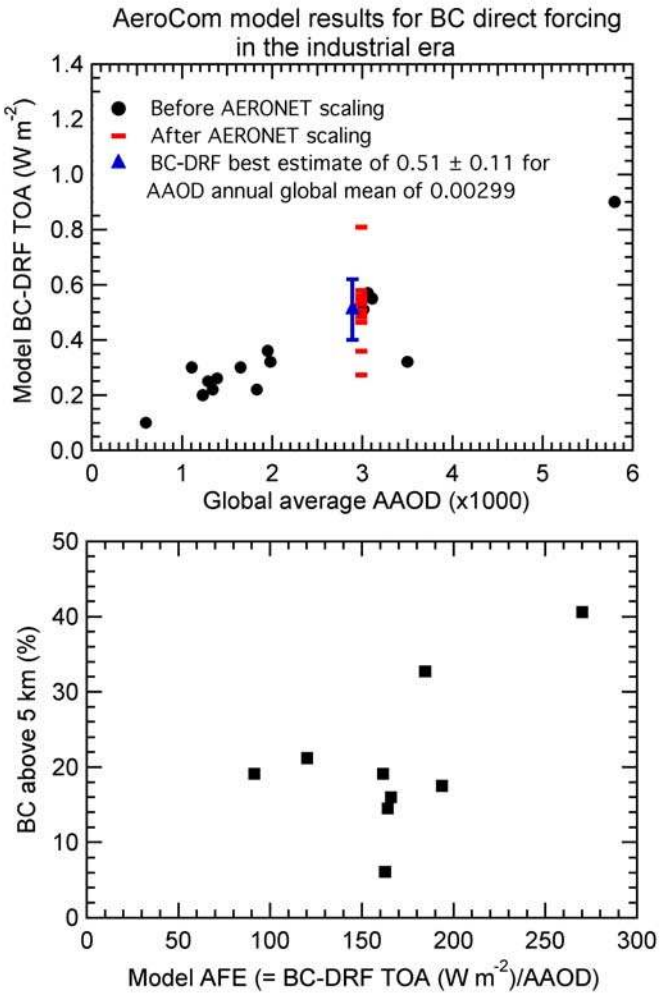

Figure 5.6. AeroCom model results for BC direct radiative forcing (DRF) in the industrial era. Top: Unscaled Aerocom BC-DRF versus global average AAOD in each model (circles) and scaled BC-DRF values (short lines) plotted at the AeroCom median AAOD value (0.00299). AAOD is a measure of the amount of BC in the atmosphere. Unscaled models with higher AAOD generally have higher radiative forcing. When DRF from each model is scaled to the AAOD global mean value of 0.00299, the resulting DRF has a mean and standard deviation of 0.51 ± 0.12 W m^{-2} (blue triangle slightly offset for clarity). Bottom: The percentage of BC above 5 km versus absorption forcing efficiency (AFE) in several Aerocom models. Data presented here are also provided in Tables 5.1 and 5.2. The scaling of BC DRF in AeroCom models is discussed in Section 5.7.1. The forcing average shown here is reduced for the best estimate of forcing, as discussed in Section 5.7.2.

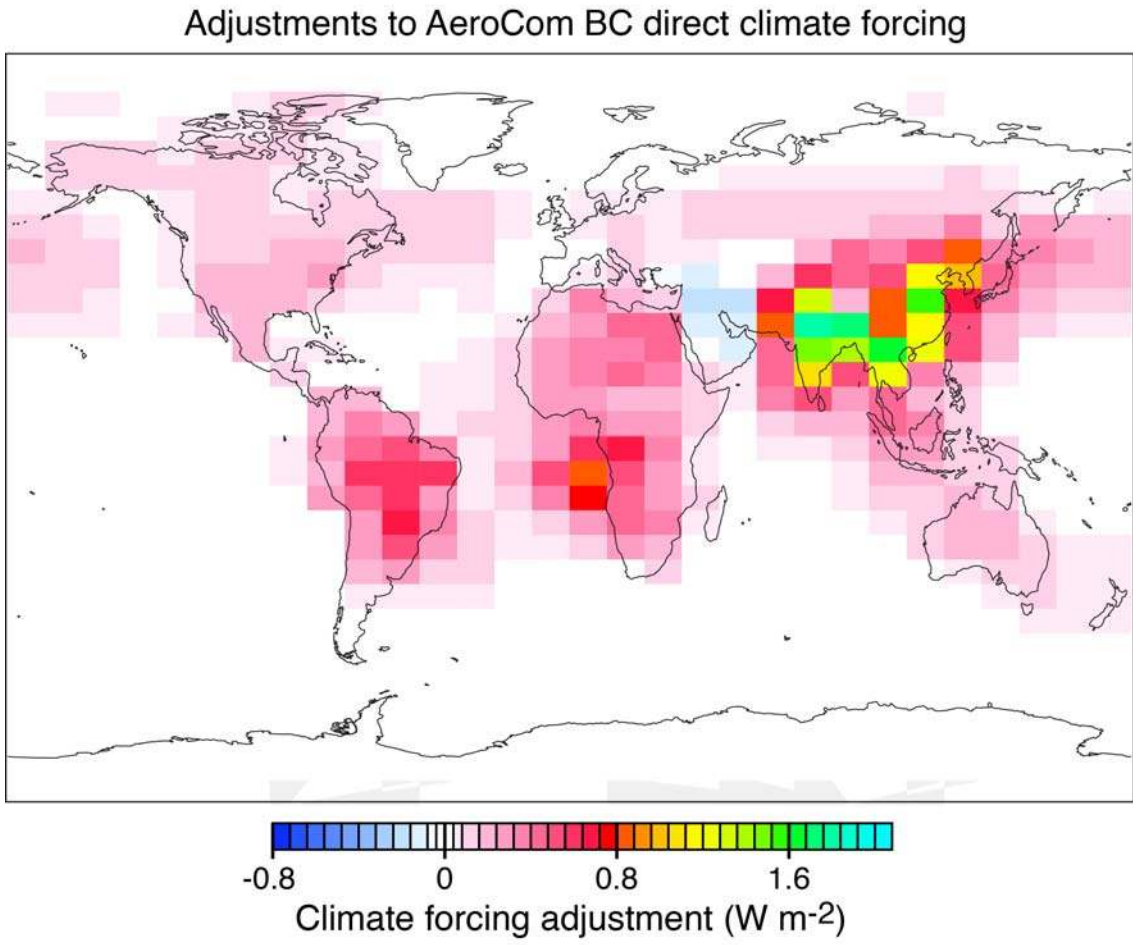

Figure 5.7. Adjustments to the annual mean, direct radiative forcing (W m^{-2}) by BC in the median AeroCom model required for consistency with the AERONET retrieved aerosol absorption optical depth (AAOD).

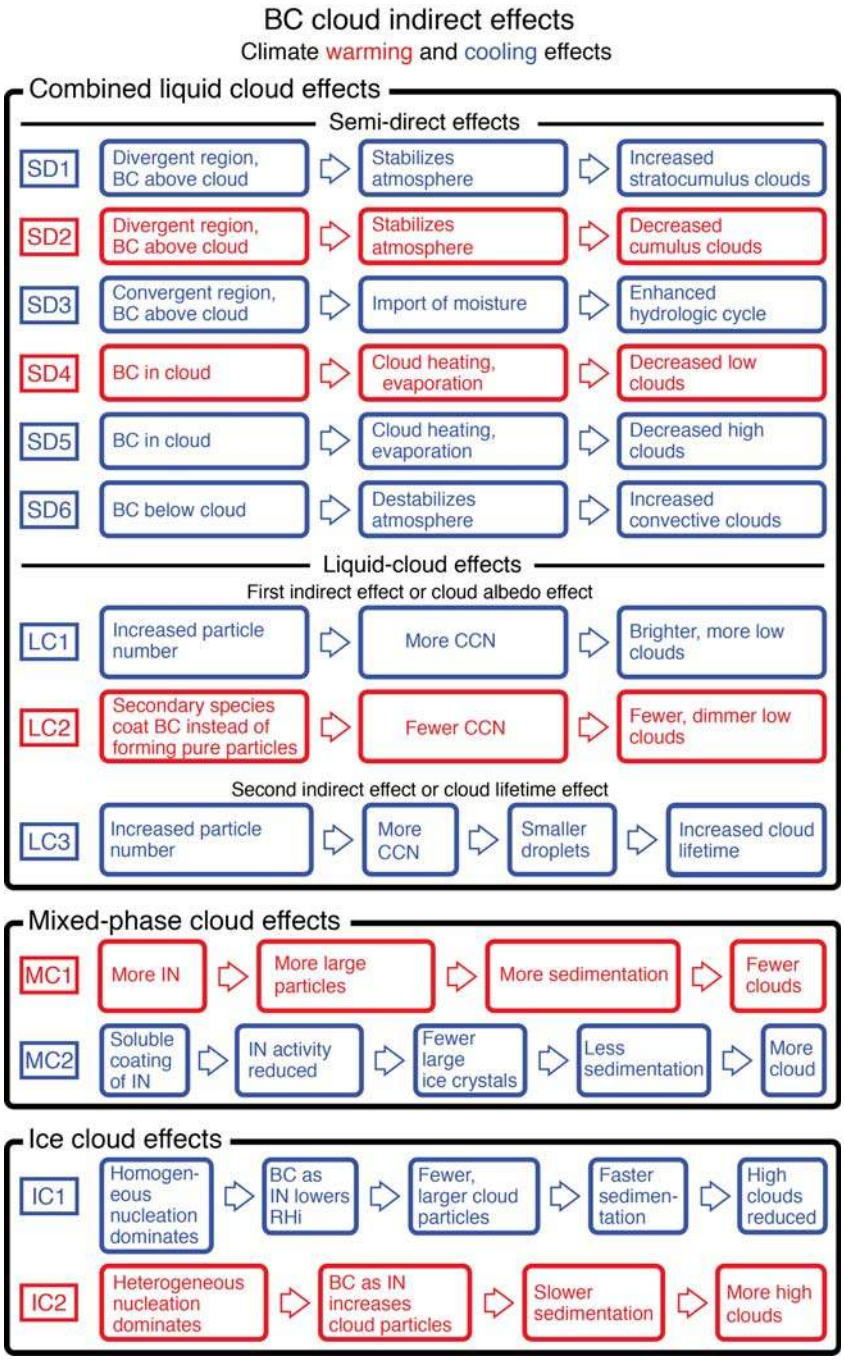

Figure 6.1. Schematic of the causes and effects that lead to cloud effects from BC emissions. Each row begins with an identifying label followed by a cause, namely an atmospheric or microphysical parameter representing a potential perturbation to cloud properties. To the right of each cause are the response(s) to the perturbation. On the far right is the associated effect, namely, the cloud parameter that changes in response to the perturbation. The single color of the components in each row indicates the climate system response, either warming (red) or cooling (blue).

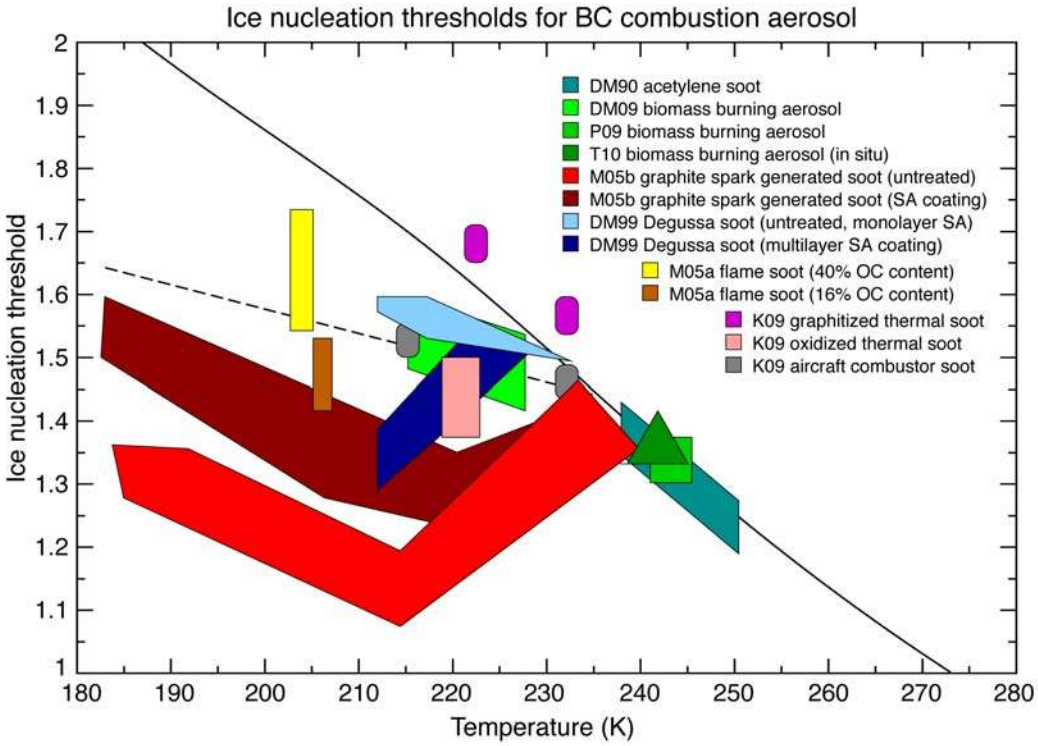

Figure 6.2. Compilation of heterogeneous ice nucleation thresholds of combustion aerosol samples from BC sources as a function of temperature. The ice nucleation threshold is the supersaturation with respect to ice at which the aerosol activates. Color-shaded regions show data from *DeMott* [1990] (DM90); *DeMott et al.* [1999] (DM99); *Möhler et al.* [2005a/b] (M05a/b); *Petters et al.* [2009] (P09); *DeMott et al.* [2009a] (DM09); *Köhler et al.* [2009] (K09); and *Twohy et al.* [2010] (T10). The dashed curve represents the equilibrium ice saturation ratio required to freeze an aqueous solution droplet of diameter 500 nm in 1 s [*Koop et al.*, 2000]. The solid curve is the water saturation curve, or the vapor pressure ratio of supercooled liquid water to hexagonal ice [*Murphy and Koop*, 2005]. Figure updated from *Kärcher et al.* [2007].

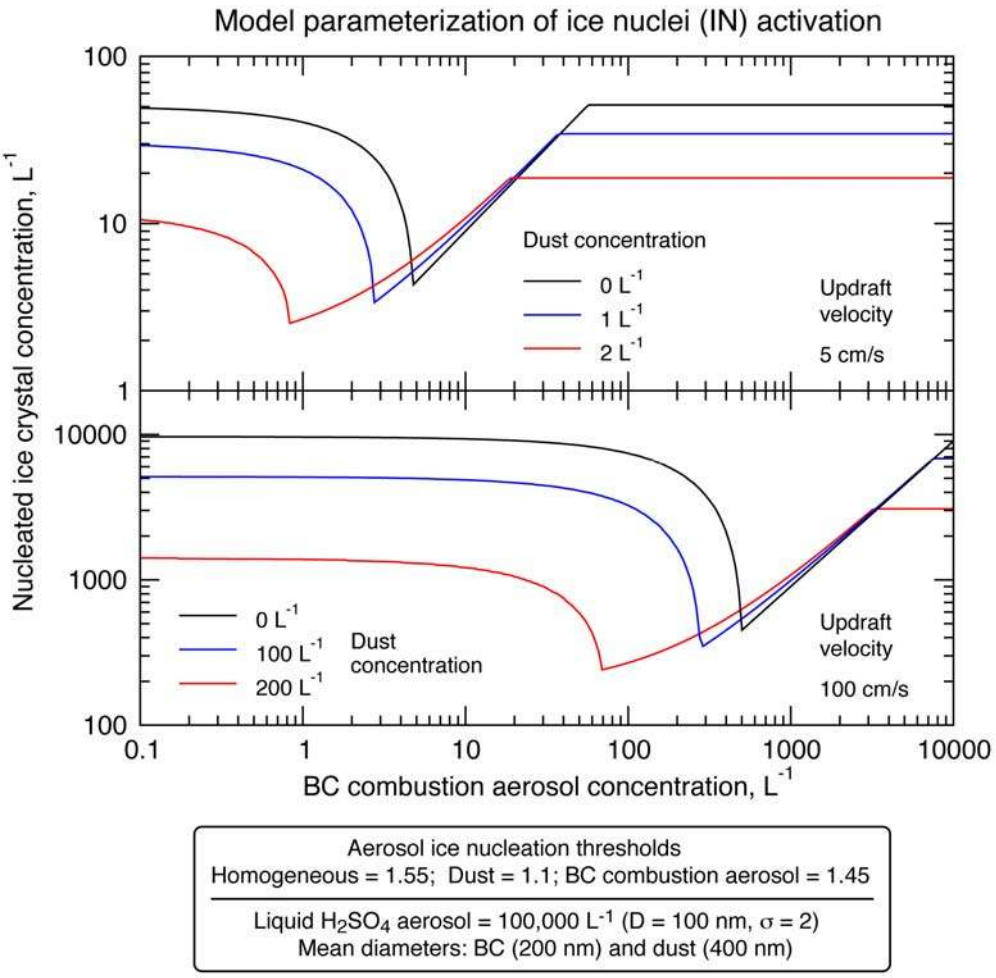

Figure 6.3. Calculated total number concentration of nucleated ice crystals as a function of BC combustion particle number concentration. Ice particle number results from the competition of three particle types (liquid H_2SO_4/ H_2O droplets acting as homogeneous freezing nuclei, and dust and BC particles acting as heterogeneous IN) during ice formation in adiabatically rising air parcels (sharp ice nucleation thresholds for the IN given in the legend). Results are shown for an updraft velocity of 5 cm/s (top panel, synoptic-scale vertical winds), and 100 cm/s (bottom panel, strong orographic waves or convective cells). In the simulations, air parcels start rising at 250 hPa and 220 K at ice saturation and contain mineral dust particles with concentrations noted in the legends, a wide range of BC (10^3 L^{-1} = 1 cm^{-3}) concentrations, and a fixed concentration of log-normally distributed aqueous H_2SO_4 particles. Dust and soot particles are assumed to be monodisperse. Adapted from *Kärcher et al.* [2007].

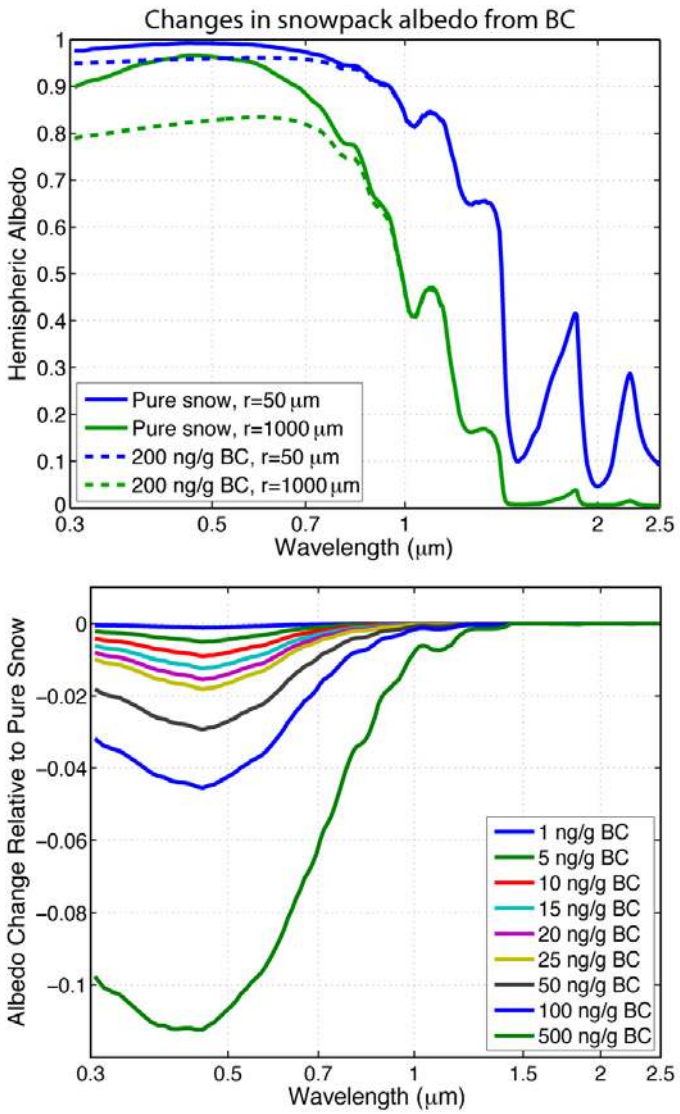

Figure 7.1. Top: Spectrally resolved, hemispheric albedo for snowpack effective grain sizes of radii (r) of 50 and 1000 μm, with and without BC mixing ratios of 200 ng/g, for a semi-infinite snowpack and with diffuse incident solar radiation. Changes in grain size most strongly affect albedo at near infrared wavelengths, whereas BC lowers albedo most strongly at visible and ultraviolet wavelengths. Bottom: the reduction in hemispheric albedo caused by various mixing ratios of BC as a function of wavelength, for a snowpack with effective grain size of 200 μm. BC optical properties are those used by *Flanner et al.* [2007, 2009] for hydrophobic (uncoated) particles, tuned to match recommendations from *Bond and Bergstrom* [2006]. Albedo calculations were made following *Flanner et al.* [2007, 2009].

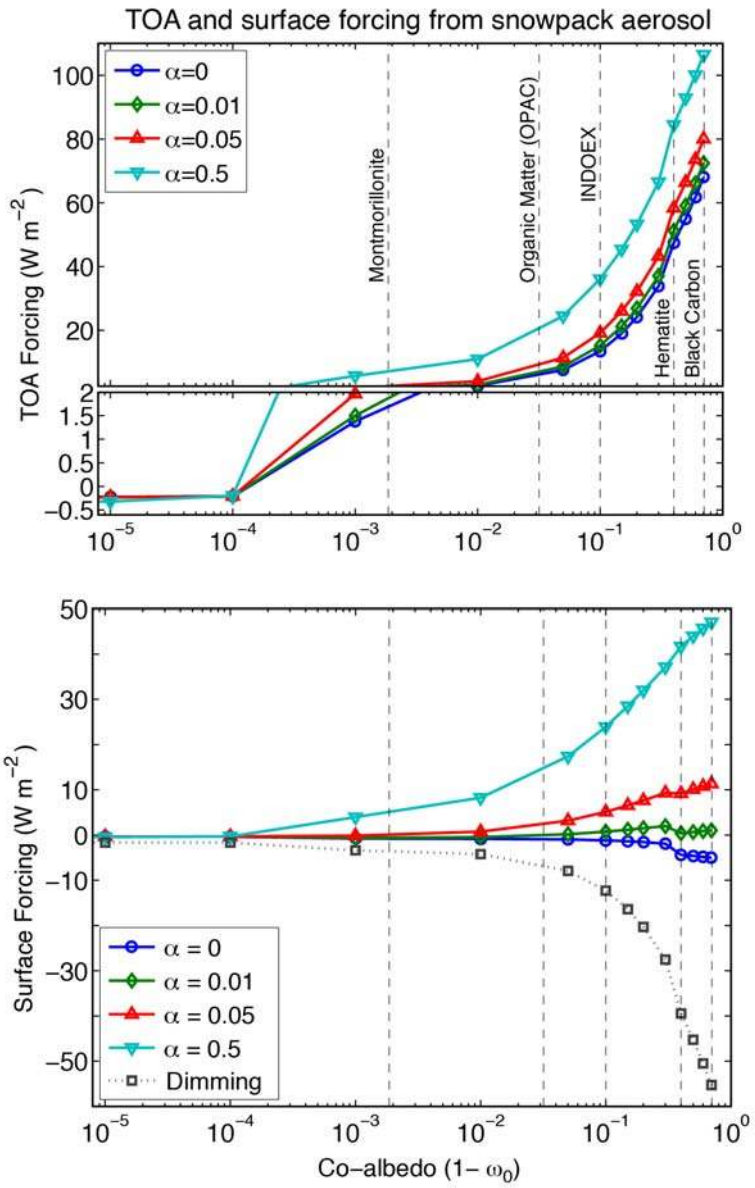

Figure 7.2. Daily-mean (top) top-of-atmosphere and (bottom) surface changes in net solar power (radiative forcing) as a function of single-scattering co-albedo ($1-\omega_o$) for all aerosol at 500 nm. Extinction optical depth of the atmospheric aerosol is fixed at 0.2 and the environment represents a clear-sky atmosphere overlying a snowpack with effective grain radius of 200 μm on 1 April at 45°N. Curves are shown for different values of α, which is the ratio of particle mixing ratio in snow to atmospheric column burden ((kg kg^{-1}) (kg·m^{-2})$^{-1}$). Radiative forcings represent the combined influence of particles in the atmosphere and snow. For reference, the change in downwelling surface insolation ('dimming') is also depicted. Vertical lines depict common co-albedo values of BC and organic matter, and that measured during the Indian Ocean Experiment (INDOEX) [*Ramanathan et al.,* 2001a]. Also shown are co-albedo values of strongly and weakly absorbing components of dust aerosols. The plot illustrates that 1) any mixture of atmospheric BC and organic matter exerts a positive ToA radiative forcing over snowpack, and 2) a small amount of aerosol mixed within the underlying snowpack exerts a darkening effect that exceeds the loss of absorbed energy from surface dimming caused by the atmospheric constituents. Figure from *Flanner et al*. [2009].

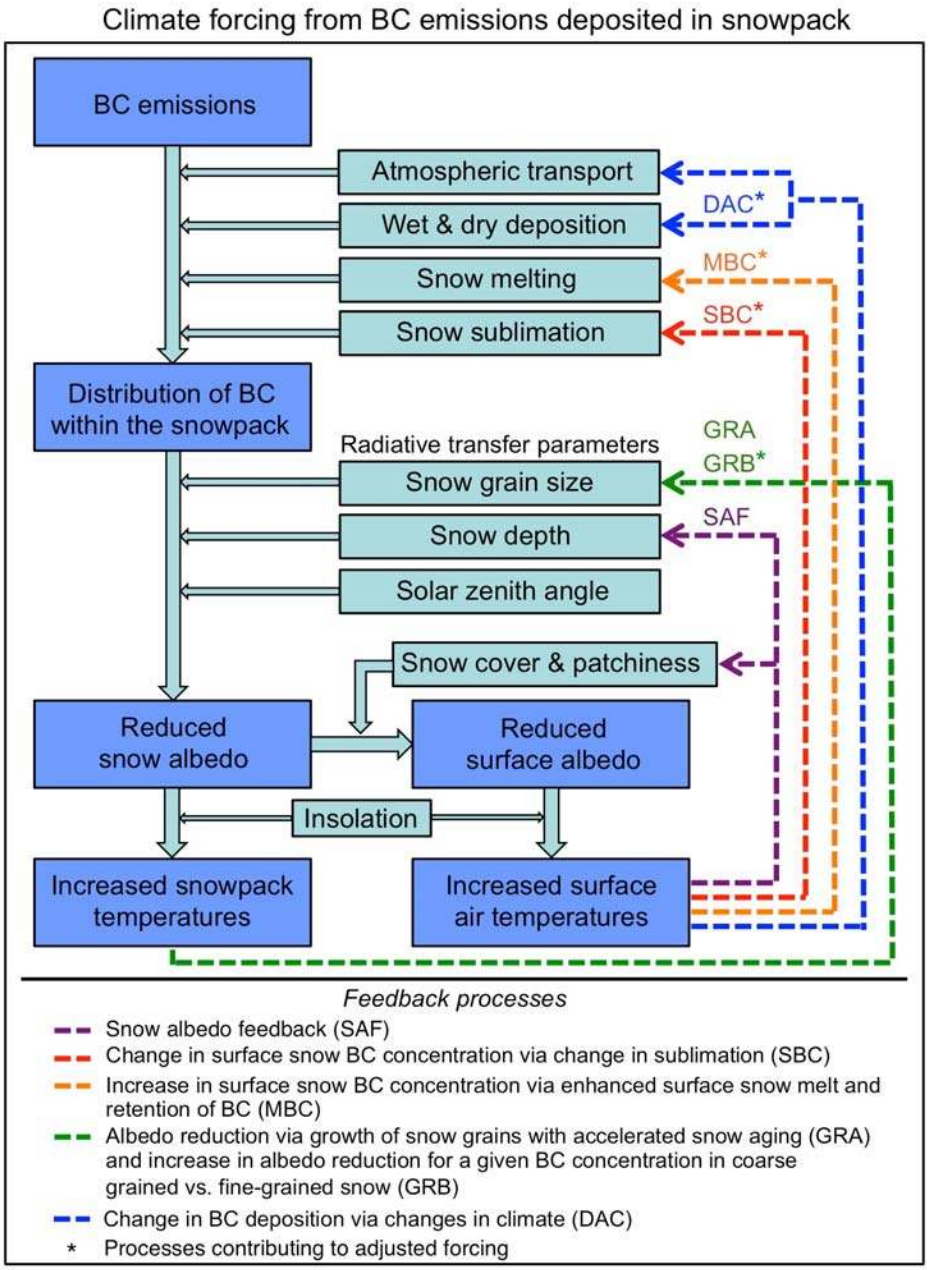

Figure 7.3. Schematic of the parameters and feedbacks that influence climate forcing by BC in surface snow. BC in the snowpack leads to reduced albedo of the snow surface, with the albedo change depending on BC amounts, snow grain size and snow depth. Reduced snowpack albedo reduces regional surface albedo and leads to increased snowpack and surface air temperatures. The temperature changes feed back to snow albedo through changes in snow parameters via several processes, as noted in the legend and discussed in the text. This figure emphasizes feedbacks specific to forcing by BC in snow. Changes in climate of any origin may also affect BC emissions, atmospheric transport, rates of BC deposition to the snowpack and snow accumulation rate.

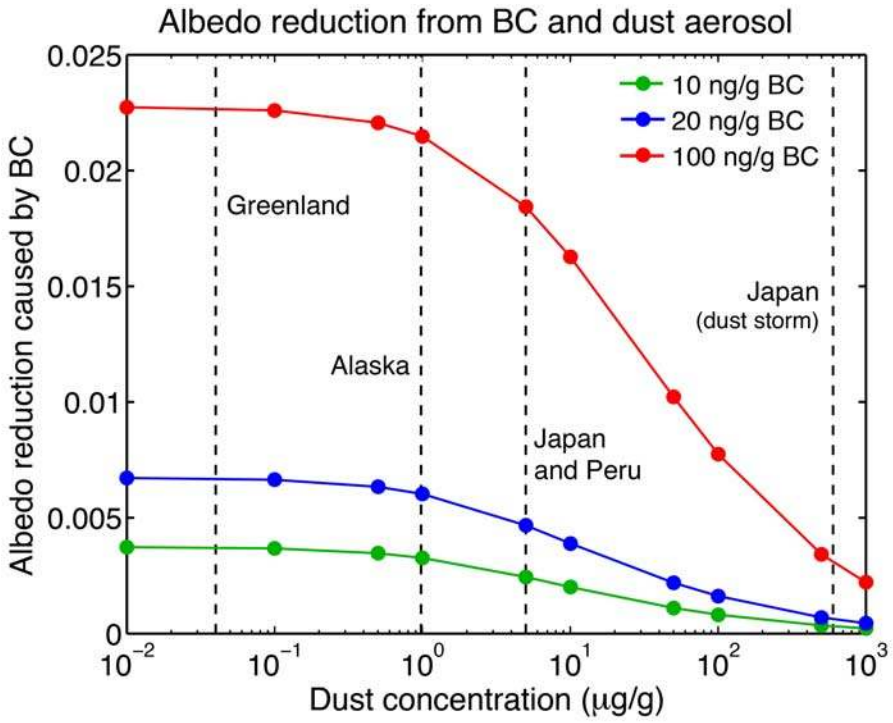

Figure 7.4. Reduction in hemispheric broadband snow albedo (0.3-5.0μm) caused by BC in the presence of varying amounts of dust. The perturbation caused by BC becomes smaller with increasing dust burden. Conditions represent a clear-sky atmosphere with solar zenith angle of 60 degrees and snowpack effective grain radius of 250 μm. Dust optical properties are similar to those listed in *Flanner et al.* [2009] for a particle effective radius of 1300 nm, and albedo calculations follow *Flanner et al.* [2009]. Vertical dashed lines depict, from left to right, dust-in-snow concentrations measured in Greenland (0.03-0.06 μg g^{-1}, *De Angelis et al.* [1997]; *Banta et al.* [2008]), Barrow Alaska (0.98 μg g^{-1}, *Darby et al.* [1974]), Hokkaido, Japan, during pre-melt and Andes, Peru (5 μg g^{-1}, *Thompson et al.* [1979]; *Higuchi and Nagoshi*, [1977]), and Hokkaido, Japan, after a dust storm (600 μg g^{-1}, *Aoki et al.* [2006]).

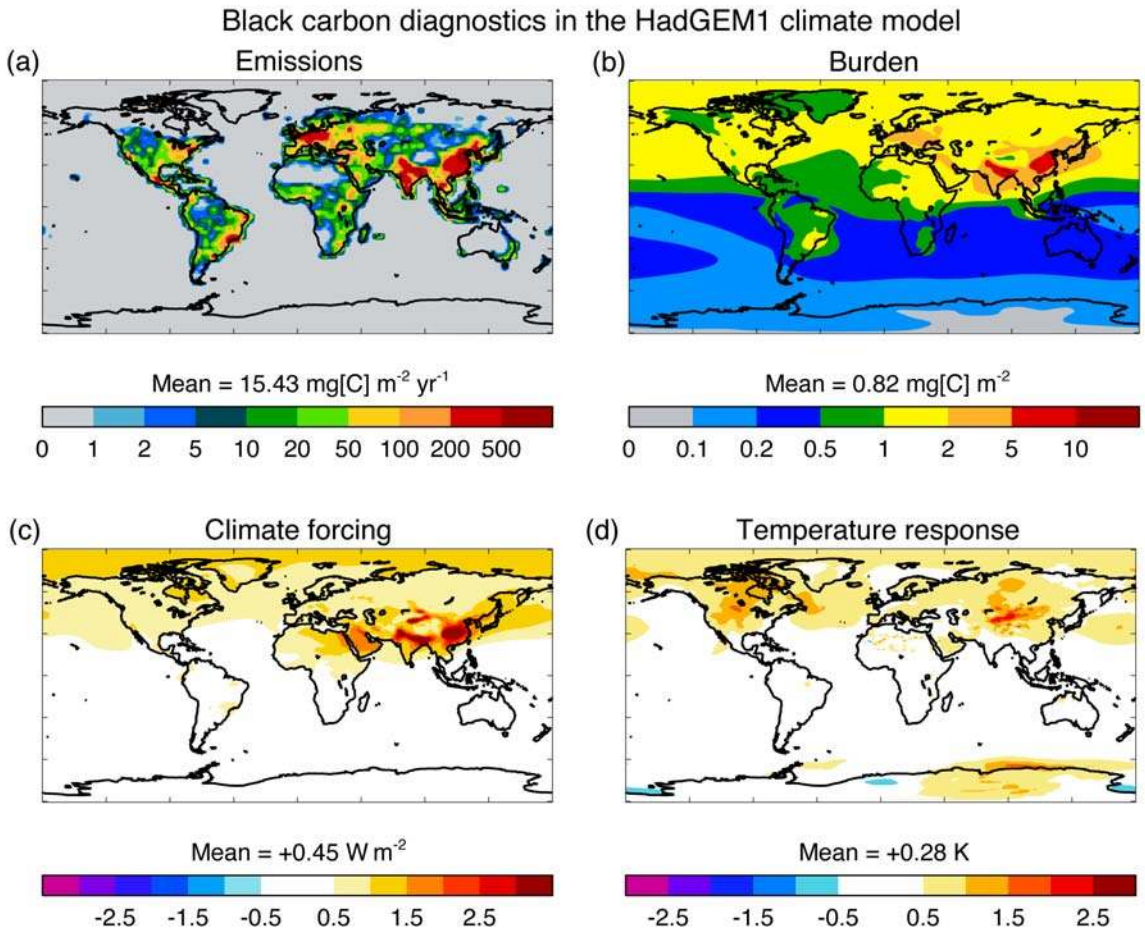

Figure 8.1. (a) Emissions of BC aerosols (mg BC m^{-2} yr^{-1}), (b) burden of BC aerosols (mg BC m^{-2}), (c) direct radiative forcing due to BC aerosols (Wm^{-2}) and (d) equilibrium surface temperature change (K) in response to the BC direct radiative forcing. Adapted from data from the Hadley Centre climate model (HadGEM1) published in *Jones et al.* [2007]. The patterns of burden, radiative forcing and surface temperature response are considered illustrative because the lifetime of BC is known to be too long in this model.

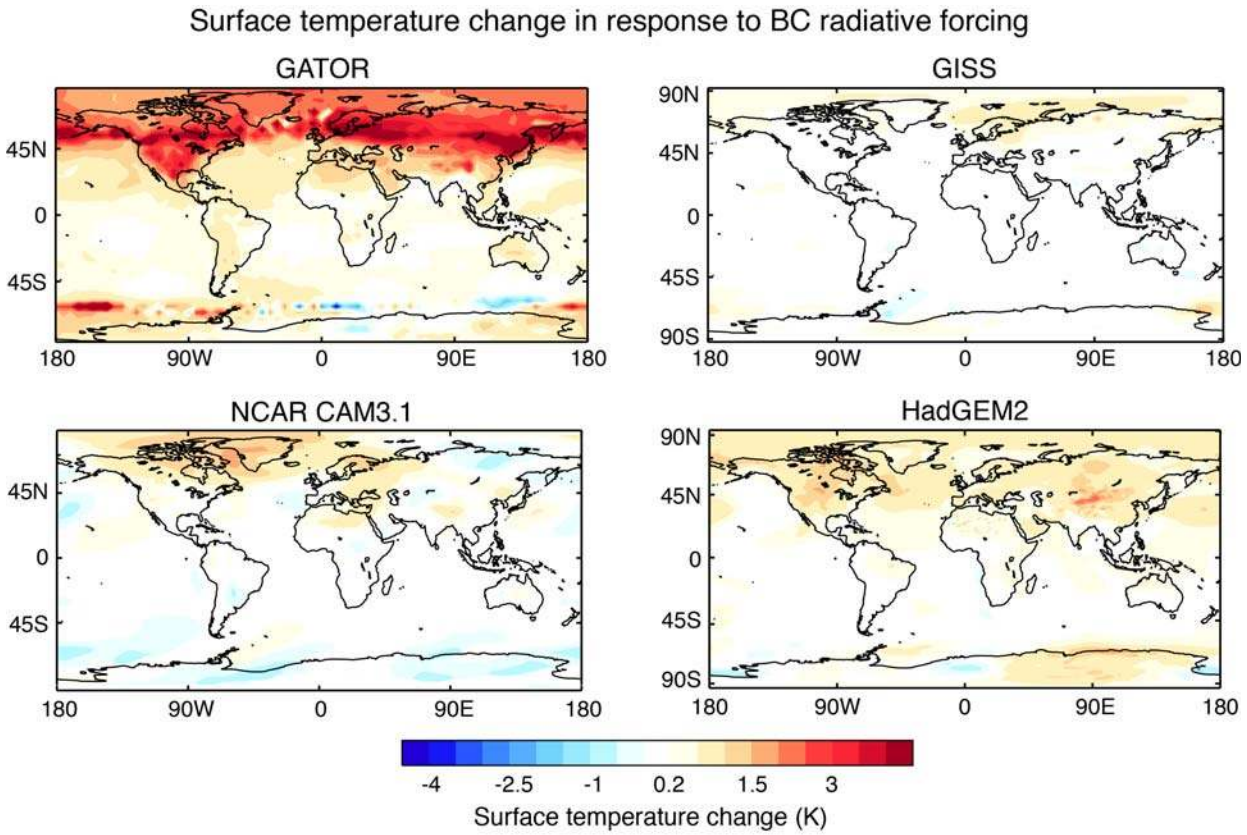

Figure 8.2. Surface temperature change in response to the BC radiative forcing in different climate models. Note that the experiments differ in their BC emissions, inclusion or not of the snow albedo and indirect effects on clouds, and setup. The panels are labeled with the model name. The details of each model and experimental setups are provided in Table 8.3.

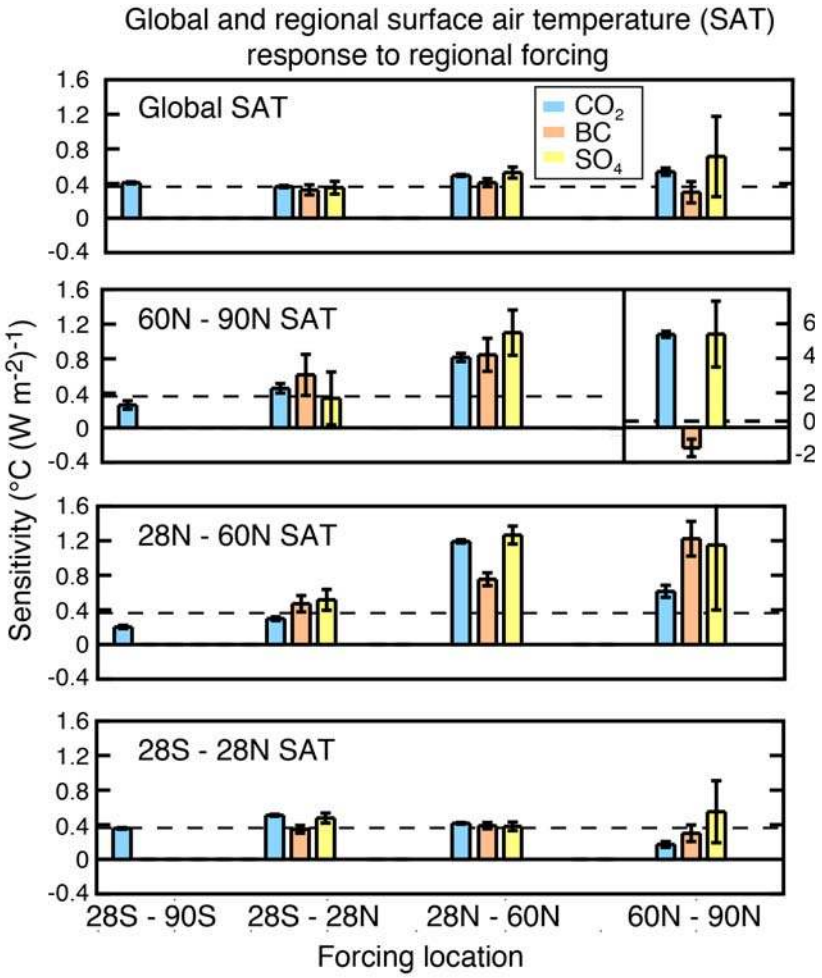

Figure 8.3. Normalized global and regional surface air temperature (SAT) changes (°C $(Wm^{-2})^{-1}$) in response to regional radiative forcings due to CO_2 (blue bars), BC aerosol (no cryosphere) (red bars) and sulfate aerosol (yellow bars). The forcing regions are defined on the horizontal axis as latitudinal bands (Southern Hemisphere mid- and high-latitudes, 28°S-90°S; tropics, 28°S-28°N; Northern Hemisphere mid-latitudes, 28°N-60°N; and Northern Hemisphere high-latitudes, 60°N-90°N). The SAT response regions are labeled in each panel. Adapted from *Shindell and Faluvegi* [2009].

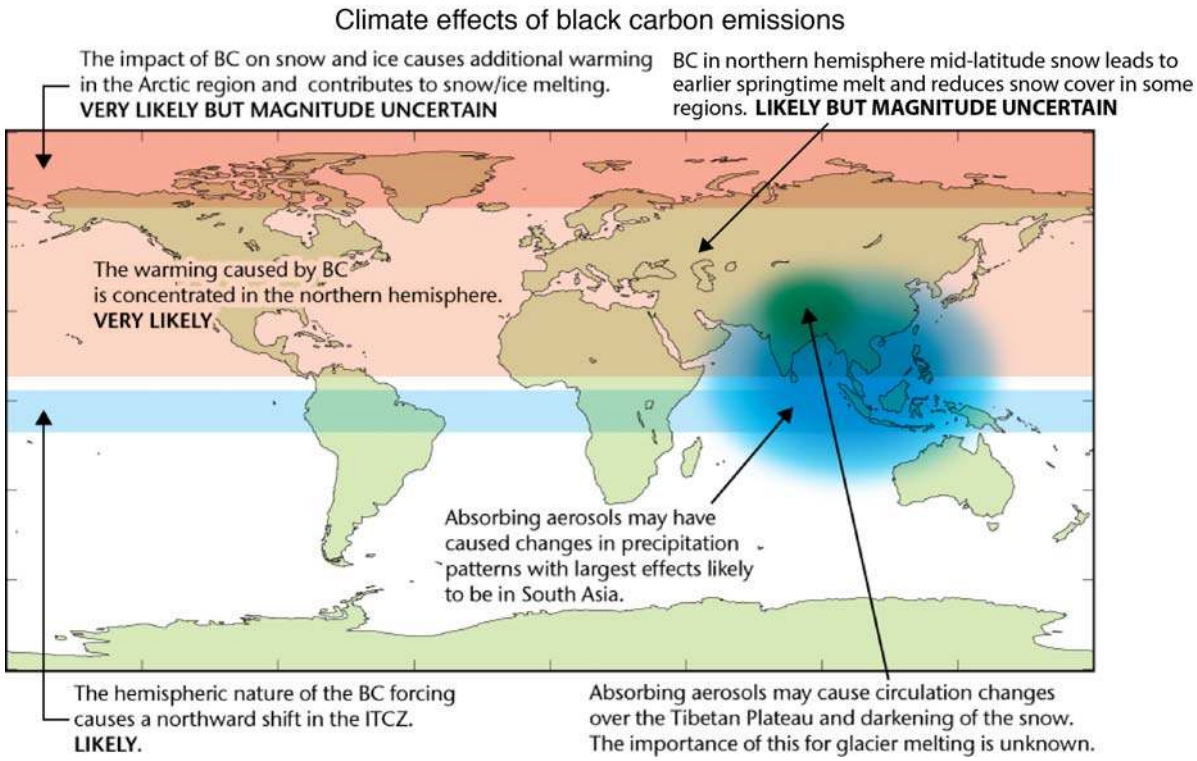

Figure 8.4. Qualitative summary of our current understanding of the global climate impacts of black carbon.

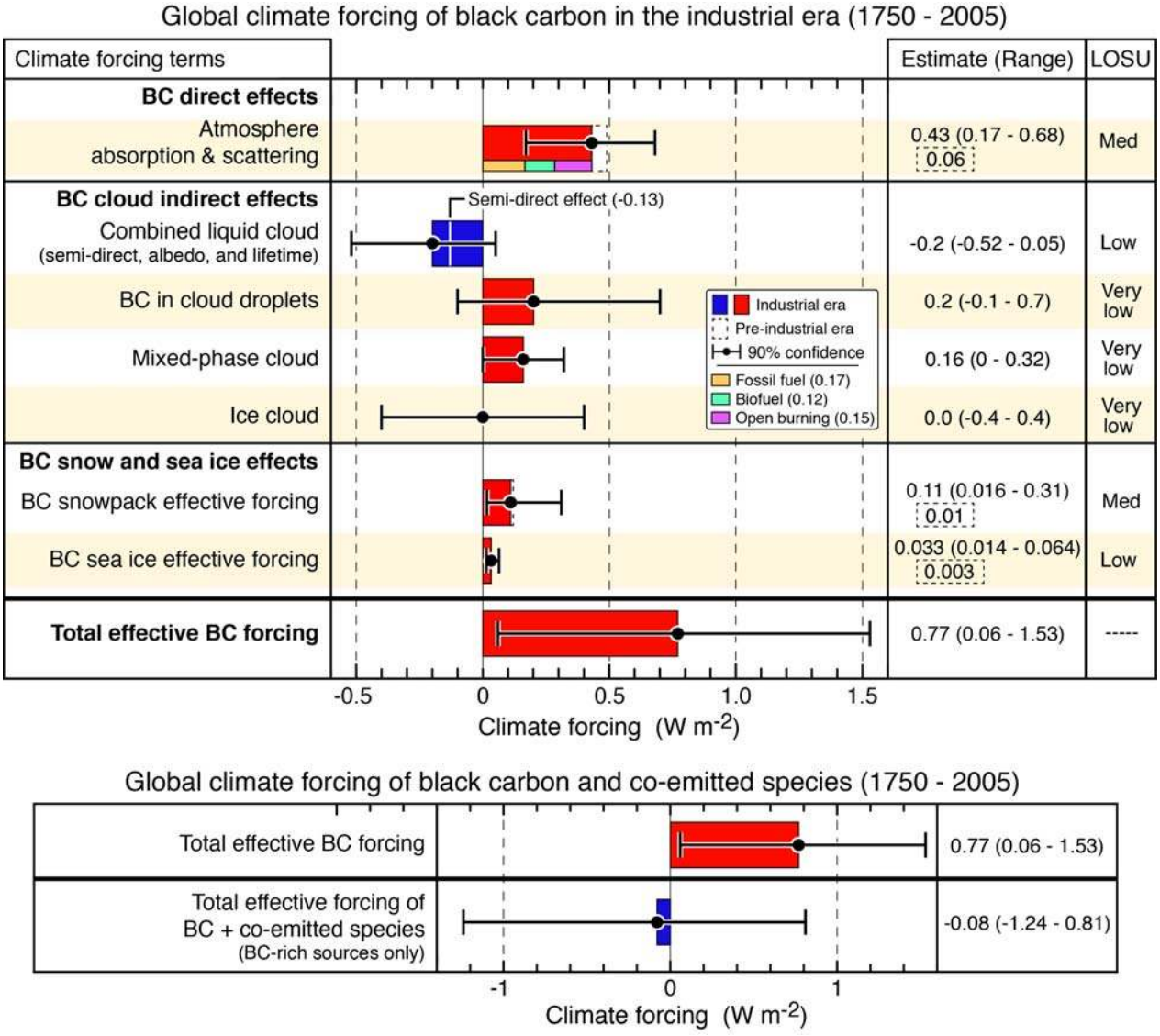

Figure 9.1. Globally averaged climate forcing in units of W m^{-2} from BC emissions in the year 2000 compared to those in 1750 (the industrial era). The top panel shows the breakdown into the different climate forcings of BC acting alone. The bottom panel compares the total forcing of BC acting alone with the combined forcing from the effect of BC plus its co-emitted species from BC-rich sources. Whiskers represent the assessed 90% uncertainty range (5% to 95%). The solid bars give best estimates for each climate forcing term. The three smaller bars added to the direct forcing bar and legend display the separate contributions to industrial-era radiative forcing from fossil fuel, biofuel and open burning emissions. The white line on the combined liquid-cloud forcing bar indicates the -0.12 ± 0.2 W m^{-2} contribution from semi-direct effects. The additional direct forcing of +0.09 W m^{-2} shown with the dashed line represents the direct radiative forcing from pre-industrial emissions (*i.e.,* prior to 1750). The combined colored and dashed bar represents our estimate of the all-source (*i.e.,* natural plus anthropogenic) direct radiative forcing, namely a +0.49 W m^{-2} best estimate with a +0.19 to +0.77 W m^{-2} uncertainty range (see Section 5). Likewise, the dashed line on the snow and sea-ice terms correspond to their additional climate forcing prior to 1750 and the combined bars give their all source forcing (see Section 7). For snow and ice effects their adjusted forcing and radiative forcings, respectively, have been scaled by their higher efficacy to give effective forcings as shown. The bottom bar on the upper panel presents our assessment of total effective forcing from all BC effects. The uncertainty for this bar is assessed using a Monte Carlo method that assumes correlated errors in some of the forcing terms (see text for details). The columns on the right give the numeric value for each climate forcing and its uncertainty; they also present a level of scientific understanding (LOSU) for each forcing term. LOSU follows IPCC practice [*Forster et al.,* 2007] and represents our assessment of confidence in our own evaluation of a given climate forcing (see Table 9.1 and Section 9 for further details). For details of the effective forcing resulting from co-emissions from BC-rich sources see Figure 10.2 and Section 10.

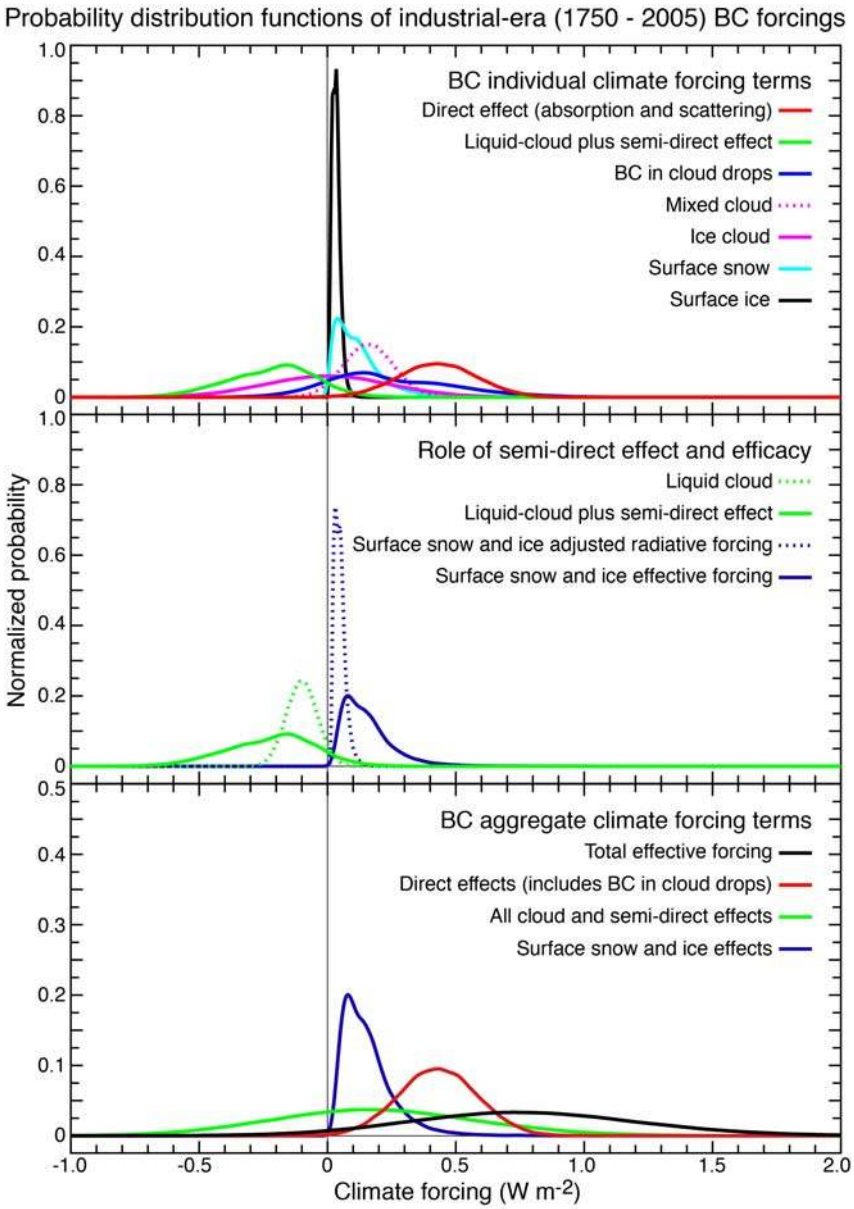

Figure 9.2. Probability distribution functions (PDFs) of industrial-era (1750 - 2000) forcings for BC climate forcing terms. Top: individual PDFs for each climate forcing term. Middle: before and after PDFs showing the role of the semi-direct effect in modifying the liquid cloud climate forcing term and the role of efficacy in modifying the BC-in-snow and BC-in-ice combined forcing term. Bottom: PDFs of the aggregated climate forcing components and the total effective climate forcing (see text for details). Probabilities are normalized to unity for all terms. Note the different vertical scale in the bottom panel.

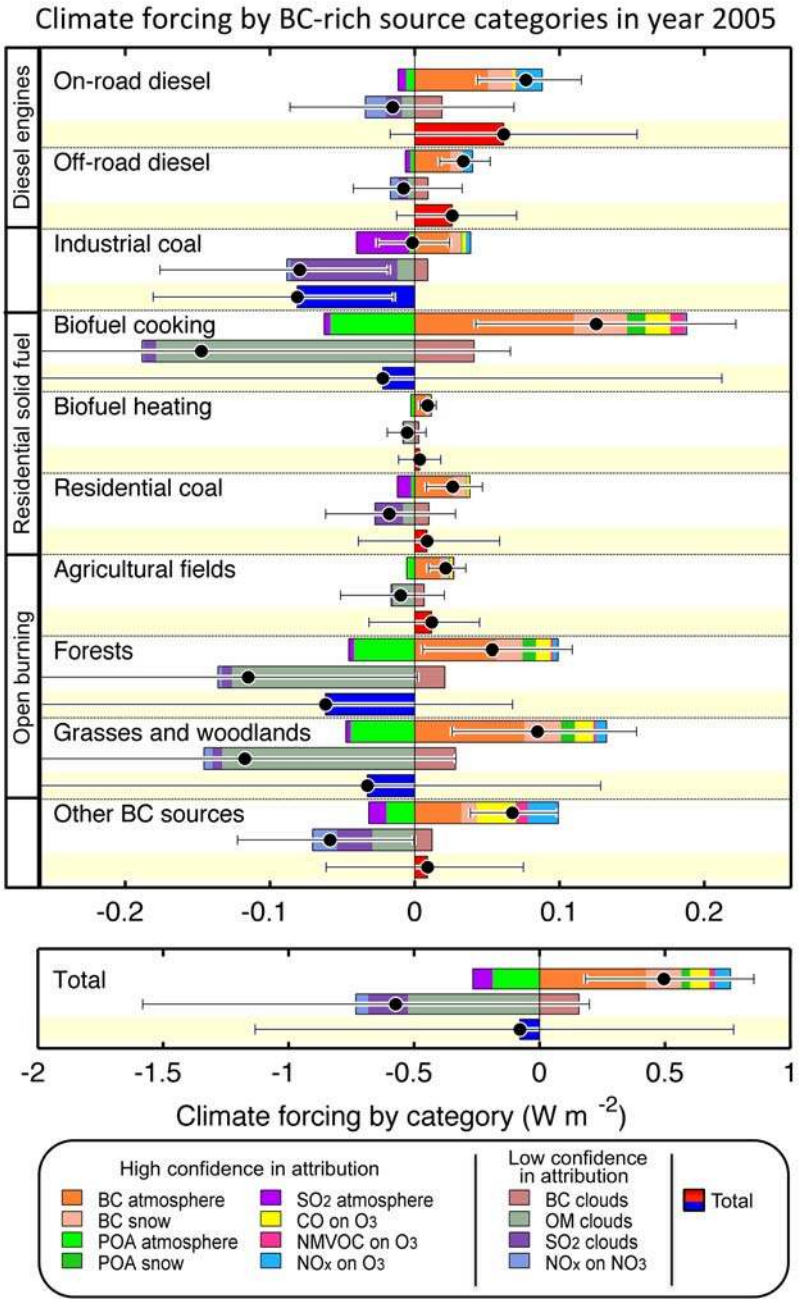

Figure 10.1. Total climate forcing for BC-rich source categories continuously emitting at year-2000 rates scaled to match observations. Three sets of climate forcings are shown for each source as bars with a best estimate (black circle) and uncertainty range. The top bar contains the components for which attribution to particular species is straightforward: direct forcing by aerosol and most gases, cryosphere forcing by aerosol (including climate feedback), and cloud response to aerosol absorption. The second bar shows the components for which there is less confidence in apportionment to individual species and, therefore, to sources. These components include all cloud indirect effects and forcing by nitrate from NO_x. The bottom bar in each group shows estimated net forcing by each emission source, combining all forcings and their uncertainties.

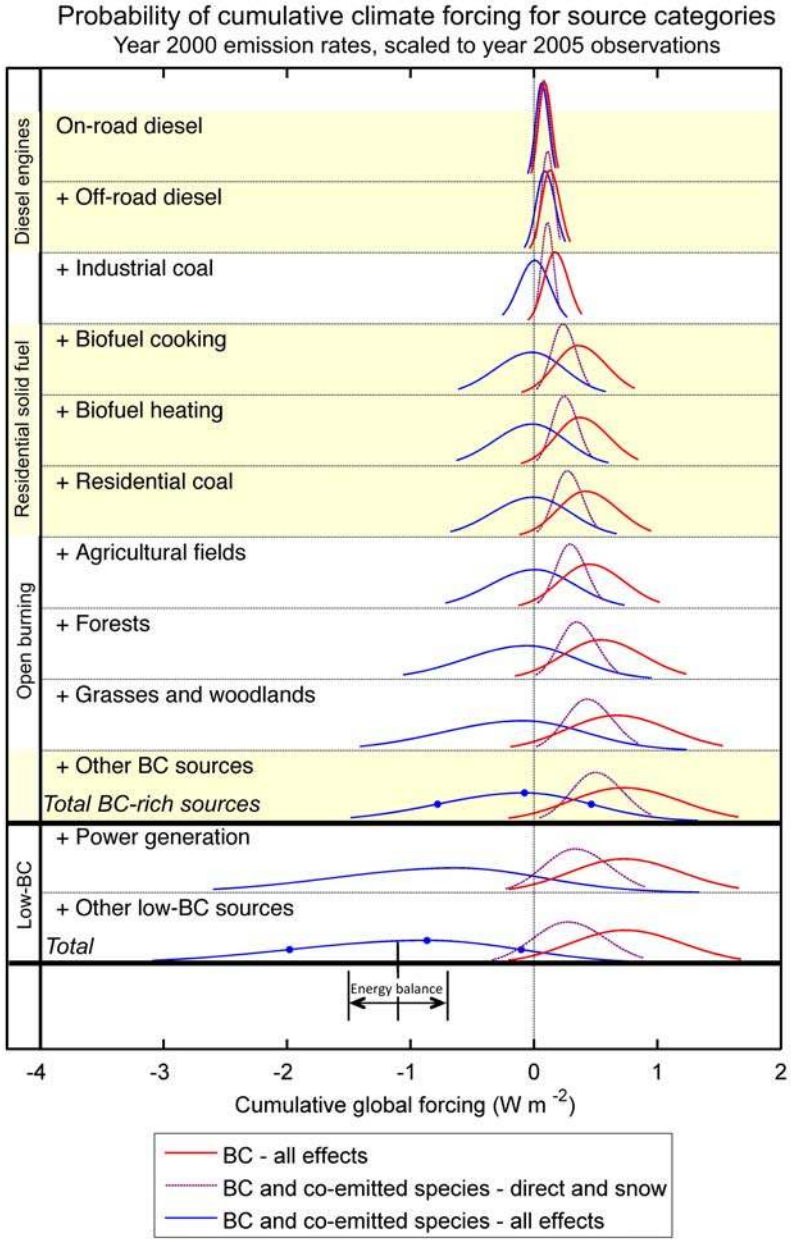

Figure 10.2. Probability density functions for effective climate forcing by emissions from the source categories and effects in Figure 10.1. Sources emit continuously at year-2000 levels, scaled to match atmospheric concentrations. Curves labeled 'BC-all effects' (red lines) show all effects attributable to BC, including cloud effects. Curves labeled 'BC and co-emitted species' (purple lines) show effects for which attribution to sources is straightforward, as described in Figure 10.1. Total climate forcing (blue lines) is the sum of forcing by all effects due to BC and co-emitted species, including clouds and nitrate forcing. Progressing from top to bottom, each curve represents forcing by the sum of the labeled category and all categories above it. The total value and its uncertainty from BC-rich sources and co-emitted species are reproduced as the bottom bar in Figure 9.1. The lowest set of curves labeled 'Other low-BC sources' represents the total effect of aerosol sources and, hence, includes first-year forcing by all aerosols, their precursors, and gaseous emissions. All curves have identical vertical scales and are normalized to unity. Blue dots on total curves represent 90% confidence intervals. Values outside of 95% confidence intervals are not plotted, so the curves do not meet the zero line. The arrow labeled 'energy-balance' represents the central value and one standard deviation of total forcing from an energy-balance calculation [*Murphy et al.*, 2009].

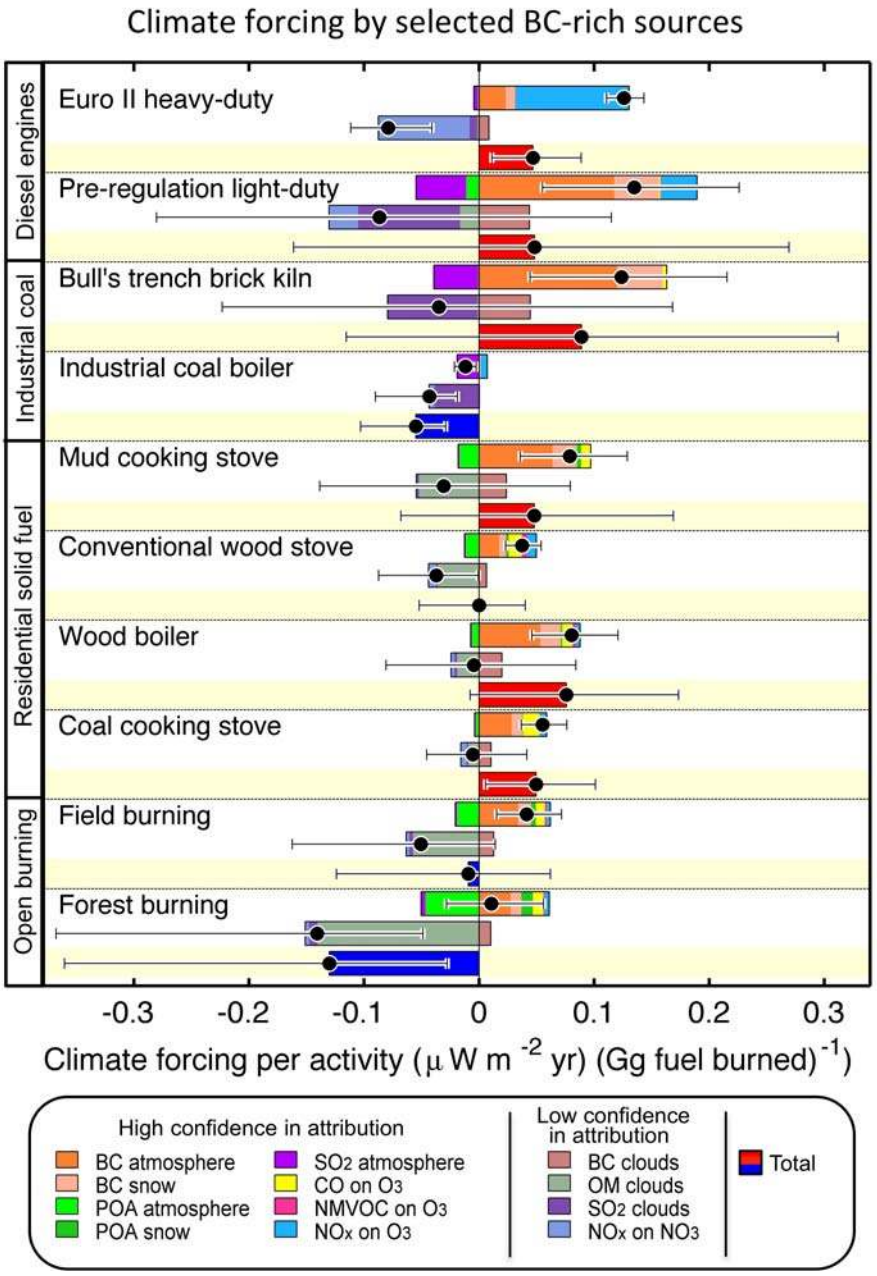

Figure 10.3. Climate forcing during the first year after emission, for selected individual sources that are subsets of the the categories in Figure 10.1. As in Figure 10.1, the three bars for each source correspond to (1) climate-forcing components for which attribution to species and sources can be done with high confidence (direct forcing by gases and aerosols); (2) components for which attribution to individual sources is difficult (cloud changes and nitrate forcing); and (3) total of all components.

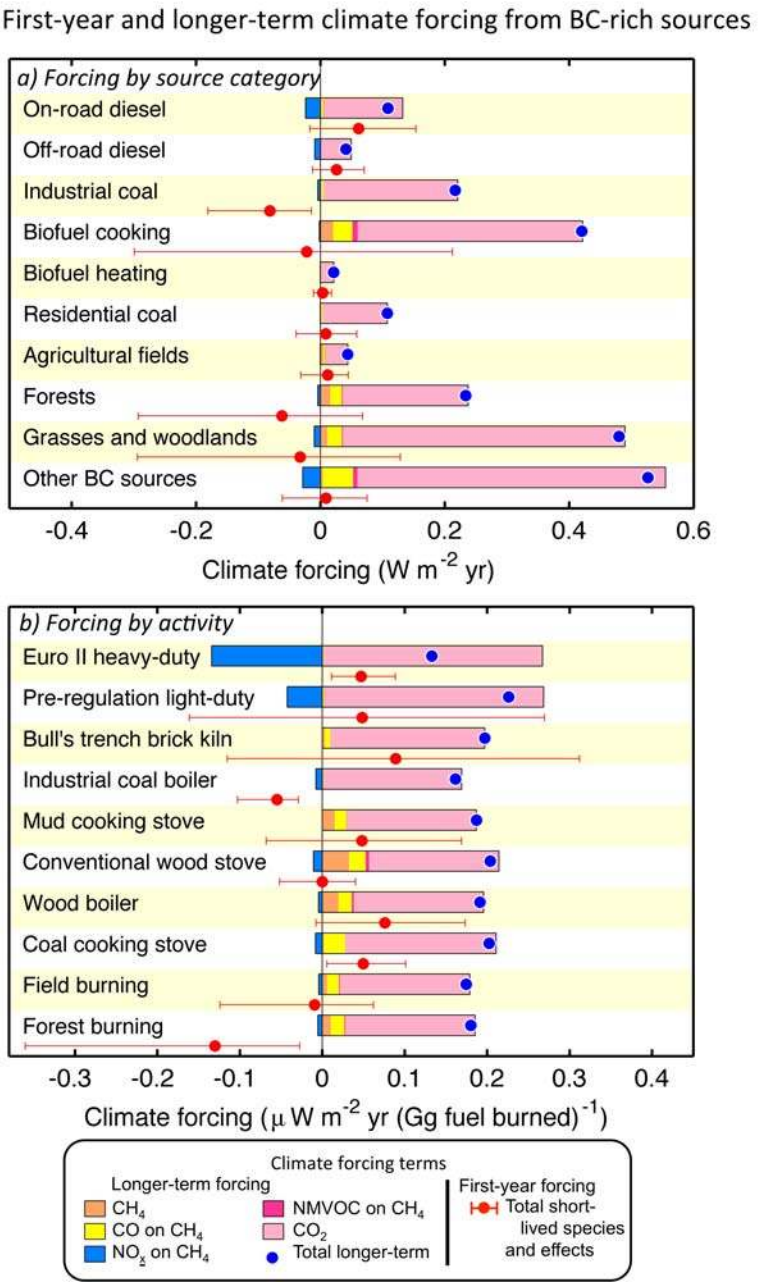

Figure 10.4. First-year and longer-term climate forcing of BC sources. The forcings are shown by category (top panel) and by source activity (bottom panel) corresponding to the categories in Figure 10.1 and 10.3. Totals and individual terms that make up integrated long-term (1-100 year) climate forcings, excluding the first-year forcing, are shown for individual terms and the total forcing with the first-year forcing excluded. The total for the first-year forcing and its uncertainty are also shown in both panels. This figure shows integrated forcing from (a) a single year of emissions (top, 2000 emission rates scaled to match atmospheric observations) or (b) a finite quantity of fuel burned, and does not assume that emissions are sustained.

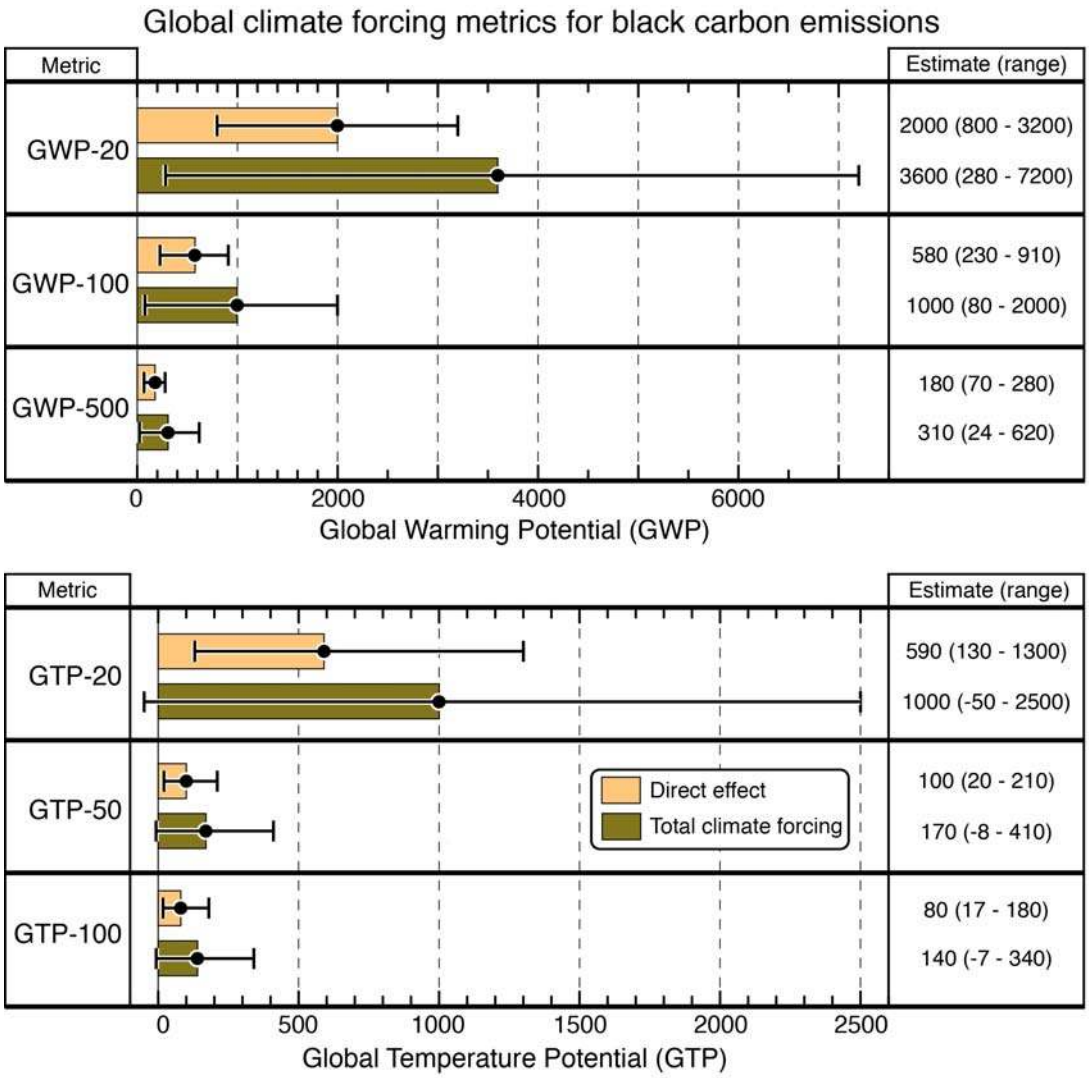

Figure 11.1. GTP and GWP values for several time horizons for BC climate forcing. Values are shown for the BC direct effect and the total climate forcing. The calculations use the industrial-era climate forcing values displayed in Figure 9.1 and an annual BC emission of 8700 Gg yr^{-1}. The whiskers represent the uncertainty range as described in the text.

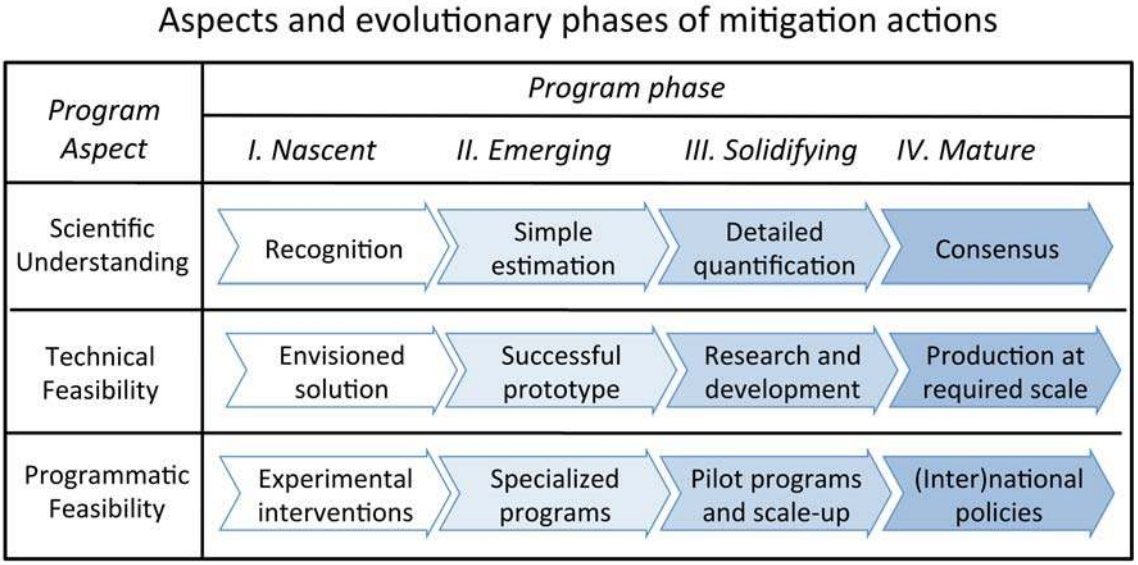

Figure 12.1. Conceptual framework for evaluating the feasibility of mitigating environmental impacts. The principal aspects are scientific understanding and technical and programmatic feasibility. Each aspect has evolutionary phases that reach maturity in several steps. Different emission sources are generally at different phases in the evolution of knowledge associated with each mitigation aspect. This assessment has primarily focused on the aspect of scientific understanding.

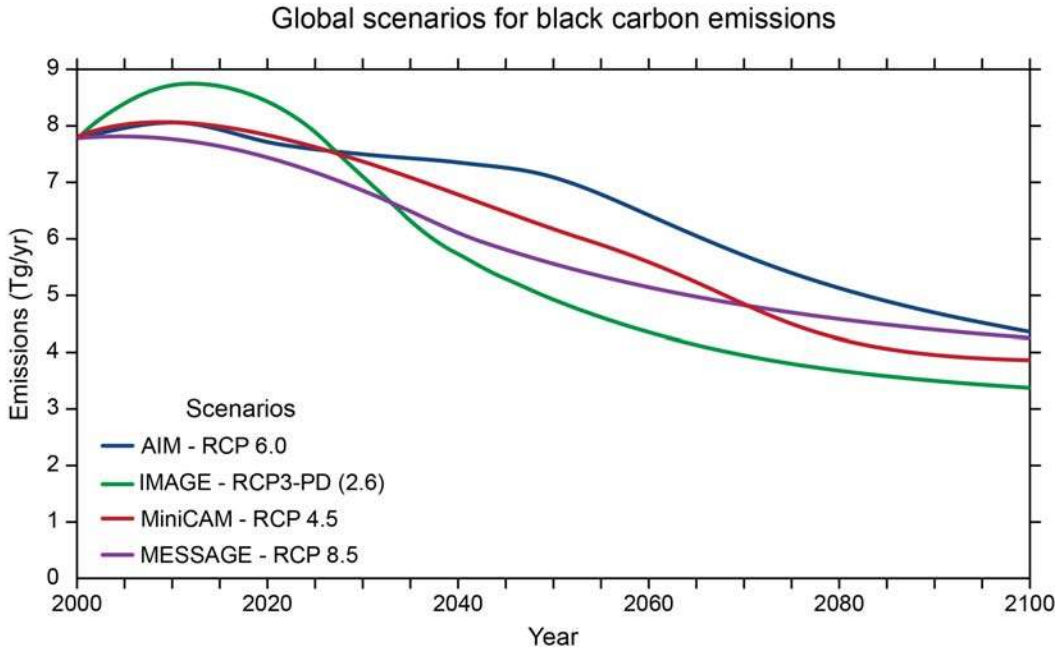

Figure 12.2. Total global BC emission projections from 2000-2100 in the four Representative Concentration Pathway (RCP) scenarios [*Moss et al.,* 2010]. These scenarios are named according to the radiative forcing in 2100, and were developed by four individual modeling groups for use in climate modeling analysis for the IPCC Fifth Assessment Report. Decreasing emissions are a result of expectations of cleaner fuels use and declining emission factors with increasing income.